PROCEEDINGS OF SPIE

Advances in X-Ray/EUV Optics and Components III

Ali M. Khounsary
Christian Morawe
Shunji Goto
Editors

11–13 August 2008
San Diego, California, USA

Sponsored and Published by
SPIE

Volume 7077

Proceedings of SPIE, 0277-786X, v. 7077

Please use the following format to cite material from this book:
Author(s), "Title of Paper," in *Advances in X-Ray/EUV Optics and Components III*, edited by Ali M. Khounsary, Christian Morawe, Shunji Goto, Proceedings of SPIE Vol. 7077 (SPIE, Bellingham, WA, 2008) Article CID Number.

ISSN 0277-786X
ISBN 9780819472977

Published by
SPIE
P.O. Box 10, Bellingham, Washington 98227-0010 USA
Telephone +1 360 676 3290 (Pacific Time) · Fax +1 360 647 1445
SPIE.org

Printed in the United States of America.

Publication of record for individual papers is online in the SPIE Digital Library.

SPIE Digital Library
SPIEDigitalLibrary.org

Paper Numbering: Proceedings of SPIE follow an e-First publication model, with papers published first online and then in print and on CD-ROM. Papers are published as they are submitted and meet publication criteria. A unique, consistent, permanent citation identifier (CID) number is assigned to each article at the time of the first publication. Utilization of CIDs allows articles to be fully citable as soon they are published online, and connects the same identifier to all online, print, and electronic versions of the publication. SPIE uses a six-digit CID article numbering system in which:

- The first four digits correspond to the SPIE volume number.
- The last two digits indicate publication order within the volume using a Base 36 numbering system employing both numerals and letters. These two-number sets start with 00, 01, 02, 03, 04, 05, 06, 07, 08, 09, 0A, 0B … 0Z, followed by 10-1Z, 20-2Z, etc.

The CID number appears on each page of the manuscript. The complete citation is used on the first page, and an abbreviated version on subsequent pages. Numbers in the index correspond to the last two digits of the six-digit CID number.

Contents

SESSION 1 MULTILAYERS

SESSION 2 MIRRORS + METROLOGY

SESSION 3 X-RAY LENSES

SESSION 4 CRYSTALS + DIFFRACTION

SESSION 5 FOCUSING

SESSION 6 X-RAY SOURCES

SESSION 7 XUV OPTICS + APPLICATIONS

SESSION 8 BEAMLINE OPTICS

POSTER SESSION

Conference Committee

Program Track Chairs

Sandra G. Biedron, Argonne National Laboratory (United States) and Sincrotrone Trieste S.C.p.A (Italy)
Massimo Altarelli, Deutsches Elektronen-Synchrotron (Germany)

Conference Chairs

Ali M. Khounsary, Argonne National Laboratory (United States)
Christian Morawe, European Synchrotron Radiation Facility (France)
Shunji Goto, Japan Synchrotron Radiation Research Institute (Japan)

Program Committee

John R. Arthur, Stanford Synchrotron Radiation Laboratory (United States)
Lahsen Assoufid, Argonne National Laboratory (United States)
Stefan Braun, Fraunhofer-Institut für Werkstoff- und Strahltechnik (Germany)
Shih-Lin Chang, National Tsing Hua University (Taiwan)
Sultan B. Dabagov, Istituto Nazionale di Fisica Nucleare (Italy)
Ralf D. Geckeler, Physikalisch-Technische Bundesanstalt (Germany)
Hans M. Hertz, Kungliga Tekniska Högskolan (Sweden)
Werner H. Jark, Sincrotrone Trieste S.C.p.A. (Italy)
Alexander Yu. Kazimirov, Cornell University (United States)
Igor V. Kozhevnikov, A.V. Shubnikov Institute of Crystallography (Russia)
George A. Kyrala, Los Alamos National Laboratory (United States)
Carolyn A. MacDonald, SUNY/University at Albany (United States)
Kazuya Ota, Nikon Corporation (Japan)
Howard A. Padmore, Lawrence Berkeley National Laboratory (United States)
Ladislav Pina, Czech Technical University in Prague (Czech Republic)
Michael James Pivovaroff, Lawrence Livermore National Laboratory (United States)
Yuriy Ya. Platonov, Rigaku/MSC, Inc. (United States)
Seungyu Rah, Pohang University of Science and Technology (Republic of Korea)
Kawal J. S. Sawhney, Diamond Light Source Ltd. (United Kingdom)
Anatoly A. Snigirev, European Synchrotron Radiation Facility (France)
Regina Soufli, Lawrence Livermore National Laboratory (United States)
Peter Z. Takacs, Brookhaven National Laboratory (United States)
Kai Tiedtke, Deutsches Elektronen-Synchrotron (Germany)

Makina Yabashi, Japan Synchrotron Radiation Research Institute (Japan)
Kazuto Yamauchi, Osaka University (Japan)
Brian W. Yates, Canadian Light Source, Inc. (Canada)

Session Chairs

1 Multilayers
Christian Morawe, European Synchrotron Radiation Facility (France)

2 Mirrors + Metrology
Ali M. Khounsary, Argonne National Laboratory (United States)

3 X-Ray Lenses
Werner H. Jark, Sincrotrone Trieste S.C.p.A. (Italy)

4 Crystals + Diffraction
Shunji Goto, Japan Synchrotron Radiation Research Institute (Japan)

5 Focusing
Ladislav Pina, Czech Technical University in Prague (Czech Republic)

6 X-Ray Sources
Carolyn A. MacDonald, SUNY/University at Albany (United States)

7 XUV Optics + Applications
Regina Soufli, Lawrence Livermore National Laboratory (United States)

8 Beamline Optics
Alexander Yu. Kazimirov, Cornell University (United States)

Focus on X-Ray Focusing Workshop
Ali M. Khounsary, Argonne National Laboratory (United States)
Christian Morawe, European Synchrotron Radiation Facility (France)
Shunji Goto, Japan Synchrotron Radiation Research Institute (Japan)

Focus on X-Ray Focusing Workshop

August 13, 2008

"Focus on X-Ray Focusing" was the title of a one-day workshop during Optics + Photonics 2008 held on August 13, 2008 in conjunction with the Advances in X-Ray/EUV Optics and Components III conference. The aim of the Workshop was to provide the audience with a comprehensive introduction and up-to-date information on various X-ray focusing techniques covering theory, development, implementation, progress and applications. The Workshop consisted of ten presentations by some of the renowned practitioners in the field, each describing one of the focusing techniques and its challenges, limitations, and prospects.

Workshop Chairs:
Ali Khounsary, Argonne National Laboratory
Christian Morawe, European Synchrotron Radiation Facility (France)
Shunji Goto, Japan Synchrotron Radiation Research Institute (Japan)

Introduction to x-ray focusing, Franz Pfeiffer, Swiss Light Source, Paul Scherrer Institute and Ecole Polytechnique Fédérale de Lausanne (Switzerland)

X-ray focusing with Kirkpatrick-Baez optics, K. Yamauchi, Osaka Univ. (Japan)

Hard x-ray focusing with curved reflective multilayers, Christian Morawe, European Synchrotron Radiation Facility (France)

Refractive x-ray lenses for hard x-ray microscopy, Chrstian G. Schroer, Technische Univ. Dresden (Germany)

Kinoform x-ray lens arrays, Werner H. Jark, Sincrotrone Trieste (Italy)

Monocapillary optics, Ladislav Pina, Czech Technical Univ. (Czech Republic) (presentation not available)

X-ray focusing with polycapillary optics, Carolyn A. MacDonald, SUNY, Univ. at Albany

Focusing of x-rays using crystal optics, Eckhart Förster, Friedrich-Schiller-Univ. Jena (Germany)

Multilayer Laue Lens for efficient nanometer focusing of hard x-rays, G. B. Stephenson, Argonne National Lab.

Diffractive focusing by zone plates, Michael Feser, Xradia, Inc.

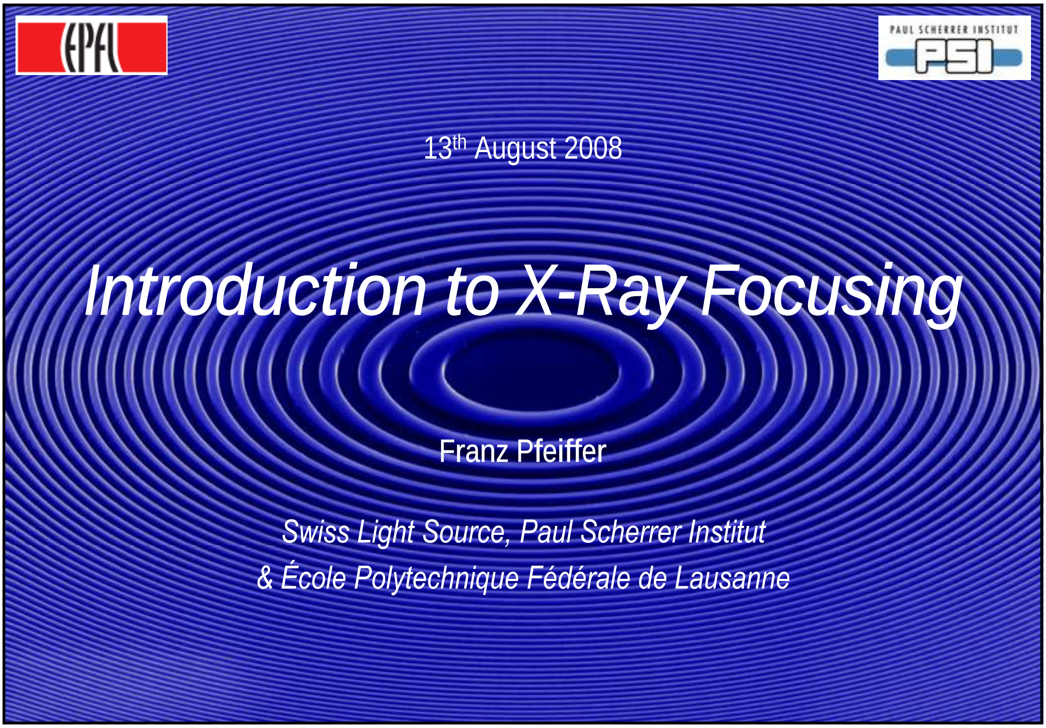

13th August 2008

Introduction to X-Ray Focusing

Franz Pfeiffer

Swiss Light Source, Paul Scherrer Institut
& École Polytechnique Fédérale de Lausanne

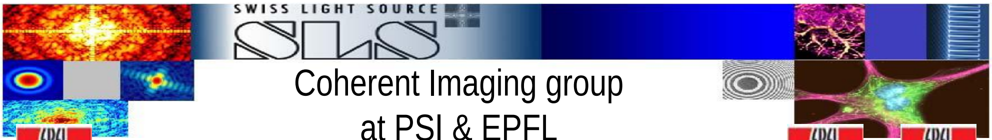

Coherent Imaging group at PSI & EPFL


Franz Pfeiffer


Oliver Bunk


Andreas Menzel


Xavier Donath


Pierre Thibault


Cameron Kewish

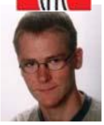
Martin Dierolf


Tobias Boehlen

Christian David, Joan Vila, Konstantins Jefimovs, Vitaliy Guzenko, Harun Solak, Sankha Sarkar,
Laboratory for Micro- and Nanotechnology, Paul Scherrer Institut, CH

Outline

1. X-ray focusing – Why
2. Methods overview – focus on X-ray waveguides
3. Recent advances at Paul Scherrer Institut
4. ‘Super-Resolution’ coherent X-ray microscopy
   & characterization of focused wave-fields

Email: franz.pfeiffer@psi.ch - Web: http://people.epfl.ch/franz.pfeiffer

---

X-ray Focusing – Why

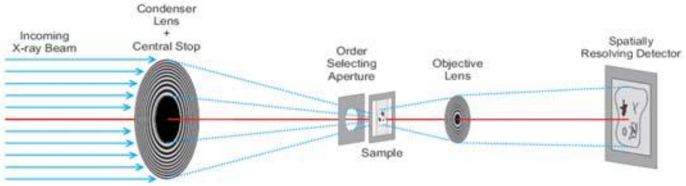

+ fast

- only x-ray transmission signal

full-field microscope

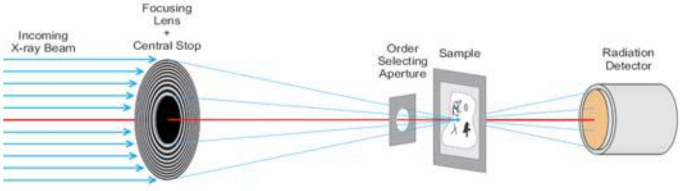

+ many detection schemes possible (elemental & chemical specificity, crystalline ordering, …)

-requires coherent illumination

scanning microscope

Email: franz.pfeiffer@psi.ch - Web: http://people.epfl.ch/franz.pfeiffer

Small-Angle X-Ray Scattering (SAXS) & Scanning Microscopy

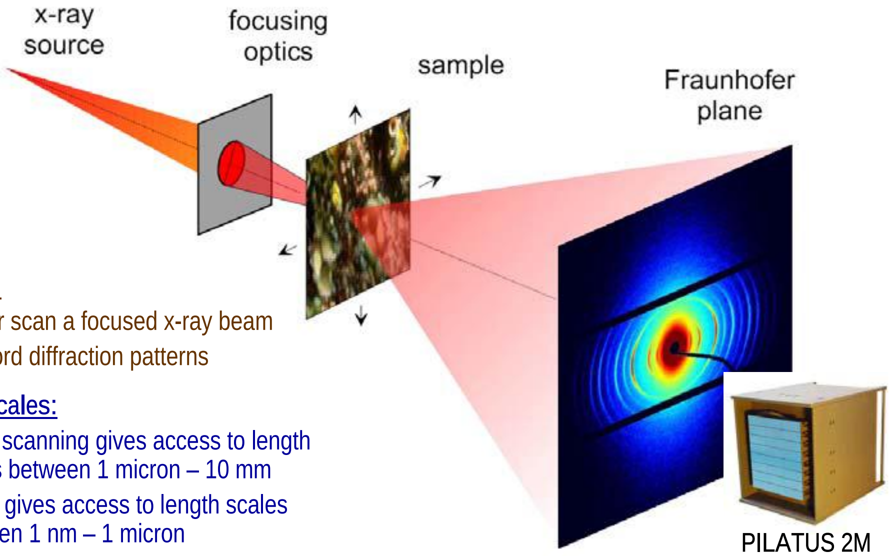

Principle:

- ➢ Raster scan a focused x-ray beam & record diffraction patterns

Length Scales:

- ➢ raster scanning gives access to length scales between 1 micron – 10 mm
- ➢ SAXS gives access to length scales between 1 nm – 1 micron

Email: franz.pfeiffer@psi.ch - Web: http://people.epfl.ch/franz.pfeiffer

---

Small-Angle X-Ray Scattering (SAXS) & Scanning Microscopy

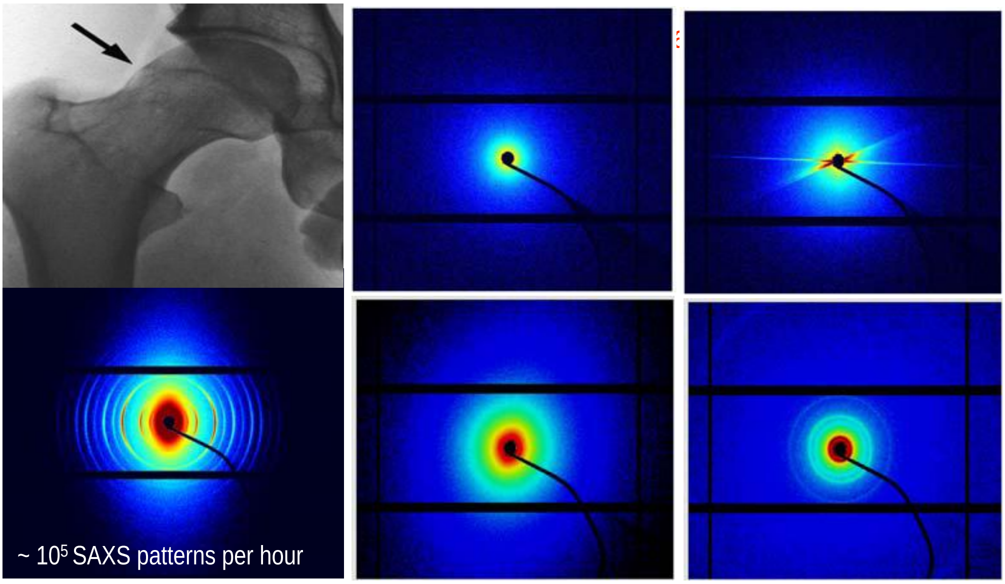

~ 10^5 SAXS patterns per hour

Email: franz.pfeiffer@psi.ch - Web: http://people.epfl.ch/franz.pfeiffer

Small-Angle X-Ray Scattering (SAXS) & Scanning Microscopy

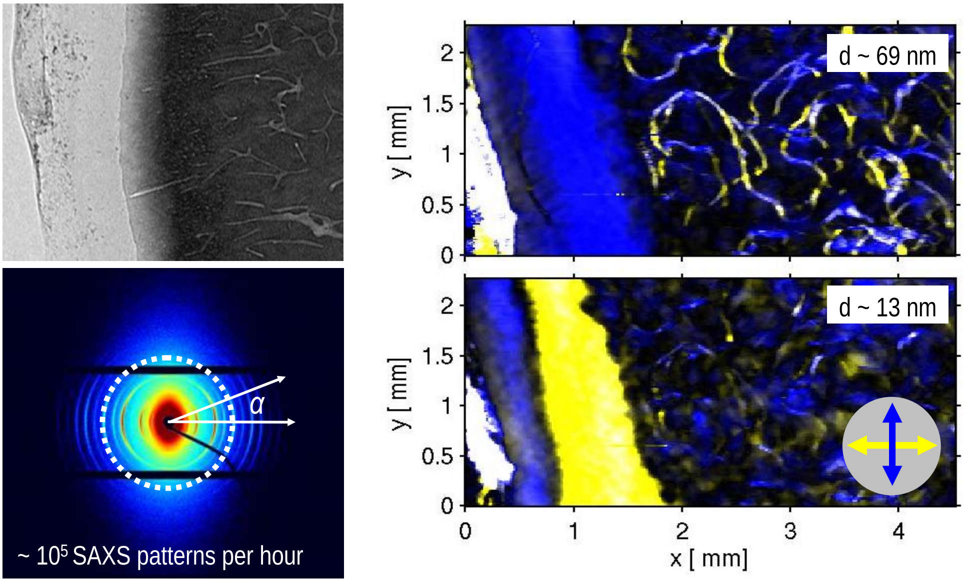

Email: franz.pfeiffer@psi.ch - Web: http://people.epfl.ch/franz.pfeiffer

---

Outline

1. X-ray focusing – Why
2. Methods overview – focus on X-ray waveguides
3. Recent advances at Paul Scherrer Institut
4. ‘Super-Resolution’ coherent X-ray microscopy
   & characterization of focused wave-fields

Email: franz.pfeiffer@psi.ch - Web: http://people.epfl.ch/franz.pfeiffer

X-Ray Focusing - HOWTO

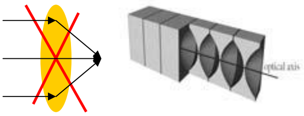

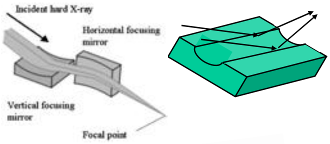

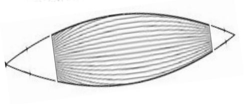

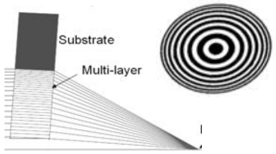

Take a lens: Yes, but ...

Compound refractive lenses [C. Schroer & W. Jark]

Reflective optics

Kirkpatrick-Baez optics [K. Yamamauchi]

Curved reflective multilayers [C. Morawe]

Bragg-reflective optics [F. Foerster]

Capillary optics

Monocapillary optics [L. Pina]

Polycapillary optics [C.A. Mc Donald]

Diffractive optics

Frensel Zone Plates [M. Feser]

Multilayer Laue Lenses [G.B. Stephenson]

...and Waveguides

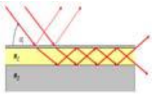

X-ray waveguides

$\lambda \sim 0.1$ nm, $d \sim 50$ nm

X-rays

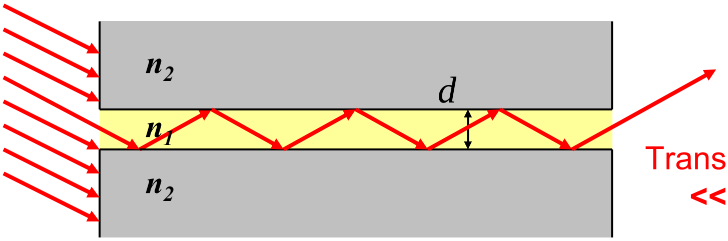

Transmission
<< 1 %

Y. P. Feng et al., Phys. Rev. Lett. 71, 537 (1993);
S. Lagomarsino et al., Appl. Phys. Lett. 71, 2557 (1997);
S. Di Fonza et al., Nature 403, 638 (2000).

Resonant beam coupling waveguides

$$\alpha_{c,\,n_1} < \alpha_i < \alpha_{c,n_2}$$

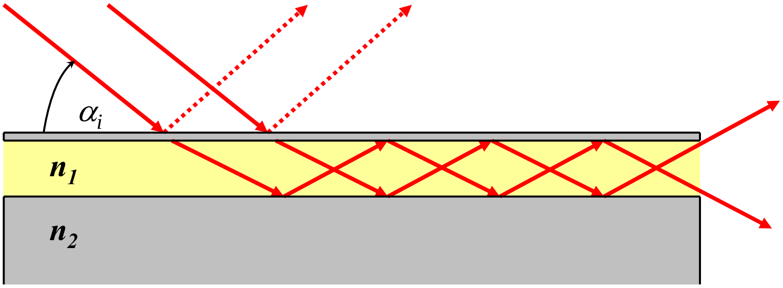

F. Pfeiffer et al., Physical Review B 62(24), 16939-16943 (2000)

Email: franz.pfeiffer@psi.ch - Web: http://people.epfl.ch/franz.pfeiffer

---

Field distribution in 1D resonant beam coupling waveguides

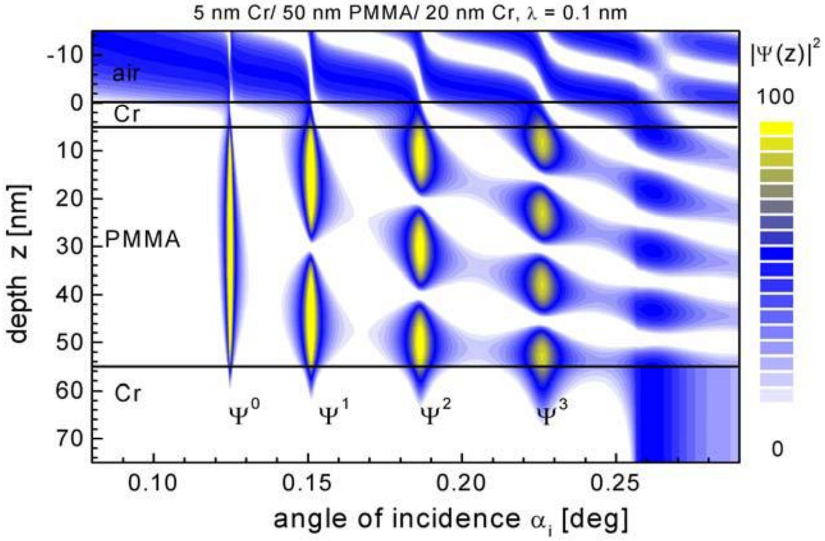

F. Pfeiffer et al., Physical Review B 62(24), 16939-16943 (2000)

Email: franz.pfeiffer@psi.ch - Web: http://people.epfl.ch/franz.pfeiffer

2D Waveguides

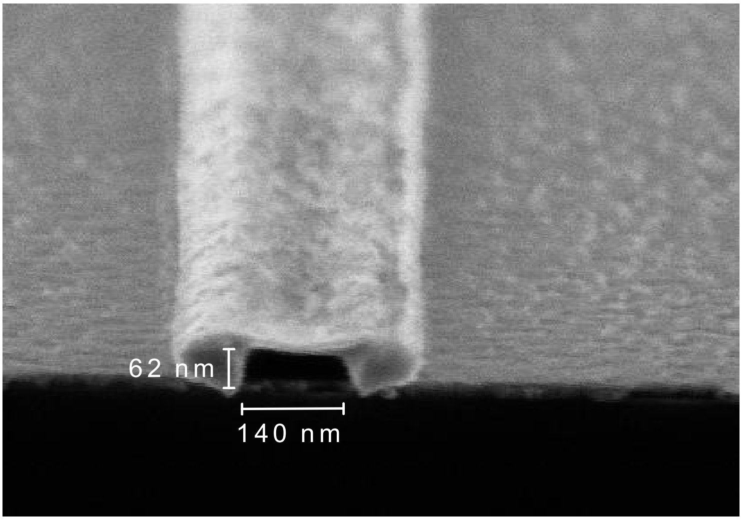

F. Pfeiffer, et al., Science 297, 205 (2002)

Farfield pattern of modes in 2D x-ray waveguides

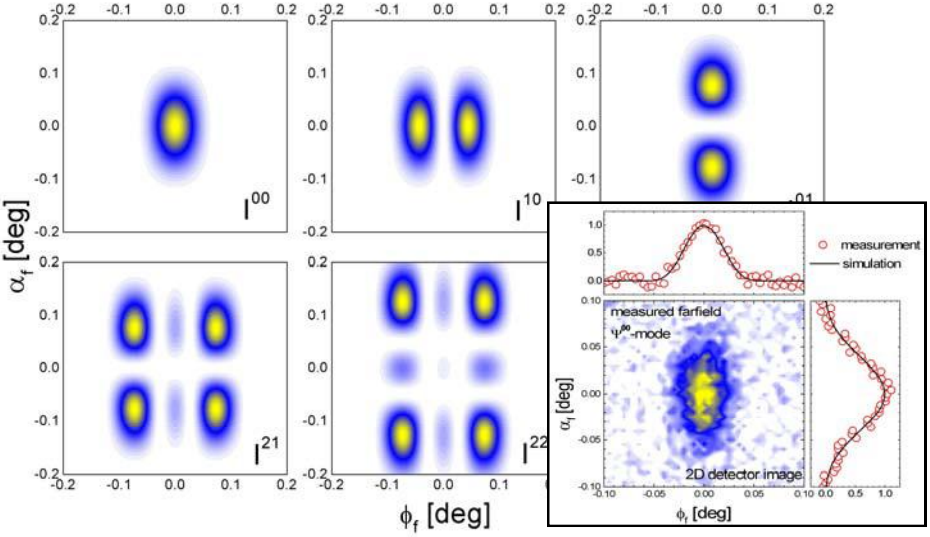

F. Pfeiffer, et al., Science 297, 205 (2002)

Waveguide based 'Holo-Microscopy' – slide from T. Salditt

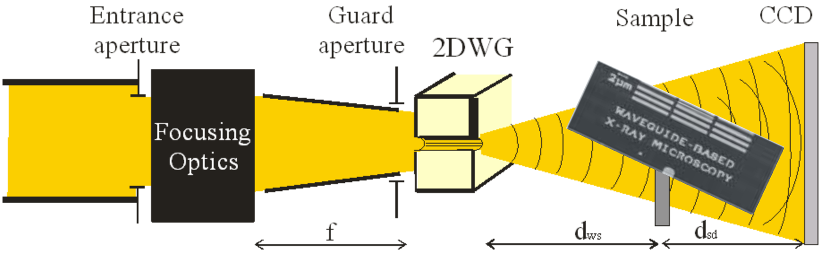

raw data

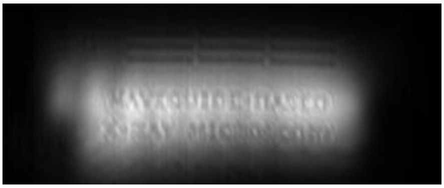

holography reconstruction

ESRF data, 10.4 keV

C. Fuhse et al., Appl. Phys. Lett. 85 (2004) & C. Fuhse et al., Phys. Rev. Lett. (2006)

Outline

1. X-ray focusing – Why
2. Methods overview – focus on X-ray waveguides
3. Recent advances at Paul Scherrer Institut

   > Fresnel Zone Plate fabrication by EUV inference lithography

   > Zone-doubling technique for ultra-high resolution FZP
4. 'Super-Resolution' coherent X-ray microscopy

   & characterization of focused wave-fields

Spatial resolution limit in x-ray microscopy

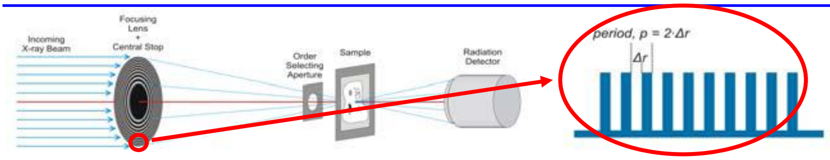

$\delta_{res} \sim \Delta r = p/2$

e-beam lithography limits

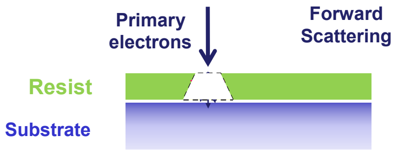
Primary electrons

Forward Scattering

Resist

Substrate

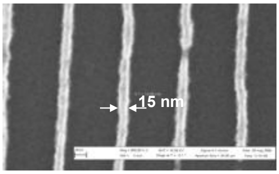

Isolated
10 — 20 nm lines ✓

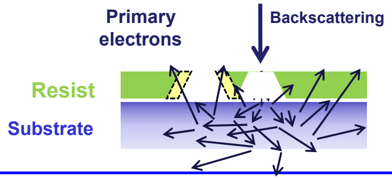
Primary electrons

Backscattering

Resist

Substrate

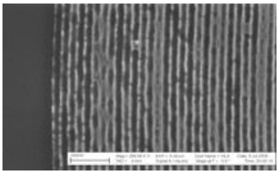

Dense
10 — 20 nm lines ✗

Possible solutions

W. L. Chao et al. NATURE 435 (2005) 1210-1213

Figure 2 | An illustration of the overlay nanofabrication technique for micro zone plate fabrication.

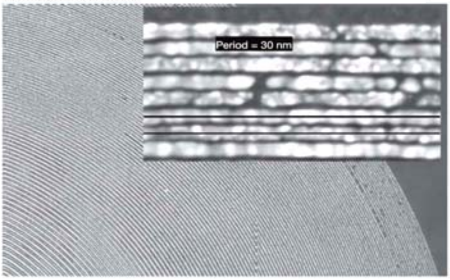

Figure 3 | Scanning electron micrograph of a zone plate with 15 nm outermost zone. Shown in the inset is a more detailed view of the outermost zones. The zonal period, as indicated by the two black lines, is measured to be 30 nm. The zone placement accuracy is measured to be 1.7 nm.

H. C. Kang et al. PRL96 (2006) 127401

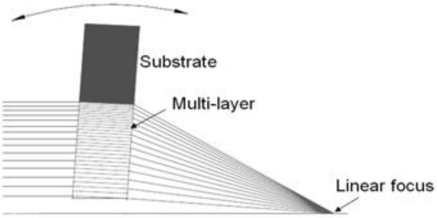

The Swiss alternatives:

- **FZP fabrication by EUV inference lithography**
- **Zone-doubled FZP**

FZP fabrication by EUV inference lithography (H. Solak)

work by Sankha S. Sarkar, Yasin Ekinci, and Harun Solak @ PSI

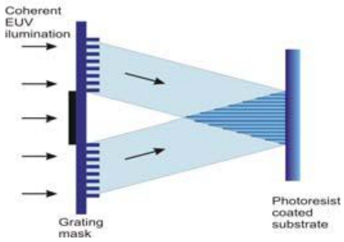

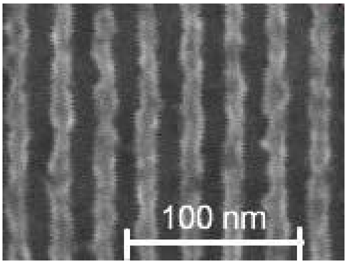

Solak HH, Ekinci Y, Kaser P, Park S
Photon-beam lithography reaches 12.5 nm half-pitch resolution.
JOURNAL OF VACUUM SCIENCE & TECHNOLOGY B **25, 91 (2007)**

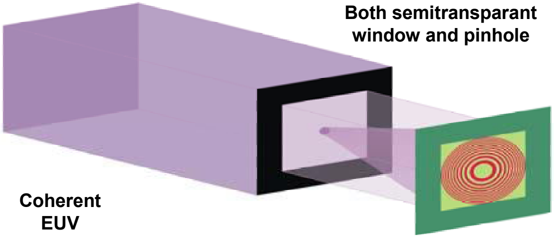

Both semitransparant window and pinhole

Coherent EUV Illumination

Advantages in relation to e-beam lithography:

- **Parallel writing**
- **No Proximity effect**
- **No Finite pixel size**

Email: franz.pfeiffer@psi.ch - Web: http://people.epfl.ch/franz.pfeiffer

---

FZP fabrication by EUV lithography

work by Sankha S. Sarkar, Yasin Ekinci, and Harun Solak @ PSI

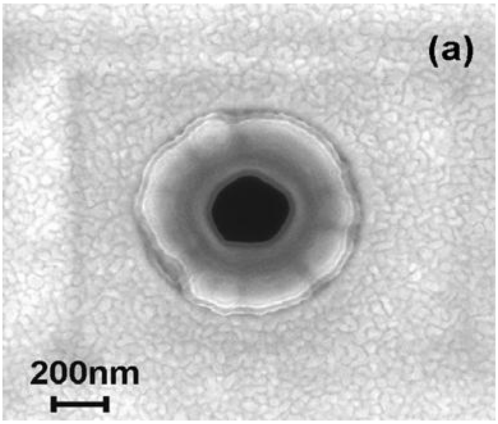

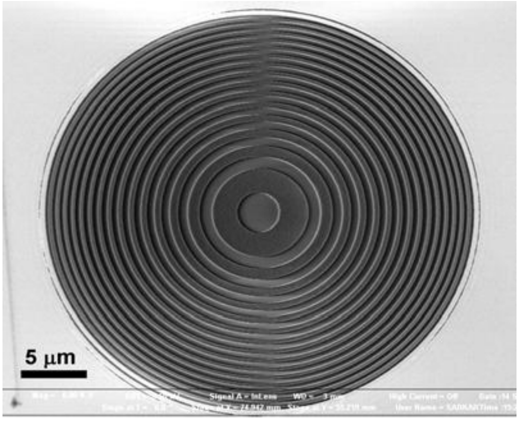

Pinhole Diameter ~ 300 nm

Distance from mask ~ 600 µm
N = 30, D ~ 32 µm
Δr_N ~ 260 nm

Email: franz.pfeiffer@psi.ch - Web: http://people.epfl.ch/franz.pfeiffer

Zone-doubling for high resolution FZP (slides J. Vila)

work by J. Vila, K. Jefimovs, and C. David @ PSI

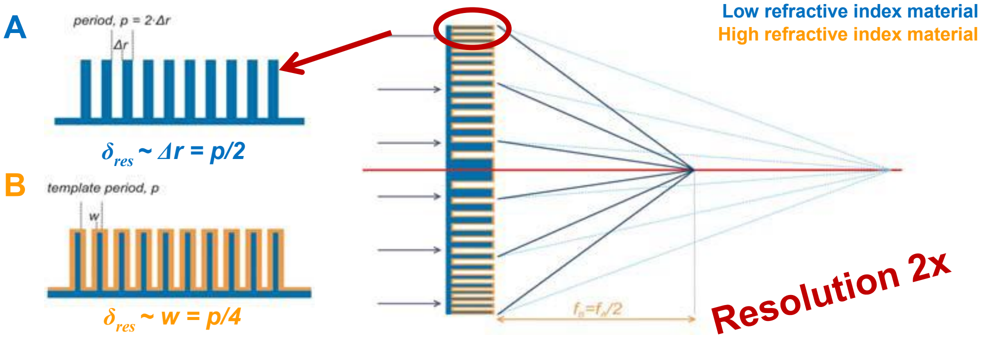

Resolution 2x

Manufacturing advantages:

- ✓ **No alignment required**
- ✓ **One single EBL exposure**

FZP pattern generation is simple and reproducible!

K. Jefimovs et al., Phys. Rev. Lett. 99, 264801 (2007)

Zone-doubling for high resolution FZP (slides J. Vila)

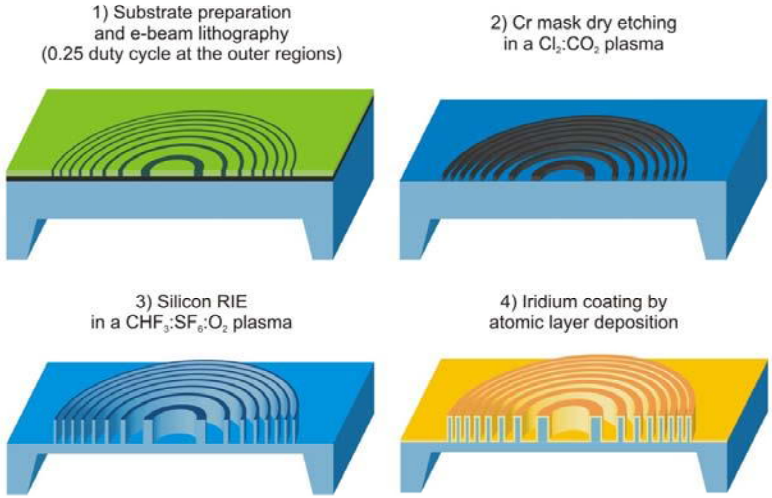

Low refractive index material → Silicon

High refractive index material → Iridium

ALD
Deposition
@
University of
Helsinki
T. Pilvi &
M. Ritala

Zone-doubling for high resolution FZP *(slides J. Vila)*

FZP with D = 100μm, Δr = 20 nm

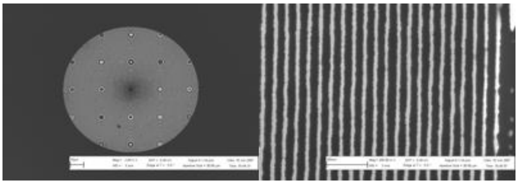

FZP with D = 100μm, Δr = 15 nm

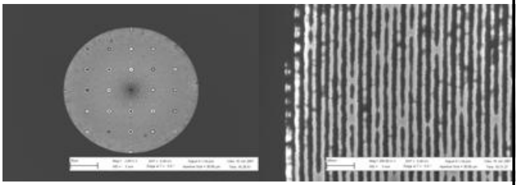

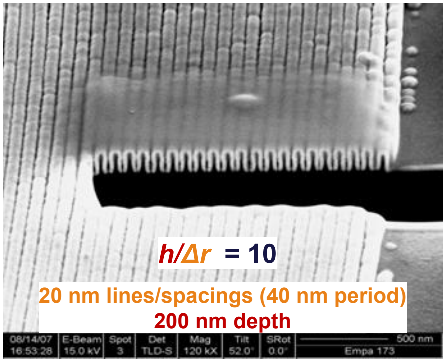

h/Δr = 10

20 nm lines/spacings (40 nm period)

200 nm depth

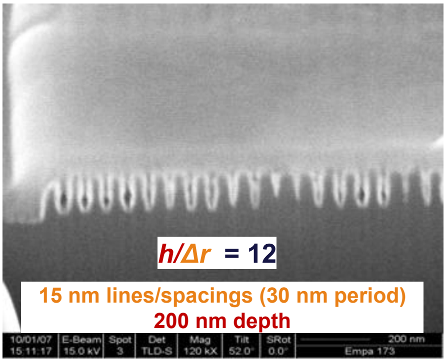

h/Δr = 12

15 nm lines/spacings (30 nm period)

200 nm depth

Email: franz.pfeiffer@psi.ch - Web: http://people.epfl.ch/franz.pfeiffer

---

Zone-doubling for high resolution FZP *(slides J. Vila)*

FZP with D = 100μm, Δr = 20 nm

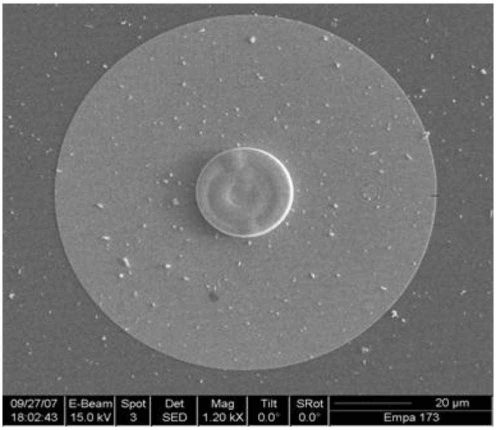

FZP with D = 100μm, Δr = 15 nm

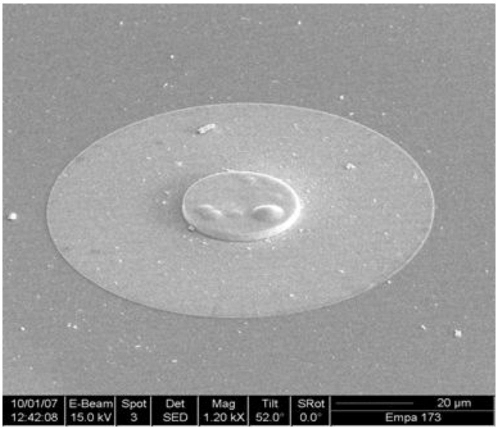

20 μm diameter central stops made of 1.5 μm thick layer of Pt by FIB induced deposition.

Email: franz.pfeiffer@psi.ch - Web: http://people.epfl.ch/franz.pfeiffer

STXM @ PolLux beamline of SLS (J. Raabe & G. Tzvetkov)

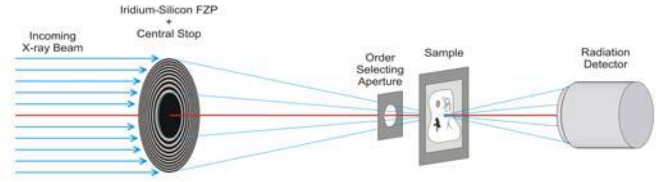

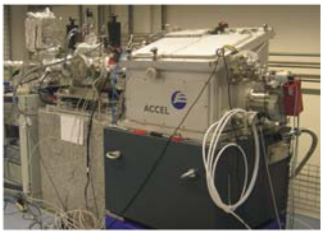

Email: franz.pfeiffer@psi.ch - Web: http://people.epfl.ch/franz.pfeiffer

---

STXM @ PolLux beamline of SLS (J. Raabe & G. Tzvetkov)

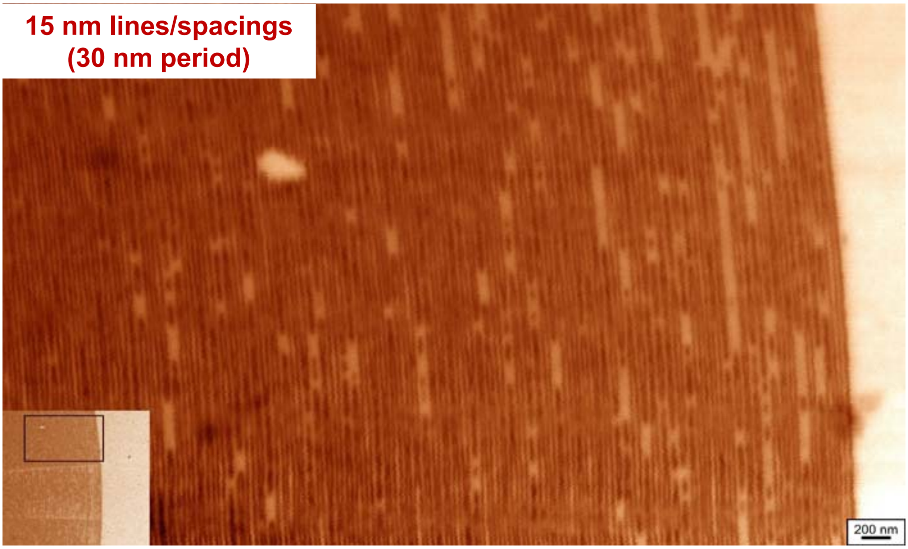

15 nm lines/spacings
(30 nm period)

1.0 keV photon energy

Email: franz.pfeiffer@psi.ch - Web: http://people.epfl.ch/franz.pfeiffer

Outline

1. X-ray focusing – Why
2. Methods overview – focus on X-ray waveguides
3. Recent advances at Paul Scherrer Institut
4. ‘Super-Resolution’ coherent X-ray microscopy & characterization of focused wave-fields

---

‚Super-Resolution‘ Coherent Scanning X-Ray Microscopy

Principles:

- In standard scanning x-ray microscopy, resolution is limited to probe size
- Collect coherent diffraction patterns while scanning the spot (Ptychography)
- Phase and amplitude of the object can be retrieved with *enhanced resolution*

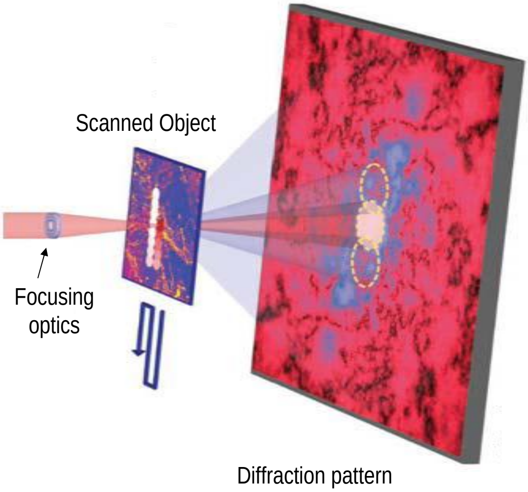

P. Thibault, M. Dierolf, A. Menzel, O. Bunk, C. David, F. Pfeiffer, SCIENCE 321, 379-382 (2008)

‚Super-Resolution‘ Coherent Scanning X-Ray Microscopy

Principles:

- ➢ In standard scanning x-ray microscopy, resolution is limited to probe size
- ➢ Collect coherent diffraction patterns while scanning the spot (Ptychography)
- ➢ Phase and amplitude of the object can be retrieved with *enhanced resolution*

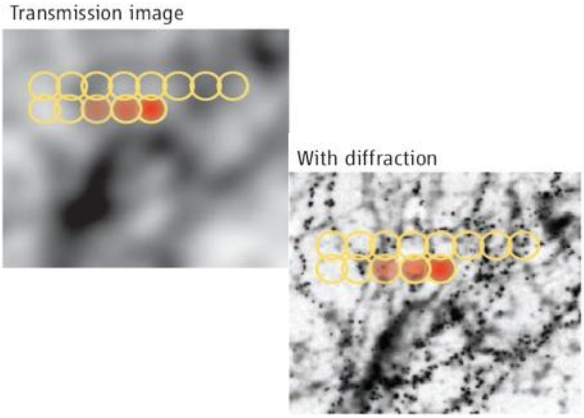

P. Thibault, M. Dierolf, A. Menzel, O. Bunk, C. David, F. Pfeiffer, SCIENCE 321, 379-382 (2008)

Email: franz.pfeiffer@psi.ch - Web: http://people.epfl.ch/franz.pfeiffer

---

Ptychographic phase retrieval

- ➢ W. Hoppe, Acta Cryst. A 25, 508 (1969).
- ➢ R. Hegerl, W. Hoppe, Ber. Bunsen-Ges. Phys. Chemie 74, 1148 (1970).

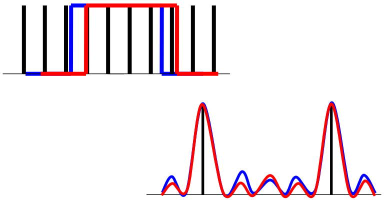

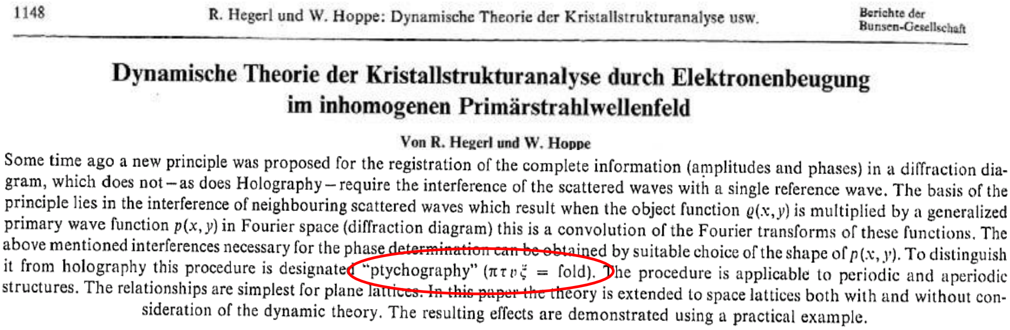

1148 R. Hegerl und W. Hoppe: Dynamische Theorie der Kristallstrukturanalyse usw. Berichte der Bunsen-Gesellschaft

Dynamische Theorie der Kristallstrukturanalyse durch Elektronenbeugung im inhomogenen Primärstrahlwellenfeld

Von R. Hegerl und W. Hoppe

Some time ago a new principle was proposed for the registration of the complete information (amplitudes and phases) in a diffraction diagram, which does not – as does Holography – require the interference of the scattered waves with a single reference wave. The basis of the principle lies in the interference of neighbouring scattered waves which result when the object function $\varrho(x,y)$ is multiplied by a generalized primary wave function $p(x,y)$ in Fourier space (diffraction diagram) this is a convolution of the Fourier transforms of these functions. The above mentioned interferences necessary for the phase determination can be obtained by suitable choice of the shape of $p(x,y)$. To distinguish it from holography this procedure is designated "ptychography" ($\pi\tau\upsilon\xi$ = fold). The procedure is applicable to periodic and aperiodic structures. The relationships are simplest for plane lattices. In this paper the theory is extended to space lattices both with and without consideration of the dynamic theory. The resulting effects are demonstrated using a practical example.

Email: franz.pfeiffer@psi.ch - Web: http://people.epfl.ch/franz.pfeiffer

Ptychographic phase retrieval

- W. Hoppe,
  Acta Cryst. A 25, 508
  (1969).
- R. Hegerl, W. Hoppe, Ber.
  Bunsen-Ges. Phys. Chemie
  74, 1148 (1970).

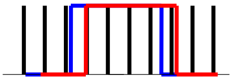

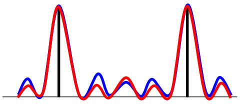

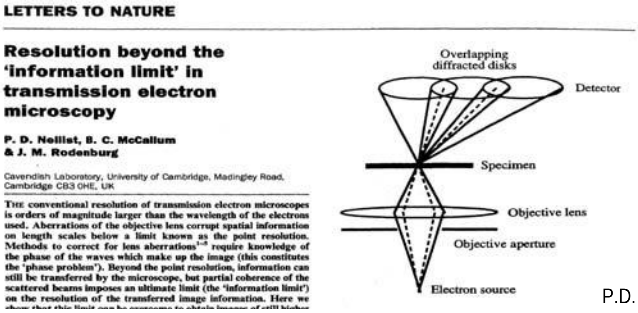

LETTERS TO NATURE

Resolution beyond the 'information limit' in transmission electron microscopy

P. D. Nellist, B. C. McCallum & J. M. Rodenburg

Cavendish Laboratory, University of Cambridge, Madingley Road, Cambridge CB3 0HE, UK

THE conventional resolution of transmission electron microscopes is orders of magnitude larger than the wavelength of the electrons used. Aberrations of the objective lens corrupt spatial information on length scales below a limit known as the point resolution. Methods to correct for lens aberrations[1-8] require knowledge of the phase of the waves which make up the image (this constitutes the 'phase problem'). Beyond the point resolution, information can still be transferred by the microscope, but partial coherence of the scattered beams imposes an ultimate limit (the 'information limit') on the resolution of the transferred image information. Here we

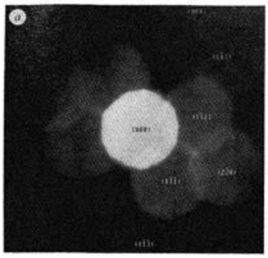

P.D. Nellist et al., Nature 374, 630 (1995)

A test case: far-field phase retrieval with laser light

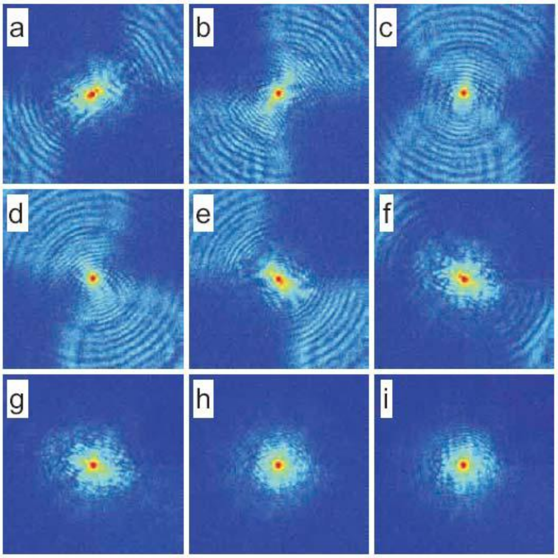

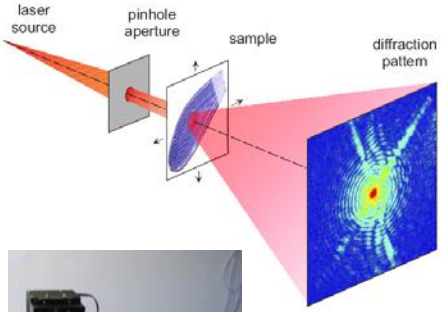

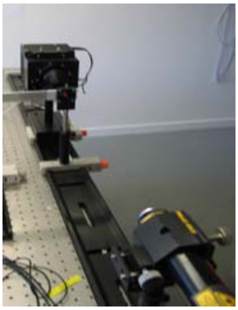

M. Dierolf et al., Europhysics News 39, 22 (2008)

'Super-Resolution' Scanning X-Ray Transmission Microscopy

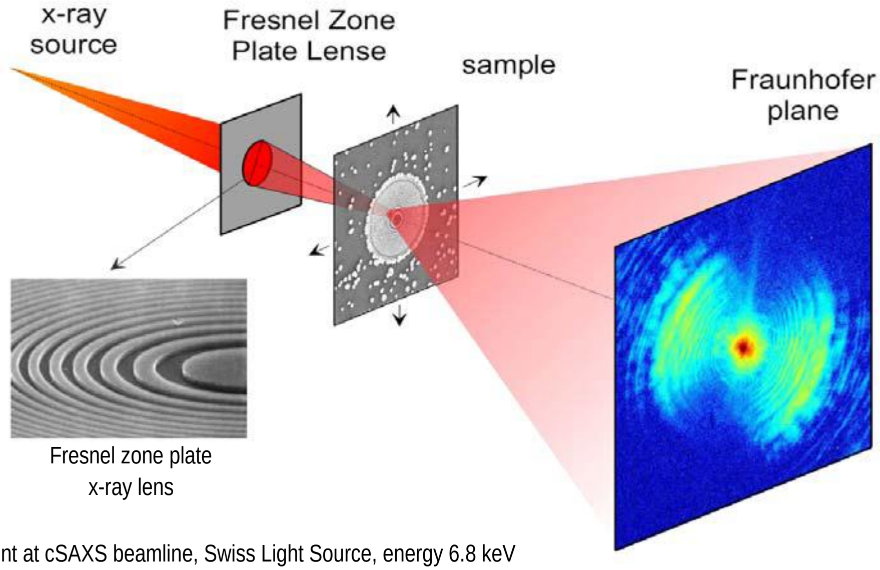

Experiment at cSAXS beamline, Swiss Light Source, energy 6.8 keV

'Super-Resolution' Scanning X-Ray Transmission Microscopy

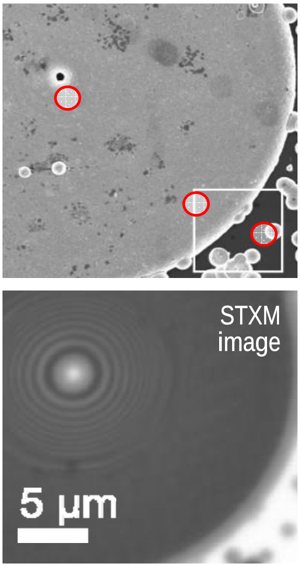

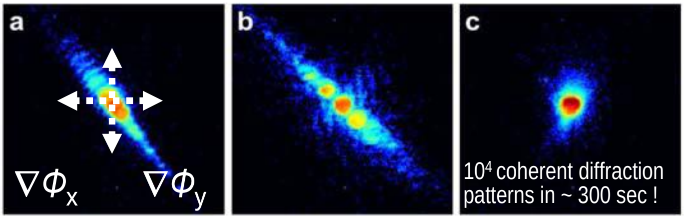

10^4 coherent diffraction patterns in ~ 300 sec !

'conventional' STXM analysis of > 10^4 diffraction patterns yields 'low-resolution' absorption & phase-contrast images

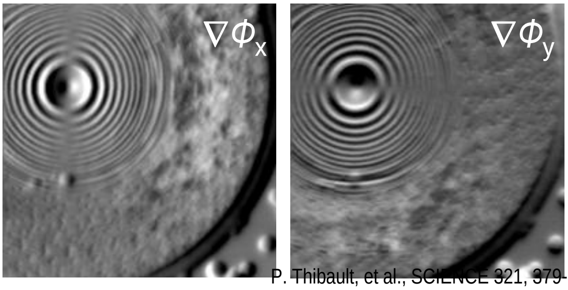

P. Thibault, et al., SCIENCE 321, 379-382 (2008)

'Super-Resolution' Scanning X-Ray Transmission Microscopy

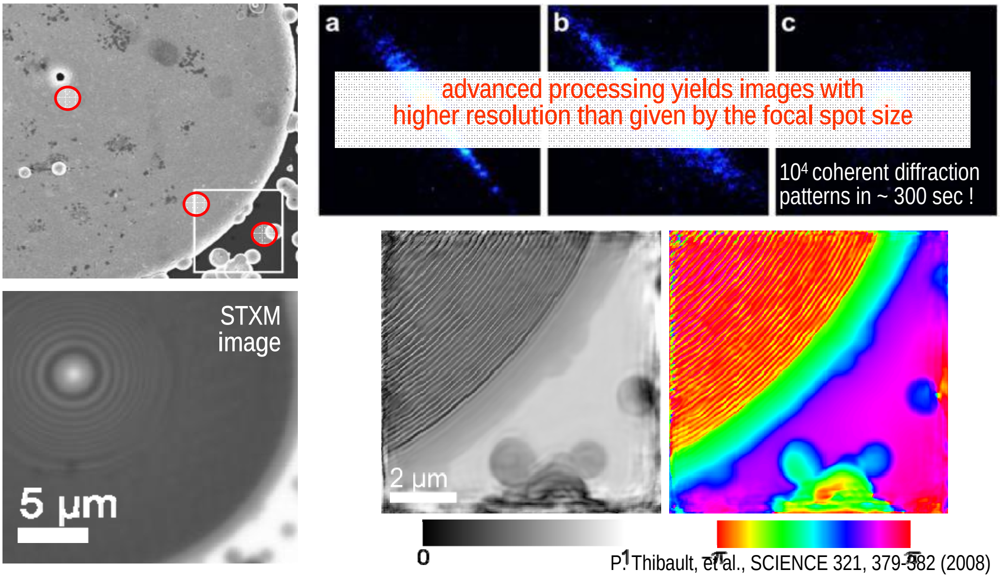

advanced processing yields images with
higher resolution than given by the focal spot size

10^4 coherent diffraction patterns in ~ 300 sec !

P. Thibault, et al., SCIENCE 321, 379-382 (2008)

Simultaneous reconstruction of probe & specimen

P. Thibault, et al., SCIENCE 321, 379-382 (2008)

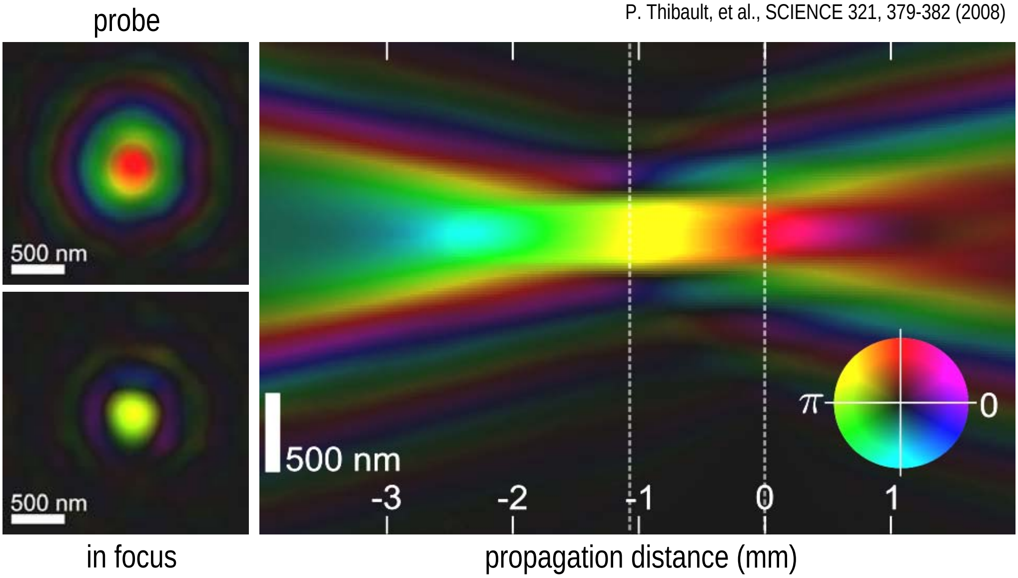

‘Super-Resolution’ X-Ray Microscopy

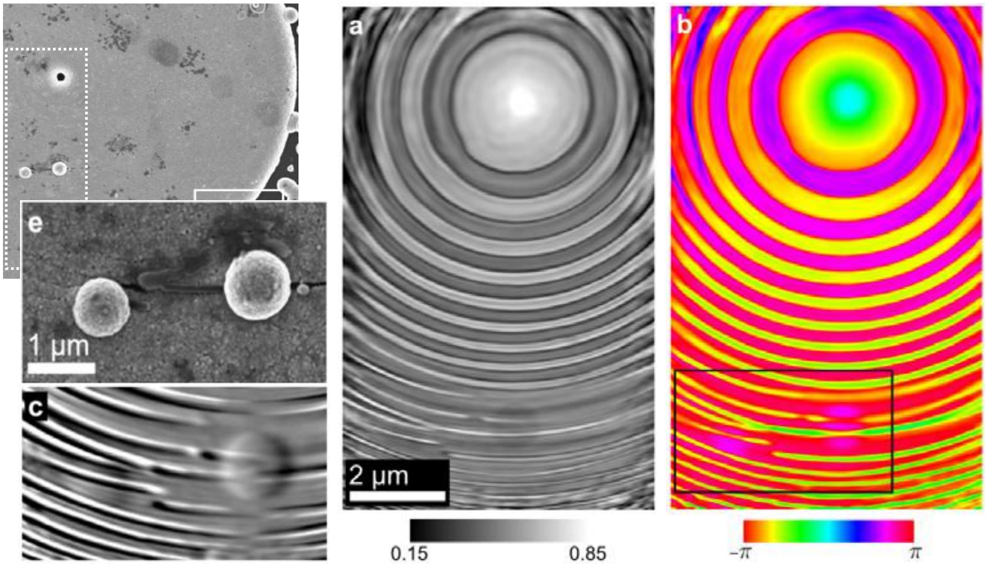

Near future: High-resolution x-ray imaging of cells ?

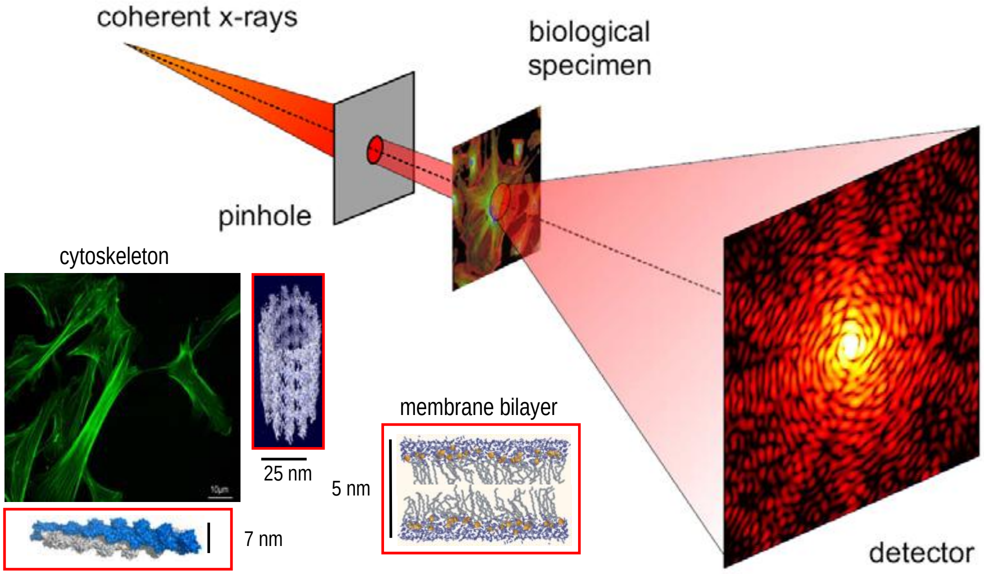

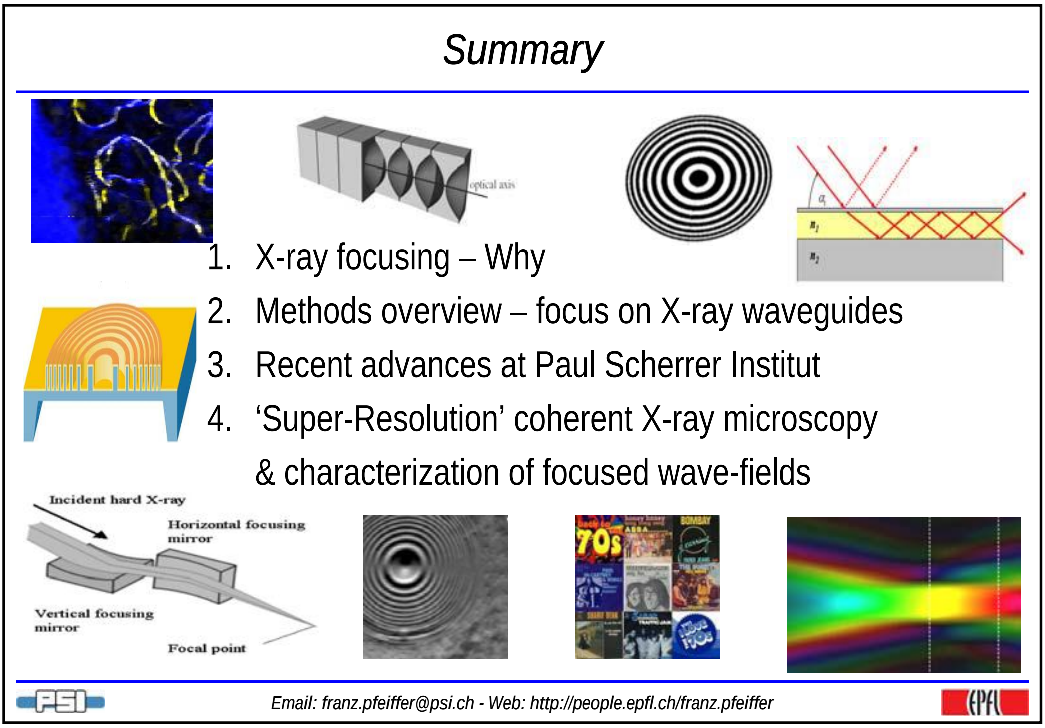

Summary

1. X-ray focusing – Why
2. Methods overview – focus on X-ray waveguides
3. Recent advances at Paul Scherrer Institut
4. ‘Super-Resolution’ coherent X-ray microscopy & characterization of focused wave-fields

Email: franz.pfeiffer@psi.ch - Web: http://people.epfl.ch/franz.pfeiffer

Coherent Imaging group at PSI & EPFL

Franz Pfeiffer	Oliver Bunk	Andreas Menzel	Xavier Donath	Pierre Thibault	Cameron Kewish	Martin Dierolf	Tobias Boehlen

Christian David, Joan Vila, Konstantins Jefimovs, Vitaliy Guzenko, Harun Solak, Sankha Sarkar,
Laboratory for Micro- and Nanotechnology, Paul Scherrer Institut, CH

X-ray focusing with Kirkpatrick-Baez optics

K. Yamauchi
Osaka University

Contents

Advantages of KB mirror optic

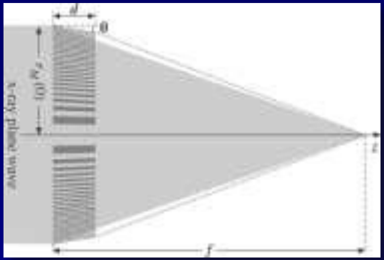

Fresnel zone plate

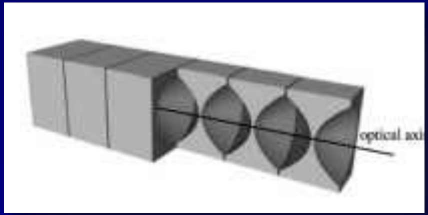

Refractive lens

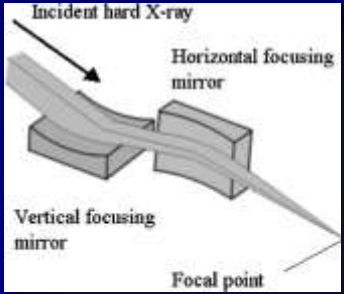

K-B mirror optics

Achromatic optic (total reflection mirrors)

High efficiency >90%

Large aperture ≈500µm

Long working distance 10mm ～500mm

Recent achievement in 50nm-level focusing

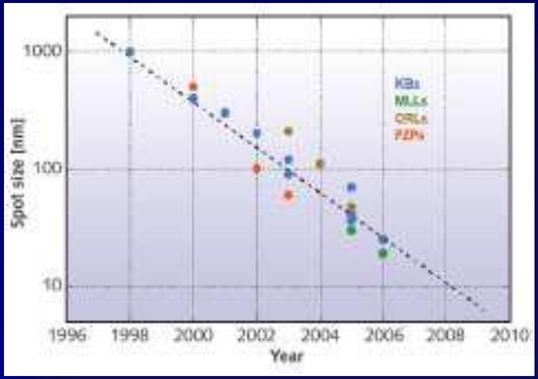

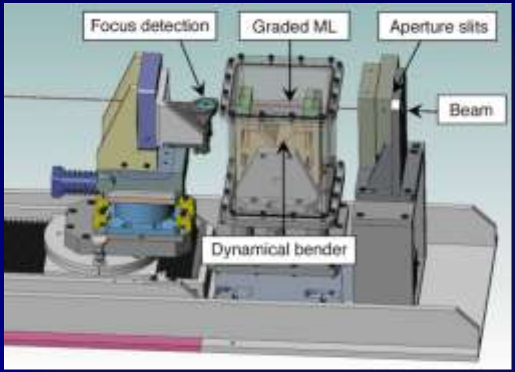

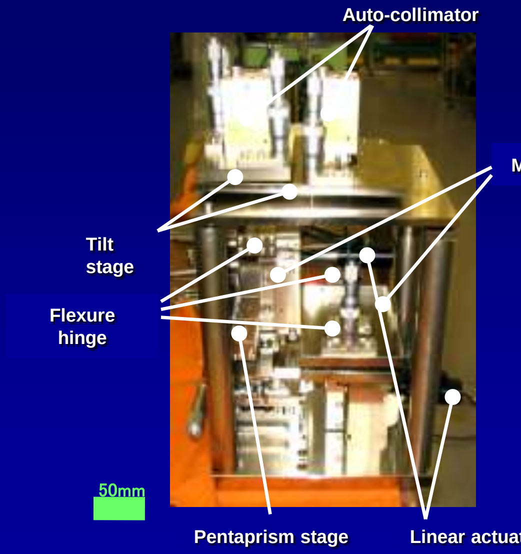

90nm x 90nm, 45nm focusing were achieved at **ESRF** by
a graded multilayer coating and a fine bending system
Efficient sub 100 nm focusing of hard x rays
O. Hignette, P. Cloetens, G. Rostaing, P. Bernard and C. Morawe
Rev. Sci. Instrum. 76, 063709 (2005)

Ch. Morawe et al,
Proc. SPIE 6317 (2006

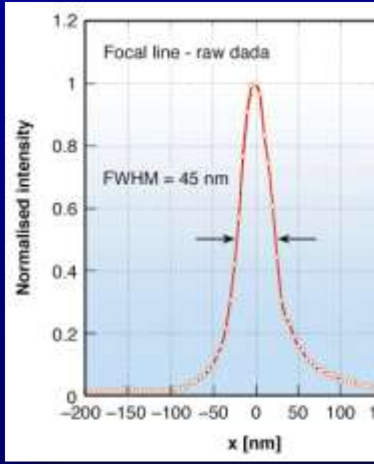

75nm x 85nm focusing was achieved at **APS** by
a optical figuring and a differential deposition.
Short focal length Kirkpatrick-Baez mirrors for a hard x-ray nanoprobe
W. Liu, G. Ice, J. Tischler, A. Khounsary, C. Liu, L. Assoufid
and A. Macrander, Rev. Sci. Instrum. 76 (11), 2005, p.113701

36nm x 48nm, 25nm focusing were achieved by **SPring-8** and
Osaka Univ. group by EEM, P-CVM, MSI and RADSI.

H. Mimura et al., Hard X-ray Diffraction-Limited Nanofocusing with Kirkpatrick-Baez Mirrors, Japanese Journal of Applied Physics Part 2, 44 (18), L539-L542 (2005).
H. Mimura et al., Efficient focusing of hard x rays to 25 nm by a total reflection mirror, Applied Physics Letters 90, 051903 (2007).

Required accuracy for nano-focusing under D-limited condition

Kirkpatrick-Baez mirrors

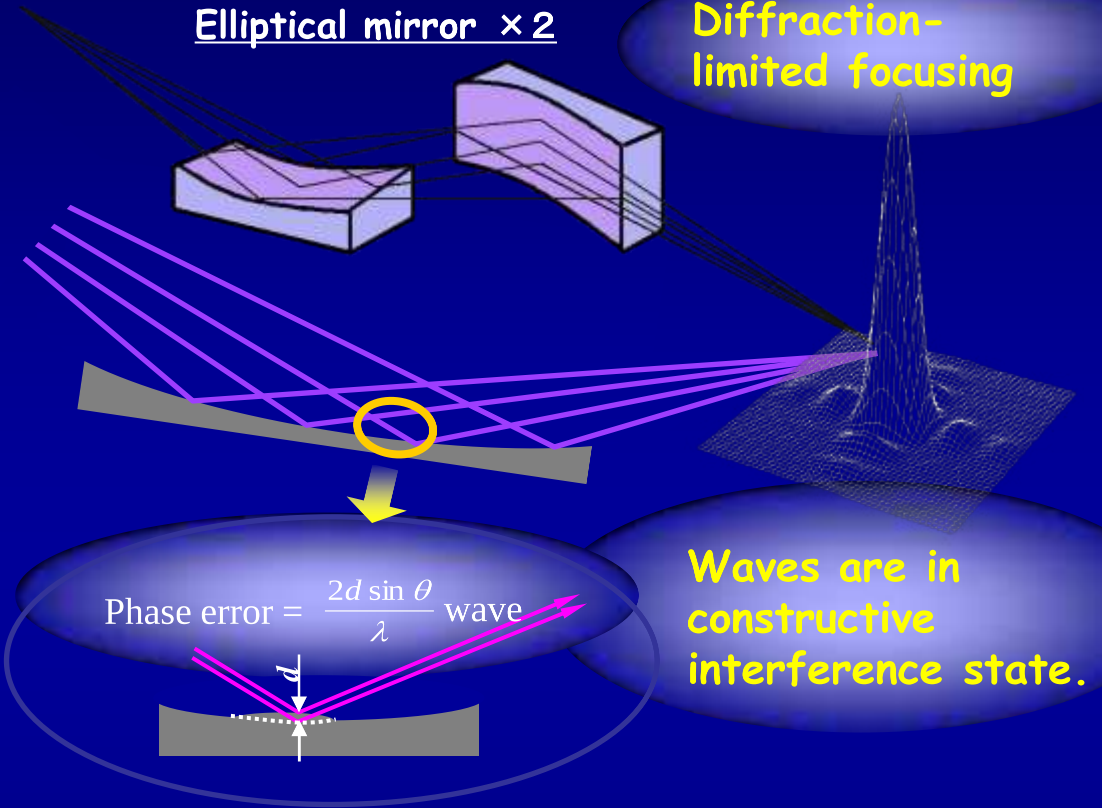

Phase error = $\frac{2d\sin\theta}{\lambda}$ wave

Waves are in constructive interference state.

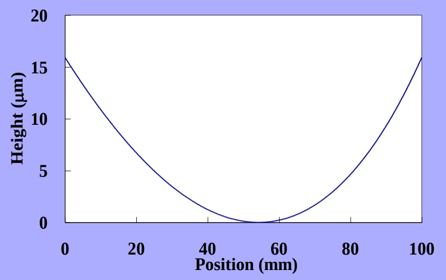

Designed profile (ellipse)

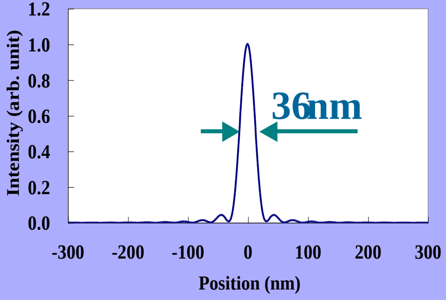

Beam profile

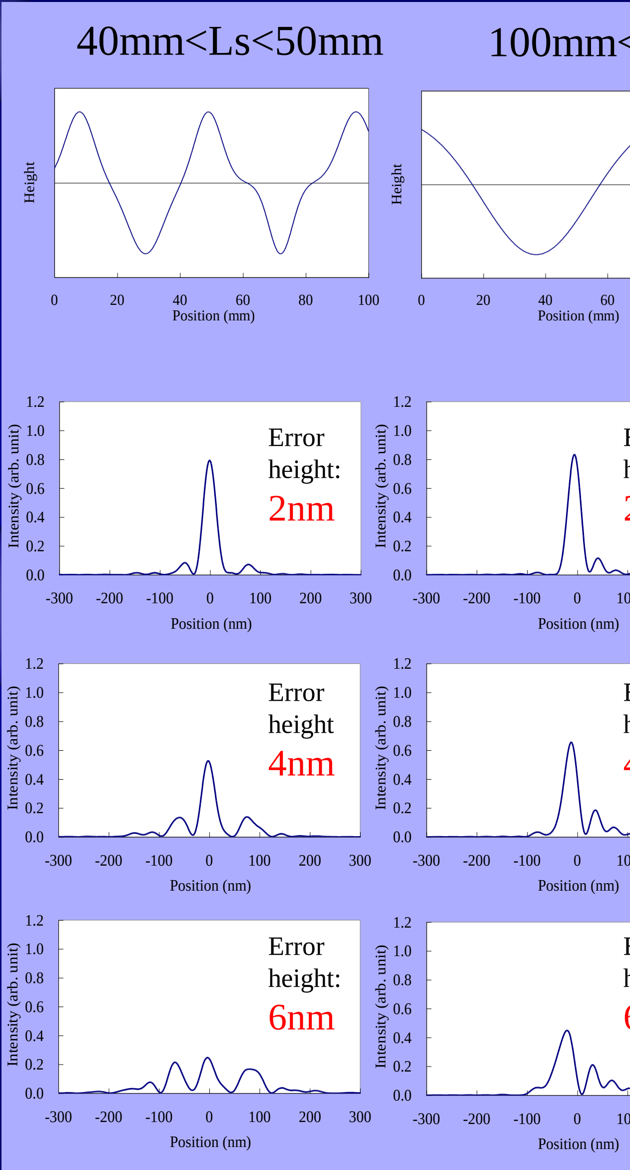

Fabrication and figure testing technologies of Osaka University

◎ Plasma CVM (chemical vaporization machining)

→ Rough figuring (Rapid figuring with sub-10nm (P-V) accuracy)

K. Yamamura et al., Rev. Sci. Instrum. 71 (2000), 4627

◎ EEM (elastic emission machining)

→ Final figuring and smoothing (Fine figuring and atomic smoothness)

K. Yamauchi et al., Rev. Sci. Instrum. 73 (2002), 4028

◎ MSI (microstitching interferometry)

→ Figure tester with spatial resolution close to 1μm

K. Yamauchi et al., Rev. Sci. Instrum. 74 (2003), 2894

◎ RADSI (relative-angle determinable stitching interferometry)

→ Figure tester for steeply curved ellipse of large NA mirror

H. Mimura et al., Rev. Sci. Instrum. 76 (2005), 045102

J-tec URL http://www.j-tec.co.jp

Sub-100nm focusing mirrors have already been commercially available

Plasma CVM (Chemical Vaporization Machining)

A chemical removal process utilizing reactive species generated in the ***atmospheric pressure plasma***

- ***High density reactive species ⇒ High removal rate***
- ***Chemical reaction ⇒ No damage on the surface***
- ***Non contact ⇒ Insensitive against external disturbanc***

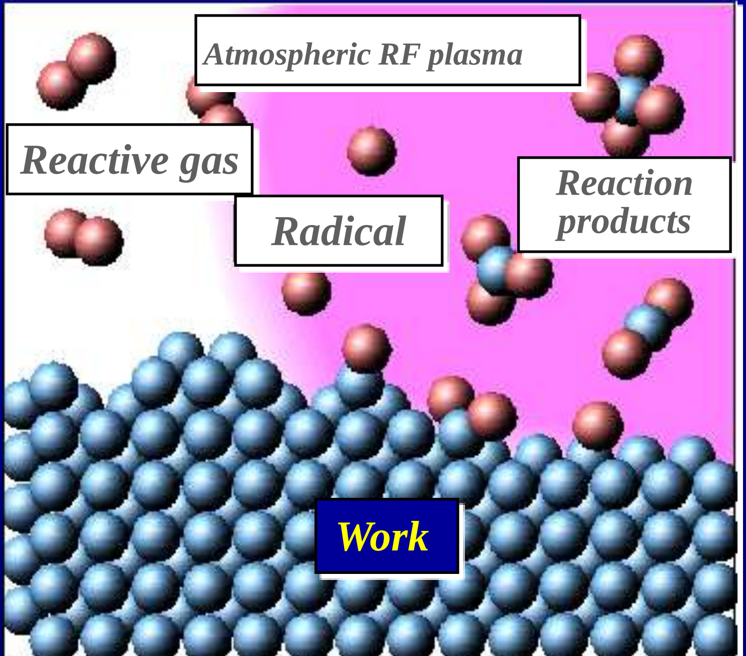

Material	Removal rate (μm/min)
Fused silica	170
Silicon	94
Molybdenum	36
Tungsten	32
Silicon carbide	6.4
Diamond	2.5

Plasma CVM (continued)

Atmospheric pressure plasma

Plasma is localized around the electrode

High spatial resolution figuring is possible without mask

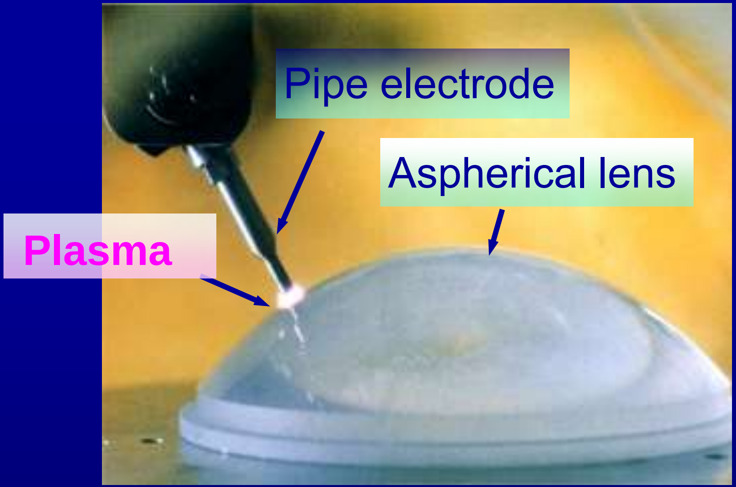

Pipe electrode is utilized for high-spatial resolution figurin

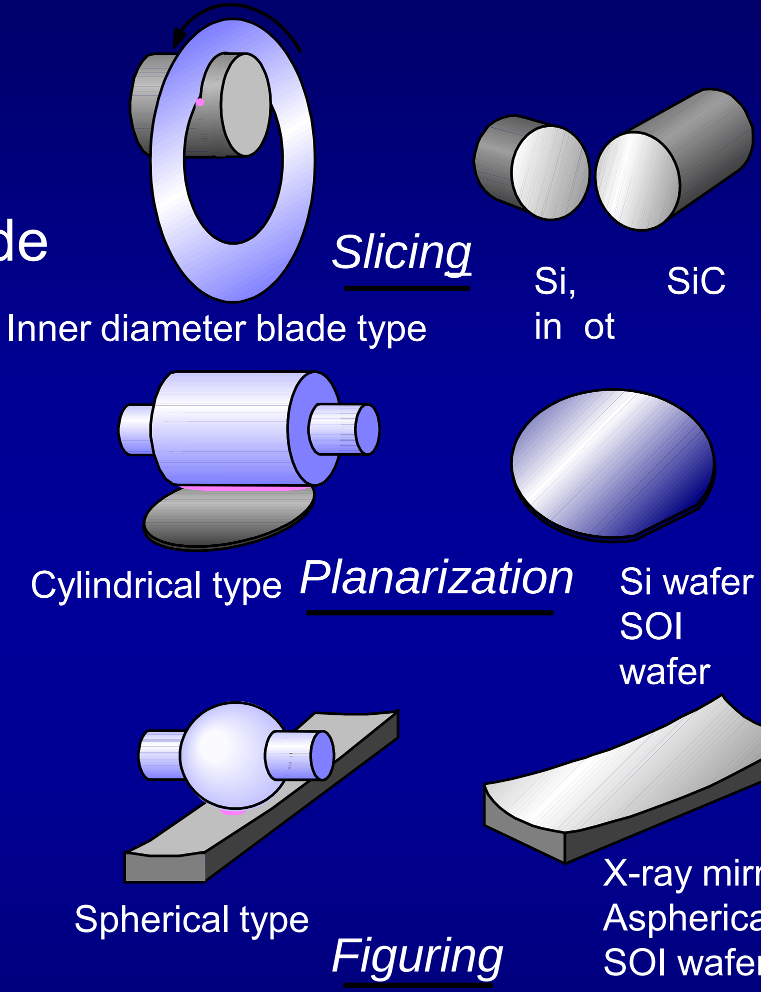

Rotary electrode is utilized fo high-efficiency machining

Figuring by Numerically Controlled Plasma CVM

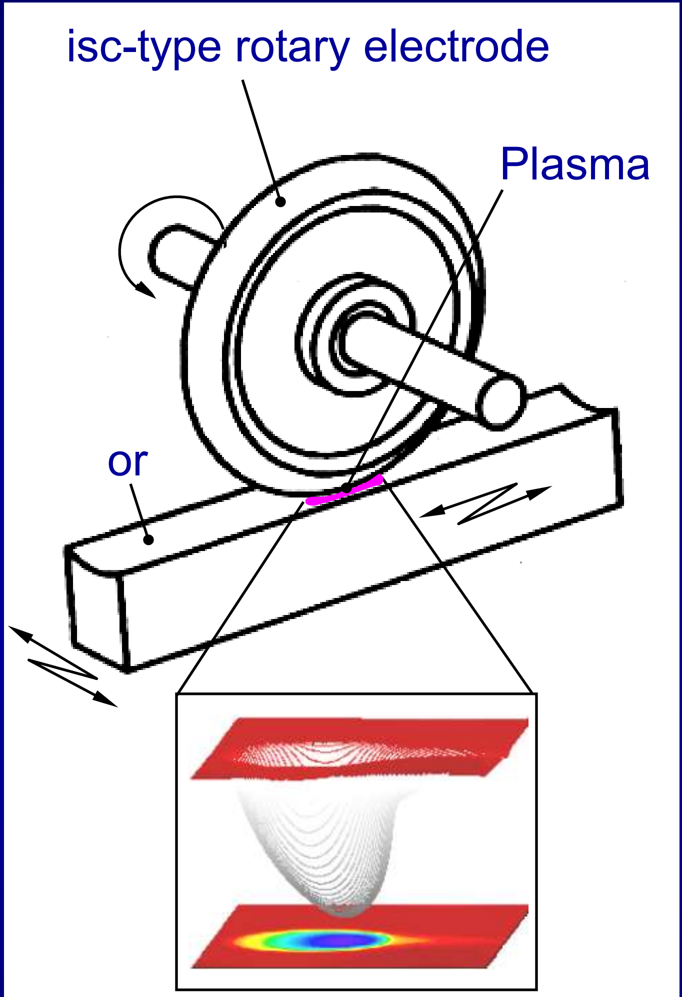

Shape of the removal spot

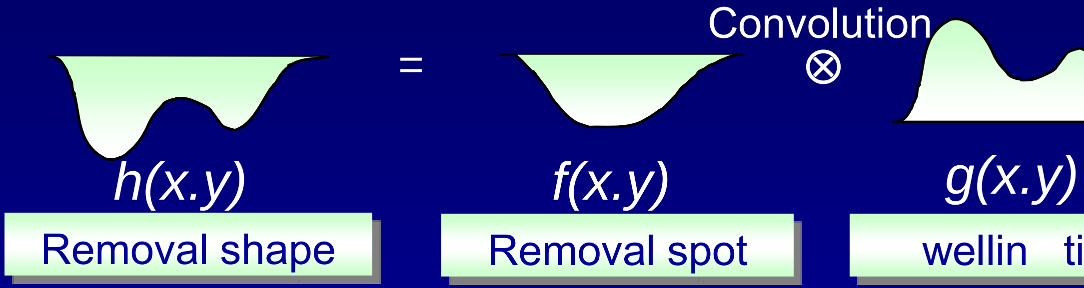

Convolution

$h(x.y) = f(x.y) \otimes g(x.y)$

Removal shape

Removal spot

wellin ti

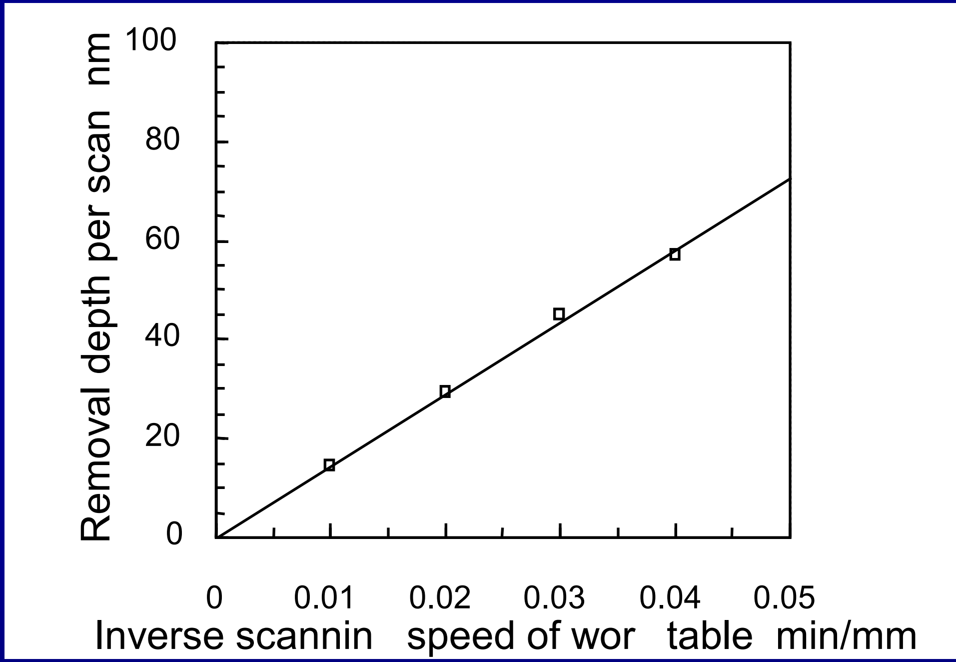

Removal depth is proportional to dwellin time so that figuring is controlled by scanning speed.

EEM (Elastic Emission Machining)

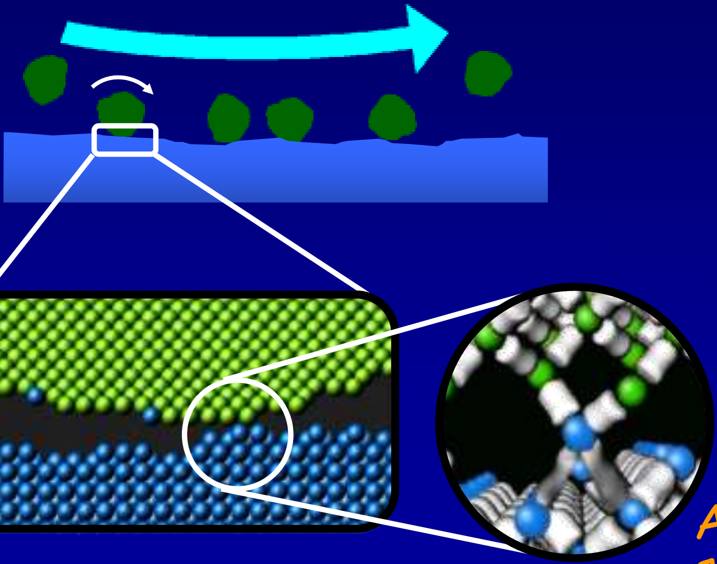

The ultra-fine particle is supplied to the work surface by ultrapure water flow

In EEM, chemical reaction between sol surfaces is utilized.

Atom removal occurs selectively at the top site of the work surfa

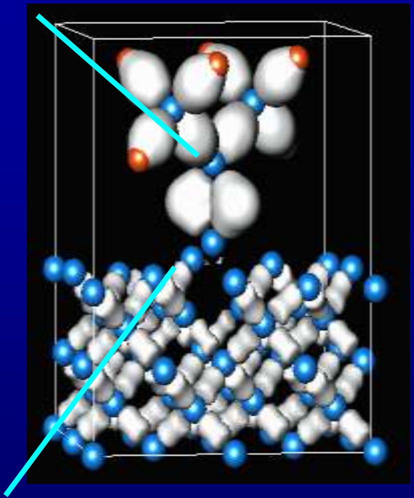

Bump site is preferentially removed

Atomically flat surface can be obtain

Removal mechanism is verified to be chemical by first-principles molecular dynamics simulatio

Surfaces smoothing properties in EEM

P-V 1.603 nm
RMS 0.183 nm

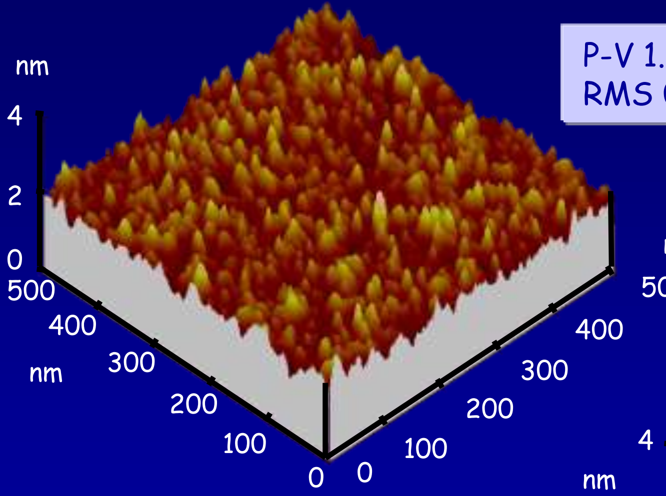

Pre-machined surface

P-V 0.910 nm
RMS 0.100 nm

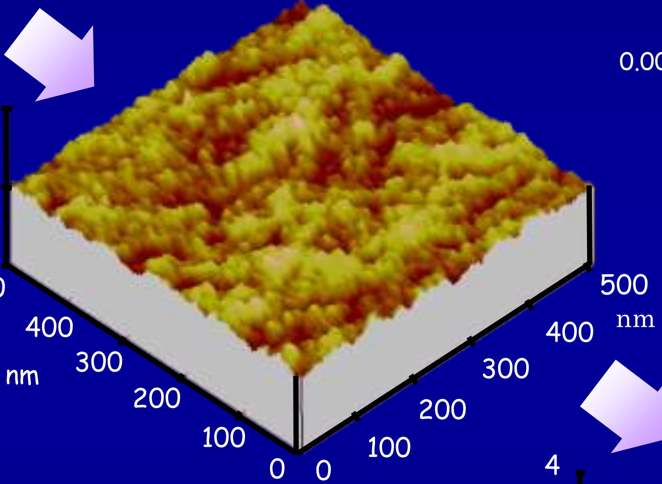

EEM surface (Removal depth:2nm)

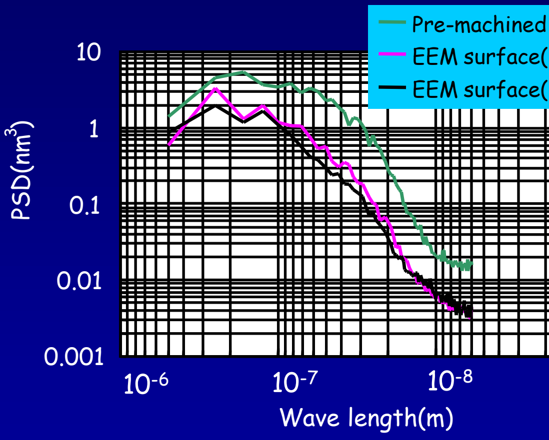

PSD analysis

P-V 0.769 n
RMS 0.087

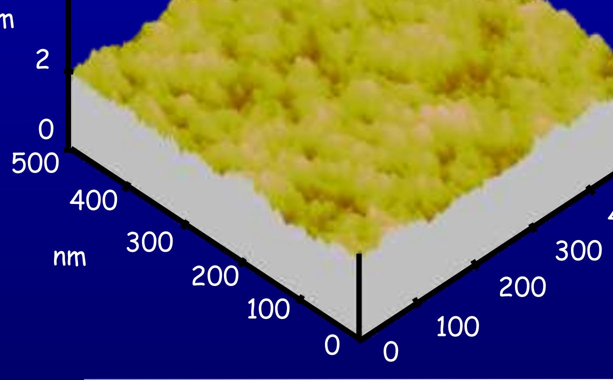

EEM surface (Removal depth

The roughness of about 2nm(P-V) can be flattened with the removal of 2nm thickness.

The bump site is selectively removed.

STM image of EEM processed surface

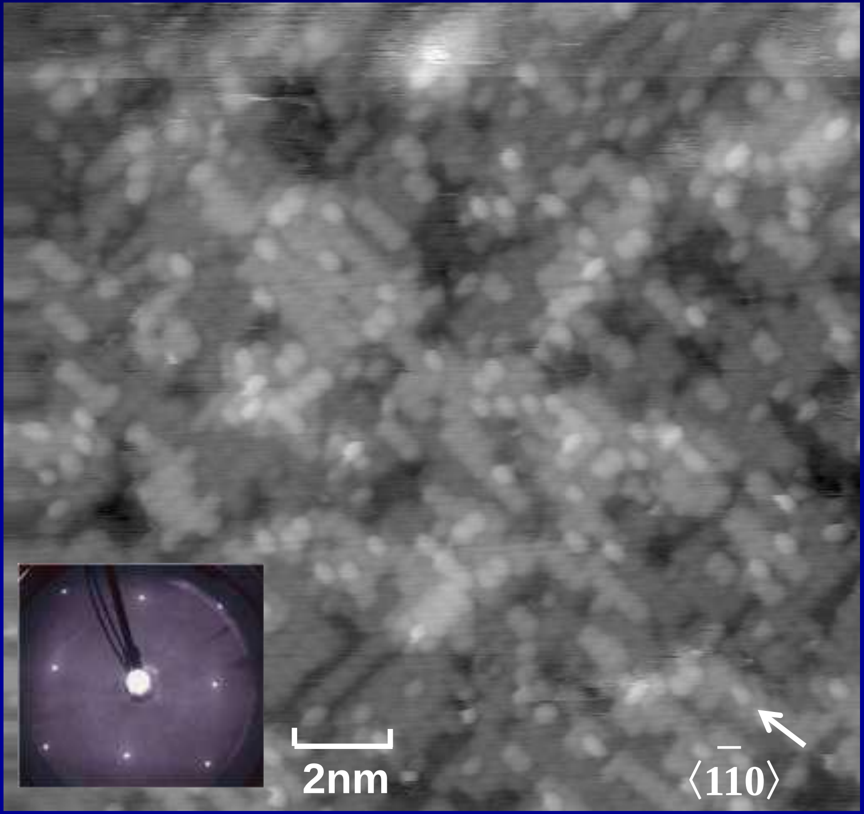

EE pattern

STM image
(20nm × 20nm)

95% of the EEM processed surface is constructed with only 3 atomic layers.

K. Arima et al,

Distribution of atom classified for every atomic layer

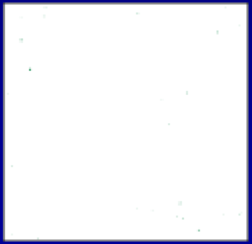

1st layer (0.034%)

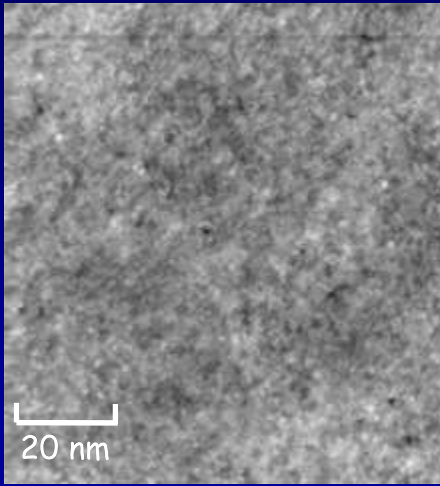

STM image (100nm × 100

2nd layer (1.4%)

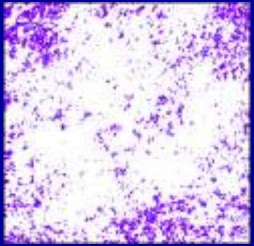

3rd layer (16.0%)

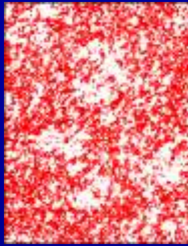

4th layer (47

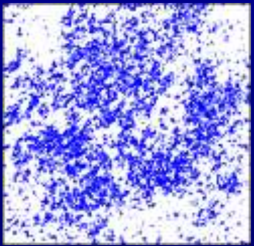

5th layer (30.7%)

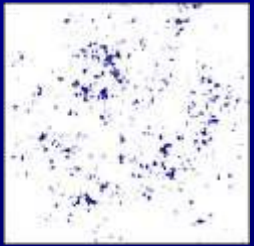

6th layer (4.0%)

Others (0.1

Typical figuring properties using EEM

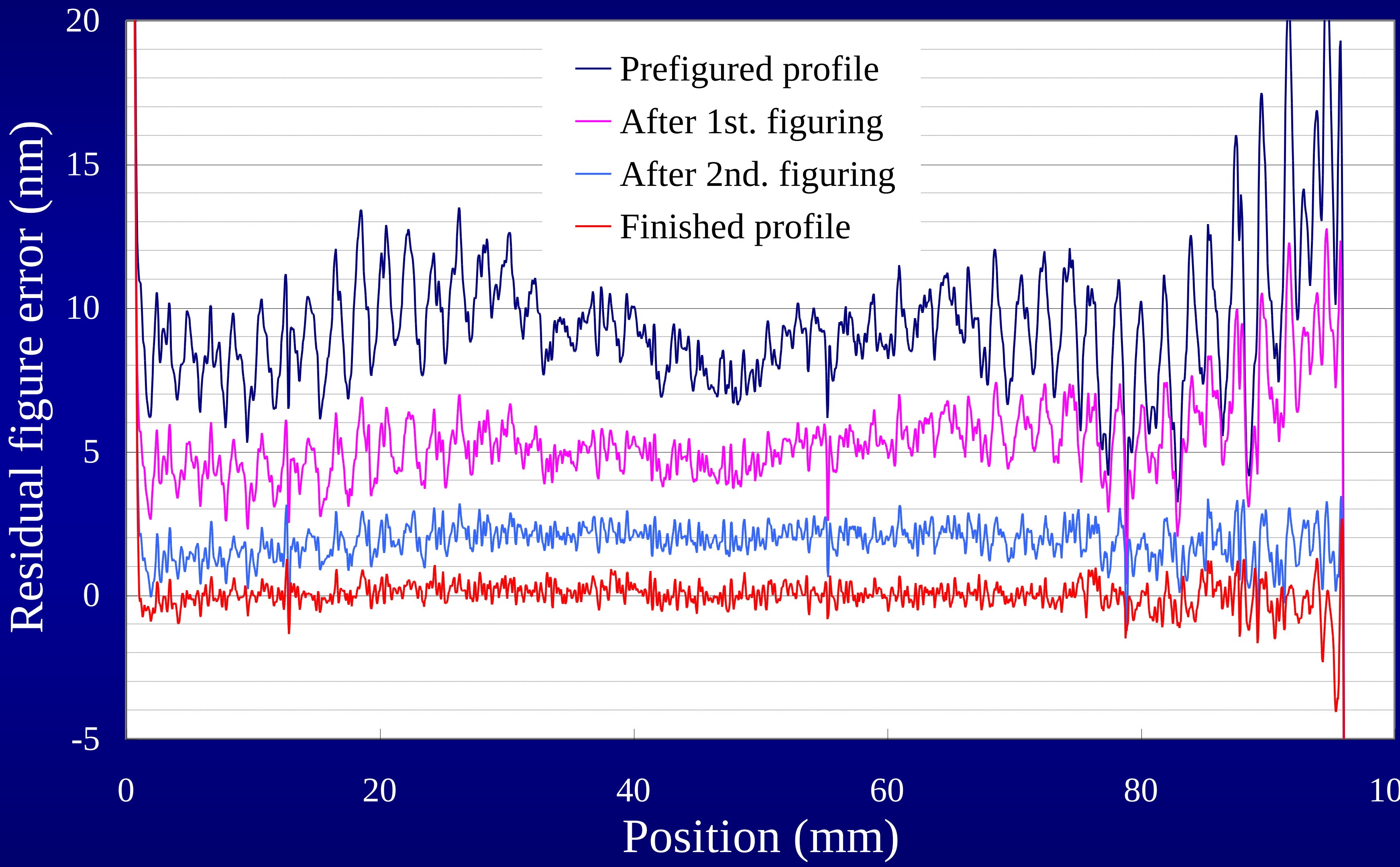

Sub-30nm focusing

Designed configuration

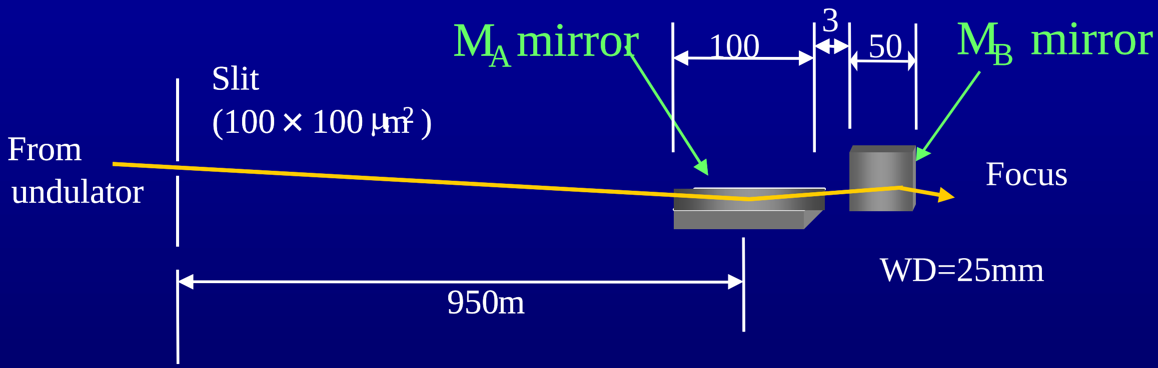

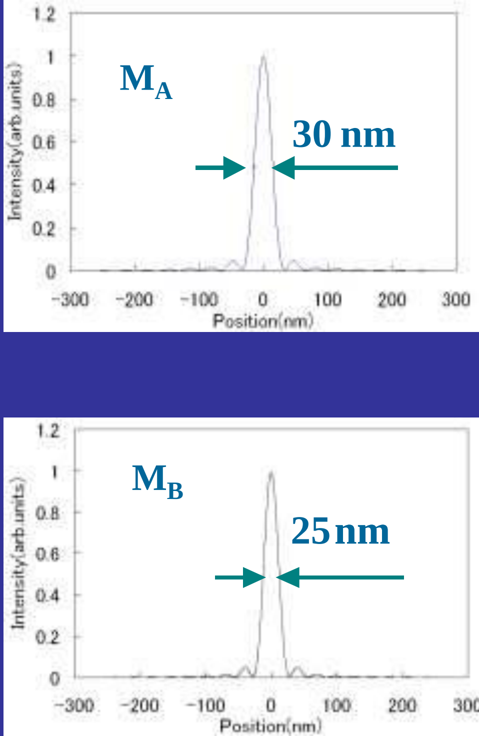

< Wave-optically expected beam profile >

Focusing performance

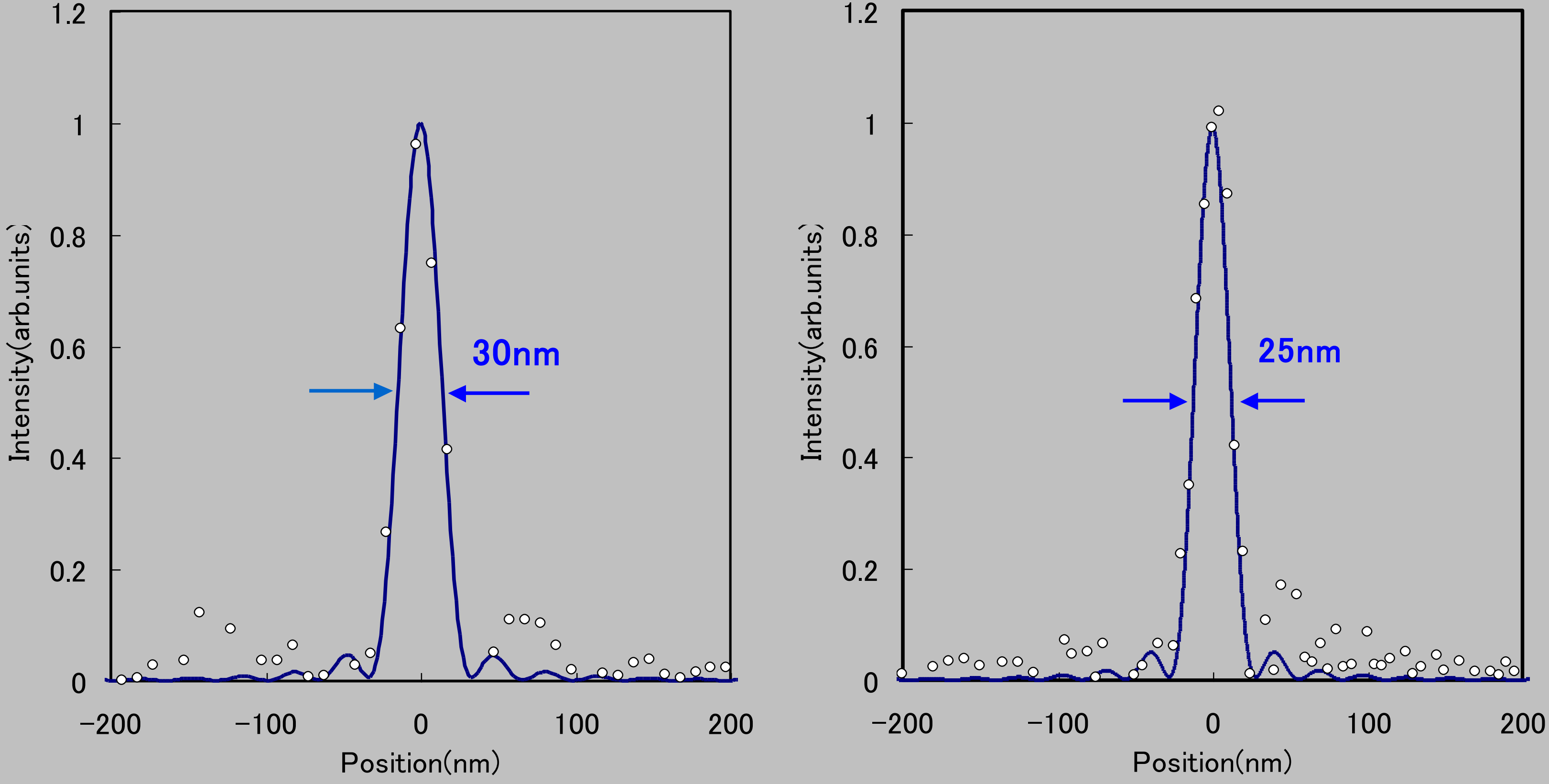

Beam waist structures

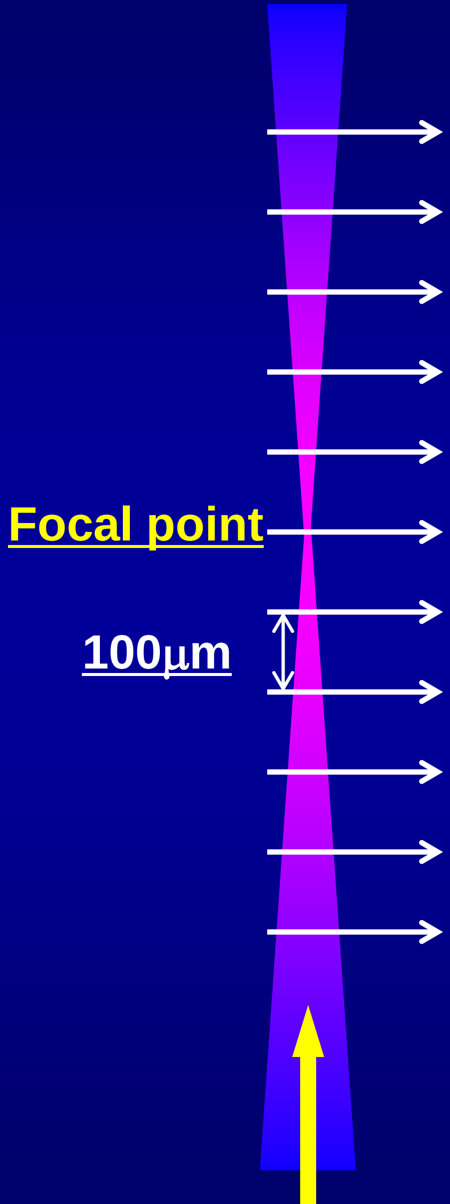

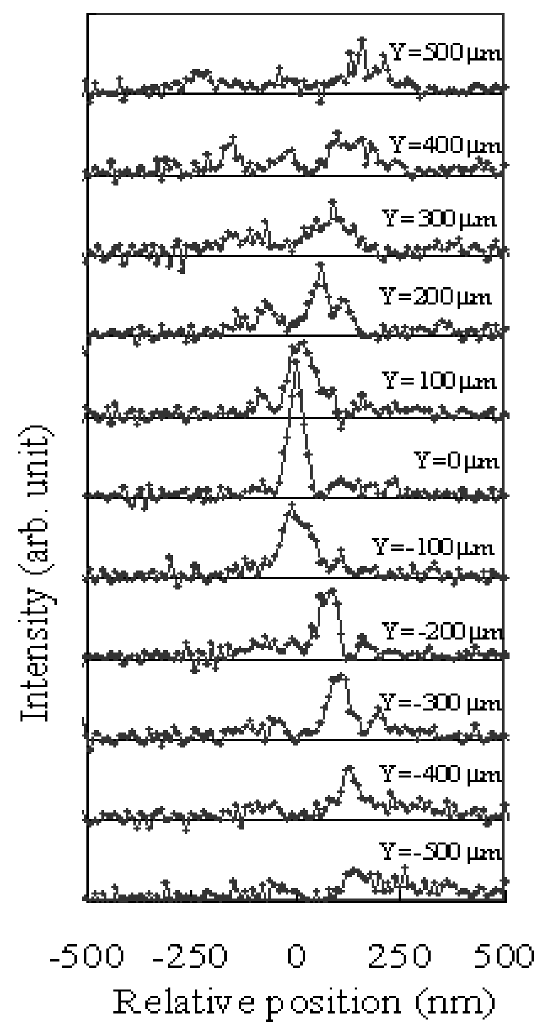

Measured profile

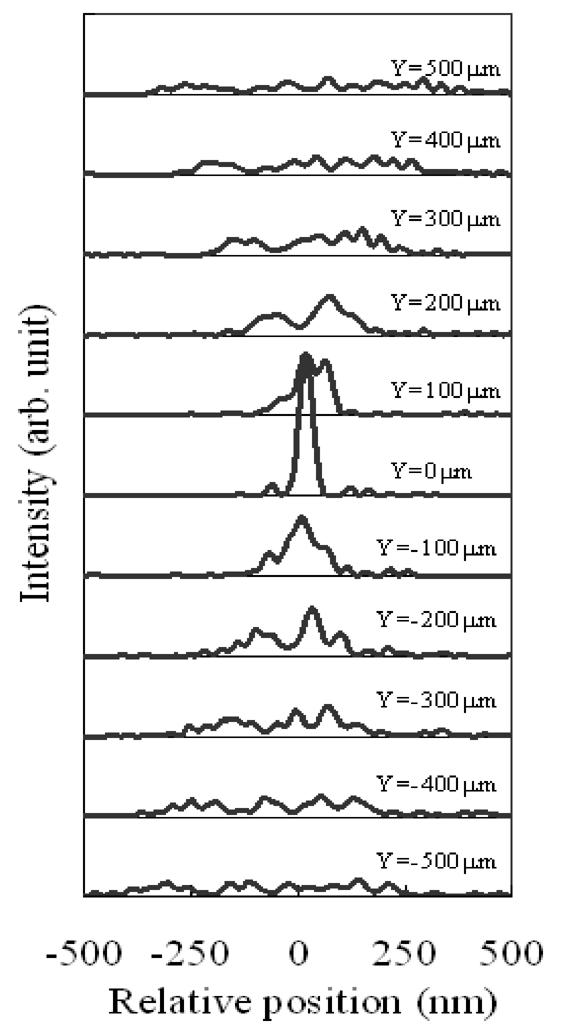

Calculated profile
using measured shape

Tunability of beam size and photon flux

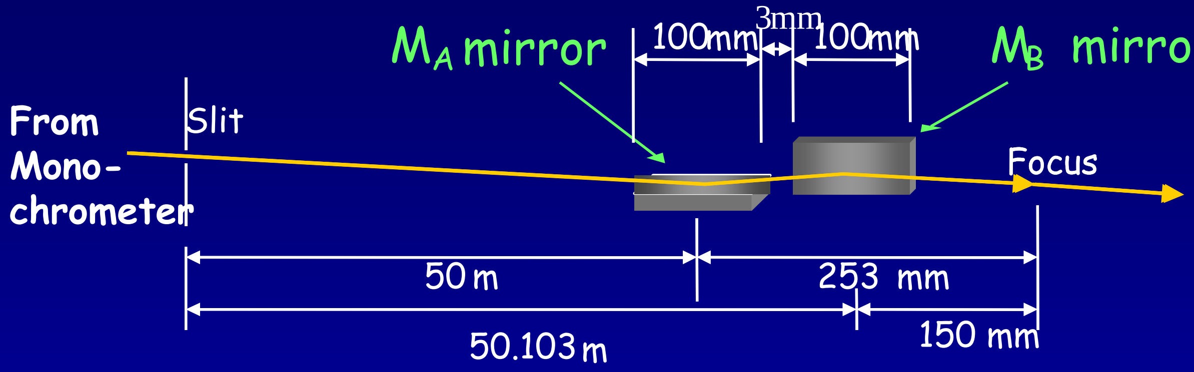

Photon flux:

$5 \times 10^9 \sim 10^{12}$ (1/s)

Installed in a new hutch of BL29

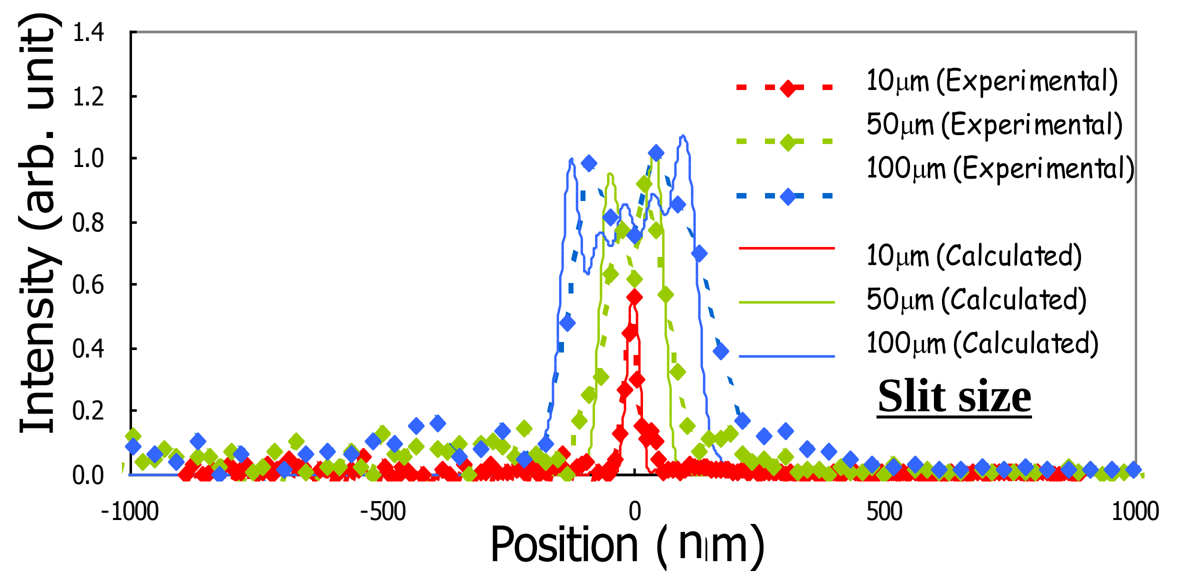

S. Matsuyama et al.
Rev. Sci. Instrum., 77, 103102 (2006)

emonstration of oomin performance

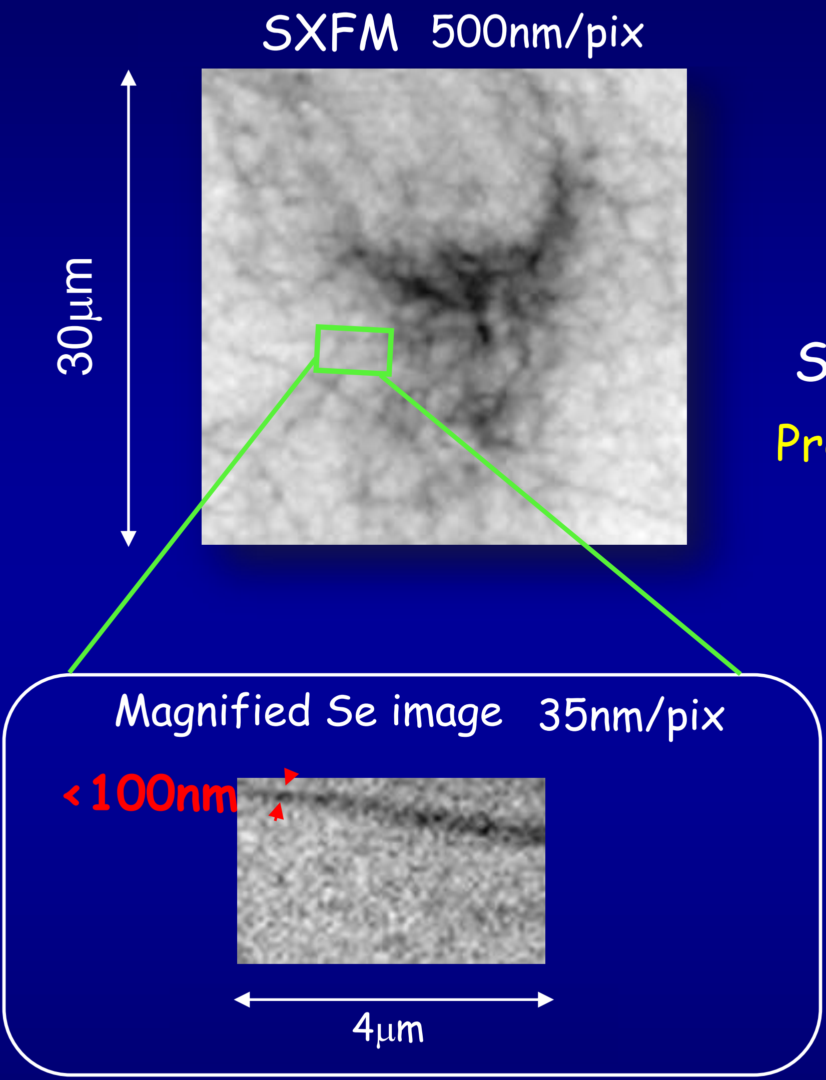

Se image

Probe X-ray : 15keV

Mouse cell tubulin was stained with nanocrystals of CdSe/ZnS.

“Hard-X-ray sub-10nm focusing By KB mirrors”

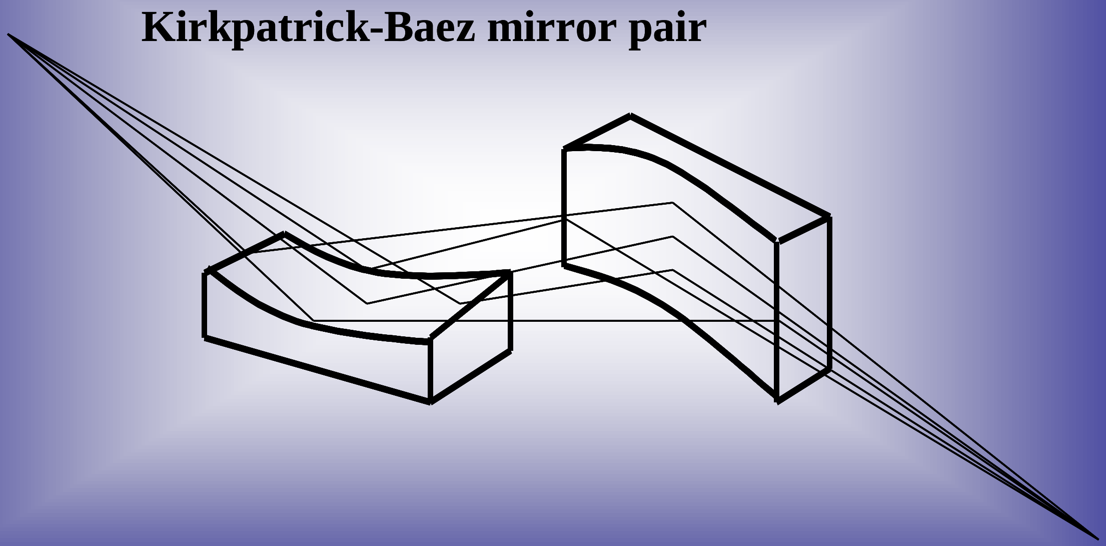

To realize Sub-10nm focusing K-B mirrors

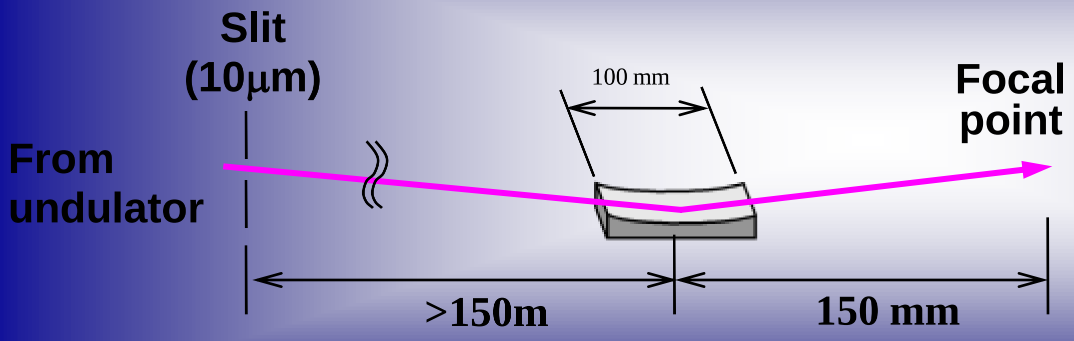

X-ray energy : 20keV

Focal length : 150mm

Acceptance width : 1.1mm

Incidence angle : <u>11.1mrad</u>

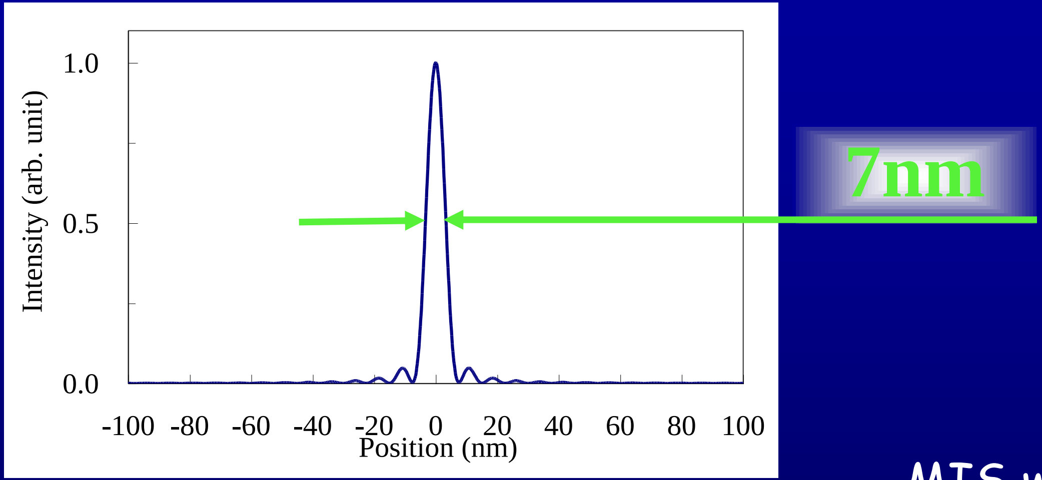

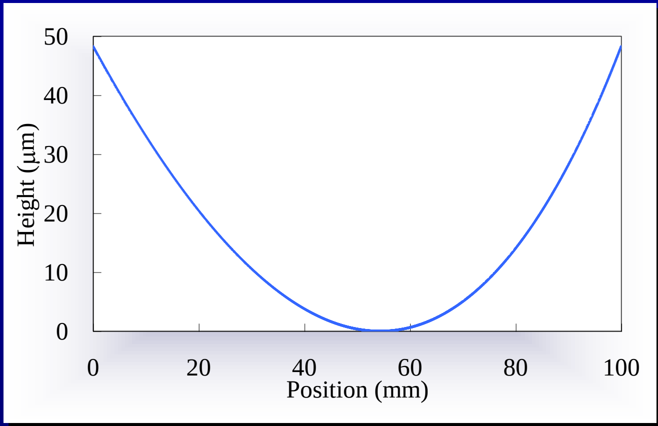

<u>MIS with RADSI and EEM can prepare</u>

surface figure within 1～2nm (P-V) err

Required accuracy

@20keV Mirror length: 100mm, Focal length: 150mm

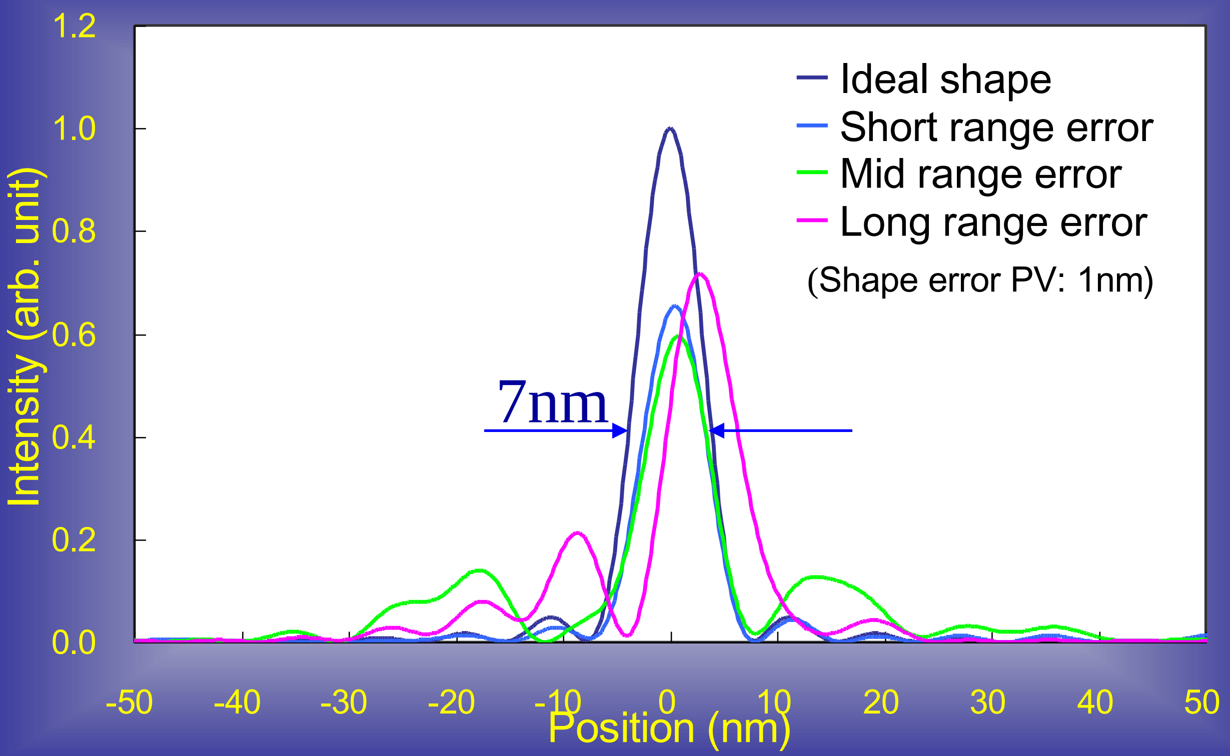

Figure error of 1nm is not allowable in this case

Off-line figure testing might be impossible?

Multi-layer technology is needed to realize large NA

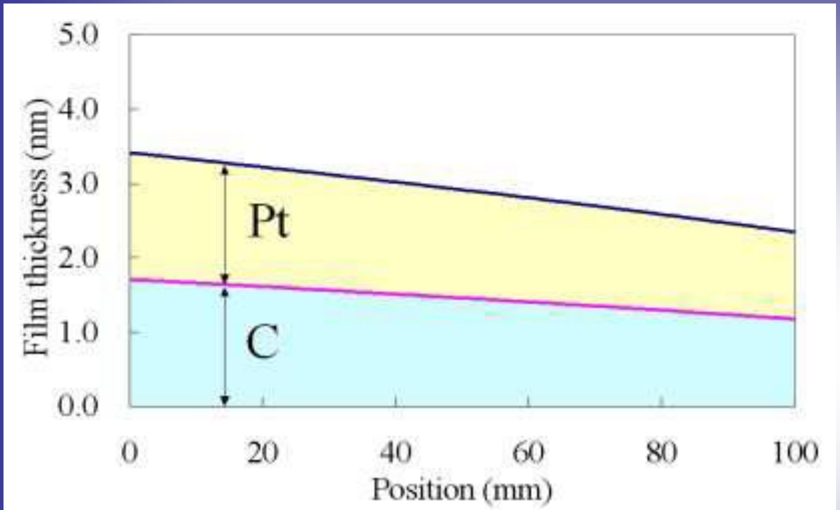

Graded multi-layer

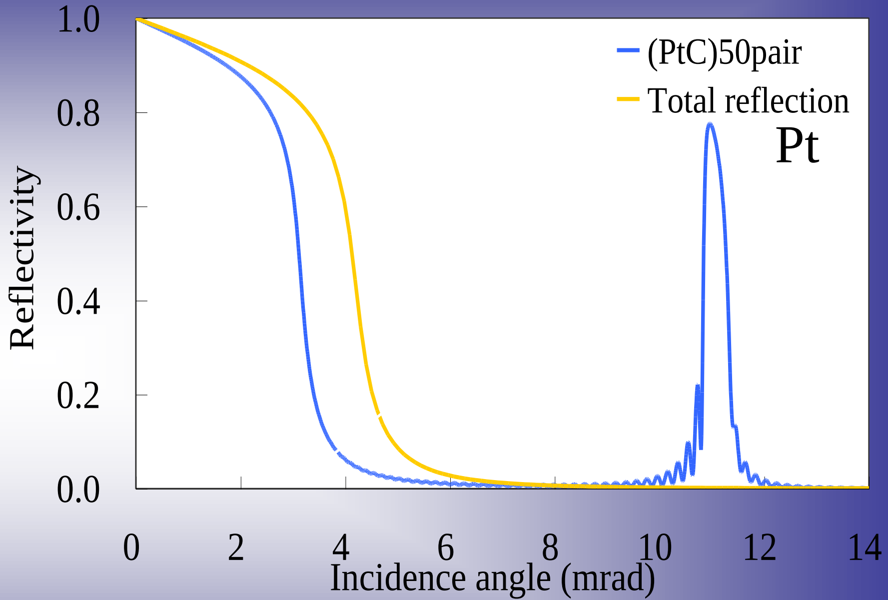

Reflectivity

Not only figure error but also thickness deviation of the multilayer induce the wavefront phase error.

At-wavelength phase-retrieval interferometry

lue : nov

Red : un

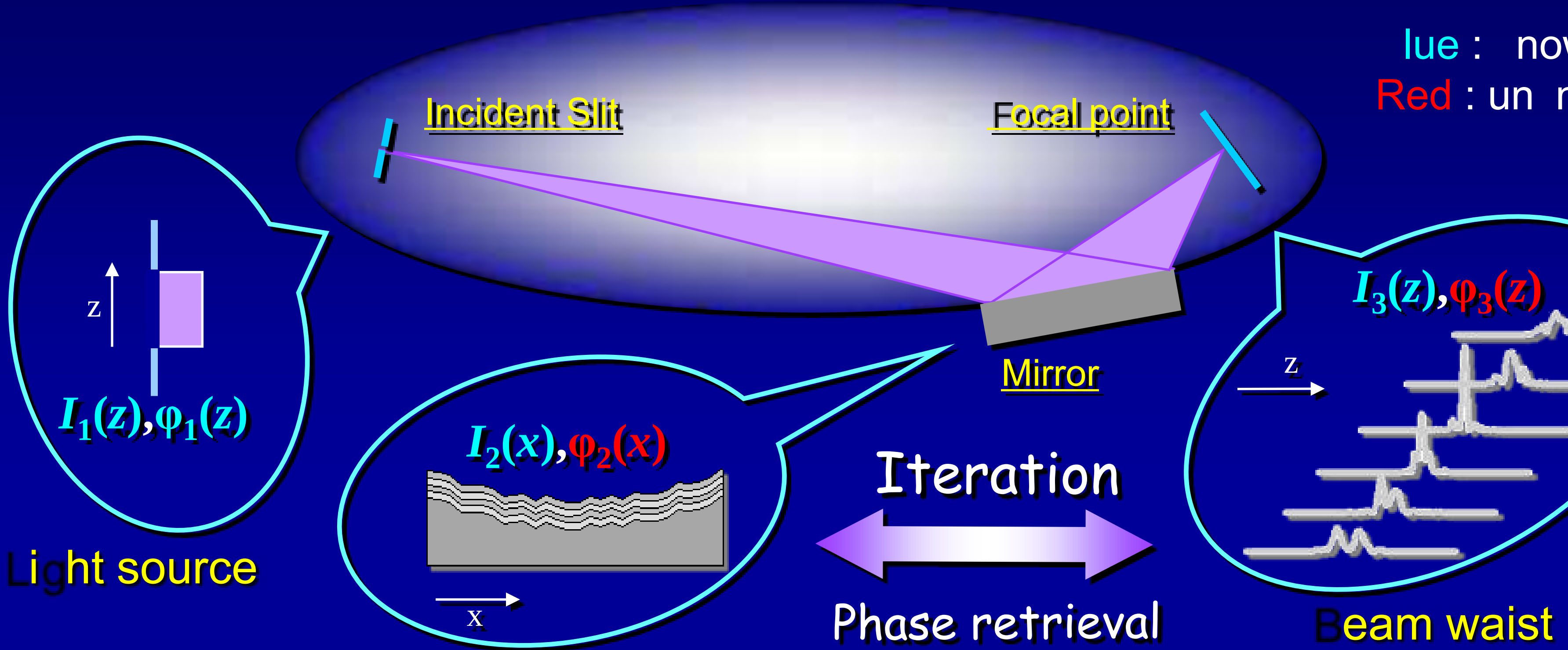

Mirror surface

(Phase error originates in errors of surface profile and ML thickness)

Phase error compensation

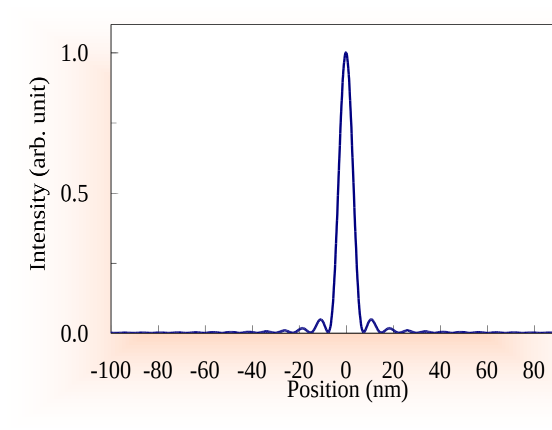

A strategy to fabricate KB mirrors for 10 nm hard X-rays focusing,
K. Yamauchi, X-Ray Optics: A Roadmap for the Next 10 Years

Phase retrieval properties

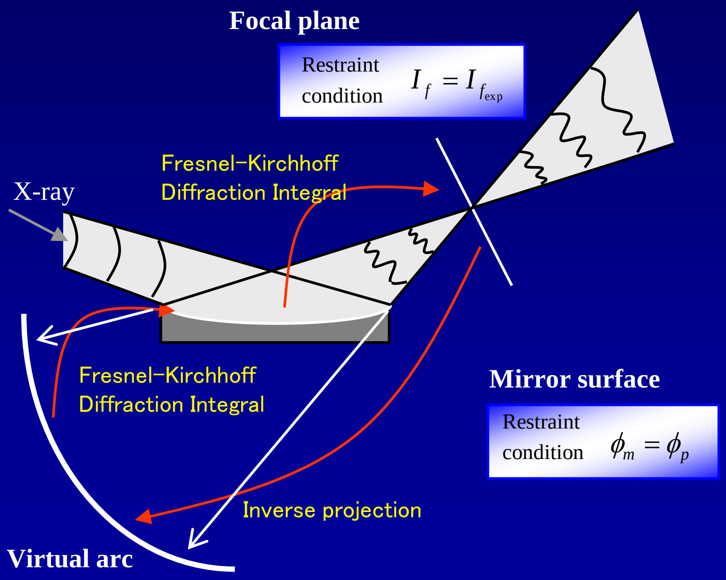

Focal plane

Restraint condition $I_f = I_{f_{\exp}}$

Fresnel−Kirchhoff Diffraction Integral

X-ray

Fresnel−Kirchhoff Diffraction Integral

Mirror surface

Restraint condition $\phi_m = \phi_p$

Inverse projection

Virtual arc

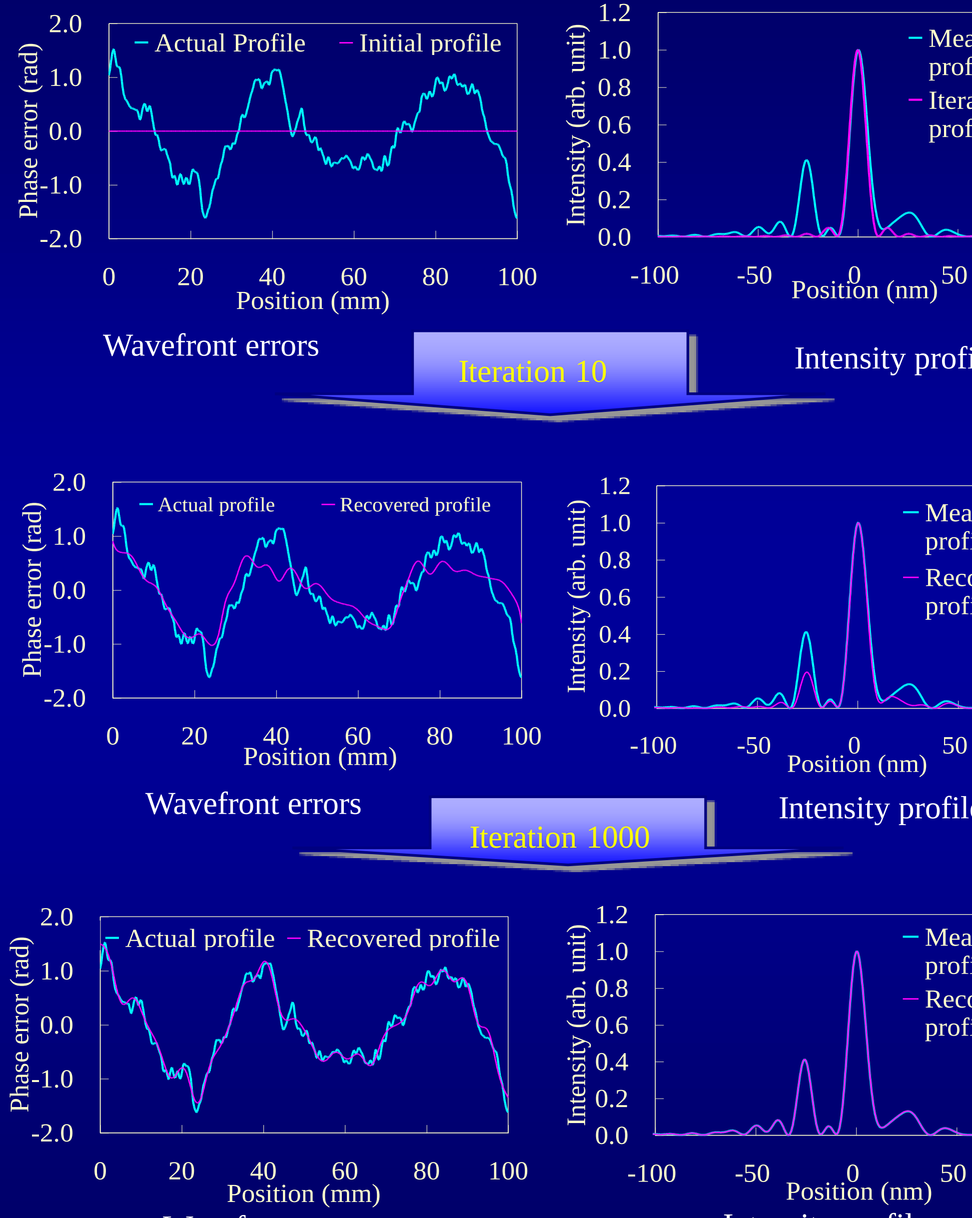

On focal plane

Intensity is changed to experimental value.

Phase is kept to be recovered value.

On mirror surface

Intensity is changed to theoretical value.

Phase is kept to be recovered value.

H. Yumoto et al.,
Review of Scientific Instruments 77, 063712 (2006)

New knife-edge method

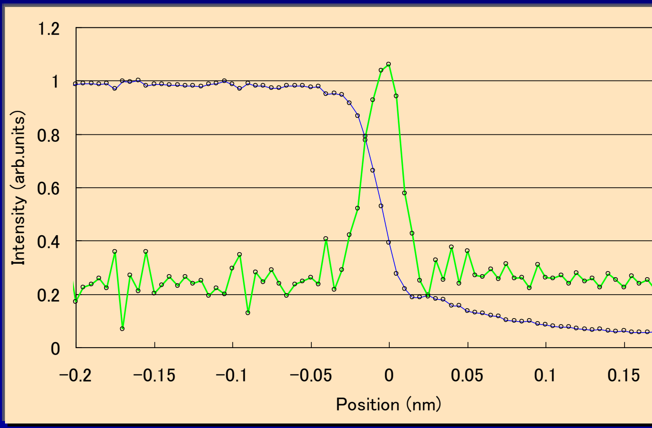

Conventional knife-edge method

New method

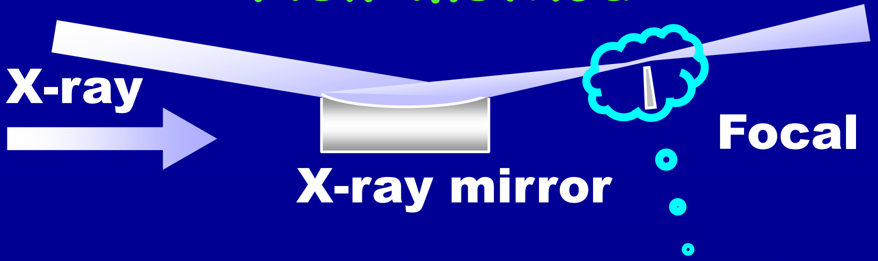

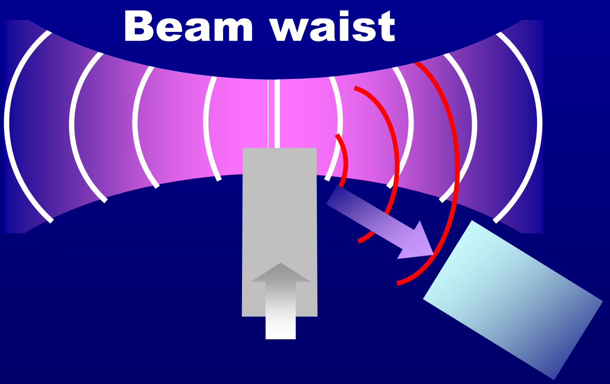

Y. Suzuki et al., Jpn. J. Appl. Phys. Part 1 44, 199

Details of the new knife-edge method

Beam waist

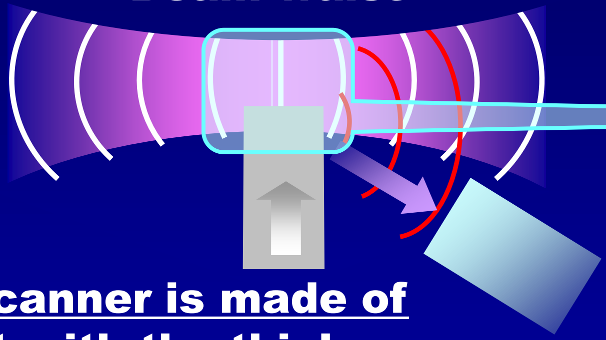

Scanner is made of Pt with the thickness of 2.5μm.

Spherically diffracted X-ray

X-ray detector

Scanner is acting as a phase object

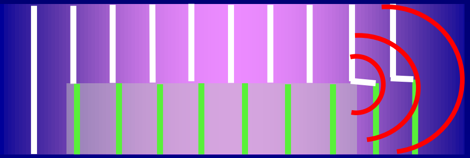

Modified wavefront

Phase is shifted with λ/2

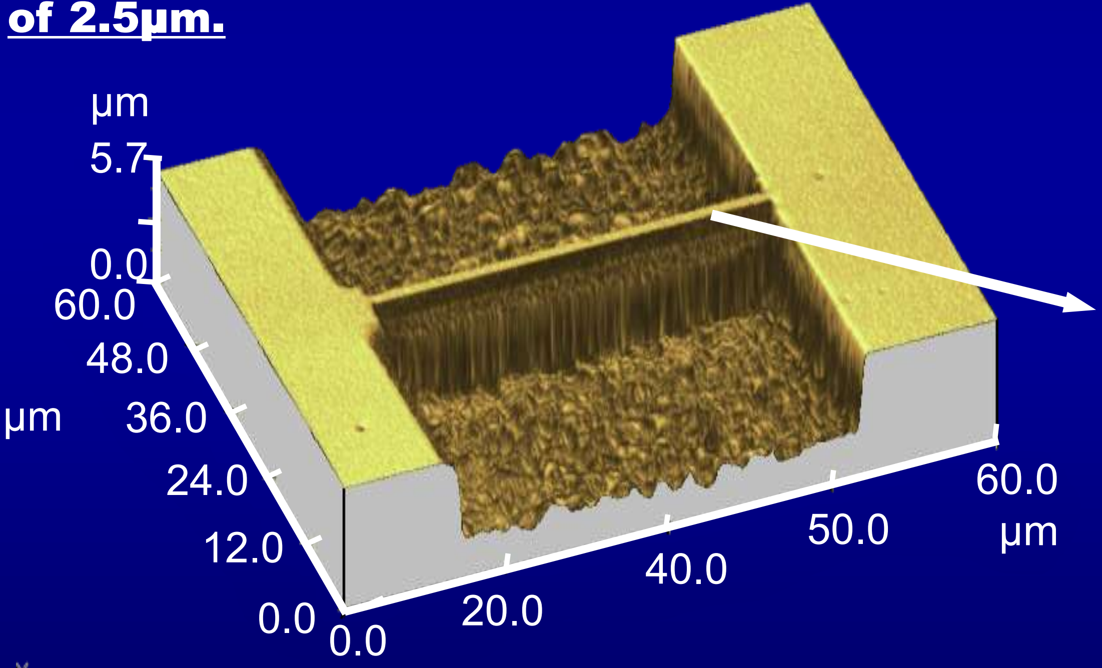

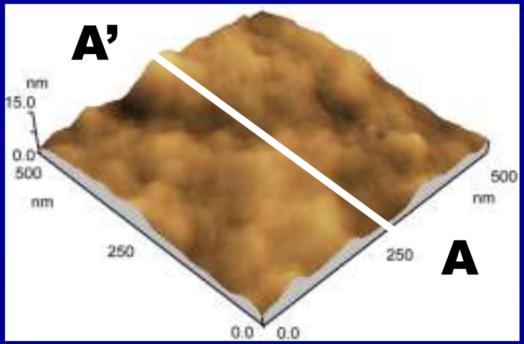

Microroughness at the bridge

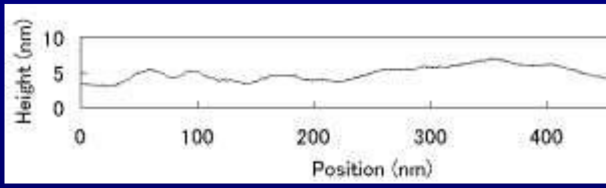

A-A' profile

H.Mimura et al., Phys. Rev. A 77 015812 (2008)

A demonstration of at-wavelength measuremen
(30nm-focusing mirror was employed)

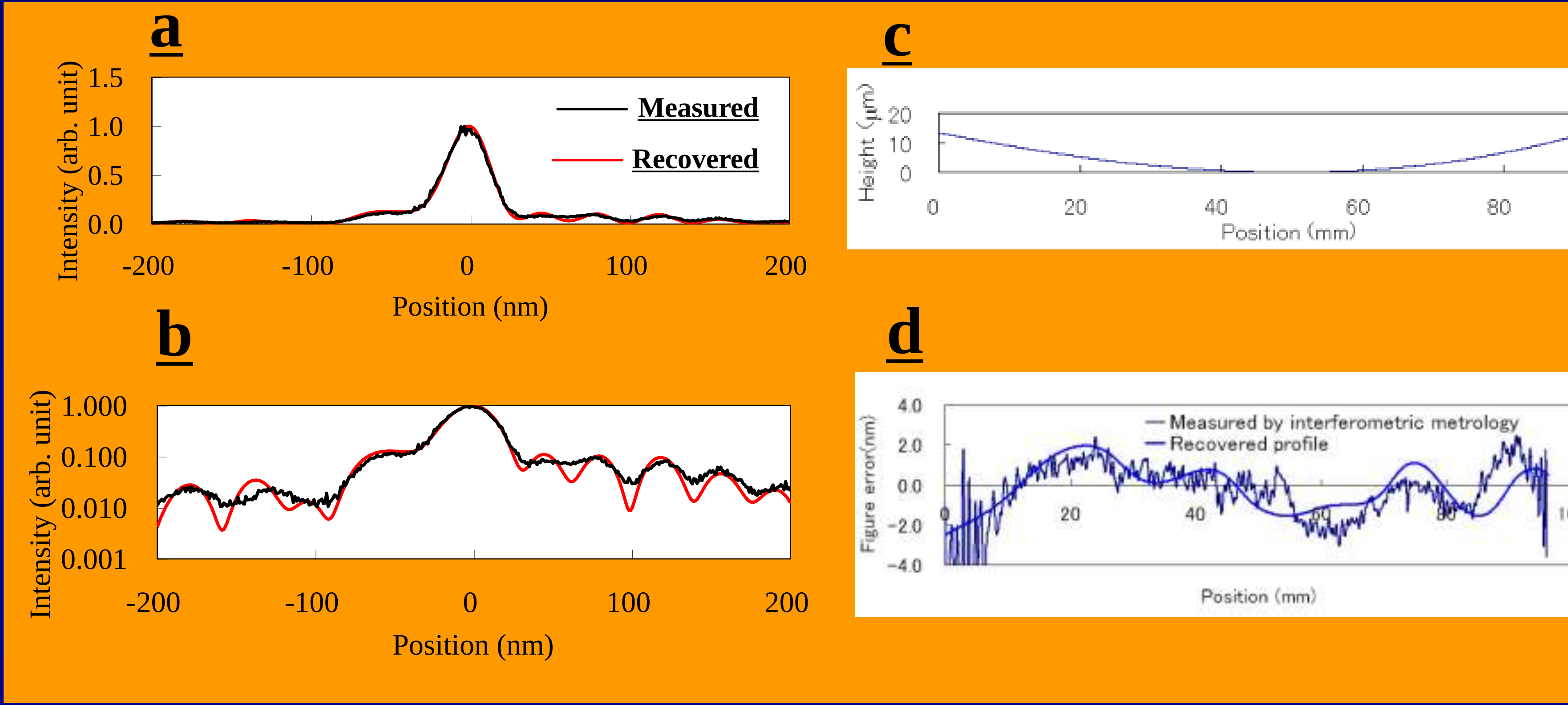

FIG. 3. Results of measuring intensity profiles in the focal plane and phase retrieval calculations. A Intensity profiles in the focal plane. The black line is the profile measured by scanning the microbridge, while the red line was obtained using phase retrieval calculations for determining the mirror surface profile. The plot interval is 1 nm. b Single logarithmic plot of graph in a. c Ideal profile of x-ray mirror. d Comparison of measured and reconstructed figure error profiles.

H.Mimura et al., Phys. Rev. A 77 015812(2008)

To avoid local-minimum problem

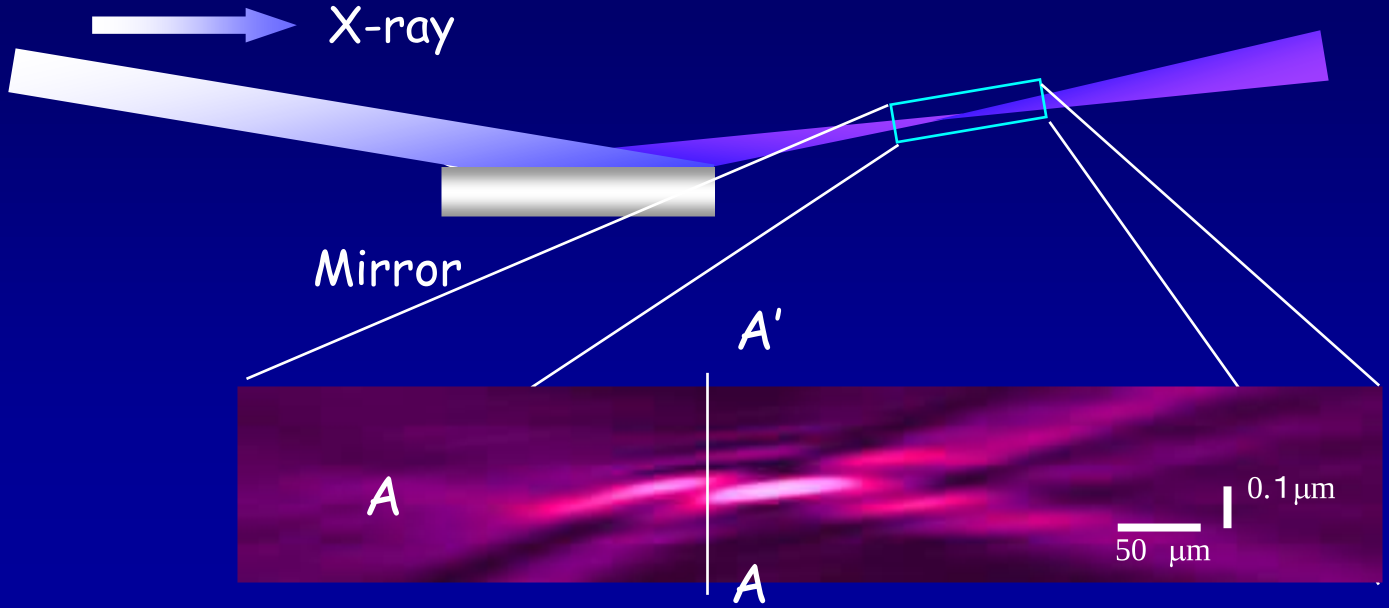

Intensity distribution at beamwaist

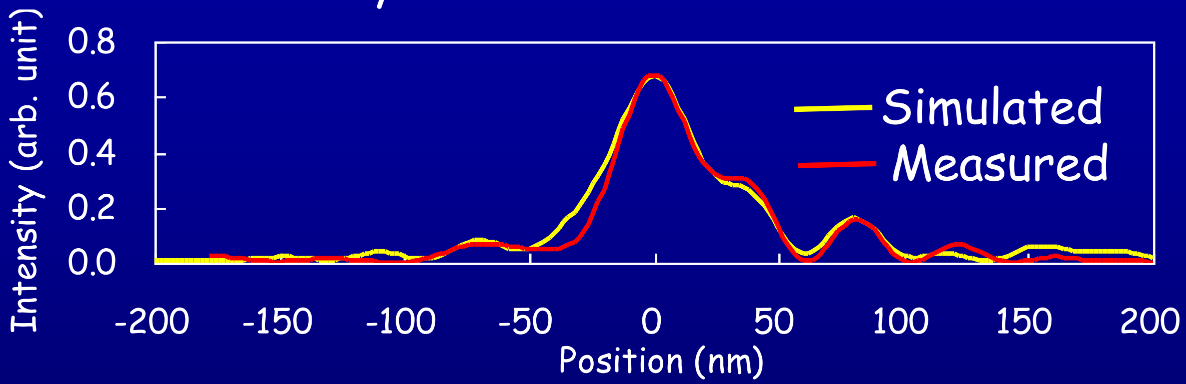

Calculated and measured intensity profiles on A-A' line.
(50μm upstream from the focal point)

H.Mimura et al., Phys. Rev. A 77 015812

On-line compensation of wavefront

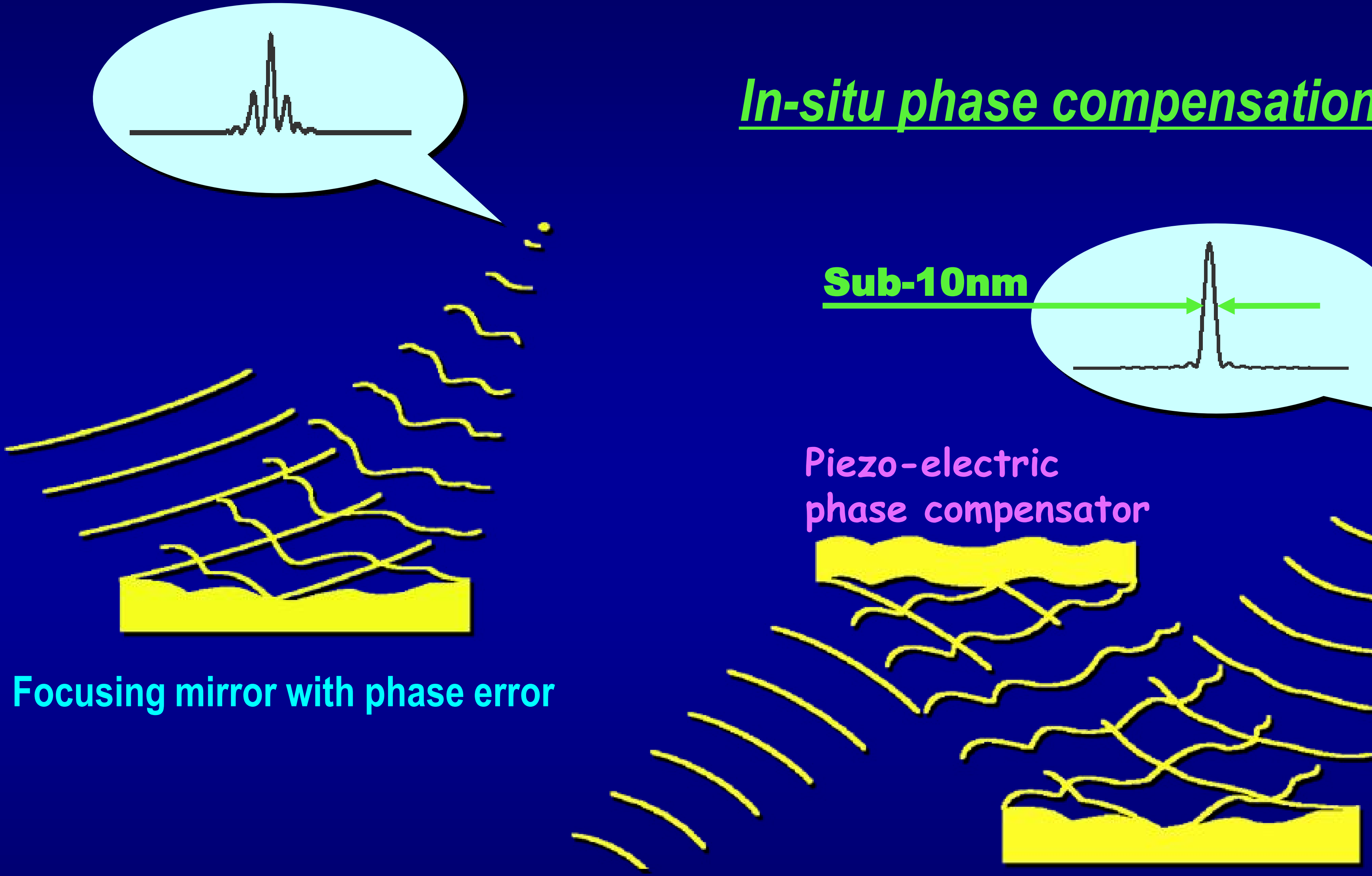

In-situ phase compensation

Sub-10nm

Piezo-electric phase compensator

Focusing mirror with phase error

Focusing mirror with phase

Designing 1 (reduction of required accuracy)

Phase error = $2kd\sin\theta$

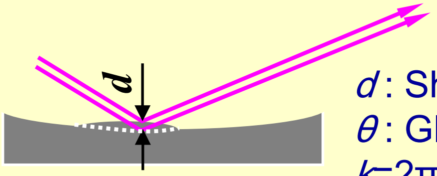

d : Shape error
θ : Glancing angle
$k=2\pi/\lambda$: Wave number

An example

Glancing angle of
10nm-level focusing mirror: 7 [mra
Glancing angle of
active mirror: 1.0[mrad]

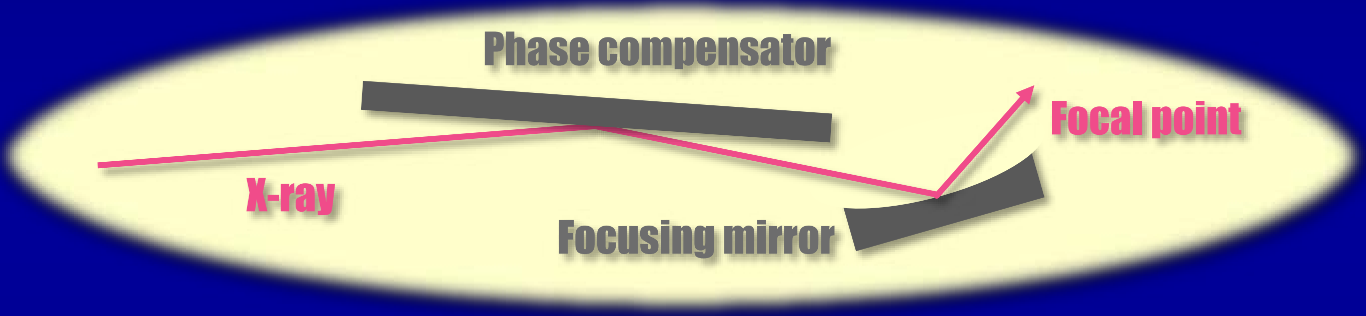

★ Required figure accuracy of the 10nm-level focusing mirror is 0.7nm (PV).

★ Glancing angle of the active mirror is 7 times smaller than that of the focusing mi

Required figure accuracy of the active mirror becomes 4.9nm (PV).

Designing 2 (How many waves should be generated by the active mirror?)

Spatial wavelength of the figure error and the positio of the satellite peak are wave-optically correlated.

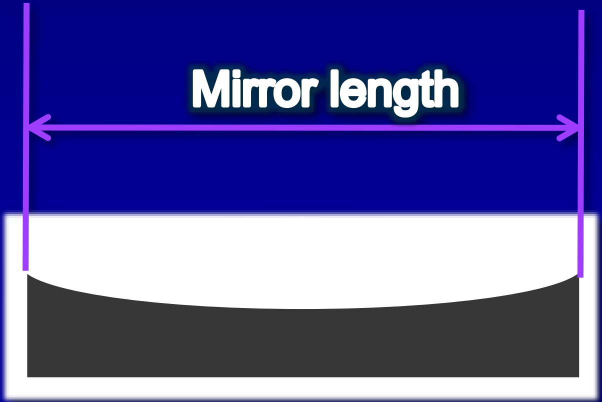

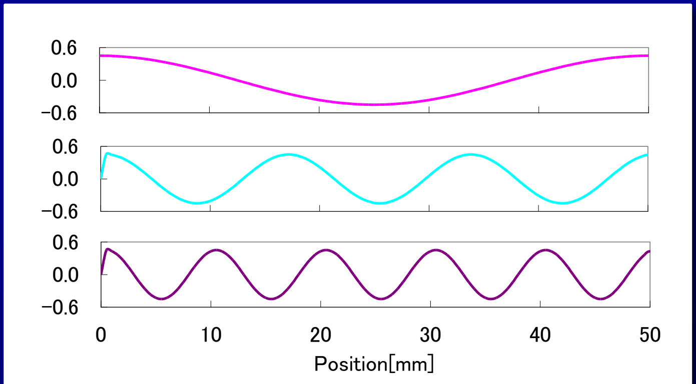

Shape error profiles

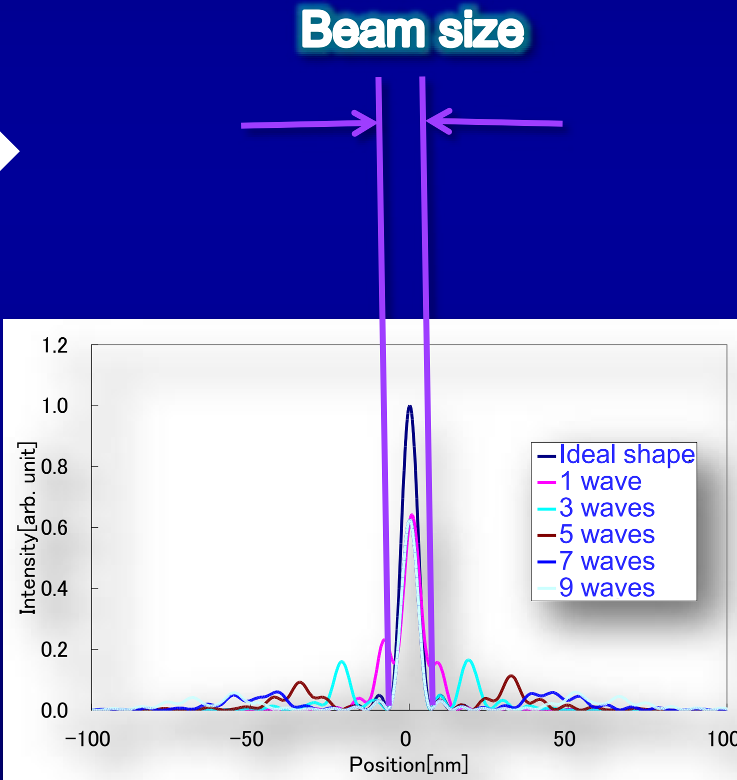

Phase compensator

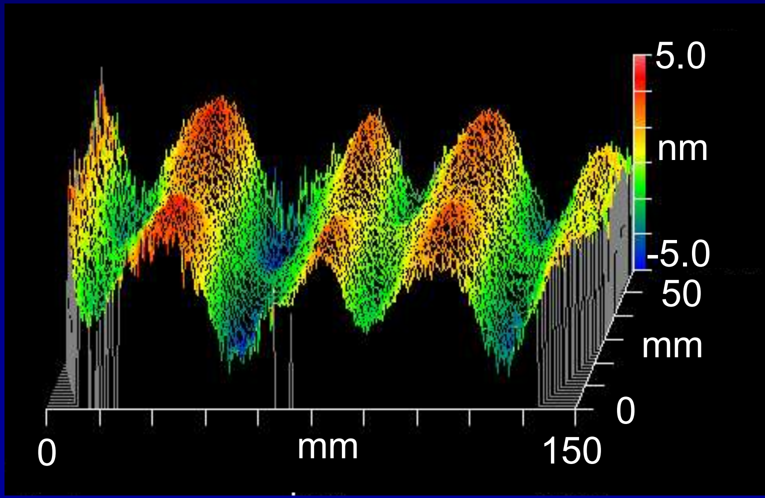

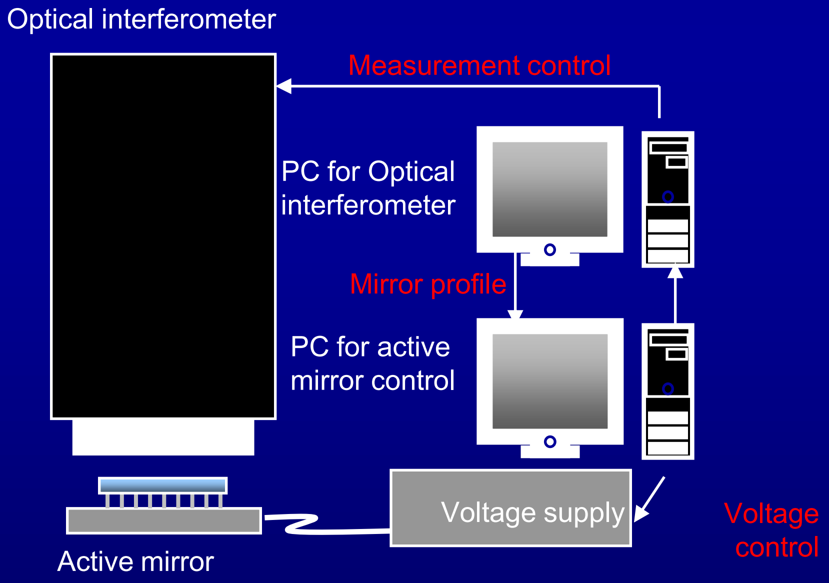

Optical interferometer

Measurement control

PC for Optical interferometer

Mirror profile

PC for active mirror control

Voltage supply

Voltage control

Active mirror

Feedback system

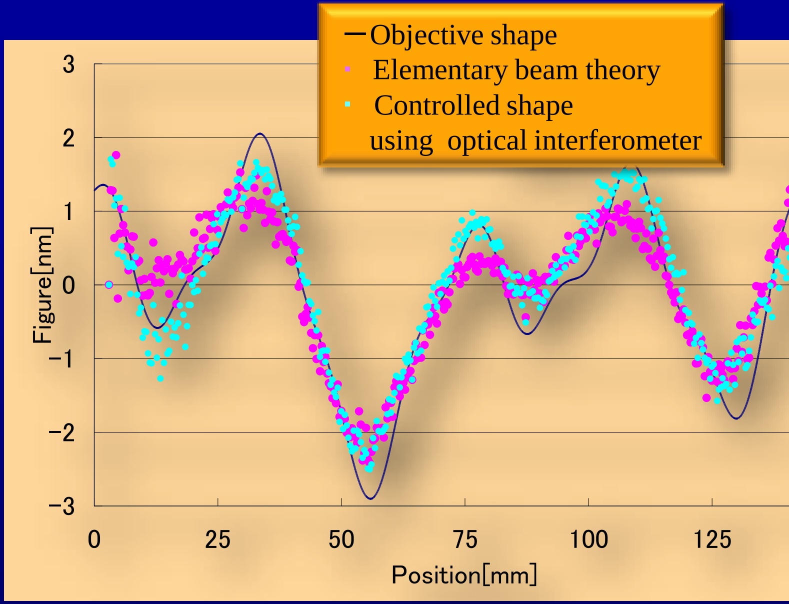

Optical configuration of 10nm-level focusing with AM

Compensator (AM: Active mirror)

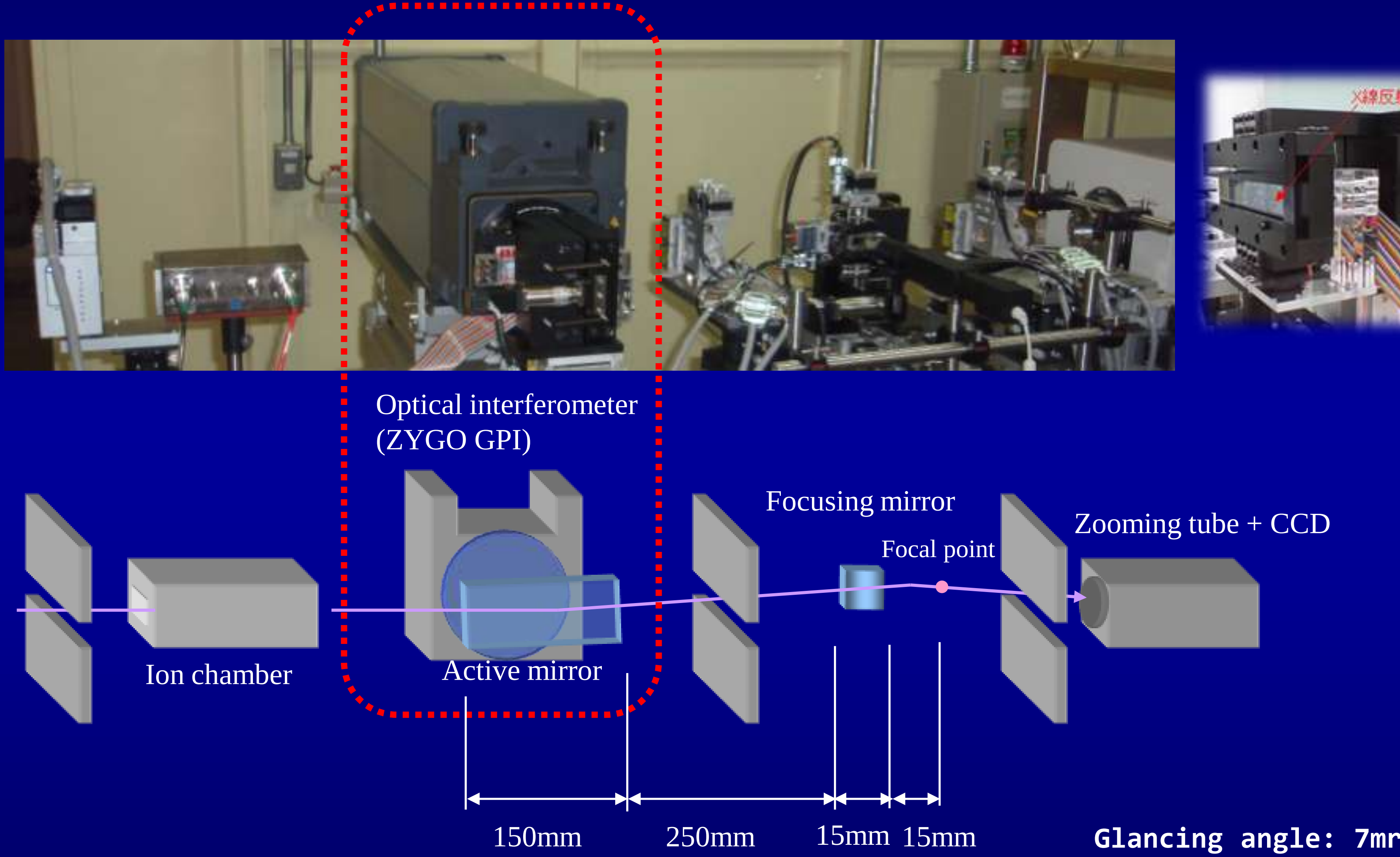

Glancing angle: 7mr
(Graded multilayer (Pt/C) coate

Glancing angle: 1mrad

Achieved beam size at Spring-8

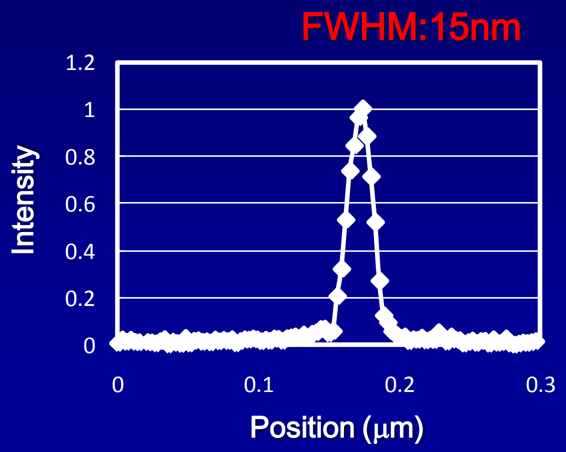

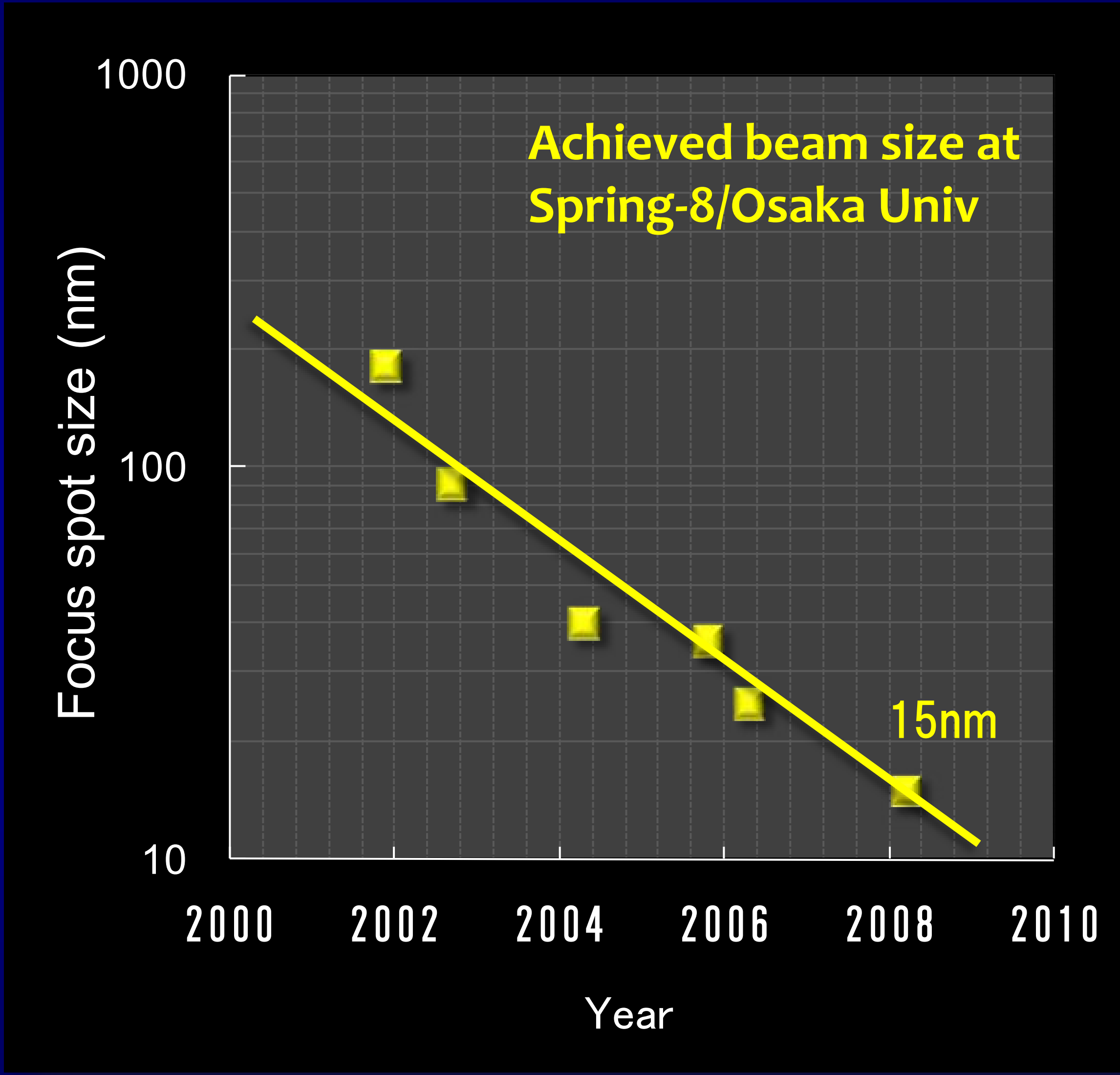

400mm-long mirror for XFEL

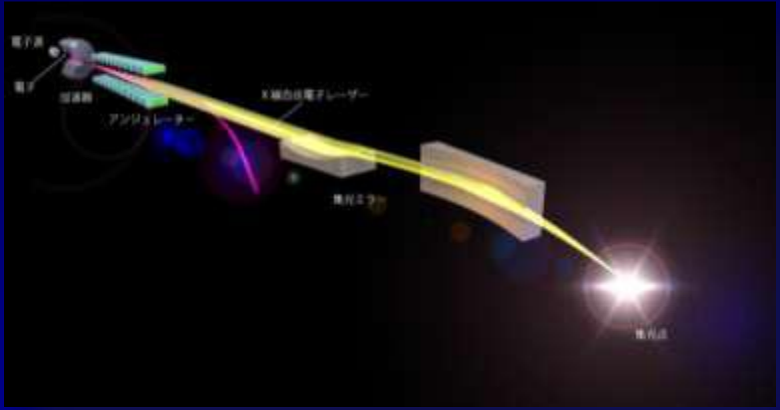

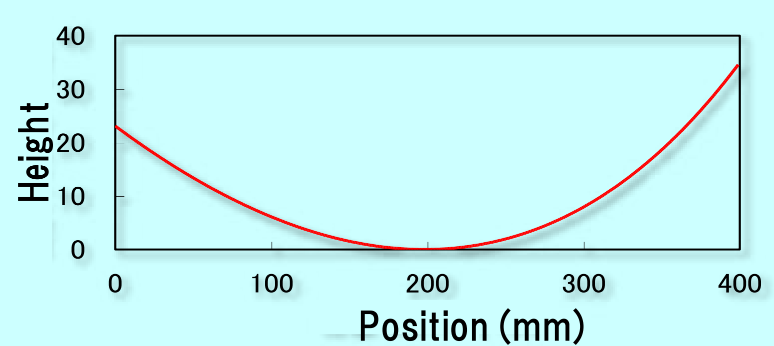

WD: 350m

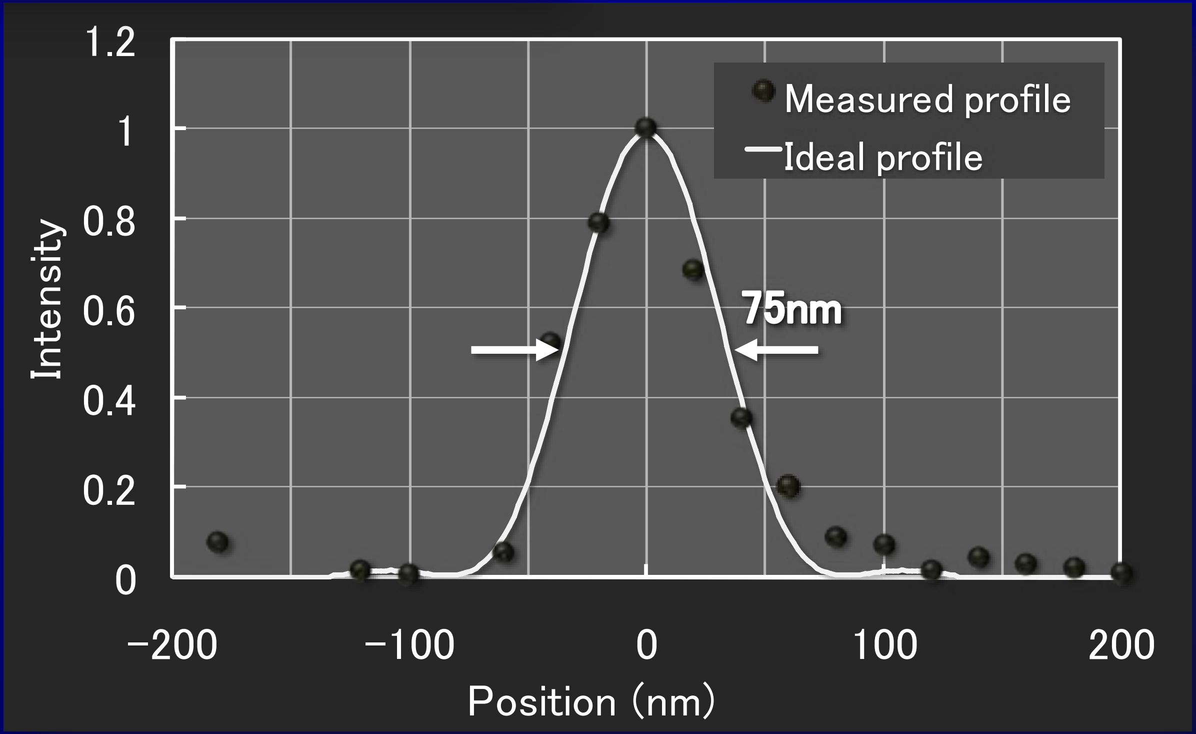

Mimura et al., Rev. Sci. Instrum., 79, 083104 200

Conclusion

1. Mirror optic has many advantages against the other optics, such as long WD, no chromatic aberration (in case of total reflection mirror), high focusing-efficiency, and relatively lar aperture.
2. Diffraction-limited focusing performance has been already realized in mirror focusing.
3. Sub-50nm focusing mirrors become ordinary devices.
4. Phase retrieval interferometry will become a possible technique for the mirror surface testing.
5. Active mirror can control wavefront phase with 0.1λ-level accuracy.
6. 10nm-level X-ray beams will be realized in the near future.

Acknowledgement

Co-workers

H. Mimura[a], H. Yumoto[a], S. Matsuyama[a], S. Handa[a], T. Kimura[a], Y. Sano[a], K. Yamamura[a],
Y. Nishino[b], M. Yabashi[c], K. Tamasaku[b], and T. Ishikawa[b,c]

a: Osaka University b: RIKEN/SPring-8
c: JASRI/SPring-8

This research was supported by

A Grant-in-Aid for Specially Promoted Research 18002009, 2006 from the Ministry of Education, Sports, Culture, Science and Technology, Japan,

A 21st Century COE Research, Center for Atomistic Fabrication Technology, 2003 from the Ministry of Education, Sports, Culture, Science and Technology, Japan,

A Global COE Research, Center for Atomically Controlled Fabrication Technology, 2008 from the Ministry of Education, Sports, Culture, Science and Technology, Japan,

The use of BL29XU of the SPring-8 was supported by RIKEN.

Hard X-ray focusing with curved reflective multilayers

Ch. Morawe, ESRF (France)

Outline:

- **Basic focusing considerations**
- **Theoretical models**
- **Multilayer properties**
- **Technological options**
- **Experimental progress**
- **Summary**

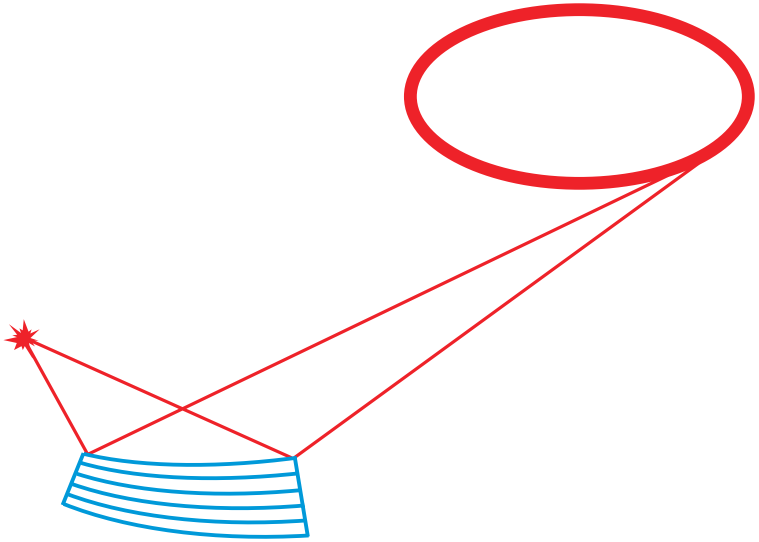

Basic considerations

Diffraction limit $D_{FWHM} = C\dfrac{\lambda}{NA}$

Numerical aperture $NA = n \cdot \sin\varepsilon$

Straight aperture $C = 0.44$

Source size limit $D = \dfrac{q}{p} \cdot S$

Further physical limitations

- Volume diffraction
- Scattering

Technological limitations

- Non-trivial design
- Fabrication accuracy
- Alignment

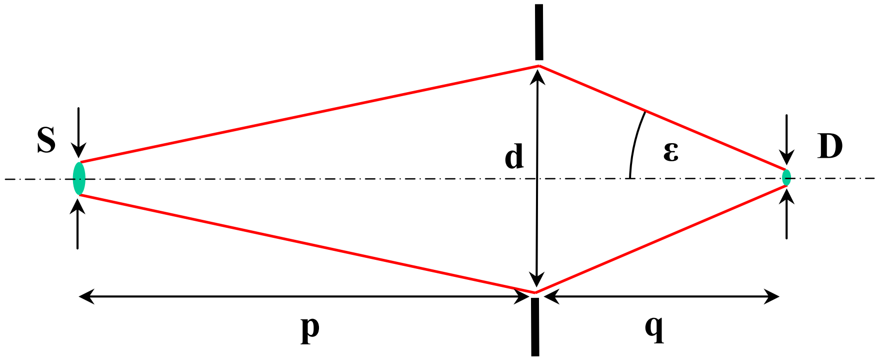

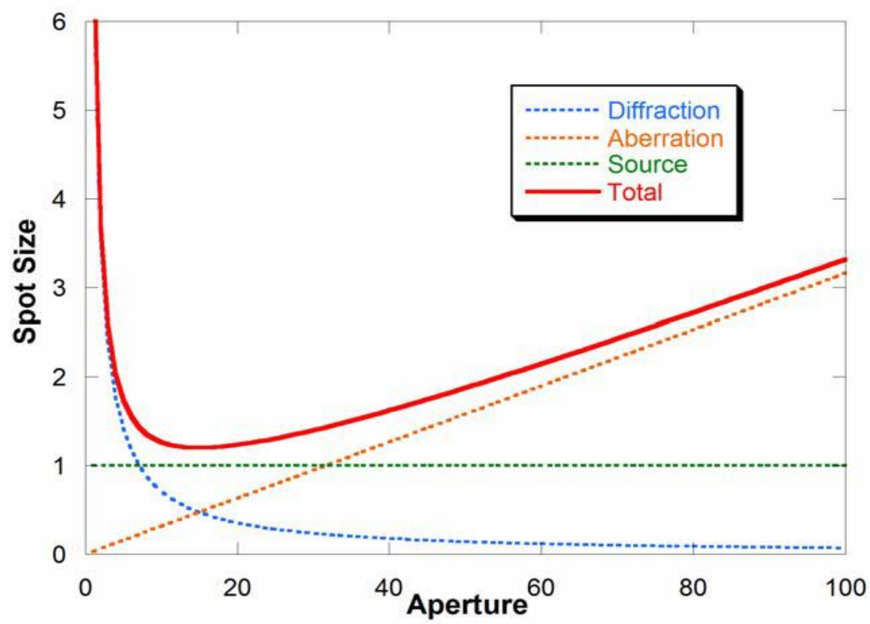

Geometrical approximation

Total reflection mirrors

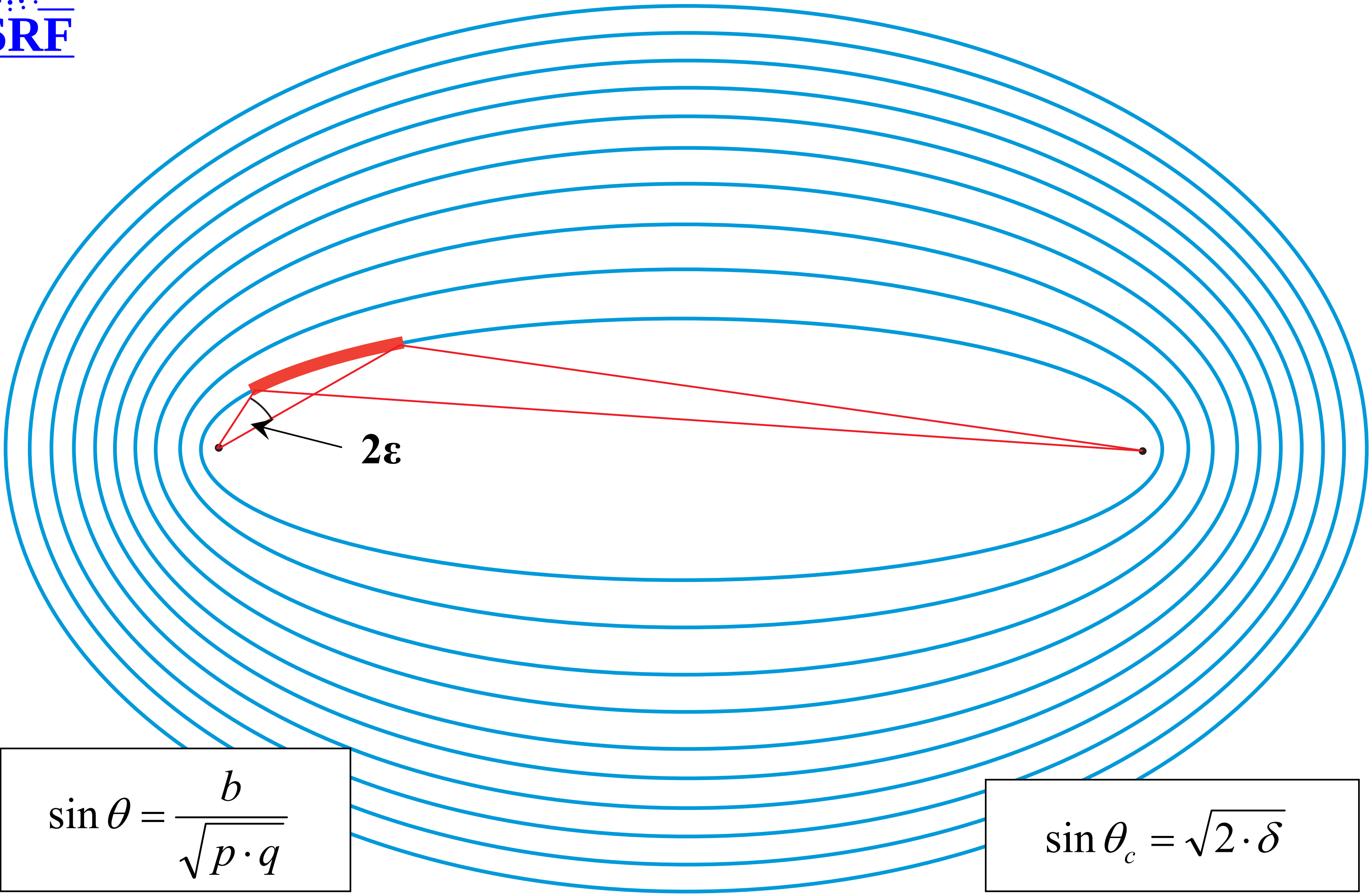

$$\sin\theta = \frac{b}{\sqrt{p \cdot q}}$$

$$\sin\theta_c = \sqrt{2\cdot\delta}$$

Geometrical approximation

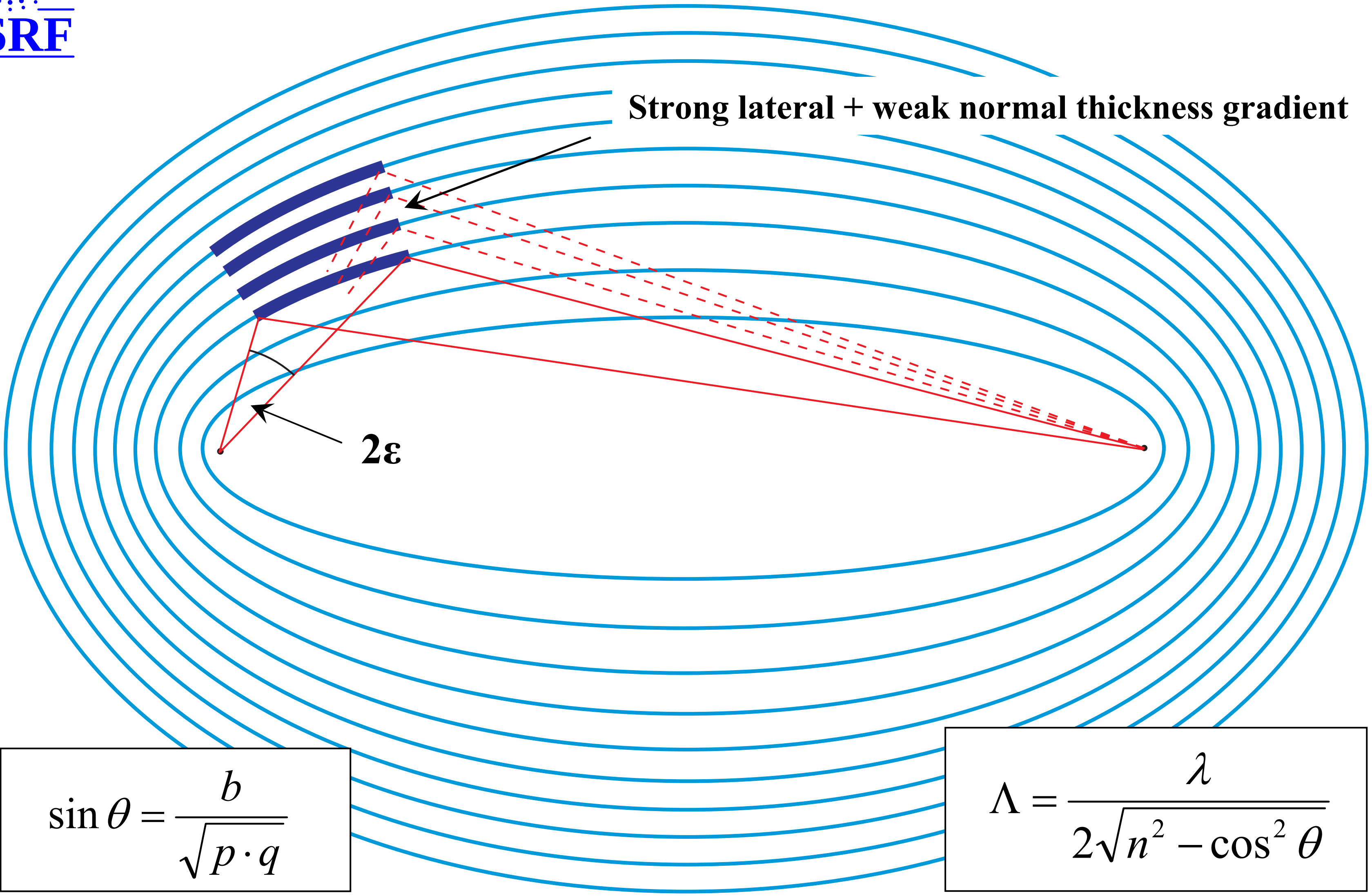

Strong lateral + weak normal thickness gradient

2ε

$$\sin\theta = \frac{b}{\sqrt{p \cdot q}}$$

$$\Lambda = \frac{\lambda}{2\sqrt{n^2 - \cos^2\theta}}$$

Basic considerations

Ellipse geometry

$$2\varepsilon = \varphi_q(\theta_2) - \varphi_q(\theta_1)$$

$$\sin\varphi_q = \frac{p \cdot \sin 2\theta}{2 \cdot c}$$

↓

$$NA = n \cdot \sin\varepsilon$$

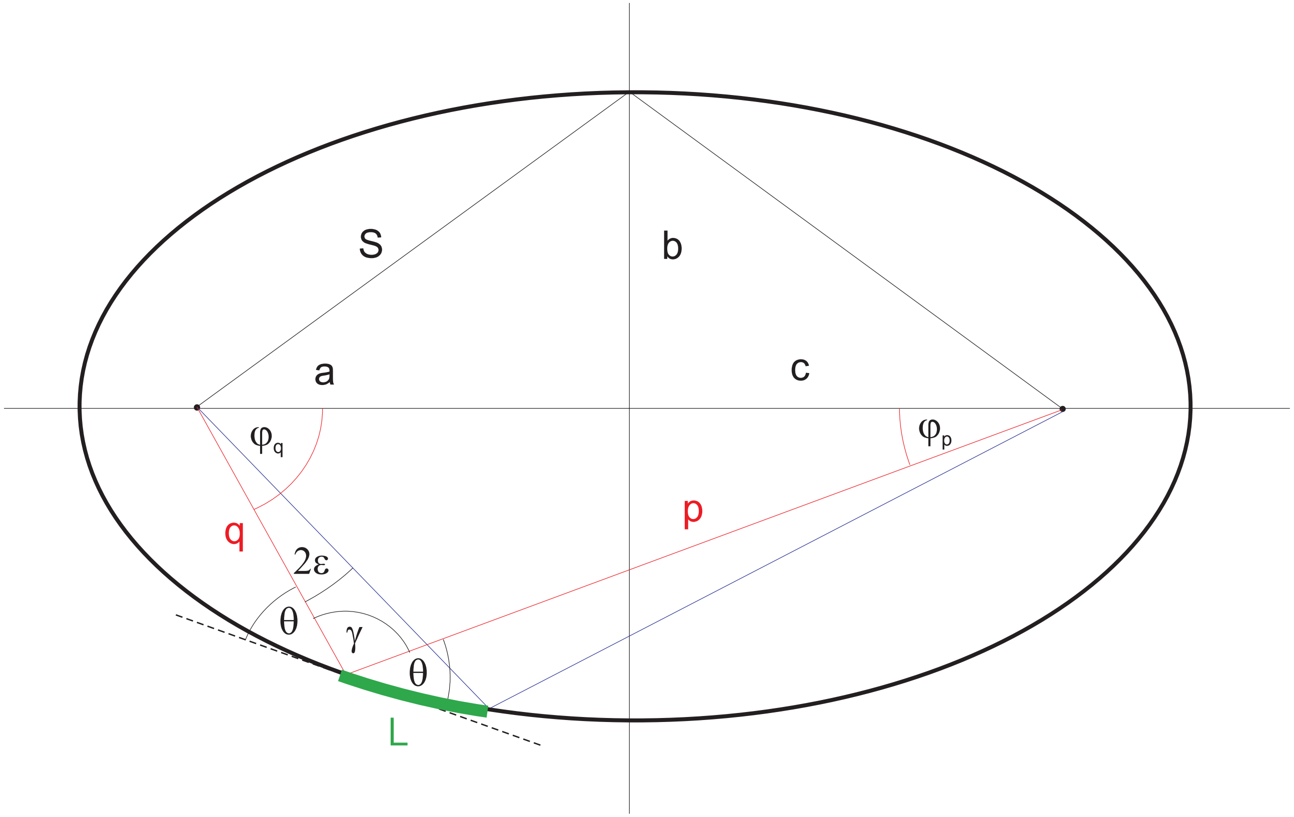

Correct only for flat aperture !

Basic considerations

Simple approximation:

a) Total reflection mirror

$$\sin\varepsilon \approx \frac{1}{4}\sin\theta_c = \frac{\sqrt{2\cdot\delta}}{4} = \frac{\lambda}{4}\sqrt{\frac{r_0\rho_e}{\pi}}$$

$$\Rightarrow D_{FWHM} \approx 1.76\cdot\sqrt{\frac{\pi}{r_0\rho_e}}$$

$D_{FWHM} \approx 25$ nm (Pt)

b) Multilayer mirror

$$\sin\varepsilon = \frac{1}{4\cdot c}\left(p_2\cdot\sin 2\theta_2 - p_1\cdot\sin 2\theta_1\right)$$

$$\sin 2\theta \approx 2\cdot\sin\theta \approx \frac{\lambda}{\Lambda}, p \approx 2\cdot c$$

$$\Rightarrow \sin\varepsilon \approx \frac{\lambda}{2}\left(1/\Lambda_2 - 1/\Lambda_1\right)$$

$$\Rightarrow D_{FWHM} \approx \frac{0.88}{1/\Lambda_2 - 1/\Lambda_1}$$

$D_{FWHM} \approx 5$ nm

No explicit energy dependence !

Theoretical models

Geometrical phase shift due to height/slope errors

$$\varphi_h = \frac{4\pi \cdot \sigma \cdot \sin\theta}{\lambda}$$

σ: height error

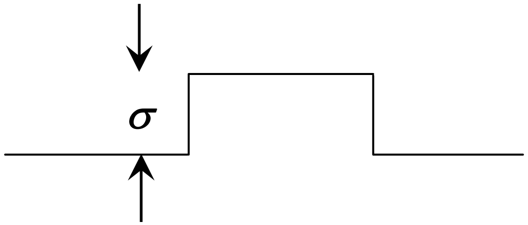

Reasonable values for ML mirrors with 80% flux in focal spot

$$\sigma_{RMS} \le \frac{\lambda}{27 \cdot \sin\theta} \approx \frac{\Lambda}{13.5} \quad \Rightarrow \sigma_{RMS} \overset{!}{<<} 1\ \text{nm}$$

O. Hignette et al, SPIE 4501 (2001)

Similar results from wave optical simulations

H. Yumoto et al, SPIE 6317 (2006)

Challenge for fabrication and metrology !

Theoretical models

Geometrical ray tracing

- **Analytical approach**
- **Parabolic/elliptic shape**
- **ML ≅ Two-interface slab**
- **Linear approximation for refraction**
- **Simple expressions for caustic and beam intersections**

Goals

- **Caustic shape**
- **Beam intersections**
- **Chromatic behavior**

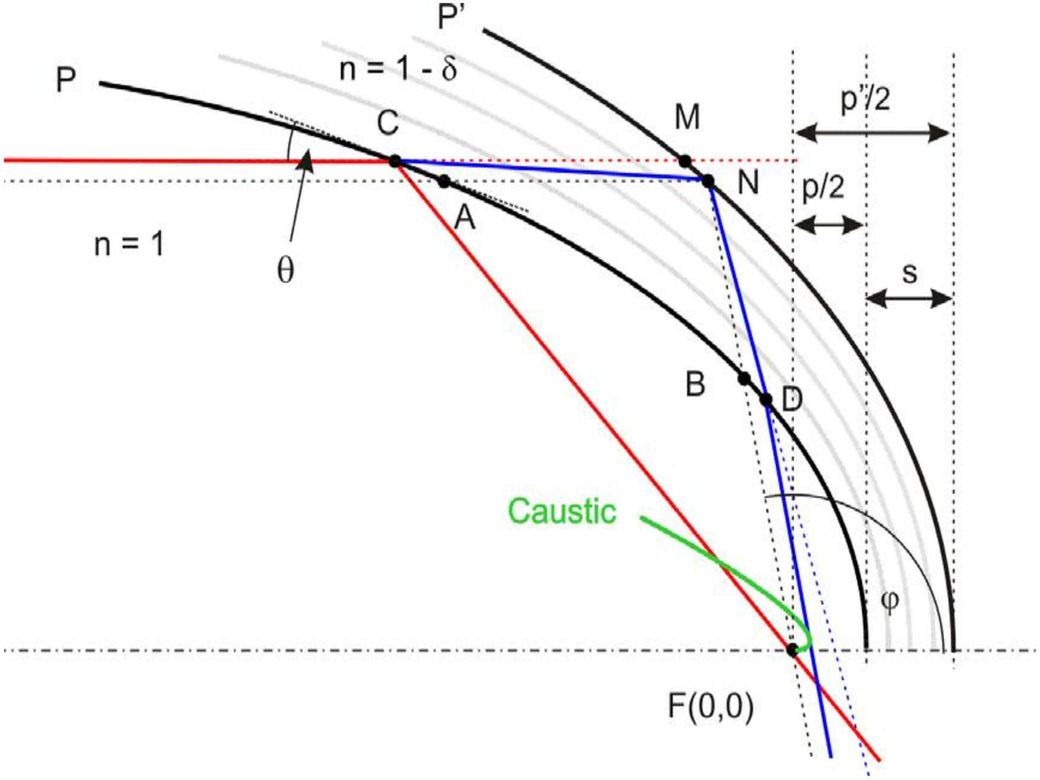

J-P. Guigay et al, Opt. Express 16, 12050 (2008)

Theoretical models

Caustic and beam intersections

- **x and y diverge at grazing incidence**
- **Refraction and penetration amplify the effect**
- **Reduced aberration for increased angles of incidence**
- **Order of magnitude:**

Δx ≤ 1000 nm

Δy ≤ 10 nm

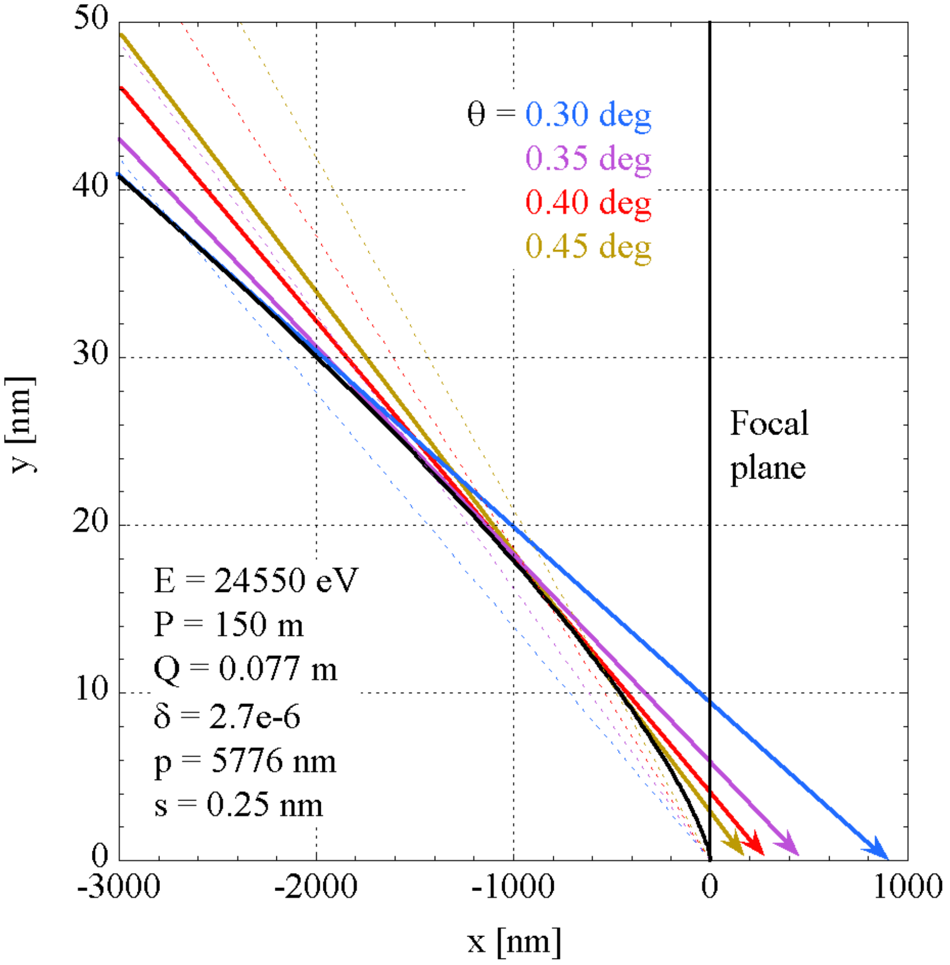

Theoretical models

Exact ray tracing

- **Snell's law**
- **No approximations**
- **Good agreement with analytical model**
- **Linear approach for refraction fails near critical angle**
- **Agreement ESRF – Osaka**

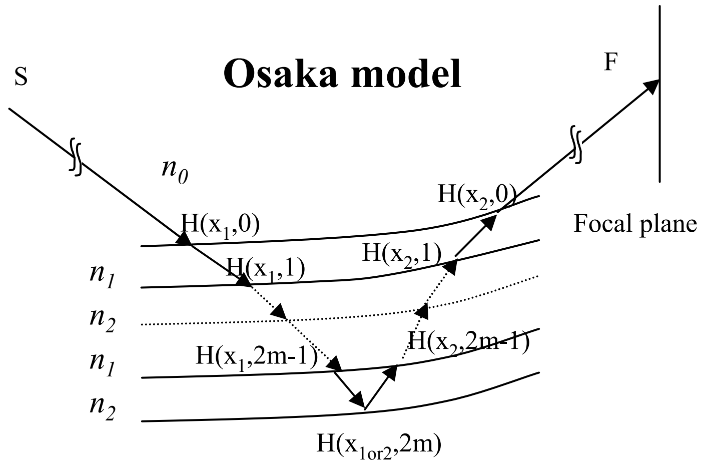

Osaka model

H. Mimura et al, SPIE 67050L (2007)

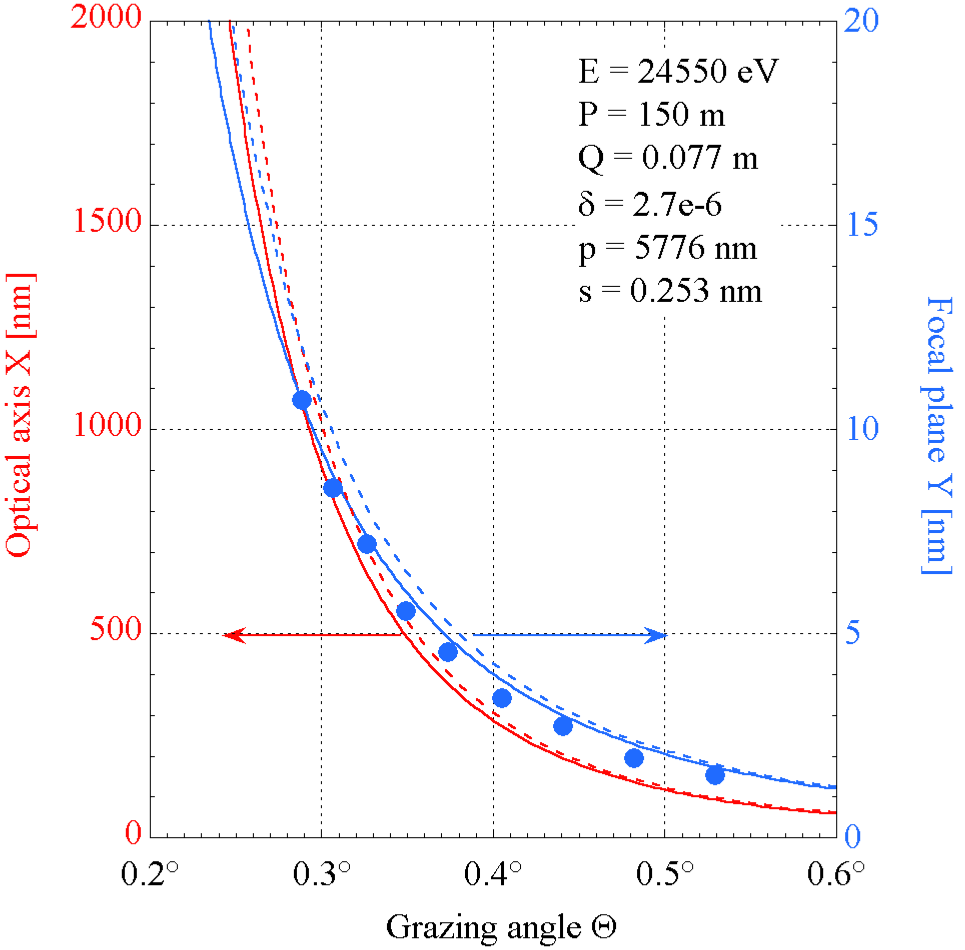

Theoretical models

Chromaticity

$$\delta \sim \frac{1}{E^2} \longrightarrow \left|\frac{df}{dE}\right| = 2 \cdot \frac{\Delta f}{E}$$

$$D_{tot}^2 = D_{diff}^2 + D_{chrom}^2 \overset{!}{\leq} 2 \cdot D_{diff}^2$$

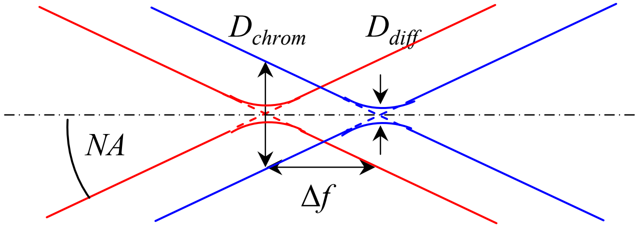

	FZP	CRL	RML
$\frac{dE}{E}$	$\frac{D_{tot}^2}{1.76 \cdot f \cdot \lambda}$	$\frac{D_{tot}^2}{3.52 \cdot f \cdot \lambda}$	$\frac{D_{tot}^2}{3.52 \cdot \Delta f \cdot \lambda}$

Secondary effect on focus !

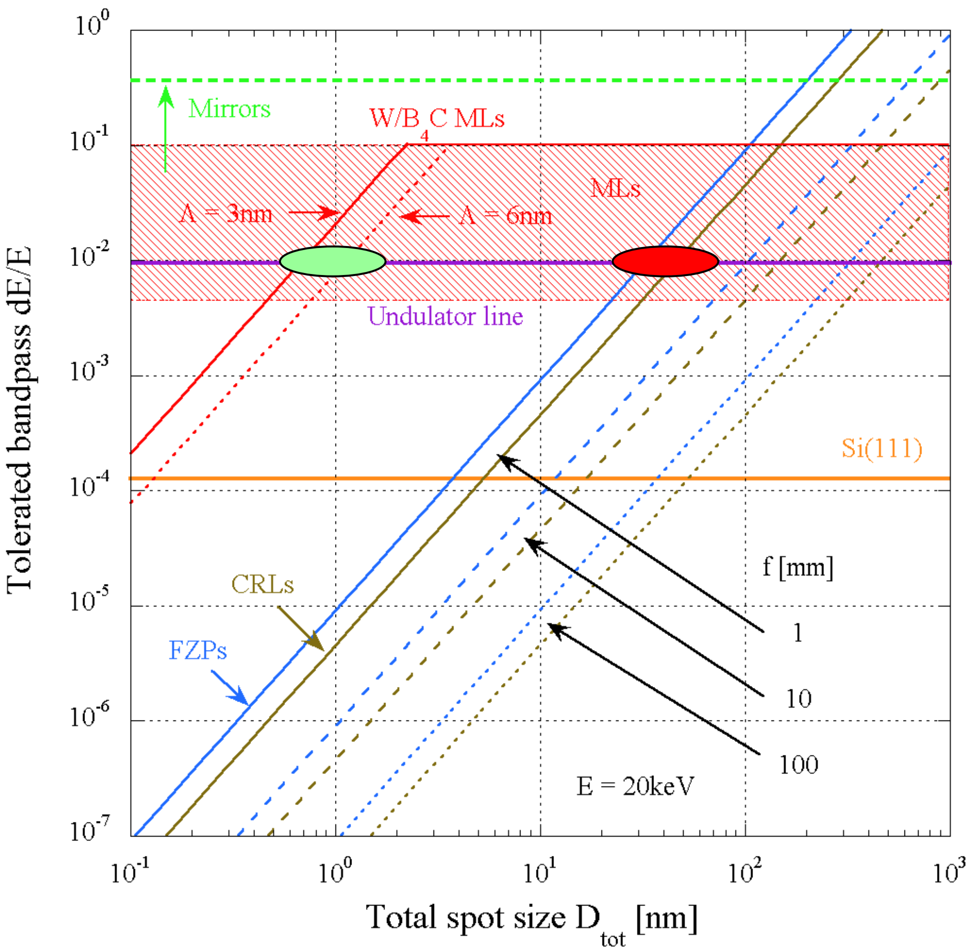

Theoretical models

Are we already doing better ?

- ML design via corrected Bragg law

$$\Lambda = \frac{\lambda}{2\sqrt{n^2 - \cos^2\theta}} \left(\approx \frac{\lambda}{2 \cdot \sin\theta} \right)$$

- Refraction implicitly considered
- ML interface shapes not elliptic (except for surface layer)
- Difficult analytical access
- Aberrations reduced/suppressed ?

Need for wave optical calculations !

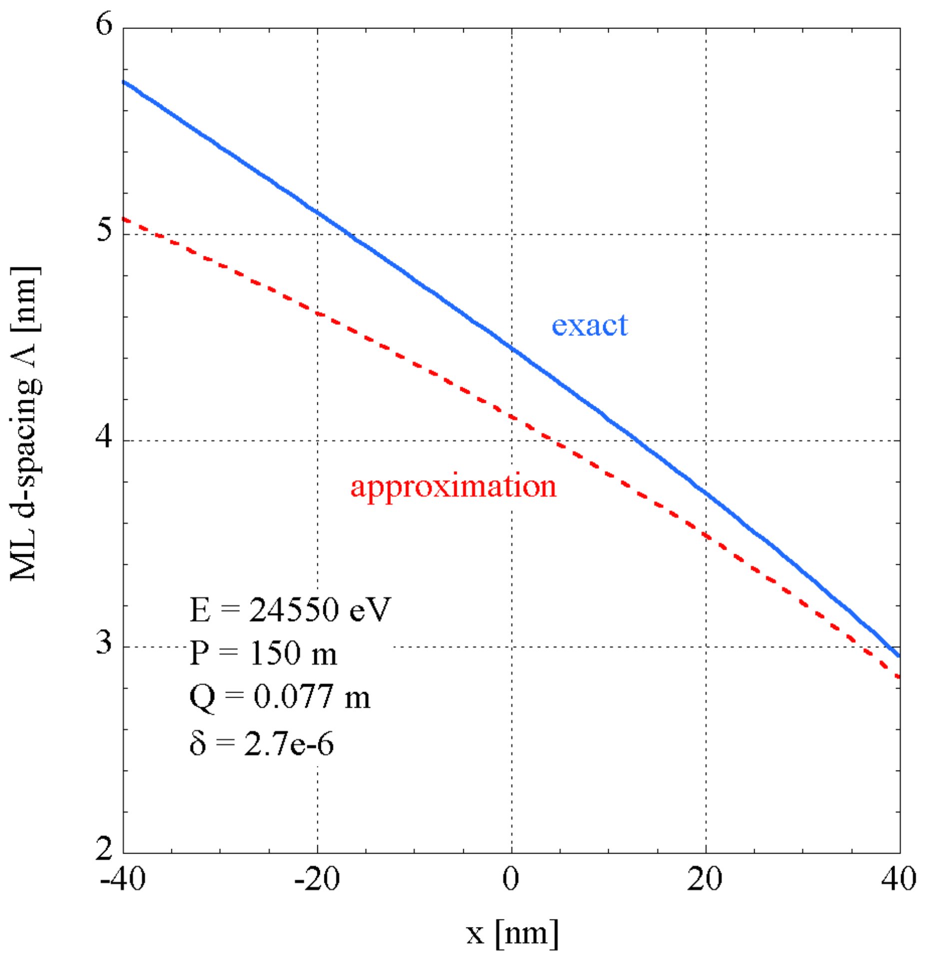

Theoretical models

Alternative approach

- **ML design via numerical simulation (Osaka University)**
- **ML ray tracing and optical path optimization**
- **Equivalent to corrected Bragg equation (?)**

$$\Lambda = \frac{\lambda}{2\sqrt{n^2 - \cos^2\theta}}$$

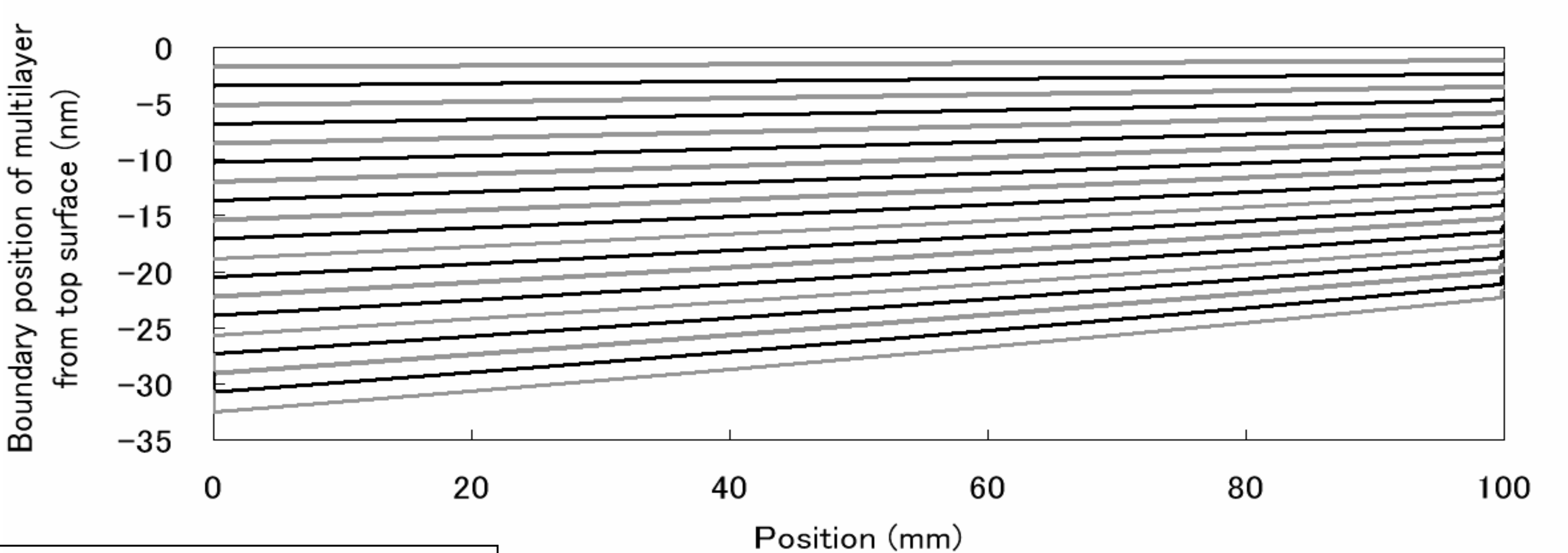

H. Mimura et al, SPIE 67050L (2007)

Theoretical models

Results of numerical optimization

H. Mimura et al, SPIE 67050L (2007)

Single deep reflection

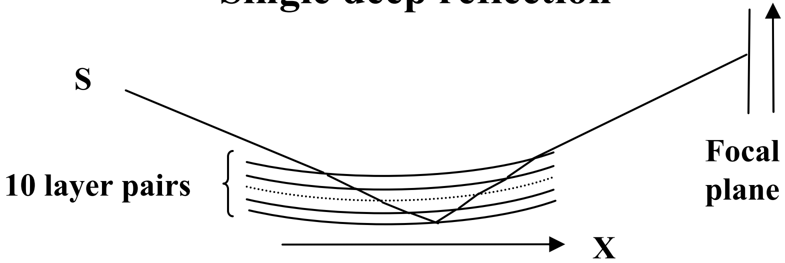

Multiple shallow reflections

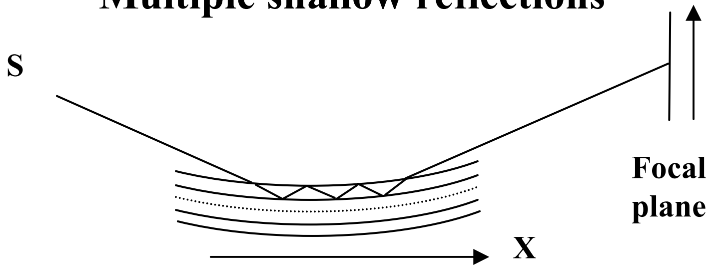

Focal spot blurring < 1 nm !

Theoretical models

Wave optical simulations

- Exist for CRLs, FZPs, and MLLs
  - predict diffraction limited focusing
  - spot size down to nm dimensions
- Not yet available for reflecting MLs
- Space for future investigation

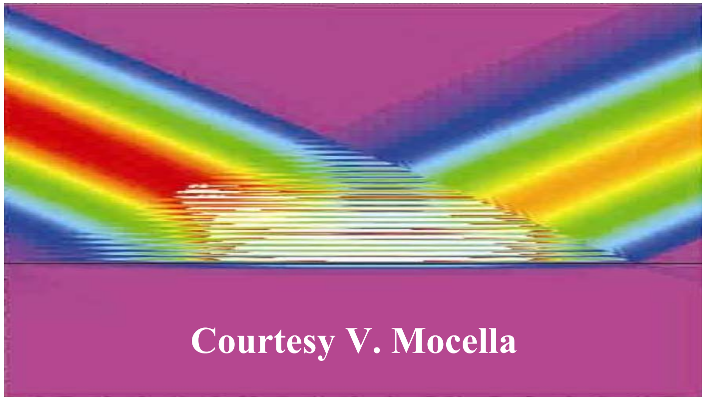

Courtesy V. Mocella

PhD project ESRF/Univ.Göttingen

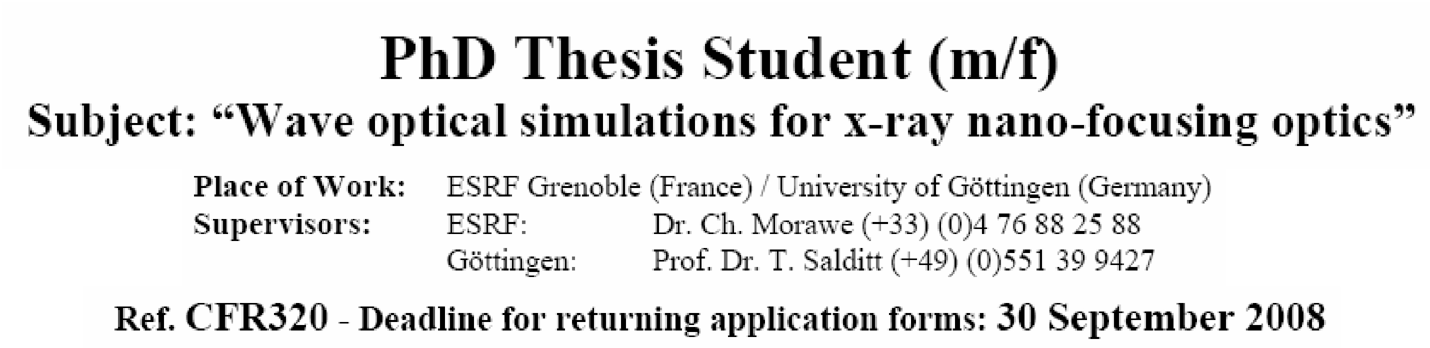

PhD Thesis Student (m/f)

Subject: "Wave optical simulations for x-ray nano-focusing optics"

Place of Work: ESRF Grenoble (France) / University of Göttingen (Germany)

Supervisors: ESRF: Dr. Ch. Morawe (+33) (0)4 76 88 25 88

Göttingen: Prof. Dr. T. Salditt (+49) (0)551 39 9427

Ref. CFR320 - Deadline for returning application forms: 30 September 2008

Multilayer properties

Numerical calculations: Dynamical theory of flat MLs

L.G. Parratt, Phys. Rev. 95, 359 (1954)

- Bragg peaks and fringes due to interference
- Positions depend on E and Λ
- Intensities depend on Δρ, N, σ…

Corrected Bragg equation

$$m \cdot \lambda = 2 \cdot \Lambda \cdot \sqrt{n_2^{\,2} - n_1^{\,2} \cos^2 \theta}$$

For $\theta \gg \theta_C \rightarrow \quad m \cdot \lambda \approx 2 \cdot \Lambda \cdot \sin\theta$

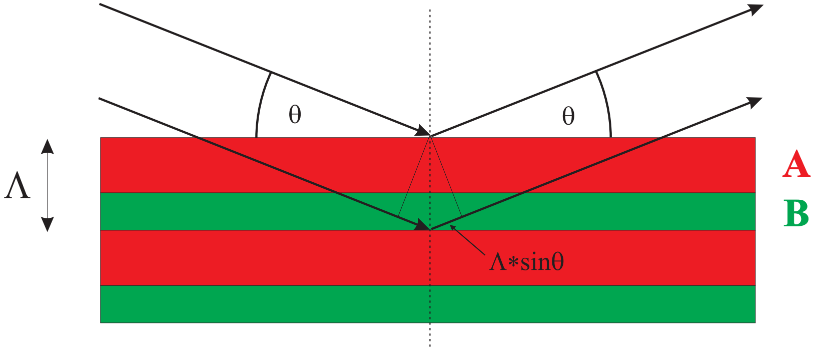

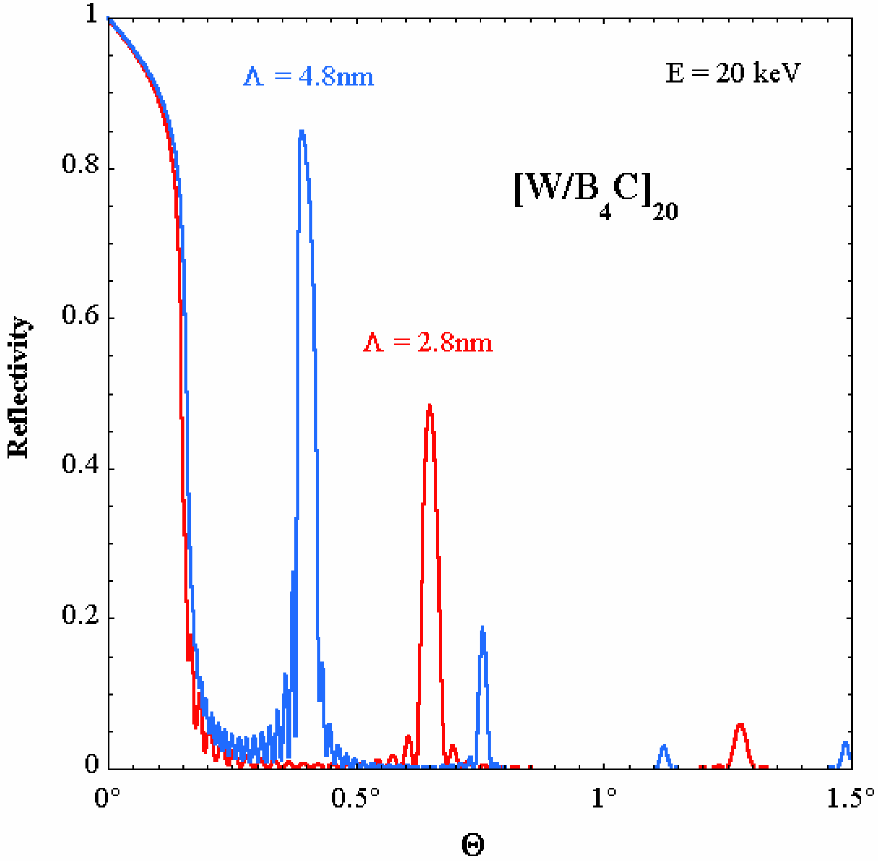

Multilayer properties

Materials choice – Basic rules:

1. Select low-Z spacer material with lowest absorption (β_{spacer})
2. Select high-Z absorber material with highest reflectivity with spacer ($\delta_{abs} - \delta_{spacer}$)
3. In case of multiple choices select high-Z material with lowest absorption (β_{abs})
4. Make sure that both materials can form stable and sharp interfaces (lower d-spacing limit)

Computational search algorithms

- Soft X-rays: A.E. Rosenbluth (1988)
- Hard X-rays: K. Vestli (1995)

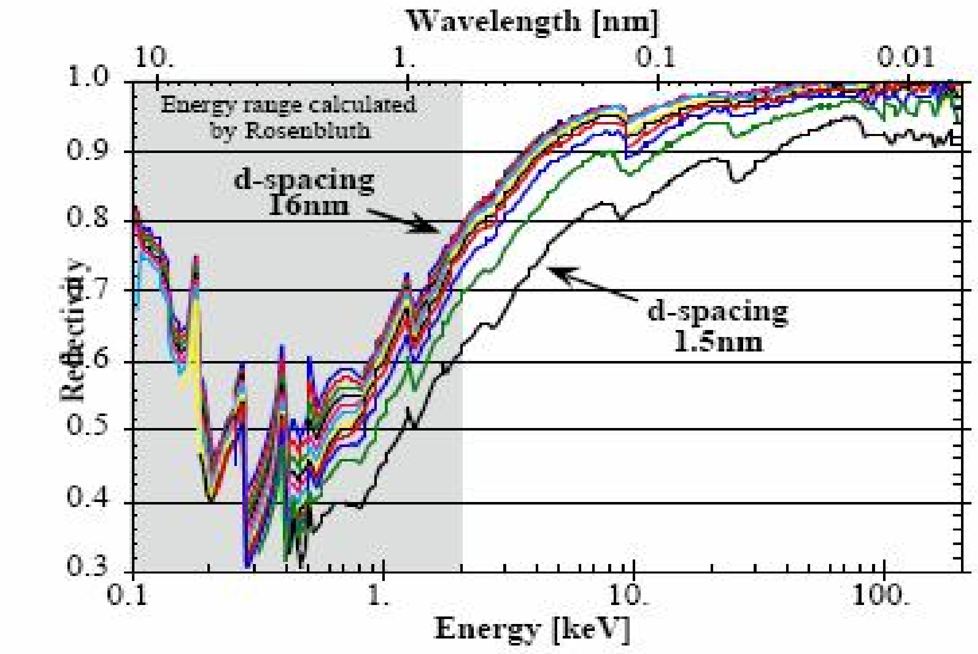

K. Vestli et al, Rev. Sci. Instr. 67, 3356 (1996)

Multilayer properties

Period number N:

Peak versus integrated reflectivity:

- **R_{peak} increases with N up to extinction**
- **ΔE/E decreases ~ 1/N in kinematical range**
- **R_{int} is maximum before extinction**

High and low resolution MLs

Optimize N according to needs !

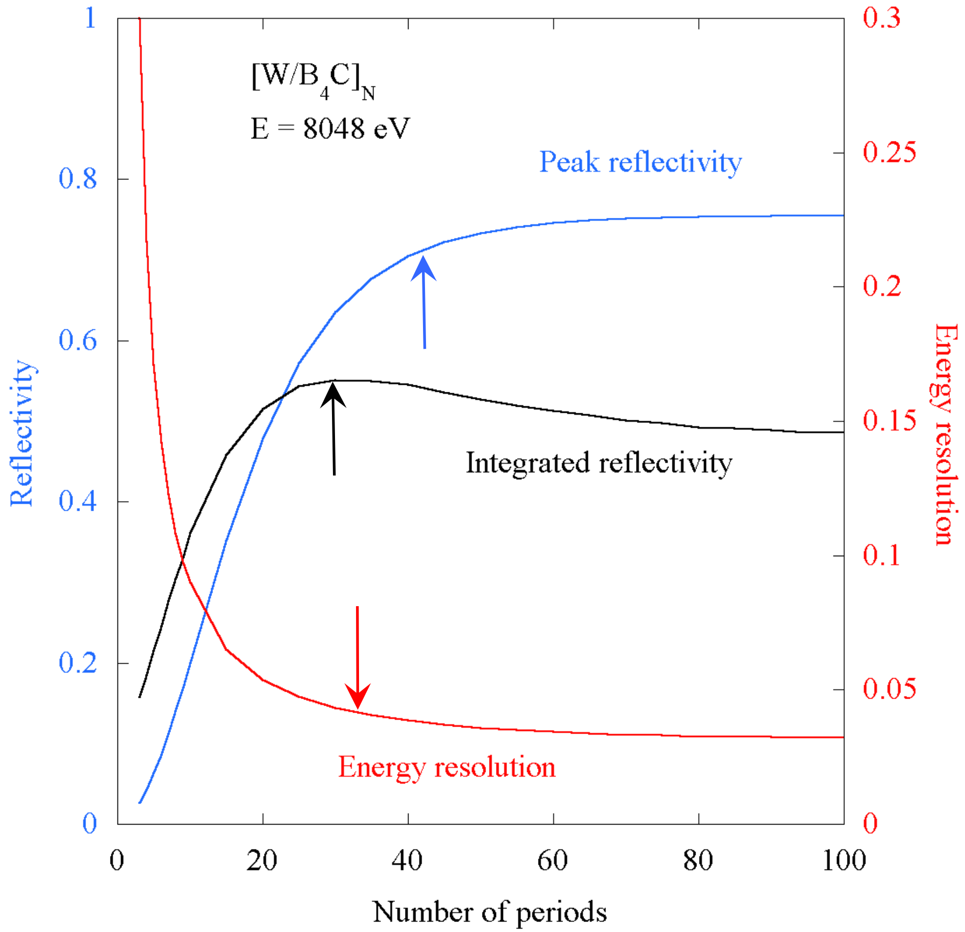

Multilayer properties

Filling factor $\Gamma = t_{abs}/\Lambda$

- **Harmonics suppression**
- **Reflectivity enhancement**

Optimum Γ for large N

A.V. Vinogradov et al, Appl. Opt. 16, 89 (1977)

$$\tan(\pi \cdot \Gamma_{opt}) \approx \pi \cdot \left(\Gamma_{opt} + \frac{\beta_{abs}}{\beta_{abs} - \beta_{spacer}} \right)$$

Best Γ drops with growing N !

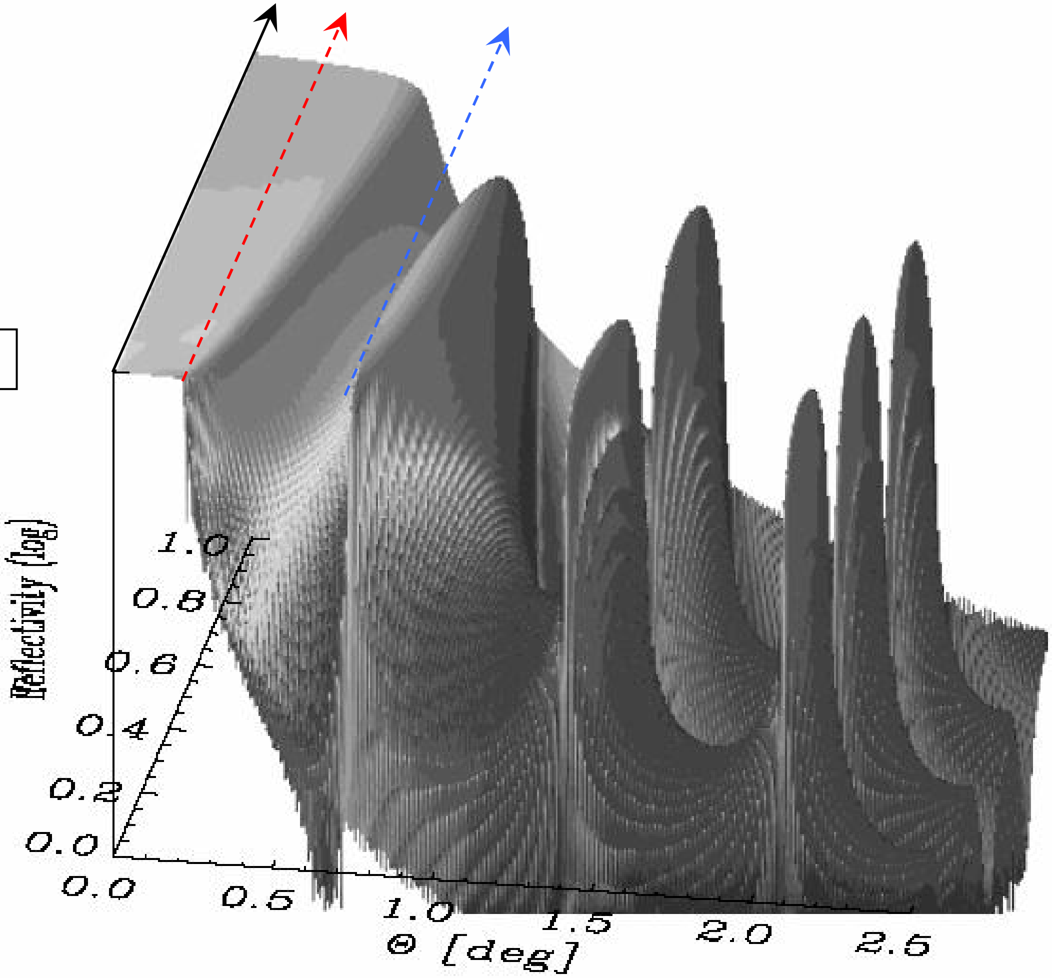

Multilayer properties

Non-periodic stacks:

Ch. Morawe et al, Nucl. Instr. ànd Meth. A 493, 189 (2002)

- Ni/B_4C structure
- R(θ) = const over 20% bandwidth

Theoretical design

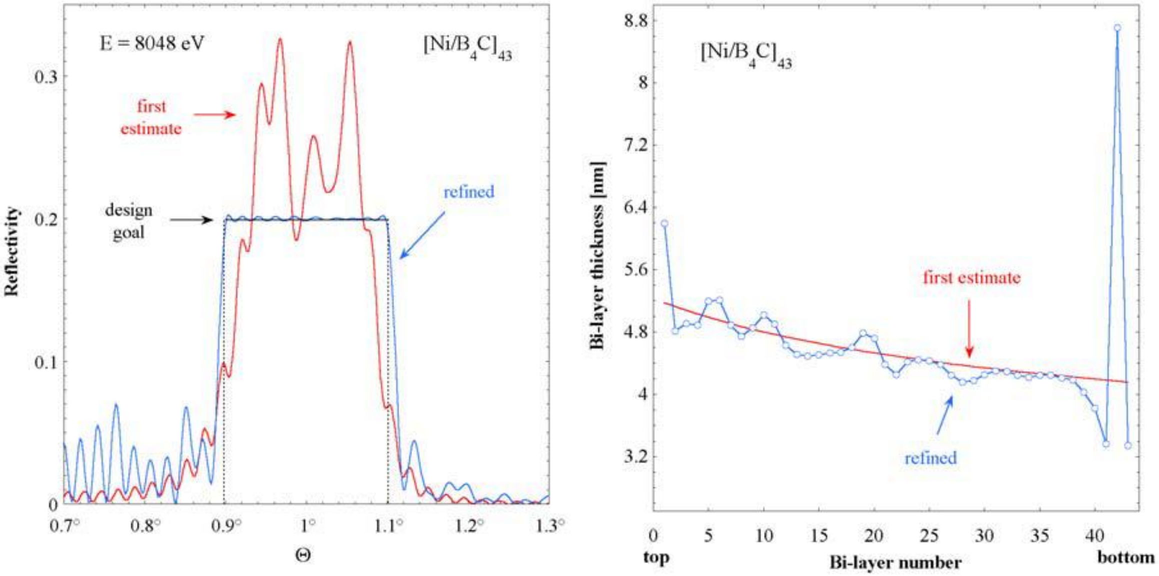

Experimental result

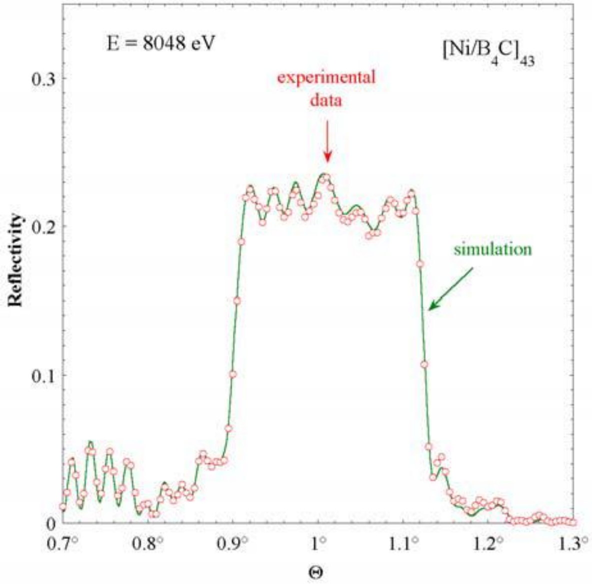

Multilayer properties

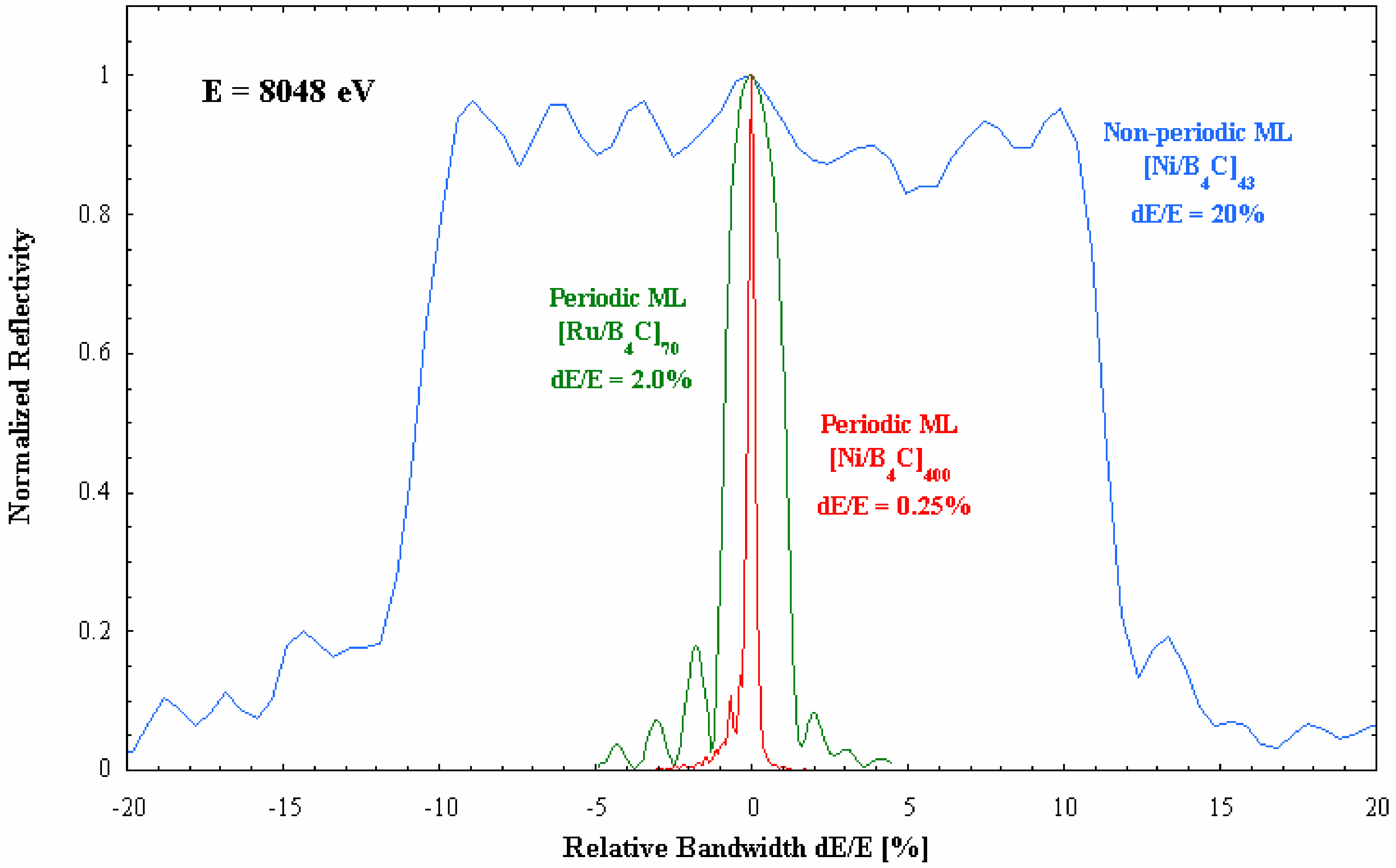

Multilayer properties

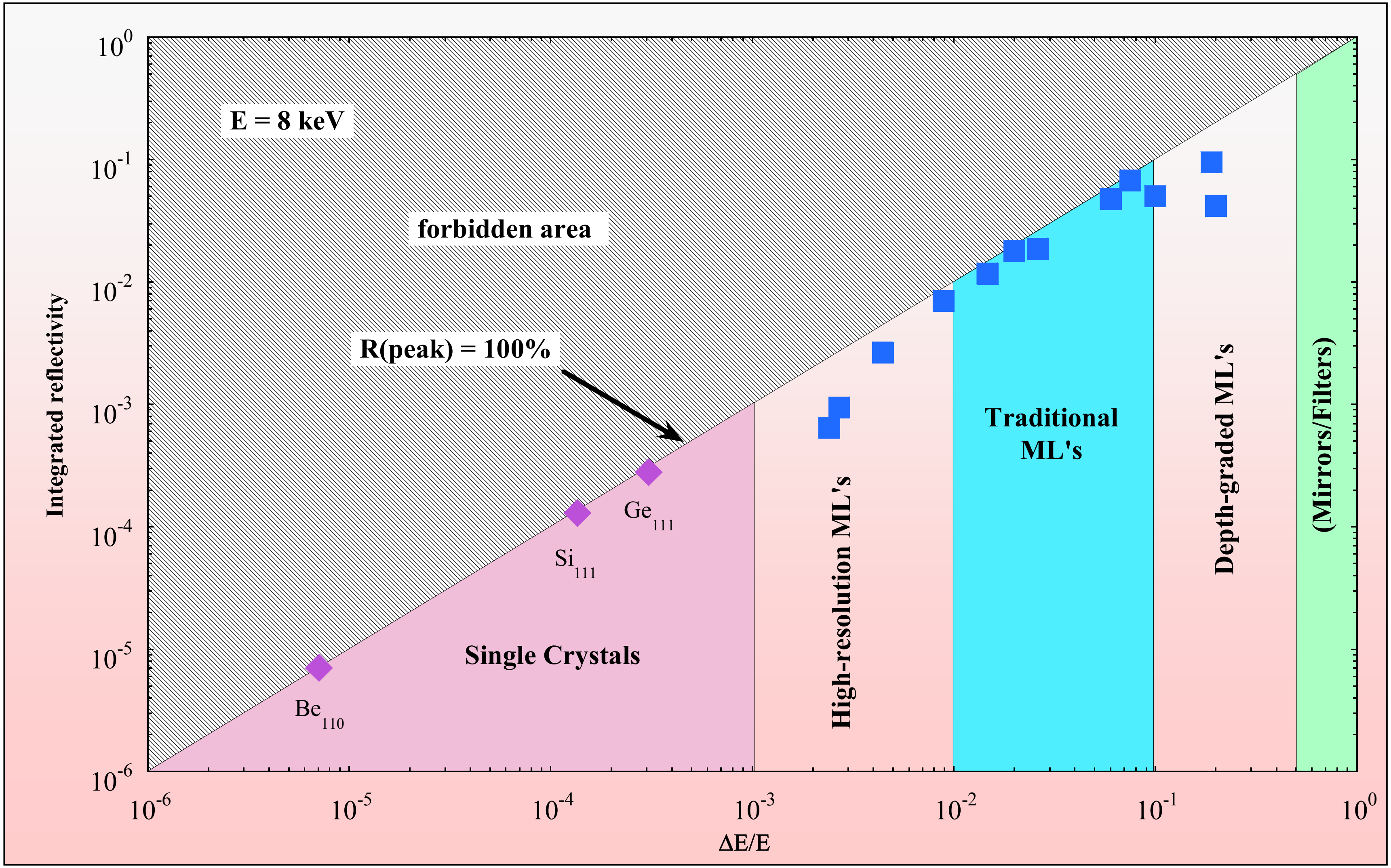

Multilayer properties

Energy dispersion:

Bragg equation: $E(\theta) = \dfrac{h \cdot c}{2\Lambda\sqrt{n^2(E) - \cos^2\theta}}$

Elliptic mirror: $\sin^2\theta = \dfrac{b^2}{p \cdot q}$ $\quad p + q = 2 \cdot a$

$$\downarrow$$

$$\boxed{E(q) = \frac{h \cdot c}{2\Lambda\sqrt{n^2(E) - 1 + \dfrac{b^2}{(2a-q)q}}}}$$

Dispersion "along ML mirror"

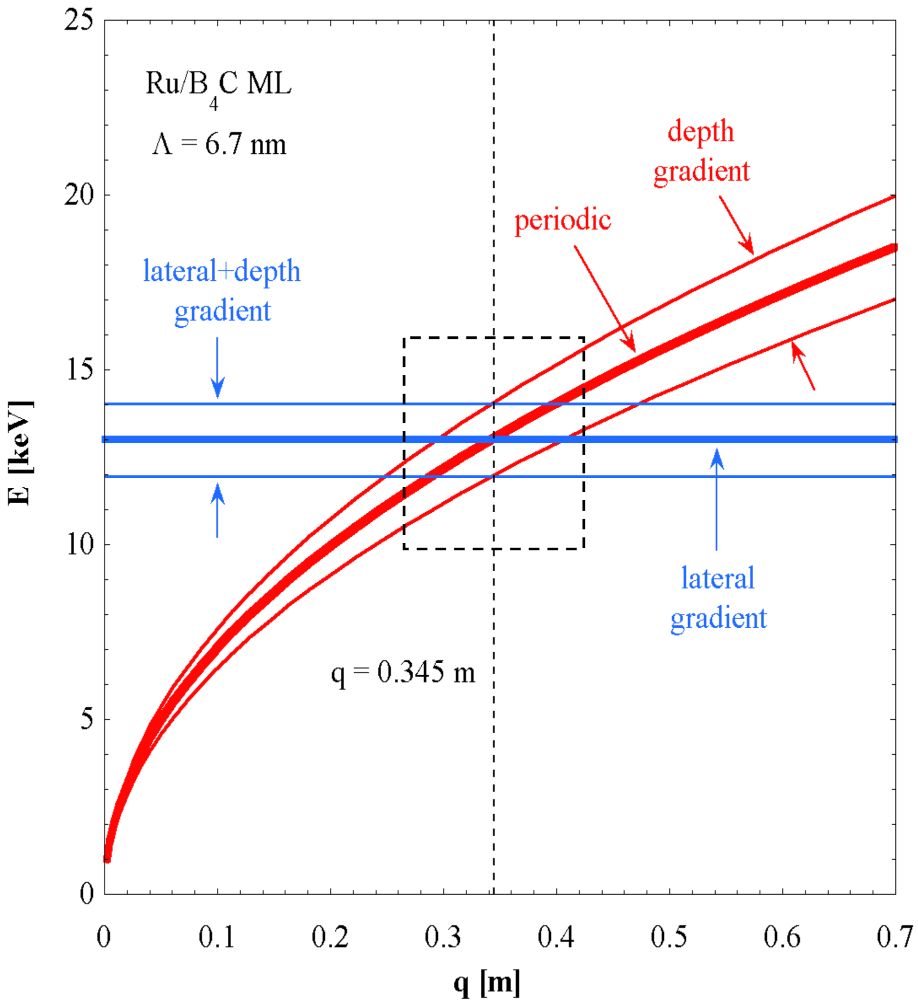

Multilayer properties

<u>Intensity profiles:</u> (Kirkpatrick-Baez multilayer optics on ESRF BM05)

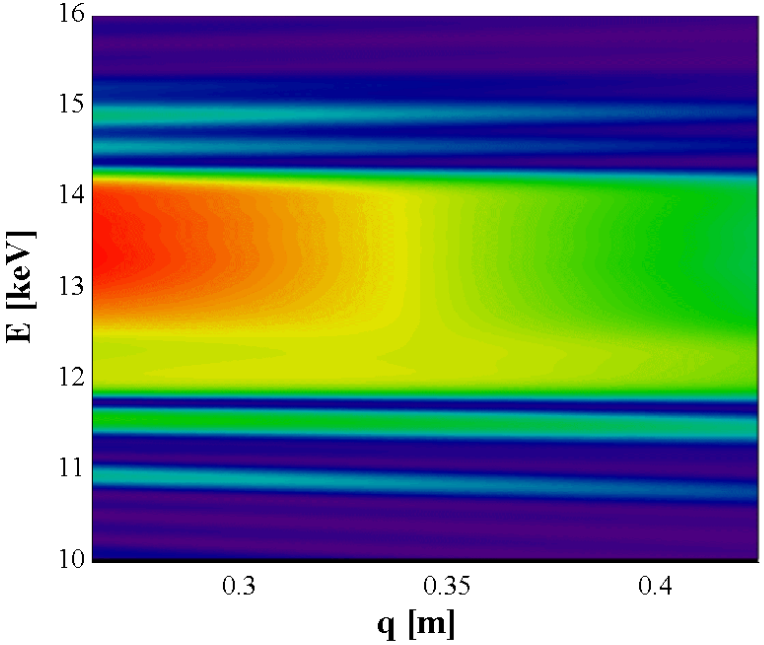

Theory

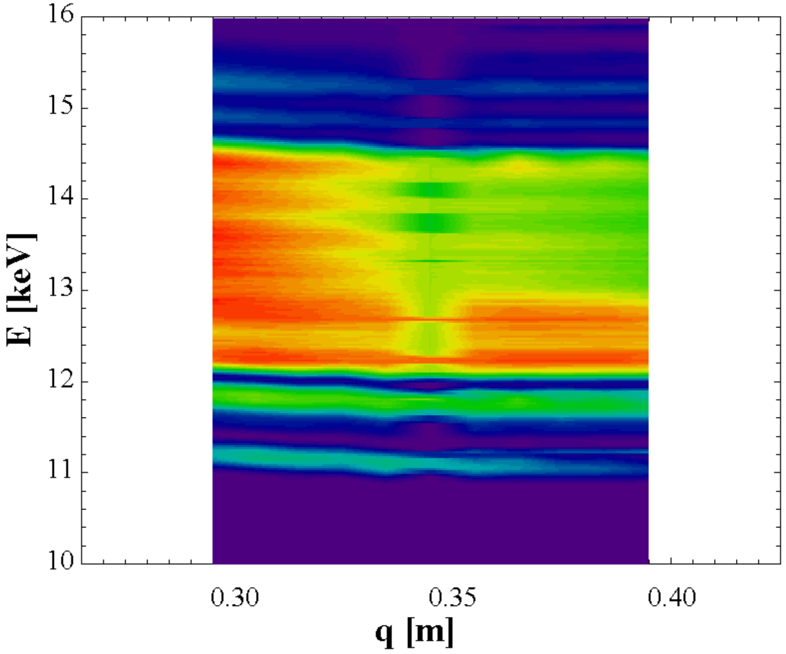

Experiment

Ch. Morawe et al, SPIE 5537, 115 (2004)

Technological options

Deposition techniques	Vacuum	Particle energy	Deposition rate	Deposition area
Thermal evaporation	HV (UHV)	Low	Low	Small
E-beam evaporation	UHV	Low	Low	Small
Magnetron sputtering	HV (+Gas)	High	High	Large
DECR sputtering	HV (+Gas)	High	Low	Medium
Ion beam sputtering	UHV (+Gas)	Very high	High	Medium
Pulsed laser deposition	HV	Very high	High	Medium

- **Characteristics may vary depending on equipment and application**
- **Magnetron sputtering most widely used for X-ray multilayer fabrication**
- **High particle energy favors very thin and uniform layers**

Technological options

Large area coatings (uniform, gradient)

- Relative motion source - substrate
- Masking techniques

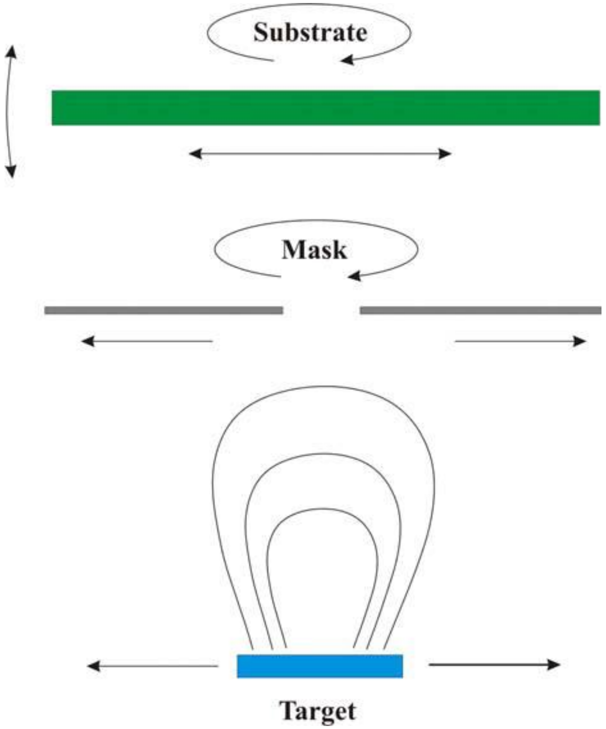

$$t(\vec{r}) = \int \varphi(\vec{r},\vec{r}\,')\frac{d\vec{r}\,'}{v(\vec{r}\,')}$$

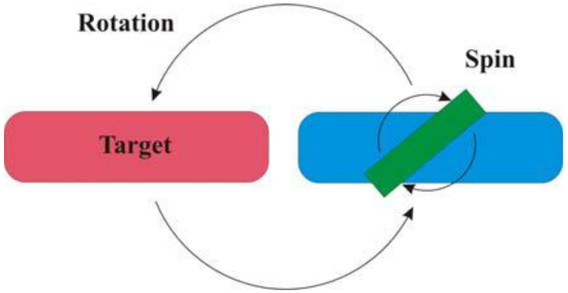

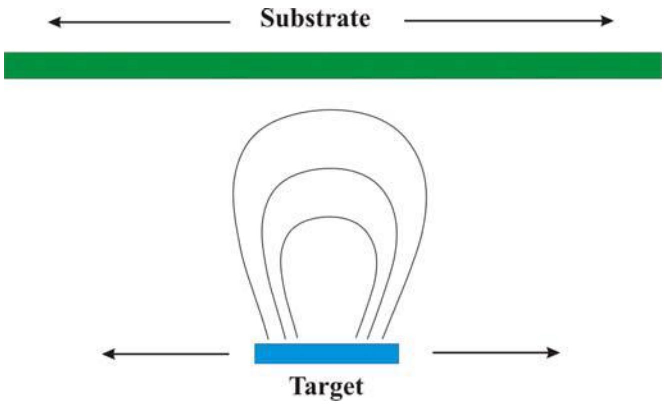

Technological options

Technology and engineering

Curved MLs

- Figured substrates or bending techniques ?
- Surface finishing (deterministic polishing/etching/coating)

Stability and stress

- Intrinsic stress after coating
- Thermal and radiation load (white beam)
- Sample environment (vacuum/He/N_2)

Metrology

- Ex-situ techniques reaching limits
- On-line metrology (intensity, phase retrieval)
- Phase correction elements

Several solutions commercially available!

APS profile coating

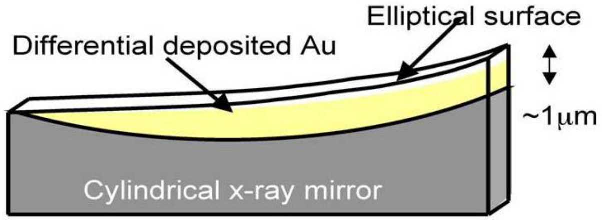

ESRF bender

Osaka EEM technology

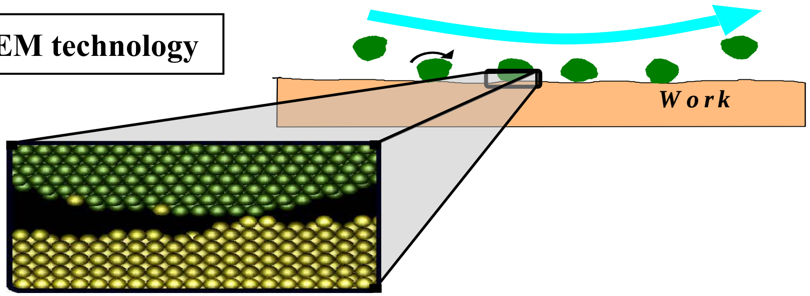

Experimental progress

Example: [W/B_4C]$_{25}$ ML @ 24550 eV

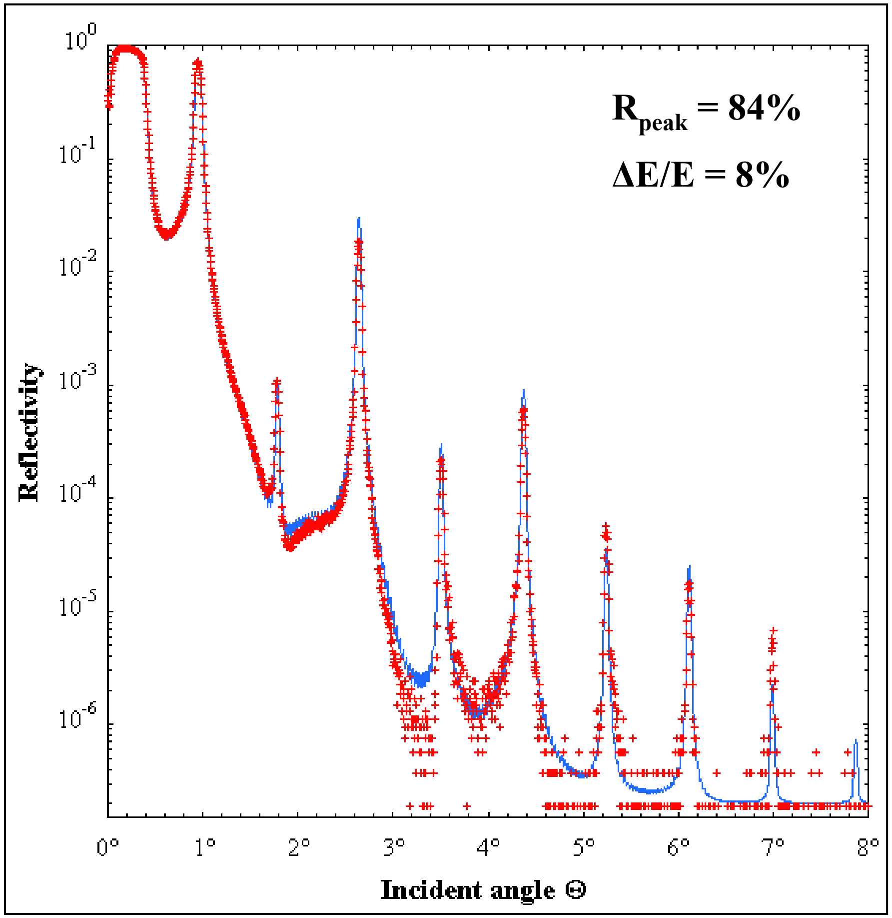

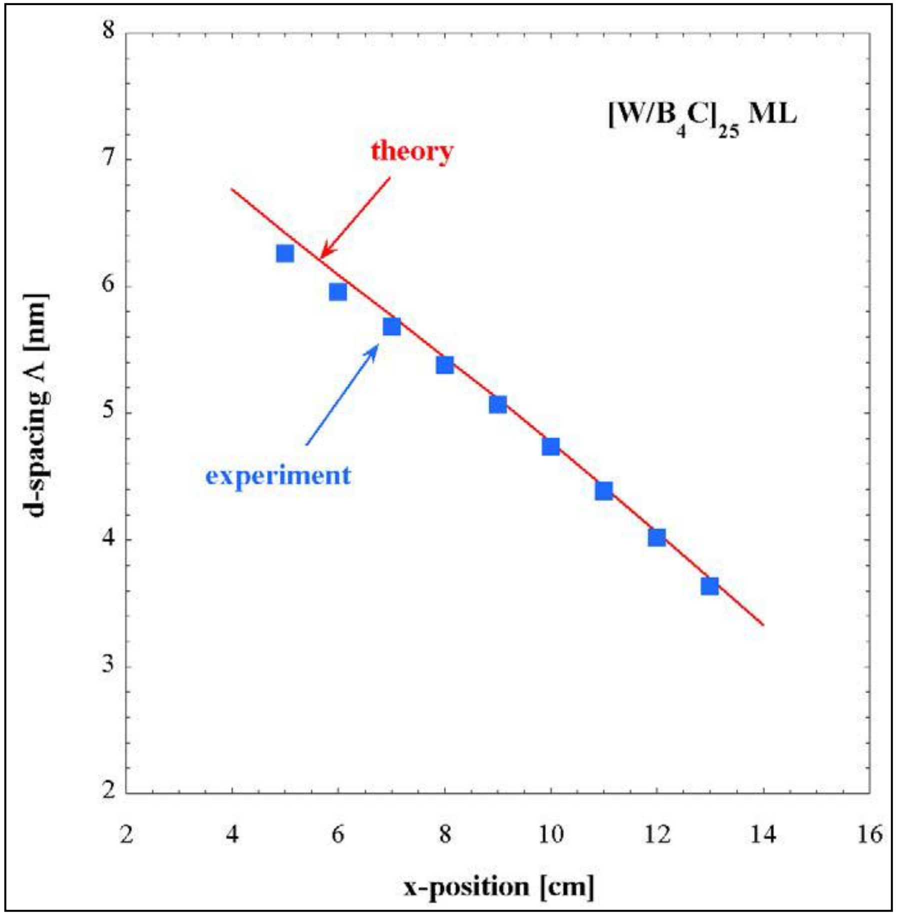

Experimental progress

ESRF focusing experiment

- **Full undulator spectrum**
- **P = 150 m, Q = 77 mm**
- **Vertical line focus**
- **Raw data 45 nm FWHM @ 100 µm aperture**

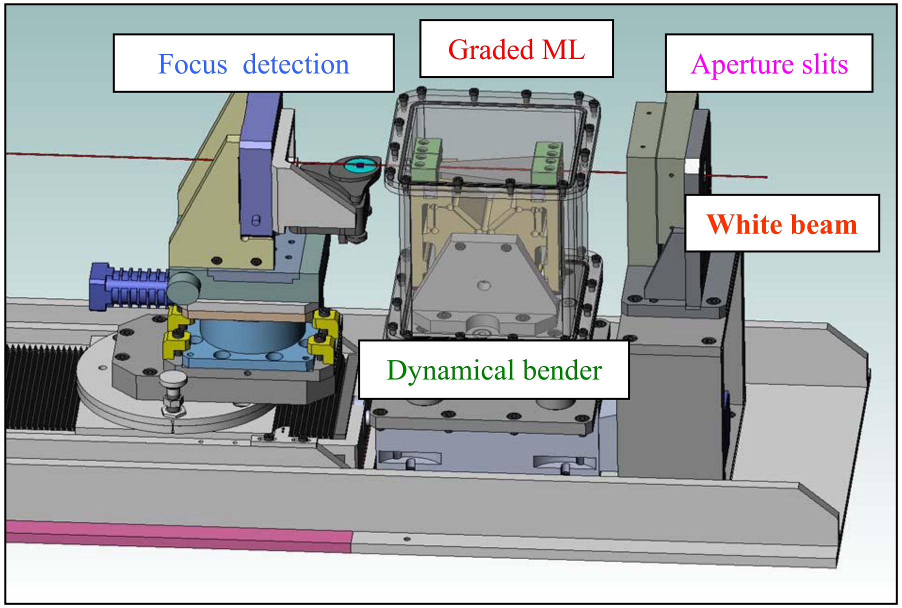

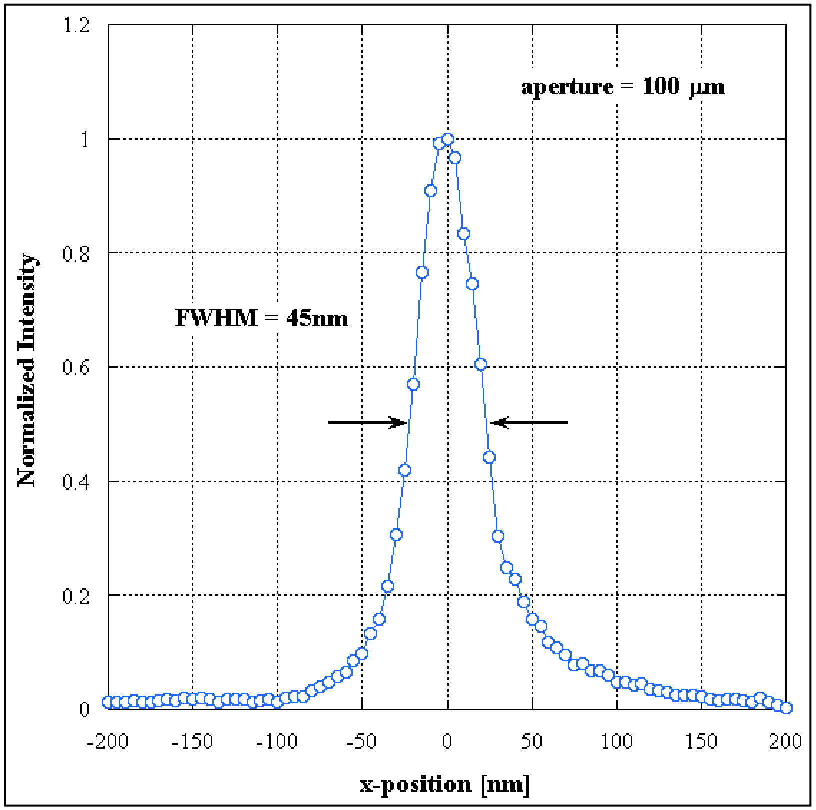

Ch. Morawe et al, Proc. SPIE 6317 (2006)

Experimental progress

ID19: low β @ 150 m, E = 15…24 keV
86*83 nm^2: 2*10^{11}ph/s @ 80mA

ID22: high β @ 60 m, slit source, E = 17 keV
76*84 nm^2: 10^{9}ph/s @ 200mA
150*100 nm^2: 10^{12}ph/s @ 200mA

3*10^5 ph/s/mA/nm^2

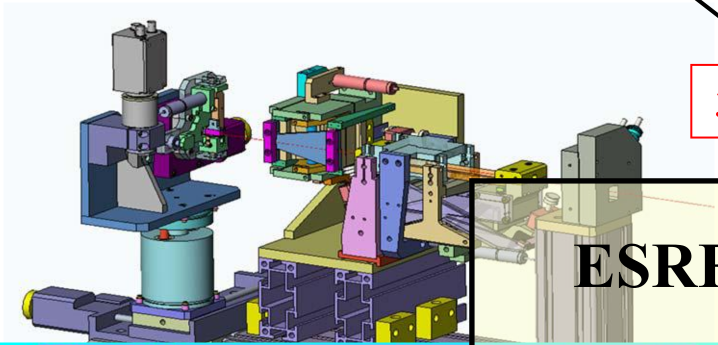

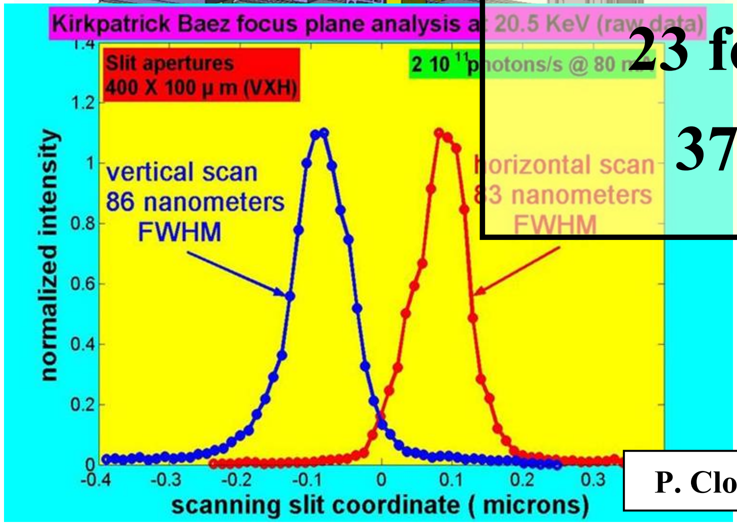

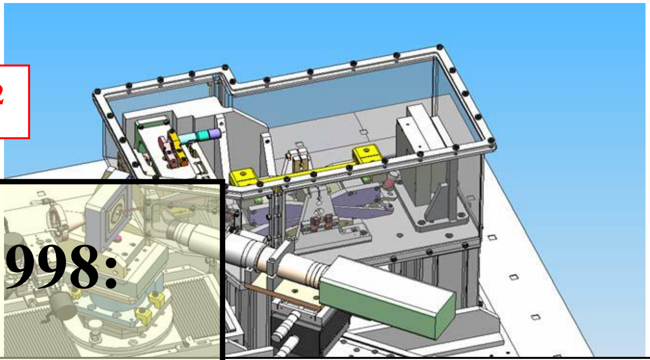

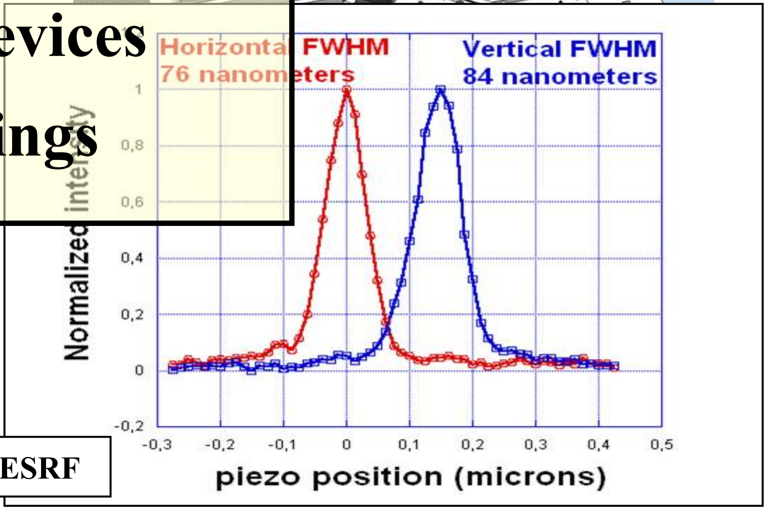

ESRF BLs since 1998:

23 focusing devices

37 ML coatings

P. Cloetens, O. Hignette, ESRF

Summary

ML - KB “Data Sheet”

Energy range	5…100 keV
Peak reflectivity	50…90% (per reflection)
Energy bandpass	0.5…20%
Minimum focal spot size	≈ 5 nm (expected diffraction limit) < 50 nm (proof of feasibility) < 100 nm (routine operation)
Focal distance	50…1000 mm
BL layout	Beam deflection (horizontal + vertical)
Alignment	Pre-alignment + on-line (recommended)
Available technologies	Static (fixed energy) Dynamic (tunable energy)
Principal curved ML developers	ESRF, Univ.Osaka/Spring-8, (APS)
Synchrotron optics (no MLs)	Irelec (France), JTEC (Japan), SESO (France), Xradia (USA), Zeiss (Germany)
Lab optics or coatings only	AXO (Germany), Incoatec (Germany), Osmic/Rigaku (USA), WinlightX (France), Xenocs (France)

TECHNISCHE
UNIVERSITÄT
DRESDEN

Refractive x-ray lenses for hard x-ray microscopy

Christian G. Schroer

Institute of Structural Physics, Technische Universität Dresden
D-01062 Dresden

e-mail: schroer@nanoprobe.de
http://www.nanoprobe.de

Collaboration

P. Boye, J. Feldkamp, R. Hoppe, J. Patommel, A. Schropp,
A. Schwab, S. Stephan
Inst. of Structural Physics, TU Dresden

M. Burghammer, C. Riekel, S. Schöder
ESRF, Grenoble

I. Vartaniants, E. Weckert
HASYLAB, DESY, Hamburg

B. Lengeler
II. Phys. Institut, RWTH Aachen

A. van der Hart
ISG, Research Center Jülich

M. Küchler
Fraunhofer IZM, Chemnitz, Germany

bmb+f
Großgeräte
der physikalischen
Grundlagenforschung

Hard X-Ray Microscopy & Tomography

Full-field microscopy:

- transmission imaging
- contrast generated by attenuation and refraction
- large 3D-images of the sample (tomography)

Scanning microscopy:

- scan sample with nanobeam (< 100 nm lateral size)
- different contrasts:
  - fluorescence
  - absorption (XAS)
  - diffraction (SAXS, WAXS, CXDI)
  - ...

K

- scanning: relatively slow
- tomography: local inner structure of sample

Optics for Hard X-Rays

Full-field microscopy:

- objective lens for imaging free of aberrations
- condensor lens to concentrate x-rays on sample

Scanning microscopy:

- generate an intensive x-ray microbeam

Variety of x-ray optics available today:

- Fresnel zone plates and multilayer Laue lenses
- refractive lenses [Snigrev, et al., Nature **384**, 49 (1996)]
- curved/bent mirrors and multilayers
- capillaries
- wave guides (mode filter)
- crystal optics
- ...

Refraction

$$n = 1 - \delta + i\beta, \quad \delta > 0$$

Vacuum optically denser than matter!

$$\delta = \frac{1}{2\pi} N_{\mathrm{A}} r_0 \lambda^2 \rho \frac{Z + f'}{A}$$

specific refraction:

independent of material
(away from absorption edges)

very weak

Absorption

$$n = 1 - \delta + i\beta, \quad \delta > 0$$

Lambert-Beer Law:

$$I(x) = I_0 e^{-\mu x}$$

attenuation coefficient μ:

$$\mu = \frac{4\pi\beta}{\lambda}$$

2 main contributions:

photo absorption $\tau \sim Z^3/E^3$
Compton scattering μ_c

[redacted]

For comparison: $\mu_{glas} = 10^{-7}$ cm^{-1}
for visible light

Refractive X-Ray Lenses

single lens

stack of lenses:
compound refractive lens (CRL)

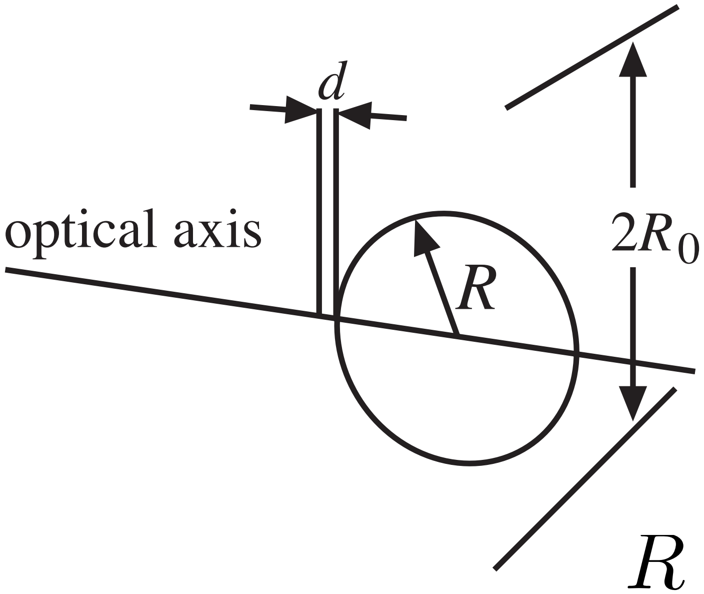

$$R = 50\ \mu\mathrm{m} - 1000\ \mu\mathrm{m}$$
$$d = 10\ \mu\mathrm{m} - 30\ \mu\mathrm{m}$$
$$2R_0 = 450\ \mu\mathrm{m} - 1000\ \mu\mathrm{m}$$

variable number of lenses: *N* = 10 ... 300

parabolic profile: no spherical aberration

→ true imaging optic

Parabolic Refractive X-Ray Lenses

Bruno Lengeler
RWTH Aachen

Full-Field Imaging

[redacted]

lenses used as objective lens in full field microscope

image distance

$$L_2 = \frac{L}{L_1}$$

numerical aperture

$$NA = \frac{D}{2}$$

Full-Field Imaging

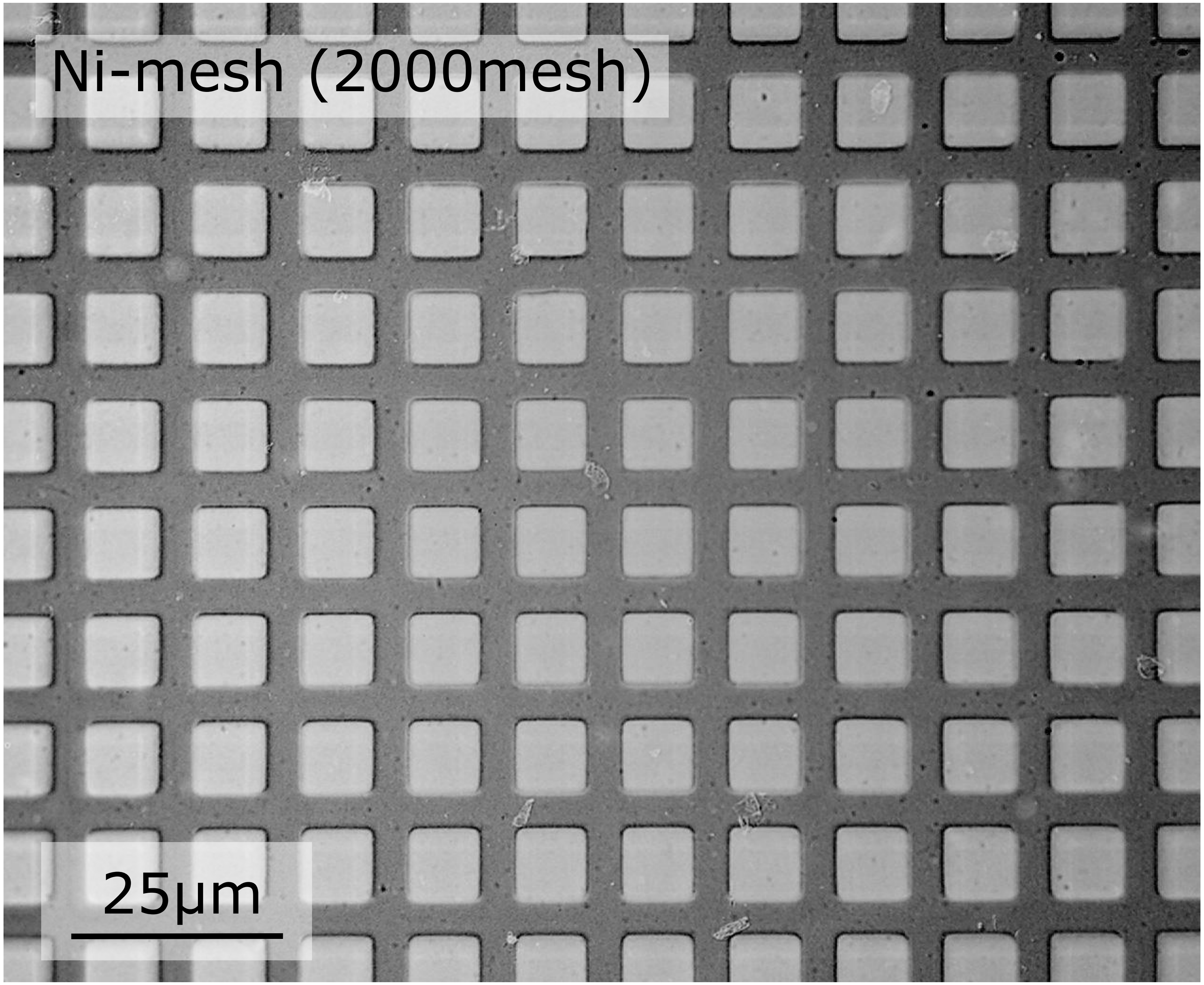

For comparison: spherical lens

(simulatio

imaging parameters:

E = 12keV
N = 91 (Be)
f = 495 mm
m = 10x

spatial resolution:

~ 100 nm

Full-Field Imaging: Spatial Resolution

expected resolution: 84 nm

line profile

deconvolve
resolution of film

(SPIE 2002)

→ resolution of x-ray optical setup: 105 nm ± 30 nm

Hard X-Ray Microbeam

source

Focus size and shape determined by:

source size
magnification L_2/L_1
diffraction limit
aberrations

lens

L_1

Flux in focus determined by:

brilliance

source size

focusing cross-section of lens

$$L_2 = \frac{L_1 f}{L_1 - f}$$

microbeam
on sample

High brilliance:

High flux per phase space volume

Ideal for nanobeams:

small source:
small geometric image
(diffraction limited focusing)

small divergence:
optic captures large fraction of emitted radiation

Be-Lens with *R* = 50µm: Microbeam

vertical focus

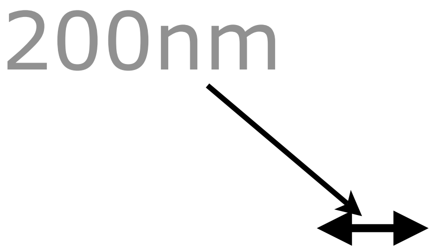

ESRF ID10

E = 8 keV
N = 31
L_1 = 60.8 m
f = 156 mm
gain ~ 10^5
flux: $3 \cdot 10^{11}$ph/s

mono: Si 111

expected focus size: 170 nm

horiz focus: 1.14 µm
(horizontal slits at 0.3mm gap)

focus source size and stability limited!

Rotationally Parabolic Refractive X-Ray Lenses

State-of-art (Be, Al):

- *R* = 50 µm [tested for focusing < 200 nm (source size limited)]
- *R* = 200 µm [tested for full field imaging with ~100 nm resolution]
- *R* = 300 µm, 500µm, and 1000µm [not tested, yet]

Lenses with *R* = 1500 µm under development

Energy range: 5 - 150 keV and higher

Application:

- hard x-ray full-field microscope (tomography)
- microbeam analysis, e. g., micro-fluorescence, XANES, SAXS also in tomography
- coherent (micro-)diffraction
- beam conditioning (moderate focusing, collimation) (white beam compatible)

⟶ Optics for X-FEL

Microprobe Example: SAXS-Tomography

Probe nanoscale structure on a virtual section through a sample

Sample:

nondestructive probe of the interior of sample

define virtual slice

obtain SAXS cross section at each location on section

injection molded PE

APL **88**, 164102 (2006)

Collab.: N. Stribeck, Univ. Hamburg

SAXS-Tomography

$$I_{\vec{q}}(r)$$

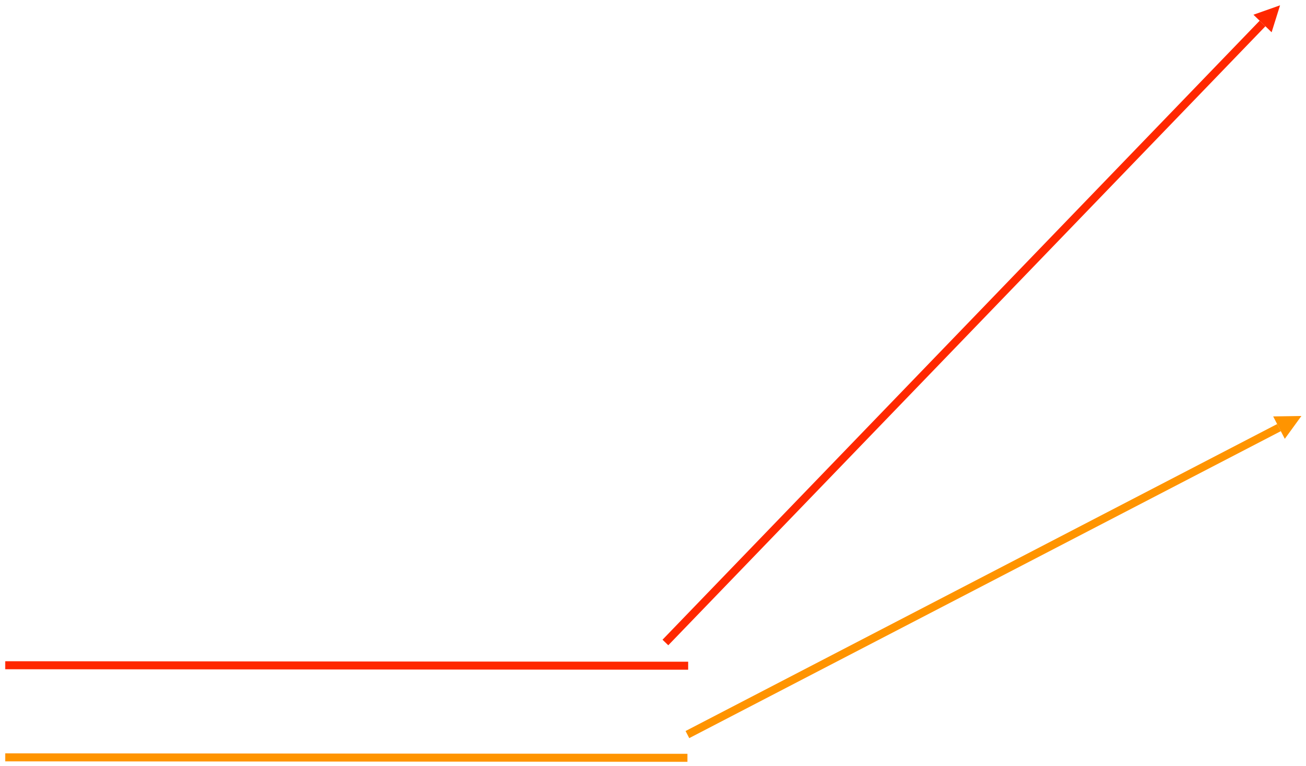

101 projections with
70 steps each
80µm step size

SAXS-Tomography

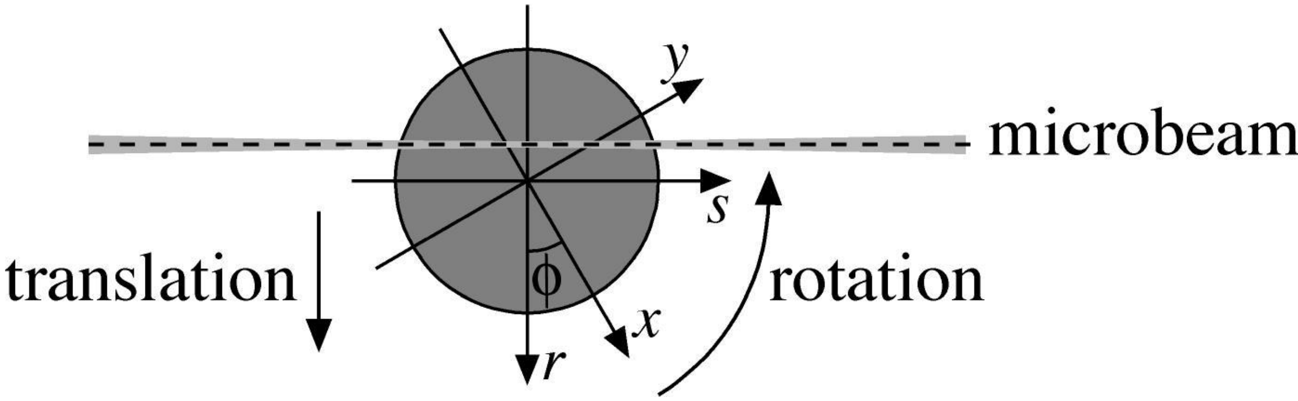

Reconstruction:

attenuation

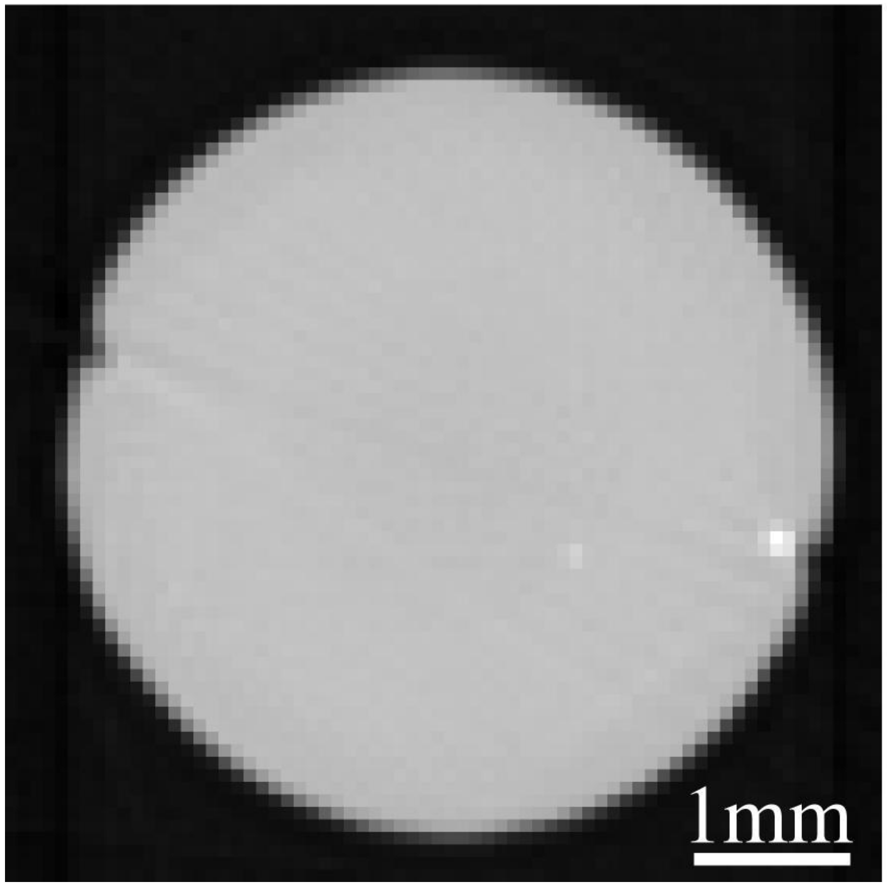

diffraction

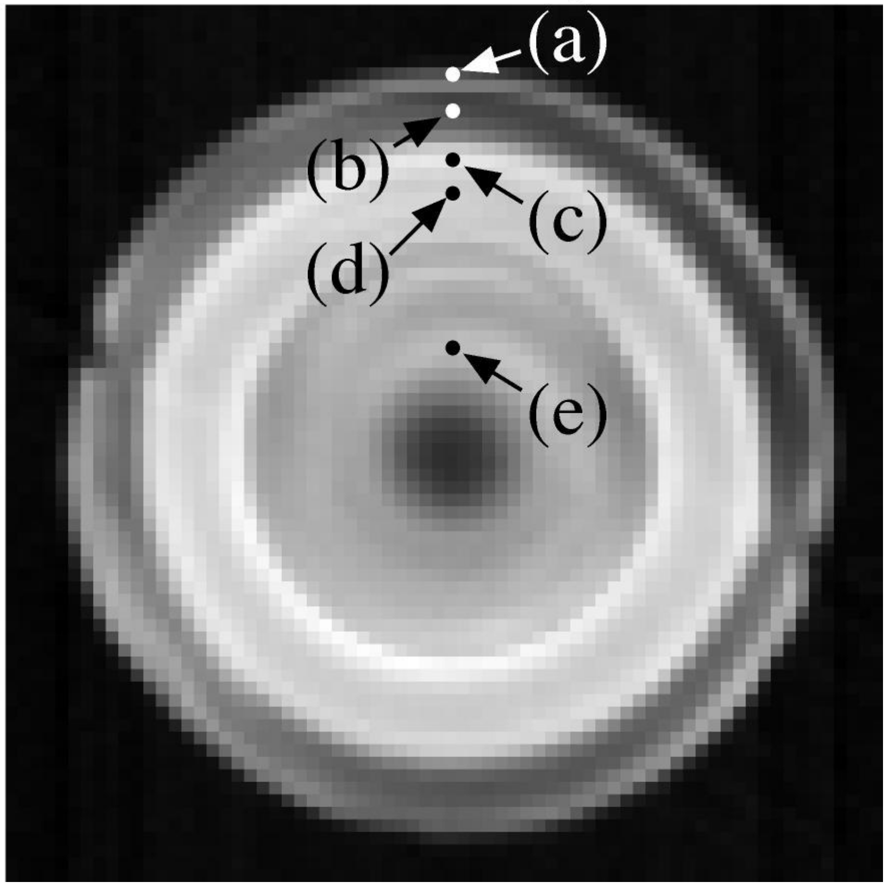

integral
scattering
along rotation
axis

$q_r = 0$

SAXS-Tomography

Sample is fibre textured:

scattering cross section

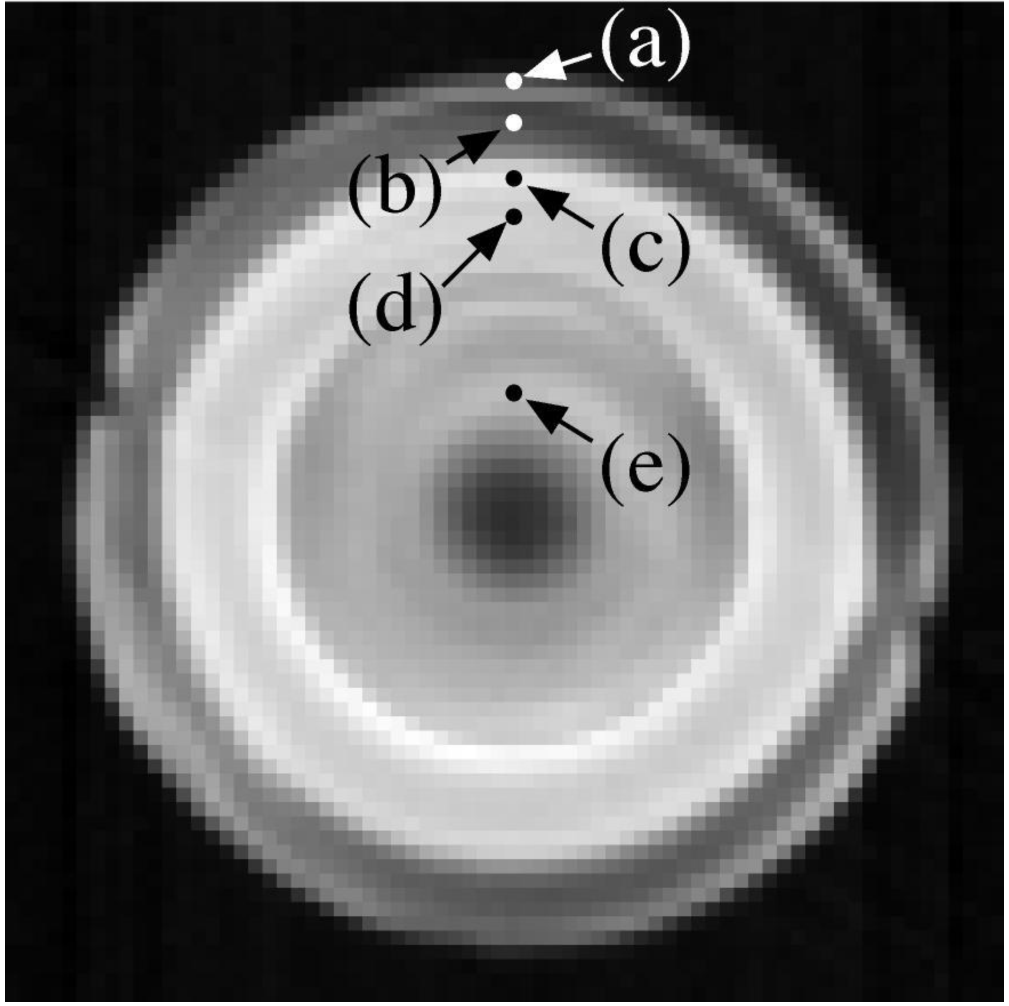

APL **88**, 164102 (2006)

scattering cross section

inhomogeneous nanostructure

In each pixel: full scattering cross section (rotationally symmetric)

interpretation: Stribeck, et al. Macromol. Chem. Phys. 207, 1139 (200

Effective Aperture and Diffraction Limit

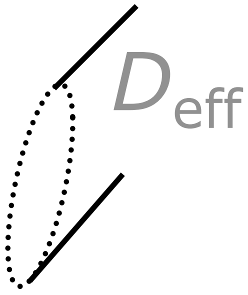

Numerical aperture:

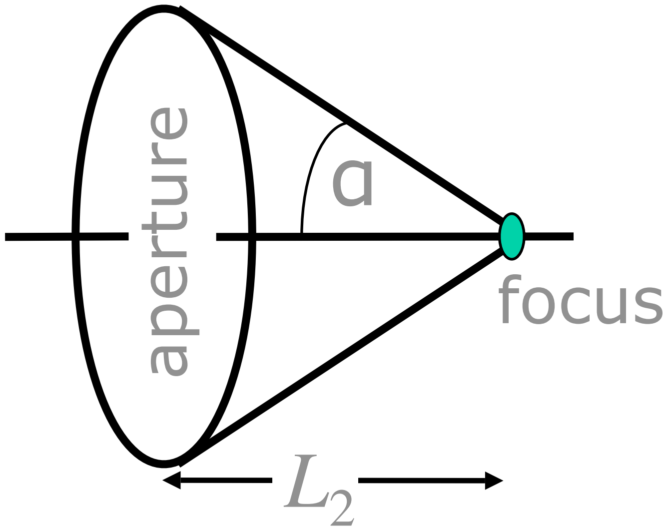

D_eff limited by:

geometric aperture $2R_0$
attenuation inside lens material
(includes Compton scattering)

→ low Z lens material

$$NA = \sin\alpha = \frac{D_\text{eff}}{2L_2}$$

Diffraction limit:

$$d_t = 0.75 \cdot \frac{\lambda}{2NA}$$

Numerical Aperture

large *f*: aperture dominated by attenuation

$$D_{\text{eff}} = 4\sqrt{\frac{f\delta}{\mu}} \propto \sqrt{f}$$

→ reduce μ/δ (low *Z* lens material)

→ $NA = D_{\text{eff}}/2f \propto 1/\sqrt{f}$: reduce focal size to minimum

→

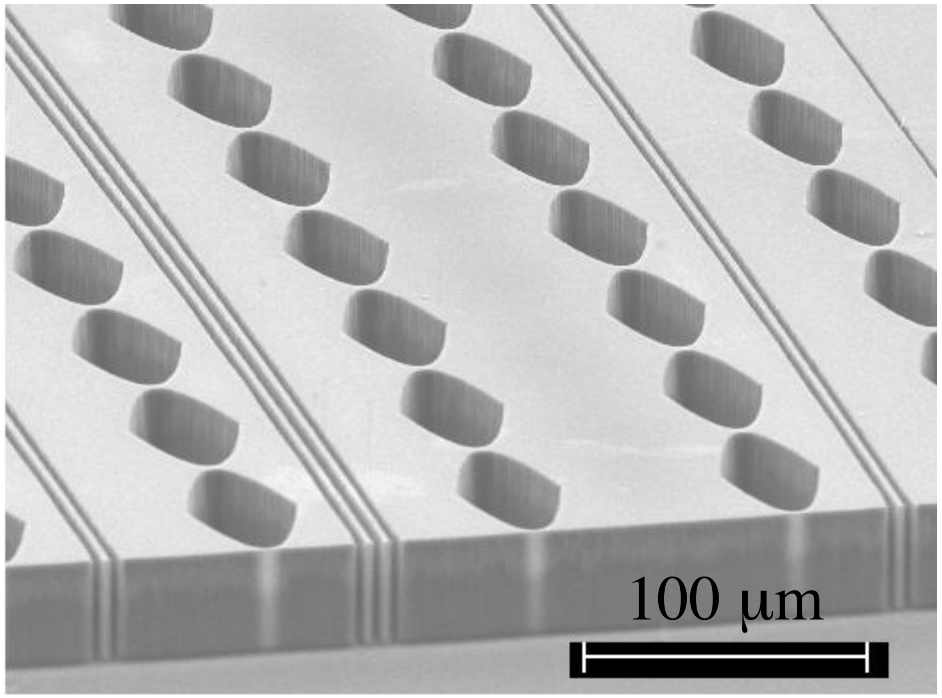

Nanofocusing Lenses (NFLs)

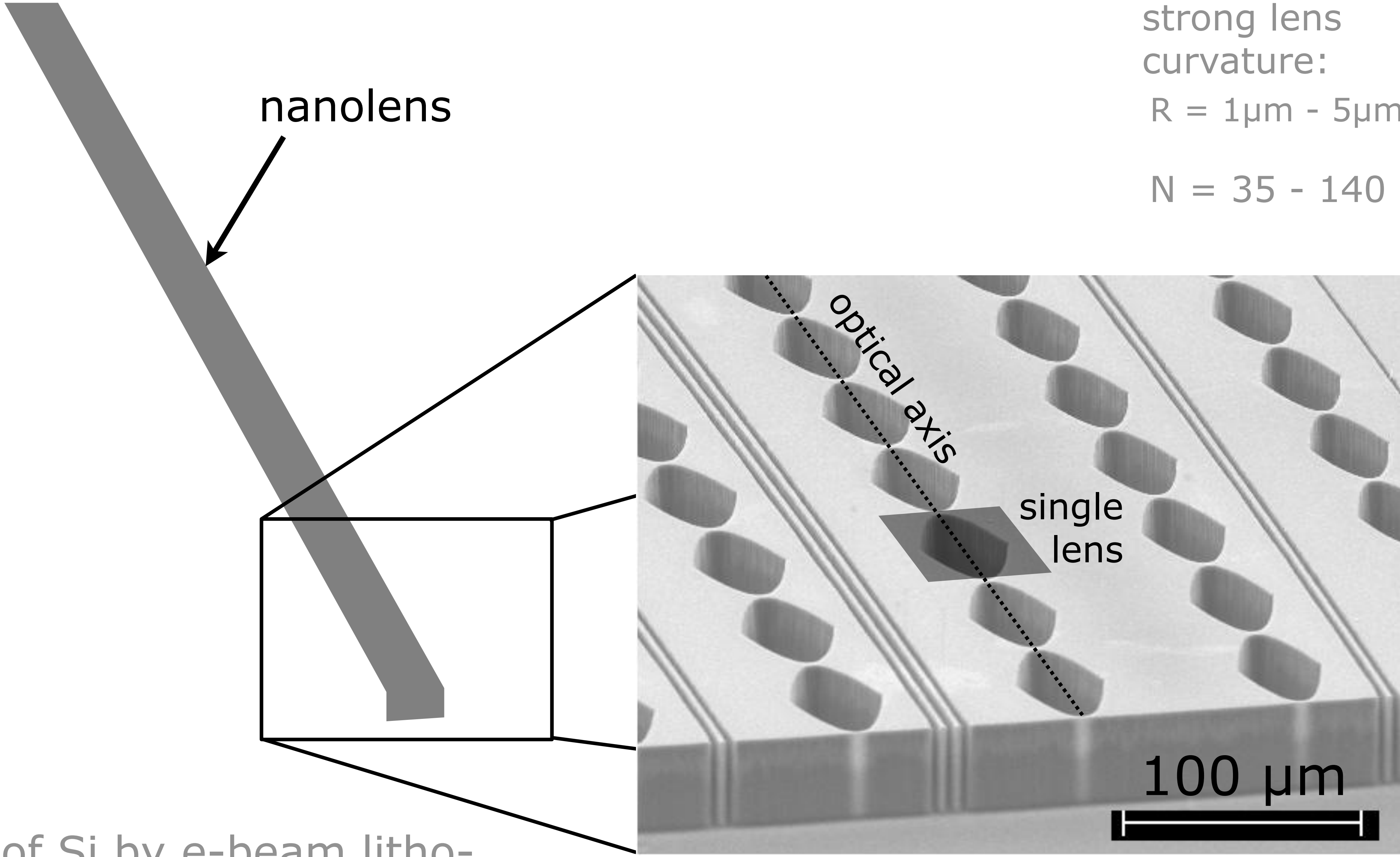

strong lens
curvature:
R = 1µm - 5µm

N = 35 - 140

lens made of Si by e-beam lithography and deep reactive ion etching!

APL **82**, 1485 (2003

Crossed Nanofocusing Lenses

Setup at ID13 of ESRF

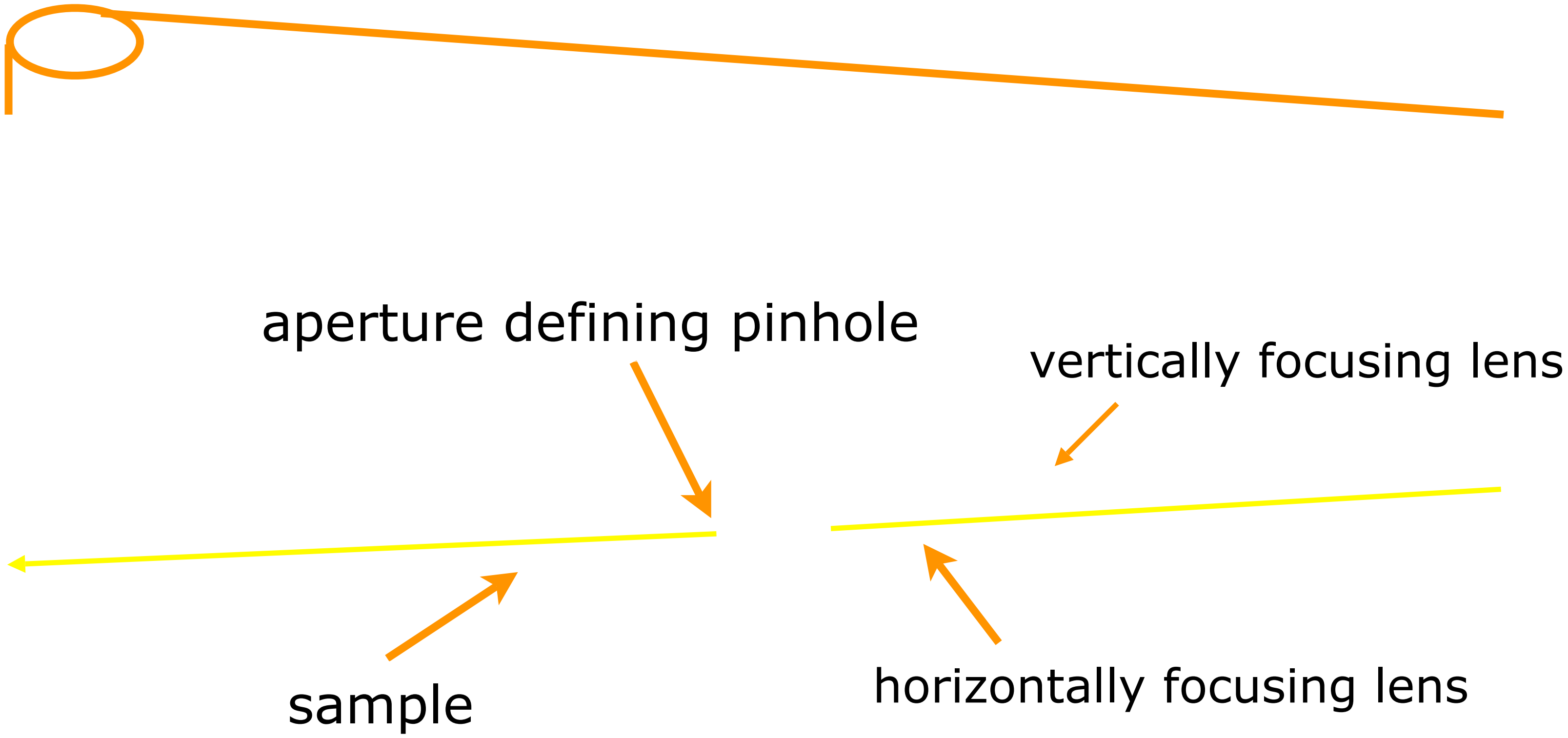

aperture defining pinhole

vertically focusing lens

sample

horizontally focusing lens

Focusing with NFLs

Si lens: E = 21keV, L_1 = 47m

source:
ID13 low-β invac. undulator

source size: 150 x 60μm^2

vertical focus: 55nm

horizontal focus: 47nm

f = 10.7mm

demagnification:
~ 2400 x 4400

flux: 1.7 ·10^8ph/s

APL **87**, 124103 (2005)

2D Scanning Mode: X-Ray Fluorescence

Arabidopsis thaliana

Fluorescence map

pollen

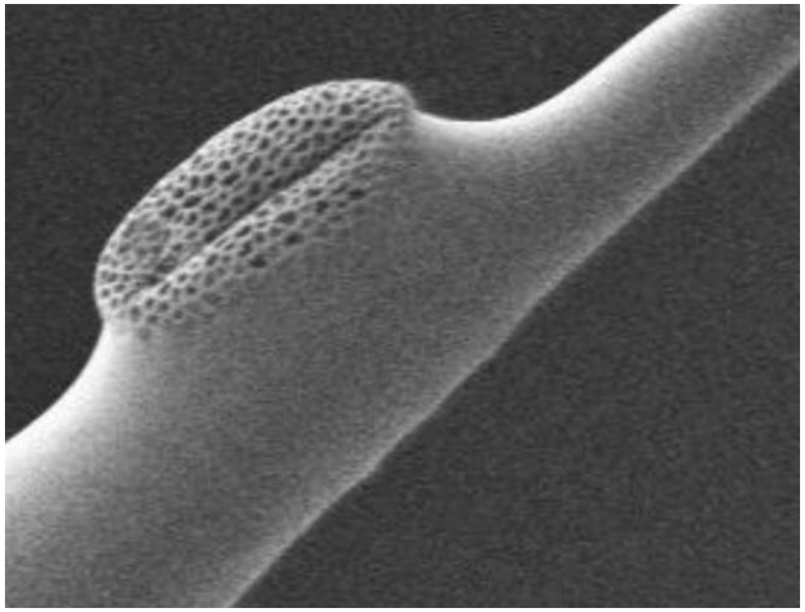

~ 100 nm resolution

E = 15.25 keV

High-Resolution Fluorescence Microtomography

Arabidopsis thaliana

trichome (leaf hair)

tip of trichome
(freeze dried)

Energy:
24.3keV

focus size:
80nm x 120nm

pixel size:
100nm

Nano-Diffraction

User experiment at ID13 carried out with prototype (Feb 2008)
M. Hanke, et al., APL **92**, 193109 (2008)

Scan single SiGe/Si(001)-islands
 (a) Ge fluorescence
 (b) light micrograph

Beam parameters:

E = 15.25 keV
beam size: 200 x 200 nm^2
flux: > 10^9 ph/s

facet-rods

Map of diffuse scattering around Si(004)-reflection

Limits of Focusing with NFLs

Diffraction limit:

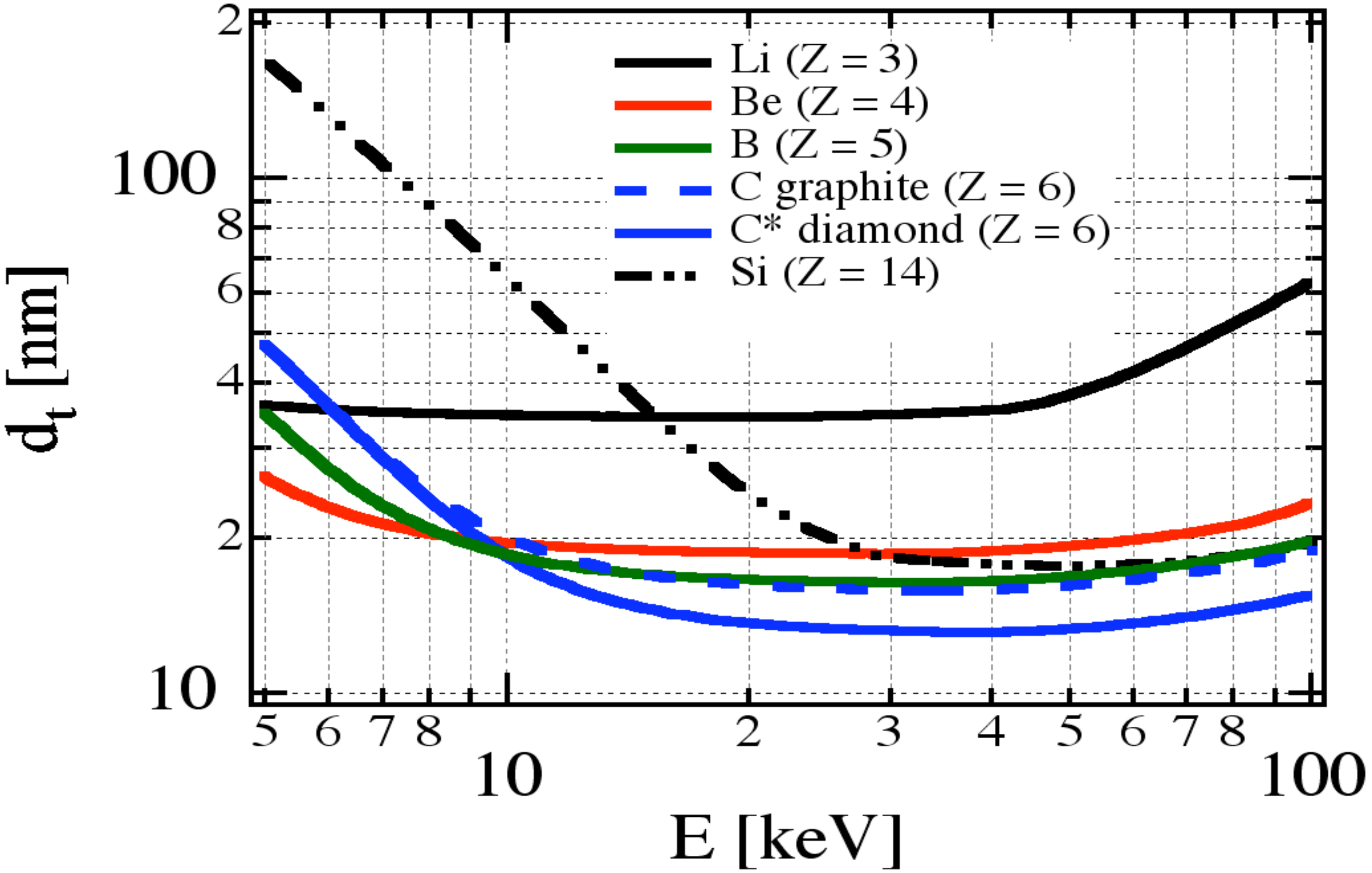

N = 100

l ≥ 0.084

R = 0.5 - 50µm

NA limited by

$$\sqrt{2\delta}$$

adapt aperture to converging beam (AFLs):

focus < 5 nm

[PRL **94**, 054802 (2005)]

Further improvement of focus size with diffractive optics (e. g., MML).

Nanoprobe: Coherent Nanodiffraction

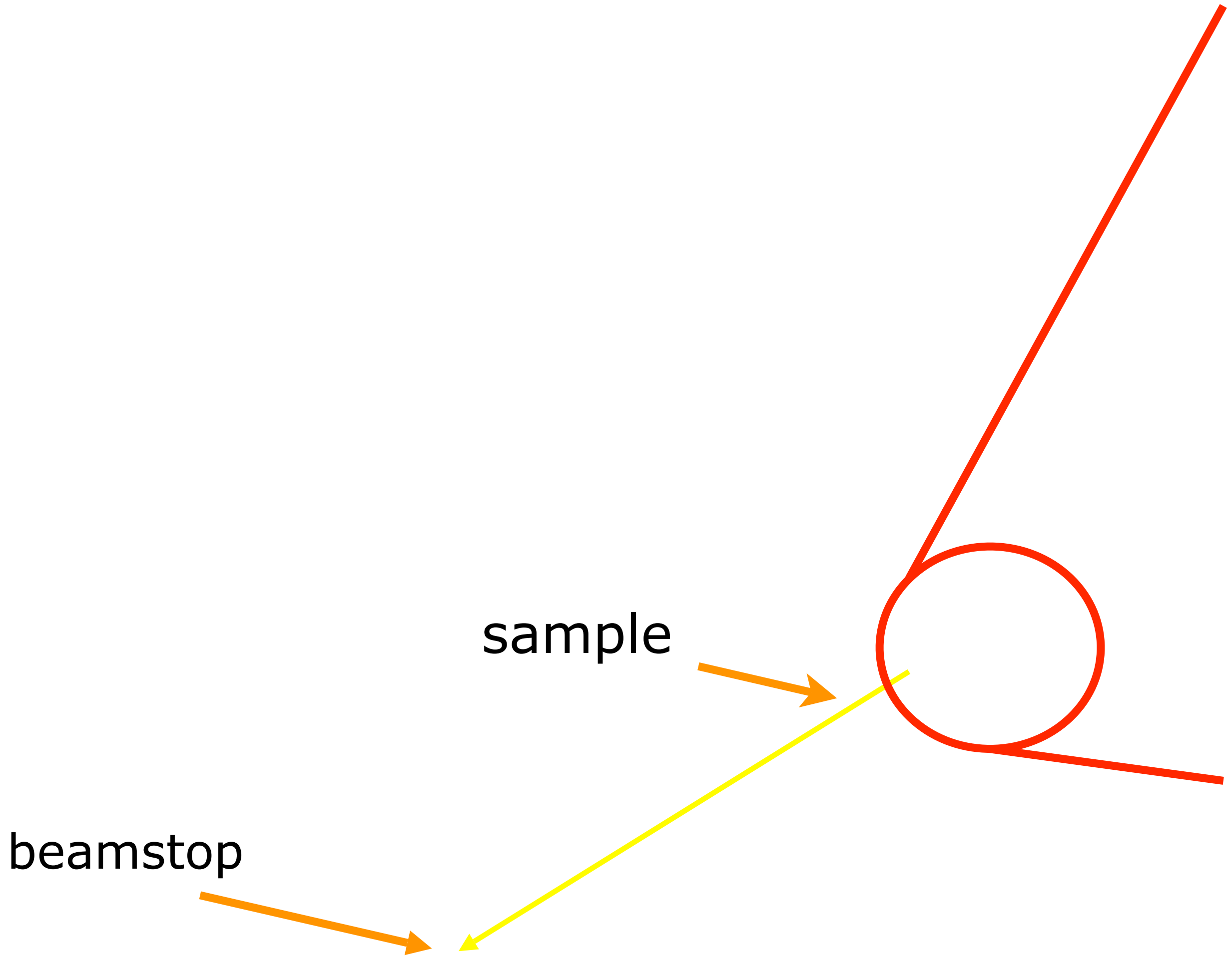

E = 15.25 keV
λ = 0.813 Å

beam size:
< 150 x 150 nm

(amplitude)

Wave Front in Diffraction Limited Focus

divergence angle:
numerical aperture

$$d_t = \frac{2\sqrt{2\ln 2}}{\pi}\,\frac{\lambda}{2NA} \approx 0.75\,\frac{\lambda}{2NA}$$

Gaussian limited plane wave

CXDI

XPCS, XFCS

Coherence in Focus

Focus size (amplitude):

$$b_{\mathrm{ampl}} = \sqrt{2b_{\mathrm{geo}}^2 + 2d_t^2}$$

lateral coherence length:

$$l_t = 2d_t\sqrt{1 + \frac{d_t^2}{b_{\mathrm{geo}}^2}}$$

So Far: No Ideal Lens...

Shape errors:

Underetching & proximity effect:

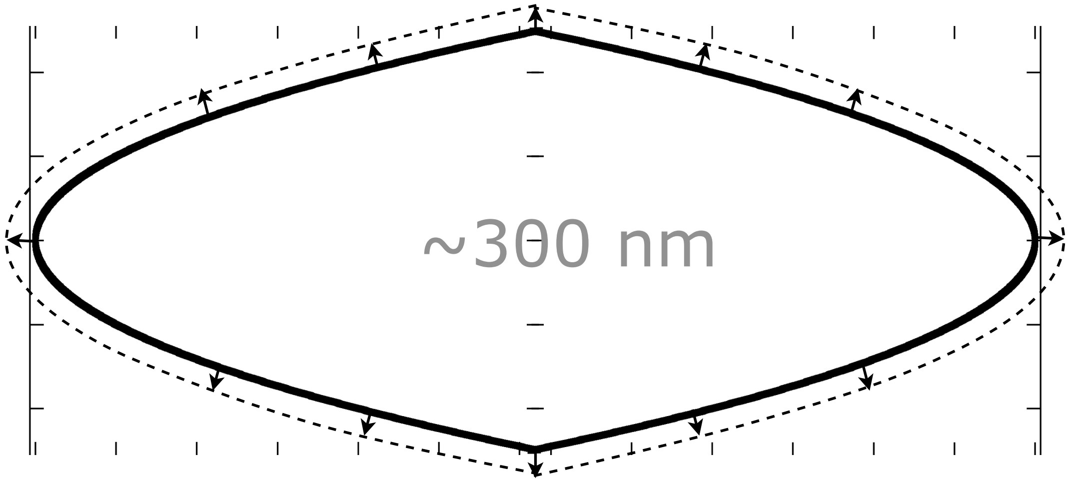

deviation from parabola

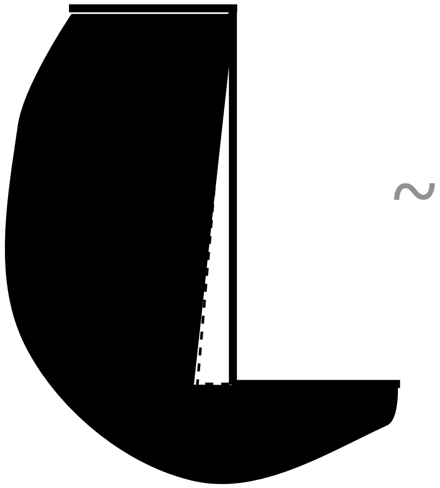

~ 10 mrad

tilted side wall

Roughness:

Shape of Wave Front in Focus

Main result:

beam flat in central speckle

In general:

Speckle size in focal plane can not be finer than diffraction limit!

Test Object: Gold Particle on Si_3N_4-Membrane

size < 100 nm

Diffraction Pattern of Gold Nanoparticle

sample-detector distance:

1250 mm (in air)

detector:

FReLoN 4K
50µm pixel size

exposure time:

10 x 60 s

intensity on sample:

3300 ph/s/nm^2

integral dose in beam:

10^{11} ph

> 2 month in fla
coherent beam

compared to 10^{12} ph/pulse at XFEL

Reconstruction

- reconstruction by HIO
- shrink-wrap
- phase left free to evolve
- 200 reconstructions
  (9 converged to wrong solutions)

reconstructions:

left-handed right-handed

averaged solution:

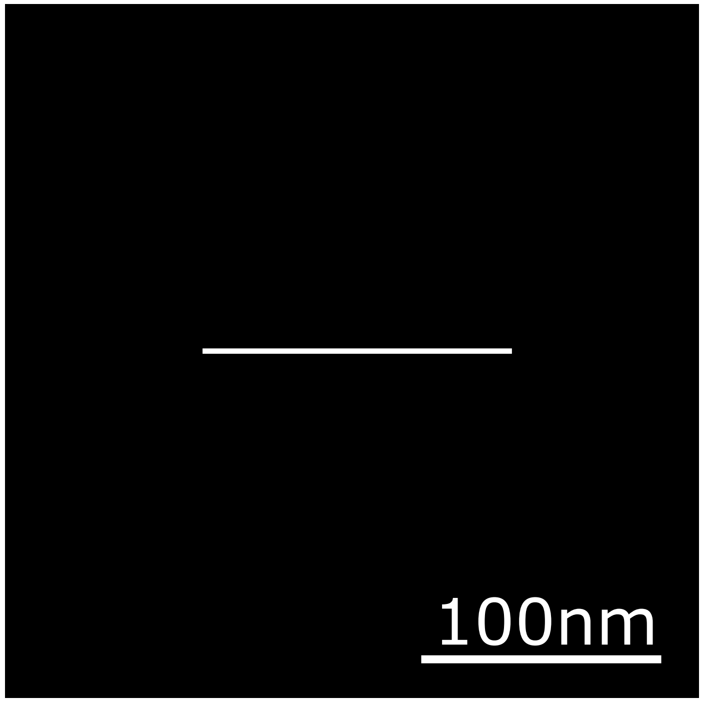

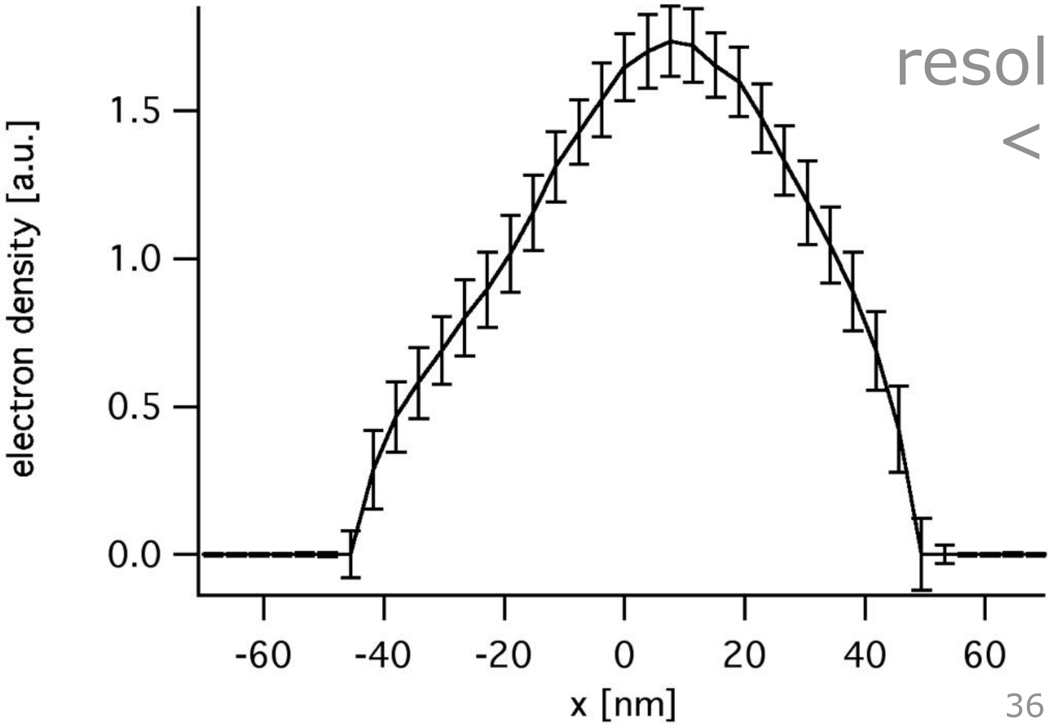

resolution:
< 5 nm

[redacted]

Conclusion

Refractive x-ray lenses:

- high resolution imaging optics
- small numerical apertures (~ mrad): aspherical lens is parabolic
- spatial resolution ~100 nm and below for different designs
- diffraction limits (theoretical):
  - < 20 nm for regular design (all lenses same size)
  - ~ 5 nm for adiabatically focusing lenses (lens size adapted to converging beam)
- diffraction limited focusing: high degree of coherence in focus

Applications:

- full-field microscopy
- scanning microscopy (fluorescence, diffraction, absorption)
- coherent diffraction imaging
- combine scanning microscopy with coherent diffraction imaging: ptychography [Thibault, et al., Science **321,** 379-382 (2008)]

Kinoform x-ray lens arrays

µXRF multilayer

Werner Jark

Sincrotrone Trieste
Basovizza (TS), Italy

werner.jark@elettra.trieste.it

www.elettra.trieste.it/experiments/beamlines/microfluo/index.html

www.elettra.trieste.it/organisation/experiments/laboratories/multilayer_technology/index.html

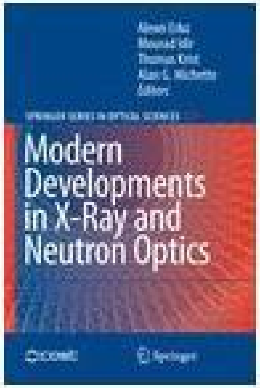

Modern Developments in X-Ray and Neutron Optics
Series: Springer Series in Optical Sciences , Vol. 137
Erko, A.; Idir, M.; Krist, Th.; Michette, A.G. (Eds.)
2008, XXIII, 533 p. 299 illus., 5 in color.
With series ad on (virtual) p. 535, 536.., Hardcover

ISBN: 978-3-540-74560-0

Read on CLESSIDRA kinoform lenses
on pages 331-351

What happens here?

μXRF
multilayer

**μXFA@ELETTRA
BL 10.1L**

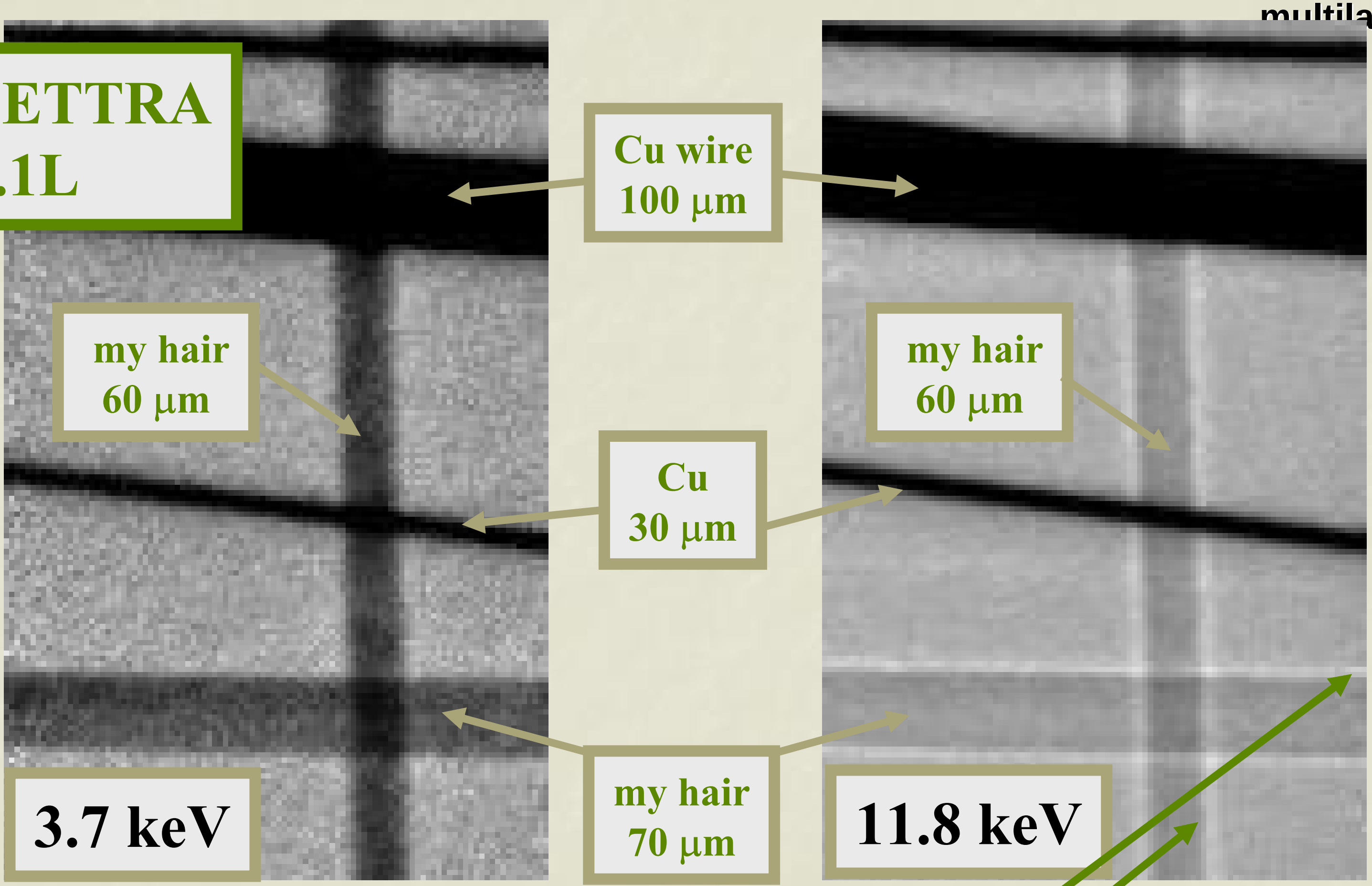

Cu wire
100 μm

my hair
60 μm

my hair
60 μm

Cu
30 μm

my hair
70 μm

3.7 keV

11.8 keV

transparent hairs can deviate (i.e. refract) x-rays

Refraction and reflection: x-rays

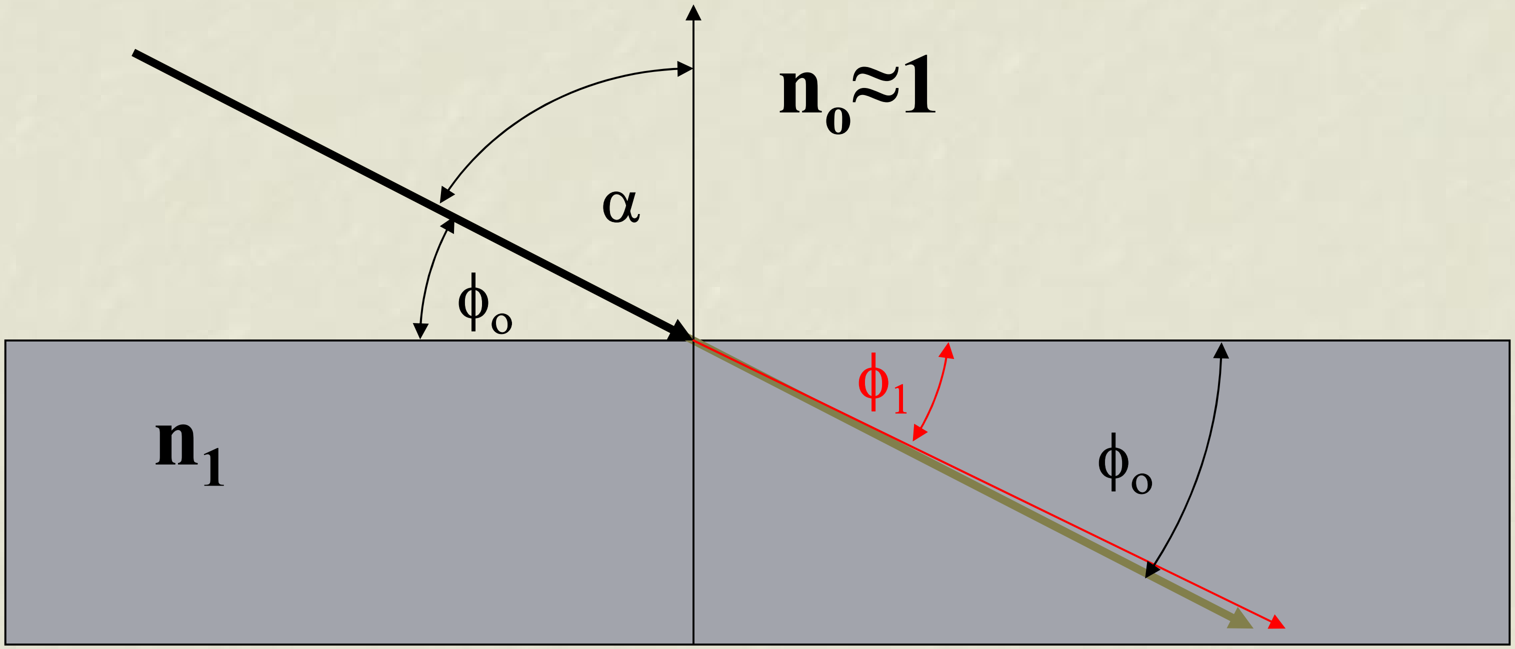

- Snell's law: $n\sin\alpha = \text{const}$ $\cos\phi_o = (1-\delta)\cos\phi_1$
- Beam deviation at one interface: $\Delta = \phi_o - \phi_1$
- with $\cos\Delta = 1$, $\sin\Delta = \Delta$: $\cos\phi_1 = \cos\phi_o + \Delta\sin\phi_o$ then $\Delta = \delta/\tan\phi_o$

Refraction in transmitted x-rays

μXRF
multilayer

$n>1.0$: convex

lens focuses

$n<1.0$: concave

lens focuses

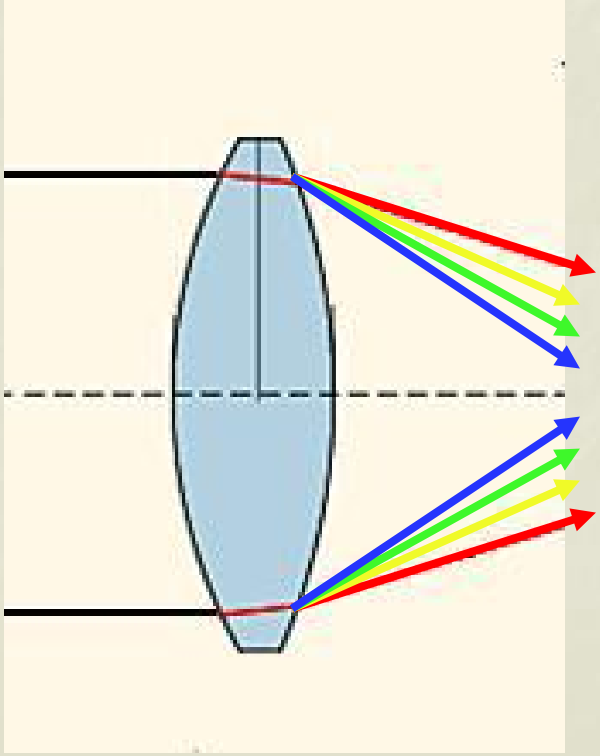

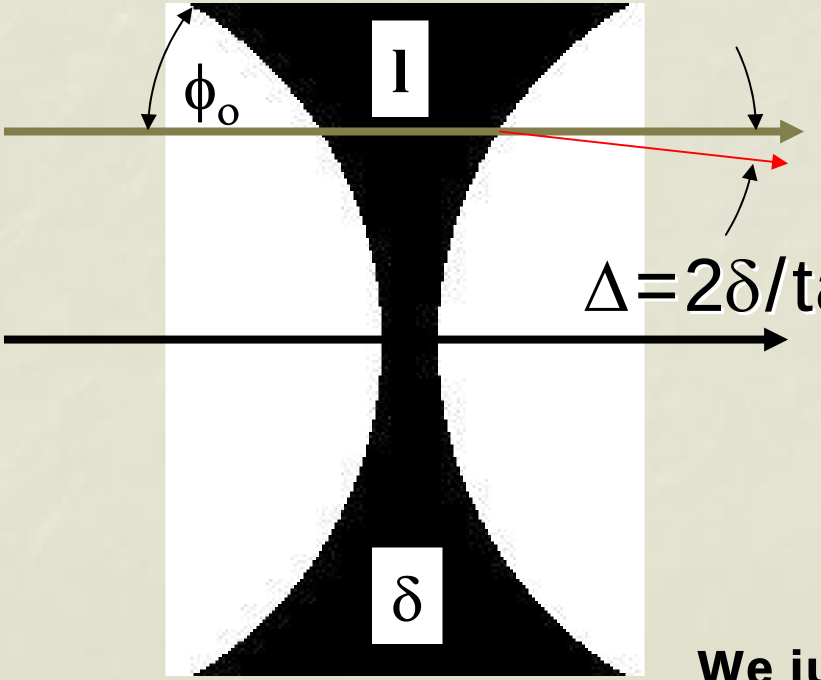

$$\Delta=2\delta/\tan\phi_o$$

We just heard it!

Refraction in transmitted x-rays

μXRF
multilayer

Back to hair and Cu wire

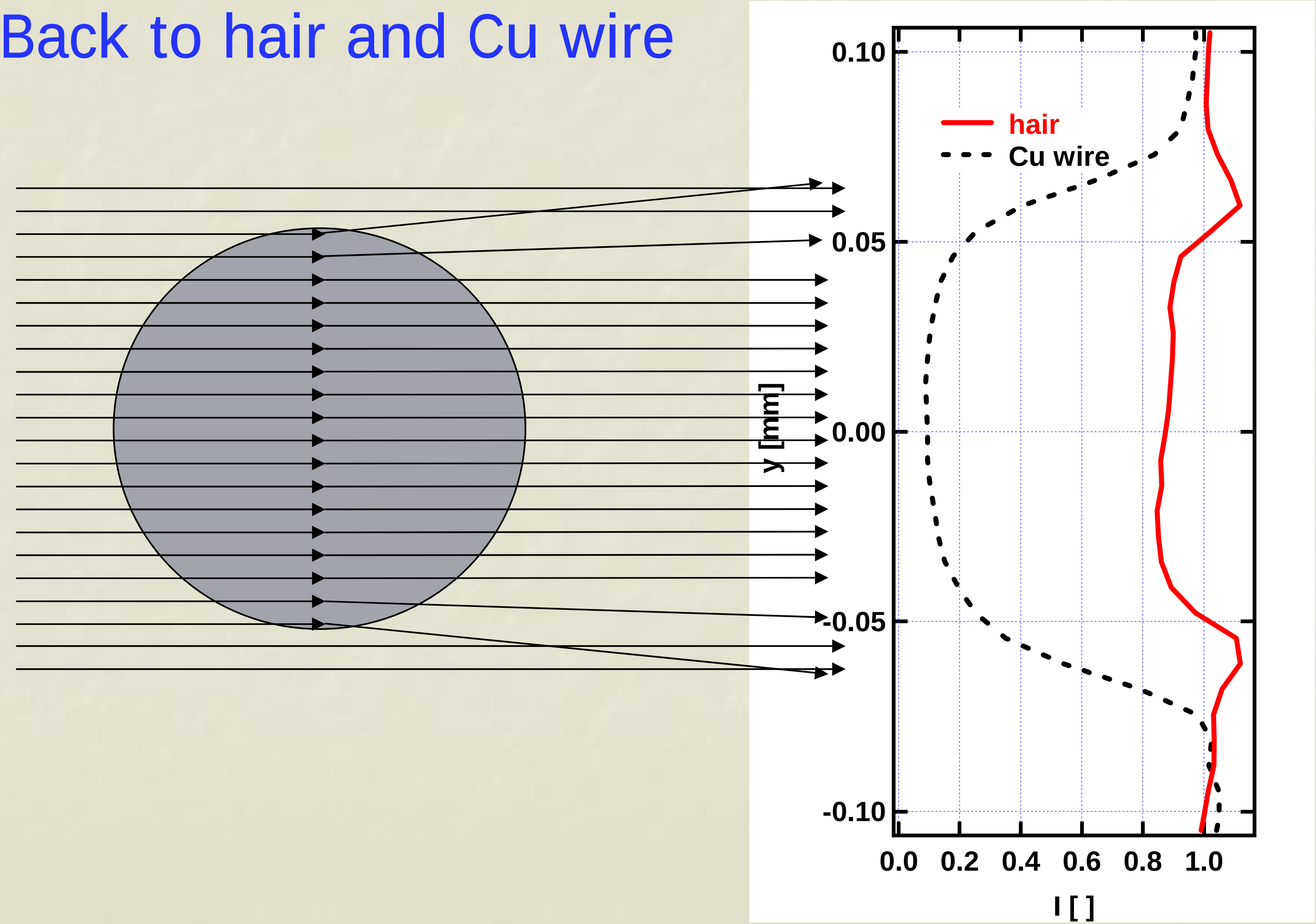

Refraction in transmitted x-rays

μXRF
multilayer

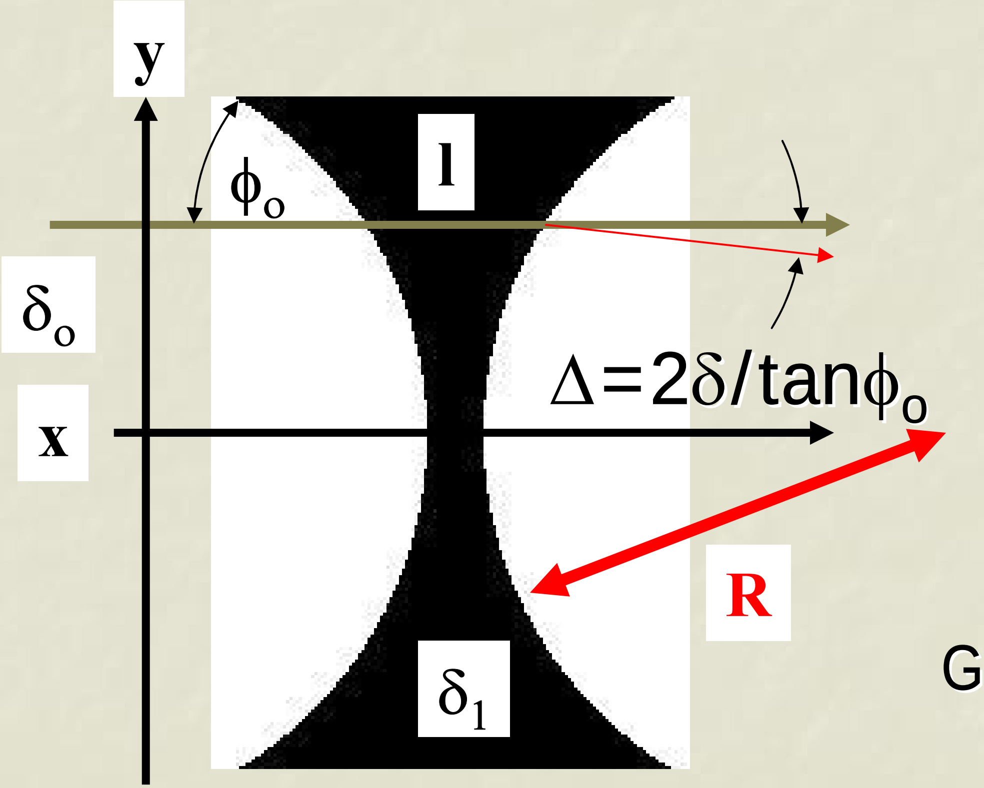

Equation for parabola

$$2R(x-x_o)=y^2$$

focal length

$$f=R/(2\delta)$$

Parabolic material increase

→

Gaussian transmission function

$$T=\exp(-y^2/(2\delta fL))$$

with L=attenuation length

Refraction in transmitted x-rays

μXRF multilayer

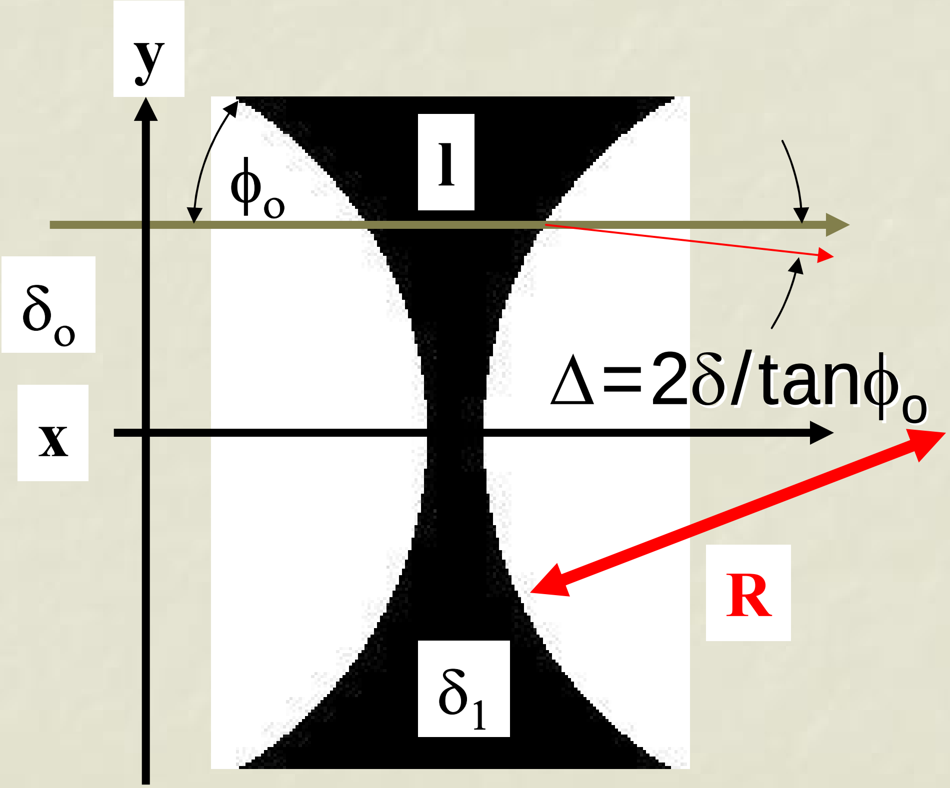

$T=\exp(-y^2/(2\delta fL))$

Optimum aperture

$A=2\mathrm{sqrt}(2f\delta L)$

Average T is 75%

Figure of merit of materials

$\mathrm{sqrt}(\delta L)$

Refraction in transmitted x-rays

μXRF multilayer

Figure of merit sqrt(δL)

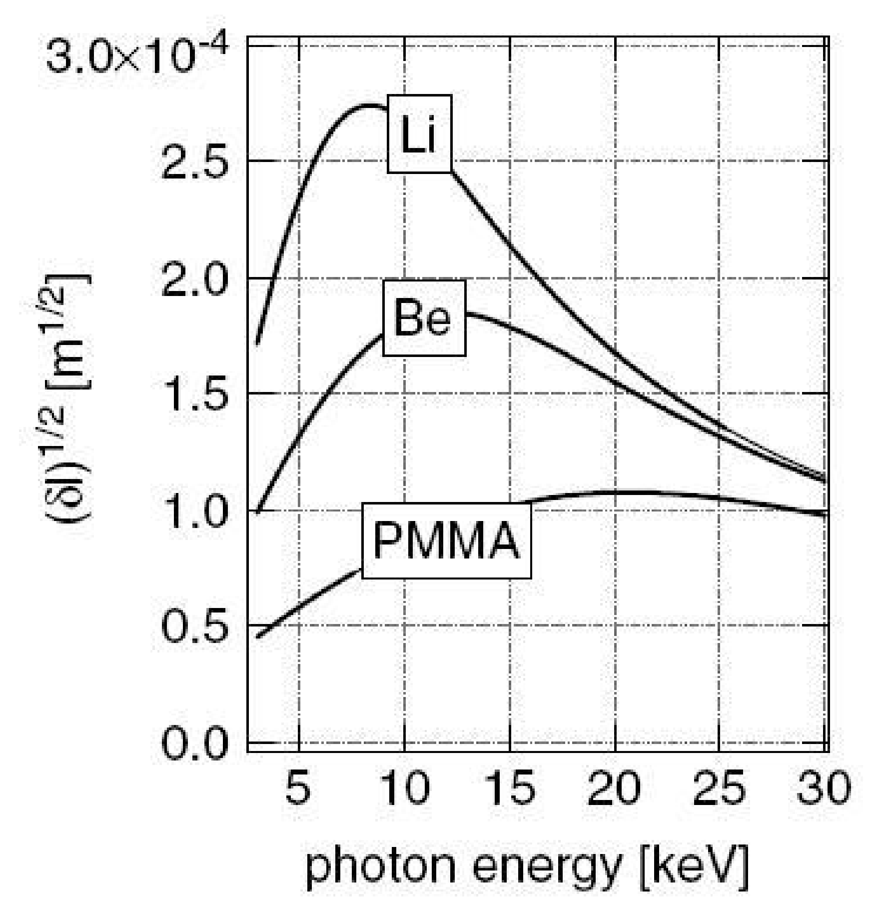

Difficult Li, very interesting Be, but also plexiglass (pmma)

Compton scattering dominates at higher energies (>30 keV):

all materials have similar figure of merit

Can we “lighten” the lens?

A.J. Fresnel made the CONVEX lenses for the Cordouan lighthouse in 1822 lighter

Strategy: <u>Refraction</u> only on transmission through inclined surfaces

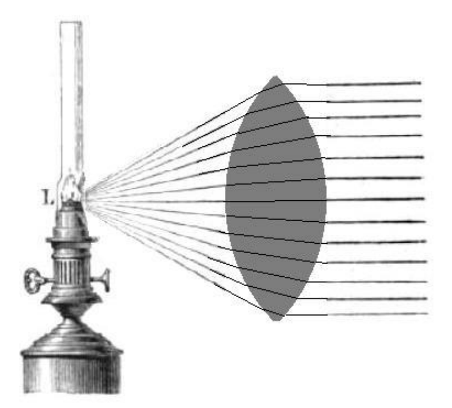

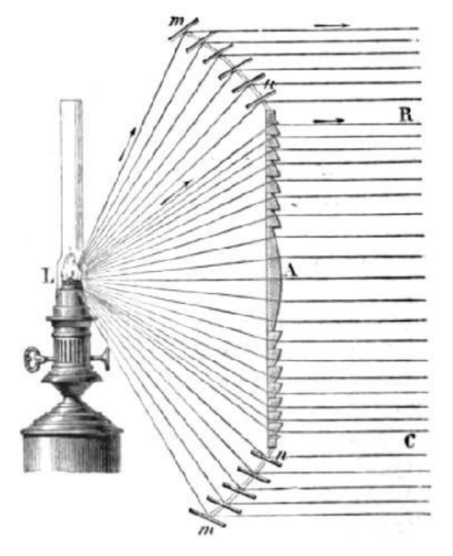

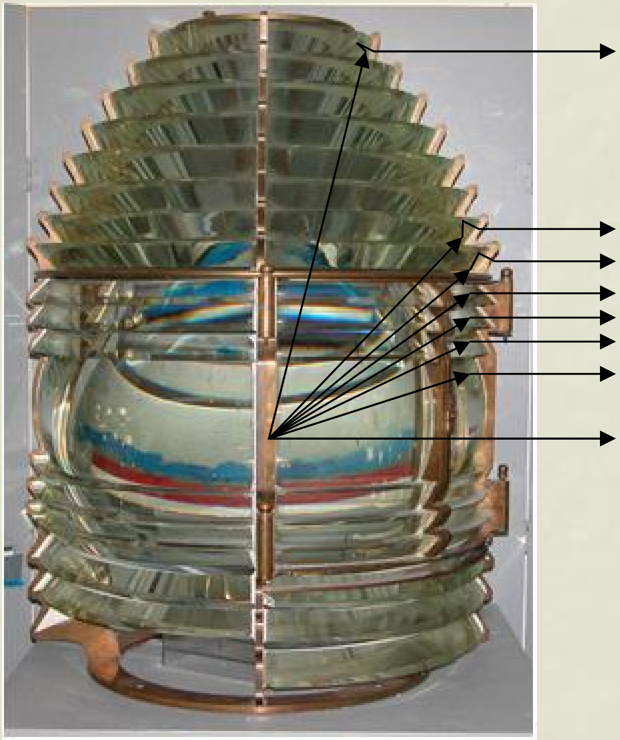

remove “useless” rectangular blocks

increase angles by refraction – reflection – refraction in prisms

To "lighten" a CONCAVE lens

μXRF
multilayer

History:

Prior to introduction of compound refractive lenses (CRL)!

Suehiro et al, Nature 352, 385 (1991): proposal in letter without picture (lathe)
Michette, Nature 353, 510 (1991): critically comments the idea
Yang, NIM A328, 578 (1993): more detailed elaboration

T. Tomie, "X-ray lens",
Japanese patent 6-045288
(18 Febr 1994)
Covering compound
refractive lenses and
"lightened" lenses

FIG.9(b)

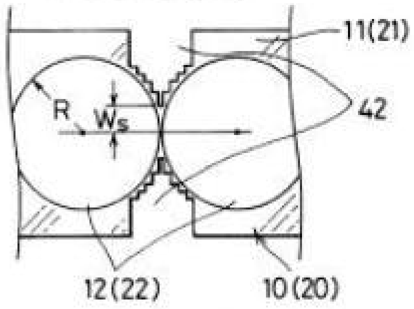

U.S. Patent Jan. 14, 1997 Sheet 8 of 8 5,594,773

Never made this way

First realisation:
Aristov et al, APL 77, 4058 (2000)

To “lighten” a CONCAVE lens

µXRF
multilayer

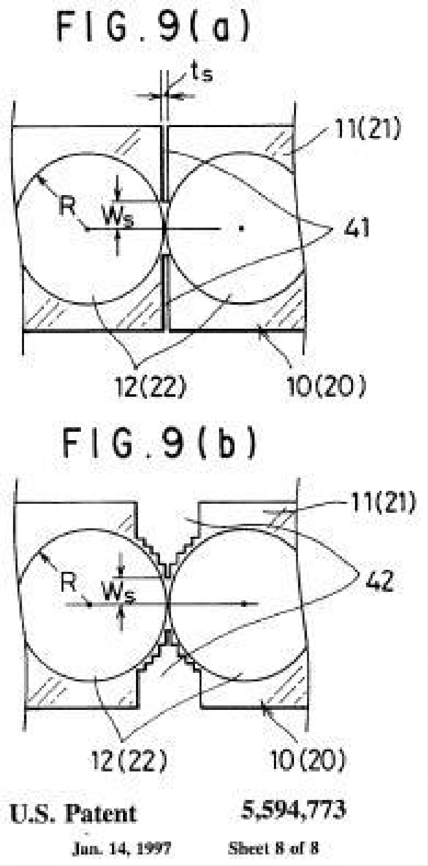

U.S. Patent Jun. 14, 1997 Sheet 8 of 8 5,594,773

Tomie 1994

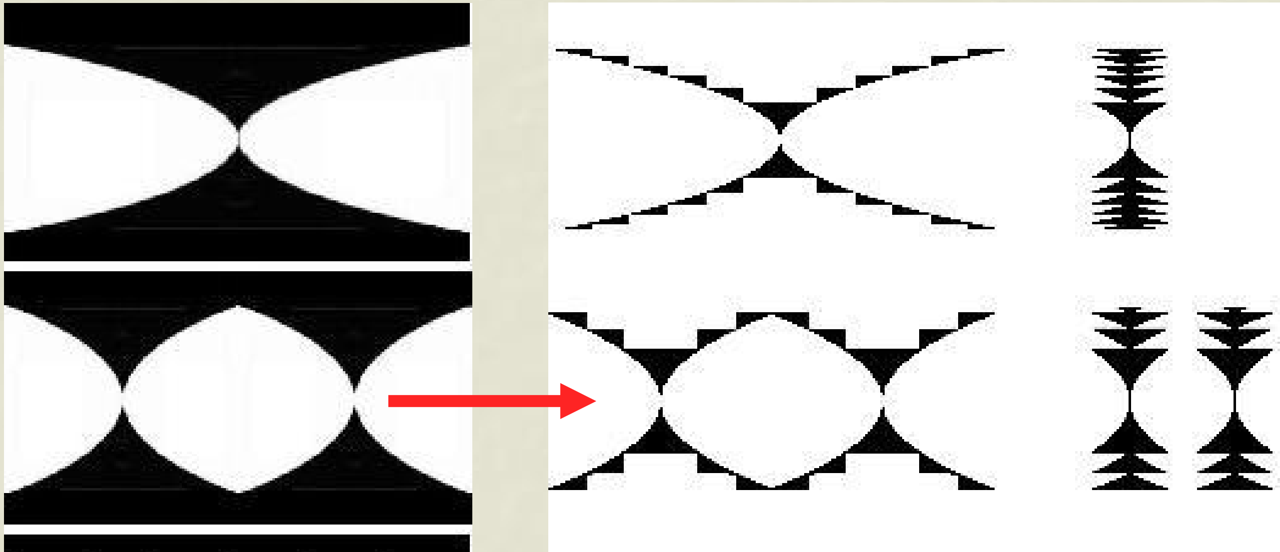

Without restrictions?

Restrictions

μXRF
multilayer

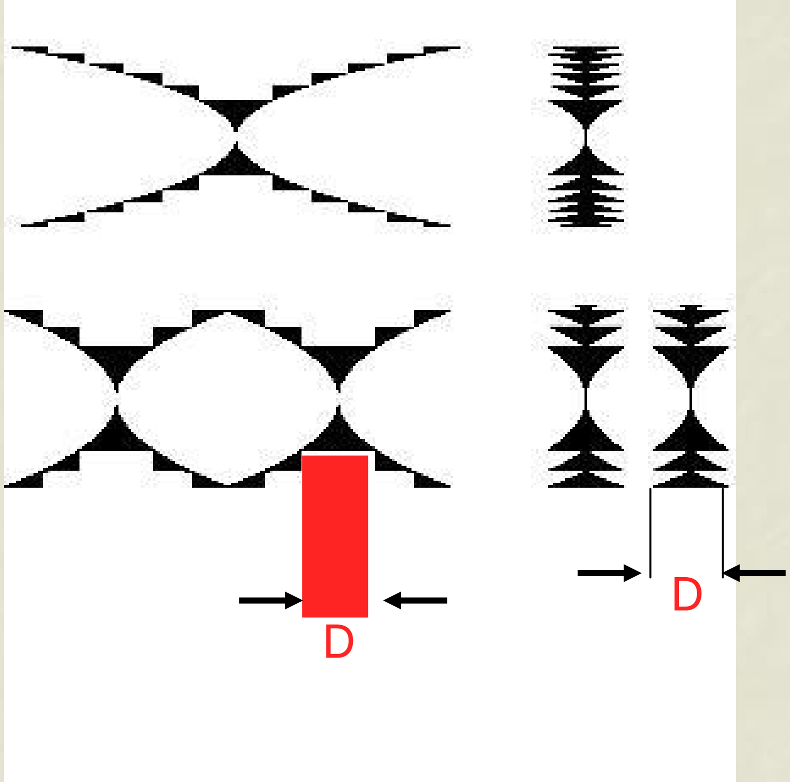

Do not distort the passing wave
Keep planes of equal phase continuous

Make use of longitudinal field periodicity:

Remove blocks, which shift phase by integer multiple of 2π!

$$D = m\lambda/\delta$$

m = integer multiple
λ = wavelength
δ = refractive index

Reduced material!!

First prototype: Aristov et al, APL 77, 4058 (2000)

These are kinoform lenses produced by lithography

μXRF multilayer

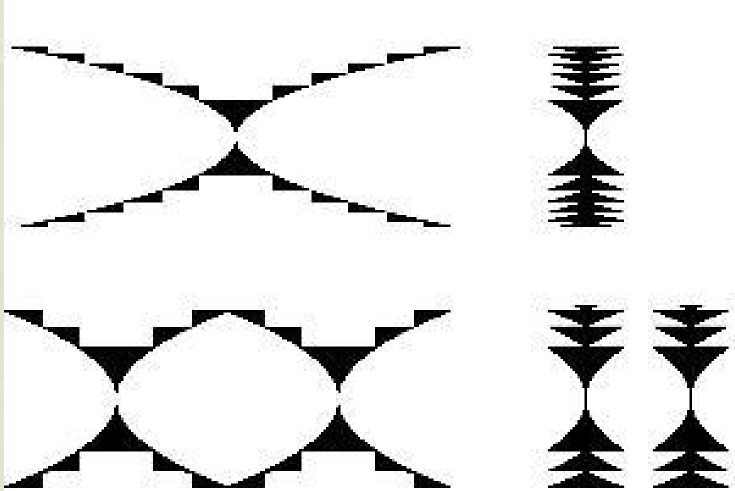

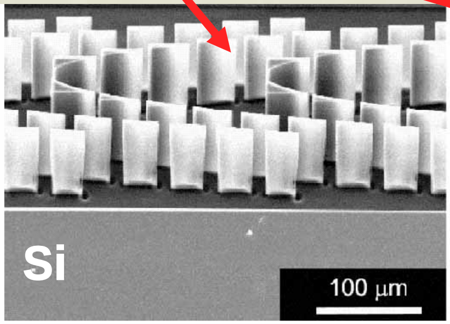

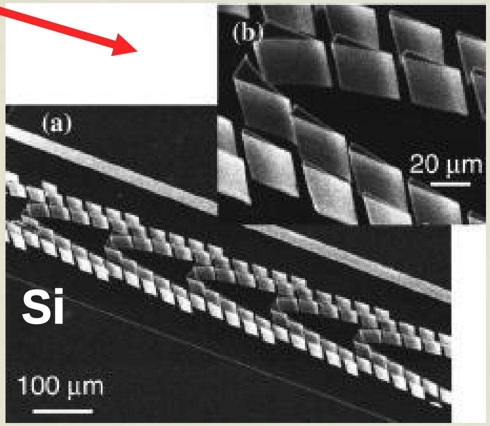

D=mλ/δ≈40 μm
For Si@12 keV

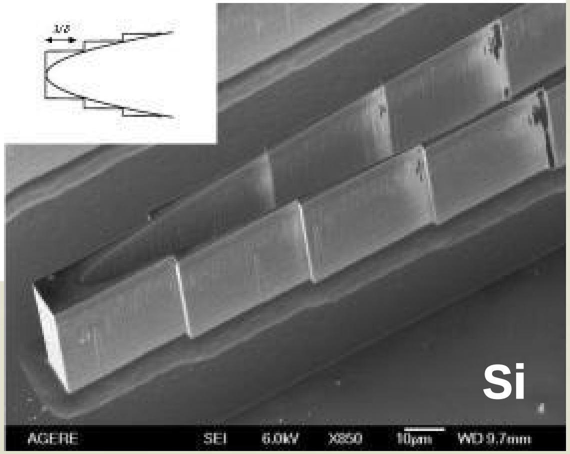

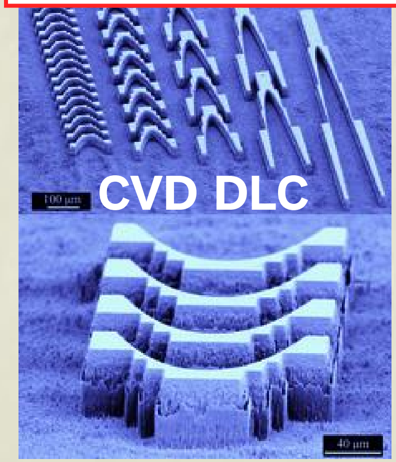

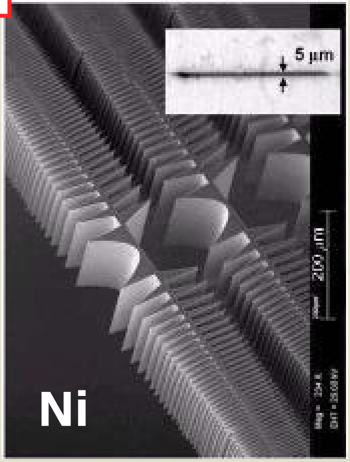

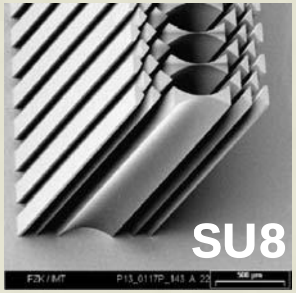

later: Evans-Lutterodt et al, Opt. Express 11, 919 (2003), Nöhammer et al, JSR 10, 168 (2003), Nazmov et al, NIM B217, 409 (2004), Alianelli et al, SPIE Proc. 6705, art. no. 670507 (2007) (single in Si)

Reduced material!!

μXRF
multilayer

Dimensions: make very good use of chip mass production techniques

BUT lithography can only shape linear structures

Need crossed lens pair for bi-dimensional focusing: match height and aperture!!

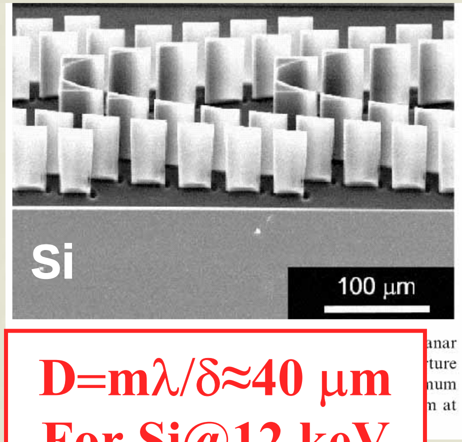

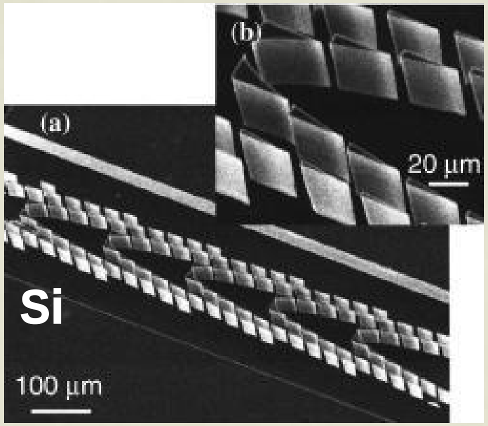

D=mλ/δ≈40 μm
For Si@12 keV

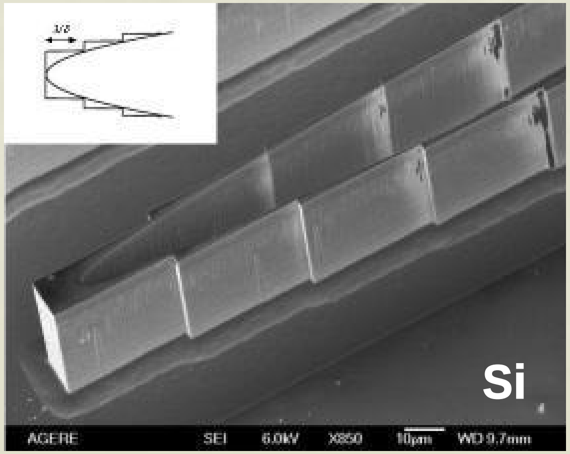

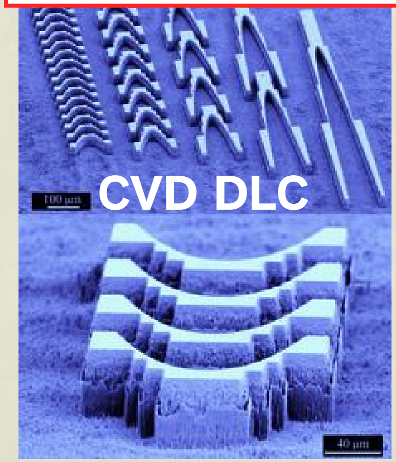

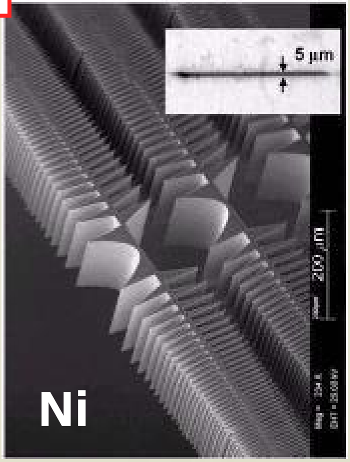

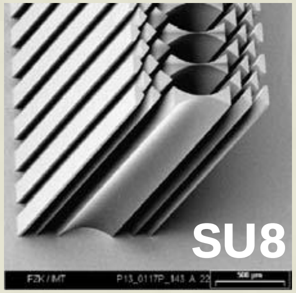

Still room for other shapes

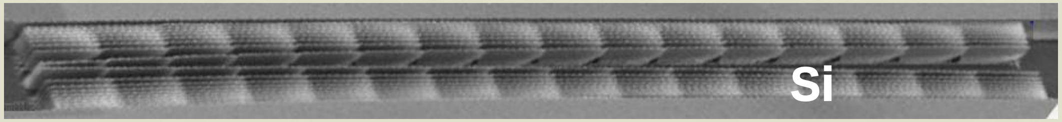

Looks good!!

µXRF
multilayer

But: More flux than center segment could provide?
Better spot size than diffraction limit of center segment?

- 🟢🟢 YES, both
- 🟢🔴 More flux, large focus
- 🔴🔴 NO, both

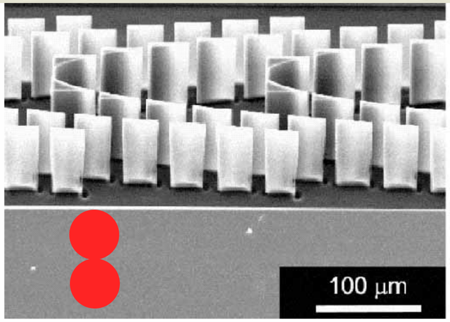

🔴🔴

Fig. 1. An SEM micrograph of a 100 µm-deep silicon planar parabolic lens with minimized absorption. The lens aperture $A = 150\,\mu\text{m}$, the number of unit lenses $p = 5$, the maximum phase variation number $M = 2$, the focal length $F = 80\,\text{cm}$ at the design wavelength $\lambda_0 = 0.071\,\text{nm}$ ($E_0 = 17.48\,\text{keV}$).

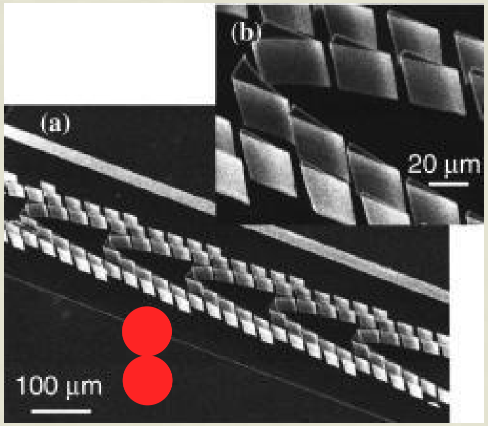

🔴🔴

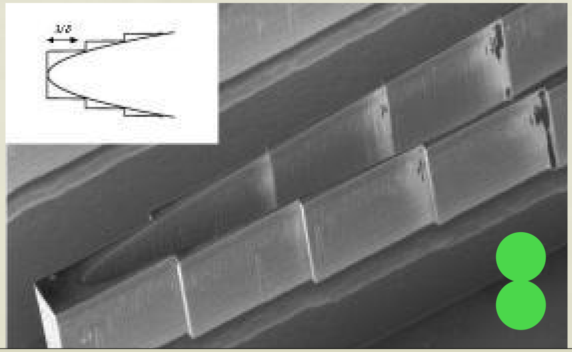

🟢🟢

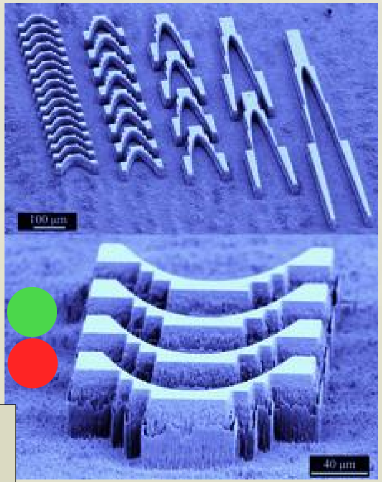

🟢🔴

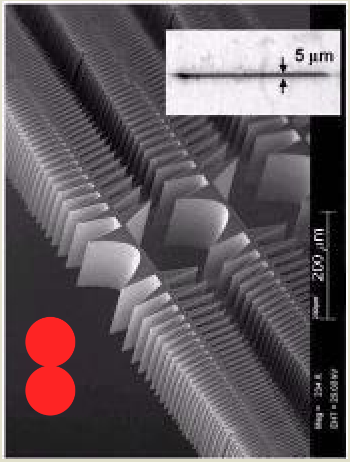

🔴🔴

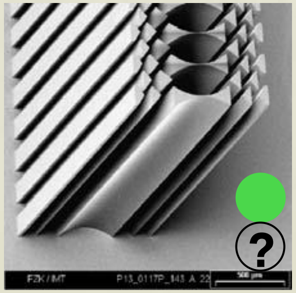

🟢 ?

IMT@FZK

Evans-Lutterodt et al, Opt. Express 11 (2003)
Alianelli et al, SPIE Proc. 6705 (2007)

Problem: small outer zones

XPE

yer

Evans-Lutterodt et al, PRL 99 (13), 134801 (2007)

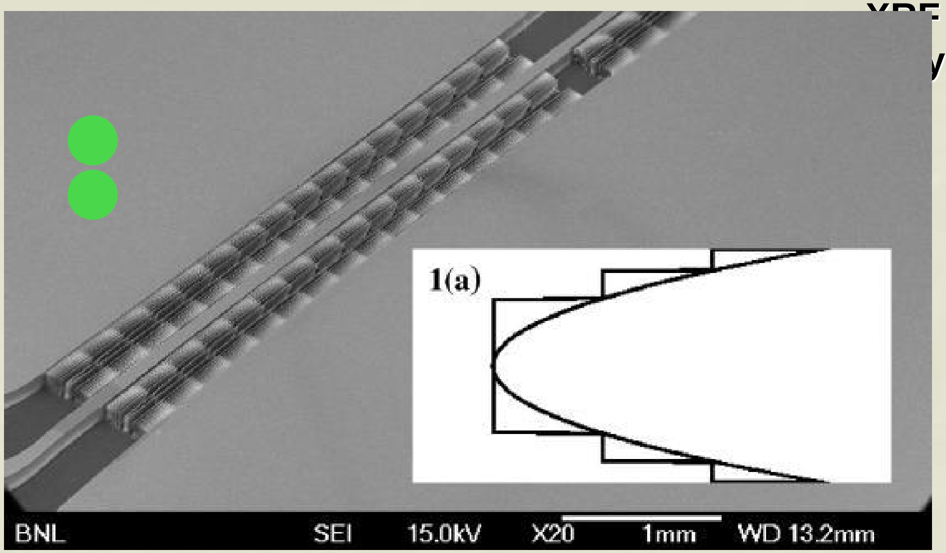

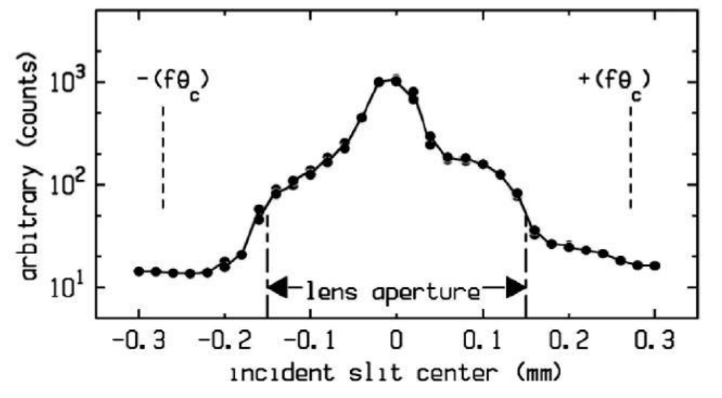

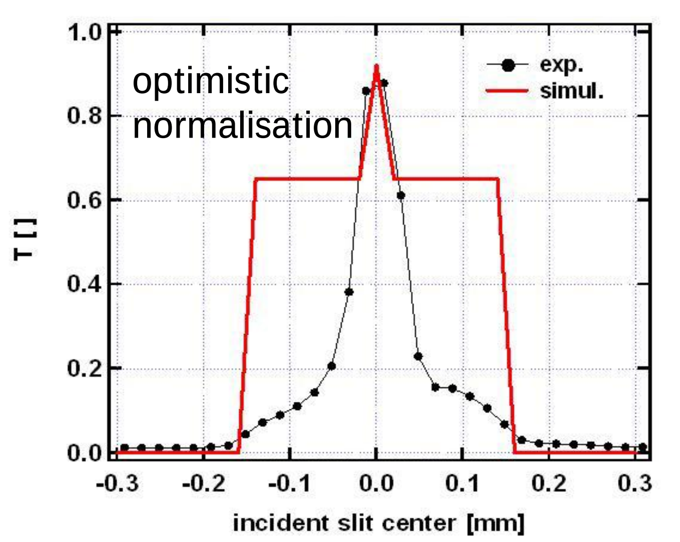

optimistic normalisation

Transmission: integrated ≤30%
i.e. ≤45% of expectation
Drops off when segment height < 2 μm

Nevertheless in single lens
smallest focus ≈320 nm fwhm
(Stein et al, JVST B26, 122 (2008))
private communication Evans-Lutterodt:
more recently <<320 nm

Alternative "lightening"

µXRF multilayer

How to keep segment HEIGHT large?

Keep it constant!

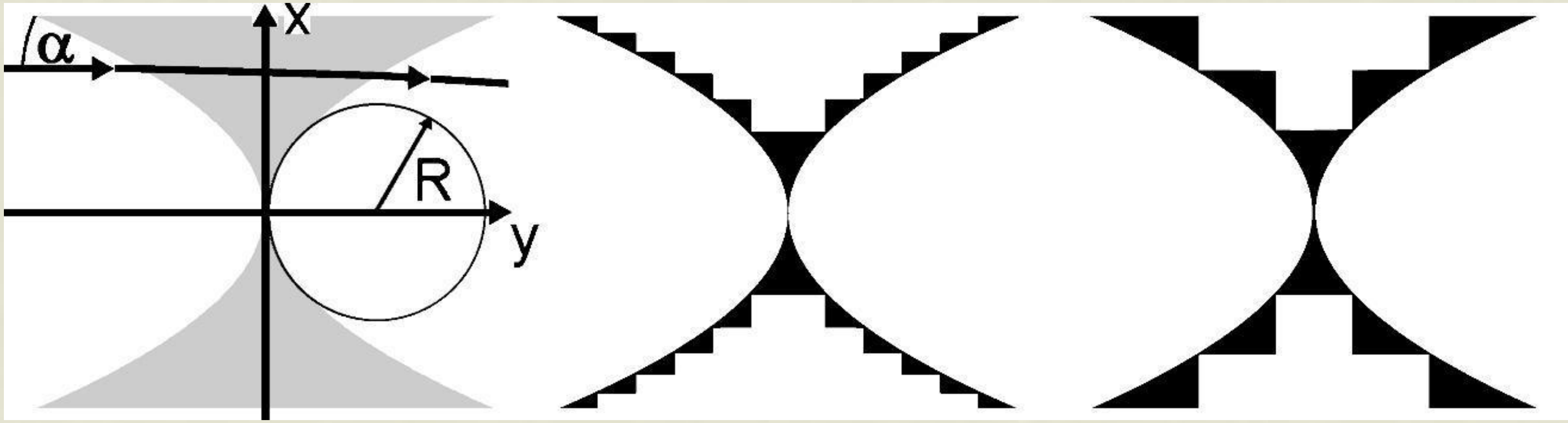

Then simplify and compact the lens

and make it

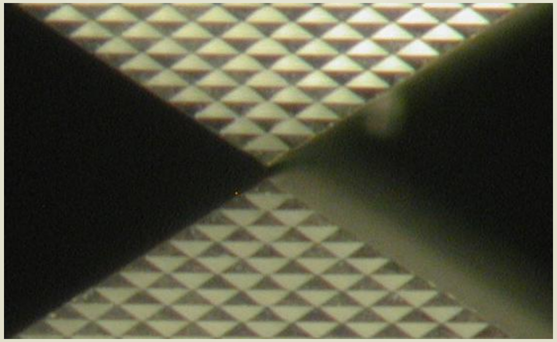

It needs a name

μXRF
multilayer

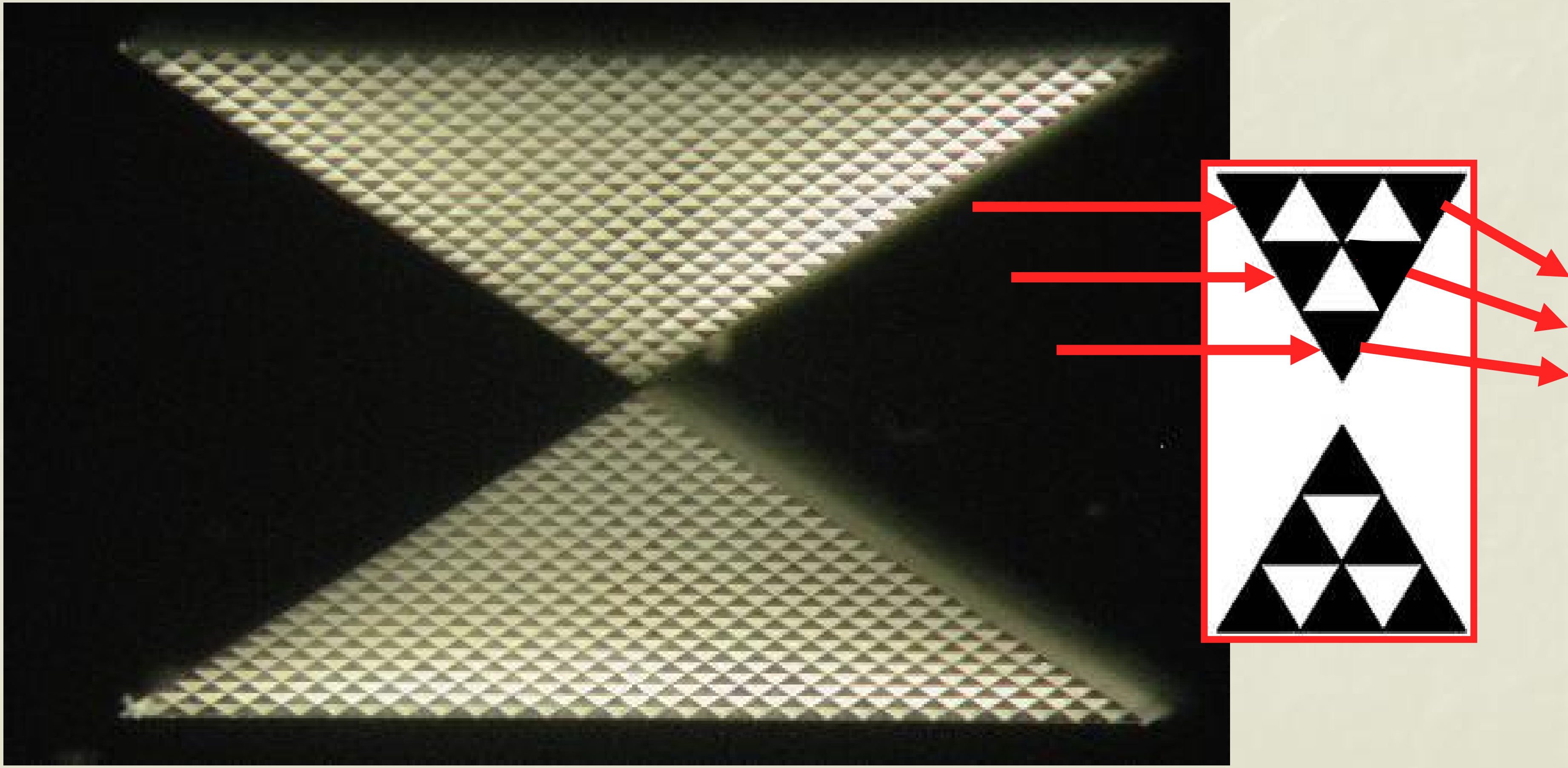

Looks good: CLESSIDRA

μXRF
multilayer

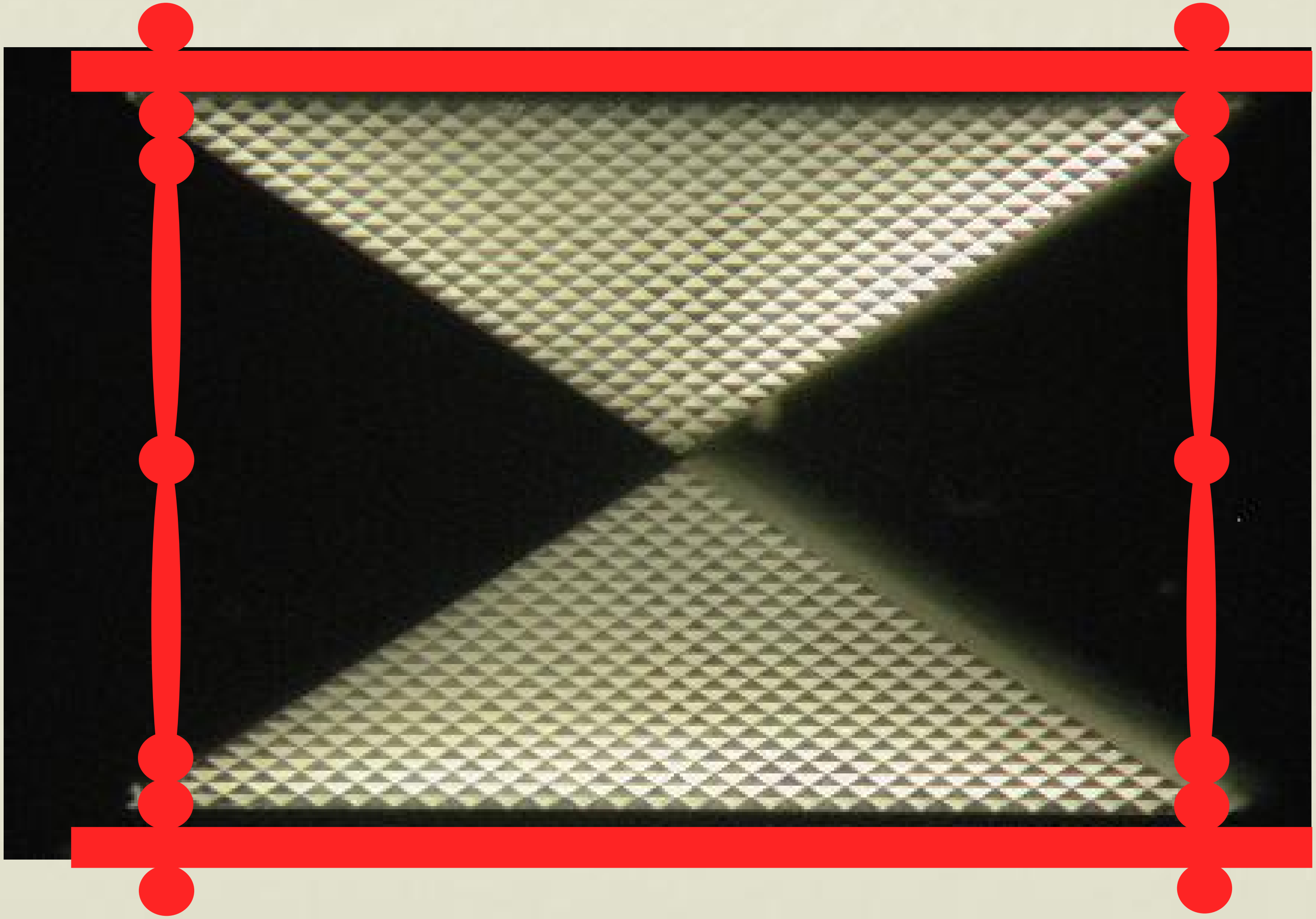

Jark et al,
JSR 11,
248 (2004)

Jark et al,
JSR 13,
239 (2006)

As before
D≈40 μm

for
SU8@8 keV
Si@12 keV

CLESSIDRA

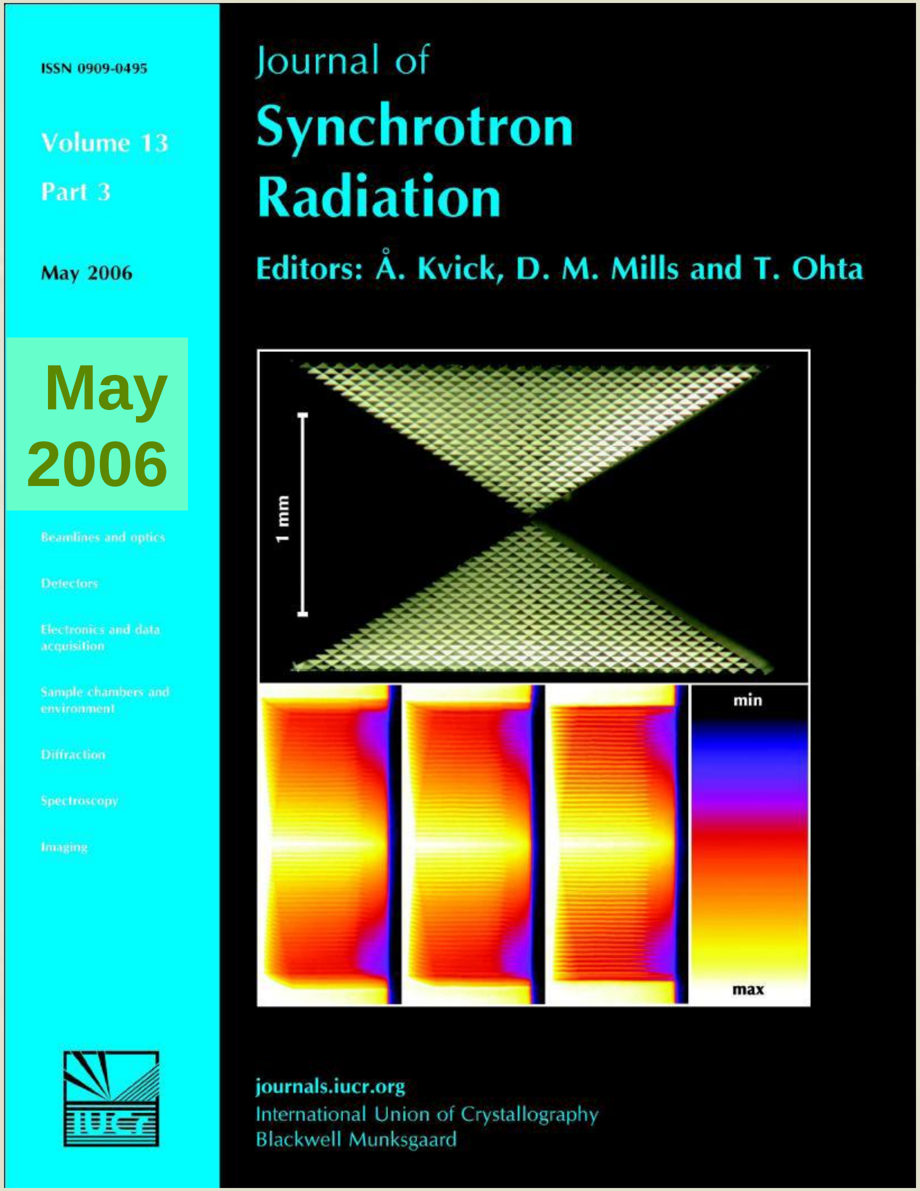

ISSN 0909-0495

Volume 13

Part 3

May 2006

Journal of Synchrotron Radiation

Editors: Å. Kvick, D. M. Mills and T. Ohta

May 2006

- Beamlines and optics
- Detectors
- Electronics and data acquisition
- Sample chambers and environment
- Diffraction
- Spectroscopy
- Imaging

journals.iucr.org
International Union of Crystallography
Blackwell Munksgaard

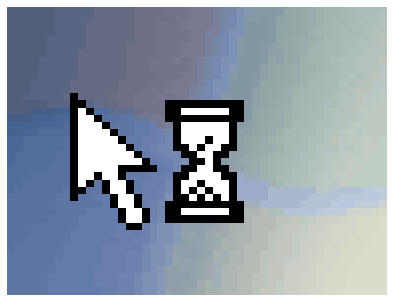

μXRF multilayer

Obviously would be a linear transmission grating

in sufficiently spatially coherent incident beam

Spatially incoherent incident beam

μXRF multilayer

CLESSIDRA is an array of tiny refracting prisms

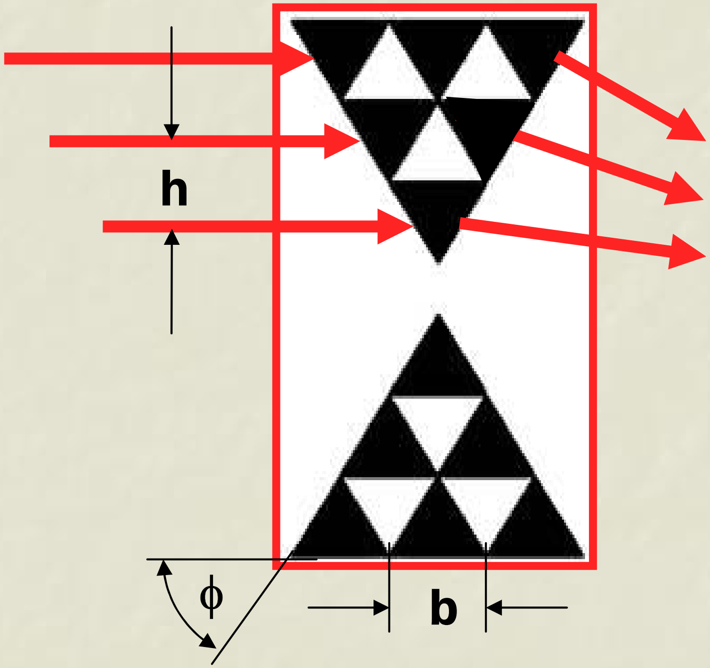

Deflection angle in prism

$$\Delta = \frac{2\delta}{\tan\phi} = \delta\frac{b}{h}$$

Distance to refractive focus

$$\Delta f = h$$

$$f_{ref} = \frac{h}{\Delta} = \frac{h\tan\phi}{2\delta} = \frac{h^2}{\delta b}$$

Can focus size be <h? NO!

We can use perfect prisms!

Rapidly alignable x-ray optics

μXRF
multilayer

Put it

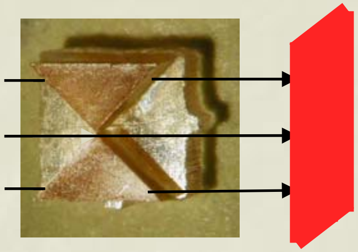

Radiography

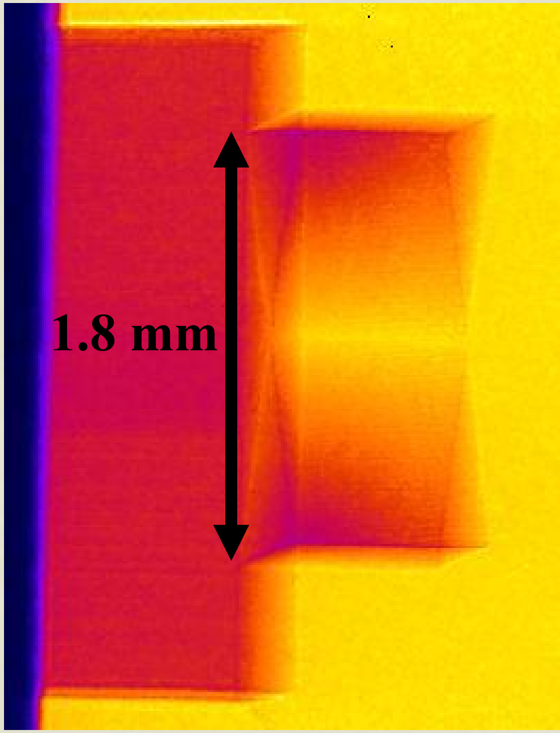

You see the clessidra shape

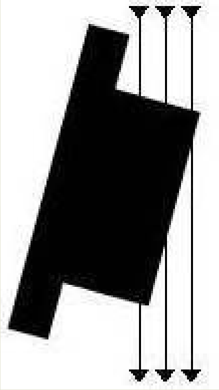

**Adjust
tilt, yaw, roll
for sharp
shadow**

SYRMEP beamline, 12 keV photon energy, CCD camera 9 μm pixel

Rapidly alignable x-ray optics

μXRF
multilayer

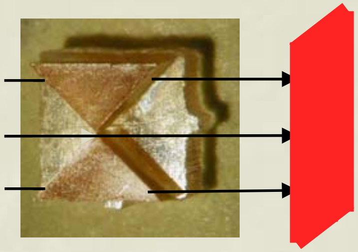

Radiography

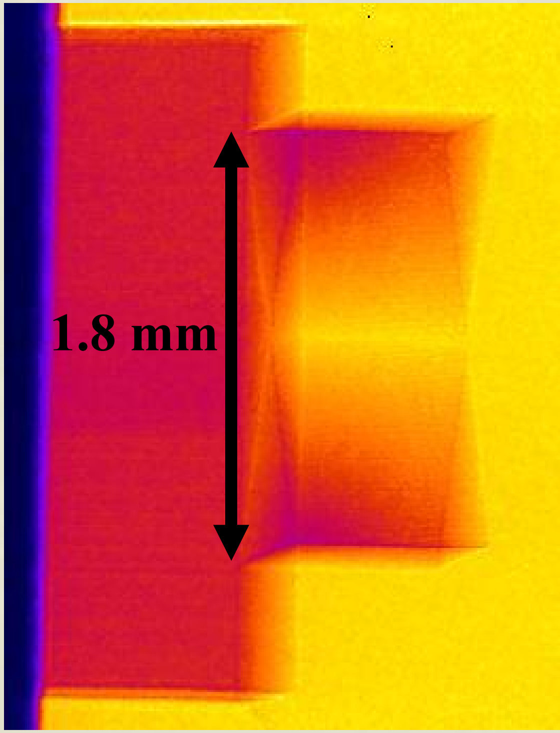

You are done.

Now you can go to refractive focus position.

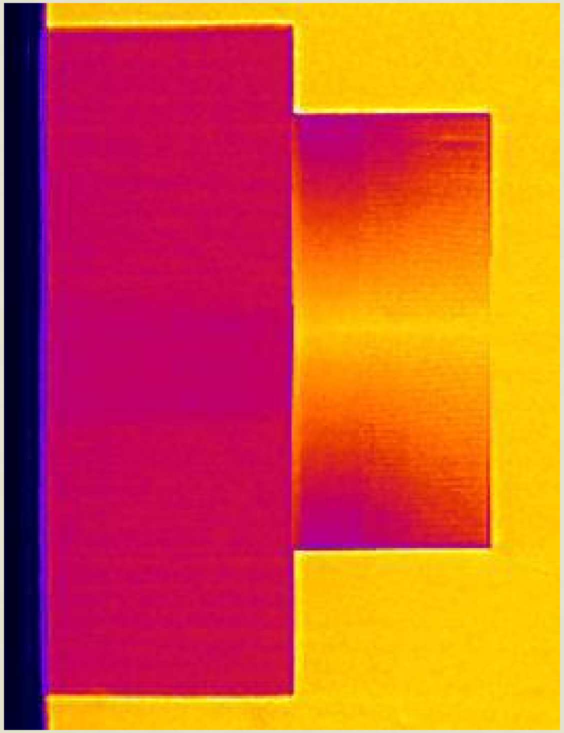

SYRMEP beamline, 12 keV photon energy, CCD camera 9 μm pixel

Rapidly alignable x-ray optics

µXRF
multilayer

10 m downstream
from lens
with h=12.83 µm

Gain in focus is 6x
Size is 110 µm (≈ hair)
lens efficiency = 25%

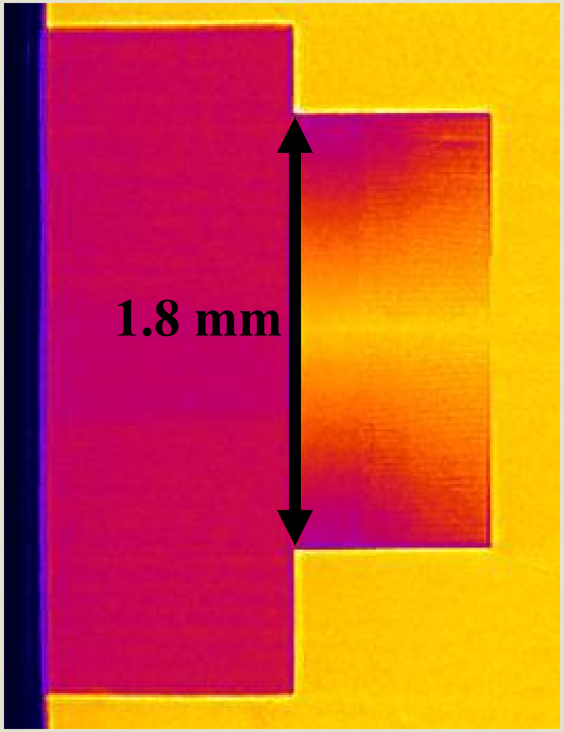

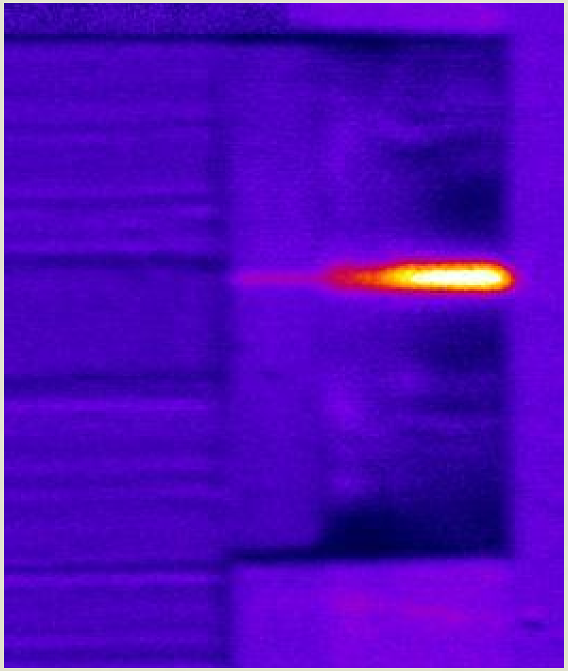

Same performance with
120 mm long mirror
with slope error <0.5”!

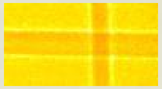

hair

See also Jark et al,
JSR 15, 411 (2008)

SYRMEP beamline, 19.5 keV photon energy, CCD camera 9 µm pixel

Rapidly alignable x-ray optics

with better beam coherence and high resolution CCD

µXRF
multilayer

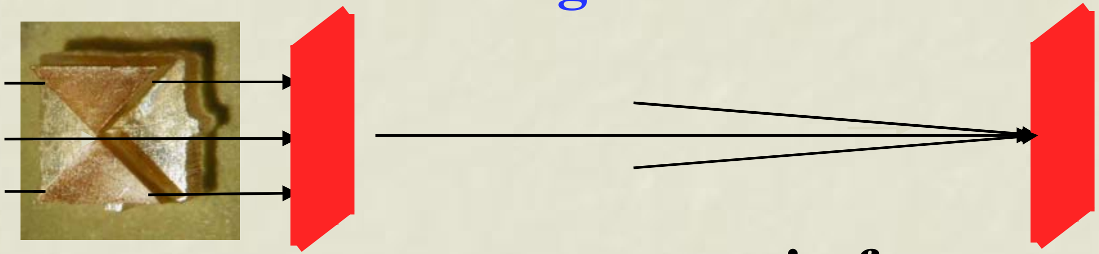

center

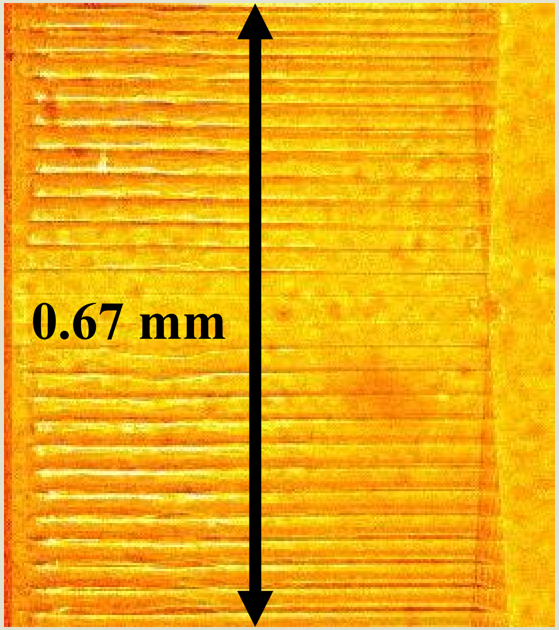

border

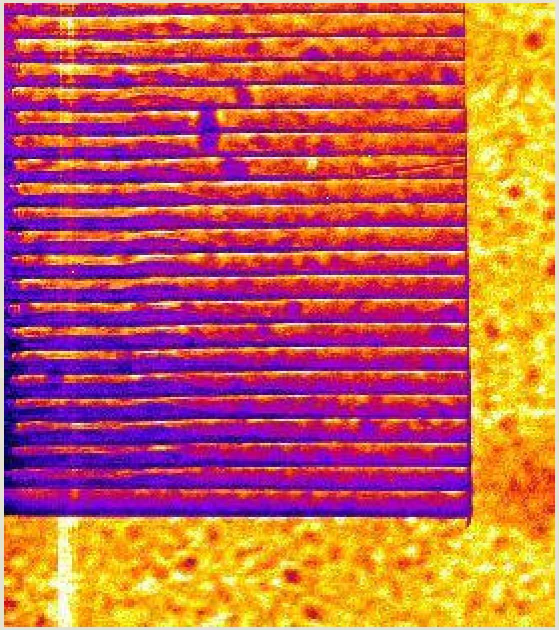

in focus (2.16 m)

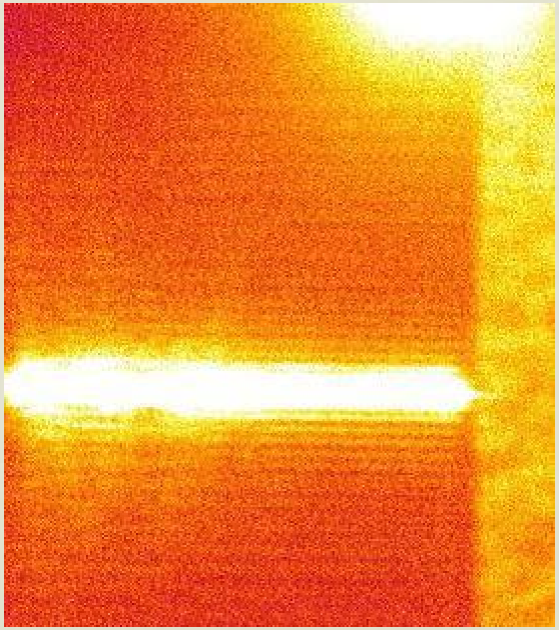

BM05(MOTB)@ESRF, 8 keV photon energy, CCD 0.65 µm pixel

Rapidly alignable x-ray optics

μXRF
multilayer

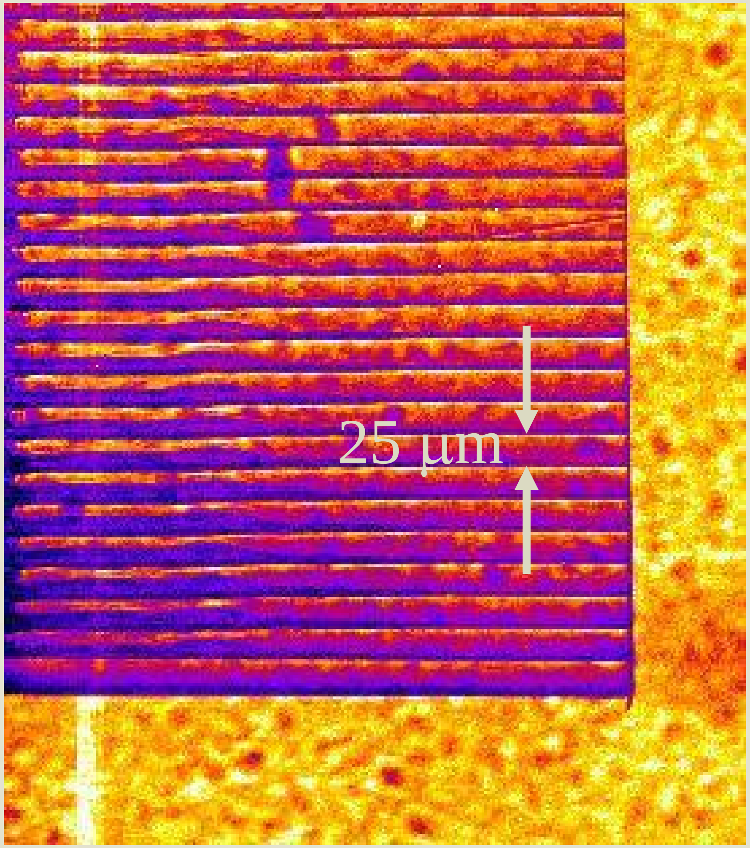

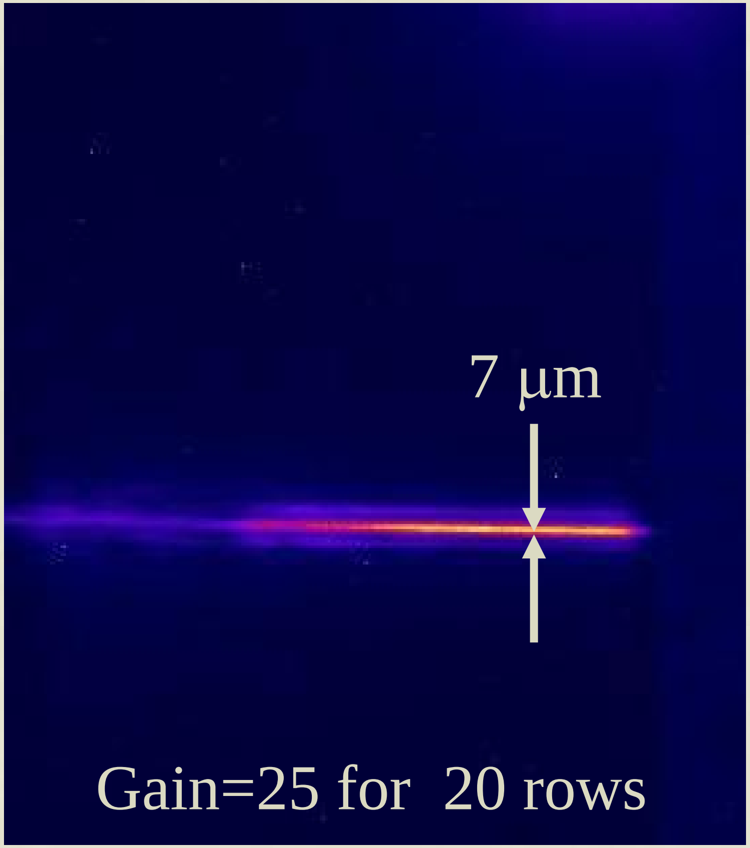

Gain=25 for 20 rows

hairs

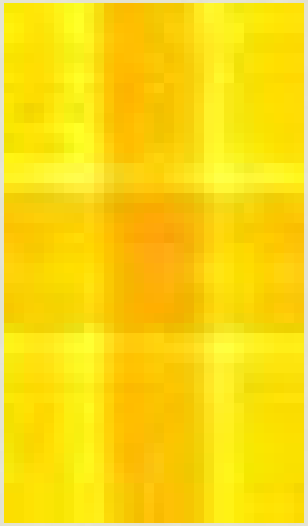

Is the focus size not correlated with prism height h??

Spatially COHERENT incident beam

μXRF multilayer

In near field or Fresnel regime an object with periodic transmission function is re-imaged at the Talbot distances

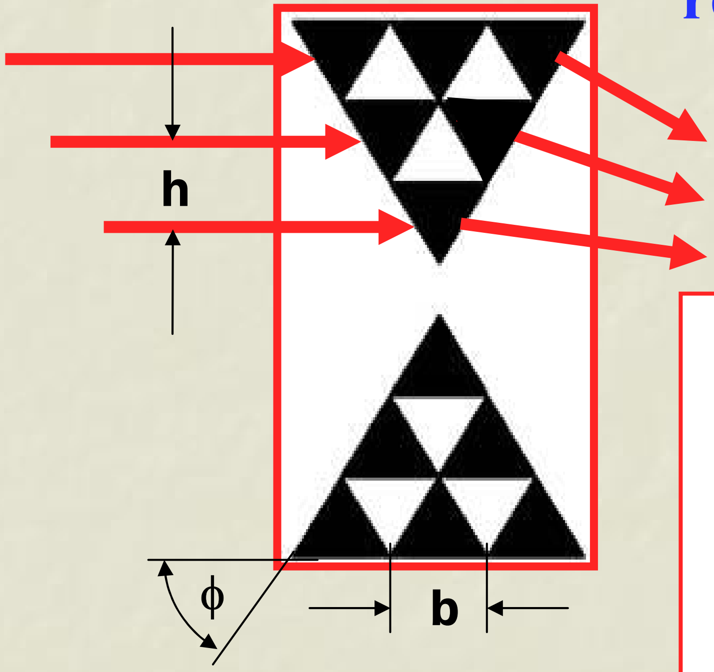

$$D_{Tal,k/l} = \frac{kh^2}{l\lambda}$$

k, l integers,
1/l demagnification factor

Now phase continuity required

$$b = D = \frac{m\lambda}{\delta}$$

fixing the refractive focal length to

$$f = \frac{h^2}{\delta b} = \frac{h^2}{m\lambda} = D_{Tal,k=1/l=m}$$

Operation restricted to discrete wavelengths

Some numbers

µXRF multilayer

f=1 m@ 8 keV
(λ=0.155 nm)

$$f = \frac{h^2}{m\lambda}$$

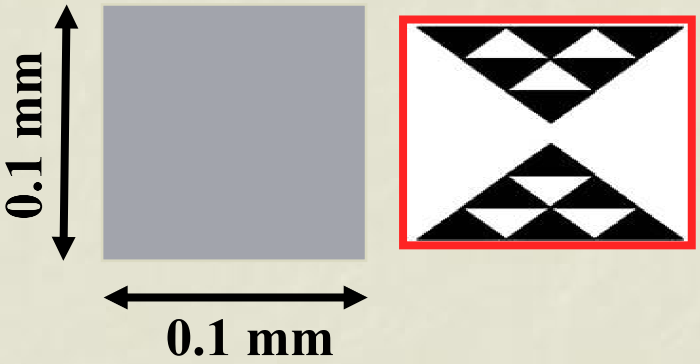

m=1

h independent of material: h= 12.45 µm

Needs lithography (we have one of few beamlines for deep x-ray lithography (DXRL) at ELETTRA)

in resists (pmma or SU8) b=36.7 µm

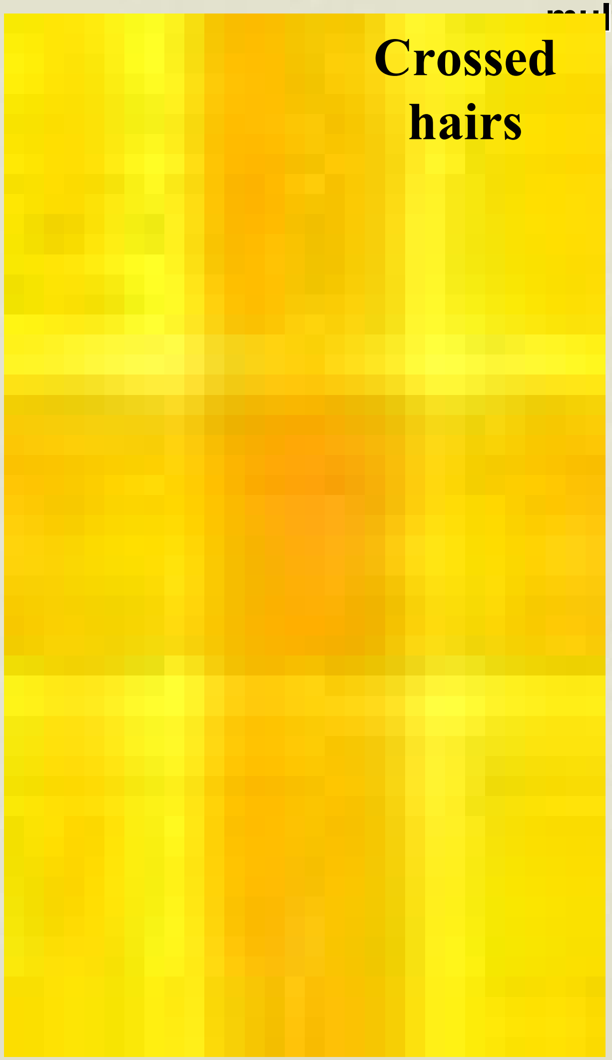

Some numbers

µXRF multilayer

Spatially coherently illuminated area:
$A=0.44\lambda q/s$

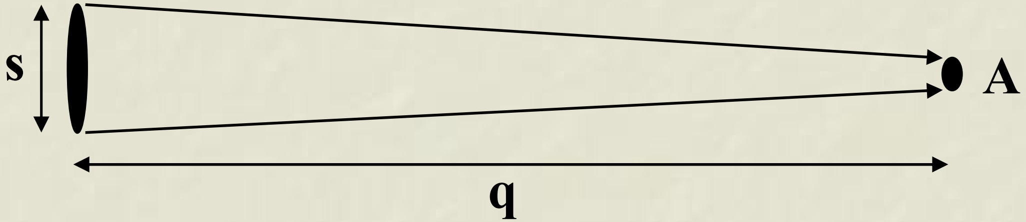

8 keV or λ=0.155 nm
SYRMEP (q=23 m, s=90 µm): A=17 µm
BM05 (q=53 m, s=85 µm): A=42 µm
ID22 (q=40 m, s=30 µm): A=91 µm

q=100m, s=23 µm: A=300 µm

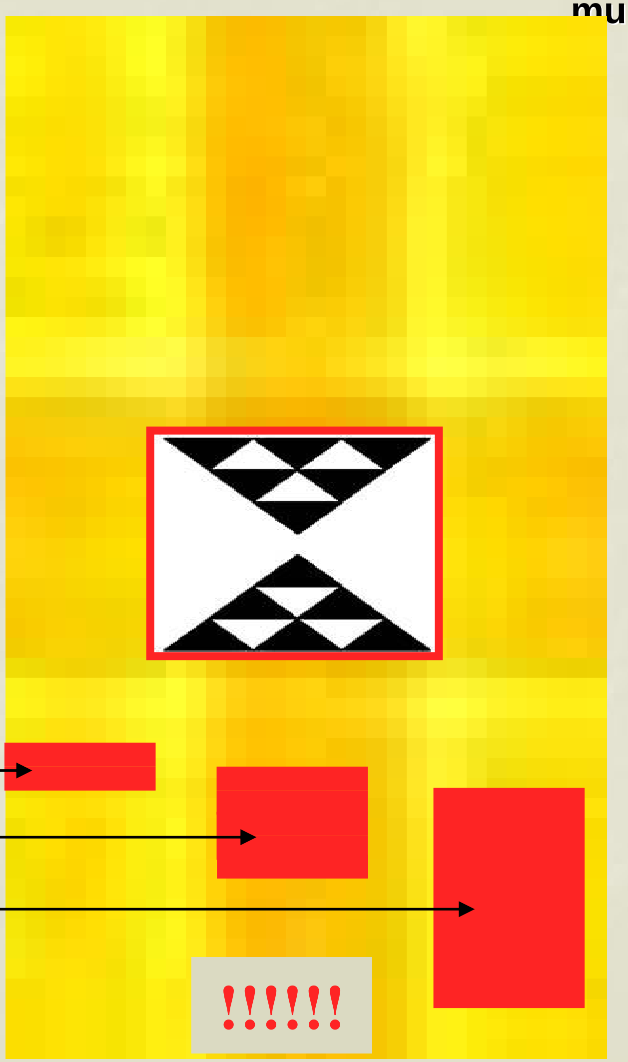

Quality control: transmission

µXRF

er

filling: 50%

pmma
h=25.7 µm
m=2, N=29

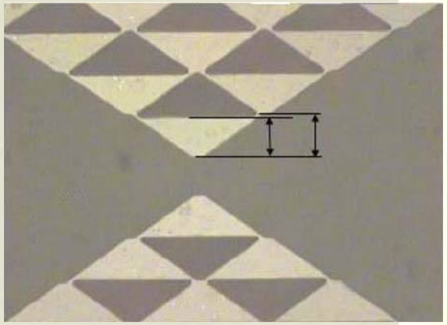

Contact radiography

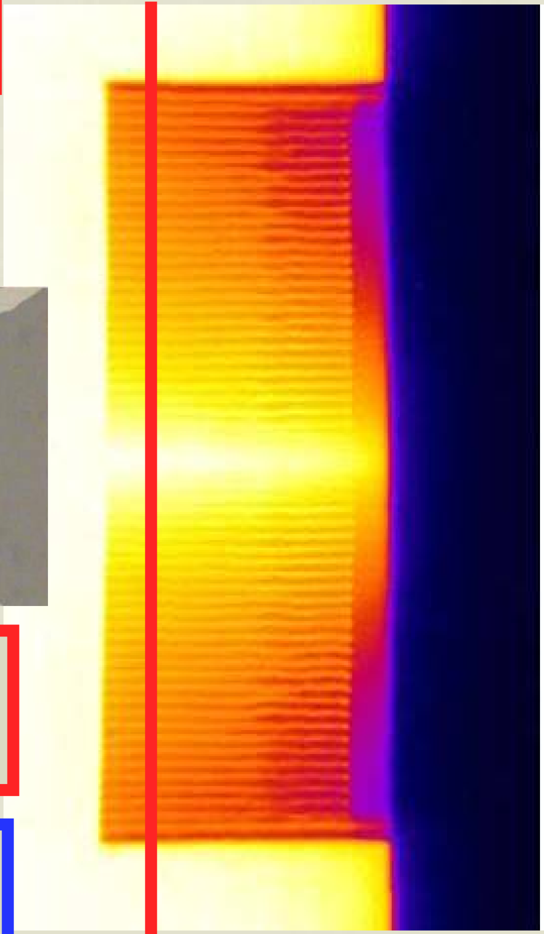

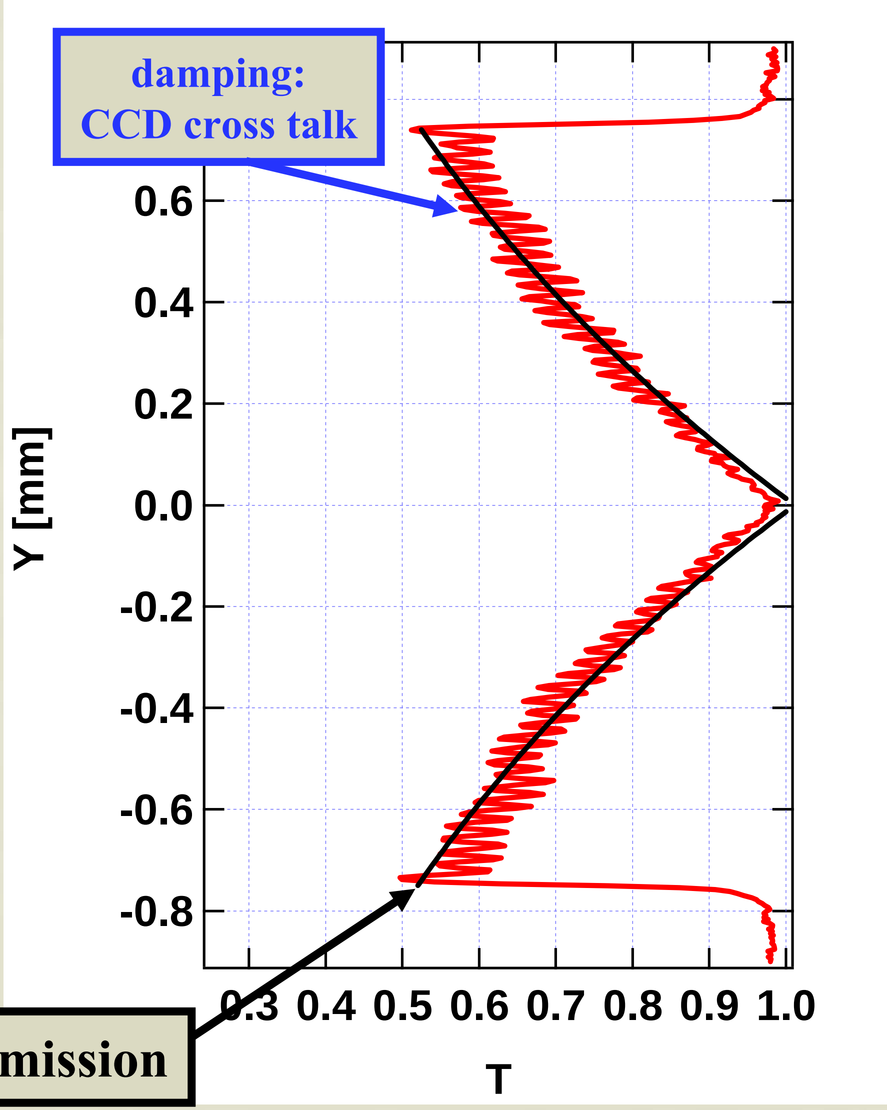

damping:
CCD cross talk

L_{exp}=1.612 mm at 8.5 keV

T variation in last row
0.25 ---- 1.0

expected average transmission

Quality control: refraction efficiency

μXRF

er

Slit scan (0.1 mm):
Flux integrated over
50 μm in focus

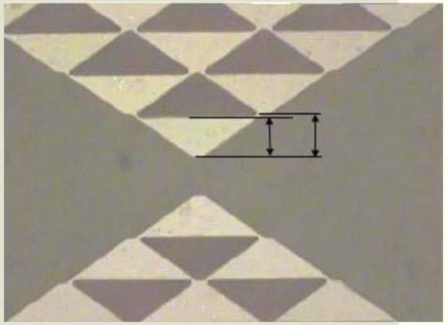

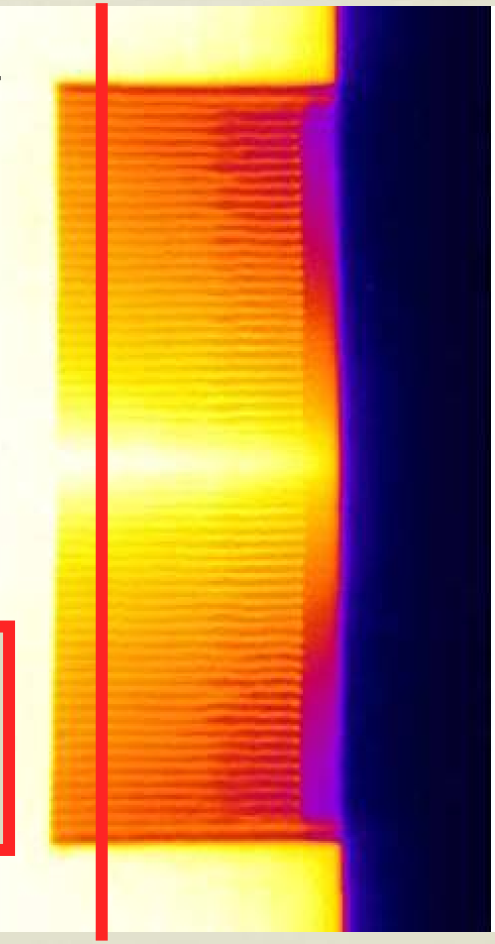

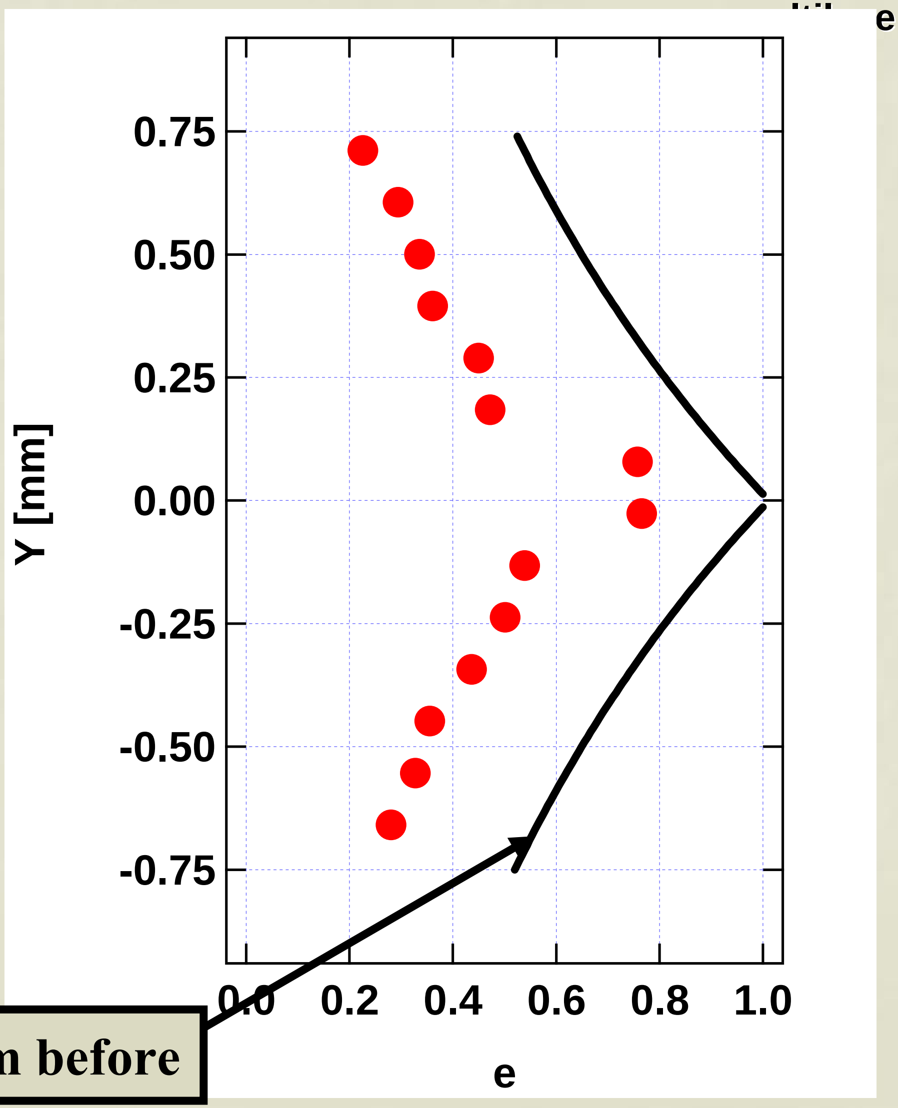

Relative efficiency
>50%
out to border

Rounding in connected prism tips

average transmission from before

Optimising the wavelength

illuminating 1.0 mm centered: 40 rows

pmma, m=2
h=25.7 μm

μXRF multilayer

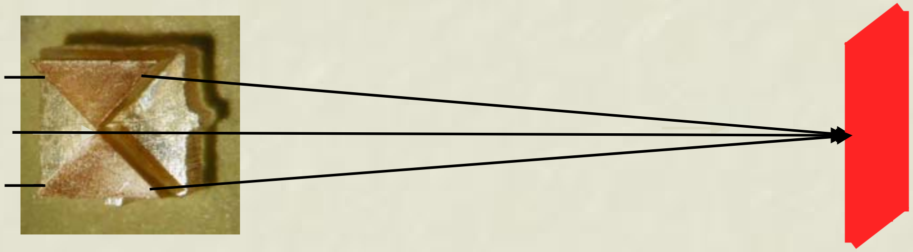

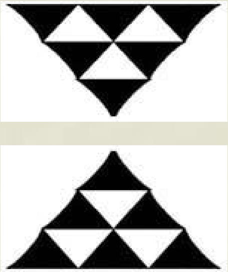

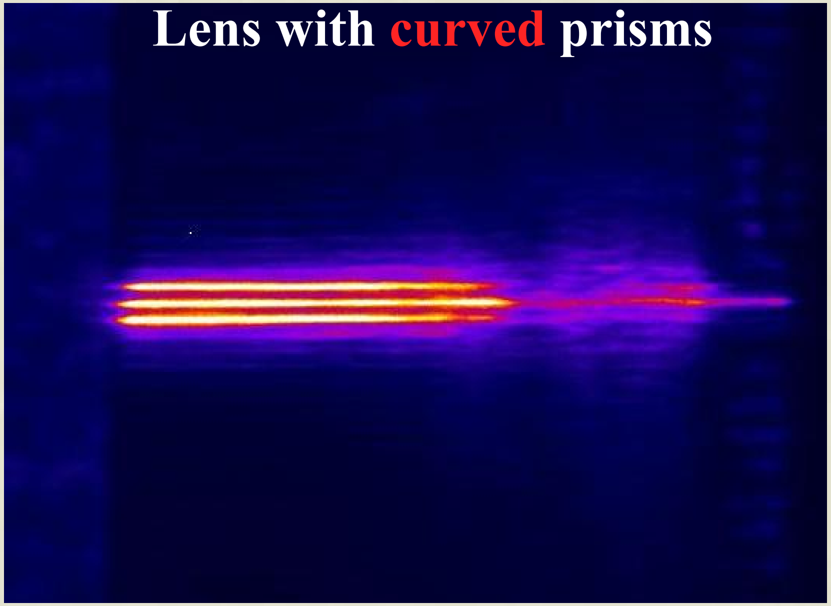

Peak width 4.0 μm

“Coherent” illumination

8.0 keV detuned

MOTB@ESRF (BM05-beamline)
CCD with 0.645 μm equivalent pixel

Optimising the wavelength

μXRF
multilayer

pmma, m=2
h=25.7 μm

illuminating 1.0 mm centered: 40 rows

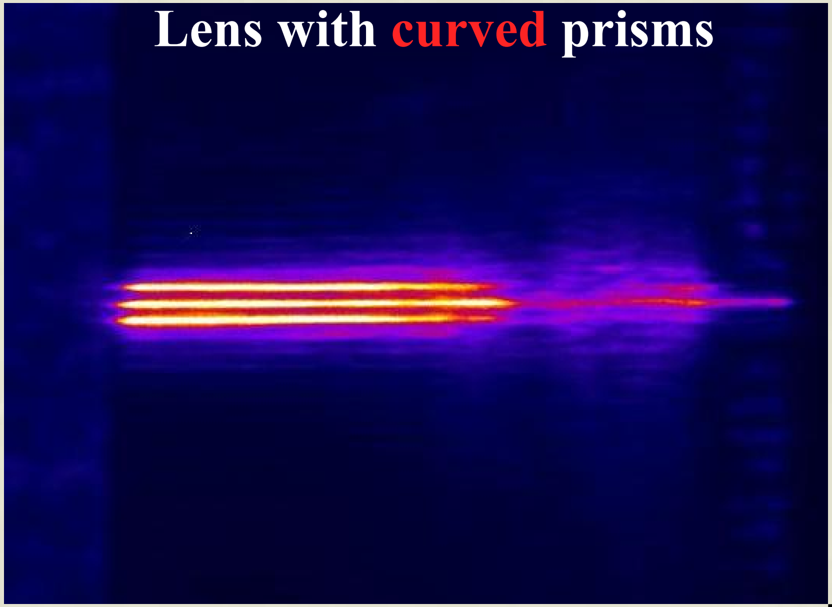

Lens with curved prisms

Distance scan: full aperture 1.5 mm

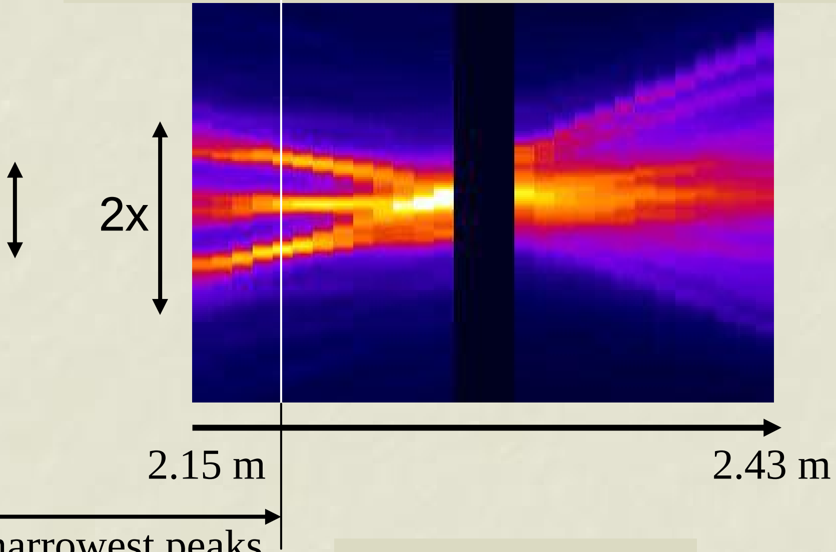

narrowest peaks

Peak width 4.0 μm

“Coherent” illumination

8.0 keV detuned

MOTB@ESRF (BM05-beamline)
CCD with 0.645 μm equivalent pixel

Optimising the wavelength

μXRF
multilayer

pmma, m=2
h=25.7 μm

illuminating 1.0 mm centered: 40 rows

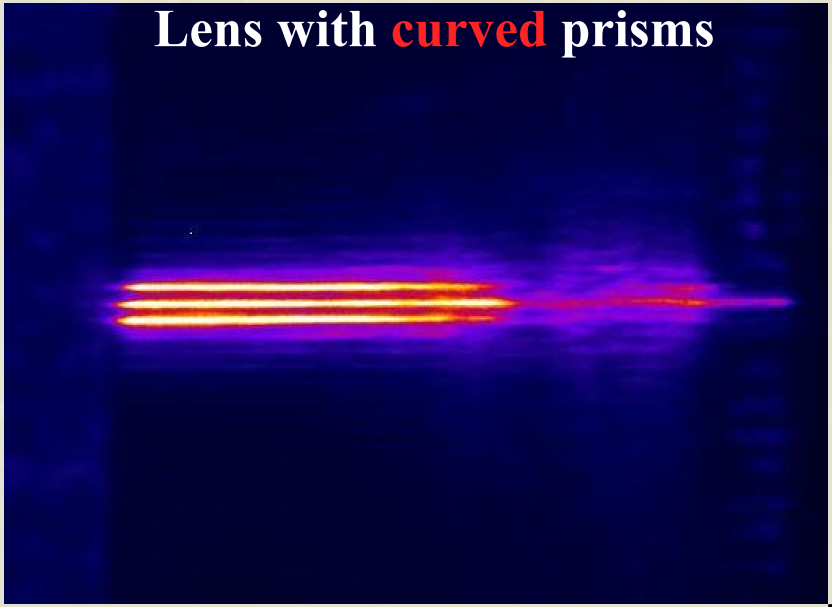

Lens with curved prisms

Distance scan: full aperture 1.5 mm

simulation

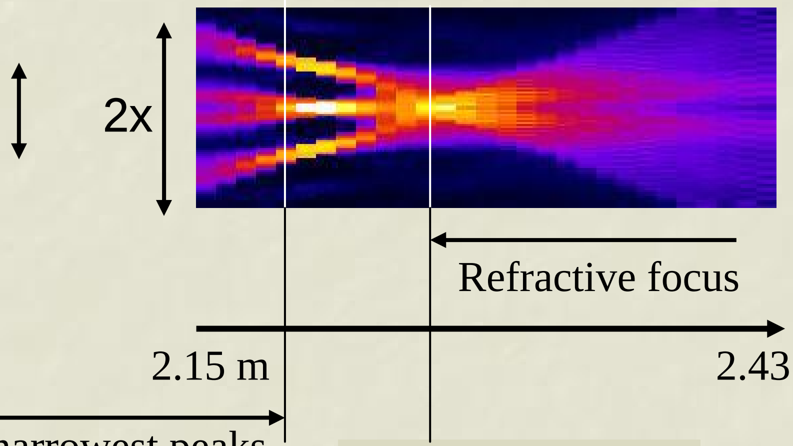

2x

Refractive focus

2.15 m

2.43 m

narrowest peaks

Peak width 4.0 μm

“Coherent” illumination

8.0 keV
detuned

MOTB@ESRF (BM05-beamline)
CCD with 0.645 μm equivalent pixel

Optimising the wavelength

μXRF multilayer

pmma, m=2
h=25.7 μm

illuminating 1.0 mm centered: 40 rows

Lens with curved prisms

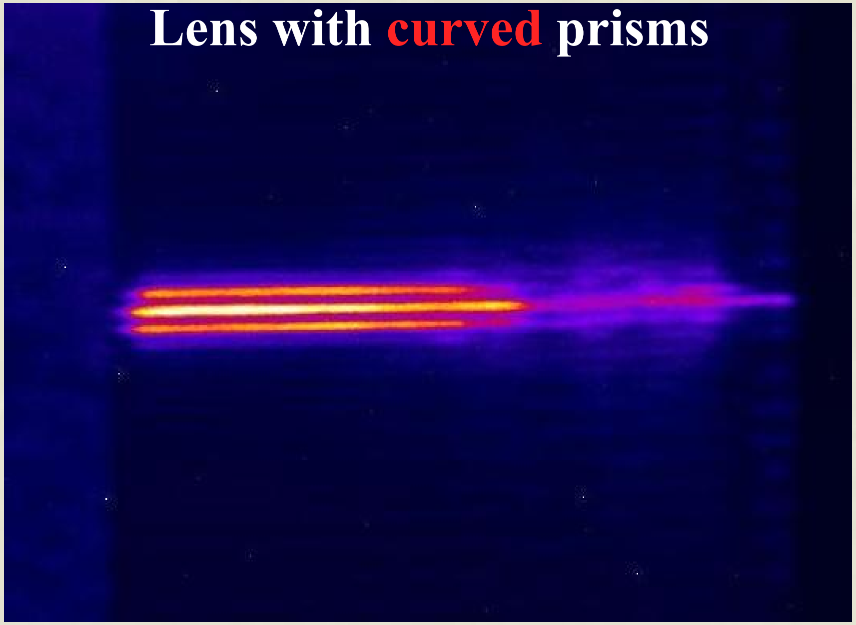

Another run (1 year later):
New monochromator
New E calibration

Vibrations:
Larger virtual source
→Wider peaks (expect 6.5 μm)
→reduced spatial coherence
(from 42 μm to 21 μm<h)

Peak width 7.3 μm

"Coherent" illumination

8.0 keV detuned

MOTB@ESRF (BM05-beamline)
CCD with 0.645 μm equivalent pixel

Optimising the wavelength

elettra
Synchrotron
Light
Laboratory

μXRF
multilayer

illuminating 1.0 mm centered: 40 rows

pmma, m=2
h=25.7 μm

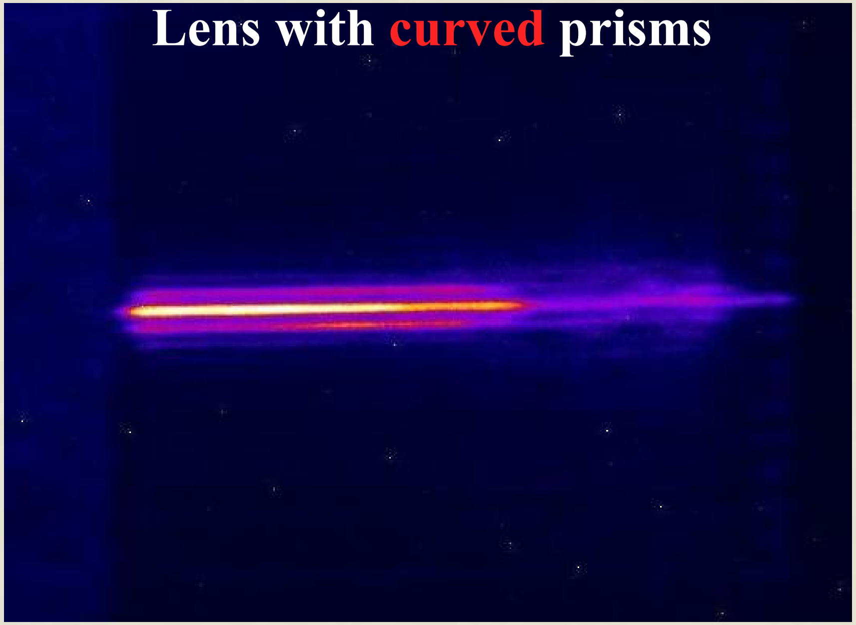
Lens with curved prisms

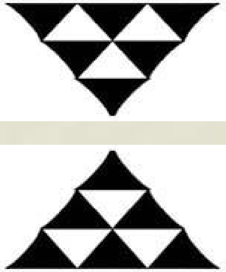

Peak width 6.6 μm

“Coherent” illumination

7.9 keV better tuned

MOTB@ESRF (BM05-beamline)
CCD with 0.645 μm equivalent pixel

Optimising the wavelength

μXRF
multilayer

illuminating 1.0 mm centered: 40 rows

pmma, m=2
h=25.7 μm

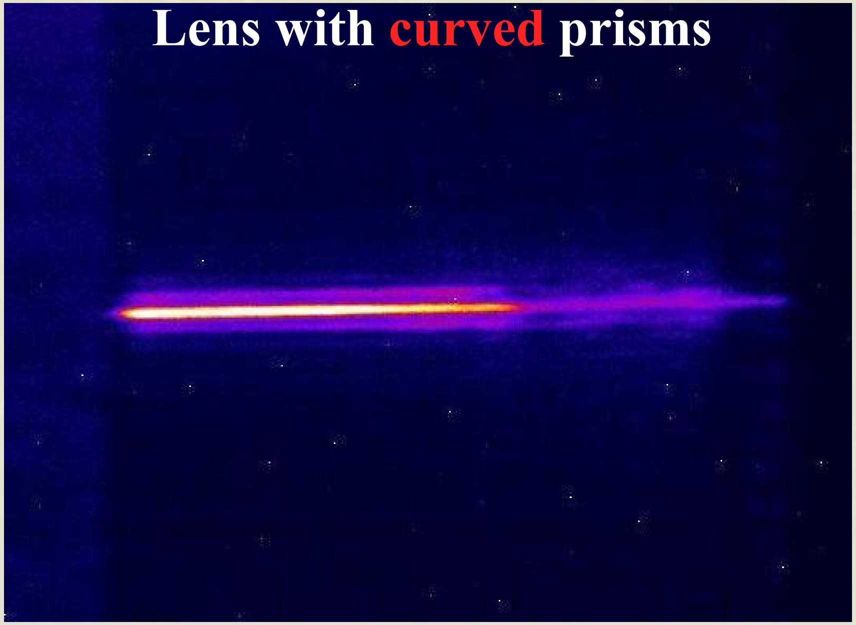
Lens with curved prisms

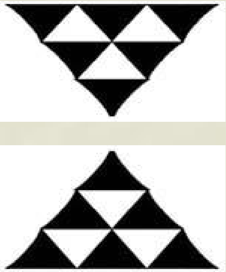

Peak width 5.7 μm

“Coherent” illumination

7.7 keV best tune

MOTB@ESRF (BM05-beamline)
CCD with 0.645 μm equivalent pixel

Optimising the wavelength

µXRF
multilayer

illuminating 1.0 mm centered: 40 rows

pmma, m=2
h=25.7 µm

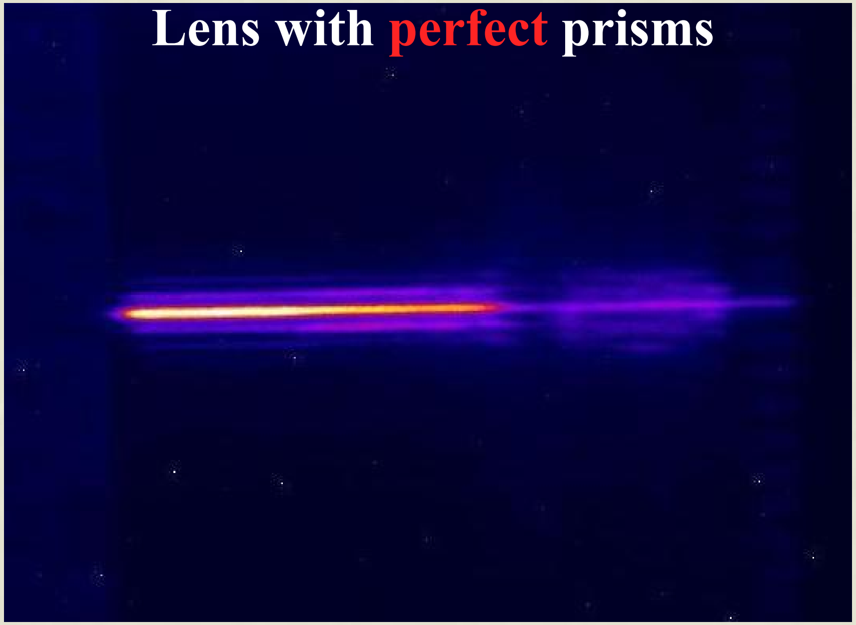

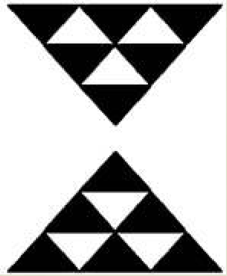

Peak width 6.5 µm

“Coherent” illumination

7.9 keV best tune

MOTB@ESRF (BM05-beamline)
CCD with 0.645 µm equivalent pixel

Optimising the wavelength

μXRF
multilayer

pmma, m=2
h=25.7 μm

illuminating 1.0 mm centered: 40 rows

Focusing horizontal source size

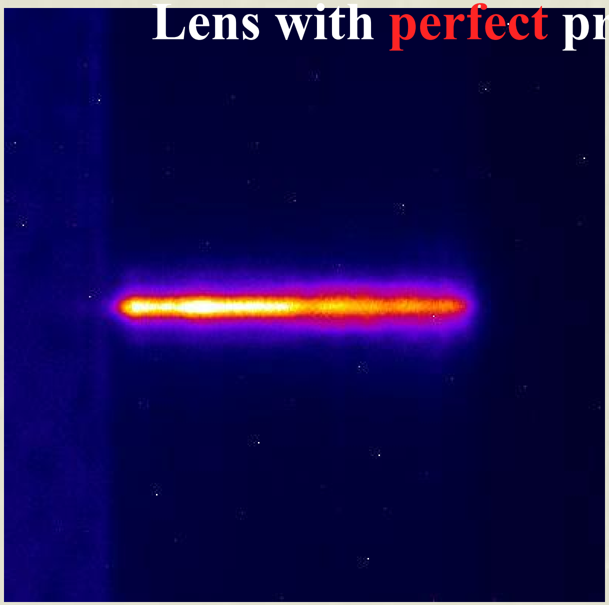

reduced spatial coherence
(from 21 μm to 13 μm<h)

Focus size is 12.5 μm =
expected demagnified source image
But also h/2

7.9 keV
best
tune

MOTB@ESRF (BM05-beamline)
CCD with 0.645 μm equivalent pixel

Refraction efficiency

µXRF multilayer

vertical focusing: illuminating 65 µm (3 rows) at 270 µm off-axis

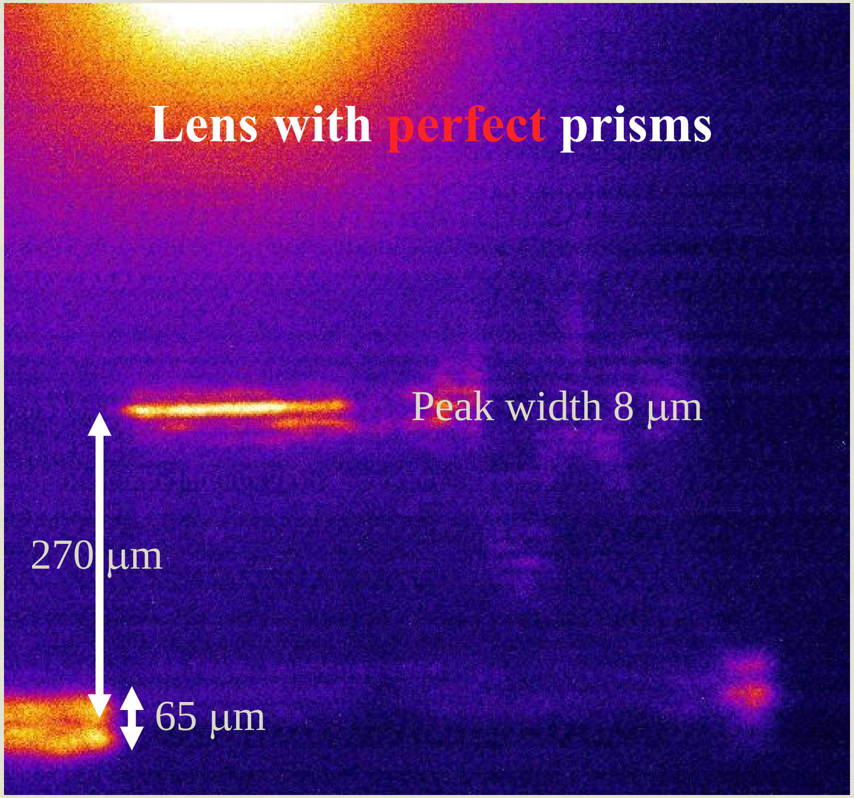

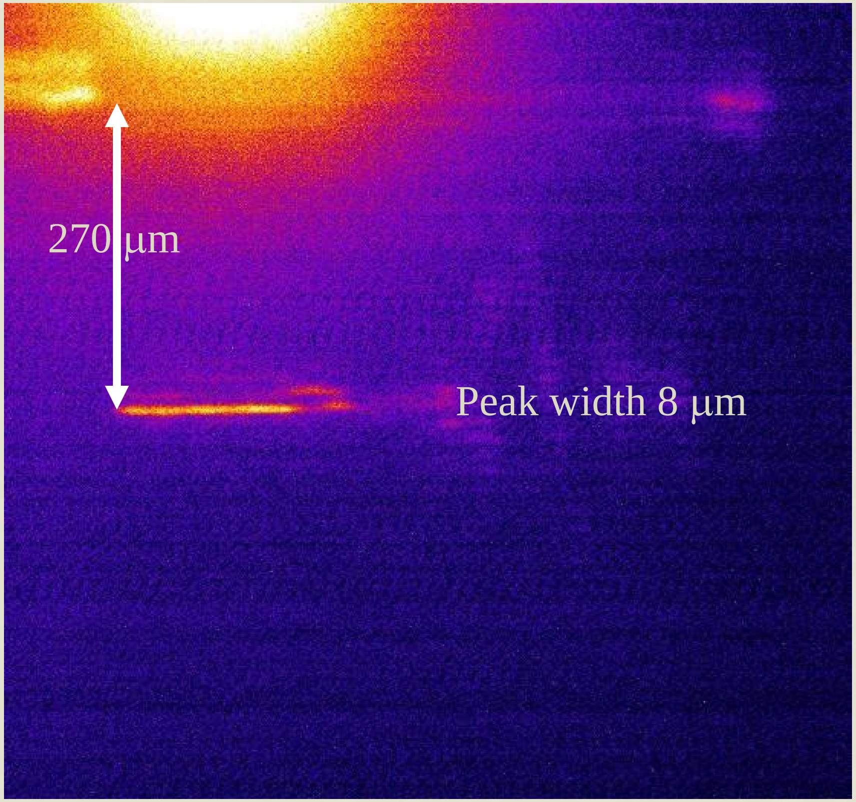

“Coherent” illumination

7.9 keV best tune

MOTB@ESRF (BM05-beamline)
CCD with 0.645 µm equivalent pixel

Refraction efficiency

µXRF multilayer

vertical focusing: illuminating 25 µm (1 row) at 270 µm off-axis

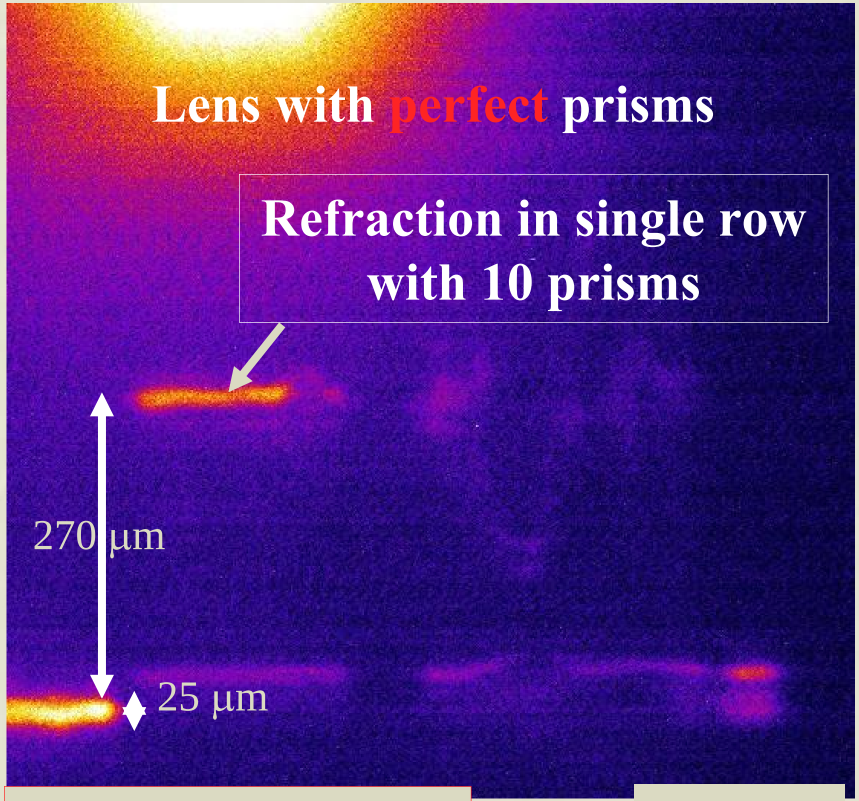

Lens with perfect prisms

Refraction in single row with 10 prisms

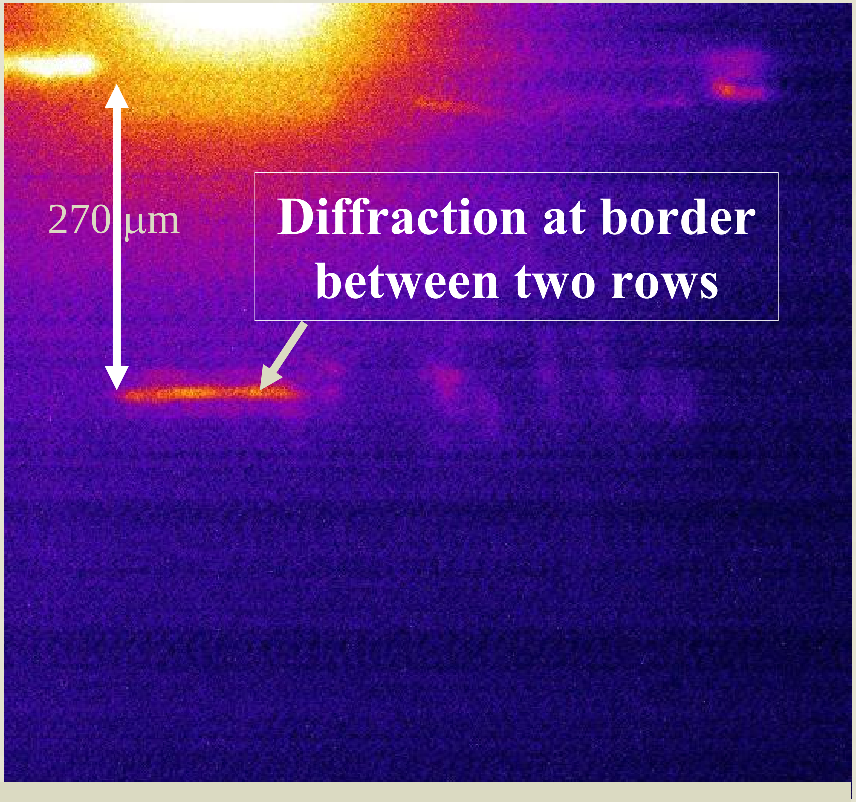

Diffraction at border between two rows

“Coherent” illumination

7.9 keV best tune

**MOTB@ESRF (BM05-beamline)
CCD with 0.645 µm equivalent pixel**

Refraction efficiency

µXRF multilayer

vertical focusing: illuminating 25 µm (1 row) at 270 µm off-axis

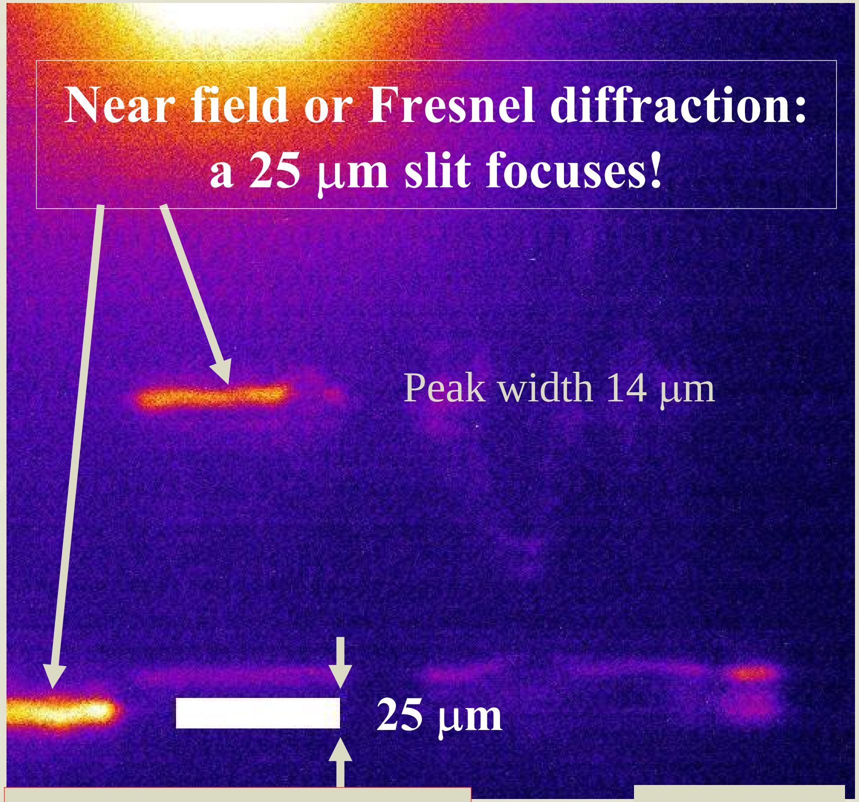

Near field or Fresnel diffraction: a 25 µm slit focuses!

Peak width 14 µm

25 µm

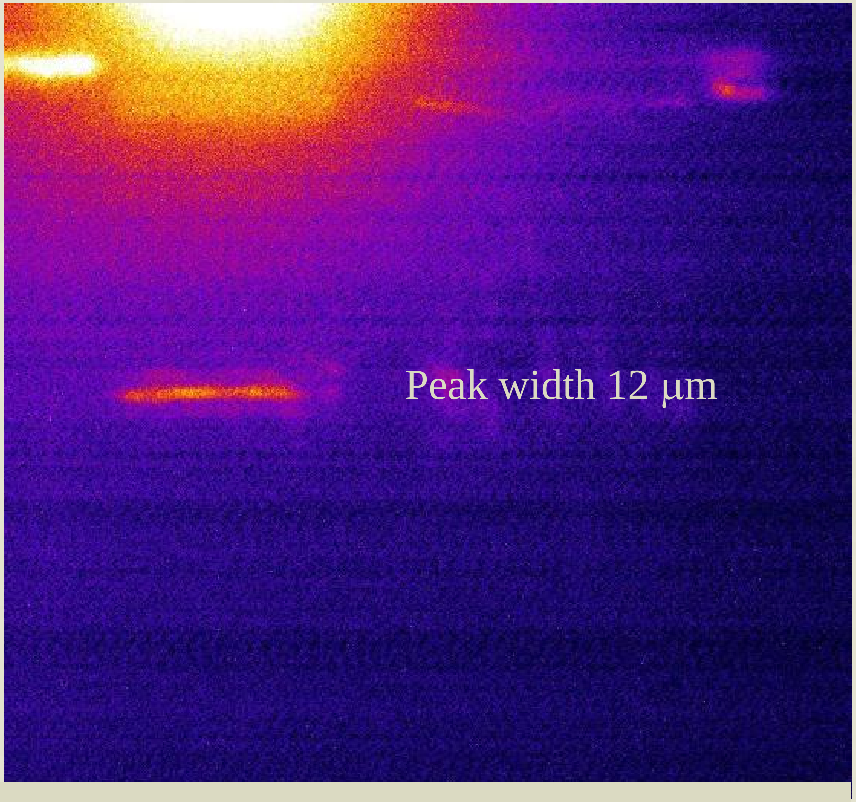

Peak width 12 µm

“Coherent” illumination

7.9 keV best tune

MOTB@ESRF (BM05-beamline)
CCD with 0.645 µm equivalent pixel

Outlook

μXRF
multilayer

De Caro and Jark, JSR 15, 176 (2008):

Found an analytical solution for the intensity distribution in focal plane for completely spatially coherent illumination!

Diffraction limited focus size identical for CLESSIDRA and concave parabolic lenses of same aperture: for aberrations corrected prisms AND for perfect prisms with m=1 and m=2!

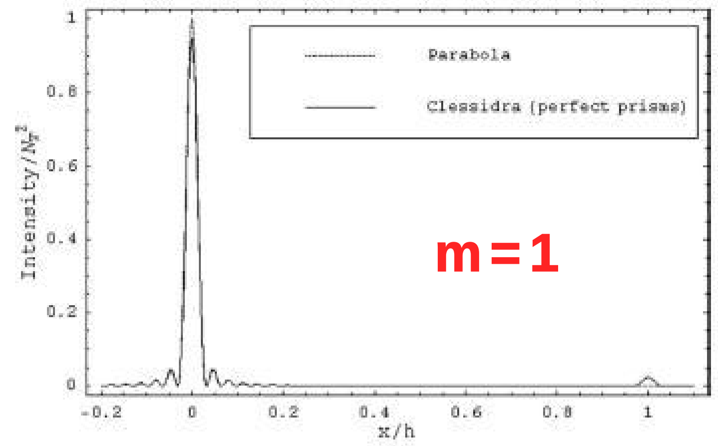

Reduction of maximum : 5%

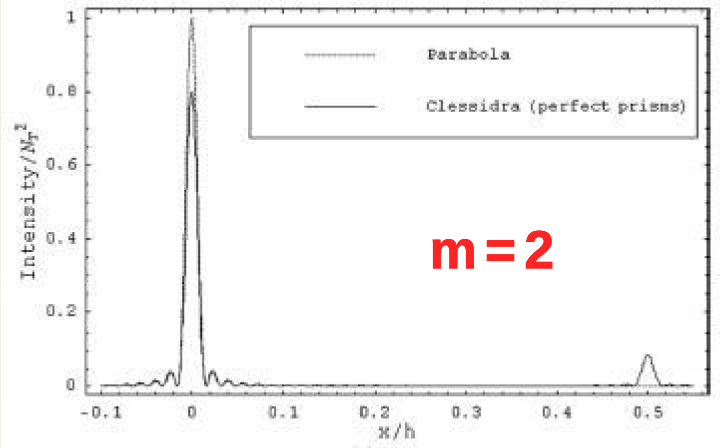

Reduction of maximum : 20%

Outlook

elettra
Synchrotron Light Laboratory

µXRF
multilayer

De Caro and Jark, JSR 15, 176 (2008):

Perfect prisms introduce periodic wavefield distortion into transmitted field. Peak-valley amplitude of distortion is λ/8 for m=1 and λ/4 for m=2!
The Rayleigh criterion for diffraction limited optics allows <λ/4 distortion!

Moderate loss of intensity into well localised secondary diffraction peaks.
To be blocked with pinholes upstream of focus.

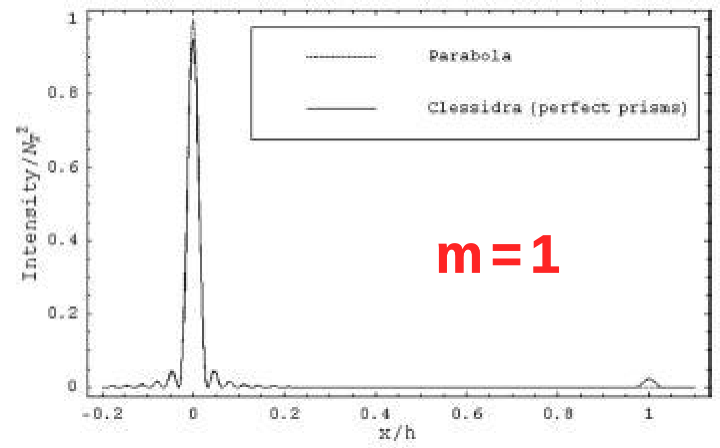

Reduction of maximum : 5%

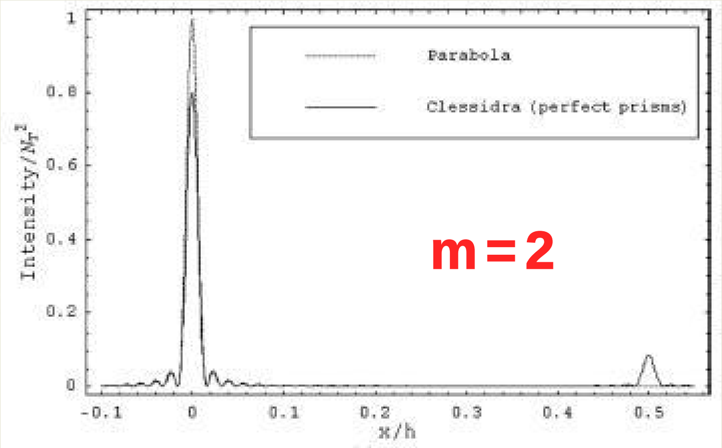

Reduction of maximum : 20%

Outlook: new concepts

B. Cederstroem et al, JSR 12, 340 (2005)

hair

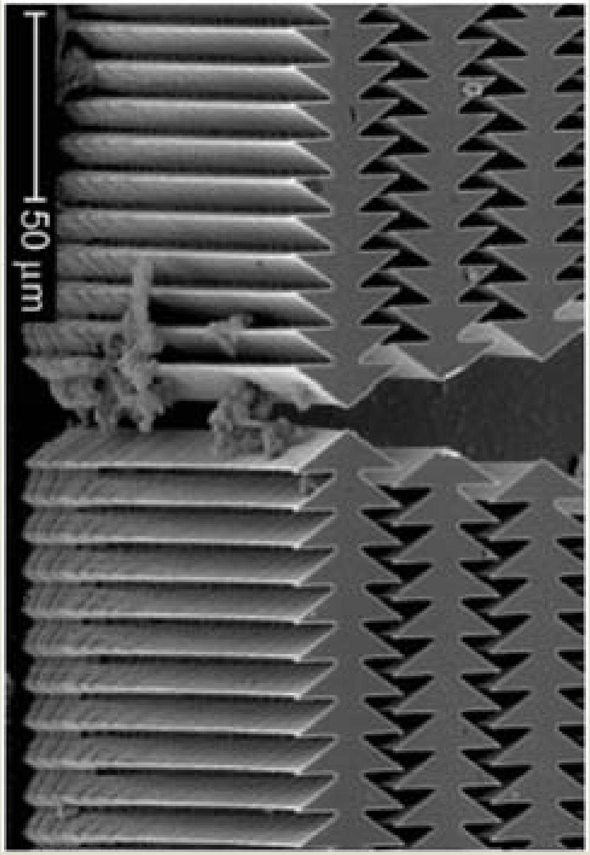

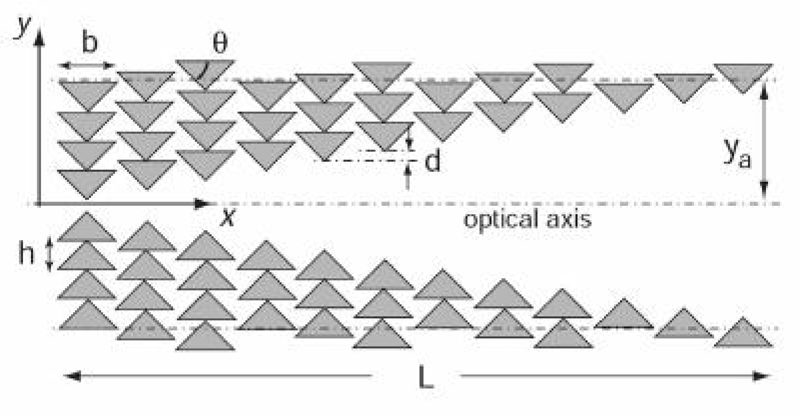

More absorbing, less distorting, larger peak separation, shorter focal length

problems in tips

Outlook: disconnect

elettra
Synchrotron Light Laboratory

µXRF
multilayer

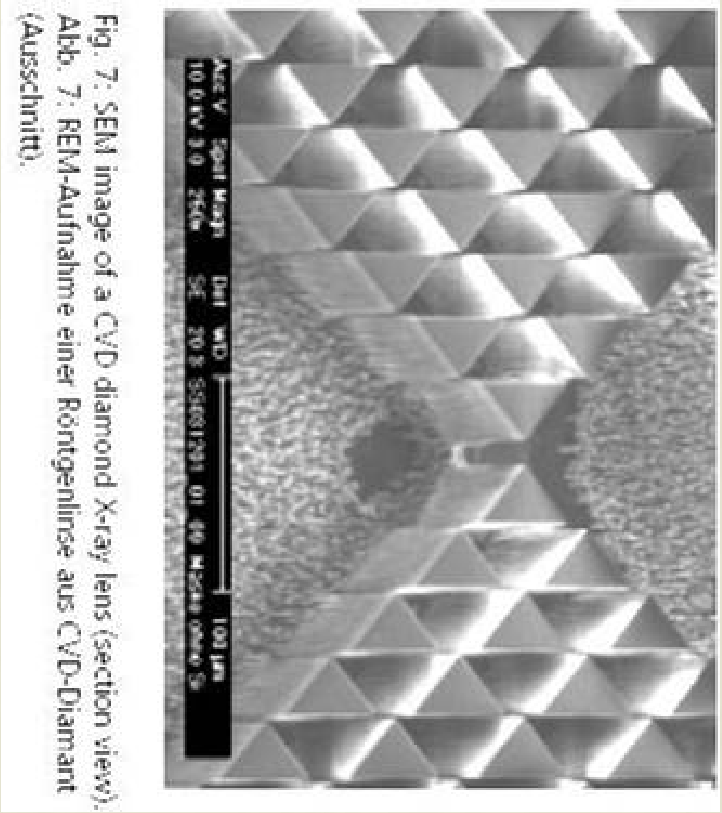

Fig. 7: SEM image of a CVD diamond X-ray lens (section view).
Abb. 7: REM-Aufnahme einer Röntgenlinse aus CVD-Diamant (Ausschnitt).

IAF, Fraunhofer, Freiburg

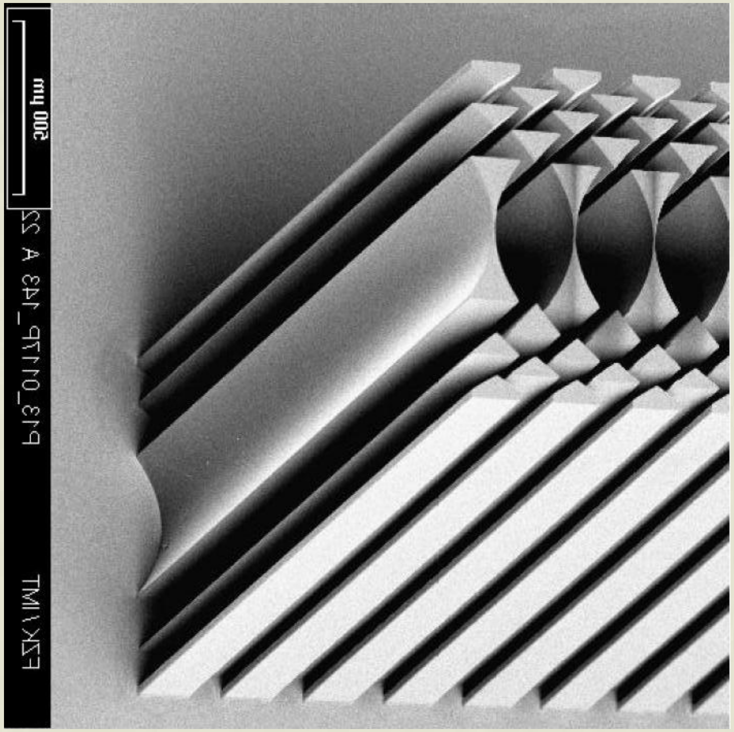

IMT @ FZK, Karlsruhe

get better tips with reduced rigidity

Outlook: depth/aperture match

This was for h=12.83 µm

Aperture is 140*h
Etching depth is only 25*h

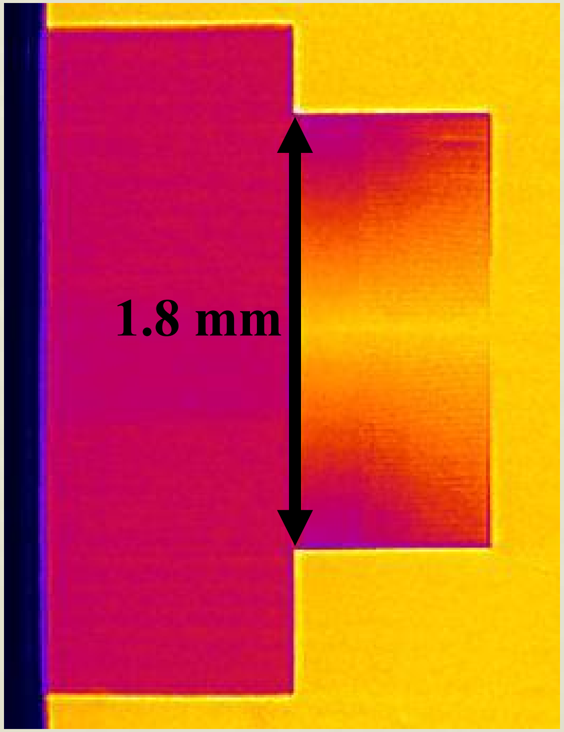

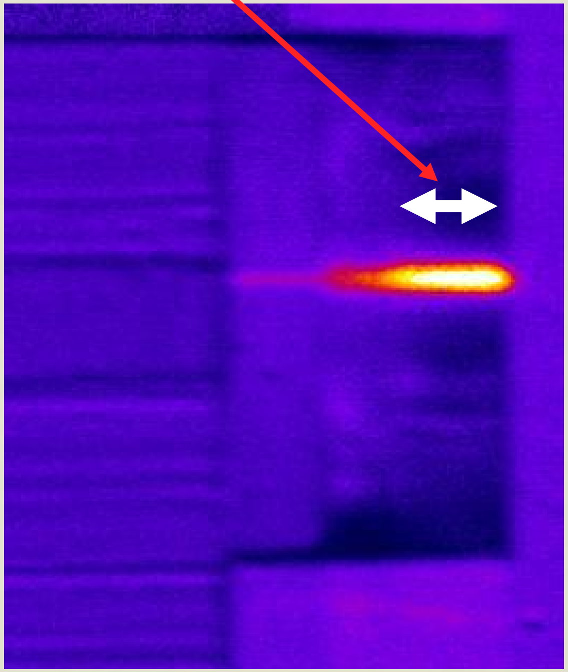

µXRF multilayer

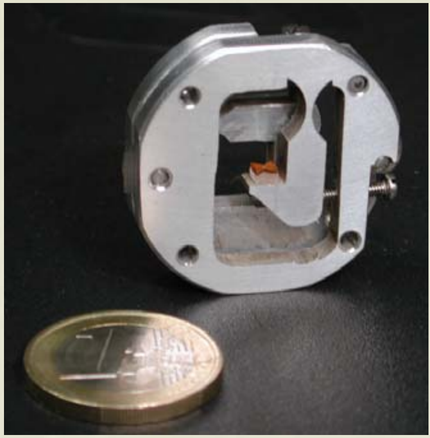

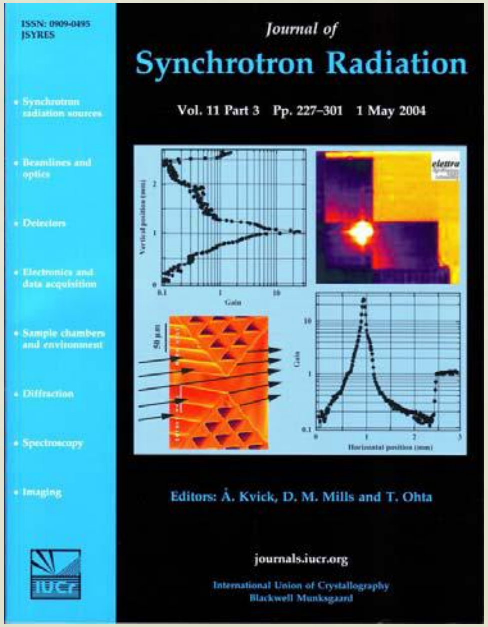

ISSN: 0909-0495
JSYRES

- Synchrotron radiation sources
- Beamlines and optics
- Detectors
- Electronics and data acquisition
- Sample chambers and environment
- Diffraction
- Spectroscopy
- Imaging

Journal of
Synchrotron Radiation

Vol. 11 Part 3 Pp. 227–301 1 May 2004

Editors: Å. Kvick, D. M. Mills and T. Ohta

journals.iucr.org

International Union of Crystallography
Blackwell Munksgaard

Conservative outlook

µXRF multilayer

Take A=25*h matched to depth of 25*h, as shown before

Stack M=2 or Cederstroem prism array

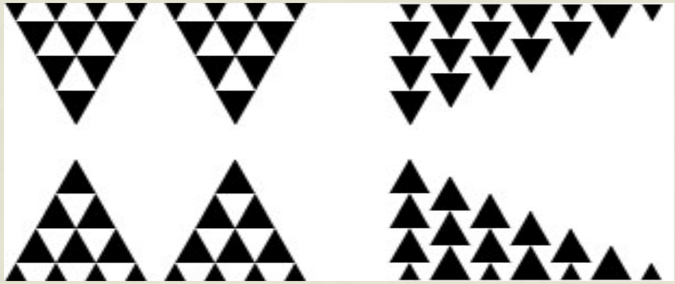

h=12 µm: A=0.3 mm and f=0.46 m @ 8 keV (λ=0.155 nm).

Spatial resolution limit r=0.88*λ*f/A r=210 nm!

!!needs spatially coherent beam, e.g. q=100 m for s=23 µm!!

image could be 110 nm

Average transmission >80%/>60% for one/bi-dimensional lens

More ambitious outlook

μXRF multilayer

Take A=50*h matched to depth of 50*h

Stack M=2 or Cederstroem prism array

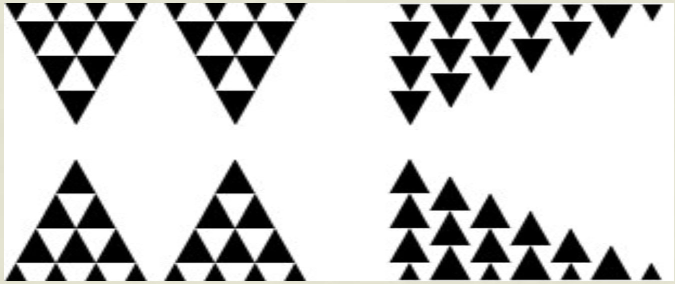

h=6 μm, A=0.3 mm and f=0.116 m @ 8 keV (λ=0.155 nm).

Spatial resolution limit r=0.88*λ*f/A r=53 nm!

!!needs spatially coherent beam, e.g. q=100 m for s=23 μm!!

image could be 27 nm

Average transmission ≈70%/≈50% for one-/bi-dimensional lens

Fresnel lens outlook

Evans-Lutterodt et al, PRL 99 (13), 134801 (2007)

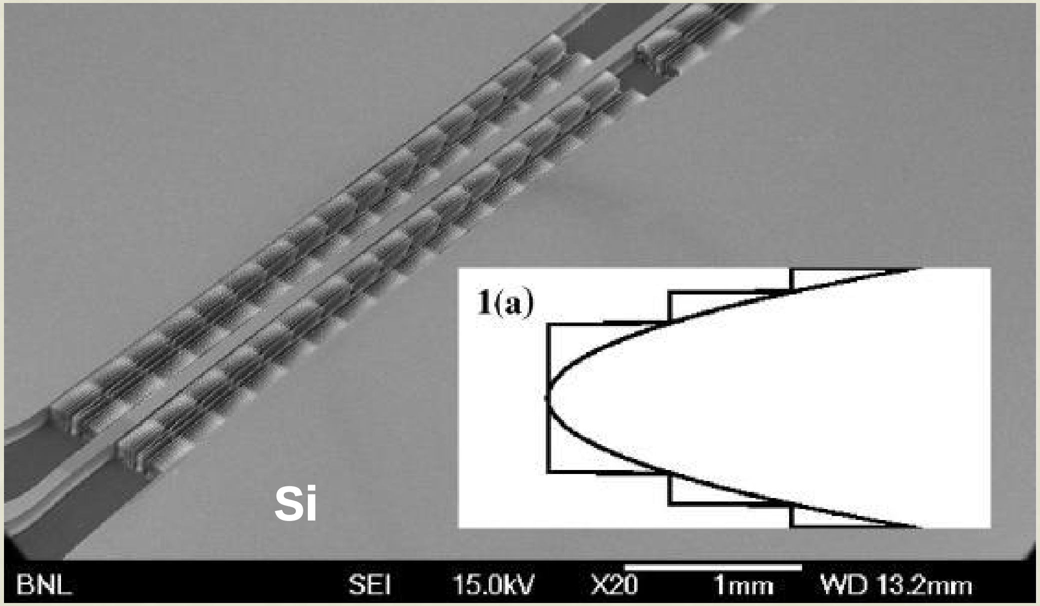

Arrived already at
A=0.3 mm, f=0.1 m
image size <<320 nm fwhm
Stein et al, JVST B26, 122 (2008),
priv. comm. Evans-Lutterodt

Only center segment is >6 μm!

Relative efficiency ≈25%
for segments ≈1.7 μm
and <10% for ≈0.7 μm

In Si better shape fidelity at smaller dimensions than in photoresist!
In turn etch depth limitation for RIE at 0.1 mm?

Fresnel lens outlook: adiabatic

Schroer et al, PRL 94, 054802 (2005)

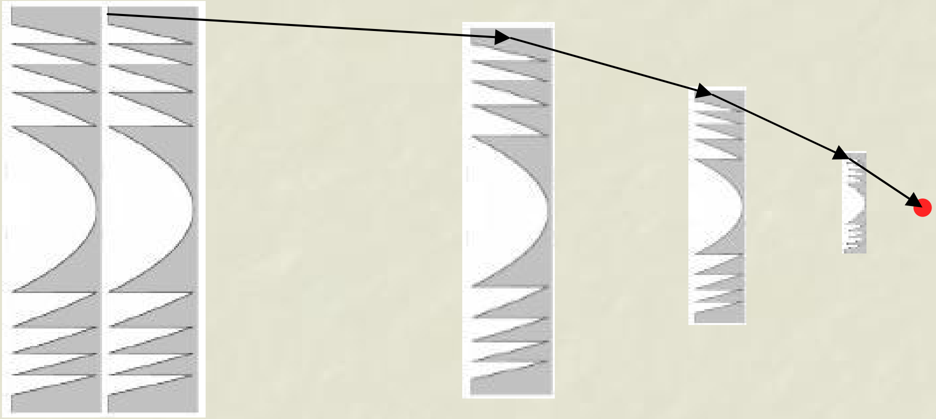

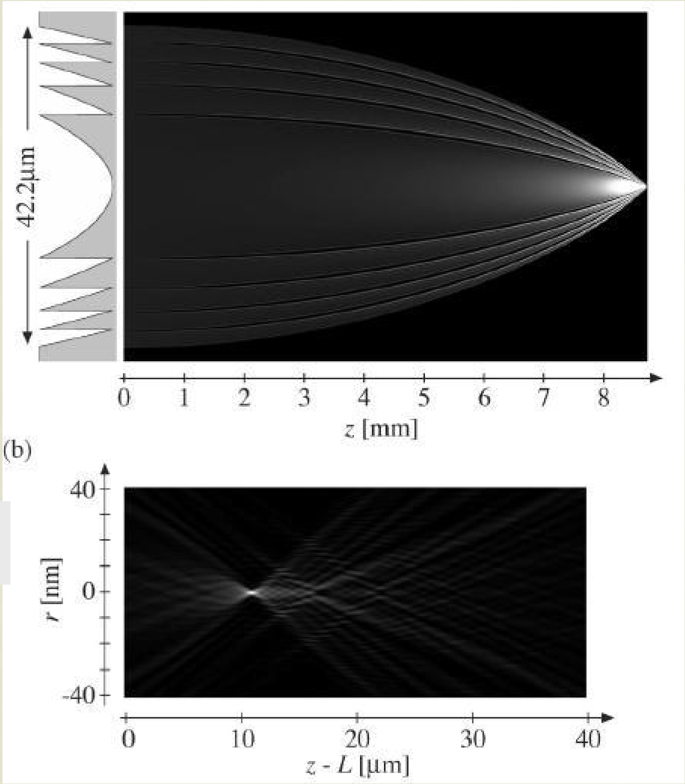

Follow adiabatically shrinking beam size

In 1166 lenses
Lens thickness: 37.8 µm … 0.100 µm
Lens aperture: 42.2 µm … 0.224 µm
Outer segment: 4.5 µm … 0.024 µm

focus r=2.21 nm @ 27.6 keV

Thank you for help

μXRF
multilayer

DXRL: Marco Matteucci, Fréderic Pérennès, Benedetta Marmiroli

IMM (Mainz): Laurence Singleton, Abdi Tunayar (EU action: EMERGE)

SYRMEP: Lucia Mancini, Giuliana Tromba, Luigi Rigon, Francesco Montanari, Ralf Hendrick Menk, Diego Dreossi
workshop: Gilio Sandrin, Ivan Cudin

IC-CNR: Liberato De Caro

ESRF-ID22: Jean Susini, Andrea Somogyi, Remi Tucoulou, Sylvain Bohic
ESRF-BM05: Anatoly Snigirev, Irina Snigireva

More about project:
http://www.elettra.trieste.it/experiments/beamlines/microfluo/docs/clessidra.pdf

Carolyn MacDonald

UAlbany Center for X-ray Optics

Outline

Structure of Polycapillaries
- Physics of Reflection, Bending Limits
- Divergence
- Alignment and Characterization
  - → Source Angle
  - → Transmission vs Energy
  - → Spot Size
- Gain and Liouville's Theorem
- Defect Analysis
- Applications
  - → MicroXR
  - → XR
  - → Astronomy
  - → Therapy

Polycapillary Optics

COLLIMATING

multifiber

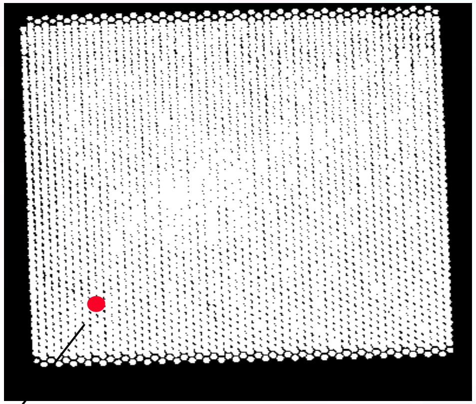

50 mm x 50 mm output
250 mm input focal length
12 µm channel

FOCUSING

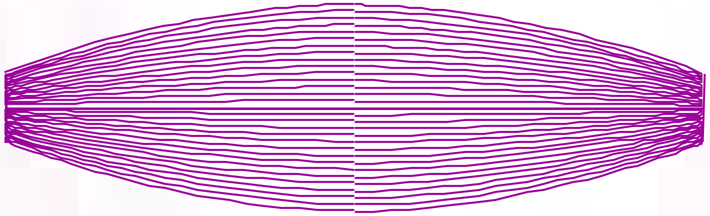

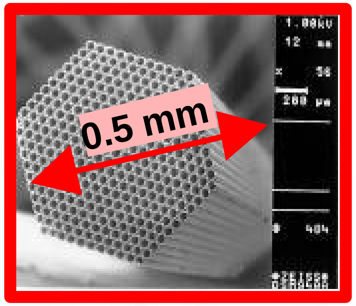

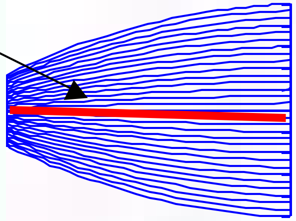

monolithic

How do they work? Maxwell's equations for a non-magnetic insulator:

$$\left.\begin{array}{l} \nabla \cdot \vec{E} = 0 \\ \nabla \cdot \vec{\ } = 0 \\ \nabla x \vec{E} = -\dfrac{\partial \vec{\ }}{\partial t} \\ \nabla x \vec{\ } = \mu_o \in \dfrac{\partial \vec{E}}{\partial t} \end{array} \right\} \Rightarrow \begin{array}{l} \dfrac{\partial^2 \vec{E}}{\partial t^2} = \dfrac{1}{\mu_o \in} \nabla^2 \vec{E} \\ v = \dfrac{1}{\sqrt{\mu_o \in}} = \dfrac{1}{\sqrt{\mu_o \in_o}} \sqrt{\dfrac{\in_o}{\in}} = \dfrac{c}{n} \end{array}$$

$$\Rightarrow \quad \text{n,index of refraction} = \sqrt{\frac{\in}{\in_o}}$$

So, given an incident plane wave of the form:

$$\vec{E} = \vec{E}_o e^{i\omega t}$$

we expect a response

$$\vec{\ } = \in \vec{E} = \in_o \vec{E} + \vec{P}$$

hence

$$\vec{\ } = \in \vec{E} = \in_o \vec{E} + \vec{P} \Rightarrow \qquad \in = \in_o + \frac{\vec{P}}{\vec{E}}$$

Need to model the response, P of the material to the EM wave

Free Electrons in one dimension:

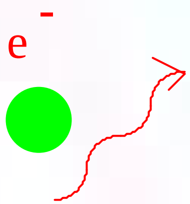

$$E = E_o \cos \omega t$$

$$P = \quad x$$

number of electrons per volume

charge on an electron

x displacement of the electron due to the electric field

$$F = m\ddot{x} = qE = qE_o \cos \omega t$$

$$x = x_o \cos \omega t$$

$$\Rightarrow -m\omega^2 x_o = qE_o \Rightarrow x_o = \frac{-qE_o}{m\omega^2}$$

$$P_o = Nqx_o = \frac{-Nq^2}{m\omega^2}E_o$$

$$\Rightarrow \in = \in_o + \frac{-\quad {}^2}{m\omega^2} = \in_o\left(1 - \frac{\frac{\quad {}^2}{m\in_o}}{\omega^2}\right)$$

$$\in = \in_o\left(1 - \frac{\omega_p^2}{\omega^2}\right)$$

Index of Refraction

$$n = \sqrt{\frac{\varepsilon}{\varepsilon_o}} = \sqrt{1-\frac{\omega_p^2}{\omega^2}} \approx 1-\frac{1}{2}\frac{\omega_p^2}{\omega^2} \quad = 1-\delta$$

$$\Rightarrow \quad \delta = \frac{1}{2}\left(\frac{30\text{ eV}}{10\quad \text{eV}}\right)^2 \approx 4.5\times10^{-6}$$

Consequences for normal incidence mirror:

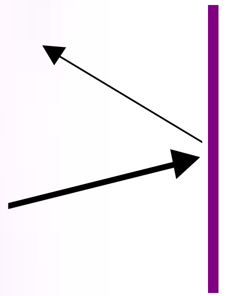

$$R(\theta=0) = \left(\frac{n_1-n_2}{n_1+n_2}\right)^2 = \frac{\delta^2}{2} \approx 10^{-11}$$ ☹

otal External Reflection

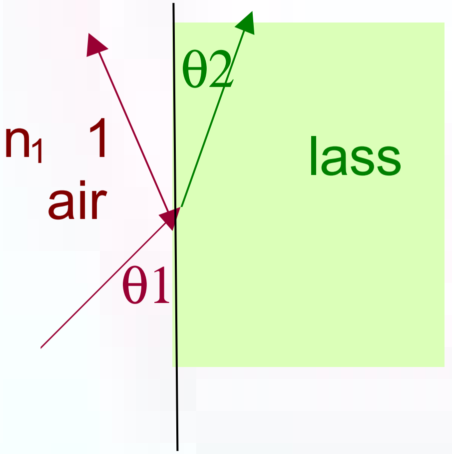

☺

$$n_1 \sin(90-\theta_1) = n_2 \sin(90-\theta_2)$$

$$(1)\cos(\theta_1) = (1-\delta)\cos(\theta_2)$$

$$(1)\cos(\theta_c) = (1-\delta)\cos(0) \quad \Rightarrow 1-\frac{\theta_c^{\,2}}{2} \doteq 1-\delta \quad \Rightarrow \theta_c \doteq \sqrt{2\delta}$$

$$\theta_c = \frac{\omega_p}{\omega} \approx 3\times10^{-3}$$ R=1

Damping

$$F = m\ddot{x} = -kx - b\dot{x} + qE$$

$$x = x_o \cos(\omega t + \phi)$$

$$n = 1 - \delta - i\beta \qquad R<1$$

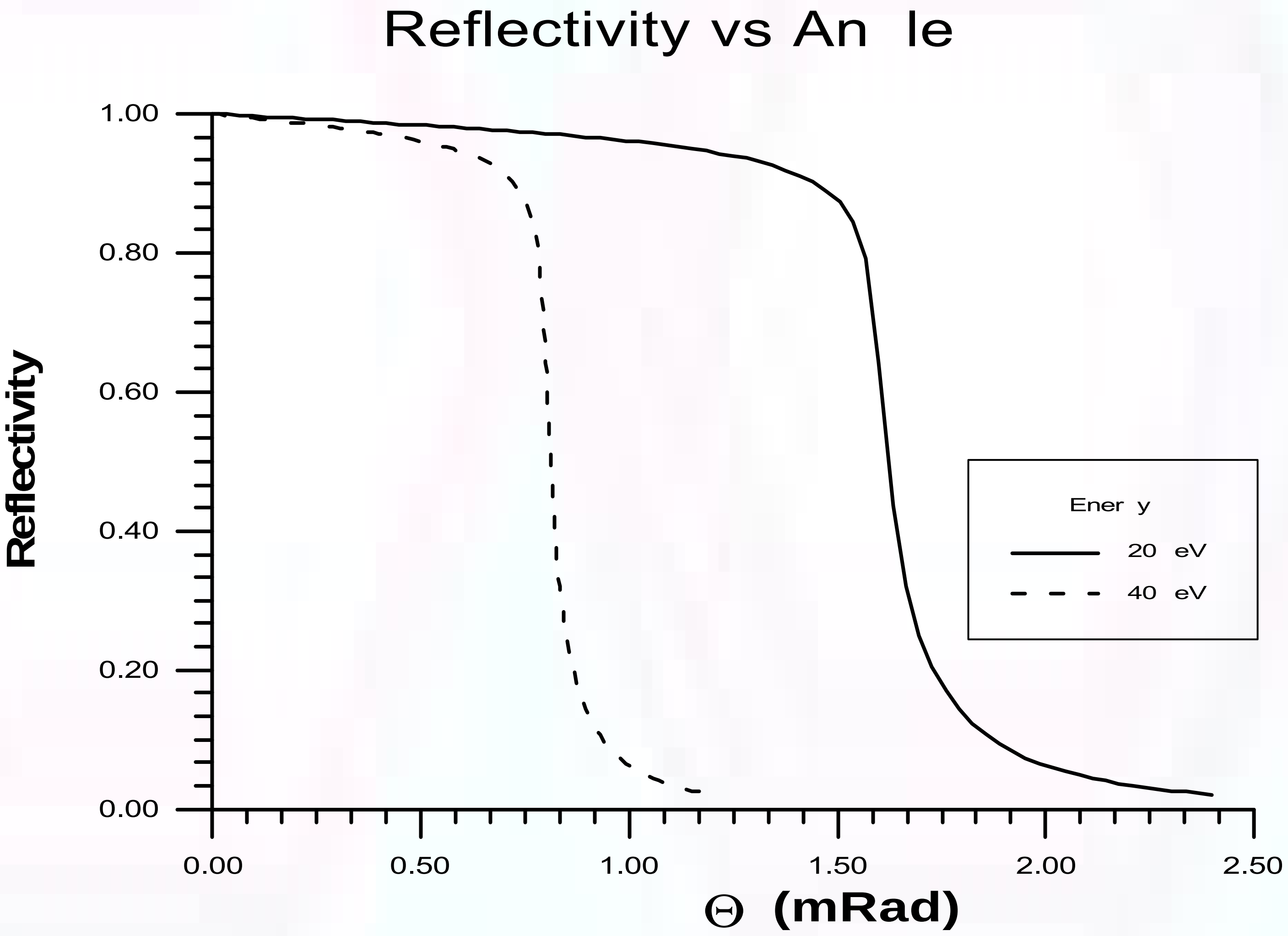

X rays in hollow capillary tubes:

Can collect

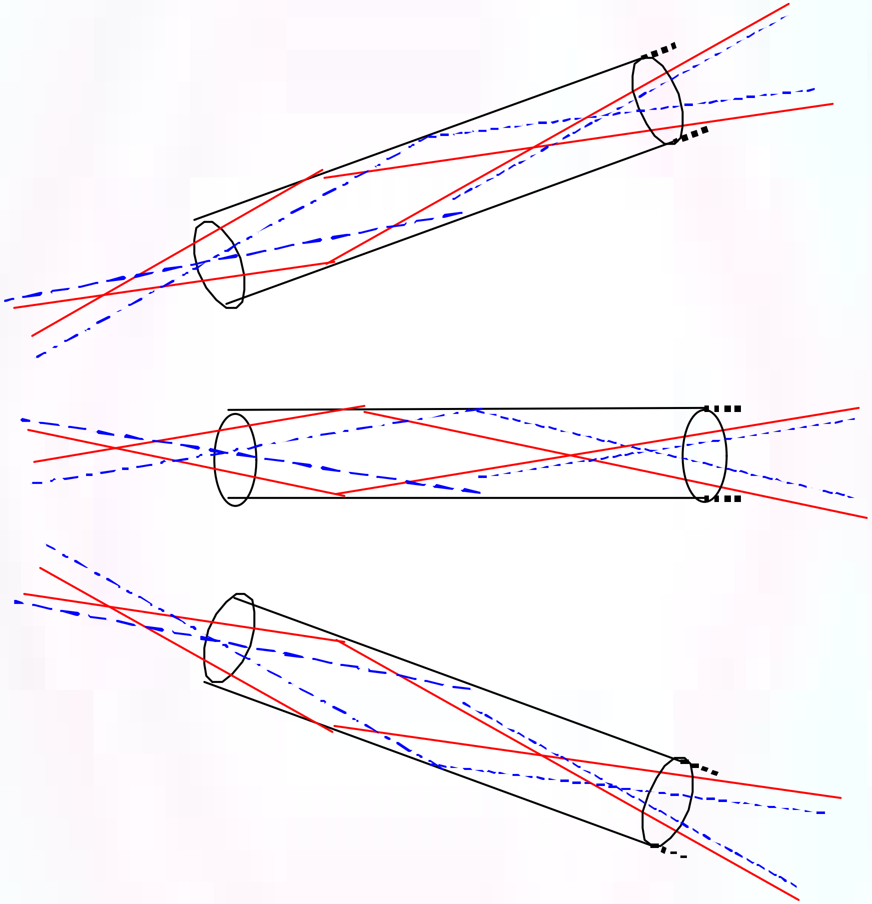

And redirect beams

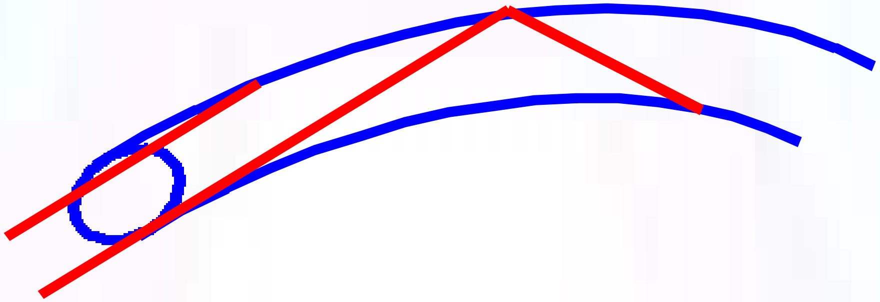

To make a lens

How much bending is required for a lens?

Approximate outermost fiber of lens as circle of radius R

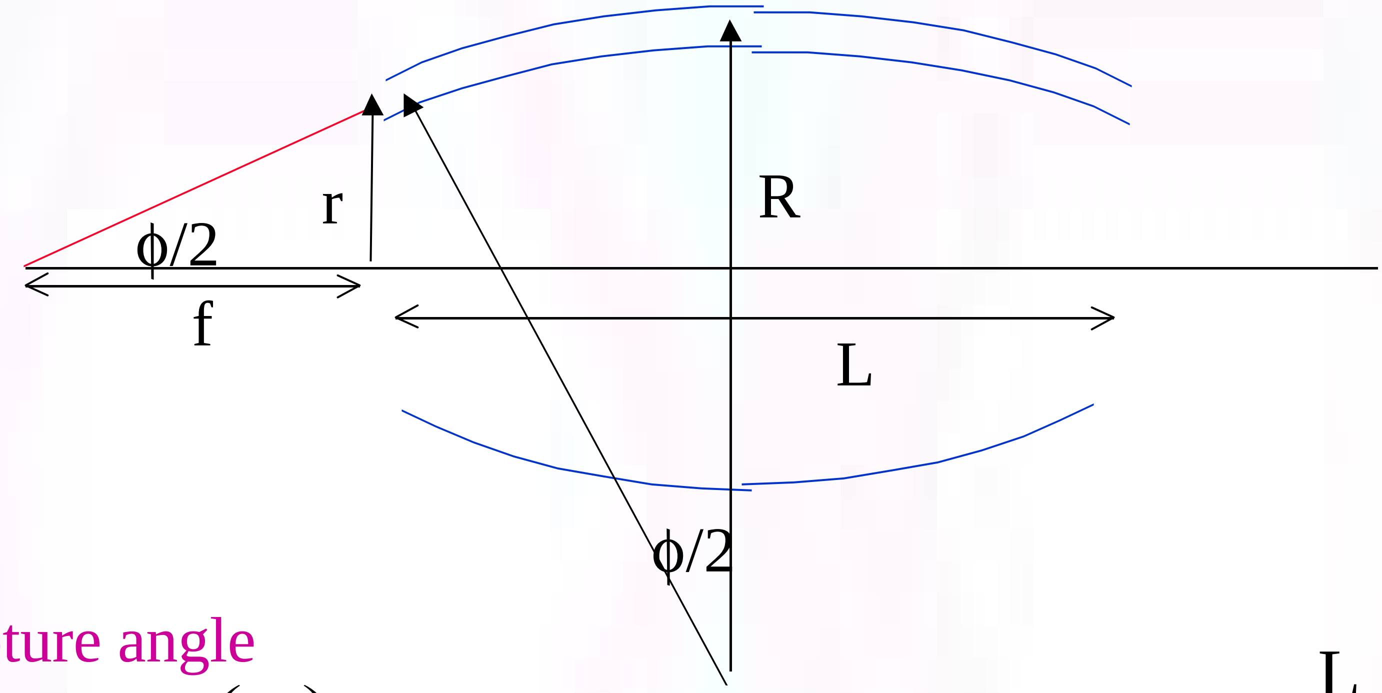

Capture angle

$$\phi = 2\,\mathrm{atan}\left(\frac{r}{f}\right)$$

$$L \approx R\phi \Rightarrow R \approx \frac{L}{\phi}$$

$$f = 50\text{ mm}, \quad r = 5\text{ mm} \quad \Rightarrow \phi = 11.5^{o} \quad L = 100\text{ mm} \quad \Rightarrow R \approx 1\text{ m}$$

Cutoff Energy dependence on bend radius and channel size

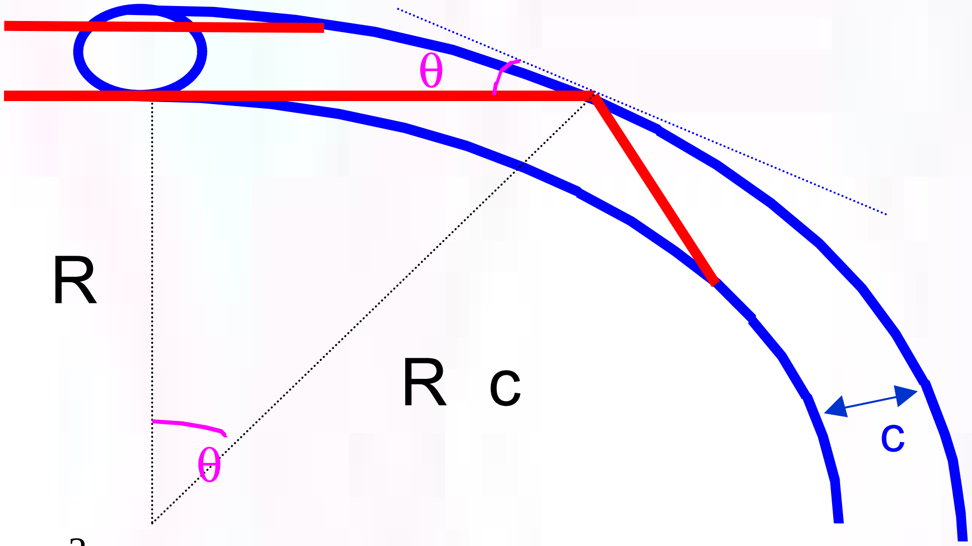

$$\cos(\theta) = \frac{R}{R+c} \Rightarrow 1 - \frac{\theta^2}{2} \approx \frac{1}{1+\frac{c}{R}} \approx 1 - \frac{c}{R}$$

$$\theta^2 \approx \frac{2c}{R} < \theta_c^2 = \left(\frac{\omega_{\text{plasma}}}{\omega}\right)^2 = \left(\frac{E_{\text{plasma}}}{E}\right)^2 \Rightarrow \quad E < E_{\text{plasma}}\sqrt{\frac{R}{2c}}$$

$$c = 2\,\mu\text{m} \quad R = 1\,\text{m} \quad E_{\text{plasma}} = 30\,\text{eV} \quad \Rightarrow \quad E < 15\,\text{keV}$$

Transmission

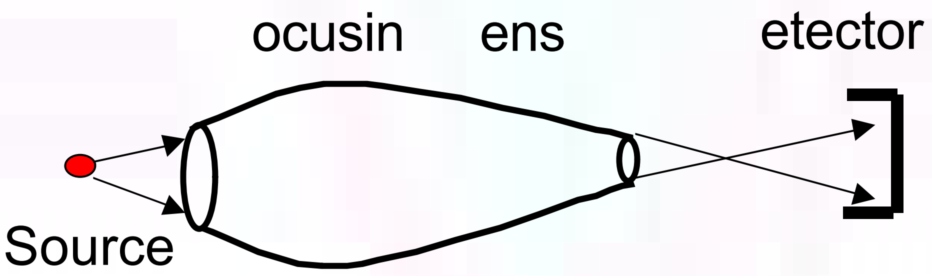

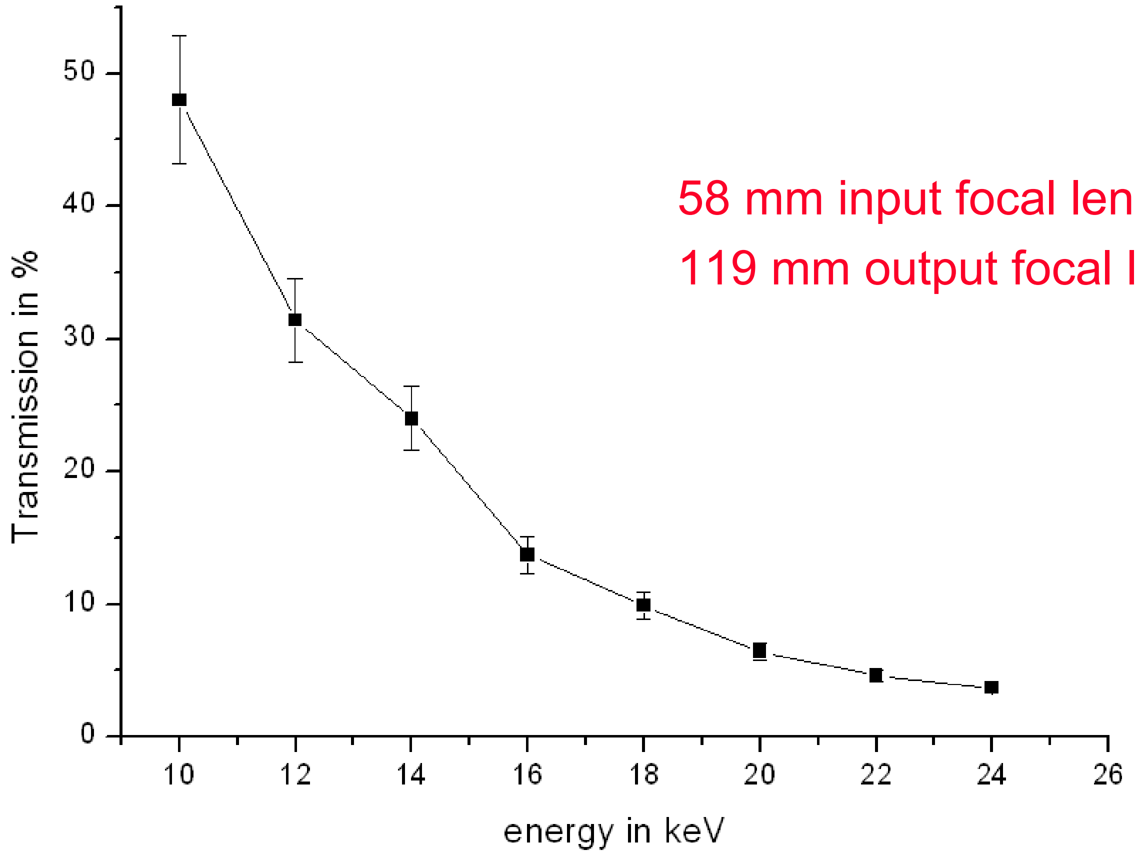

58 mm input focal length

119 mm output focal length

Beam Filtering

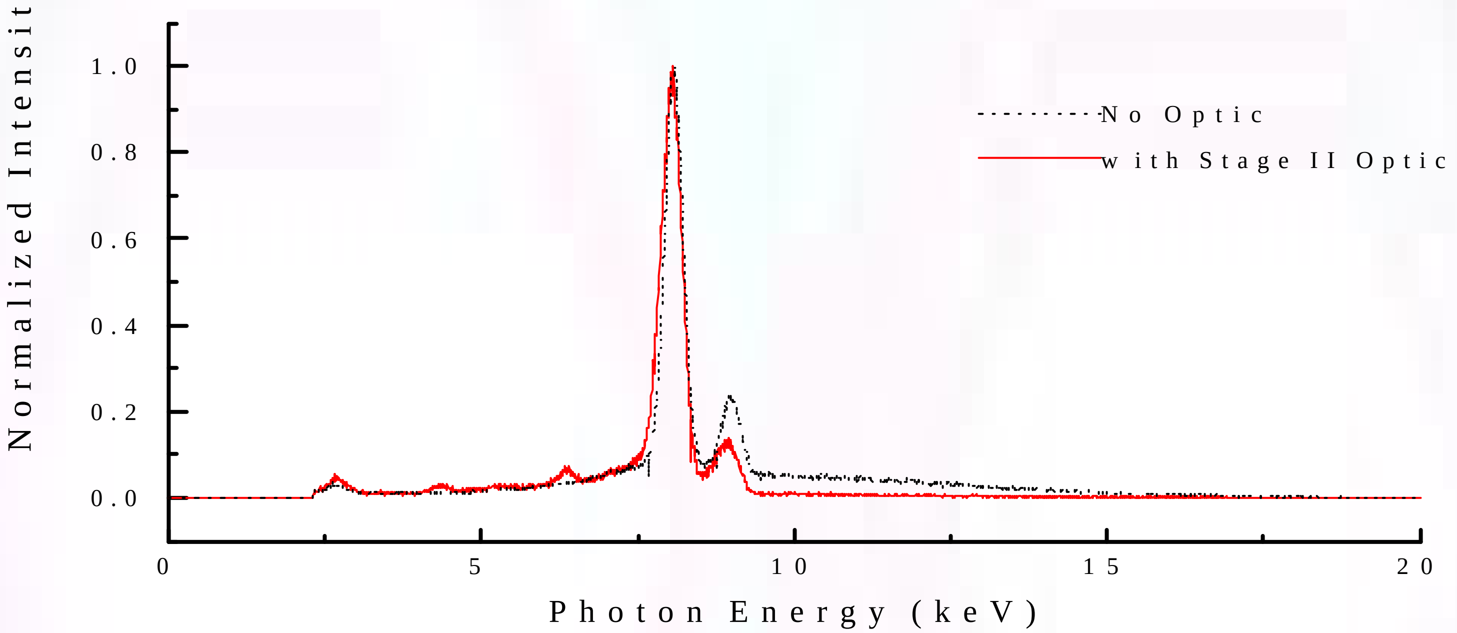

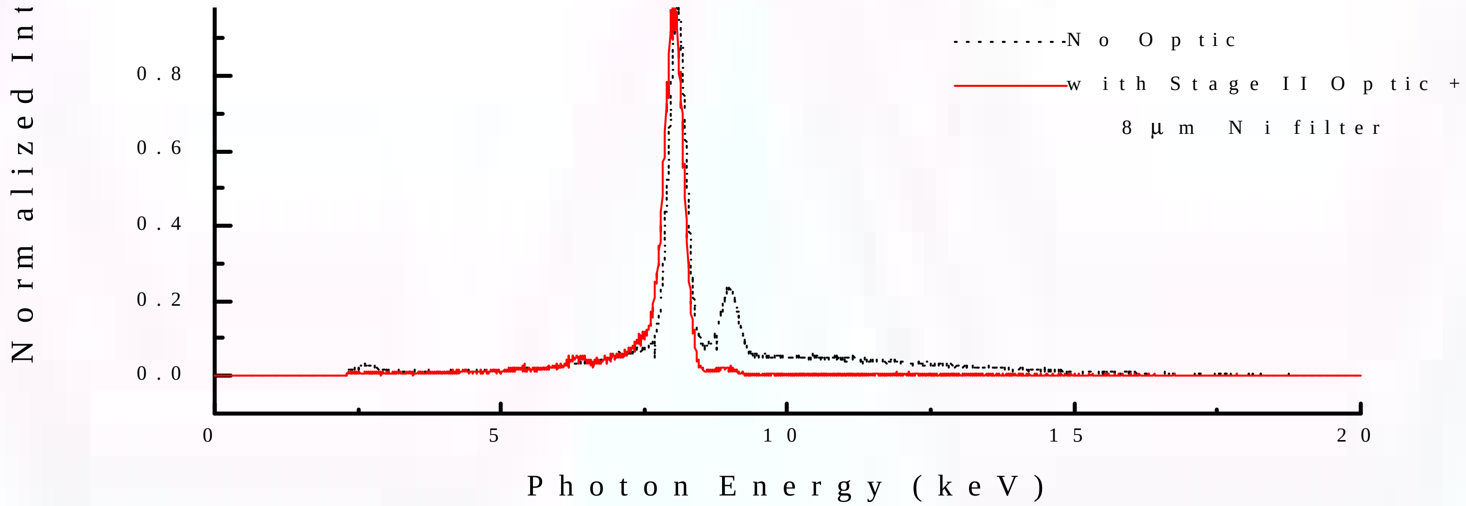

Characterization of Polycapillary Optics

Capture Angle,

ω 3º

Ω 2 millisteradian

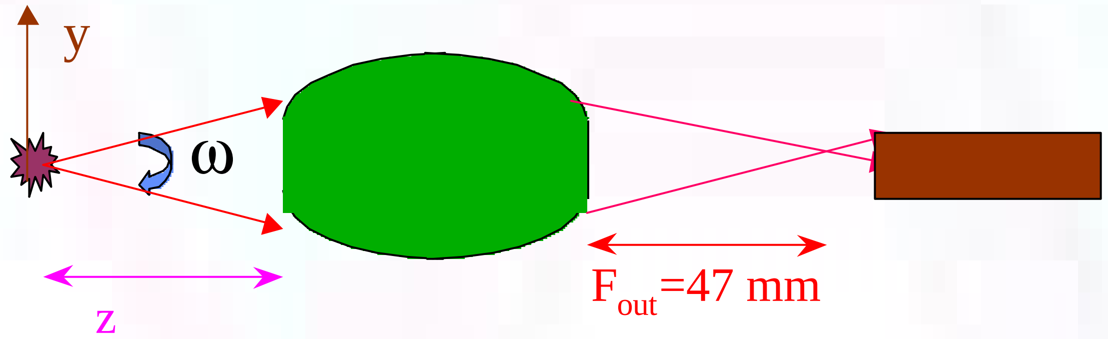

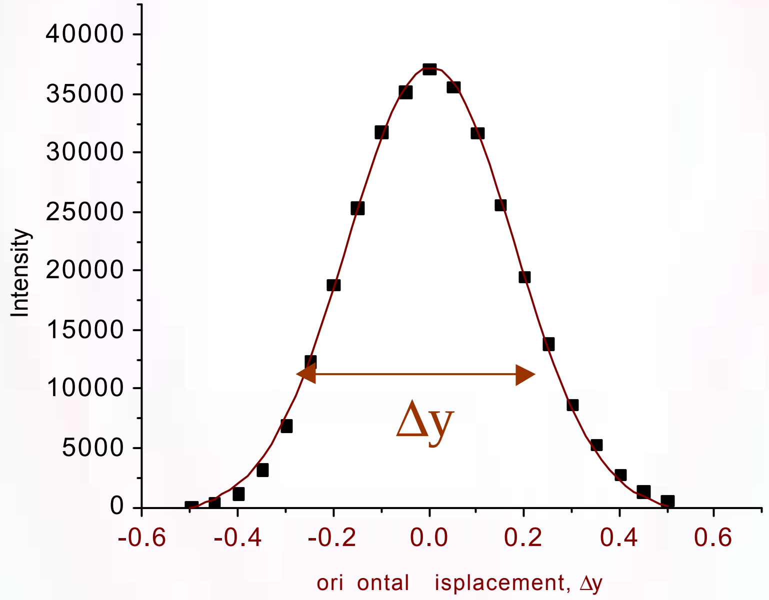

Transmission 9.9

$$\varepsilon = \frac{\Delta y}{z}$$

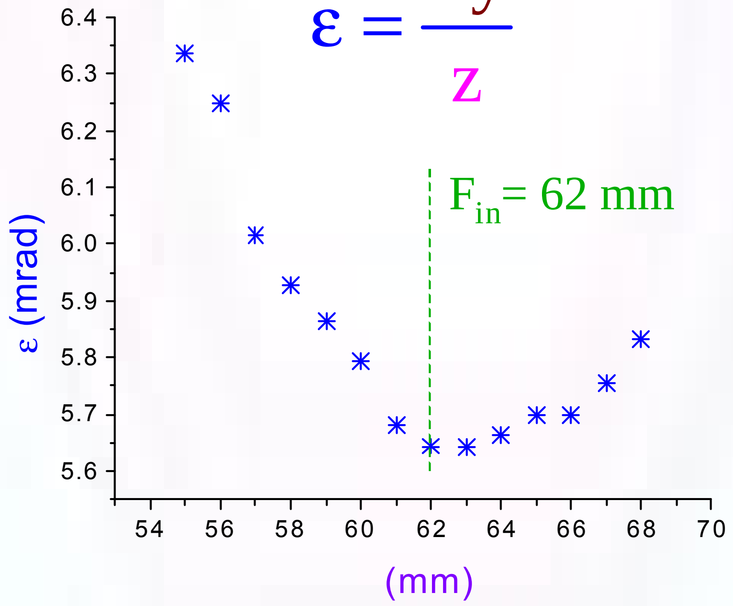

Input focal length

Focusing Lens Output Spot Measurement

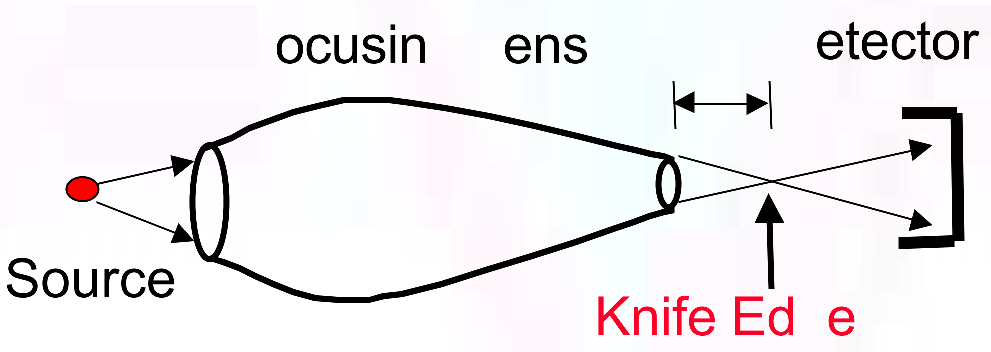

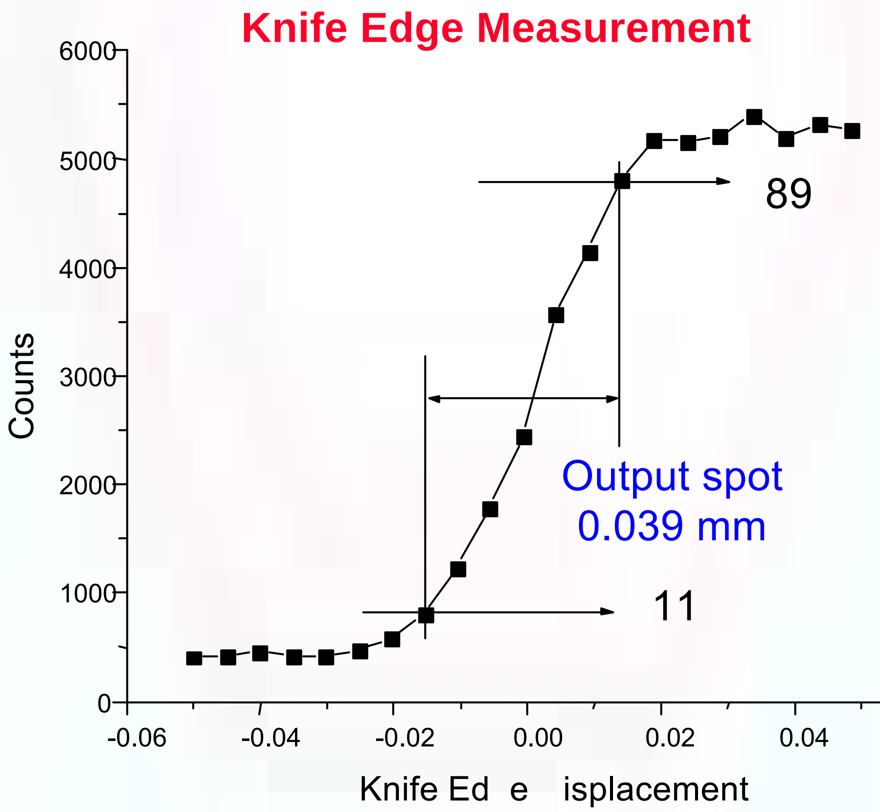

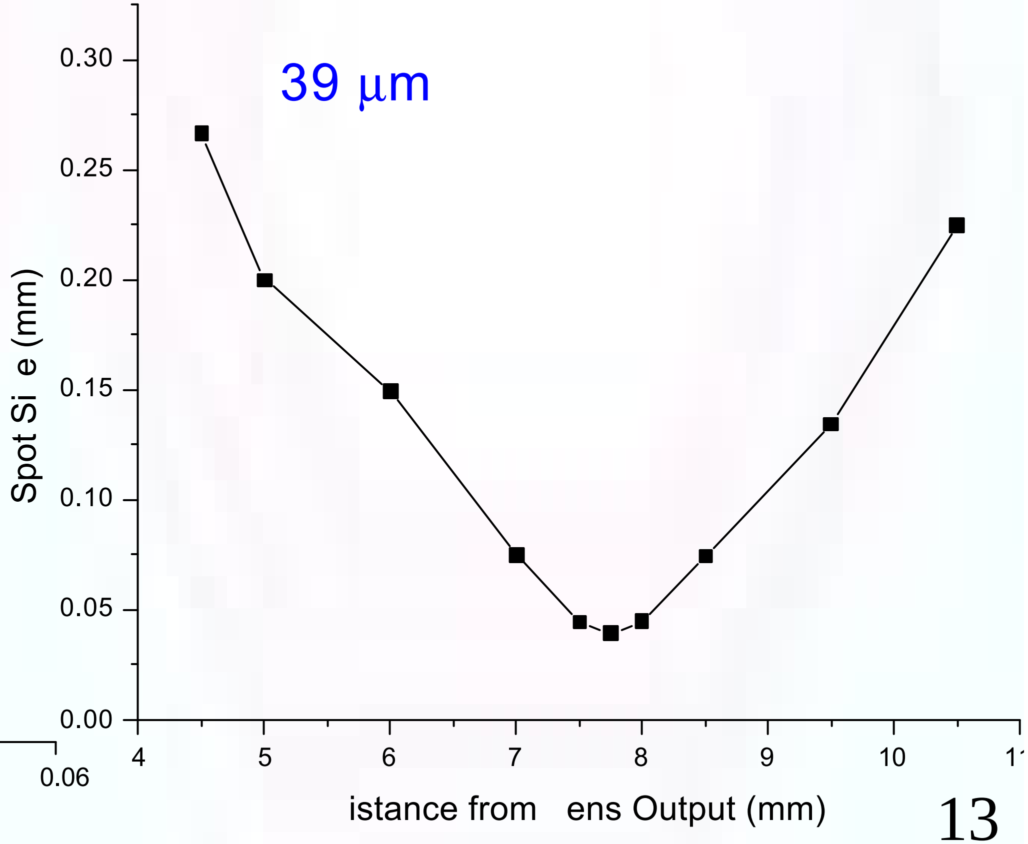

Focusing Optic Output

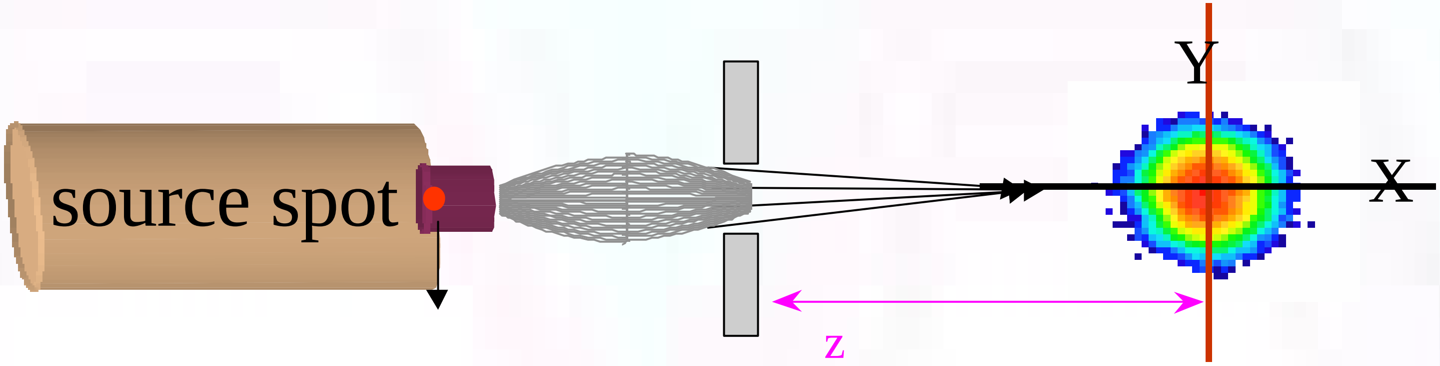

Focal spot size 0.8 mm

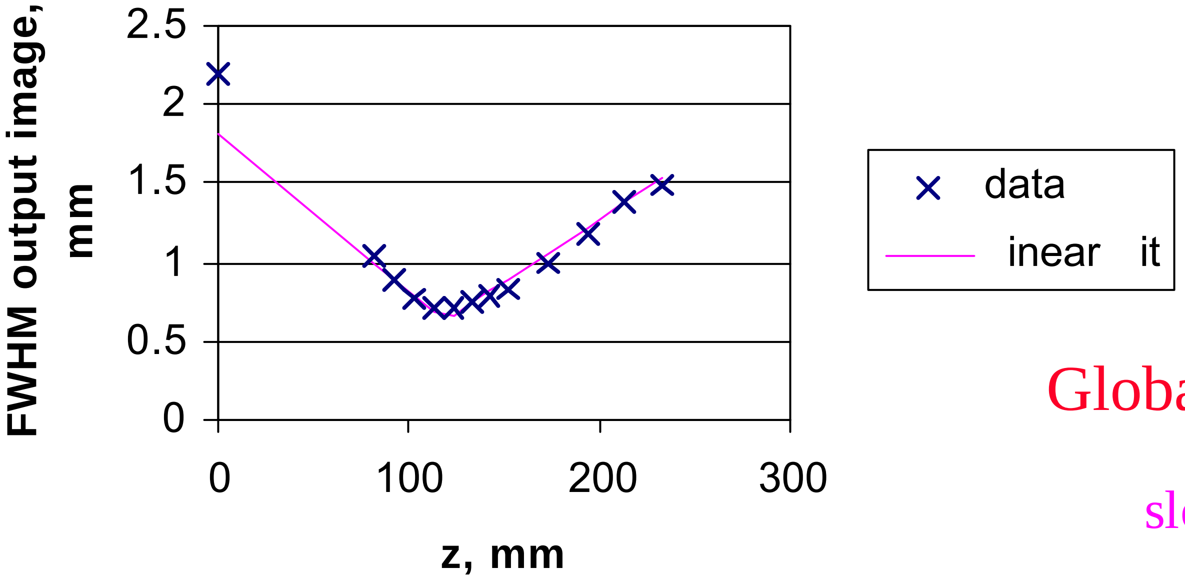

Global Divergence=

slope = $2\beta = 0.55^{o}$

FOCAL SPOT SIZE

Minimum due to Local Divergence 2a

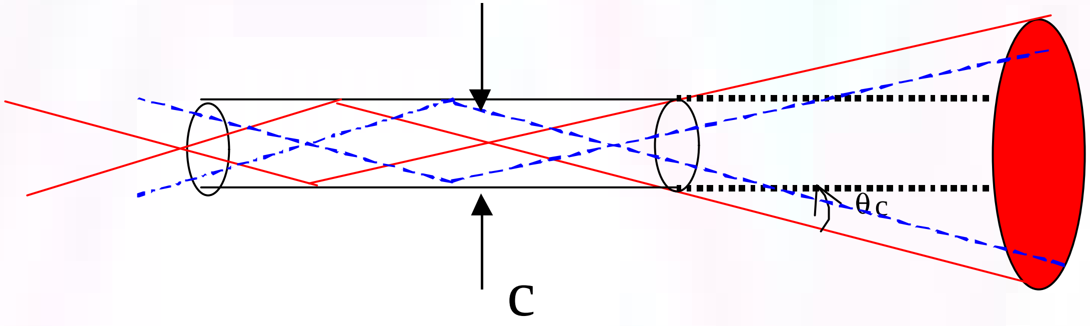

Minimum size :

$$d = c + 2\alpha f = c + 1.3\,\theta_c f$$

$$c = 5\,\mu m \quad 2\alpha = 0.28^o \quad \begin{cases} f = 50\text{ mm} & \Rightarrow d = 250\ \mu m \\ f = 5\text{ mm} & \Rightarrow d = 30\ \mu m \end{cases}$$

Rocking Curve collimating optic

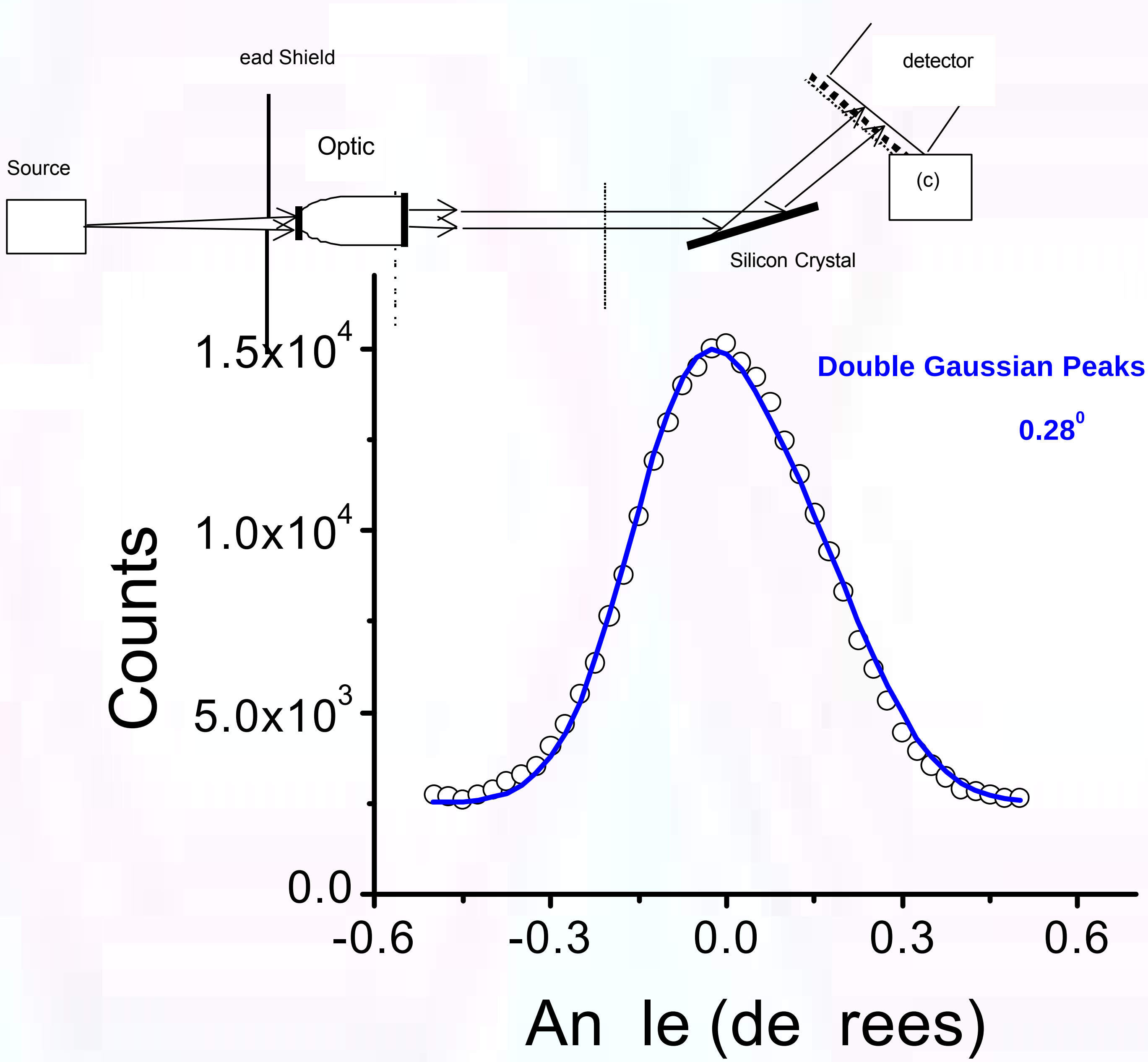

Double Gaussian Peaks of Width

0.28^0

Global divergence

Rocking Curve focusing optic

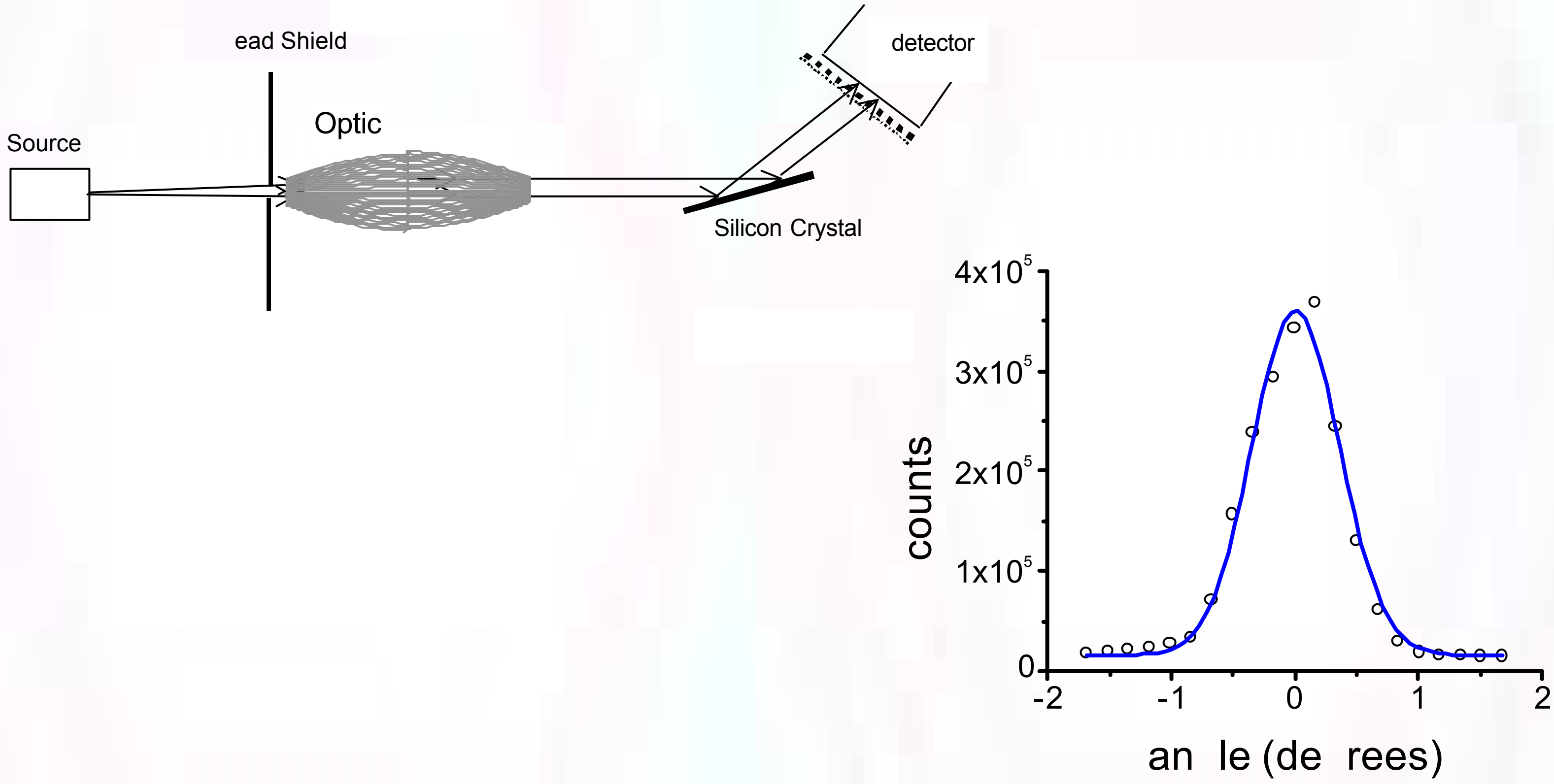

$$\text{Rocking Curve Width} = 0.83^{o} = 2\alpha + 2\beta = 0.28^{o} + 0.55^{o}$$

GAIN

Relative to What?

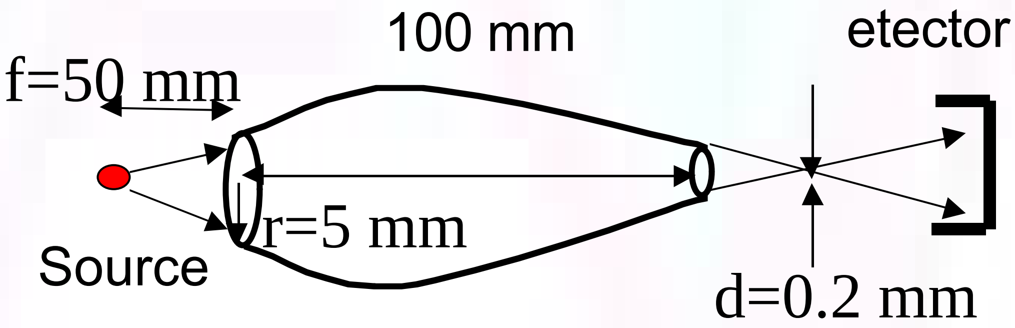

To make the optic look good: compare to flux through a pinhole of diameter < spot size compared to source at focal point:

$$F_{\mathrm{no\ optic}} = \frac{P_{\mathrm{source}}}{4\pi\left(f_{\mathrm{in}} + L + f_{\mathrm{out}}\right)^2}\pi\left(\frac{d}{2}\right)^2 \qquad F_{\mathrm{Lens}} = \frac{P_{\mathrm{source}}}{4\pi\left(f_{\mathrm{in}}\right)^2}\pi r_{\mathrm{Lens}}^2 T$$

$$\mathrm{Gain} = \frac{F_{\mathrm{Lens}}}{F_{\mathrm{no\ optic}}} = \left(\frac{f_{\mathrm{in}} + L + f_{\mathrm{out}}}{f_{\mathrm{in}}}\right)^2\left(\frac{r_{\mathrm{Lens}}}{d/2}\right)^2 T$$

$$d = 200\ \mu\mathrm{m} \quad r_{\mathrm{Lens}} = 5\ \mathrm{mm} \quad f = 50\ \mathrm{mm} \quad L = 100\ \mathrm{mm} \Rightarrow \quad \mathrm{Gain} = 8000$$

Liouville’s Theorem

Angle area product cannot decrease

$$A_f \Omega_f \geq A_o \Omega_o$$

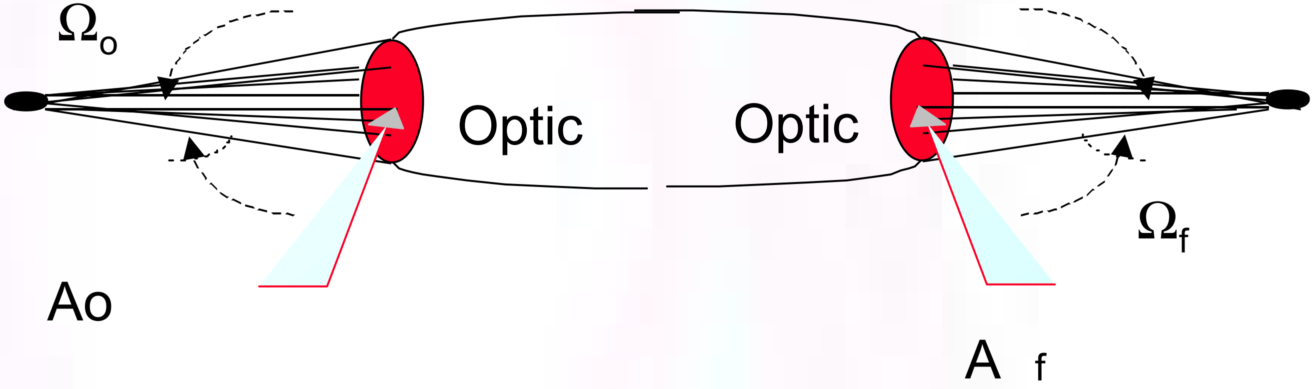

Optics Defects

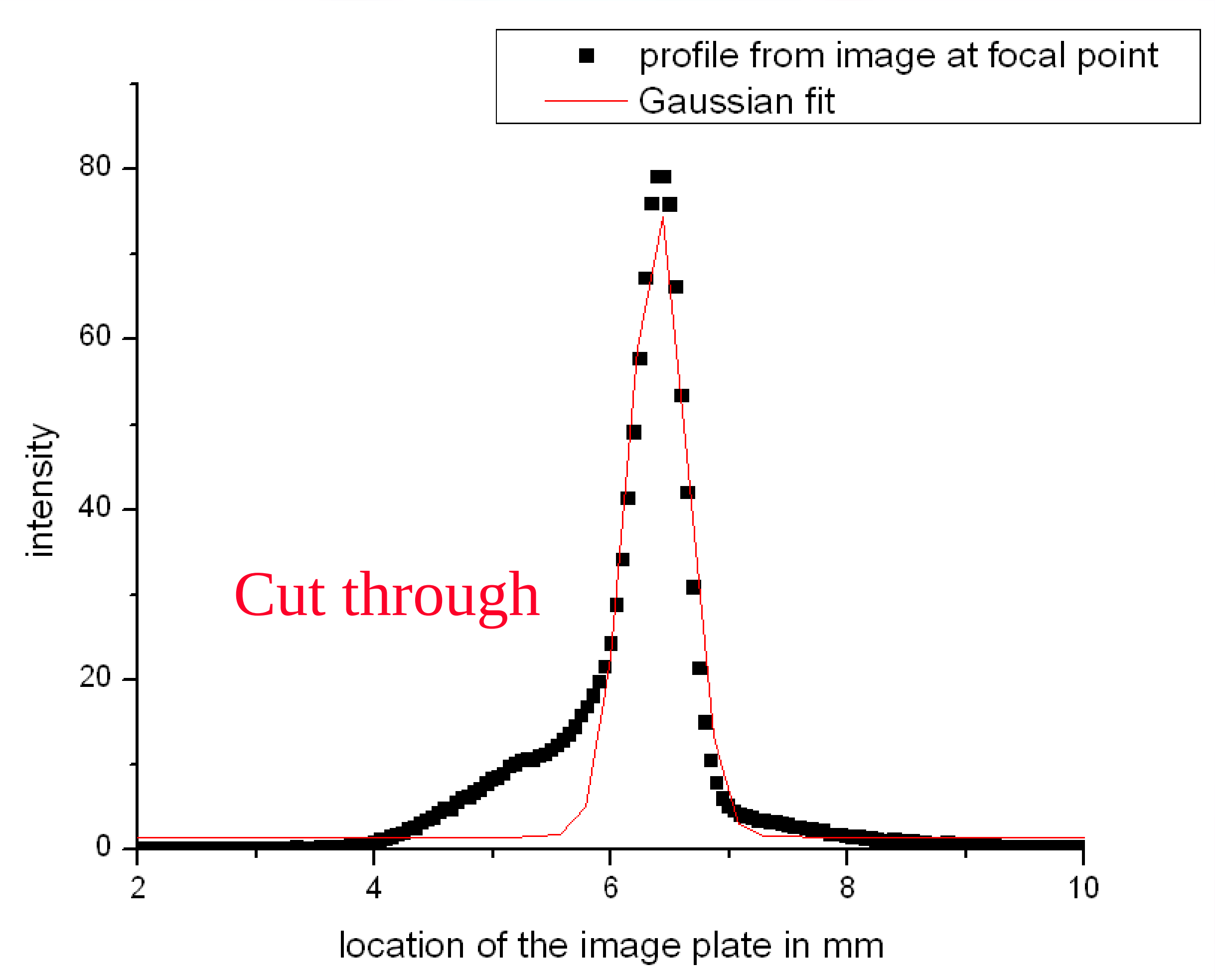

Optic defects

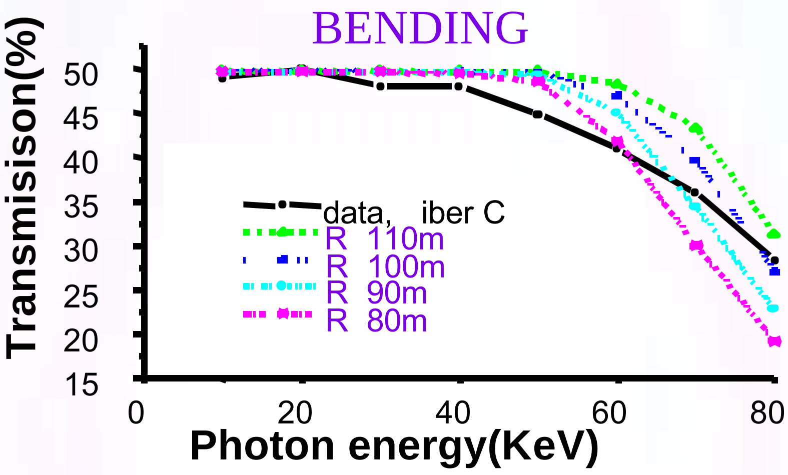

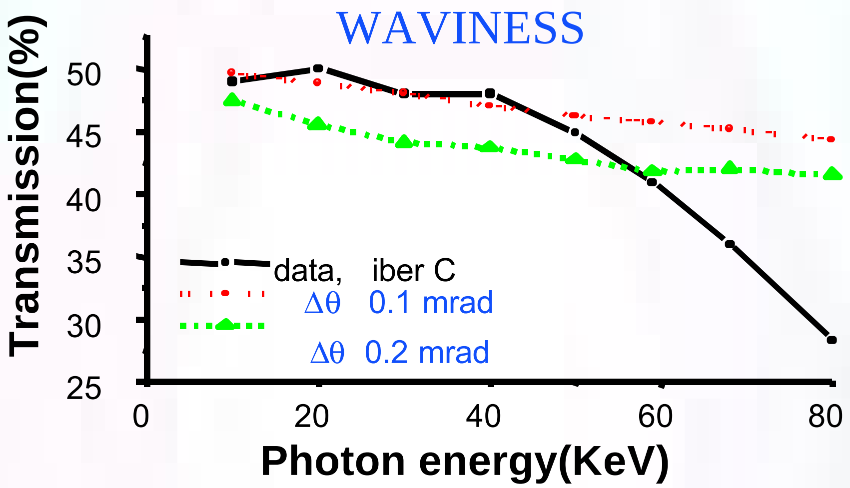

Bending:

λ_b 10 cm

parameter: bending radius, R

Waviness:

λ r λ λb
parameter:

Modeled by random angle shifts of δθ after each bounce

Optic defects

λ r 1 μm

Roughness: parameters: correlation len th
rms hei ht

Rou hness correlation

$$g(\Delta x) = \frac{1}{L}\int_0^L Z(x)Z(x+\Delta x)dx = \overline{Z}^2 e^{-\frac{|\Delta x|}{s}}$$

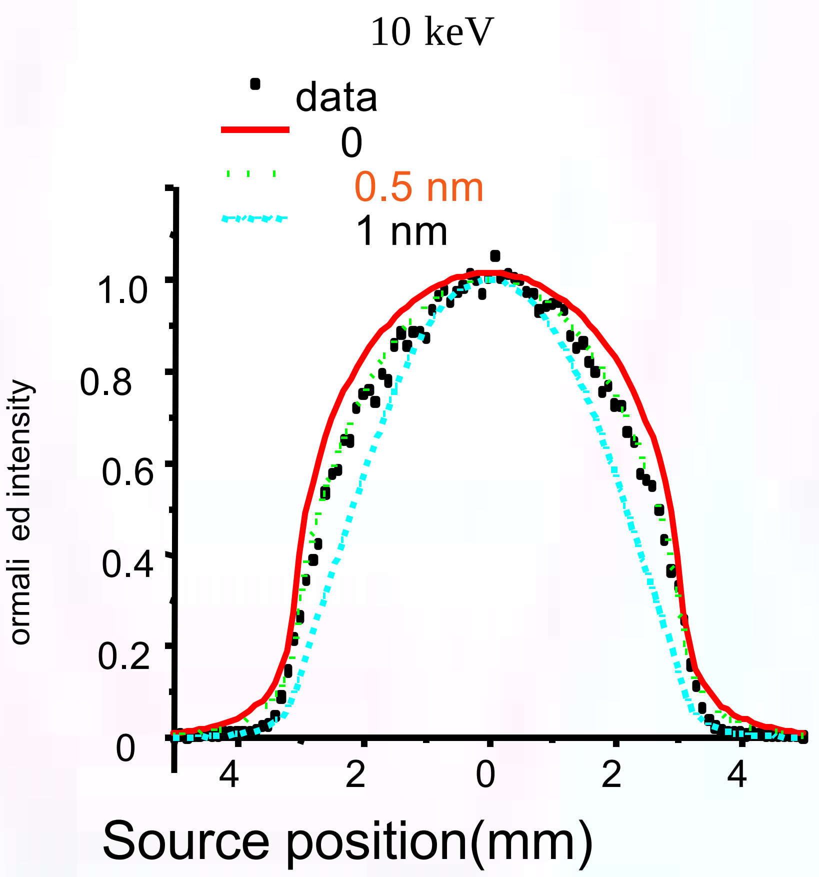

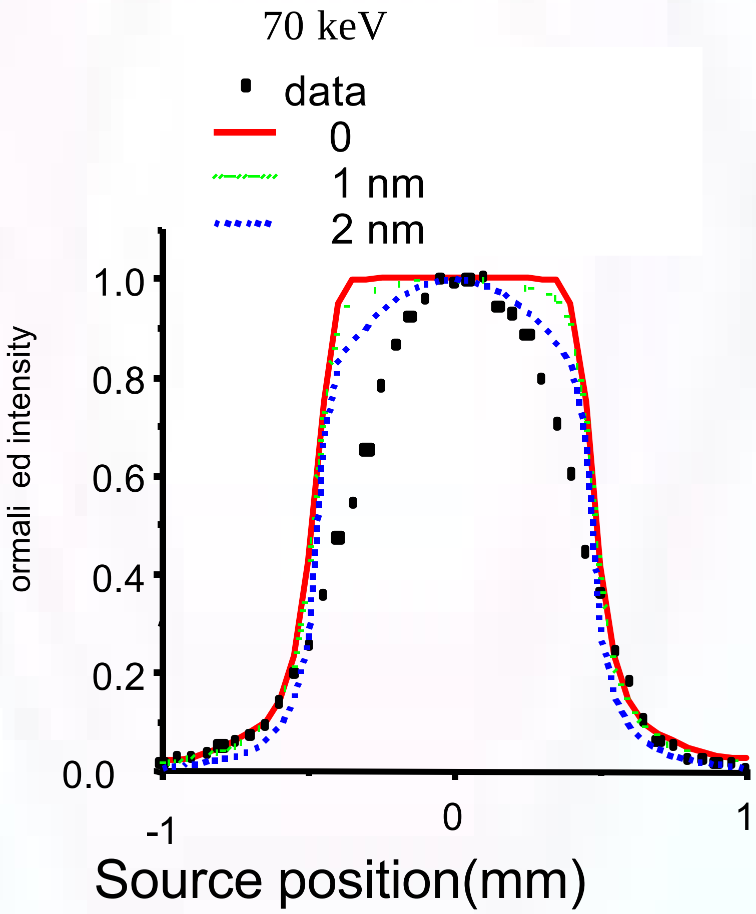

Simulation Analysis: Single Fiber

simulation with
w=0.15 mrad and
R=120 m.

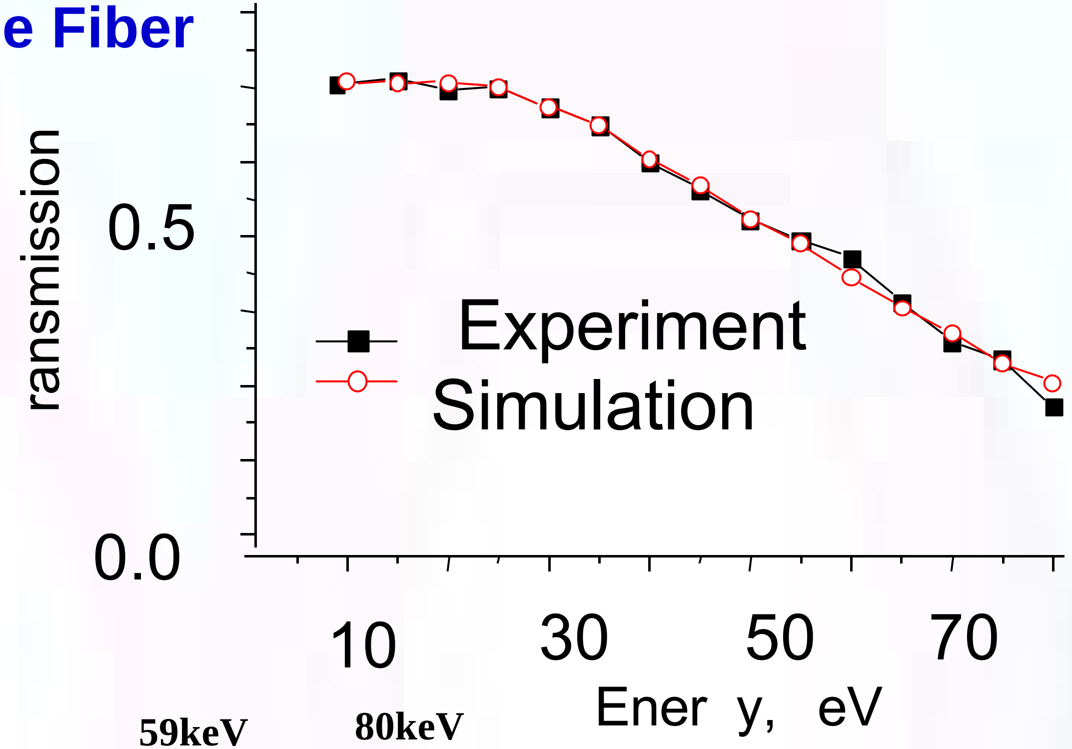

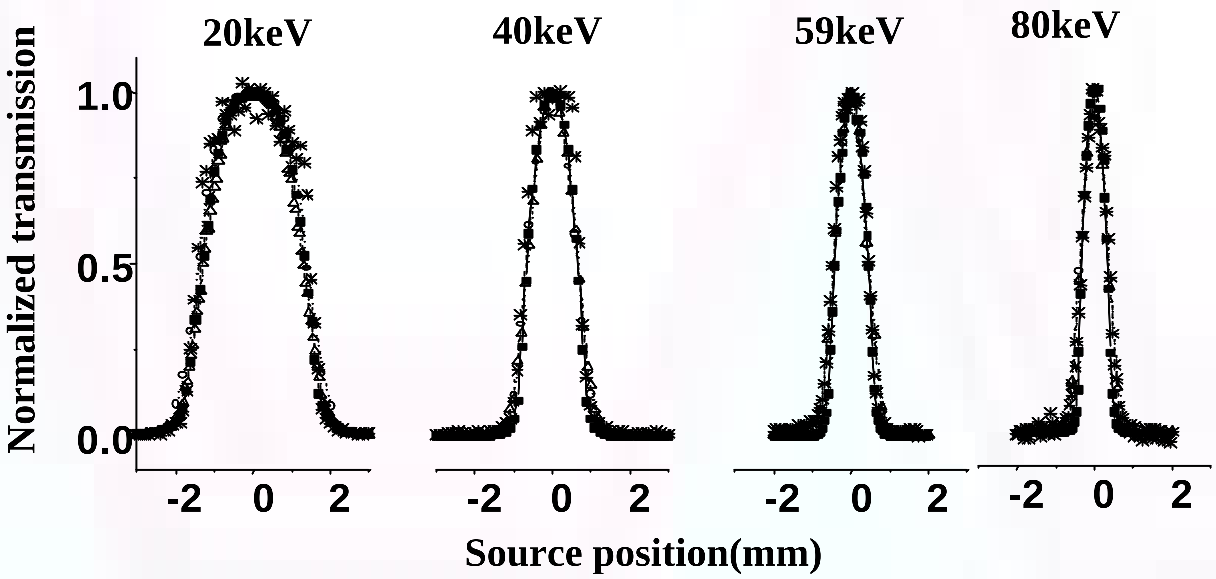

Simulation Analysis: Lens made from fibers

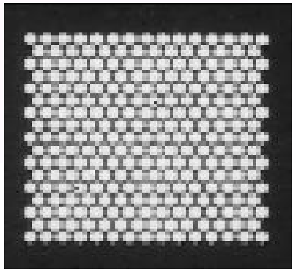

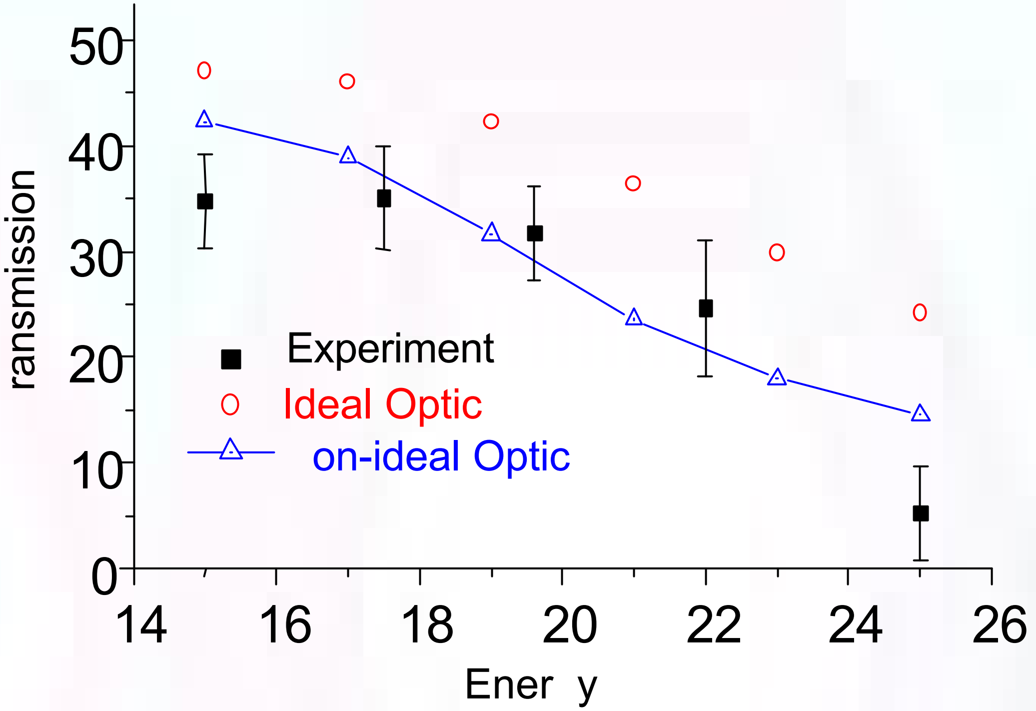

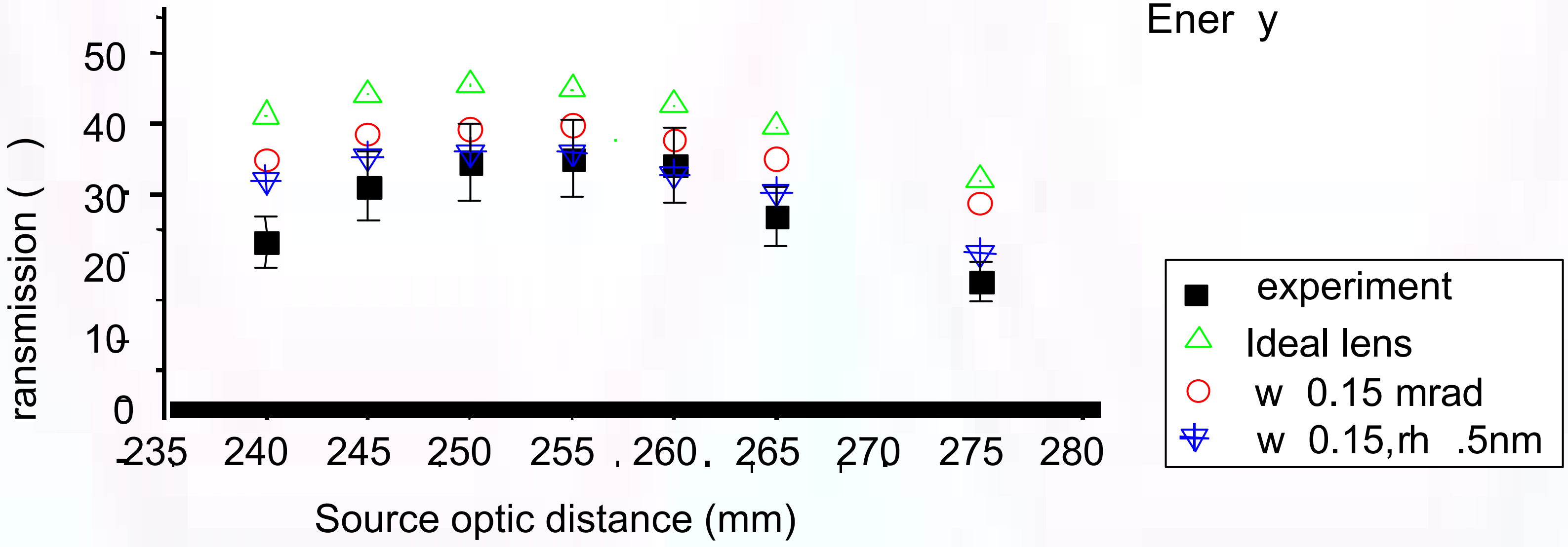

Optics Defect: Channel Blockage

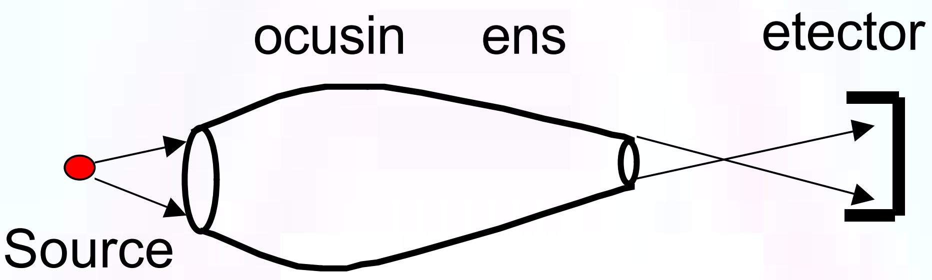

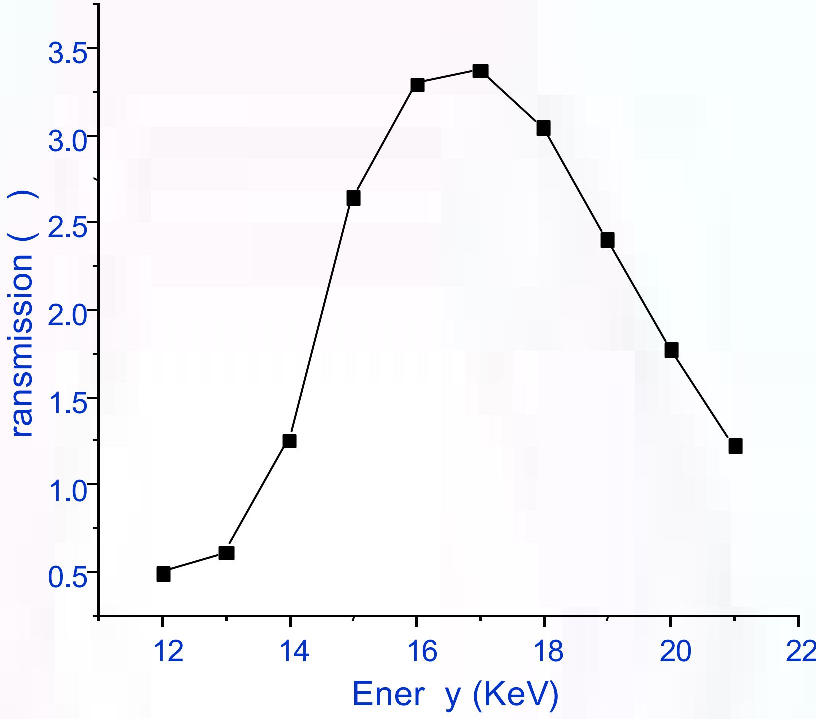

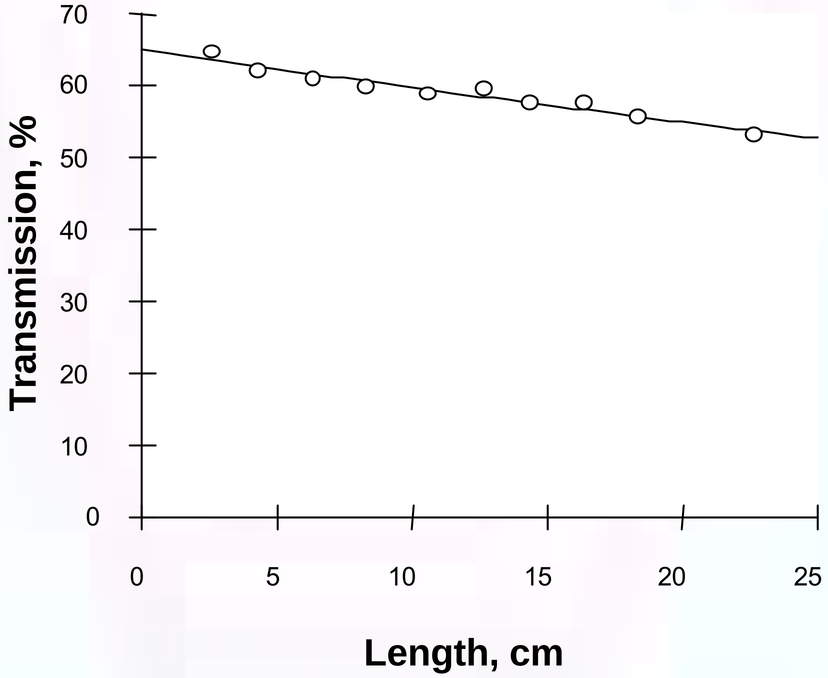

39 mm input focal length

7.8 mm output focal length

30 µm glass in length of lens

Application to Radiation Damage

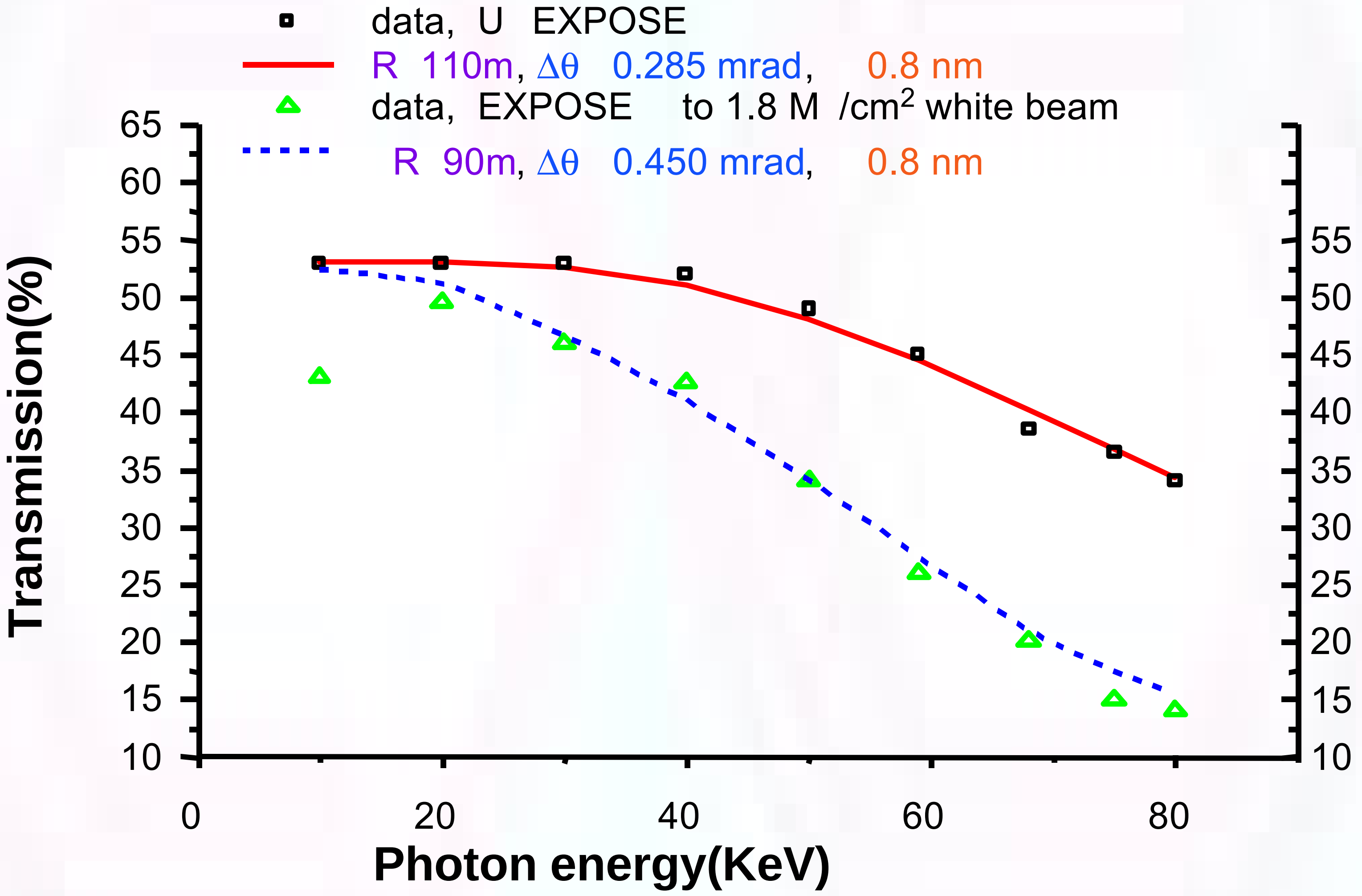

Characteristics of Polycapillary Focusing Optics:

Type Beam Focusing, Polychromatic

Useful X-ray Energy Range Typically 0.1 - 30 keV

Collection Solid Angle Up to 20 degrees

Working Distance 2.5mm 5mm 10mm 20mm 50mm 100mm

Focused beam size
(Mo Ká , FWHM, 17.4keV) 10um 18um 30um 45um 100um 180um

Gain (Compared to pinhole aperture
100 mm from source) 100x - 10000x

Applications: XRF

Spatial Resolution of MXR with 39 µm spot

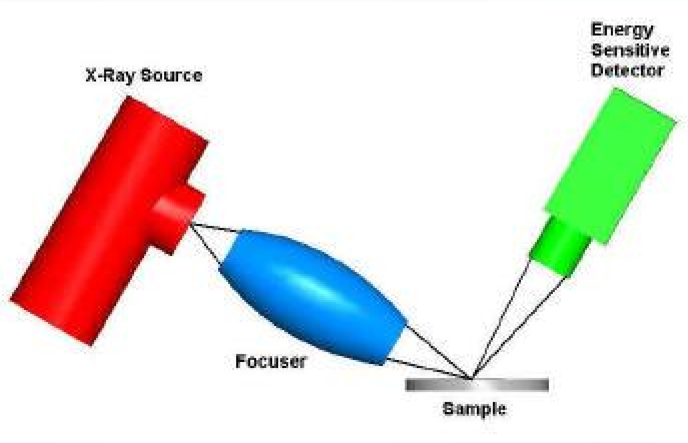

Micrograph of Cu grid

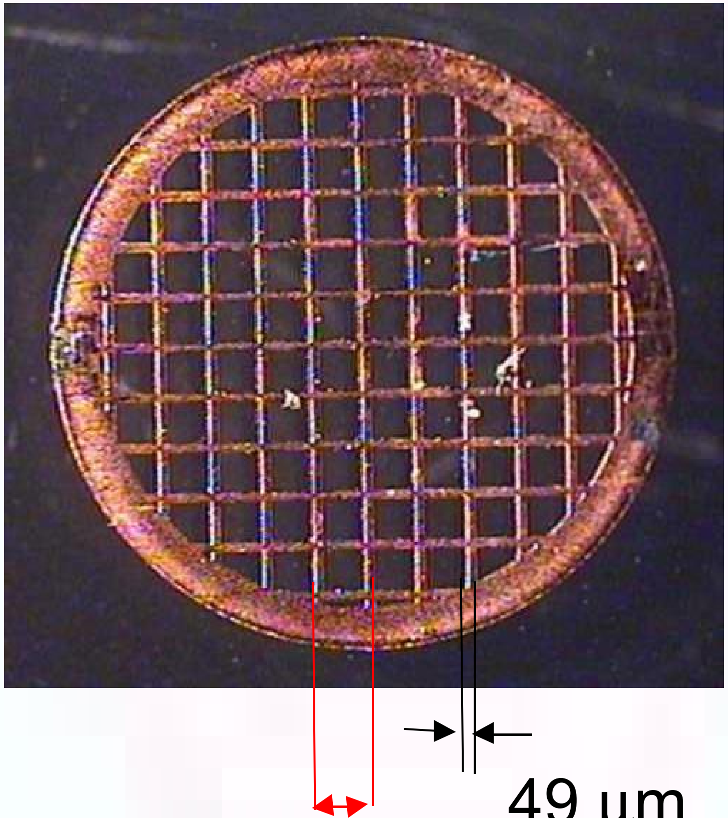

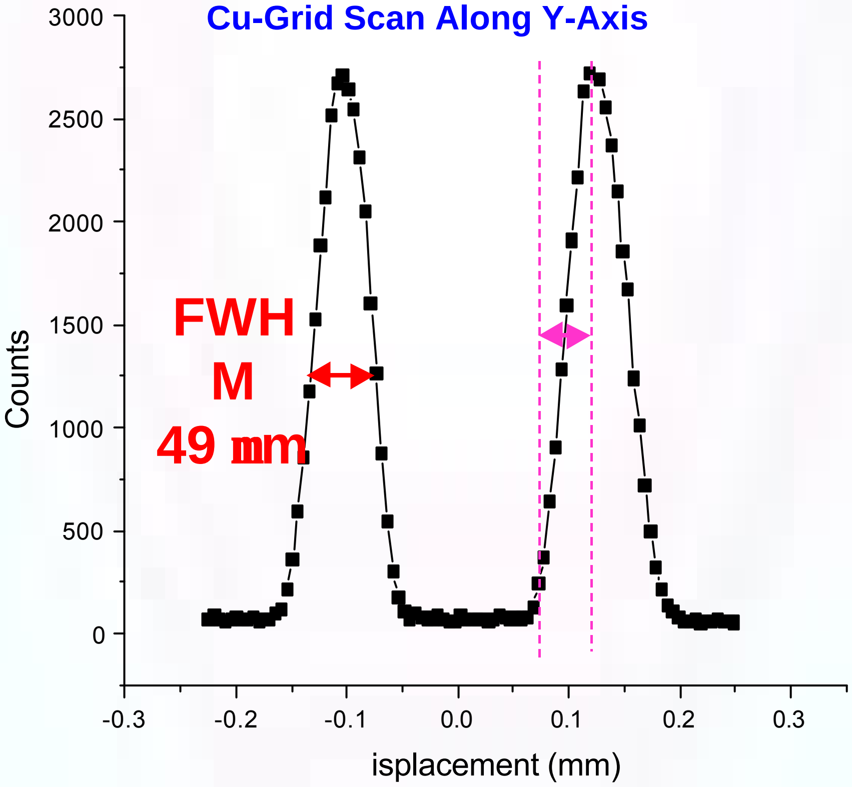

Applications: XRF

Elemental Mapping

MXRF maps of a quartz phenocryst with small volcanic glass inclusions

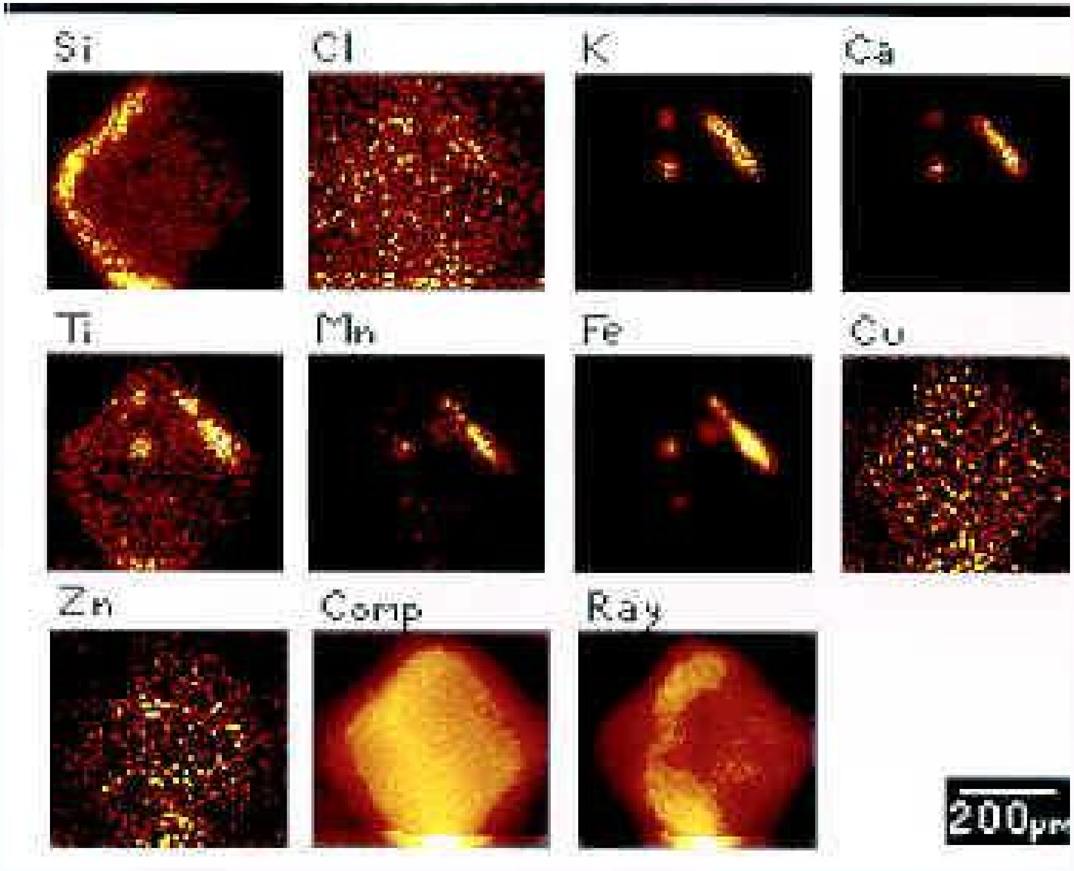

E EME	M (p)
K	4.1
i	1.5
e	0.57
n	0.28
Pb	0.52

Courtesy of Ning Gao, XOS

Applications: Protein Crystallography

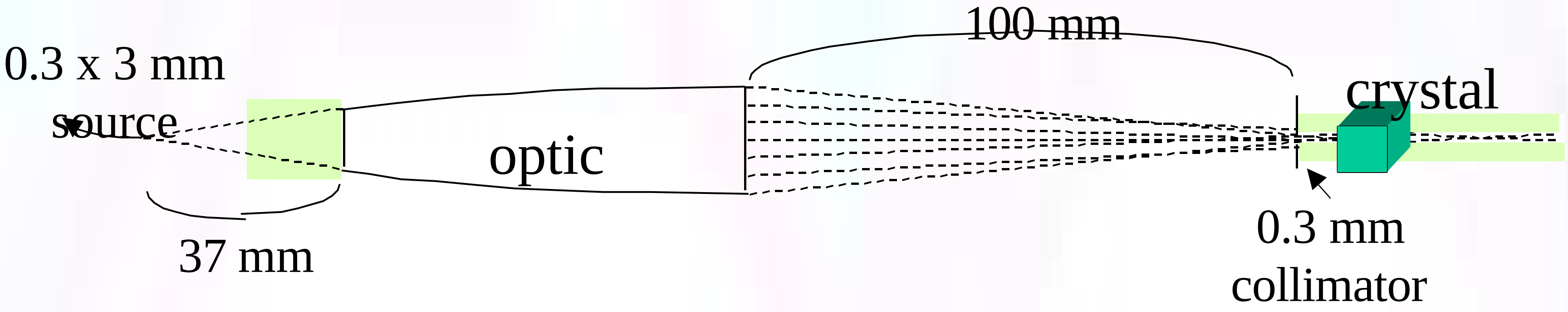

Lysozyme pattern taken in
20 seconds with 2.8
rotating anode, comparable to 30-35
min. without optic

Linear R factor without optic 6.4
with optic on same sample: 6.9

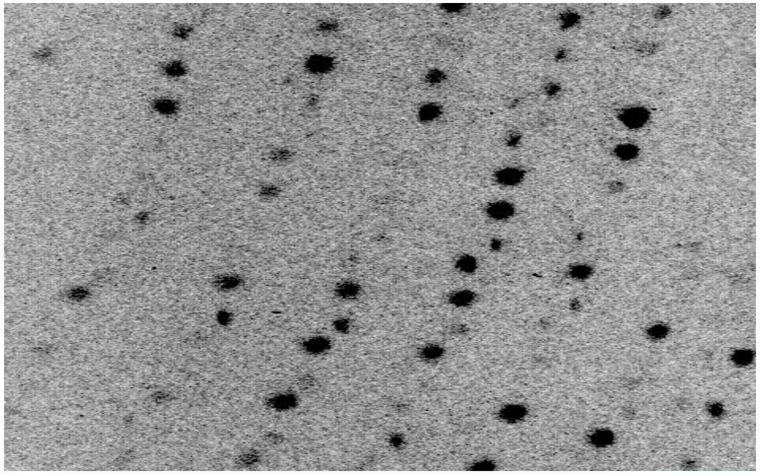

Applications: Protein Crystallography

Source: 37 kV, 25 W

Optic: 5.8 mm input, 136 mm

Crystal size	Less than 200 μm
oscillation angle	1.5 deg (44 frames)
time / frame	60 min
PINdiode intensity	3×10^{-4}
resolution	2.0 Å
R-factor	5.2%

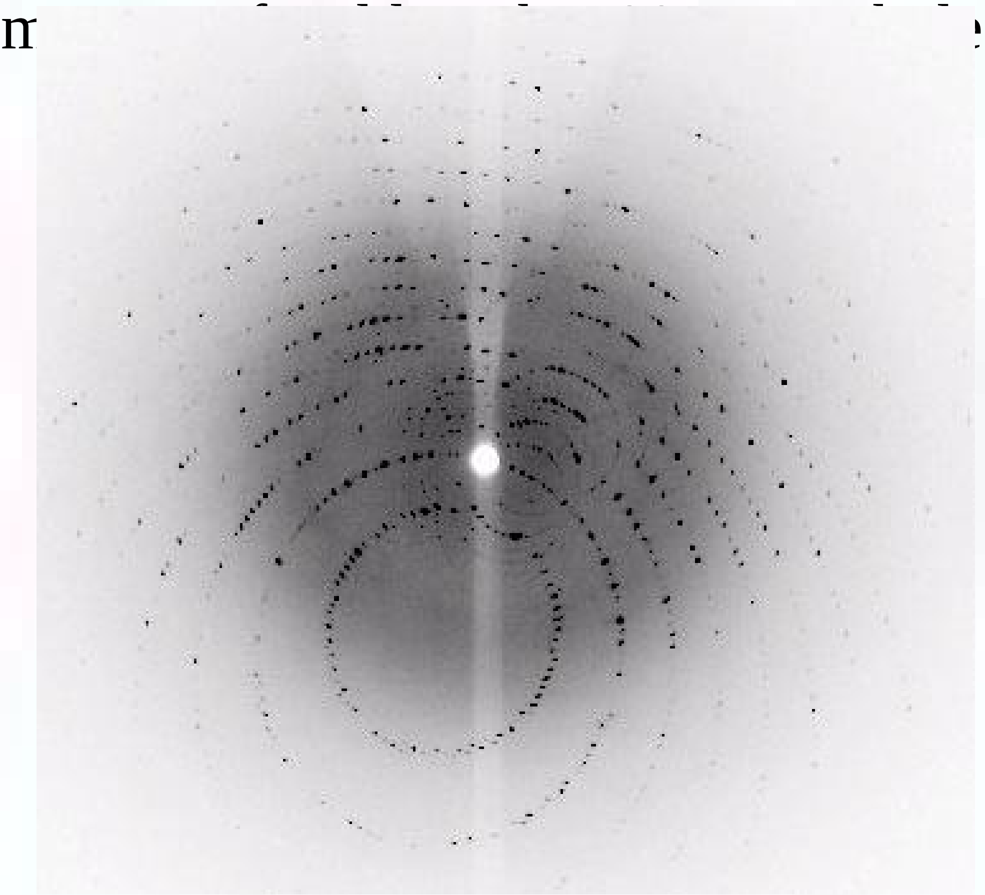

Applications: Protein Crystallography

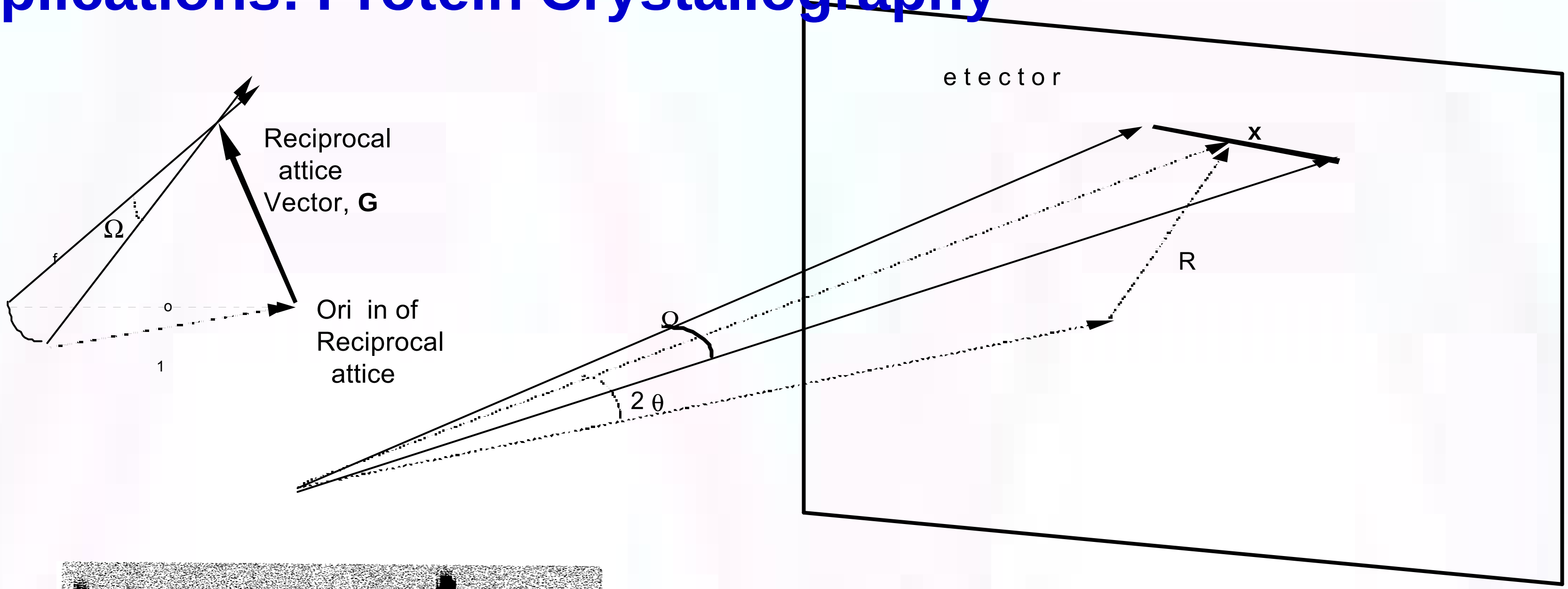
Reciprocal Lattice Vector, **G**

Origin of Reciprocal Lattice

Detector

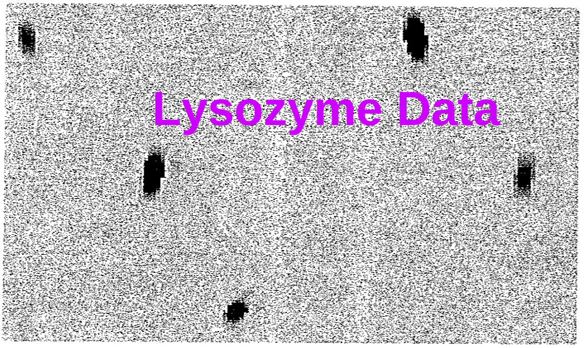
Lysozyme Data

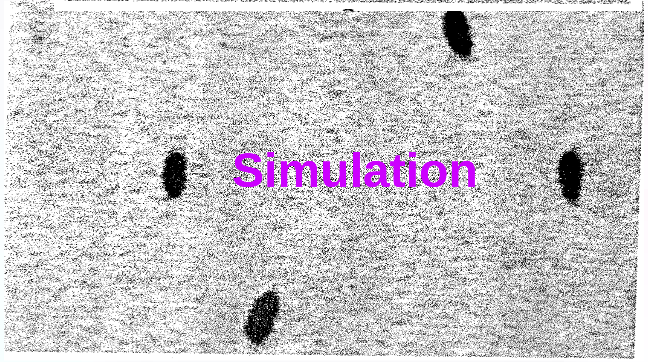
Simulation

5 min

1 mA

2.1

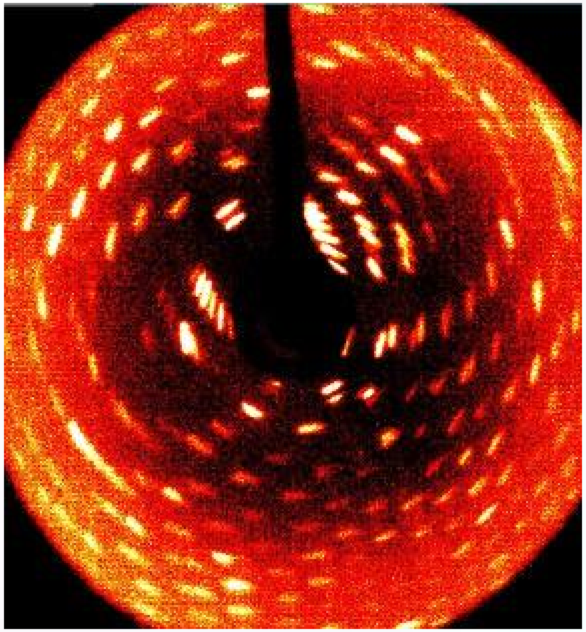

Applications: Powder Diffraction

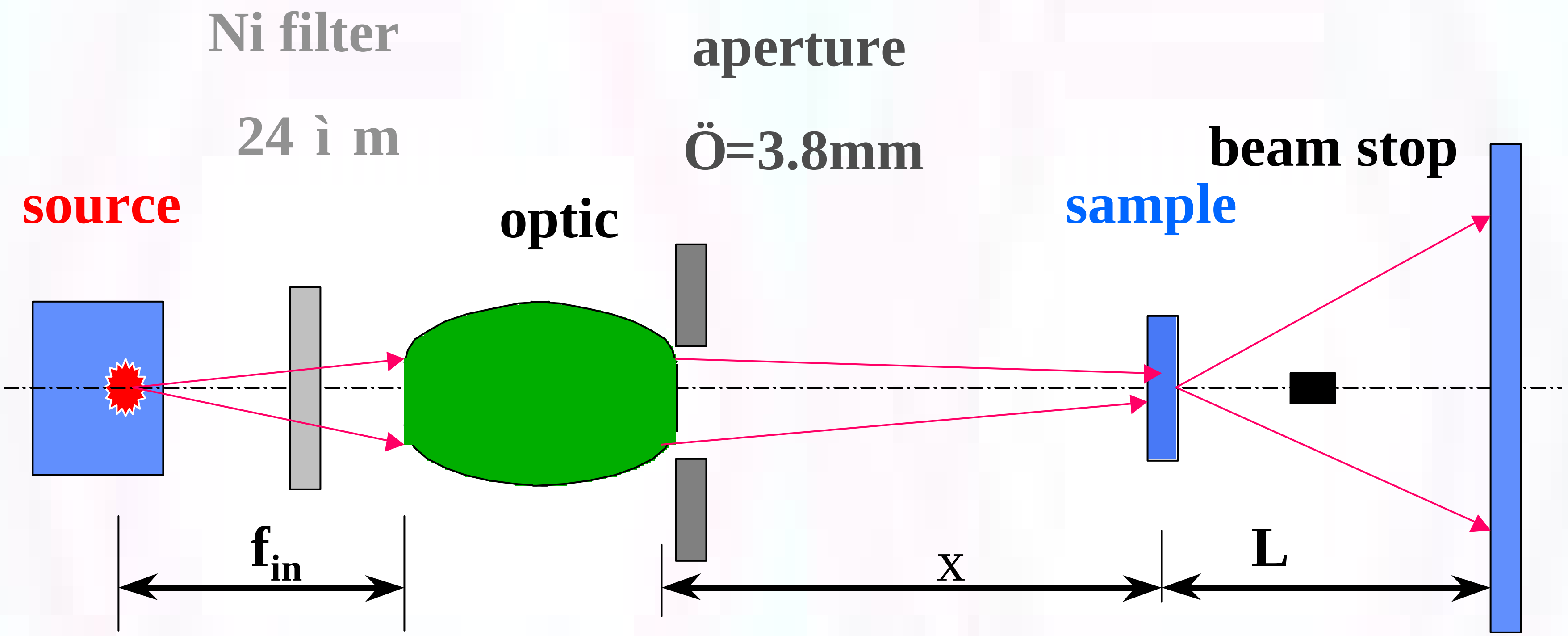

Applications: Powder Diffraction

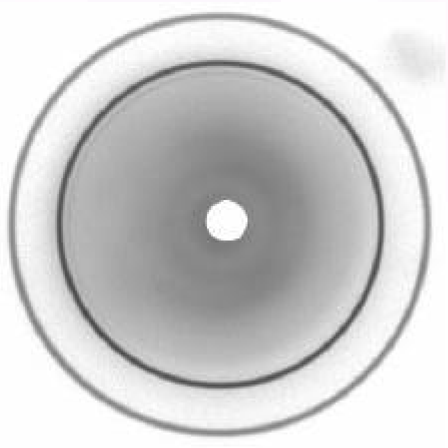

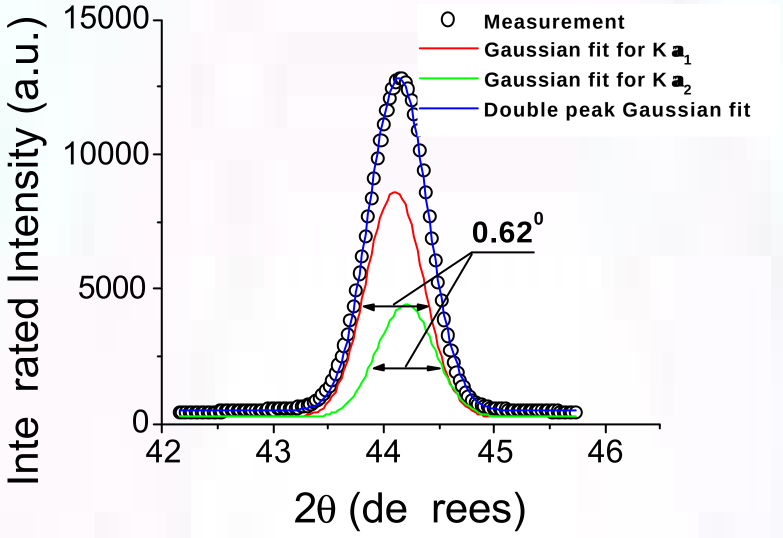

Optic Results	Relative Diffracted Beam Intensity	i sample at focus, plate at 66-75 mm	
		Peak width	Average Peak error
None	1	0.7	0.23
f 47	5	1.1	0.3
f 119	113	1.9	0.2

Applications: m-SPECT/CT

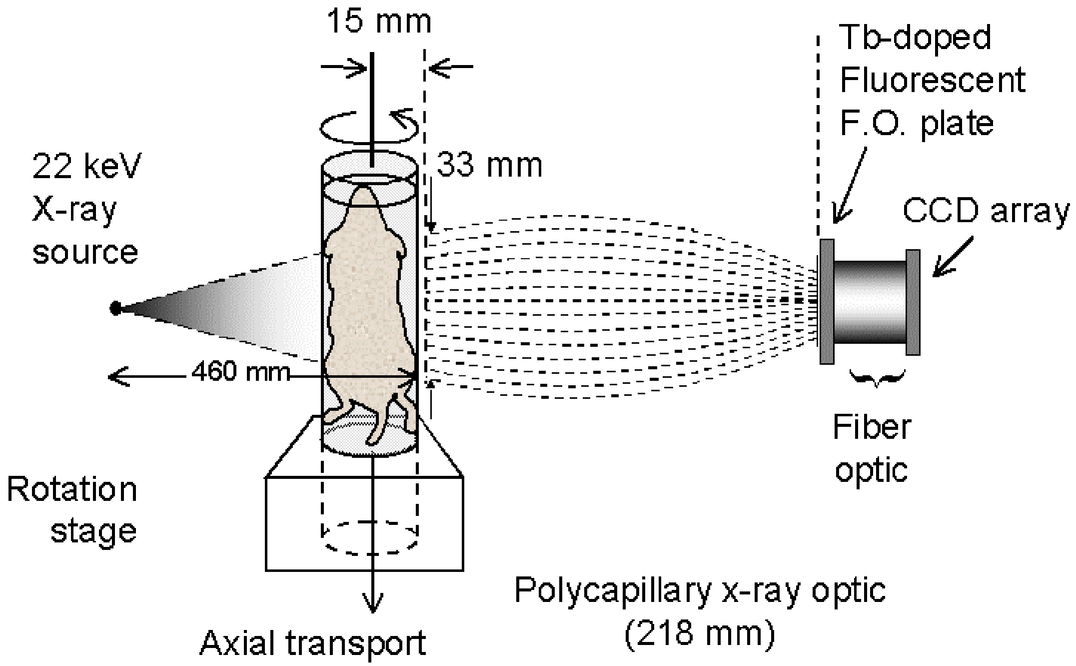

E. Ritman et al., Mayo clinic

Applications: Orthovoltage Therapy

Will the spot size increase due to intervening “tissue”?

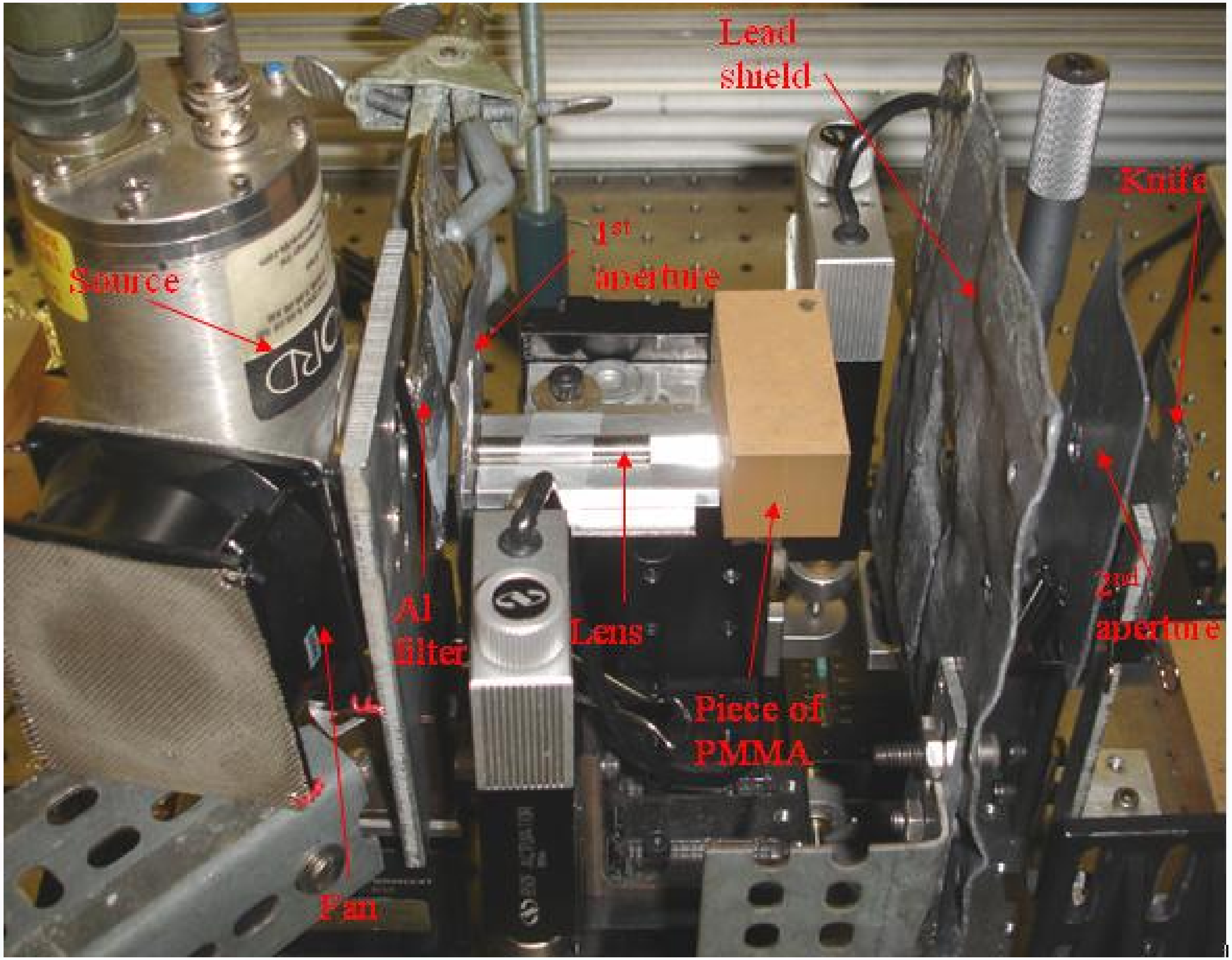

Applications: Orthovoltage Therapy

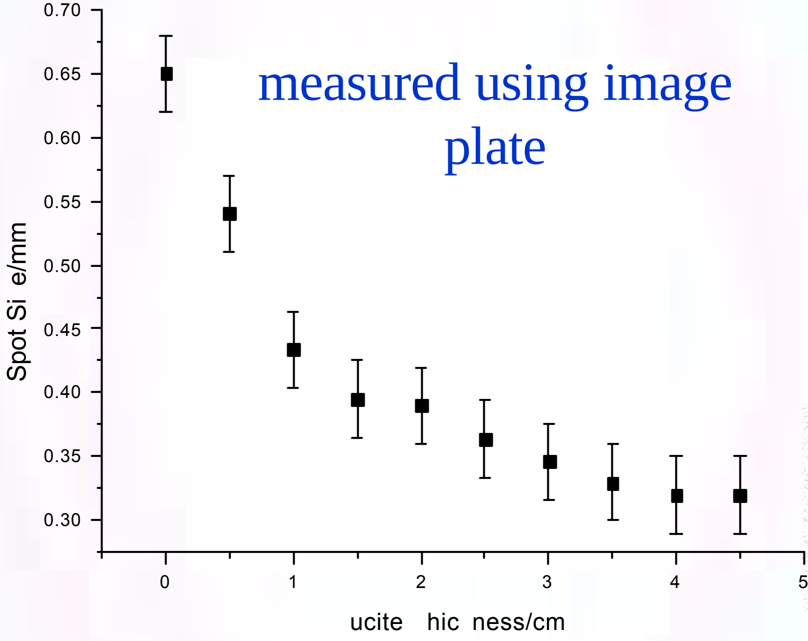

measured using image plate

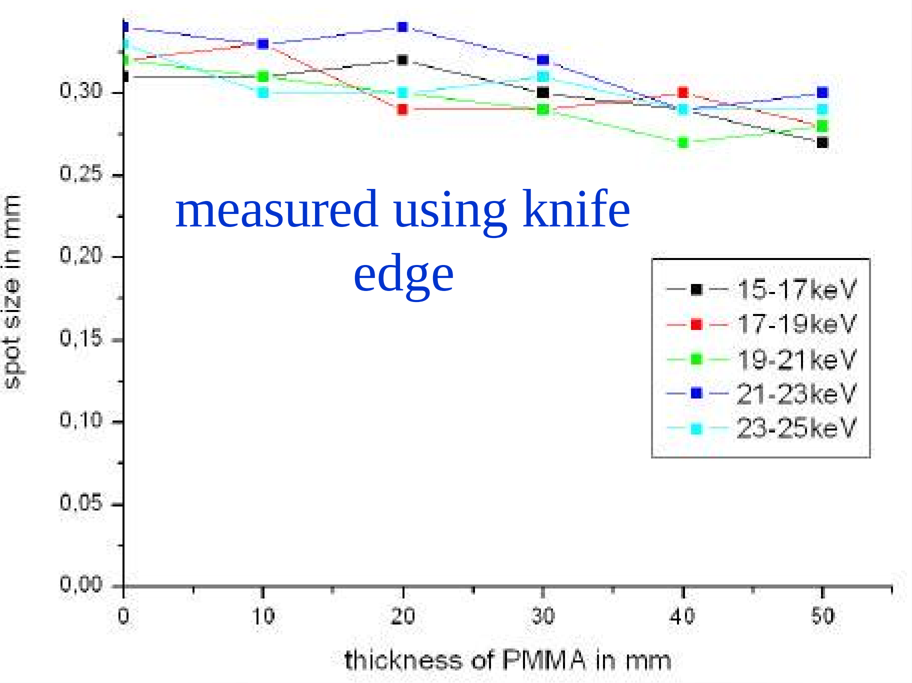

measured using knife edge

Beam hardening

Applications: Synchrotron Focusing and Astronomy

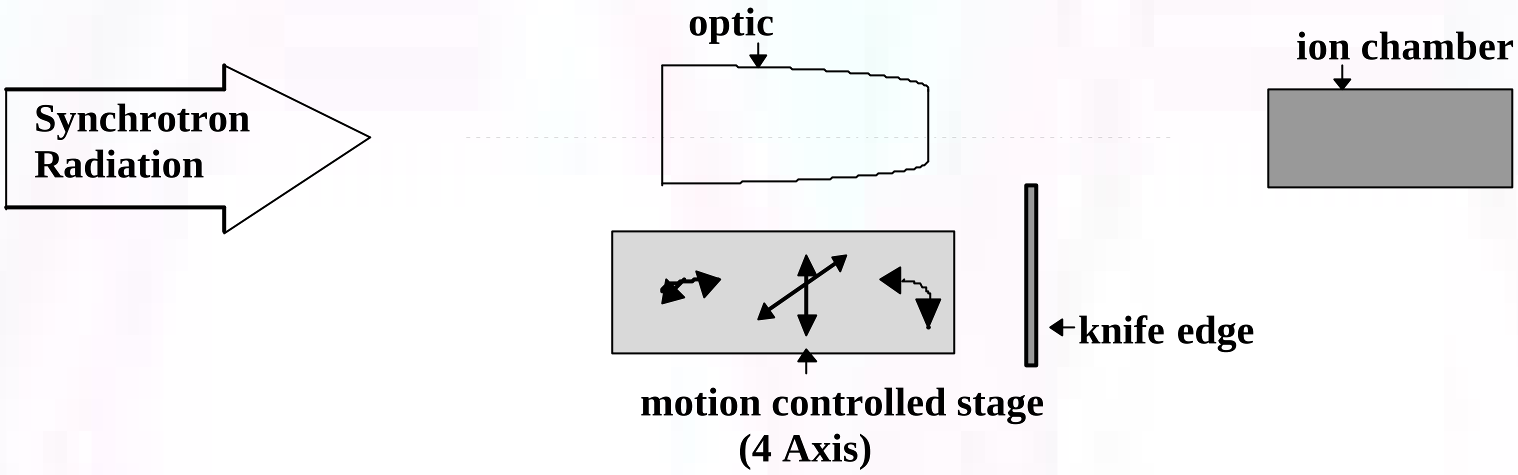

Synchrotron Radiation

optic

ion chamber

knife edge

motion controlled stage
(4 Axis)

Table 1. Results for monolithic focusing optic.

X-Ray Energy (eV)	Spot size (mm)	Trans-mission ( )	measured Gain 350 µm pinhole	calculated Gain 350 µm pinhole	calculated Gain 90 µm pinhole	calculat Gain 10 µm pinhole
6	0.09	36	78	81	645	911
8	0.08	49	96	110	933	1359
10	0.09	39	83	87	624	842
12	0.09	39	74	87	654	903
white	0.17	42	11	89	243	266

References

F.R. Sugiro, Danhong Li, C.A. MacDonald, "Beam Collimation with Polycapillary X-ray Optics for High Contrast High Resolution Monochromatic Imaging,", Med. Phys., **31**, p. 3288, 2004.

C.A. MacDonald and W.M. Gibson, "Applications and Advances In Polycapillary Optics", X-ray Spectrometry, **32 (**3), 2003, pp 258-268.

C.A. MacDonald, W.M. Gibson, and W. Peppler, "X-Ray Optics for Better Diagnostic Imaging," Technology In Cancer Research And Treatment, 1, (2), April 2002, pp 111-118.

Suparmi, Cari, Lei Wang, Hui Wang, W.M. Gibson, C.A. MacDonald, "Measurement and Analysis of Leaded glass Capillary Optic Performance for Hard X ray Applications," Journal of Applied Physics **90** (10), pp. 5363-8, 2001.

F.A. Hofmann, W.M. Gibson, C.A. MacDonald, D.A. Carter, J.X. Ho, J.R. Ruble, "Polycapillary Optic – Source combinations for Protein Crystallography," Jour. Applied Crys. **34**, pp.330-335, 2001.

C.A. MacDonald and W.M. Gibson, "An Introduction to X-ray and Neutron Optics," chapter 19 in M. Bass, ed., **Handbook of Optics, Volume III**, McGraw-Hill 2000.

C.A. MacDonald and W.M. Gibson, "Polycapillary and Multichannel Plate X-ray Optics," chapter 30 in M. Bass, ed., **Handbook of Optics, Volume III**, McGraw-Hill 2000.

J.B. Ullrich and C.A. MacDonald, "Electron Impact Sources," chapter 31 in M. Bass, ed., **Handbook of Optics, Volume III**, McGraw-Hill 2000.

C.A. MacDonald and W.M. Gibson, "Applications Requirements Affecting Optics Selection," chapter 35 in M. Bass, ed., **Handbook of Optics, Volume III**, McGraw-Hill 2000.

W.M. Gibson and C.A. MacDonald, "Summary of X-ray and Neutron Optics," chapter 37 in M. Bass, ed., **Handbook of Optics, Volume III**, McGraw-Hill 2000.

C.A. MacDonald and S.D. Padiyar, "How Photons Work," cover article, Photonics Spectra, August 2000.

C.A. MacDonald, S.M. Owens, and W.M. Gibson, "Polycapillary X-Ray Optics for Microdiffraction," Journal of Applied Crystallography, **32**, pp160-7, 1999.

B.K. Rath, W.M. Gibson, Lei Wang, B.E. Homan and C.A. MacDonald, "Measurement and Analysis of Radiation Effects in Polycapillary X-ray Optics," Journal of Applied Physics, 83, no.12, pp. 7424-7435, June 15 1998.

C.C. Abreu and C.A. MacDonald, "Beam Collimation, Focusing, Filtering and Imaging with Polycapillary X-ray and Neutron Optics," invited review article, Physica Medica, vol. XIII, N.3, 1997, pp. 79-89.

F.A. Hofmann, C.A. Freinberg-Trufas, S.M. Owens, S.D. Padiyar, C.A. MacDonald, "Focusing of Synchrotron Radiation with Polycapillary Optics," Beam Interactions with Materials and Atoms: Nuclear Instruments and Methods B, vol. **133**, 1997, pp. 145-150.

FOCUSING OF X-RAYS USING CRYSTAL OPTICS

Eckhart Förster

Friedrich-Schiller-University Jena,
Institute for Optics and Quantum Electronics,
X-Ray Optics Group
07743 Jena, Germany

Workshop: Focus on X-Ray Focusing, San Diego, August 13, 2008

X-Ray Bragg Reflection on a Flat Sample Crystal

Real space

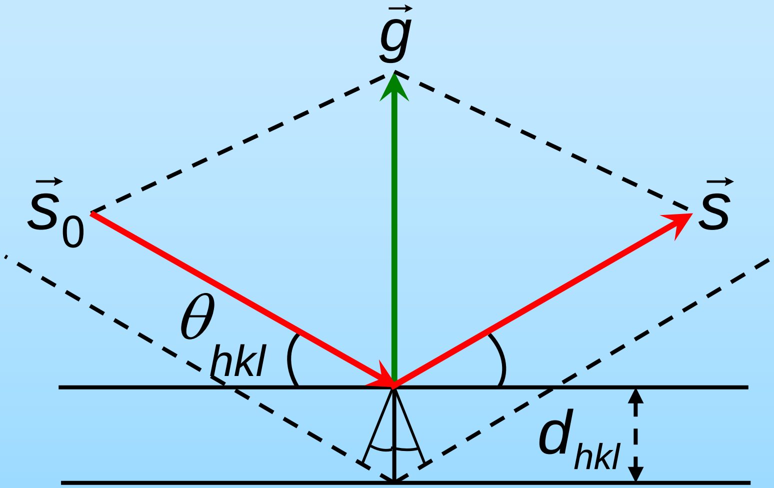

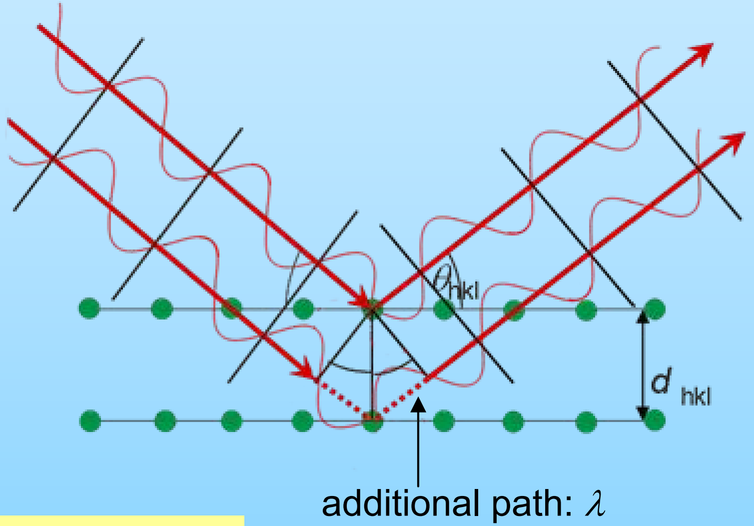

$$n \lambda = 2\, d_{\mathrm{hkl}} \sin \theta_{\mathrm{hkl}}$$

$\vec{s}_0$: incident beam wave vector

$\vec{s}$: Bragg reflected beam wave vector

θ_{hkl}: Bragg angle

d_{hkl}: distance between the reflecting planes

$\vec{g}$ normal of reflecting planes, reciprocal lattice vector

hkl indices of reflecting planes

n 1, 2, …, diffraction order

Scheme of Bragg-Reflection: DuMond-Graphs

flat crystal, symmetrical reflection

$n\,\lambda = 2\,d \sin\,\theta$

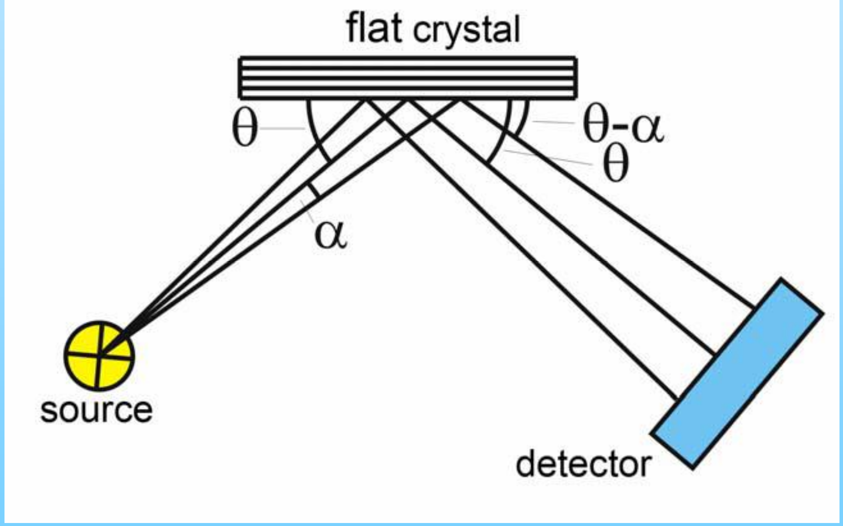

reflection curve

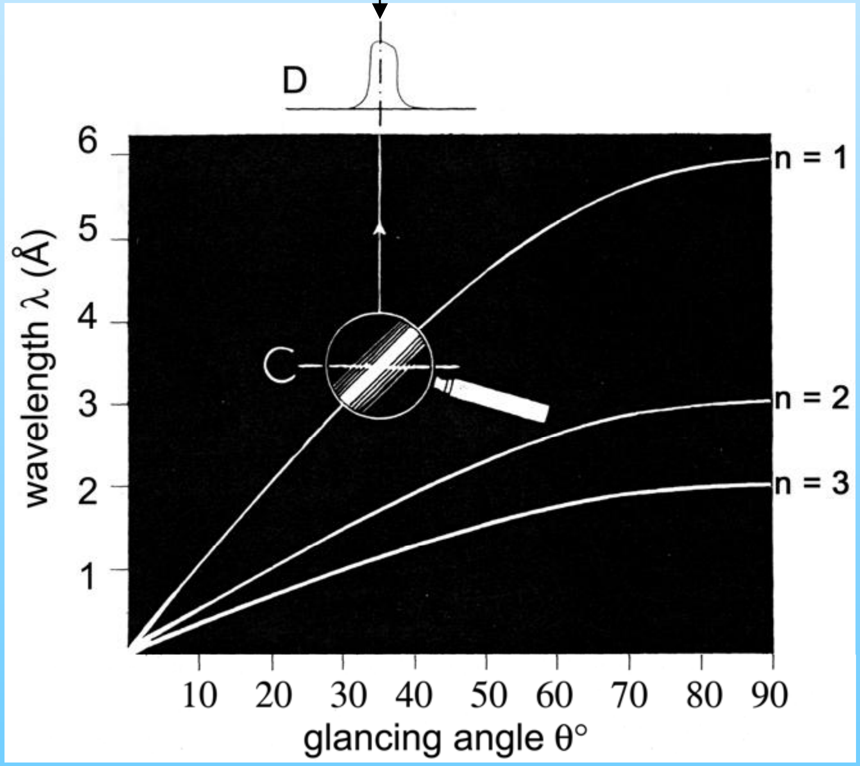

Merrill, DuMond, Annals of Physics 14 (1961), Fig. 5

X-Ray Spectrometer with Flat and Bent Crystals

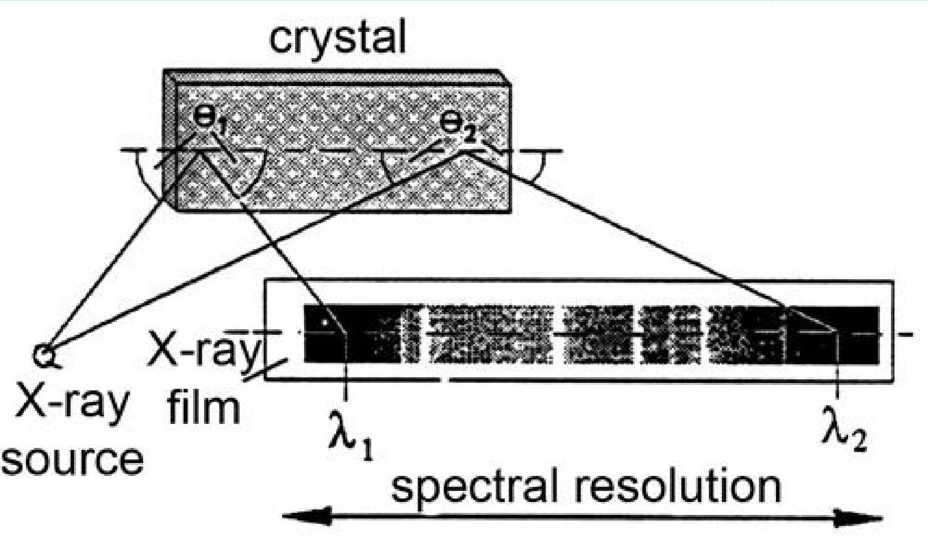

X-ray spectrometer
with a single flat crystal

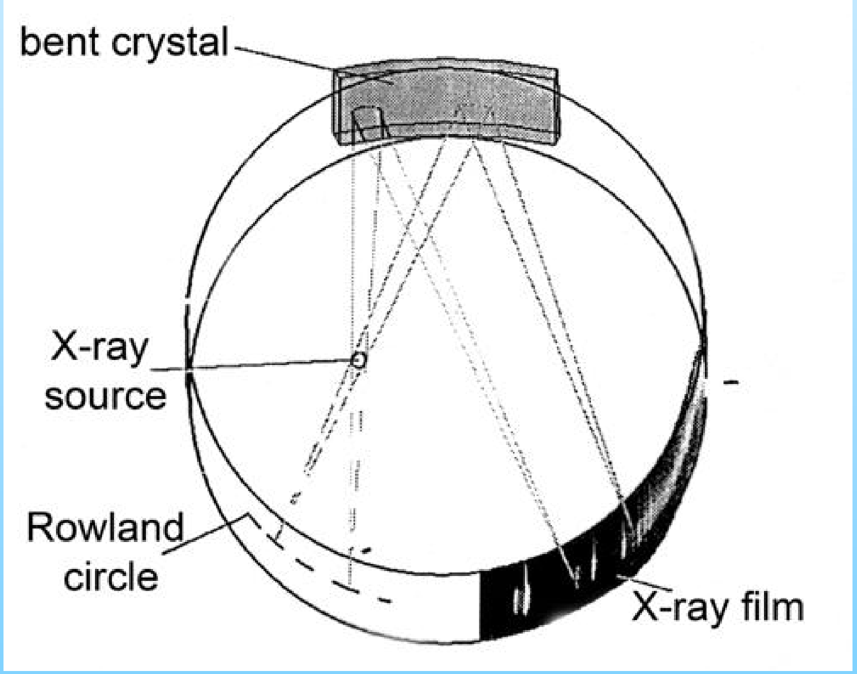

Johann spectrometer
with a bent crystal

E. Förster et al., Journal of Quantitative Spectroscopy and Radiative Transfer 51 (1994), 101

Application Range of Crystal Reflection

Application range of crystal reflection for Bragg angles 60° - 89°

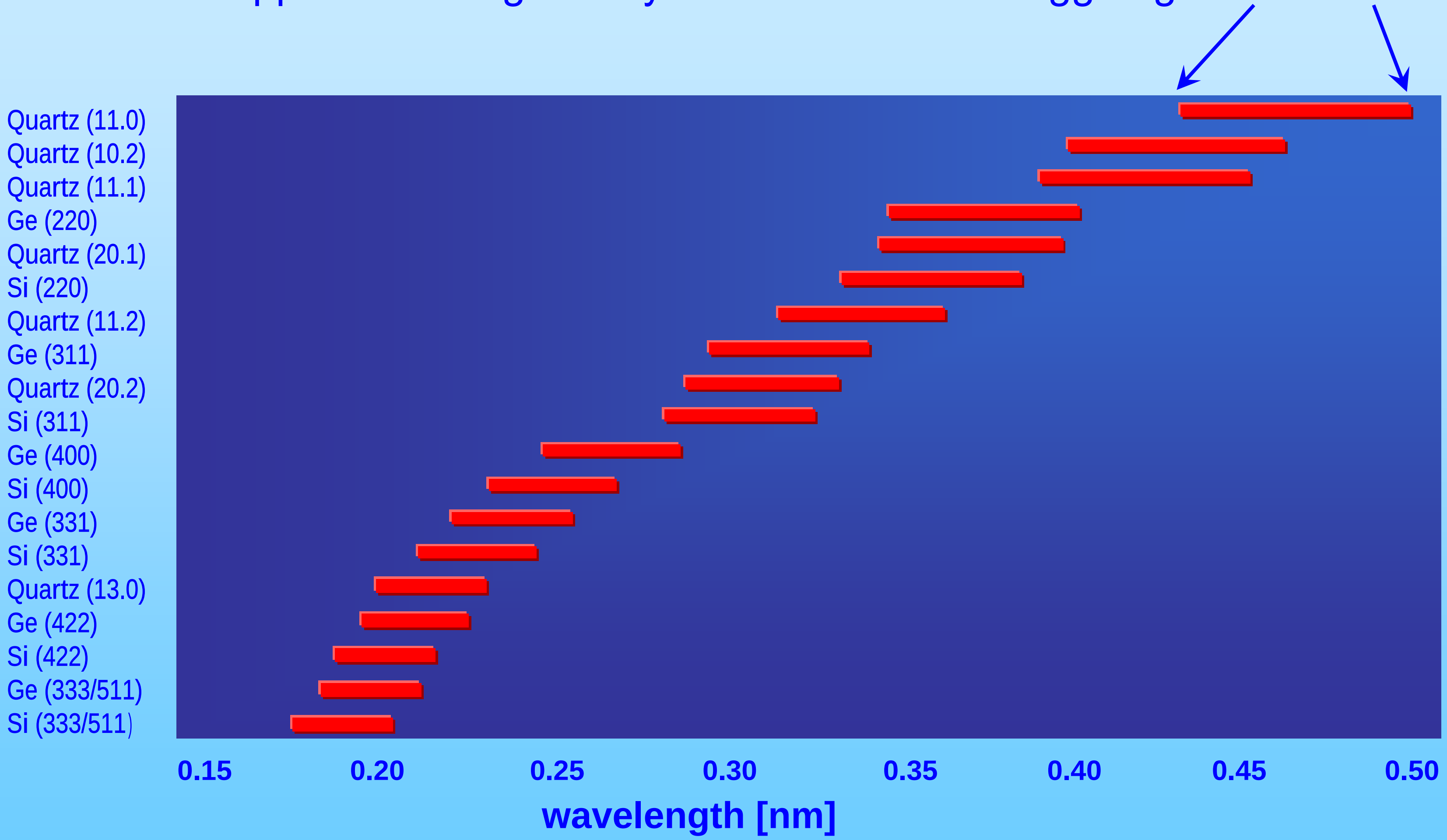

X-ray imaging is best, if θ is maximal.

N. Vollbrecht et al., Journal of Qantitative Spectroscopy and Radiative Transfer <u>58</u> (1997), 965

Toroidal Bent Crystals for Focusing of X-Ray from fs Laser Plasma

focal lengths: $f_h = (R_h/2)\cdot\sin\theta_B$

$f_v = R_v/(2\cdot\sin\theta_B)$

Point to point focussing $R_v / R_h = \sin^2\theta$

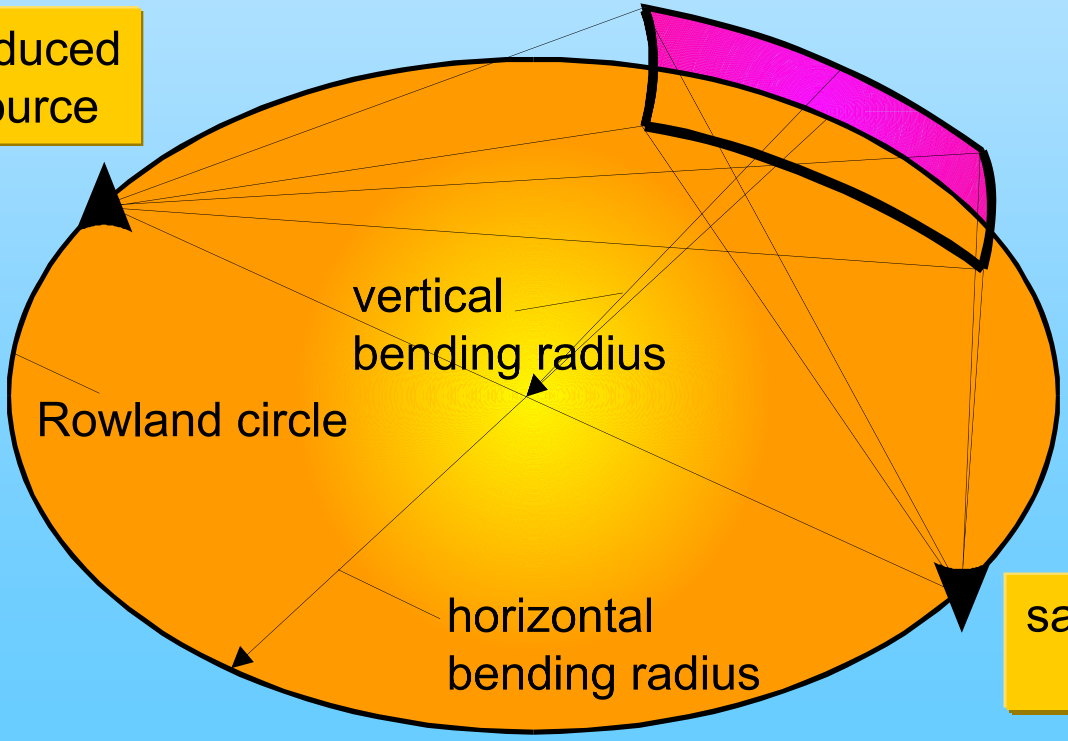

toroidally bent crystal

laser produced X-ray source

vertical bending radius

Rowland circle

horizontal bending radius

sample crystal

Fabrication and Test of Toroidally Bent Crystals

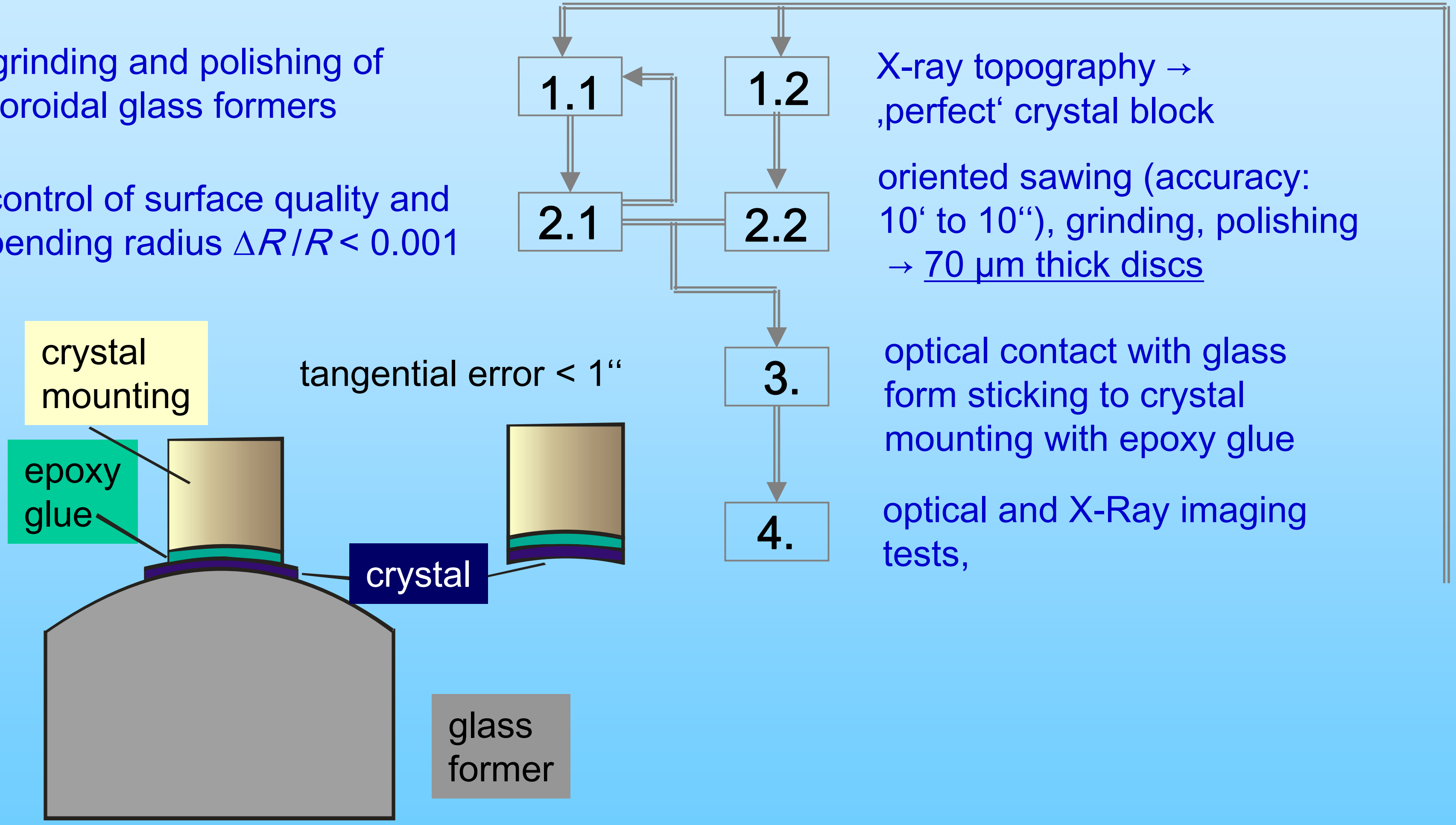

grinding and polishing of toroidal glass formers

control of surface quality and bending radius $\Delta R/R < 0.001$

X-ray topography → ‚perfect‘ crystal block

oriented sawing (accuracy: 10‘ to 10‘‘), grinding, polishing → 70 µm thick discs

tangential error < 1‘‘

optical contact with glass form sticking to crystal mounting with epoxy glue

optical and X-Ray imaging tests,

Relation of the Curvature Radii: $R_v/R_h = \sin^2\theta$

Test of Bent Crystals for Monochromatic Imaging

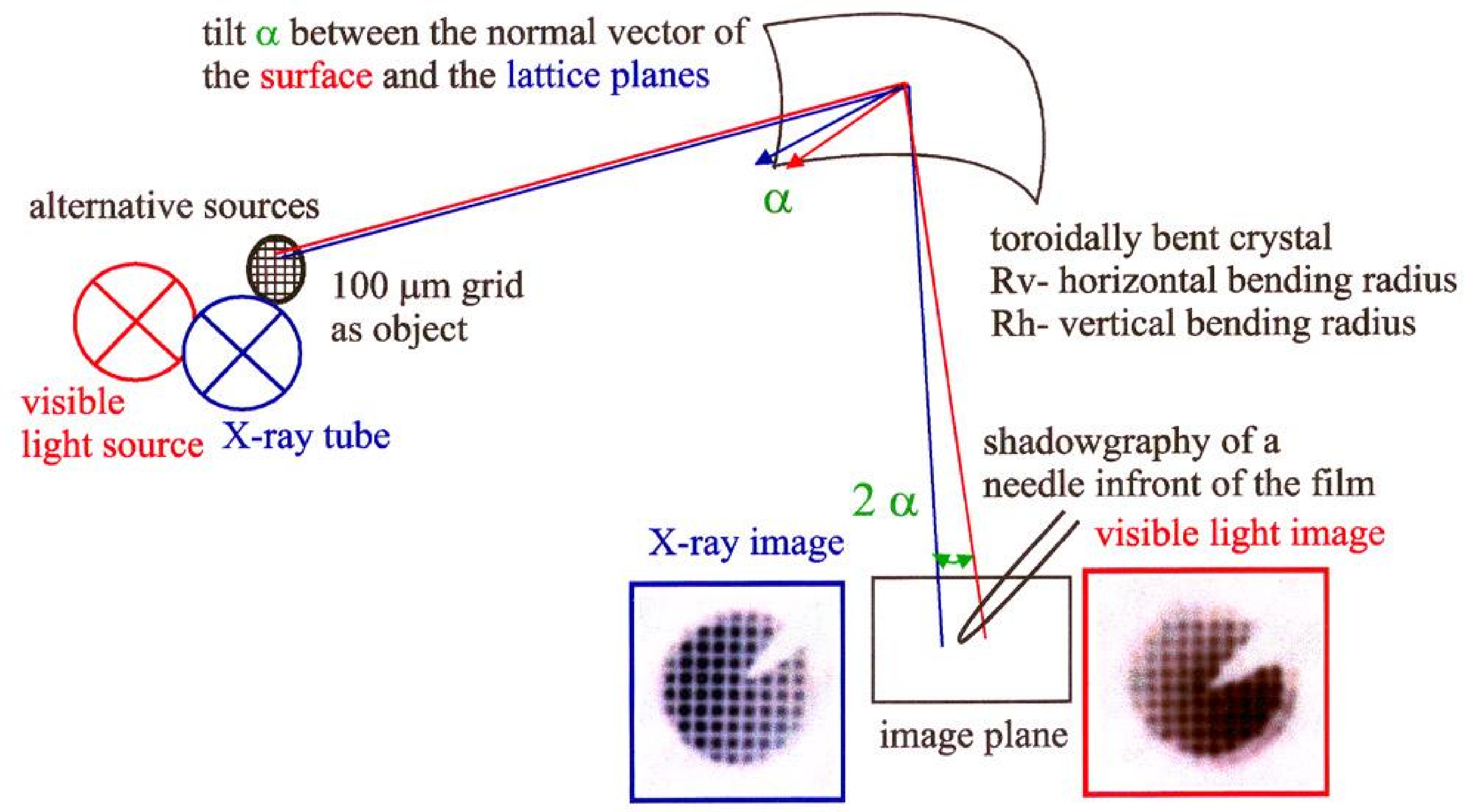

Fabrication and Test of Toroidally Bent Crystals

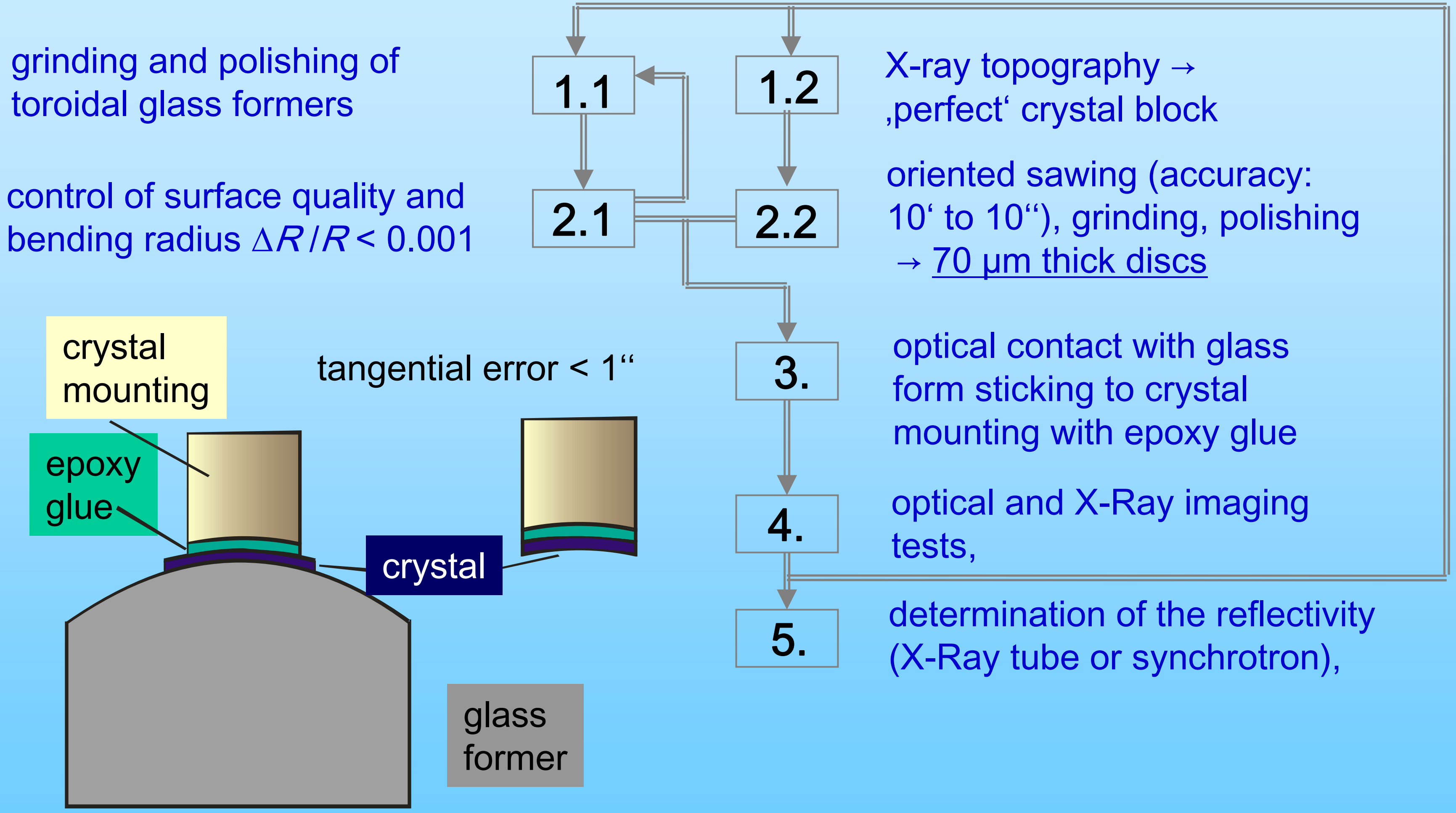

1.1 grinding and polishing of toroidal glass formers

1.2 X-ray topography → ‚perfect‘ crystal block

2.1 control of surface quality and bending radius $\Delta R/R < 0.001$

2.2 oriented sawing (accuracy: 10‘ to 10“), grinding, polishing → <u>70 µm thick discs</u>

3. optical contact with glass form sticking to crystal mounting with epoxy glue

4. optical and X-Ray imaging tests,

5. determination of the reflectivity (X-Ray tube or synchrotron),

Relation of the Curvature Radii: $R_v/R_h = \sin^2\theta$

Experimental Setup for Reflection Curve Measurement

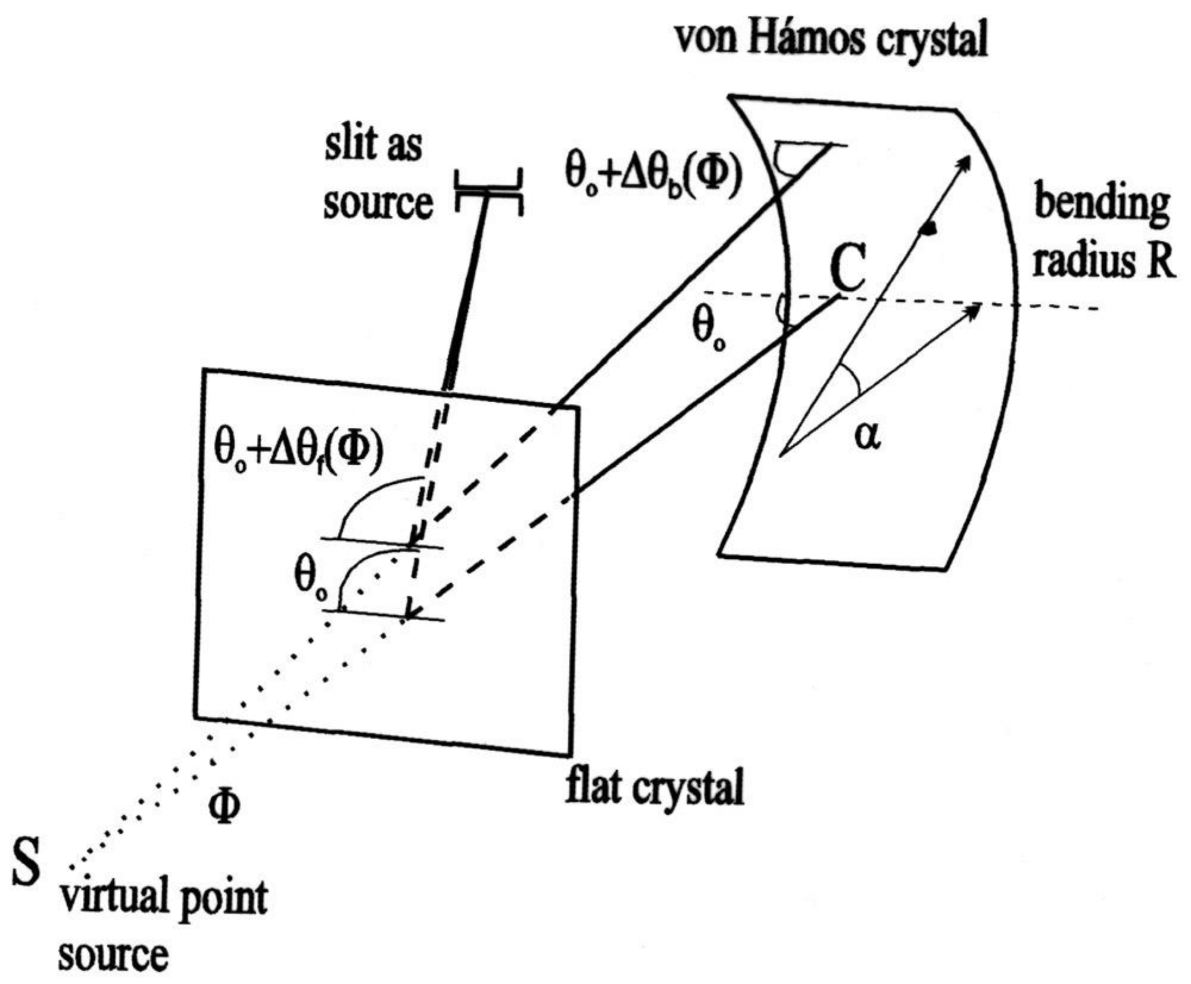

Experimental set-up for the rocking curve measurement using a flat and a cylindrically bent von Hámos – crystal, SC = *a*.

Reflection Curves of a Cylindrically Bent Quartz $40.\overline{4}$

$$E_{\text{det}} = \iiint \mathrm{d}\alpha\, \mathrm{d}\phi\, \mathrm{d}\lambda\, J_s(\alpha,\phi,\lambda) \times C\left(\sigma(\alpha,\phi) - \frac{\Delta\lambda}{\lambda}\tan\theta_0\right)$$

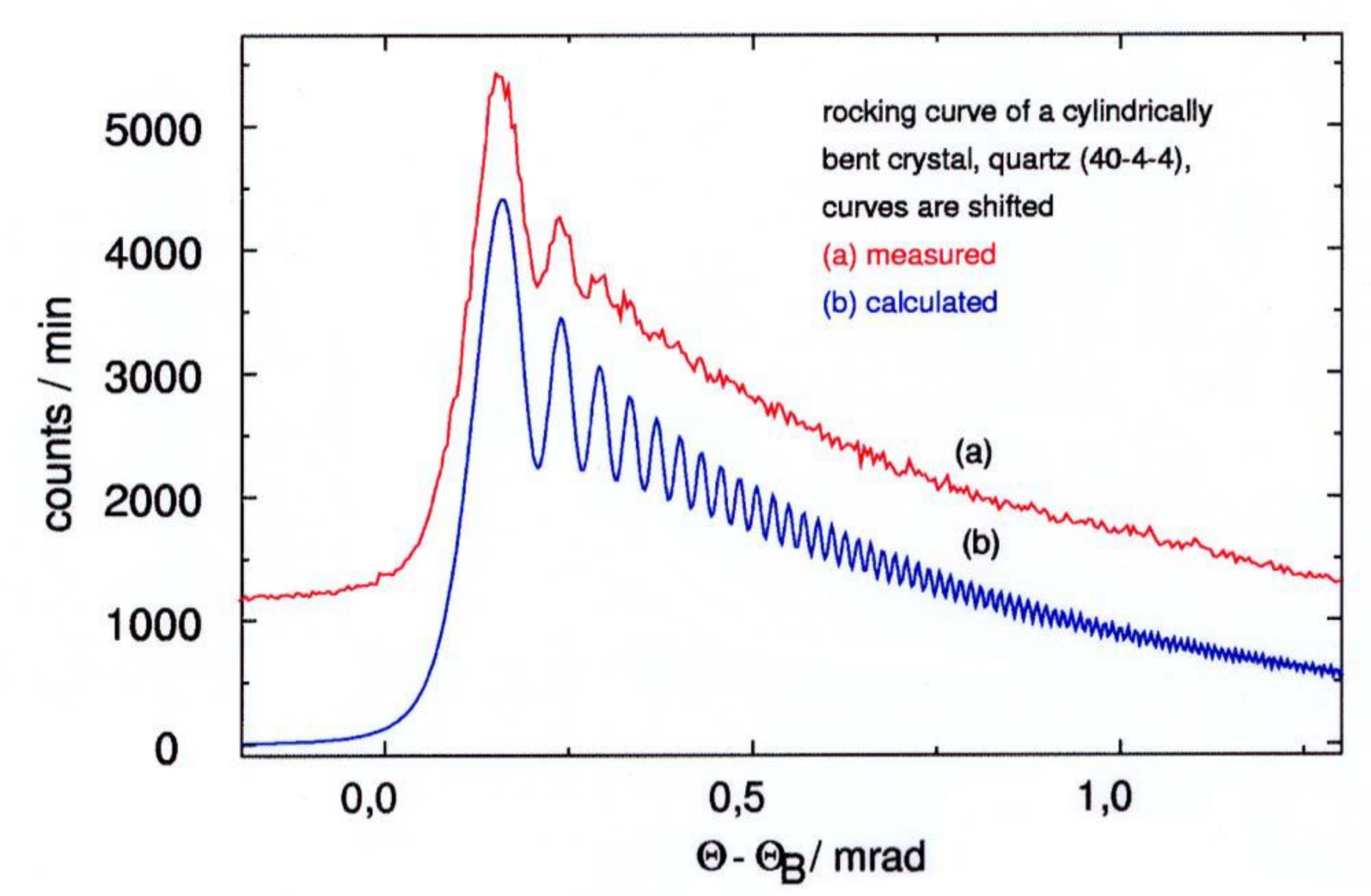

I. Uschmann, C. Malgrange, E. Förster, J. Appl. Cryst. 30 (1997), 1150

Dependency of the Reflection Power of the Curvature Radius

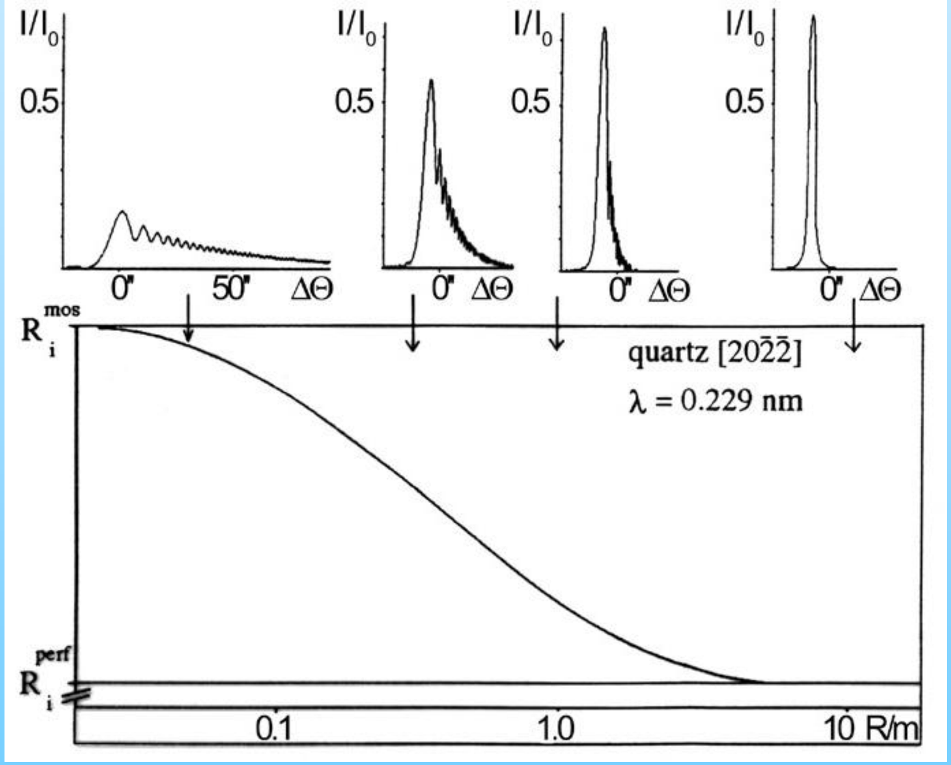

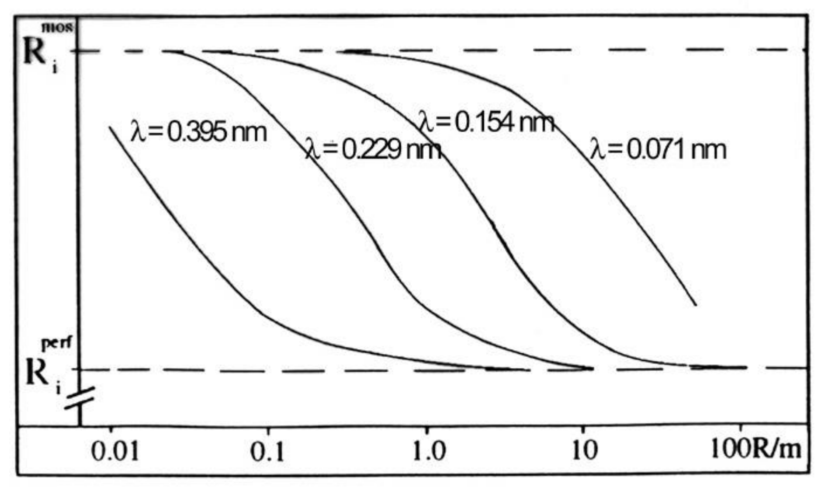

I. Uschmann et al., J. Appl. Cryst. **26** (1993), 405

Fabrication and Test of Toroidally Bent Crystals

1.1 grinding and polishing of toroidal glass formers

1.2 X-ray topography → ‚perfect‘ crystal block

2.1 control of surface quality and bending radius $\Delta R / R < 0.001$

2.2 oriented sawing (accuracy: 10‘ to 10“), grinding, polishing → 70 µm thick discs

3. optical contact with glass form sticking to crystal mounting with epoxy glue

4. optical and X-Ray imaging tests,

5. determination of the reflectivity (X-Ray tube or synchrotron),

6. use in X-Ray spectroscopy, diffractometry and X-Ray imaging

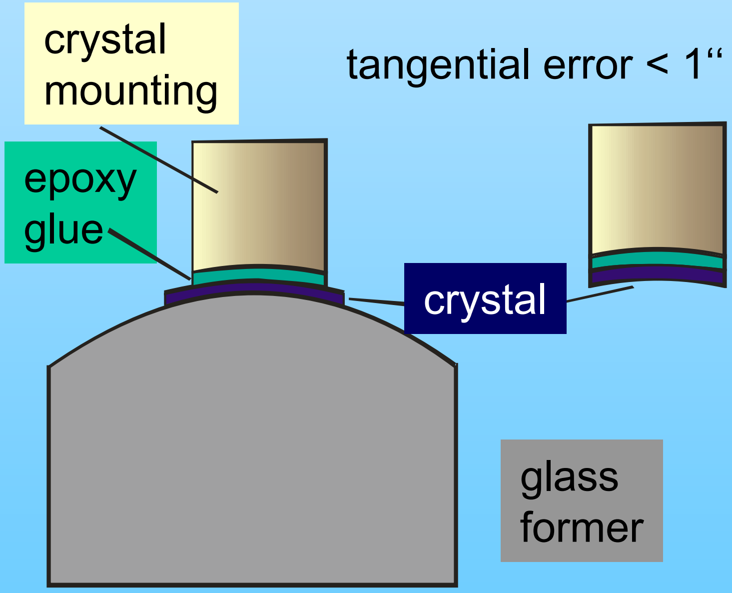

Relation of the Curvature Radii: $R_v / R_h = \sin^2\theta$

Typical Bent Crystal Parameters

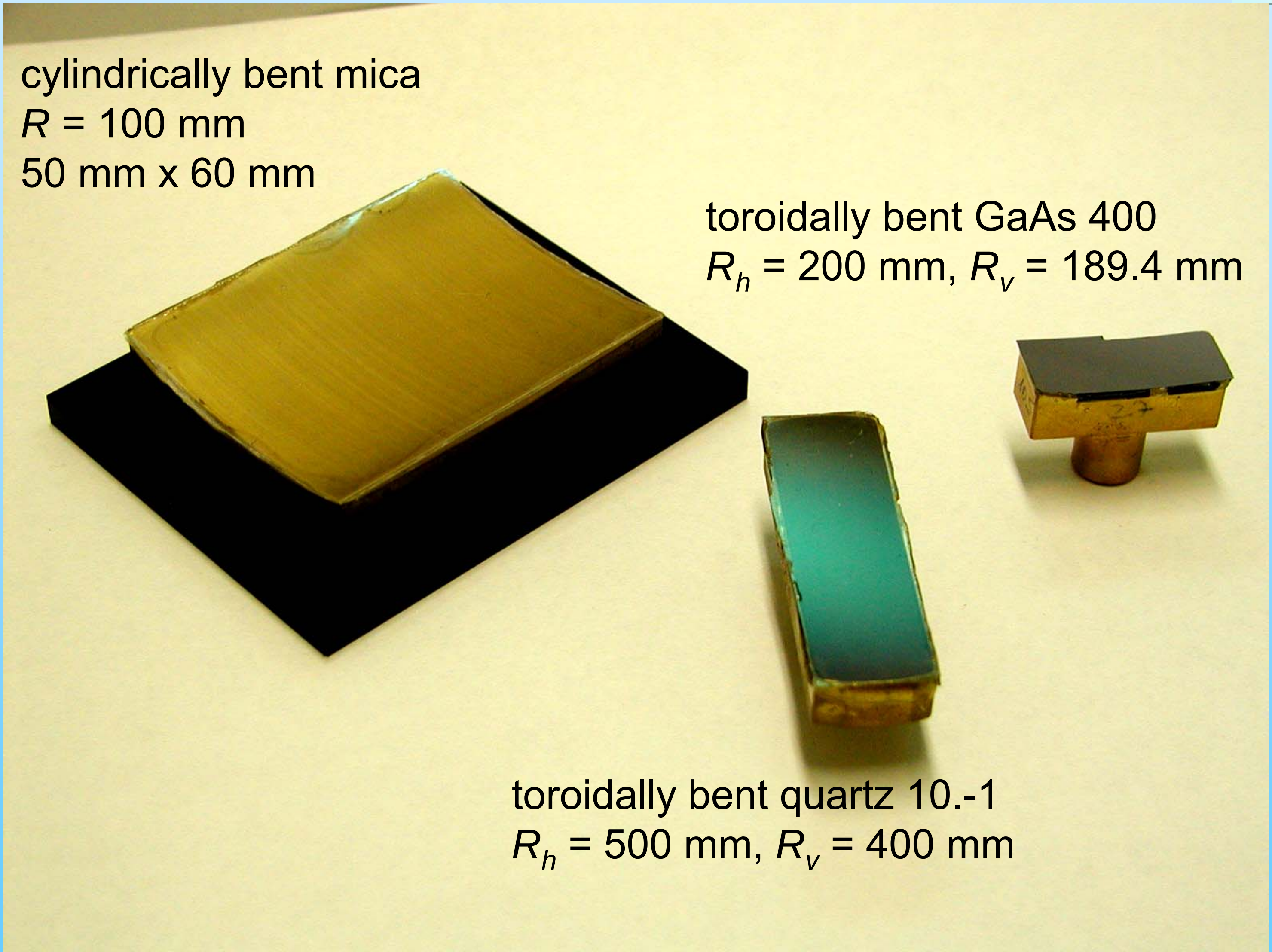

cylindrically bent mica
R = 100 mm
50 mm x 60 mm

toroidally bent GaAs 400
R_h = 200 mm, R_v = 189.4 mm

toroidally bent quartz 10.-1
R_h = 500 mm, R_v = 400 mm

X-Ray Diagnostics for Laser Fusion Experiments

High power laser**:** $E_L > 10^6$J, $\tau_L < 1$ns, $\lambda_L < 0{,}5\mu$m

main aim: supression of Rayleigh-Taylor instabilities

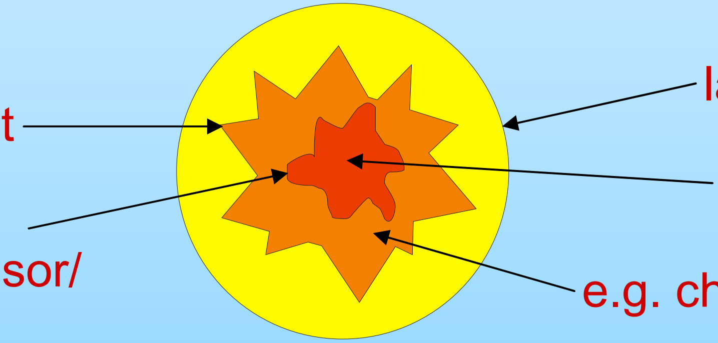

ablation front

interface

compressor/
D, T fuel

laser pusher

few % Argon
or Krypton

e.g. chlorine

$I_x\,(\lambda, x, y, z, t, \ldots)$

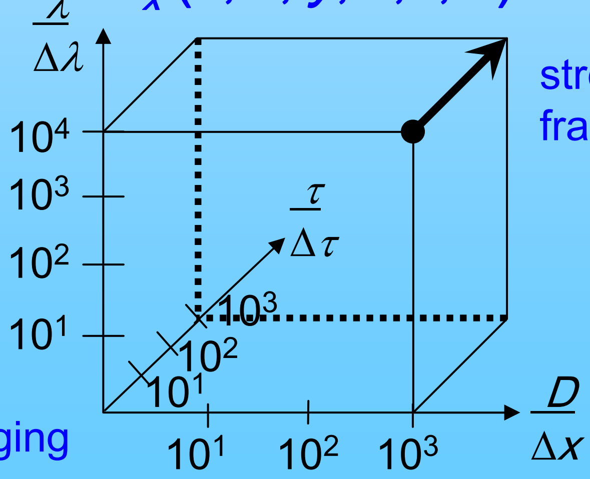

X-ray
spectrograph

streak or
framing camera

X-ray imaging
device

X-Ray Monochromatic Camera Using Two Toroidal Crystals

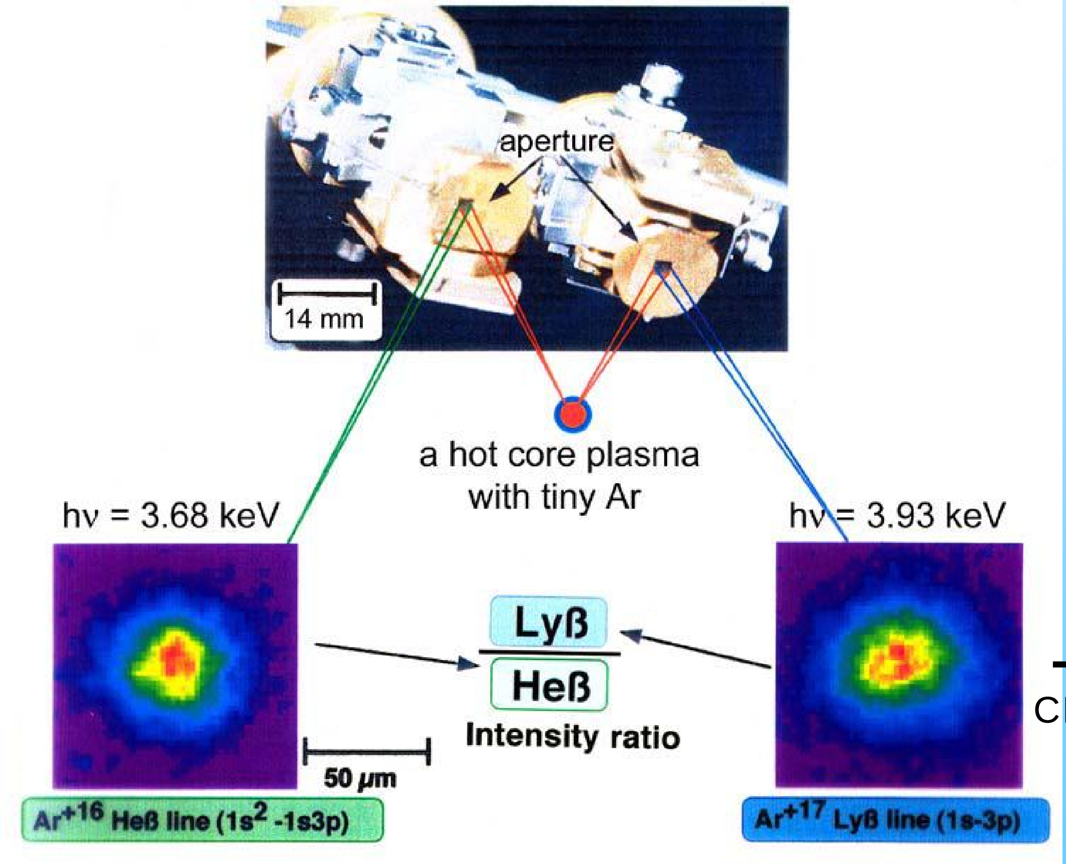

CRE model

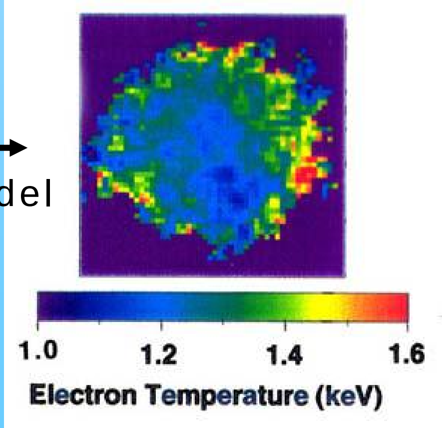

Ten Channel Imaging System

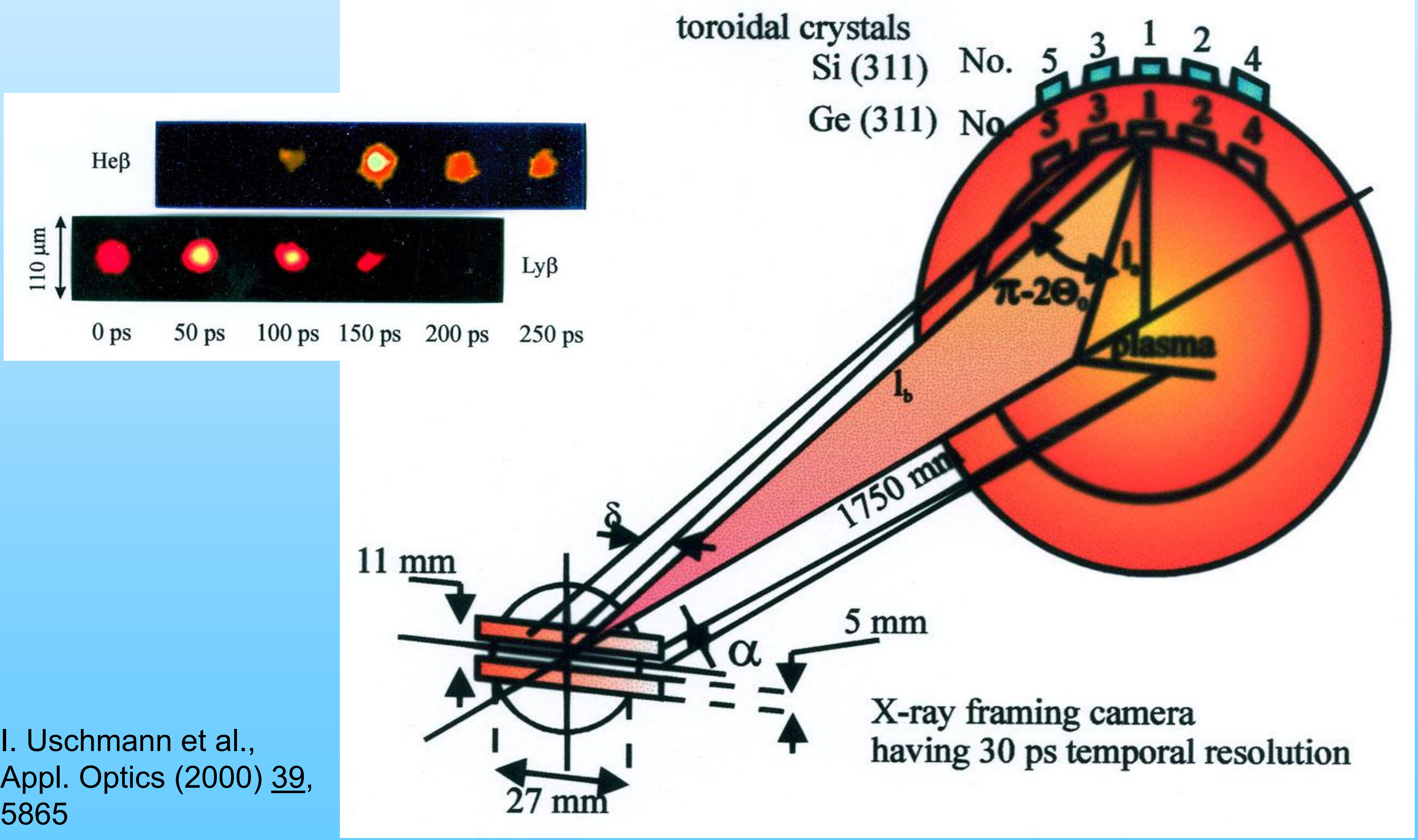

I. Uschmann et al.,
Appl. Optics (2000) 39,
5865

Abbe Sine Condition

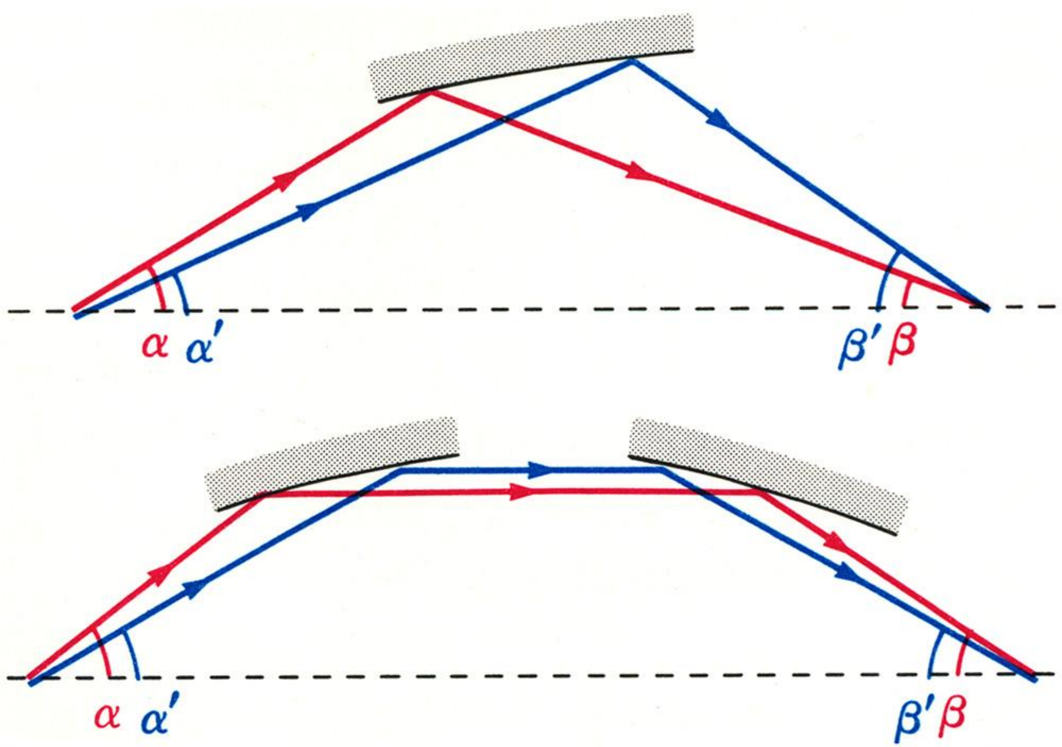

Coma can be corrected in X-ray optical systems with the use of two mirrors.
A single X-ray mirror strongly violates the Abbe sine condition, since β increases as α decreases, while the sine condition demands, that sinα / sinβ remain constant (upper diagr.). Approximate constancy of the sine ratio can be achieved through the use of two mirrors (lower diagr.), so that β increases as α increases.

James Underwood, American Scientist 66 (1978), 476 - 486

Two Crystal Scheme for X-Ray Monochromatic Imaging of Ultradense Plasmas

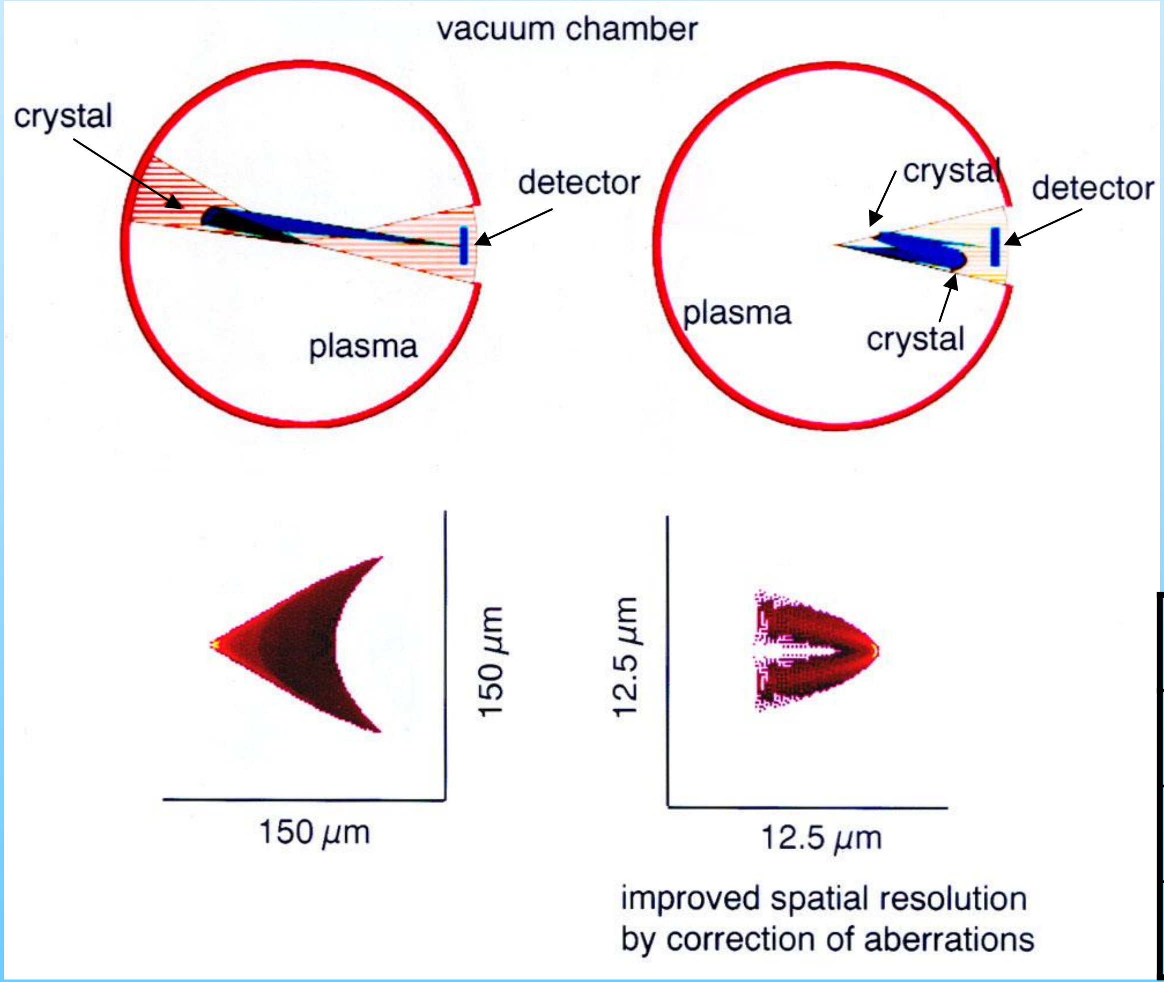

improved spatial resolution by correction of aberrations

	one crystal	two crystals
spatial resolution	14 µm	1.6 µm
spectral window ($\lambda/\Delta\lambda$)	235	6069
relative luminosity	1	1/15

Förster, Gibbon, Dirksmöller, Exp. Techn. Phys. **42** (1996), 19

Study of Ultrafast Processes in Crystalline Matter

Setup of an Optical Pump X-Ray Probe Experiment

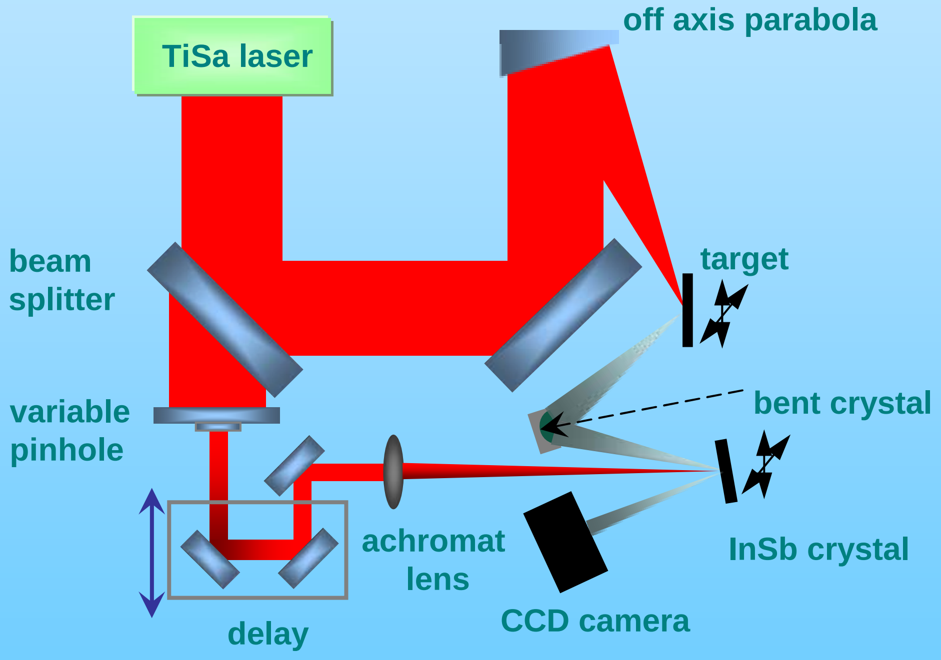

TiSa laser

off axis parabola

beam splitter

target

variable pinhole

bent crystal

achromat lens

InSb crystal

CCD camera

delay

T. Feurer et al., Appl. Phys. B (2001) 72, 15

Non-thermal Melting: InSb

X-ray signal (7 · 10^{16} W/cm^2)

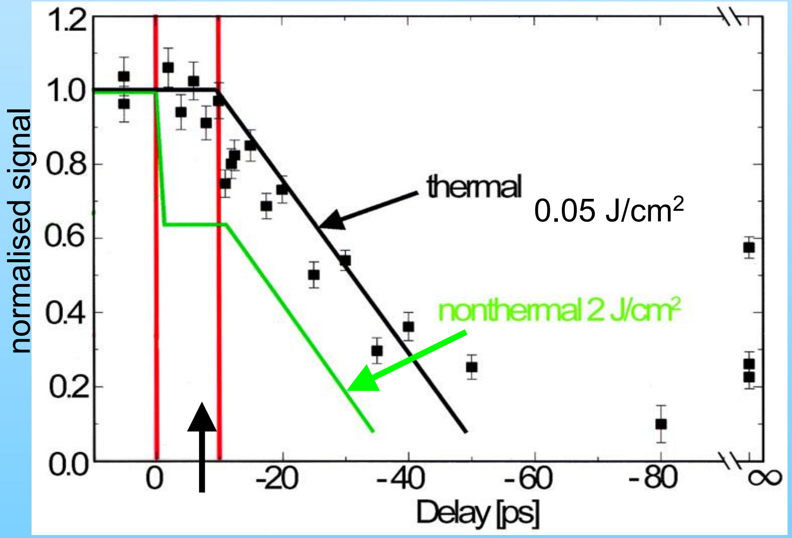

electron-phonon-coupling time 10 ps

A. Rousse et al., Nature, 410, No. 6824 (2001) 65 - 68

Schematic of Four Cu Kα Optics

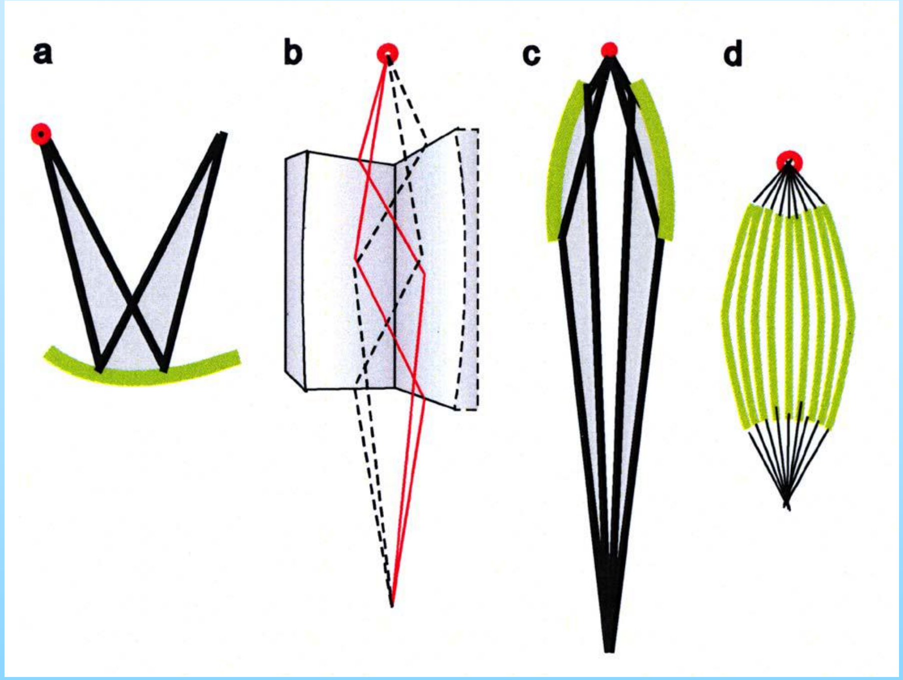

a. toroidally bent Ge crystal, 444 reflex, $\theta = 70°$,
b. two perpendicular elliptical Ni/C multilayer mirrors, $\theta \approx 3°$,
c. ellipsoidal lead-glass capillary,
d. borosilicate poly-capillaries (59,000).

M. Bargheer et al., Appl. Phys. B 80 (2005), 715

Characteristic Parameters of Cu Kα Optics

CuK_α optics	toroidal Ge	multilayer mirror system	ellipsoidal capillary	Poly-capillaries
size of focus (µm)	23	32	155	105
1D-convergence angle (deg)	1.5	0.45	0.2	3.5
solid angle (sr)	$2.3 \cdot 10^{-3}$	$8.8 \cdot 10^{-4}$	$4.0 \cdot 10^{-4}$	$1.1 \cdot 10^{-2}$
reflectivity or transmission	0.03	0.2	0.8	0.09
suppression of K_β	0.017	$5 \cdot 10^{-4}$	1.4	1.7

red – best value

pink –second best value

M. Bargheer et al., Appl. Phys. B 80 (2005), 715

Ellipsoidal HOP Graphite Crystal Reflection Curve

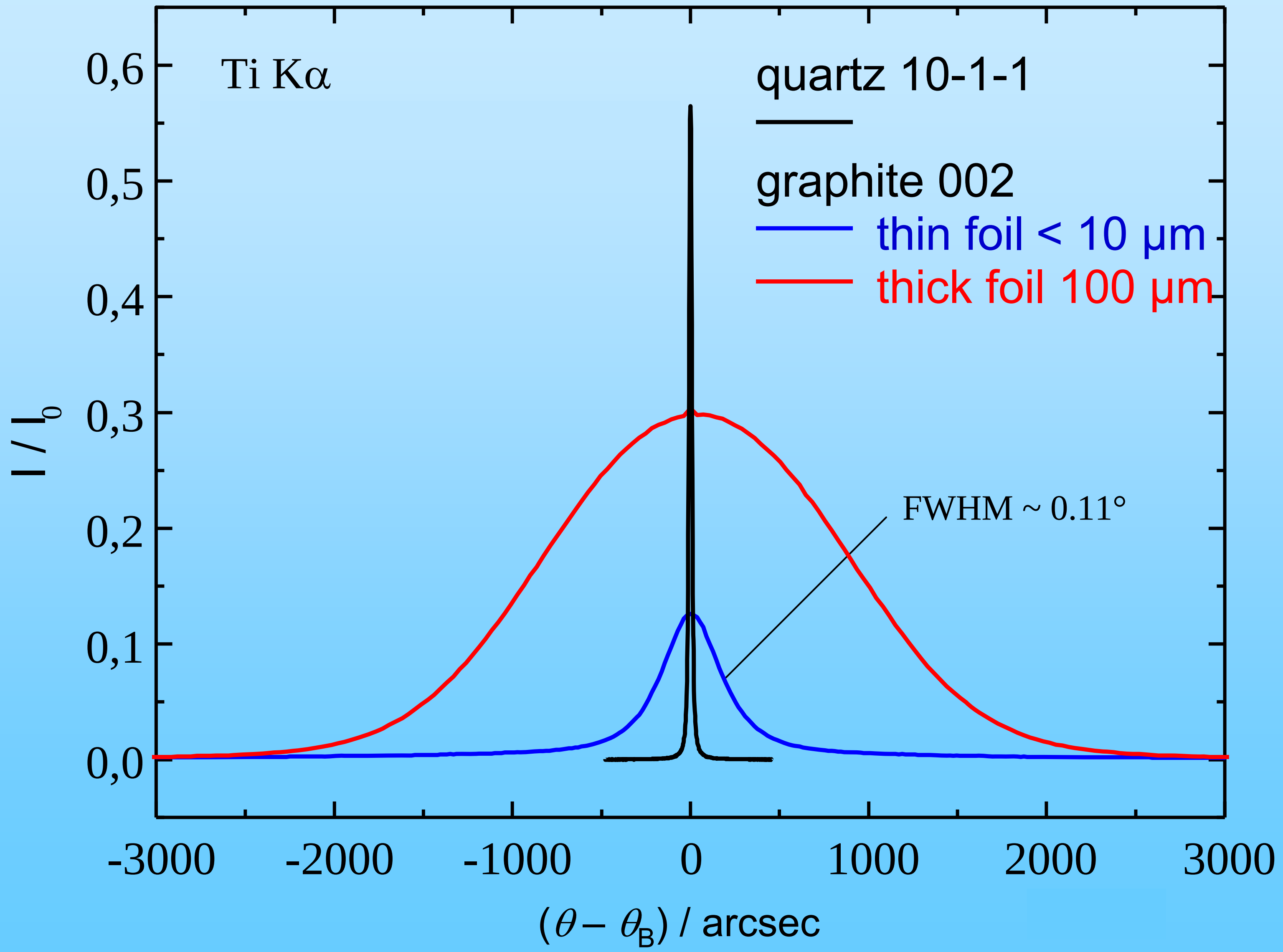

Ellipsoidal HOP Graphite Crystal X-Ray Focus Test

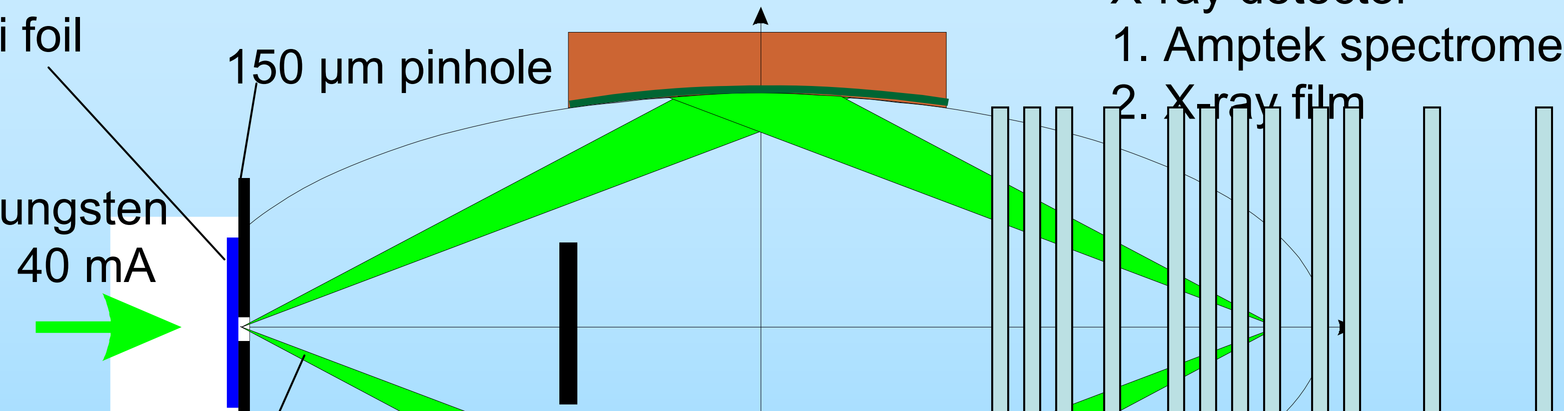

Ti foil

150 µm pinhole

X-ray detector
1. Amptek spectrometer
2. X-ray film

X-ray from tungsten tube, 10 kV, 40 mA

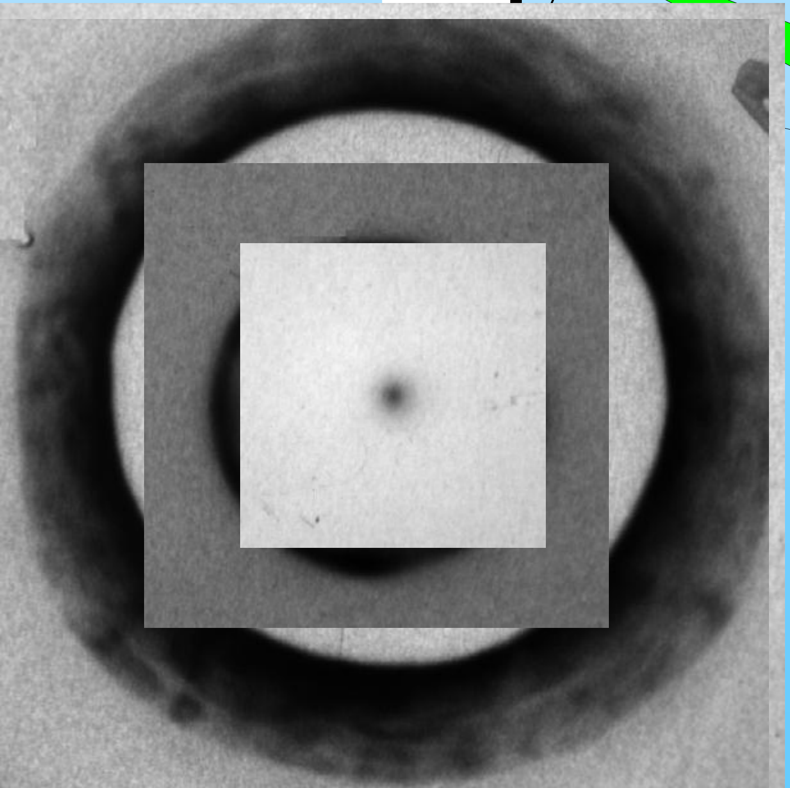

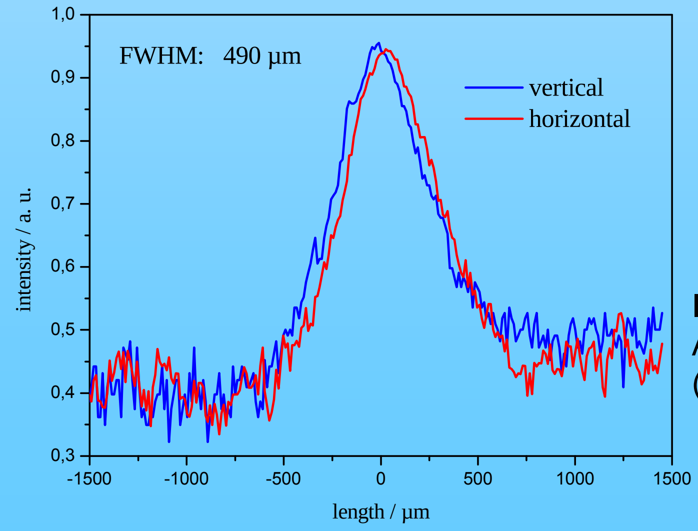

I. Uschmann et al., Appl. Optics 44, (2005), 5069

Summary
of X-Ray Crystal Optics Parameters

- Energy range: 500 eV – 40 keV (reflection case)
  20 keV – 100 keV (transmission case)

- Spectral resolution: $\Delta E / E$ = 1,000 – 10,000

- Used solid angle: 10^{-5} sr – 10^{-3} sr

- Focal size: 1 µm – 5 µm @ large θ angles,
  sub-µm for a two-crystal device

- Focal distance: 5 cm – 5 m

- Cost: 10,000 $ for one crystal

- Availability: firms of precision optics and crystal manufacturer,
  scientific institutes

Multilayer Laue Lens for Efficient Nanometer Focusing of Hard X-rays

G.B. Stephenson[1,2], H.C. Kang[2,4], H. Yan[1,5],
R.P. Winarski[1], M.V. Holt[1], J. Maser[1,3], C. Liu[3],
R. Conley[3,5], S. Vogt[3], and A.T. Macrander[3]

[1]Center for Nanoscale Materials,
[2]Materials Science Division, and
[3]X-ray Science Division,
Argonne National Laboratory

[4]Advanced Photonics Research Institute,
Gwangju Institute of Science and Technology

[5]National Synchrotron Light Source II,
Brookhaven National Laboratory

Workshop: Focus on X-ray Focusing, 2008 SPIE,
San Diego, CA, August 13, 2008

Outline

- Multilayer Laue Lens
  - Motivation and Approach
  - Status: 16 nm line focus, 31% efficiency, 19.5 keV
  - Future: Sub-nanometer focusing
- Overview of the Nanoprobe Beamline at Argonne

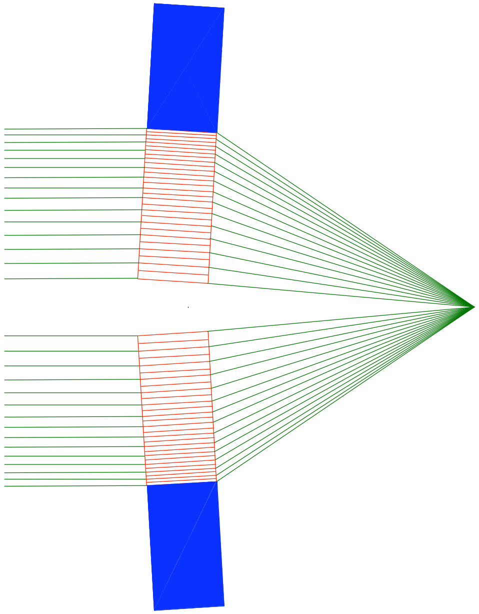

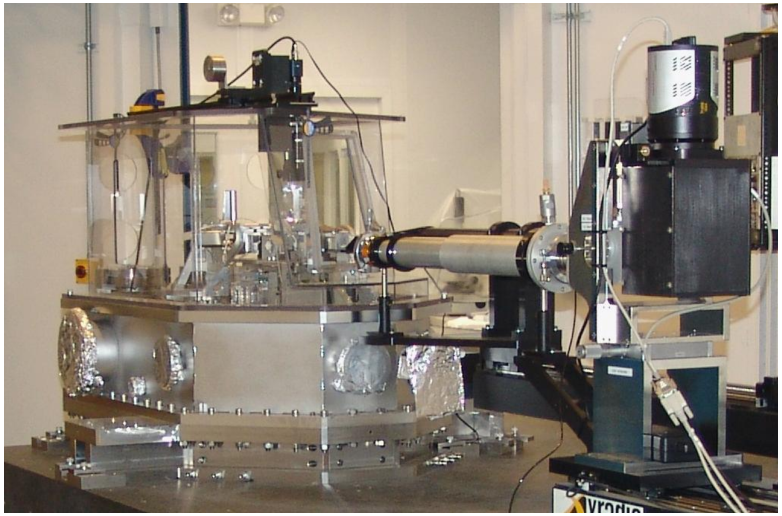

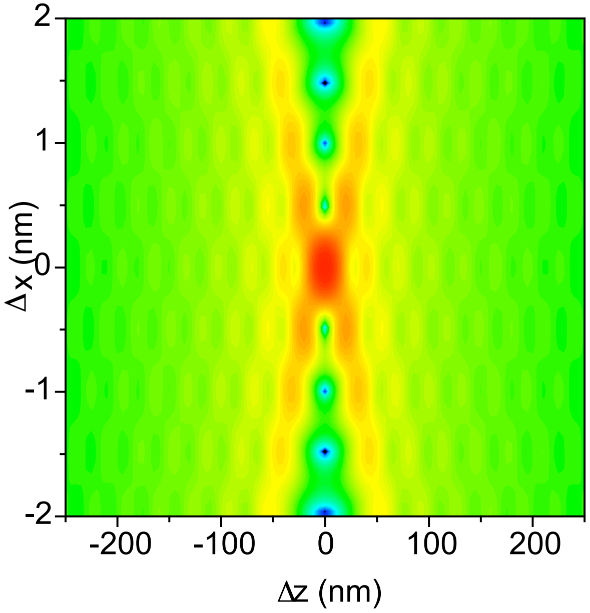

Ultimate Resolution of X-ray Focusing Optics

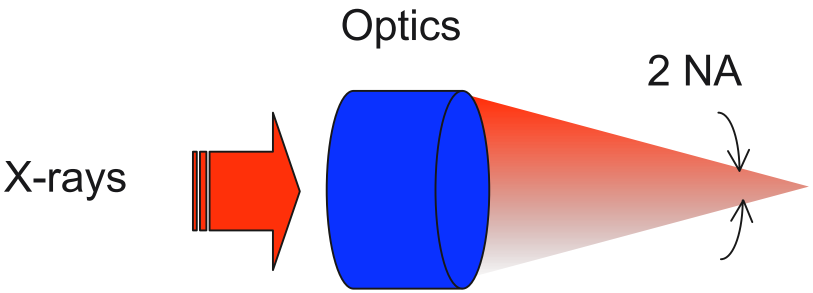

Rayleigh criterion : Best Possible Resolution = $\dfrac{\lambda}{2\ NA}$

Can x-rays be efficiently focused to the atomic scale?
--> Need larger Numerical Aperture (NA)

However, it is inherently difficult to produce large NA optics for hard x-rays

Currently, NA ~ 10^{-3}, resolution ~ 500 λ

- What type of optics will work (e.g. reflective, refractive, diffractive)?
- What is the fundamental limit using real materials ?
- Can we fabricate optics that reach the fundamental limit ?

High NA Hard X-ray Focusing Optics

- ***Refractive:* Lenses**

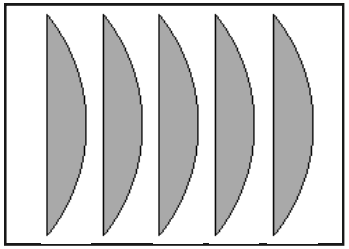

Compound refractive lens

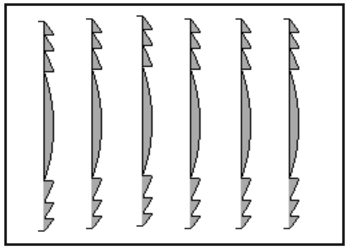

Compound Fresnel lens for high NA

- ***Reflective:* Mirrors**

  Figure by differential deposition, multilayer coated for high NA

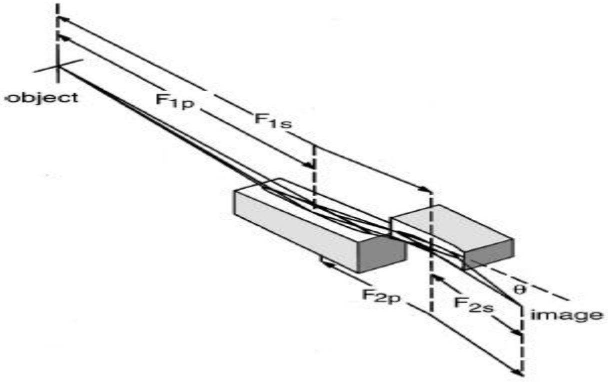

- ***Diffractive:* Zone Plates**

  High aspect ratio, tilted zones for high NA

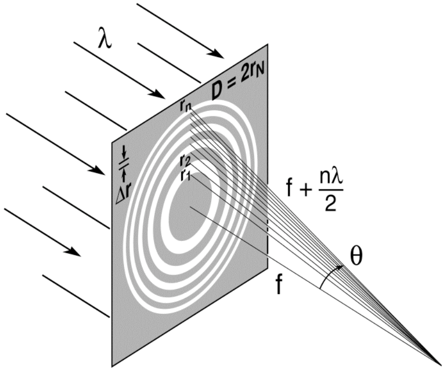

Lithographic zone plate

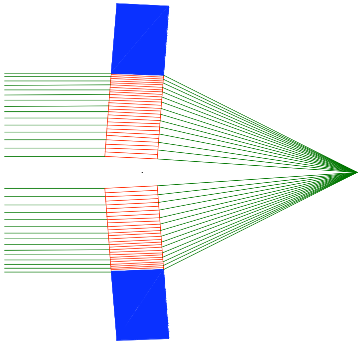

Transmission multilayer

Diffractive X-ray Optics with High NA Require High Aspect Ratio Nano-structures

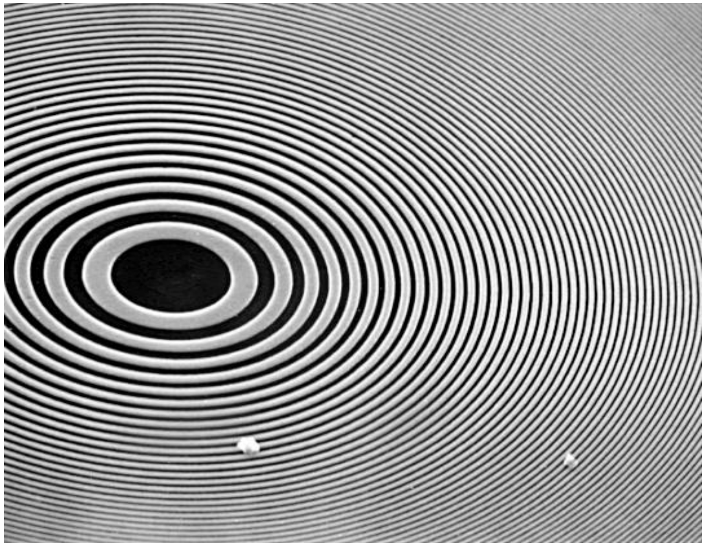

- Small focal spot sizes require small zone widths.
- Zone plate structures for hard x-rays must be several microns thick to achieve high efficiency, which implies high aspect ratios (>>100).
- It is difficult to produce such high aspect ratio structures using lithography.
- Sectioning of multilayers allows very high aspect ratios to be produced.

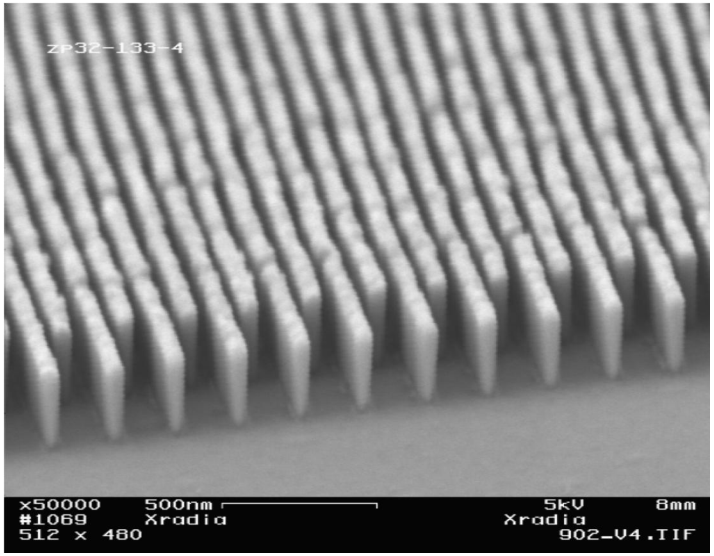

Sputtered-Sliced Fresnel Zone Plate

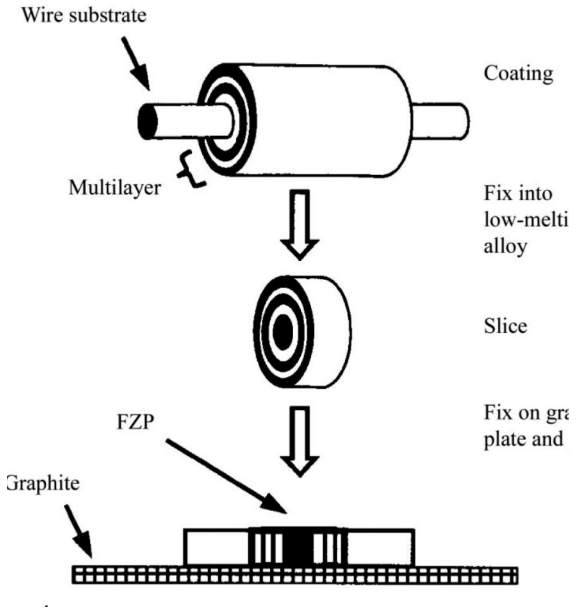

S. Tamura et al. (2002) & B. Kaulich et al. (1996)

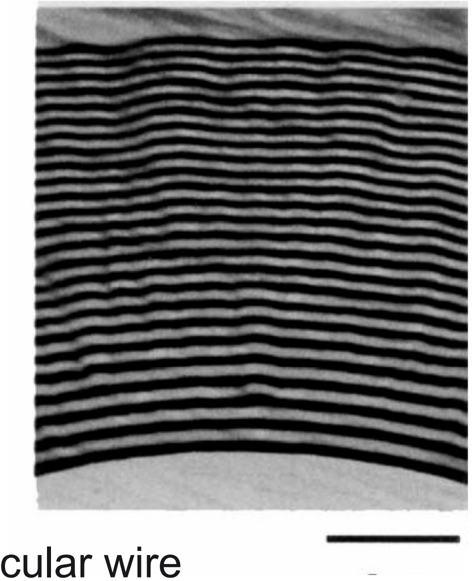

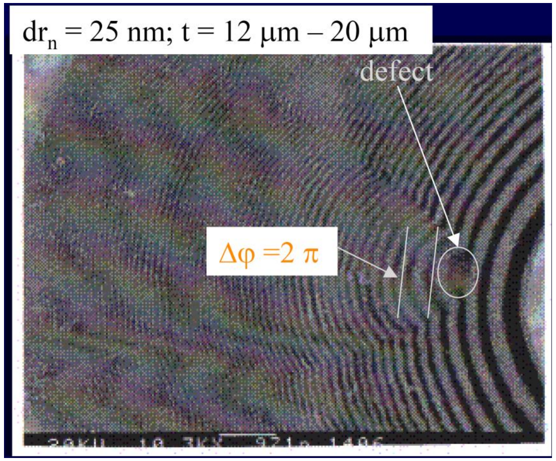

- Deposition of zone plate structure on circular wire
- Imperfections of wire are amplified
- Later coating of the outermost zones gives worse layer position accuracy in most sensitive region
- Circular geometry gives 2-D focus in one optic, but can't tilt layers to get high efficiency

- Cu-Al materials are relatively difficult to section without damage
- Focal spot size ~ 200 nm

Multilayer Laue Lens

Deposit multilayer on flat substrate to produce one-dimensional focusing optic

(1) Deposit multilayer with depth-graded spacing to form zones of linear zone plate (thinnest structures first)

(2) Make cross-sections to allow use in Laue geometry (high aspect ratio structure)

(3) Assemble sections:
two opposite to collect full NA (tilt to achieve high efficiency);
a second pair at right angles to form point focus (high efficiency allows two optics in series)

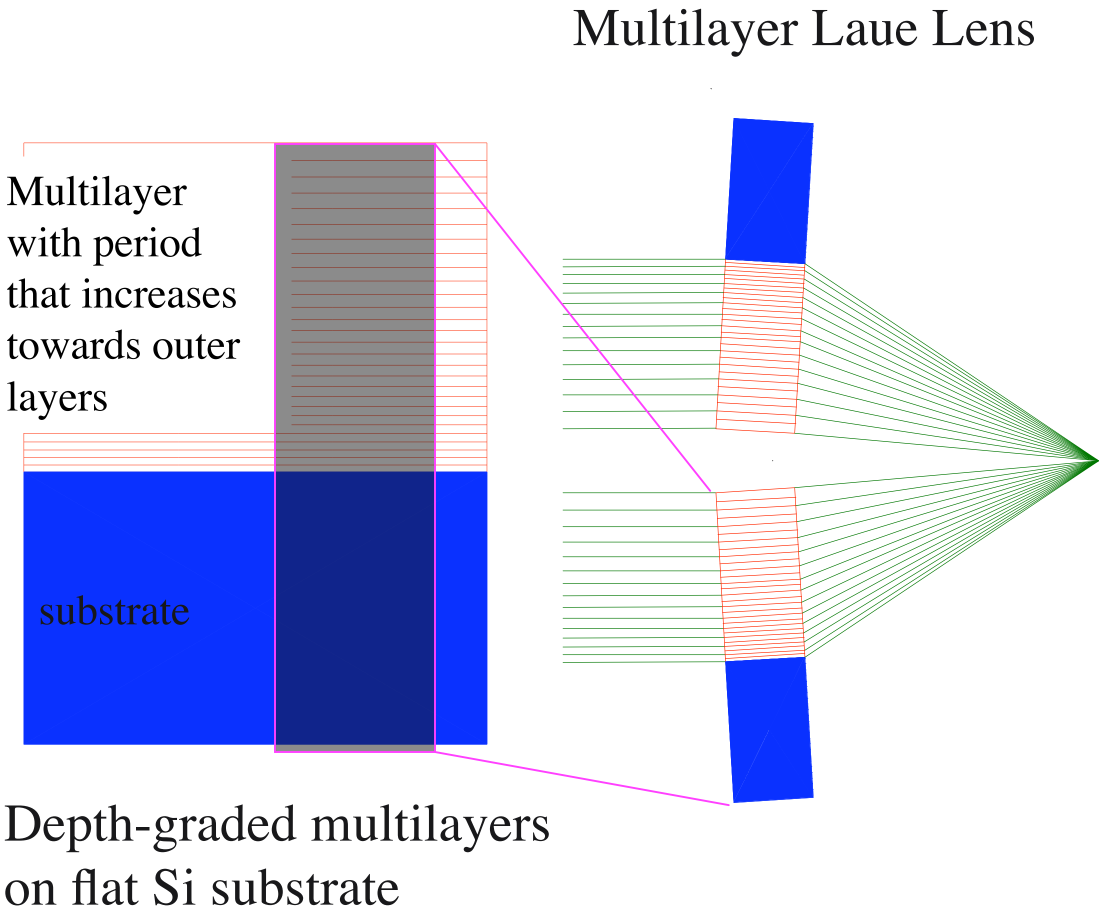

Depth-graded multilayers on flat Si substrate

Theory for MLL

- MLL’s operate in a different optical regime than standard zone plates
- Dynamical diffraction effects inside the volume of the structure are dominant
- Theory for focusing performance:
  - J. Maser et al. - Coupled wave theory (*Optics Commun.* **89**, 355 (1992); *Phys. Rev. Lett.* **96**, 127401 (2006))
  - C. Shroer - Parabolic wave equation (*Phys. Rev. B* **74**, 033405 (2006))
  - H. Yan et al. - Takagi-Taupin (*Phys. Rev. B* **76**, 115438 (2007))

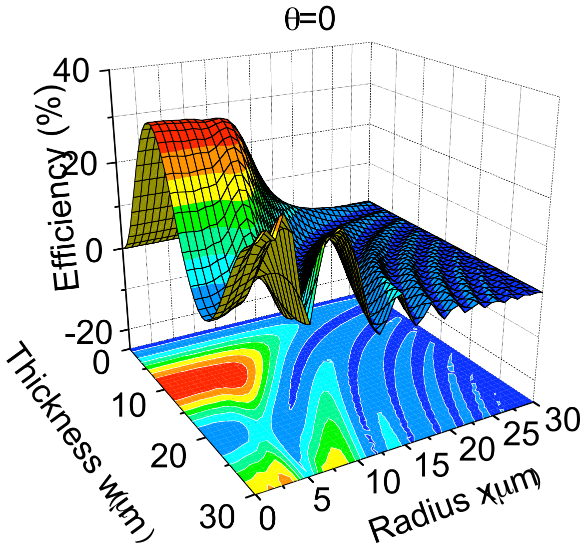
θ=0

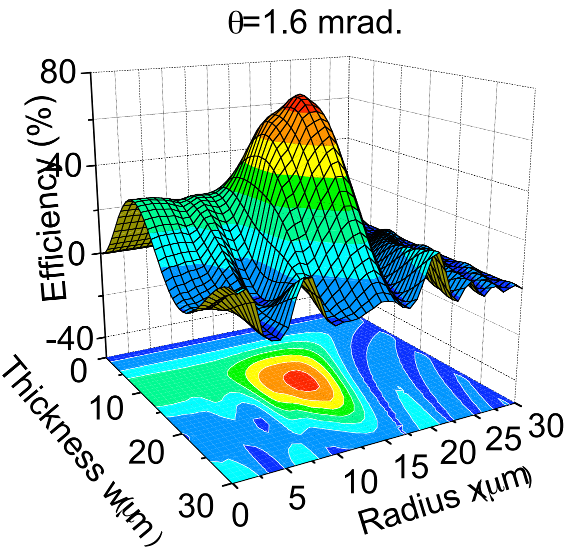
θ=1.6 mrad.

Optimum Zone Geometry

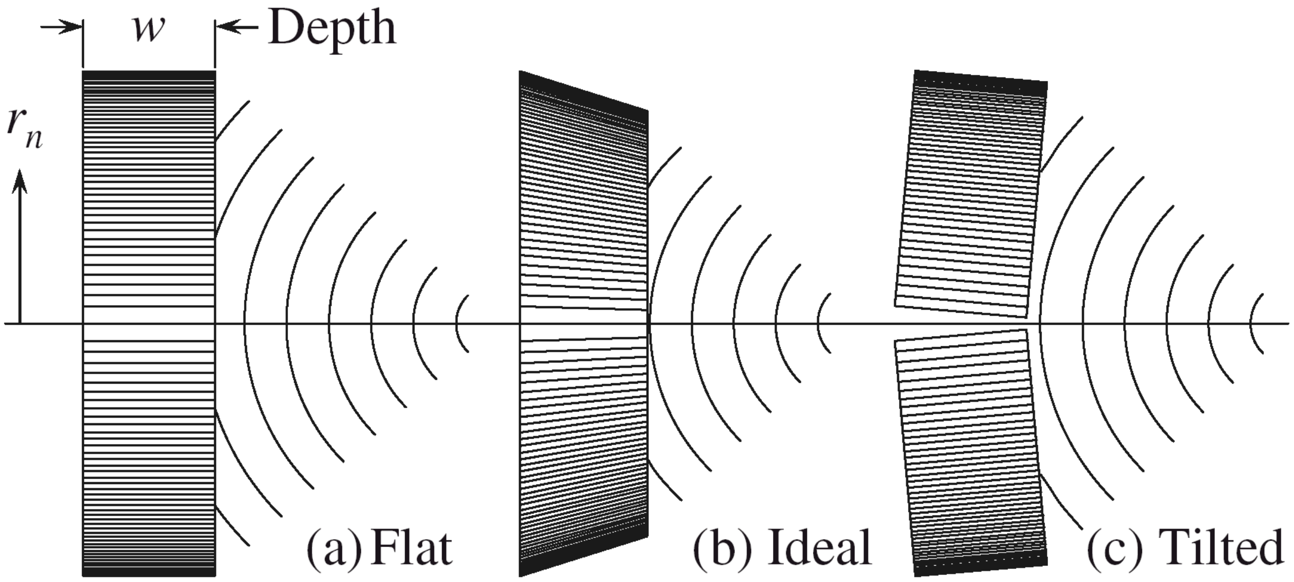

- Flat geometry with all layers parallel is standard for lithographic zone plates
- Ideal "wedged" geometry where each layer makes the Bragg angle for its spacing becomes favorable for high NA focusing
- Ideal geometry can be approximated by tilting each half of MLL

Where is the Spatial Resolution Limit?

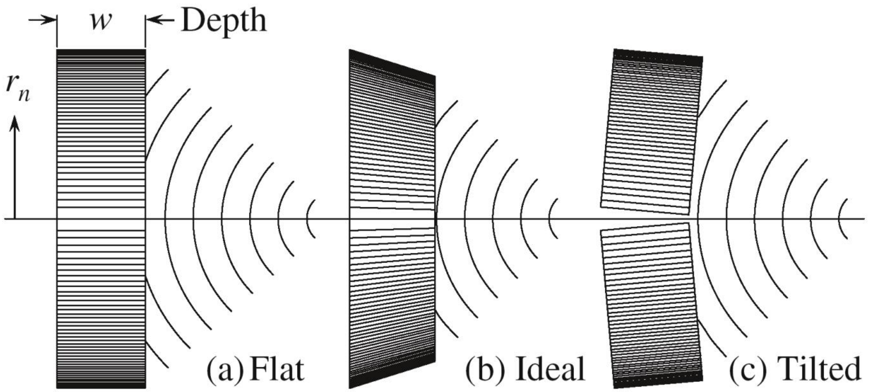

w=13.5 mm, E=19.5 keV

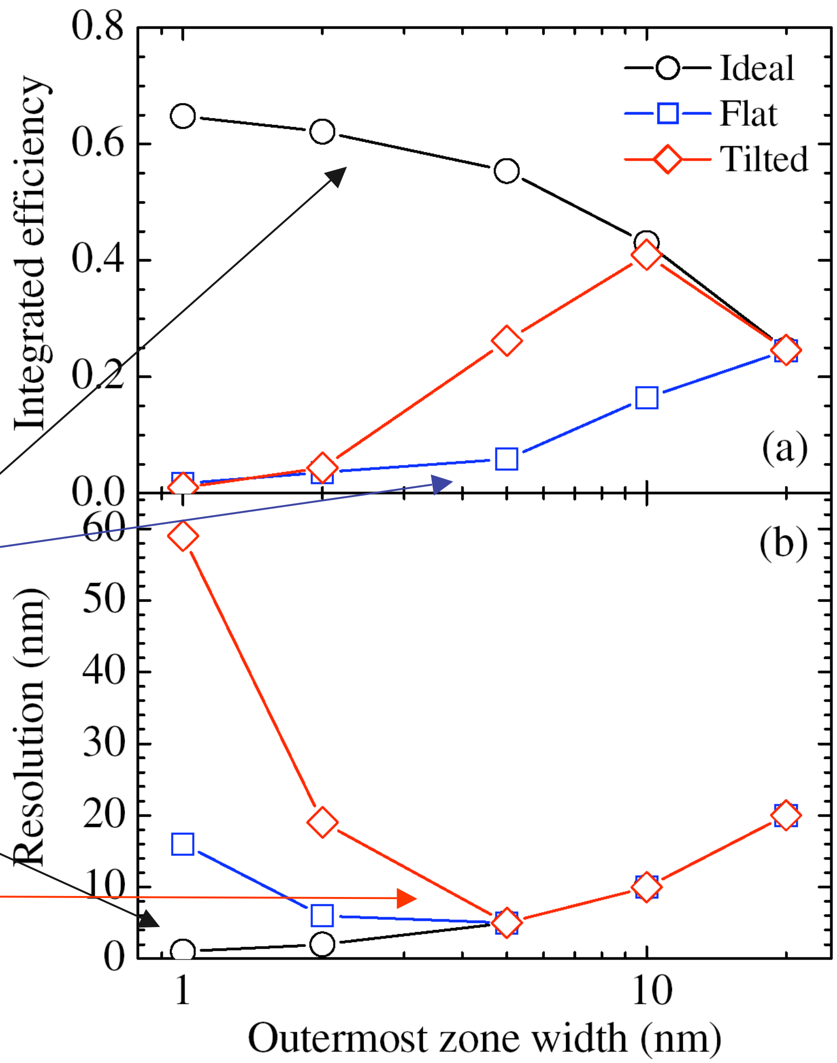

- Flat structure: loses efficiency below 10 nm
- Ideal “wedged” structure:
    - High diffraction efficiency
    - Resolution below 1 nm feasible
- Tilted MLL structure:
    - 6 nm resolution feasible

H. C. Kang et al.
Physical Review Letters **96,** 127401 (2006)

Multilayer Structure for MLL

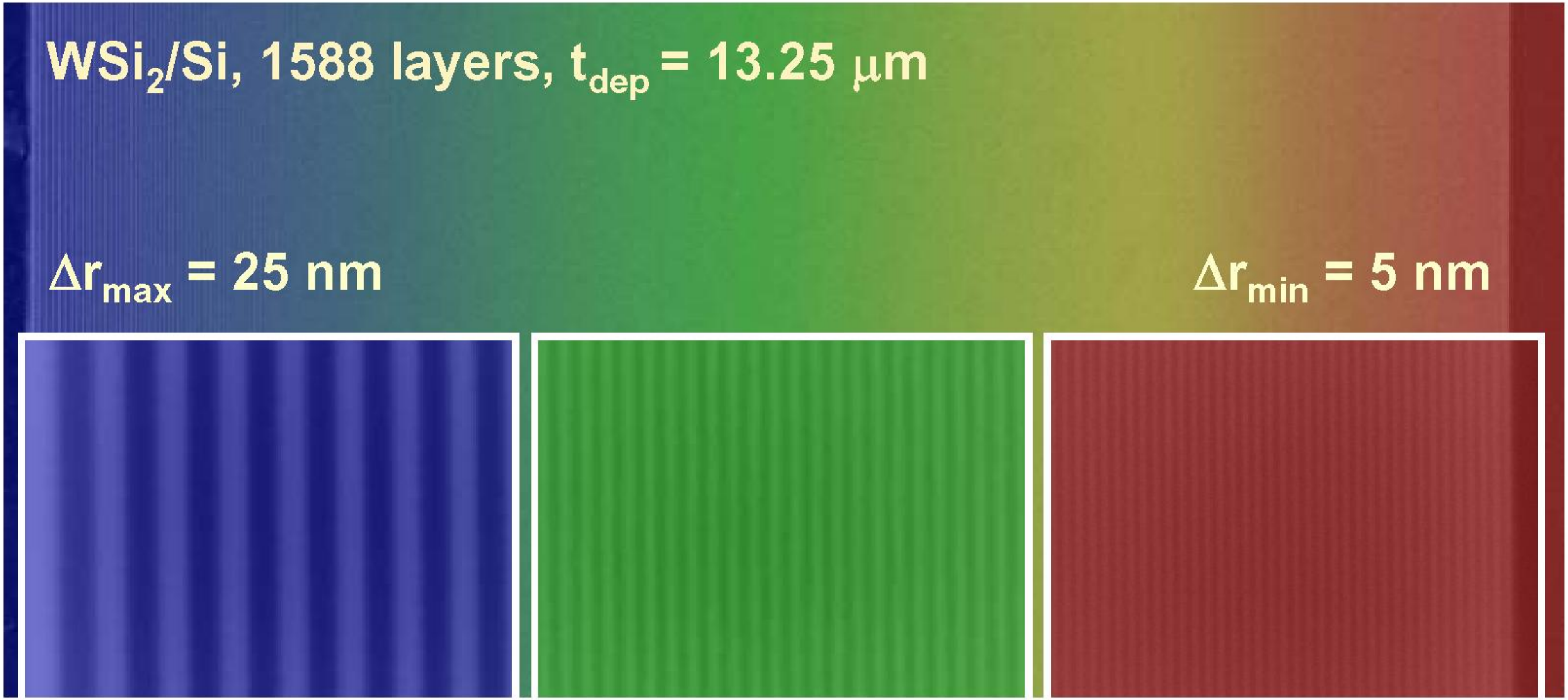

H. C. Kang et al., *Applied Physics Letters* **92**, 221114 (2008)

Measured and Calculated Performance

FWHM = 16 nm

Efficiency = 31% at 19.5 keV

Measurement of half-MLL structure agrees well with calculation

Assembly of complete MLL of this structure should give focus of 6 nm, which will be the smallest focus of photons yet achieved

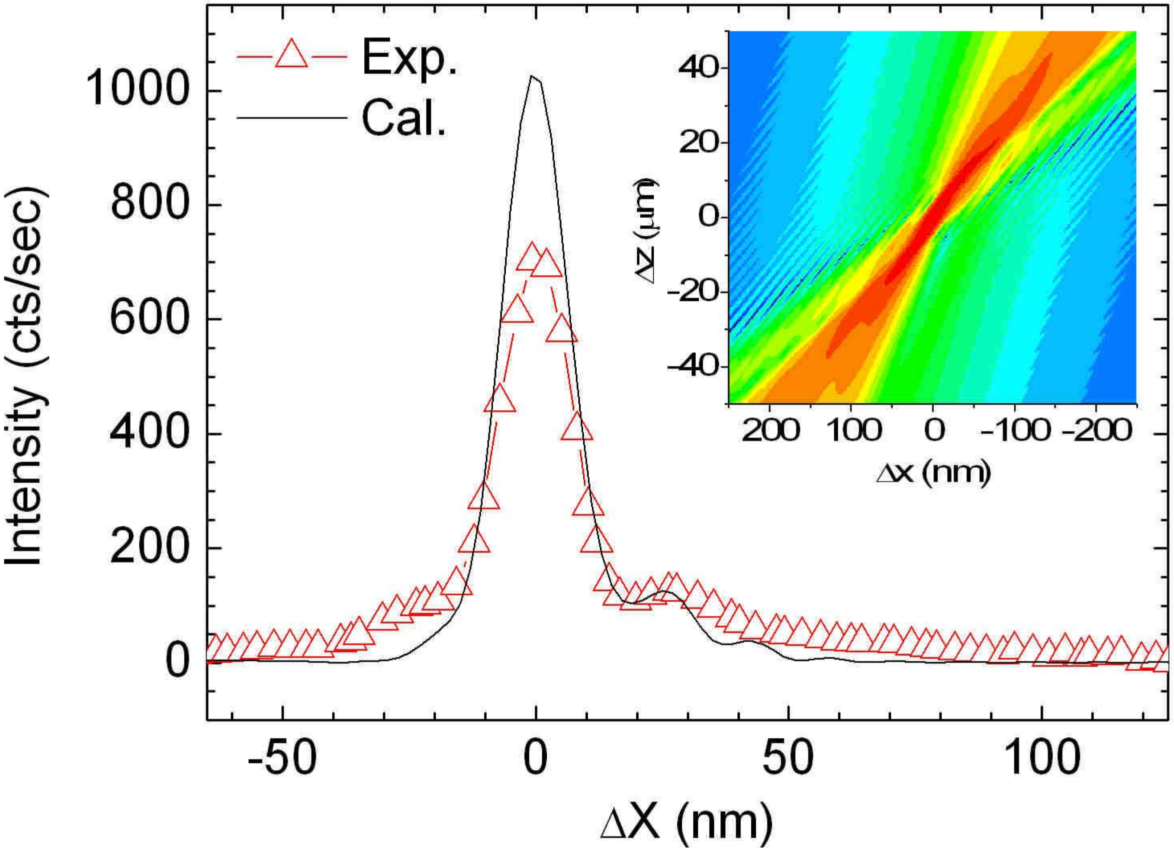

H. C. Kang et al., *Applied Physics Letters* **92**, 221114 (2008)

Near-Atomic-Scale Focusing Possible with “Wedged” MLL

Calculations show that focusing to below 1 nm is possible using “wedged” layers

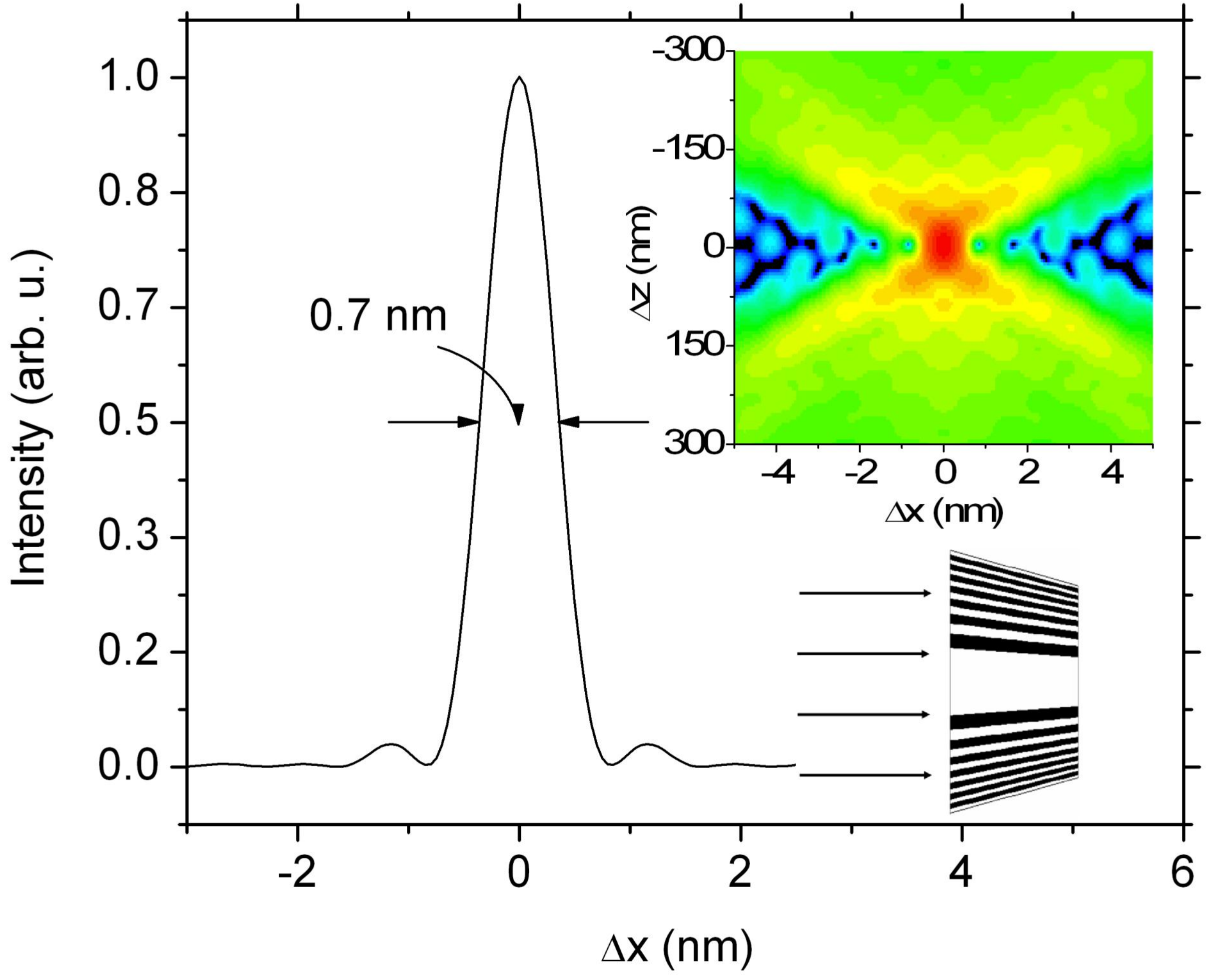

H. Yan et al., *Physical Review B* **76**, 115438 (2007)

Progress of Deposition of Wedged Multilayer Structures

- We have succeeded in depositing initial multilayer structures for a "wedged" MLL
- Examples:
  - 40% structure, outermost zone width 2.5 nm, 1588 layers, 6.6 μm tot.
  - Full structure, outermost zone width 3 nm, 6543 layers, 40 μm total
- Characterization is underway

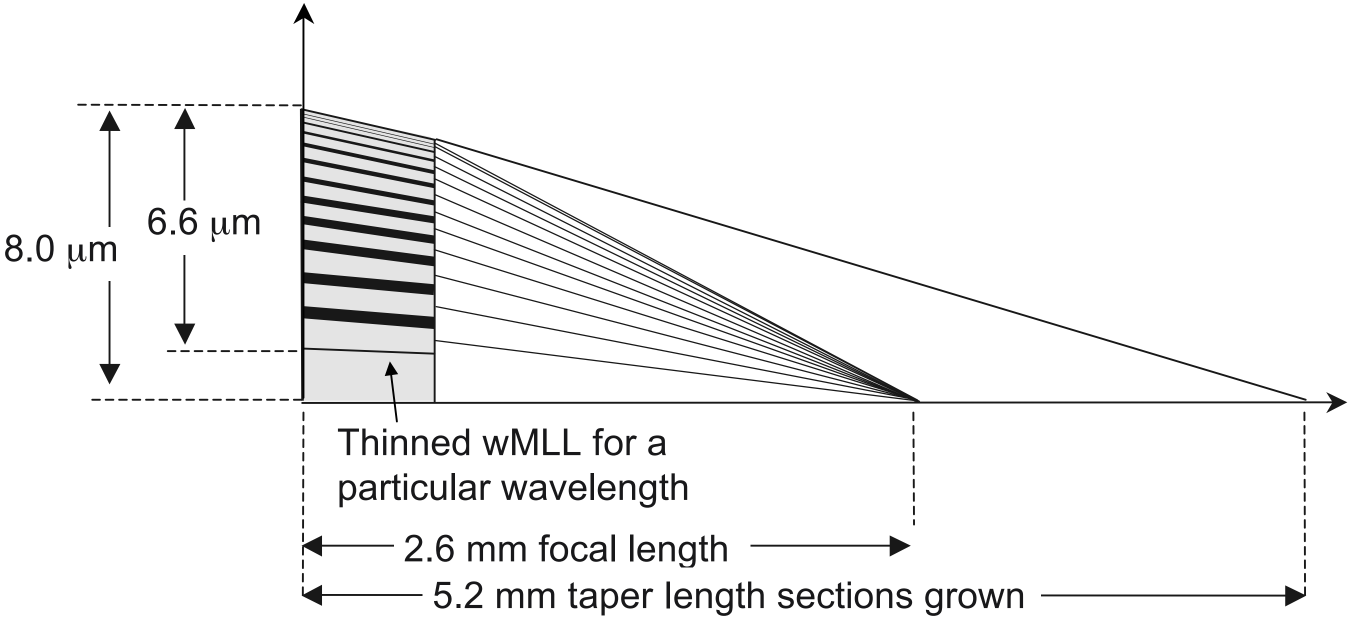

R. Conley et al., *Review of Scientific Instruments* **79**, 053104 (2008)

Future Directions for MLL

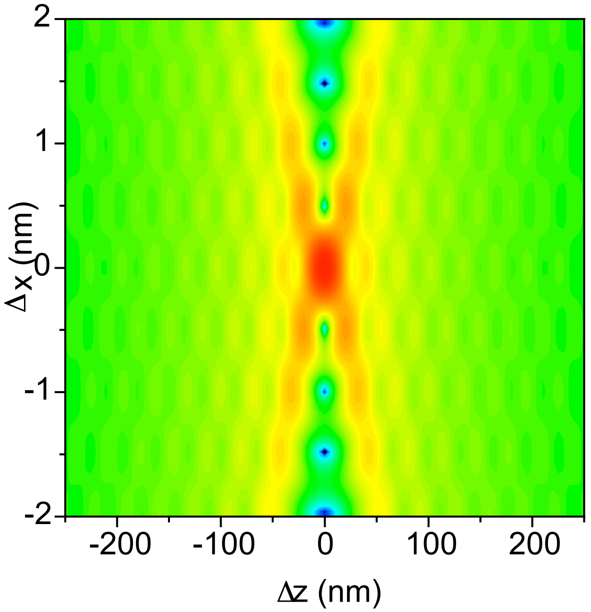

- Theory
  - Determine optimum structure and performance as f(λ)
  - Determine fabrication accuracy required
- Experiment
  - Cross two linear optics to make point focus
  - Assemble complete "tilted" structure to achieve 6 nm focus
  - Develop techniques to deposit "wedged" layers to achieve near-atomic-scale focusing

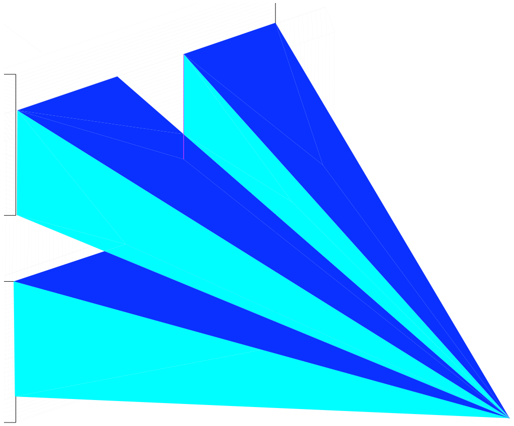

Summary of Multilayer Laue Lens Properties

- Energy range: 5 - 100 keV
- Gain: ~1000X or more in each dimension
- Focal size: 20 nm or less
- Focal distance: 2 mm or less
- Cost, availability:
  - Currently a research effort at ANL, NSLS II, GIST
  - Potentially available in a few years
  - Potentially less than $10K per optic

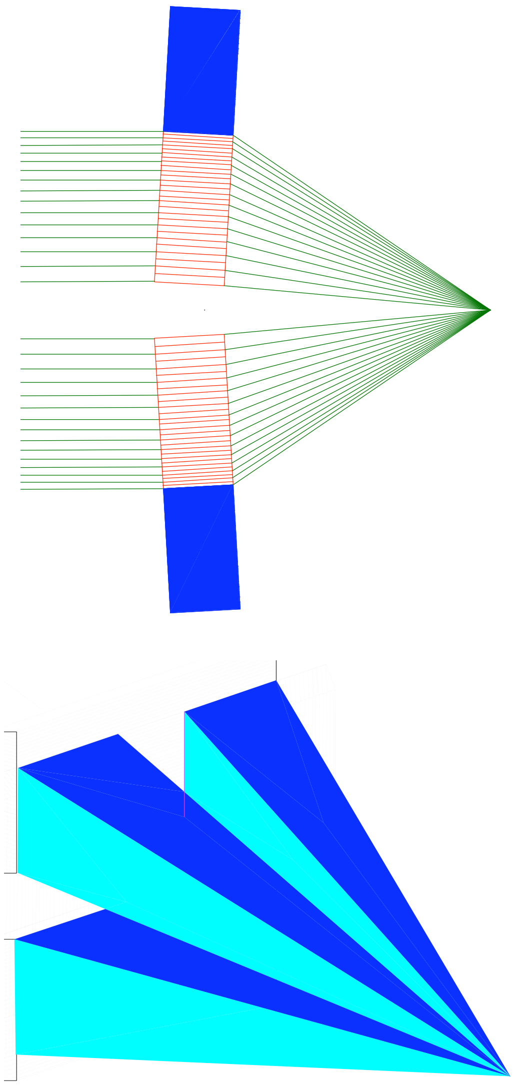

Nanoprobe Beamline at the Center for Nanoscale Materials

- Center for Nanoscale Materials
  - new nanoscience research center located adjacent to APS
- Nanoprobe Beamline
  - state-of-the-art hard x-ray microscopy beamline, built and operated in partnership between CNM and APS

Advanced Photon Source, ANL

Center for Nanoscale Materials

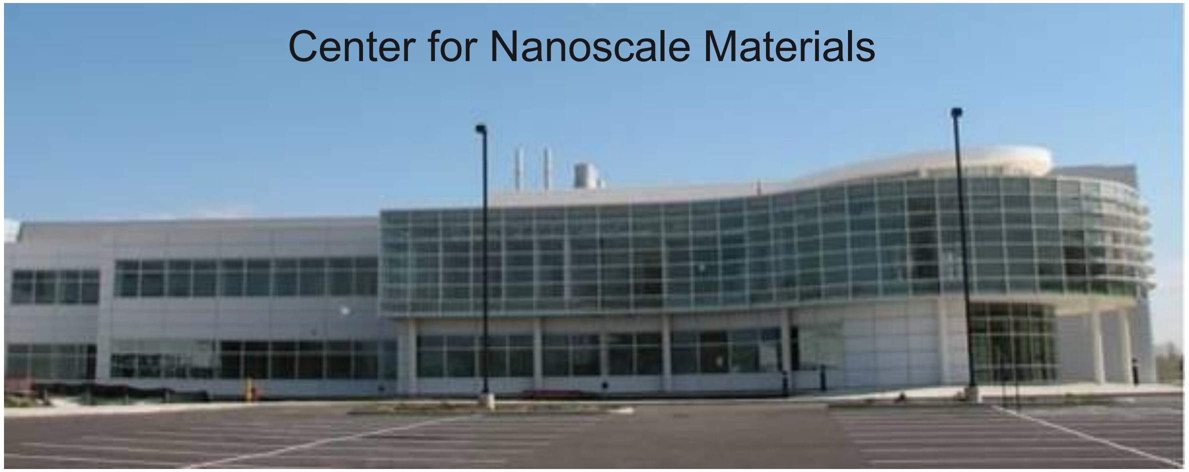

Nanoprobe Beamline: Overall Specifications

- Hard X-ray microscopy at the highest achievable spatial resolution
  - Initial spatial resolution of 30 nm using lithographic zone plates
  - Energy range 3 - 30keV (nano-spectroscopy excitation of most elements)
  - Large penetration → sample environments/fields

- Planned capabilities
  - **Fluorescence:** atto-g elemental sensitivity, chemical state sensitivity
  - **Diffraction:** sensitivity to crystallographic phase, strain, orientation
  - **Tomography:** transmission absorption / phase contrast imaging
  - **Coherent x-rays:** disorder, imaging
  - **Magnetic contrast** using polarized x-rays
  - **Dynamic studies** at 100 ps time resolution

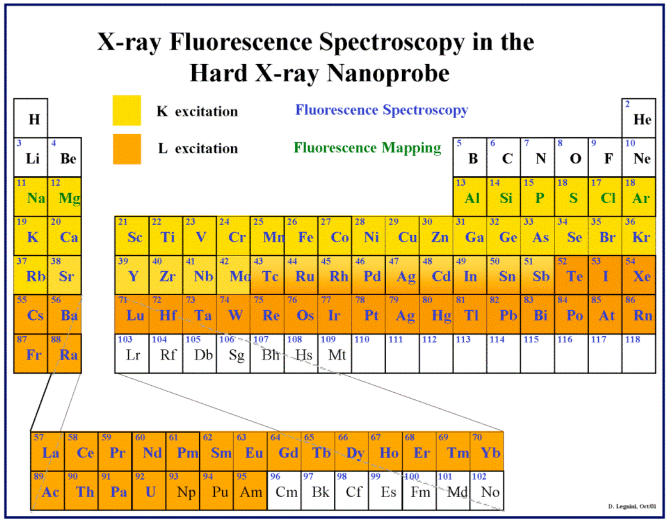

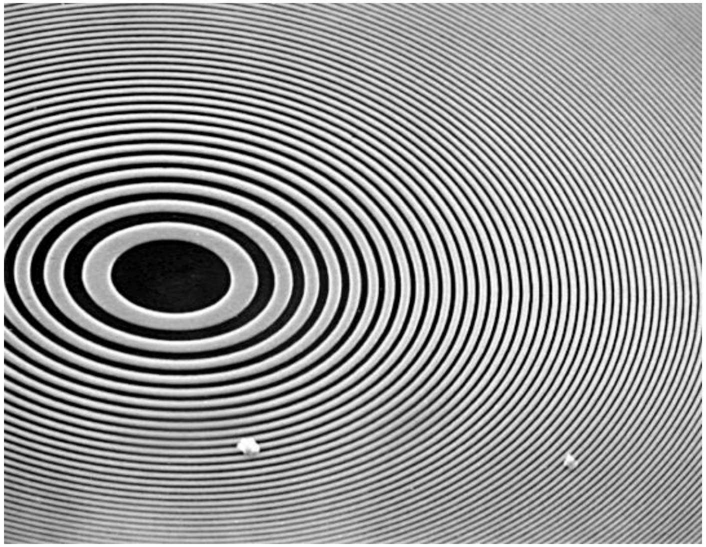

Nanoprobe Beamline Schematic

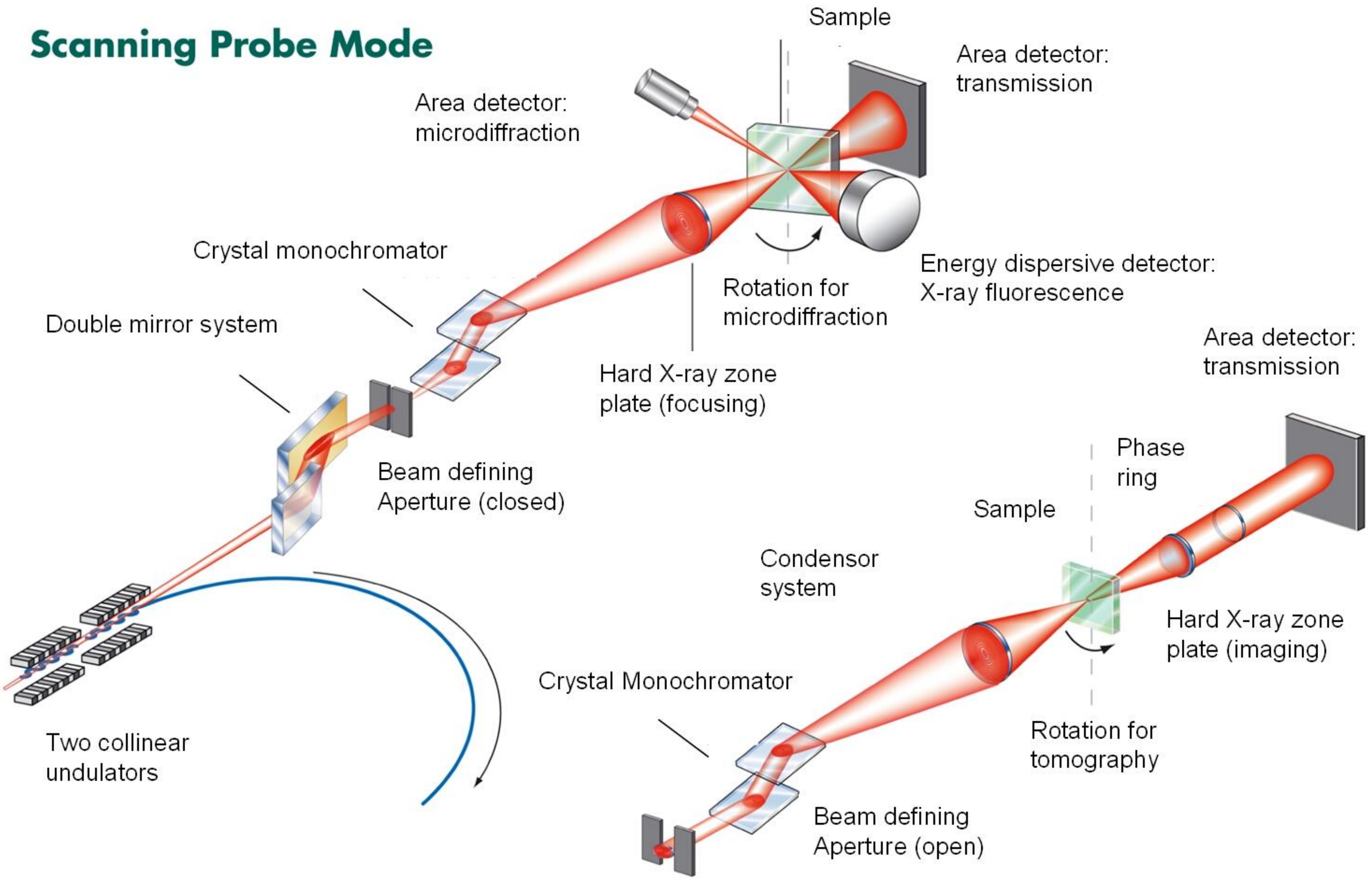

Scanning Probe Mode

Sample

Area detector:
transmission

Area detector:
microdiffraction

Crystal monochromator

Rotation for
microdiffraction

Energy dispersive detector:
X-ray fluorescence

Double mirror system

Hard X-ray zone
plate (focusing)

Beam defining
Aperture (closed)

Two collinear
undulators

Area detector:
transmission

Phase
ring

Sample

Condensor
system

Hard X-ray zone
plate (imaging)

Crystal Monochromator

Rotation for
tomography

Beam defining
Aperture (open)

Full-Field Transmission Mode

Nanoprobe Scanning Design

- Laser interferometers monitor positions of optics and sample to Angstrom precision
- Nanoscale scanning of focusing optic using piezo stages
- Feedback used to lock beam to desired position on sample at each point in scan

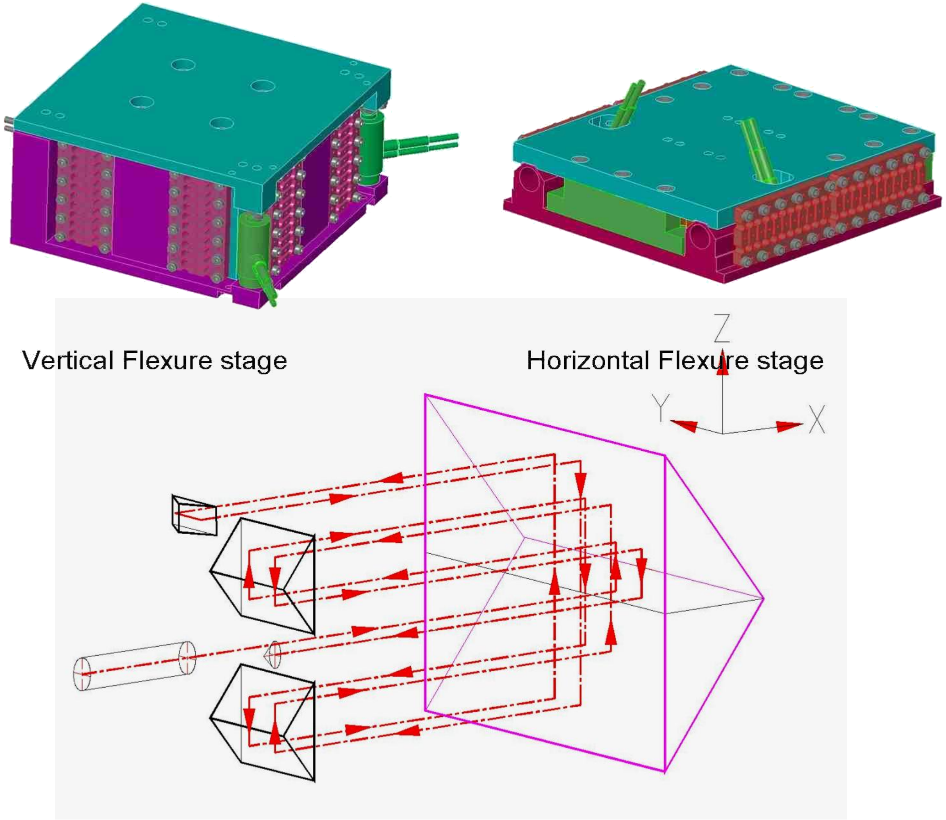
Vertical Flexure stage

Horizontal Flexure stage

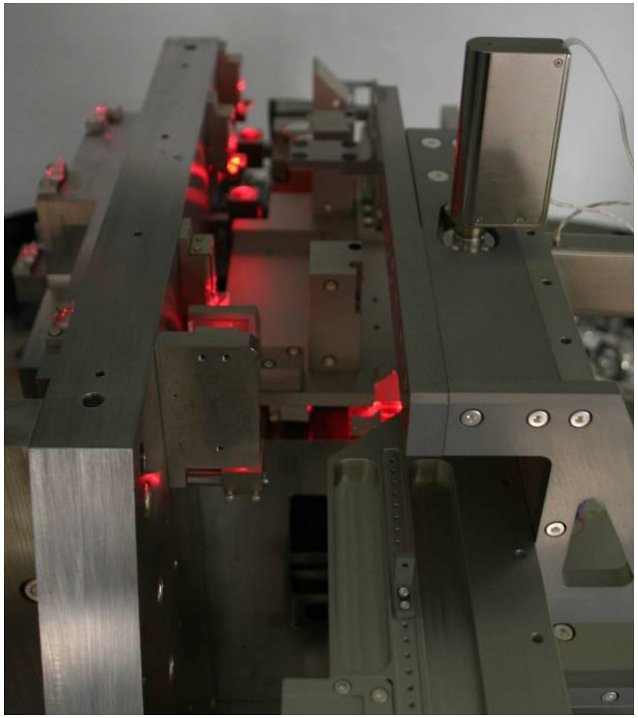

Nanoprobe Beamline Construction Complete

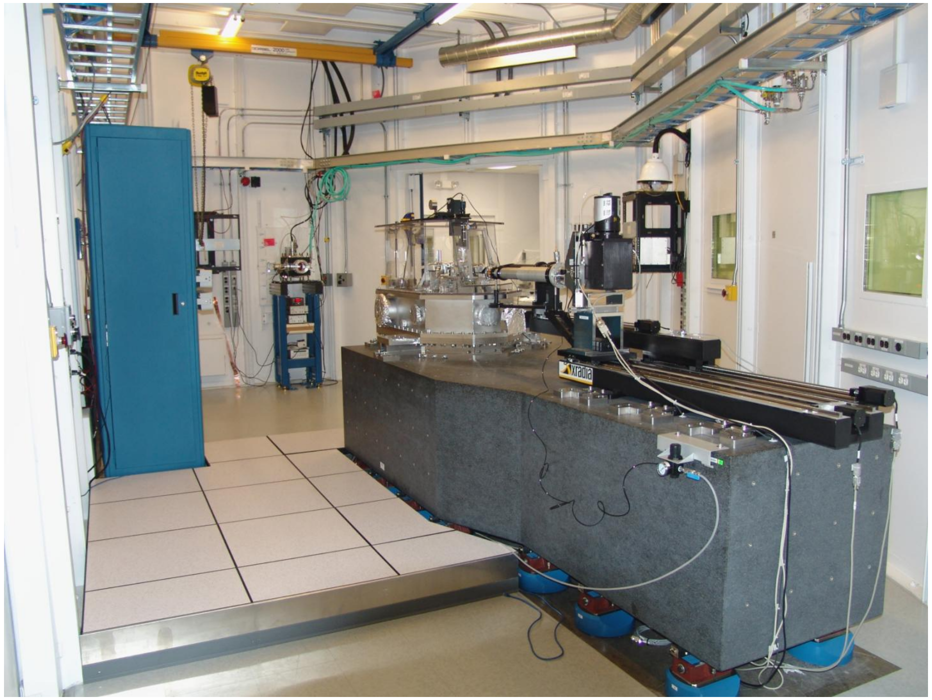

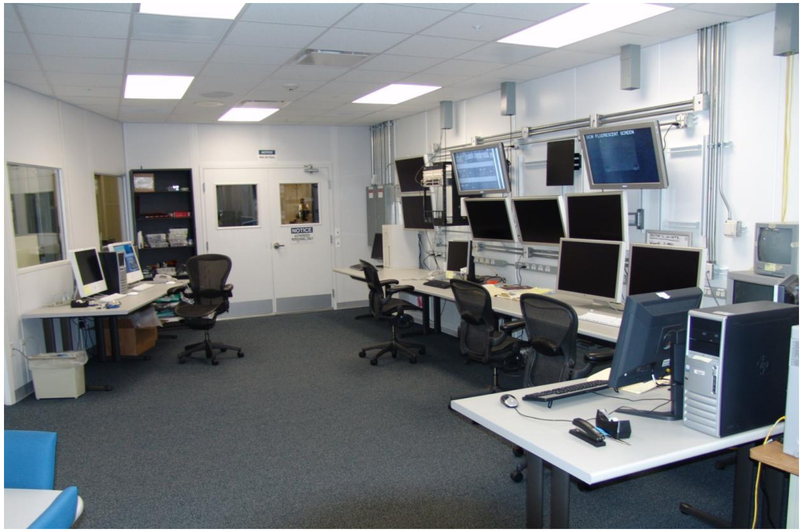

- Zone plate performance at 30 nm verified
- Beamline commissioning underway
- First user program experiments started this year

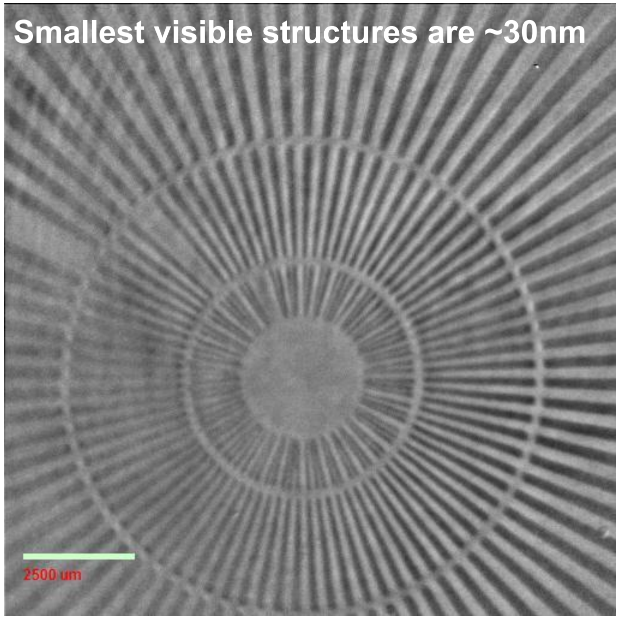

Smallest visible structures are ~30nm

Recent Example: Nanodiffraction from Strained Silicon

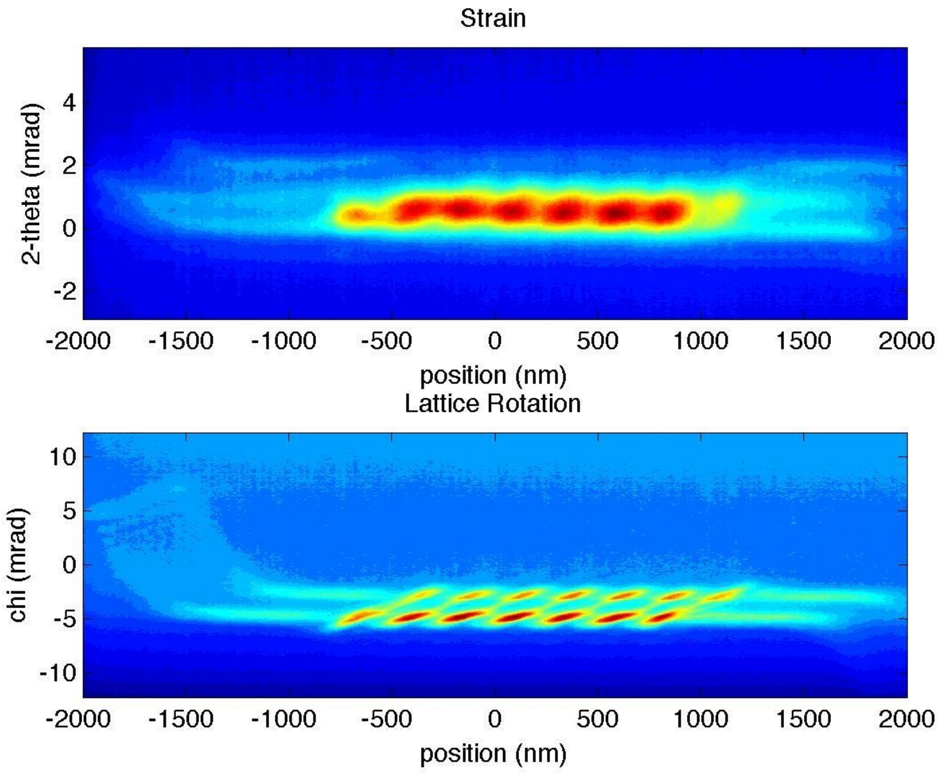

~50 nm resolution scanning diffraction maps of device features of strained silicon on insulator (SOI)

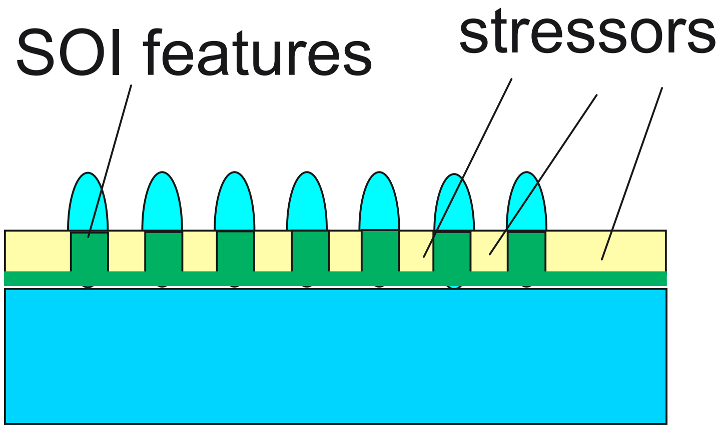

Courtesy: Conal Murray*, Sean Polvino⁺, Andrew Ying⁺, Ozgur Kalenci⁺, I.C. Noyan⁺

*** IBM, ⁺Columbia University**

Summary

- MLL
  - Achieved 16 nm FWHM line focus, 31% efficiency at 19.5 keV
  - Sub-nanometer focusing predicted
- Nanoprobe
  - Currently: 30 nm resolution zone plates
  - Plan: 10 nm resolution MLL

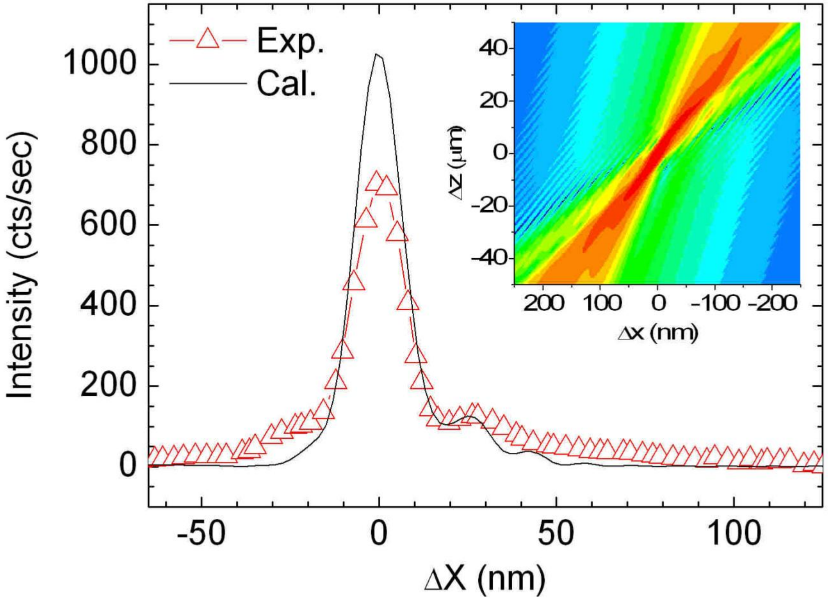

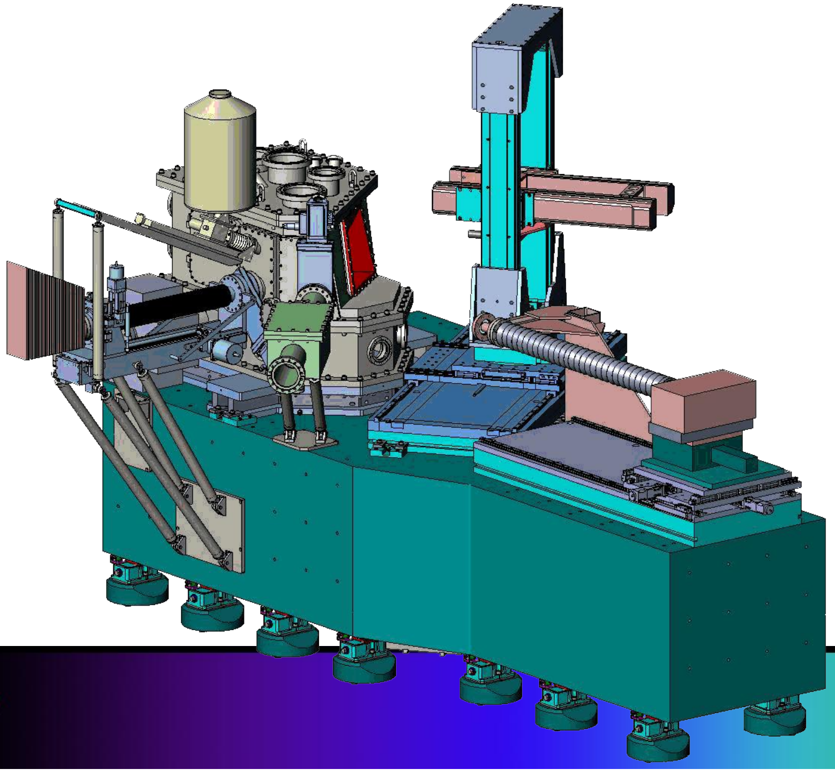

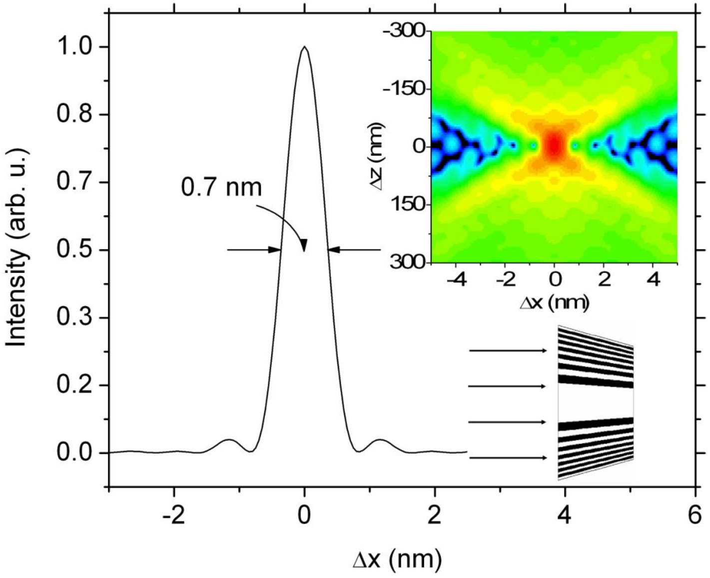

Diffractive Focusing By Zone Plates

3D X-ray Imaging for Science and Industry

SPIE X-ray
Focusing Workshop

Dr. Michael Feser
Vice President / General Manager
nano-Imaging
Xradia Inc.

High-resolution Optics: Comparison

	KB Mirror	Refractive Lens	Zone Plates (+Laue optics)
Demonstrated Resolution (nm)	<30	<50	<15 for 0.5 keV 22 for 8 keV
Flux Density Gain	>500,000	10000	>500,000
Imaging Optic	No	Yes	Yes
Chromatic Aberration	No	$1/\lambda^2$	$1/\lambda$
Theoretical resolution limit (nm)	<10	~2 ? (Schroer et al.)	~1(1) ?
Minimum focal length for 100 um aperture (mm)	~30	100 for 10 keV	0.5 for 0.5 keV 20 for 10 keV

(1) Kang et al., PRL96(2006)

Diffractive Focusing By Zone Plates
Outline

- ❑ History and working principle
- ❑ Fabrication, limitations and future developments
- ❑ Applications
  - ➢ X-ray imaging / microscopy
  - ➢ X-ray nano-probing: Diffraction, spectroscopy
- ❑ Summary and outlook

Diffraction From a Grating

- Recall diffraction from slits separated by *d*
- diffraction *maxima* for positive interference of light waves occurs when
  $d \sin \theta = n\lambda$
  n = diffraction order
  θ = diffraction angle
- Constant grating pitch acts like a prism for one diffraction order (deflects light)
- Deflection is a linear function of wavelength λ

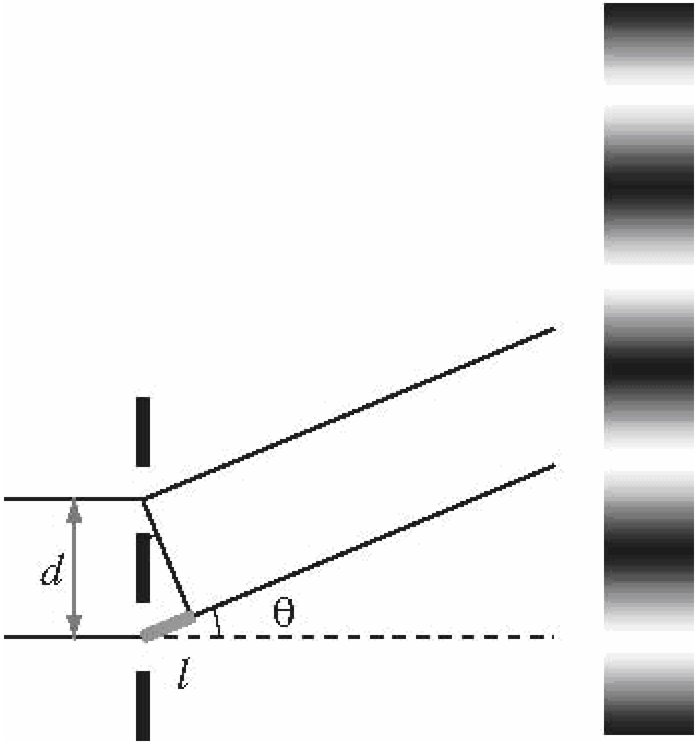

Diffraction from Circular Grating

- ❑ By varying the grating pitch radially in a circular grating, positive interference on-axis at a focal point is obtained

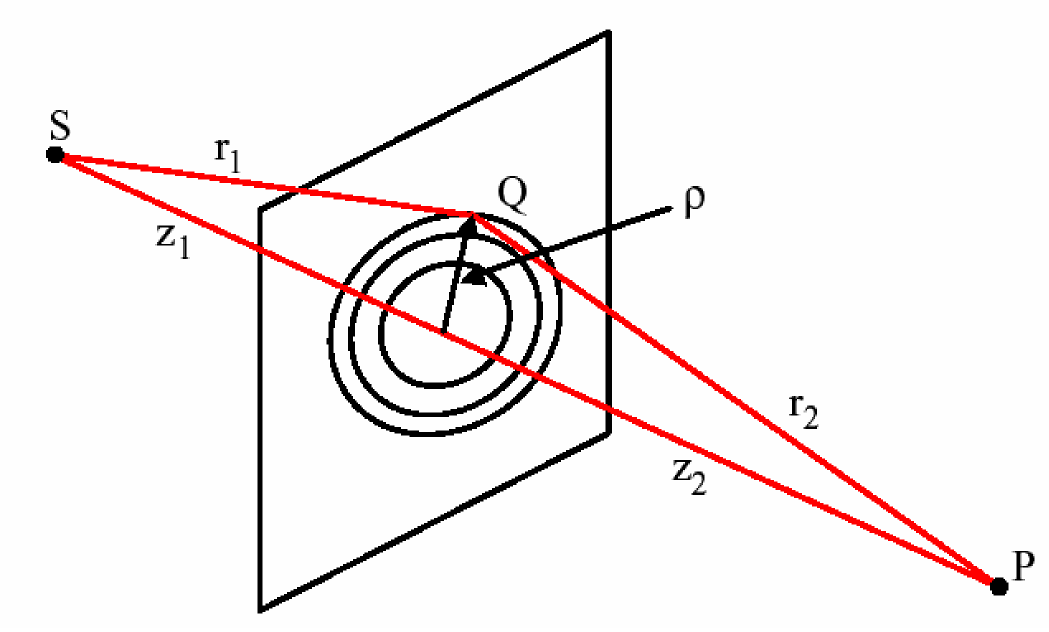

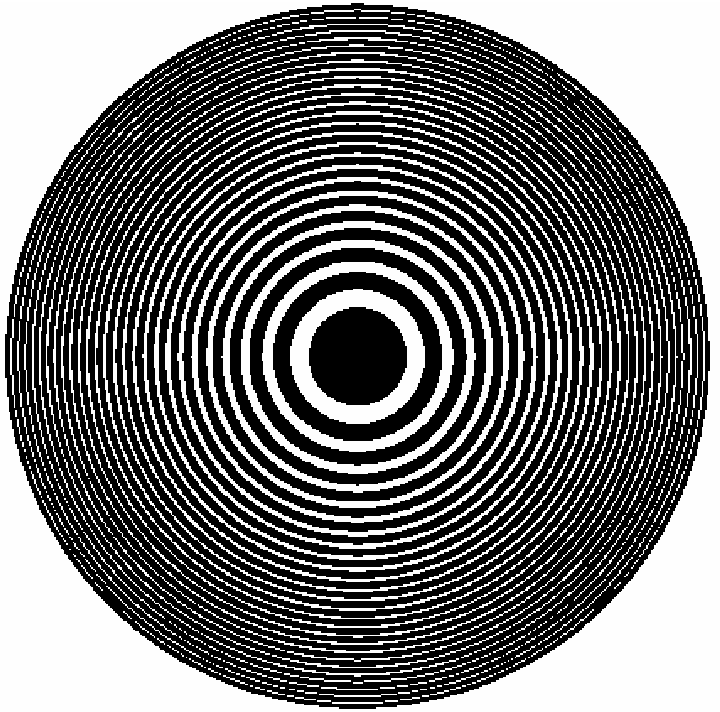

- ❑ Excellent Reference: M. Young, JOSA 62(8), pp. 972-976

Diffractive Lenses: Fresnel Zone Plates

- ❑ Focal length has a strong wavelength dependence:

$$f = \frac{OD\,\Delta R_N}{\enclose{circle}{\lambda}}$$

- ❑ Necessitates use of monochromatic beam, with bandwidth E/ΔE > number of zones
- ❑ Resolution limited by outermost zone width ΔR:

$$\text{Res} = 1.22\,\Delta R$$

Diffraction Orders of Zone Plates

- Diffractive elements have more than one diffraction order
- Directly transmitted beam: 0^{th} order
  Higher diffraction orders with decreasing intensity
  (even orders forbidden for 1:1 mark to space ratio)
- With use of apertures and stops one diffraction order can be isolated and ZP acts like a thin lens (disadvantage of zone plates)

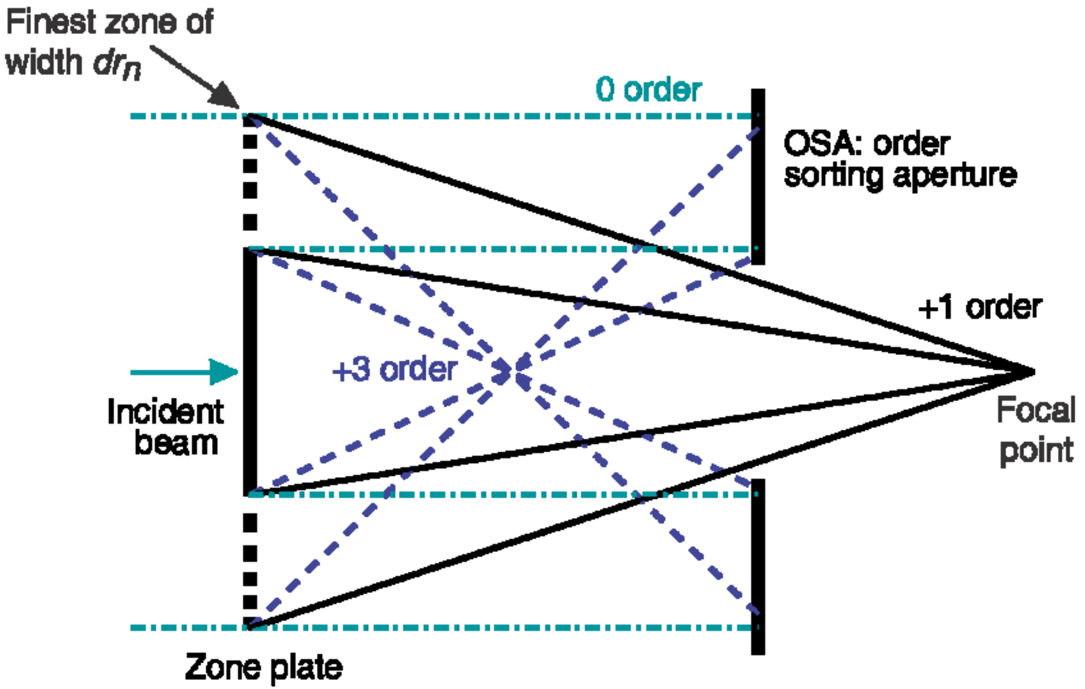

Central stop and order sorting aperture (OSA) to isolate first order focus in a nano-probing application

Zone Plates as Thin Lenses

- Works just like a thin lens, except:
  - 1st order efficiency
    - Opaque zones ~10%
    - Phase reversing zones ~40%
    - Blazed zones 100%
    - (less for real materials)
  - Need to deal with unwanted orders
  - Highly chromatic : f ~ $1/\lambda$
  - No spherical aberrations

Zone Plate Efficiency for Real Materials

Scanning Electron Micrographs of Zone Plates

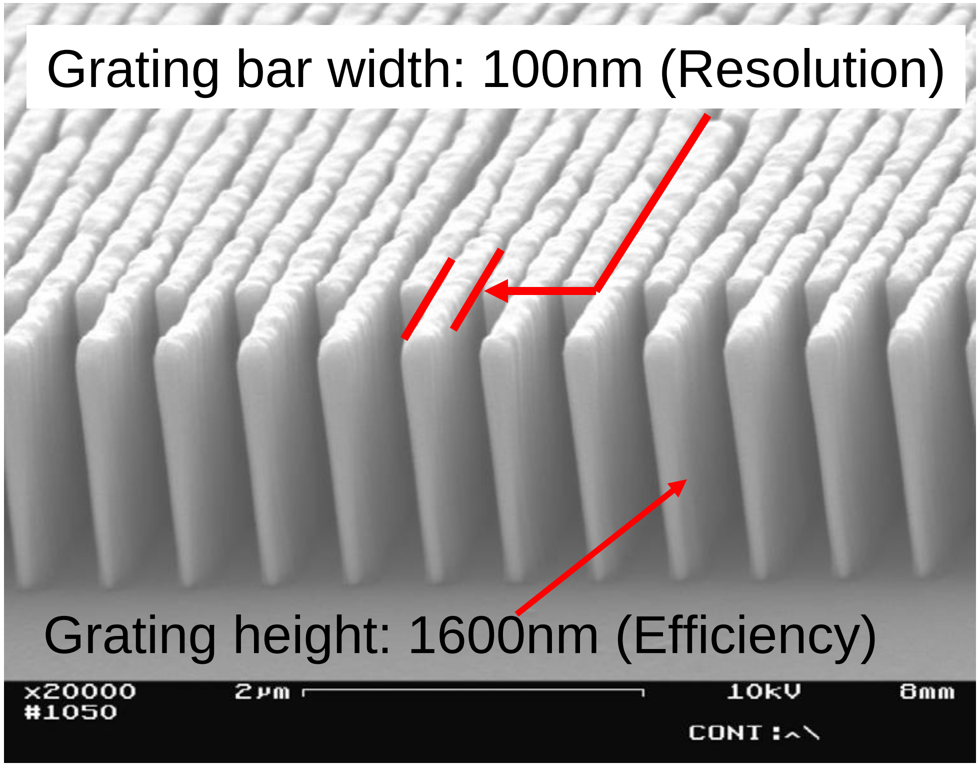
Grating bar width: 100nm (Resolution)

Grating height: 1600nm (Efficiency)

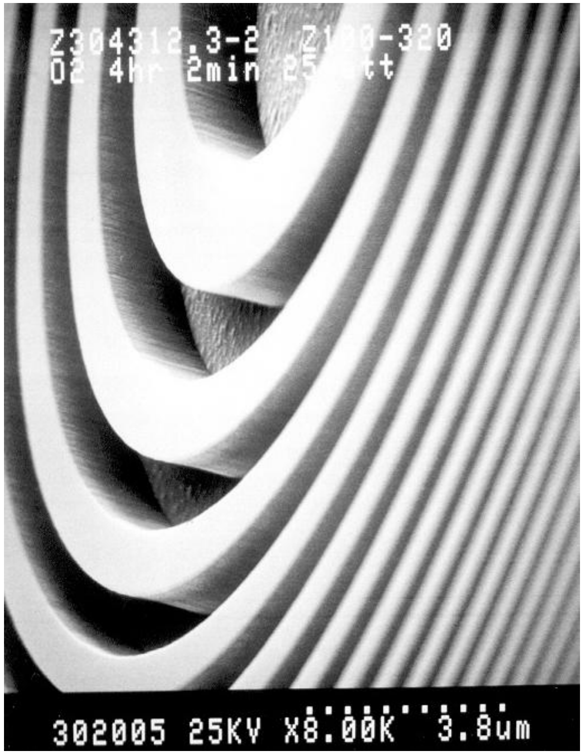

- ❑ Resolution limited to approximately the zone width ΔR
- ❑ Focusing efficiencies up to 30% for high x-ray energies

Zone Plates: Early History

- Rayleigh 1871 – unpublished
- Soret 1875 – first publication
- Rayleigh 1888 – phase zone plates
- Wood 1898 – experiments with zone plates using light

- Some simple cameras use zone plates instead of pinholes!

First Images With a Fresnel Zone Plate

- ❑R. W. Wood (1898): zone plate figure drawn with a pen and a compass! Photographically reduced

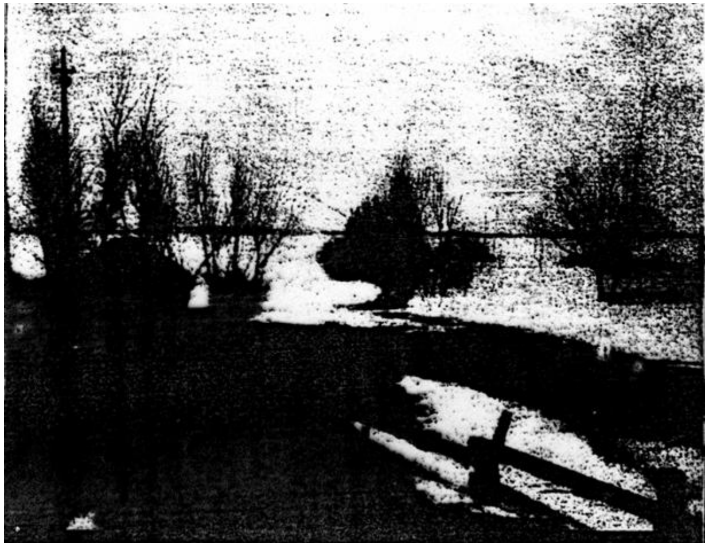

Plate 2. Zone-Plate, from a Drawing.

X-ray zone plate history

- Albert Baez (UNESCO, SAO/Cambridge)
  - “The possibility constructing a single Fresnel zone plate for x-rays should be explored” - J. Opt. Soc. Am. 42, 756 (1952) - paper on x-ray holography.
  - Demonstrated free-standing metal zone plate for X rays: “auguring well for resolution at 100 Å” - Nature 186, 958 (1960).
- Gunter Schmahl and Dietbert Rudolph (Göttingen)
  - Proposed holographic fabrication method - Optik 29, 577 (1969)
  - First TXM demonstration using synchrotron radiation - Niemann et al., Opt. Comm. 12, 160 (1974)
- Janos Kirz (Stony Brook)
  - Phase enhancement of efficiency - J. Opt. Soc. Am. 64, 301 (1974)
  - First STXM demonstration using synchrotron radiation - Rarback et al., 1983 XRM conference proceedings; Kenney et al., J. Microscopy 138, 321 (1985). Zone plates: D. Kern et al., IBM.
- E-beam zone plates:
  - Proposed by D. Sayre, IBM tech report RC 3974 (1972).
  - First demonstrated by Nat Ceglio, MIT, in E. Ash, Scanned Image Microscopy (Academic Press, 1980); J. Vac. Sci. Tech. B 1, 1285 (1983)

Zone Plate Patterning Techniques

- ❑ E-beam writing
  (Xradia, CXRO, Agere/SB, Göttingen, Trieste, Kings, etc)
  - ➢ current method of choice for high resolution patterning
  - ➢ Direct write into resist, very high resolution (<15nm demonstrated)
- ❑ Optical, Holographic Patterning (Göttingen)
  - ➢ First high resolution zone plates for x-ray imaging at synchrotron
  - ➢ Limited by diffraction of light used (wavelenth)
  - ➢ New efforts with EUV radiation at synchrotrons
- ❑ Sputtered, sliced (Göttingen, Japan)
  - ➢ Engineering challenges have proven hard to overcome
- ❑ Imprint litho (U. Texas/SB)
  - ➢ Master for imprint has to be fabricated using E-beam techniques
  - ➢ Imprint manly motivated by mass-production aspect

Zone Plates By Electron Beam Lithography

- Produces the finest possible arbitrary 2-D structure (other than what nature can be persuaded to make by itself)
- Top end machines (such as JEOL JBX-9300FS, Vistec VB300) offer ~2 nm spot size at ~1 nA and 100 kV, 500 μm field, ~1 nm positioning with 5-10 nm absolute placement on a rectangular grid. DoE nanocenters have such systems

A. Stein at the NJNC JBX-9300FS

Zone plate efficiency and thickness

- For binary zones, 1:1 mark:space ratio.
- See Kirz, *J. Opt. Soc. Am.* **64**, 301 (1974)

Gold Zone Plate Efficiency

2 aligned ZPs

Quantitative Efficiency Measurements of Zone Plates Using Laboratory Sources

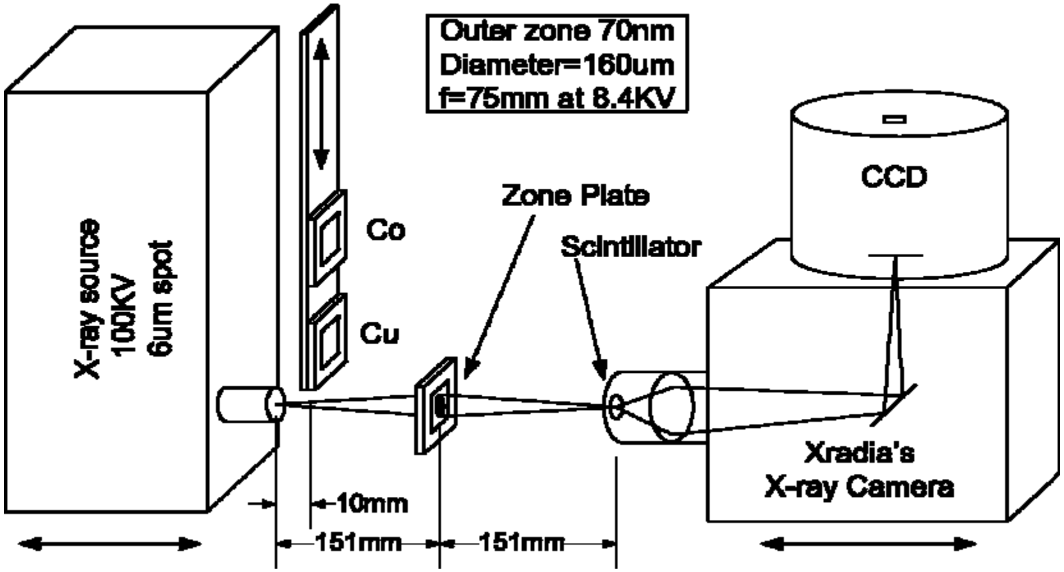

- ❑ Quantitative measurements have been restricted to synchrotron
- ❑ Balanced filter method to obtain monochromaticity with laboratory sources
- ❑ Final test and process development tool

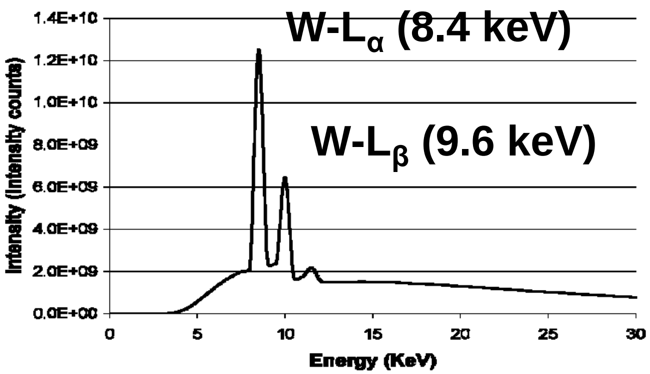

Poly-chromatic source output

Differential Filter

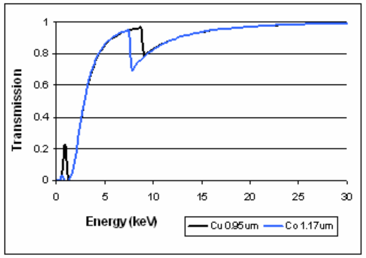

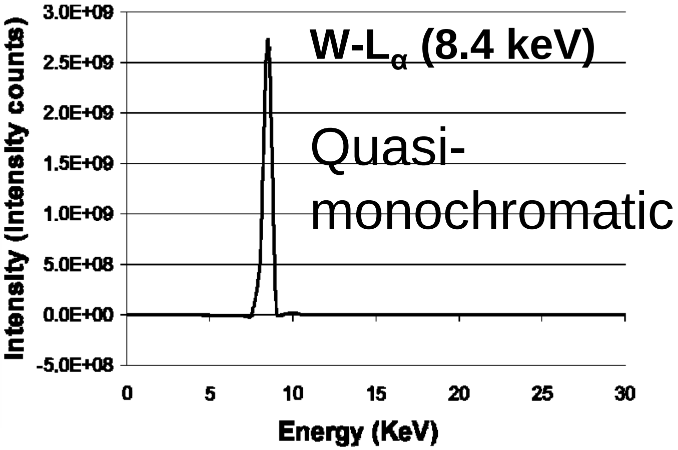

Quantitative Efficiency Measurements of Zone Plates Using Laboratory Sources

Monochromatic projection x-ray image of 70nm zone width, 160um diameter ZP

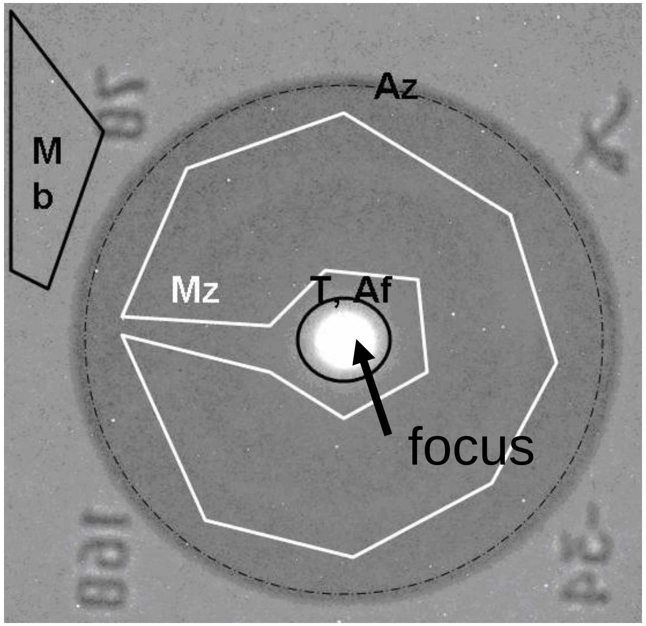

$$\boxed{Efficiency = (T - M_Z A_F) / (M_B A_Z) = 8.7\%}$$

- ❑ Quantitative measurements that agree with synchrotron measurements
- ❑ Objective measurement of zone plate efficiency
- ❑ Efficiency of 70nm zone plate 700nm zone height measured at 73% of theoretical
- ❑ Agreement with synchrotron measurements

S. Chen, et al., *Journal of x-ray science and technology*, in press

M_B Bkgd intensity (counts/pixel)	M_Z Pedestal intensity (counts/pixel)	A_Z ZP area (pixels)	T focused intensity (counts)	A_F focus area (pixels)
9.40 ± 0.1	7.00 ± 0.009	157000 ± 7100	157000 ± 400	4100 ± 300

The Proximity Effect in E-Beam Lithography

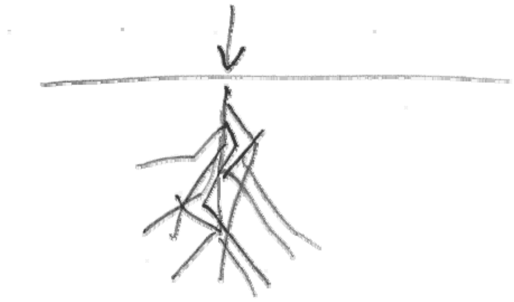

Electrons in thick resist: sidescatter

Thin resist, higher voltage: reduce sidescatter blurring

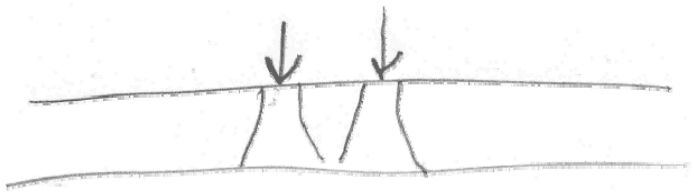

Write two lines next to each other: proximity effect

- Scattering limits the depth of structures that can be produced
- High (100keV) voltage e-beam writing preferred
- Dense gratings (such as zone plates) suffer proximity effect leading to collapse of tall structures
- Direct write to produce zone plate limited to small zone height

Avoiding the Proximity Effect

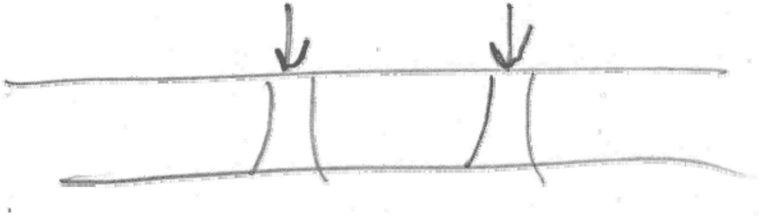

If lines are farther apart, proximity effect is reduced.

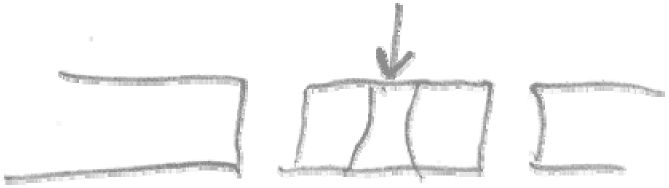

Process every other line, then go back and do the ones you missed (Chao *et al*., CXRO)

- Proximity effect can be reduced by splitting the process of producing a zone plate into two steps

Heroic efforts at Lawrence Berkeley Lab

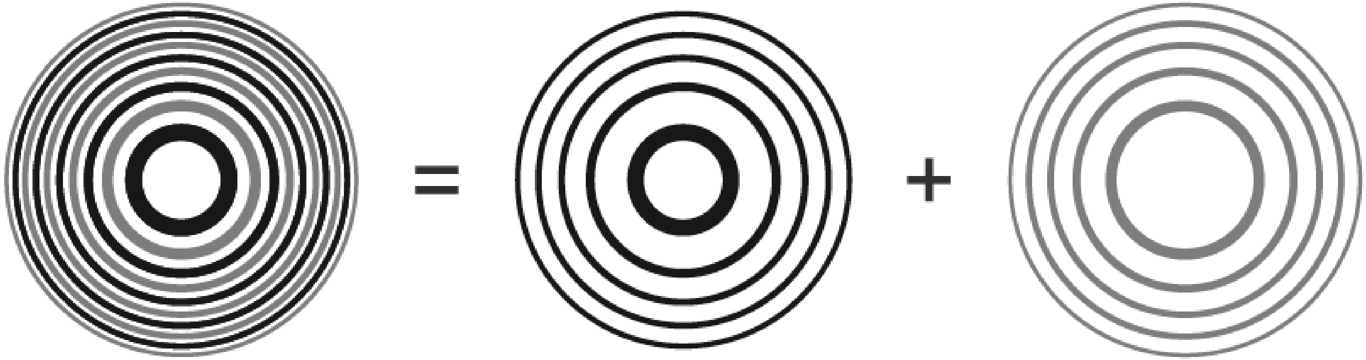

- Chao *et al*., *Nature* **435**, 1210 (2005): 15.1 nm half-pitch multilayer slice imaged with a 15 nm outermost zone width zone plate.
  - Efficiency ~3%.
  - Focal length if used at 290 eV edge: 100 µm.
- Other results: 9.2% at 20 nm: Peuker, *Appl. Phys. Lett.* **78**, 2208 (2001)

Tri-Level Processing Scheme

- Write high resolution pattern in top layer.
- Use highly directional reactive ion etching to transfer to a hard mask, and then into a secondary mask. Tennant et al., JVST 19, 1304 (1981); Schneider et al., JVST B 13, 2809 (1995); Spector et al., JVST B 15, 2872 (1997).

1. E-beam expose, develop

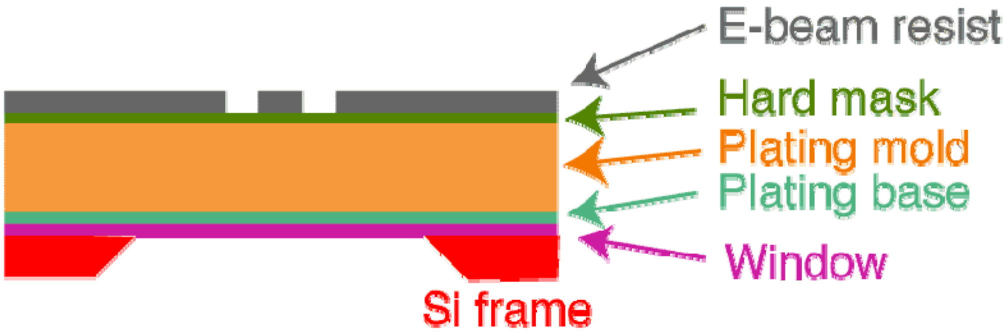

Tri-Level Processing Scheme

- Write high resolution pattern in top layer.
- Use highly directional reactive ion etching to transfer to a hard mask, and then into a secondary mask. Tennant et al., JVST 19, 1304 (1981); Schneider et al., JVST B 13, 2809 (1995); Spector et al., JVST B 15, 2872 (1997).

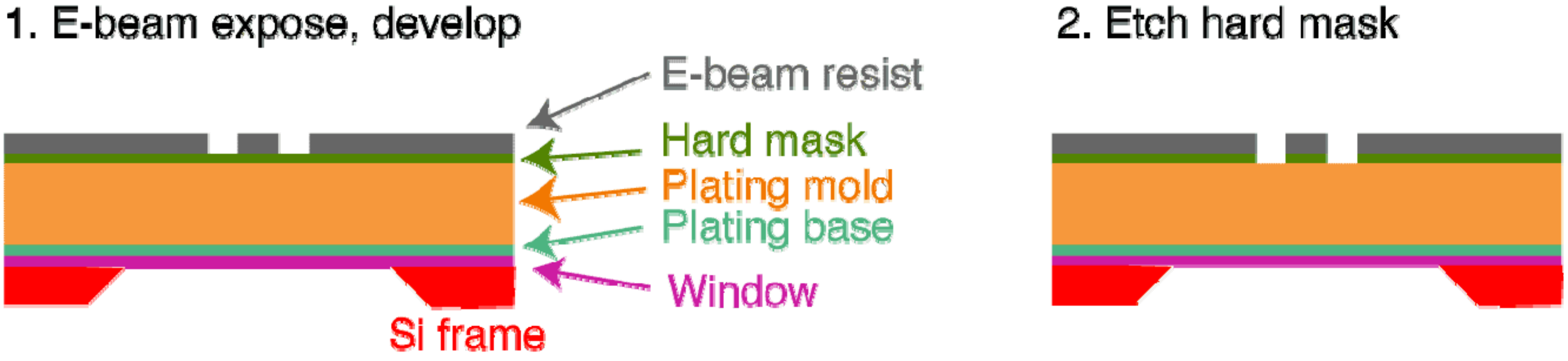

Tri-Level Processing Scheme

- Write high resolution pattern in top layer.
- Use highly directional reactive ion etching to transfer to a hard mask, and then into a secondary mask. Tennant et al., JVST 19, 1304 (1981); Schneider et al., JVST B 13, 2809 (1995); Spector et al., JVST B 15, 2872 (1997).

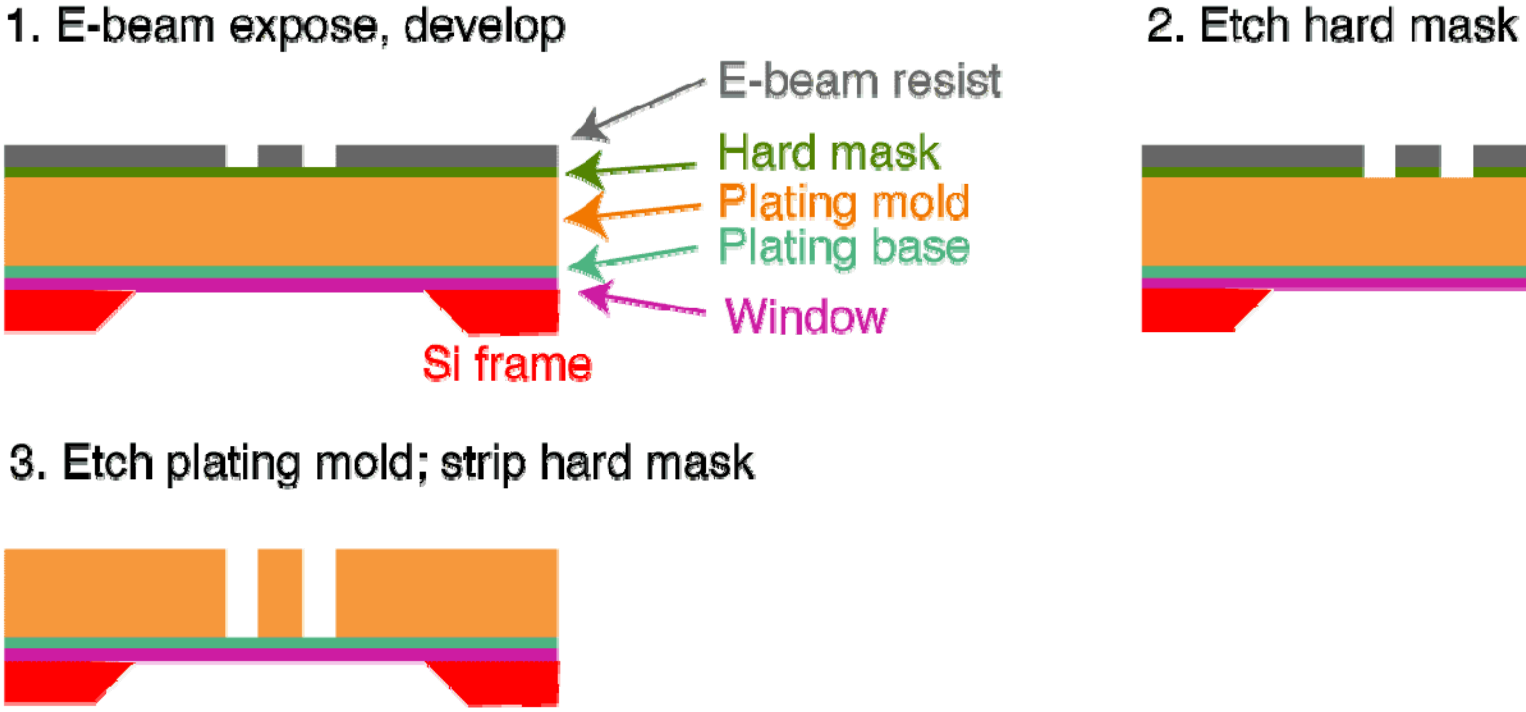

Tri-Level Processing Scheme

- ❑ Write high resolution pattern in top layer.
- ❑ Use highly directional reactive ion etching to transfer to a hard mask, and then into a secondary mask. Tennant et al., JVST 19, 1304 (1981); Schneider et al., JVST B 13, 2809 (1995); Spector et al., JVST B 15, 2872 (1997).

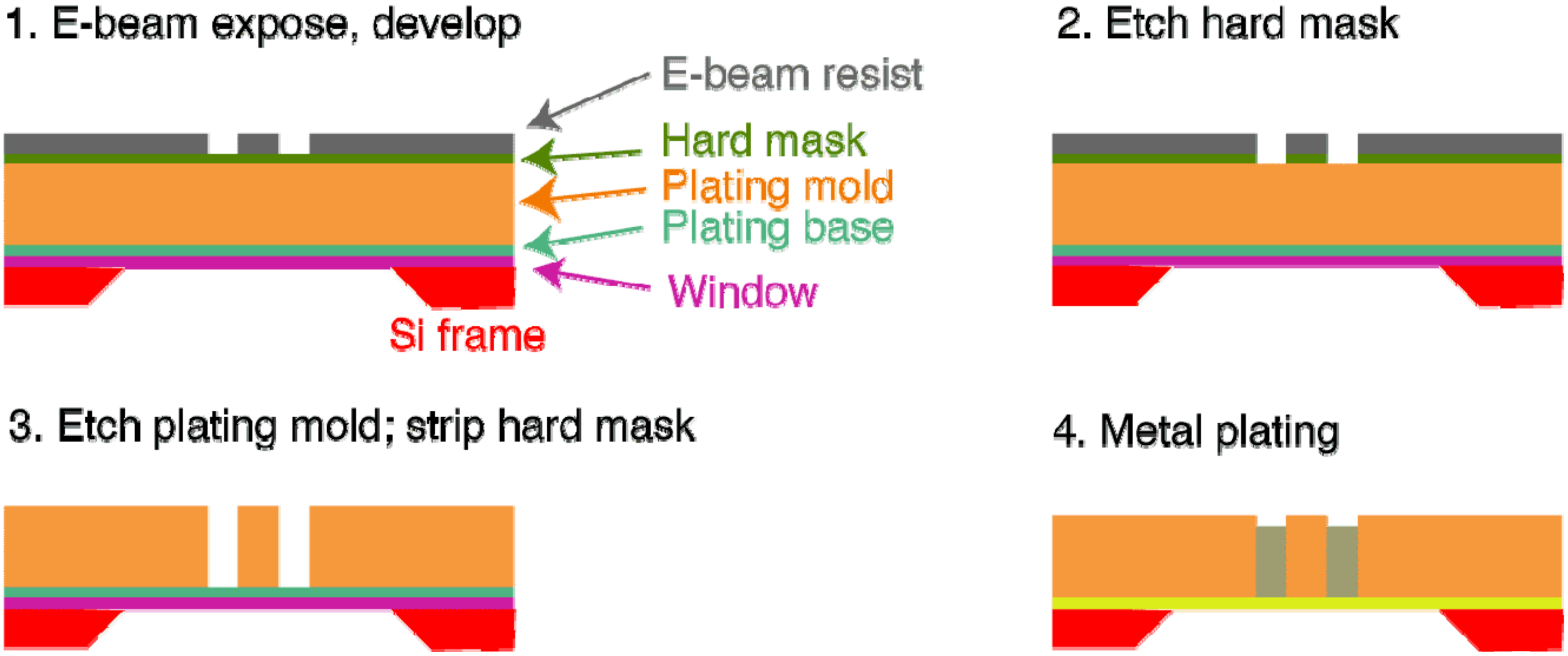

Zone Plates: Stony Brook

- Spector *et al.* [*J. Vac. Sci. Tech. B* **15**, 2872 (1997)], Stein et al. [*J. Vac. Sci. Tech. B* **21**, 214 (2003)], Lu *et al.* [*J. Vac. Sci. Tech. B* **24**, 2881 (2006)].
- Support from NSF and from BNL, collaboration with Don Tennant (Lucent/NJNC; now Cornell)

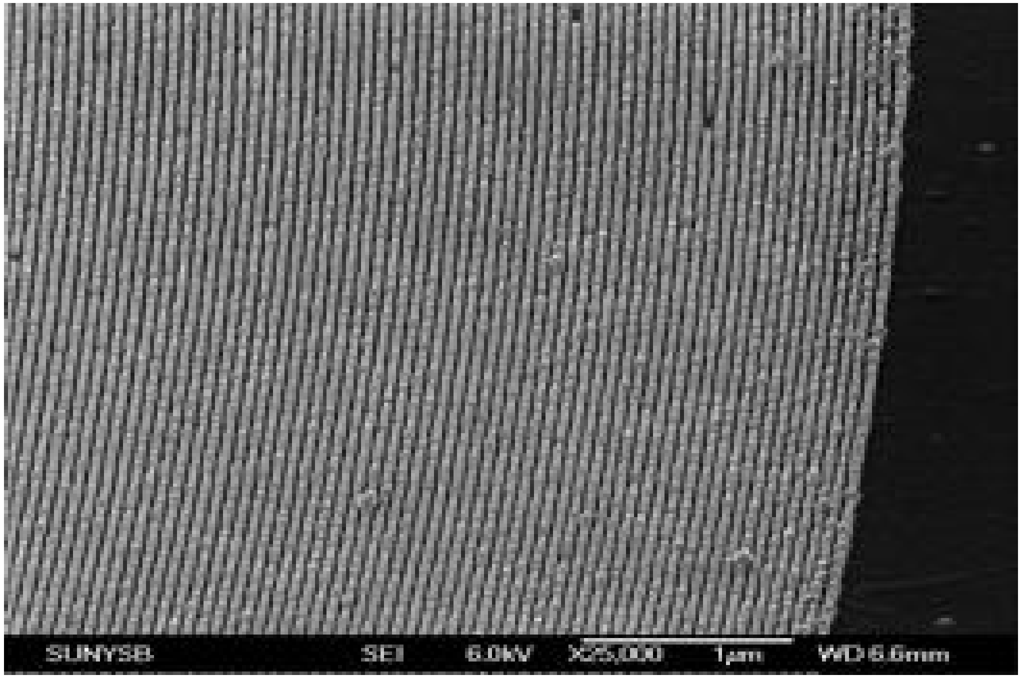

30 nm wide, 130 nm tall Ni, 160 µm diameter

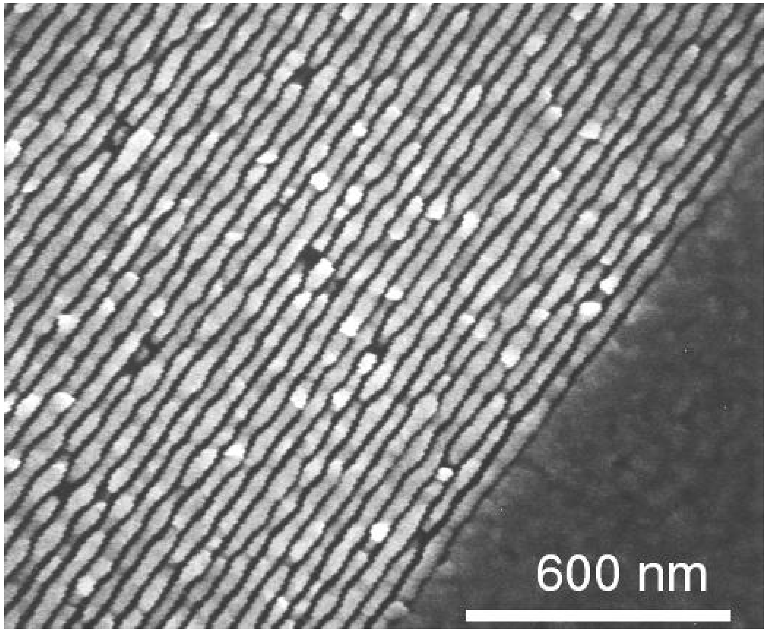

18 nm wide, 60 nm tall Ni, 80 µm diameter

Hard x-ray zone plates from Xradia Inc.

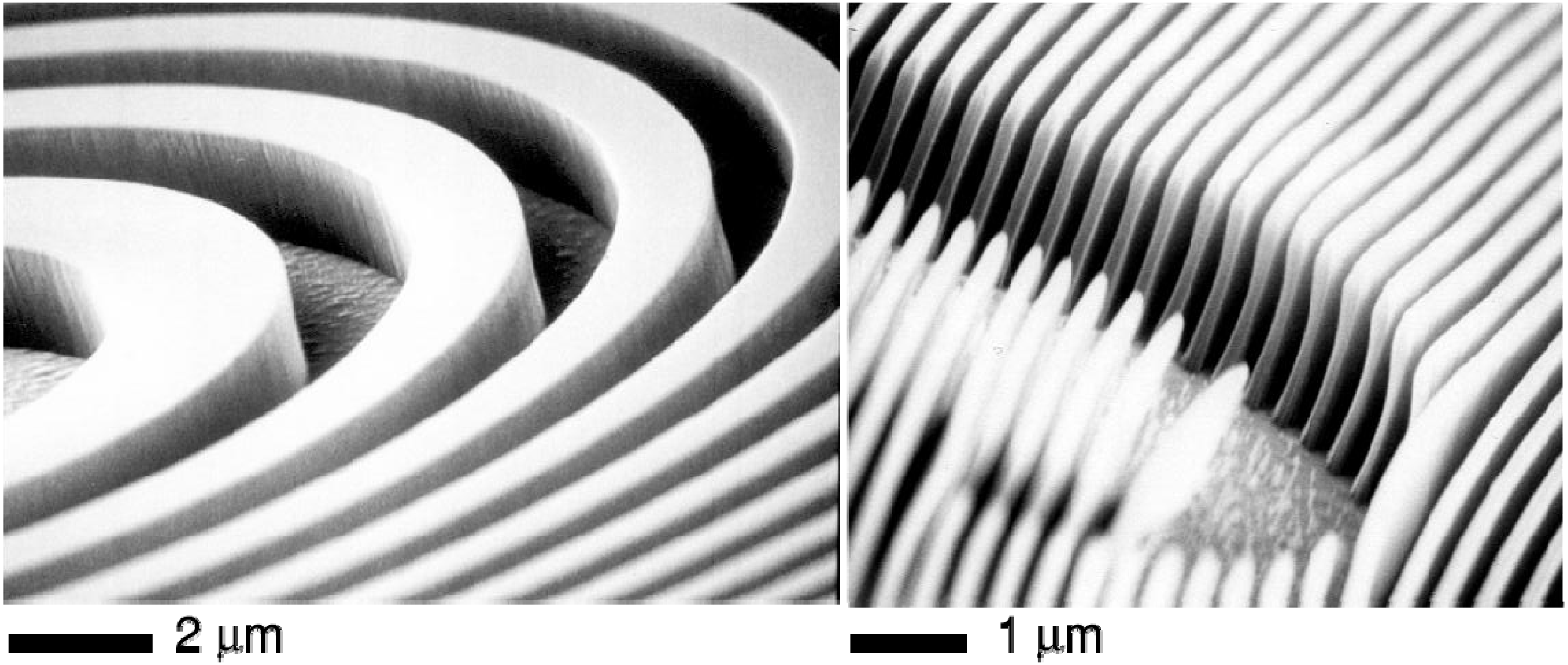

Gold zone plates, Xradia, Inc.: 70 nm outermost zones

Recent Fabrication Highlights at Xradia

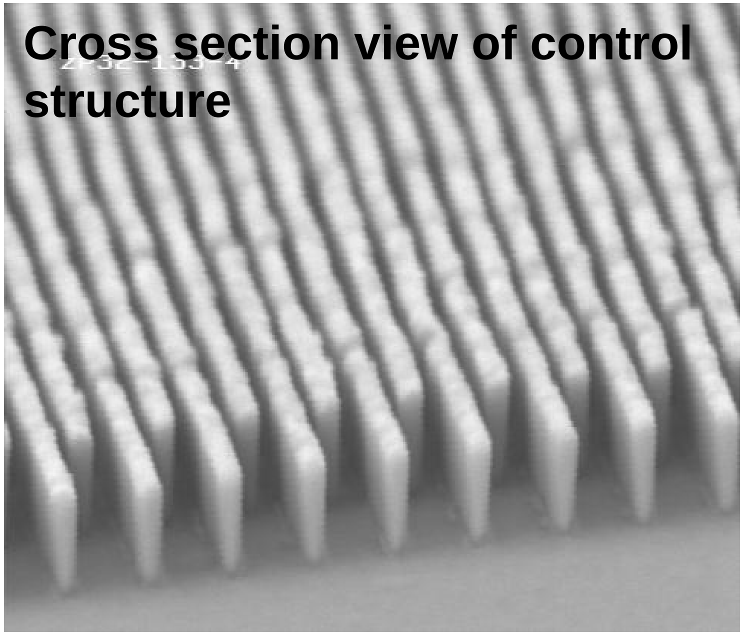

Cross section view of control structure

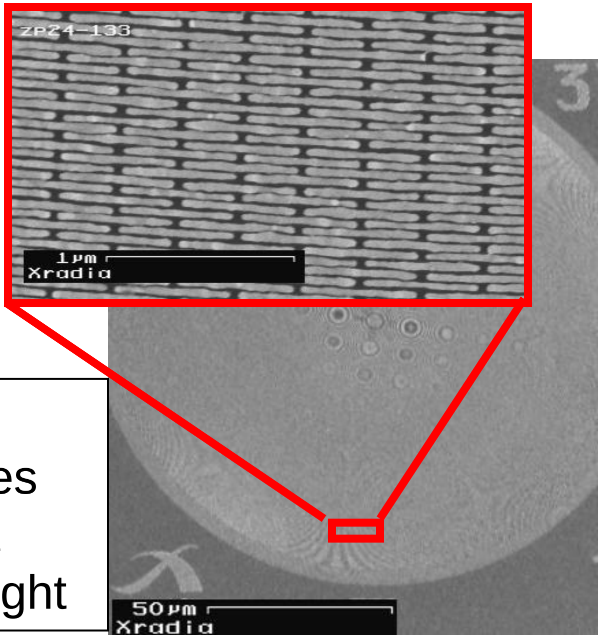

Single ZP:
24nm zones
133um dia
300nm height

- 32nm gold zone plates, 450nm thick fabricated for CNM nanoprobe project (Xradia under contract), AR=14
- 24nm available now (330nm thick, AR=14), procedure developed to align and bond two ZPs to double AR and thickness (660nm thick, AR=28)

High-resolution, High-efficiency Zone Plates
ZP Alignment

Monochromatic
X-ray

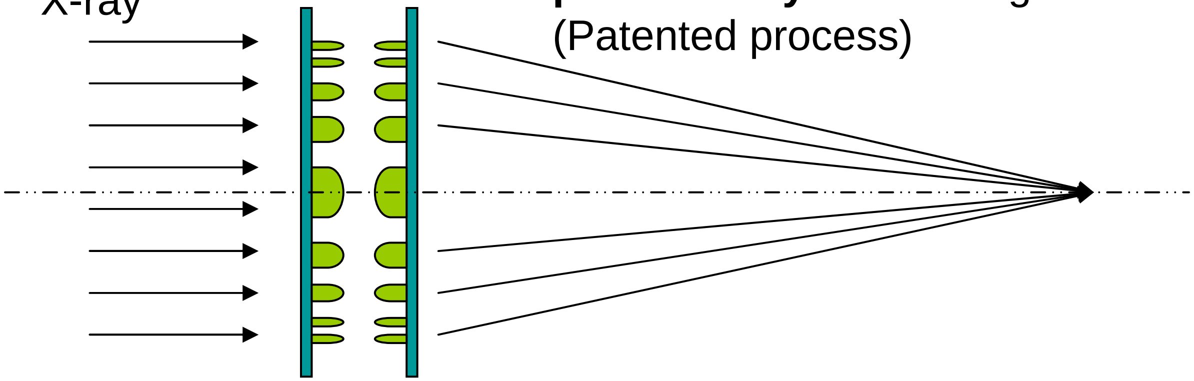

Two zone plates are aligned and **permanently** bonded together face-to-face. (Patented process)

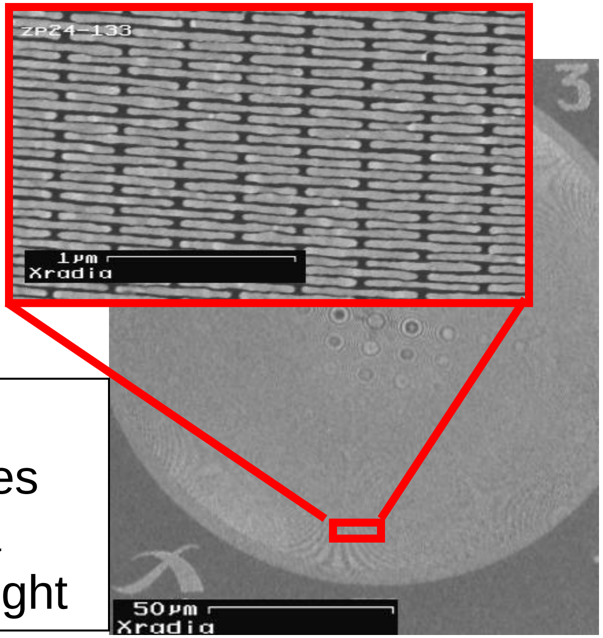

Two zone plates act effectively as one diffractive element if aligned precisely laterally and in very close proximity (within depth of focus of lens)

Single ZP:
24nm zones
133um dia
300nm height

- High-resolution zone plates usually low efficiency
- Alignment to increase zone height increases efficiency
- 24nm zone width zone plates with combined 600nm height in use at ANL ID-26 nanoprobe.

Y. Feng, et al., *Journal of vacuum science and technology B*, 25 (6), 2008

Disposable zone plates?

- Nanoimprint lithography: many cheap copies from one master.
- These slides: step-and-flash imprint lithography (SFIL) as pioneered by Wilson, Srinivasan *et al*., UT Austin

Step 1: template approaches liquid transfer layer

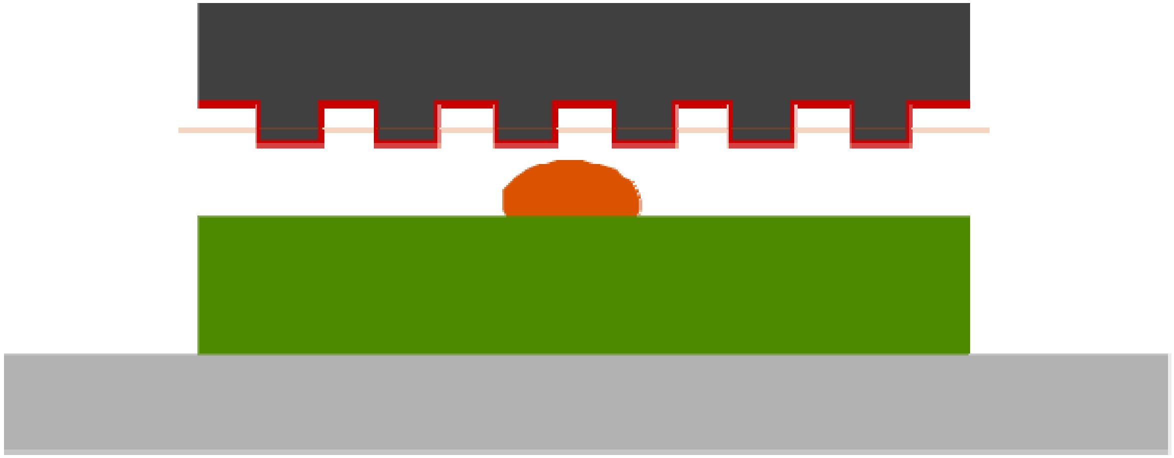

Template

Release layer

Transfer layer

Etch layer

Disposable zone plates?

- Nanoimprint lithography: many cheap copies from one master.
- These slides: step-and-flash imprint lithography (SFIL) as pioneered by Wilson, Srinivasan *et al*., UT Austin

Step 2: compress liquid transfer layer, and UV flash to harden

Template

Release layer

Transfer layer

Etch layer

Disposable zone plates?

- Nanoimprint lithography: many cheap copies from one master.
- These slides: step-and-flash imprint lithography (SFIL) as pioneered by Wilson, Srinivasan *et al*., UT Austin

Step 3: remove template

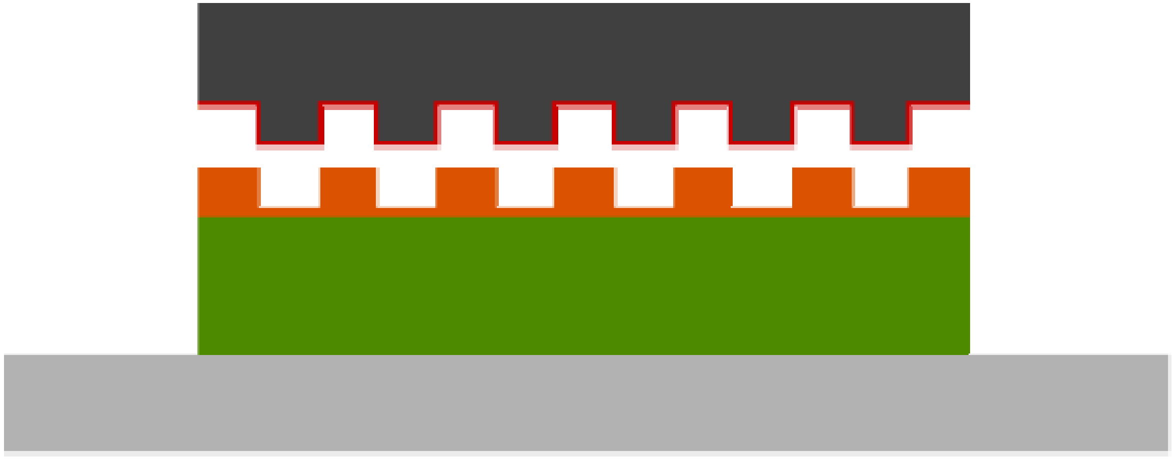

Template

Release layer

Transfer layer

Etch layer

Disposable zone plates?

- Nanoimprint lithography: many cheap copies from one master.
- These slides: step-and-flash imprint lithography (SFIL) as pioneered by Wilson, Srinivasan *et al*., UT Austin

Step 4: etch transfer layer to break through to etch layer

Template

Release layer

Transfer layer

Etch layer

Disposable zone plates?

- Nanoimprint lithography: many cheap copies from one master.
- These slides: step-and-flash imprint lithography (SFIL) as pioneered by Wilson, Srinivasan *et al*., UT Austin

Step 5: etch through the etch layer

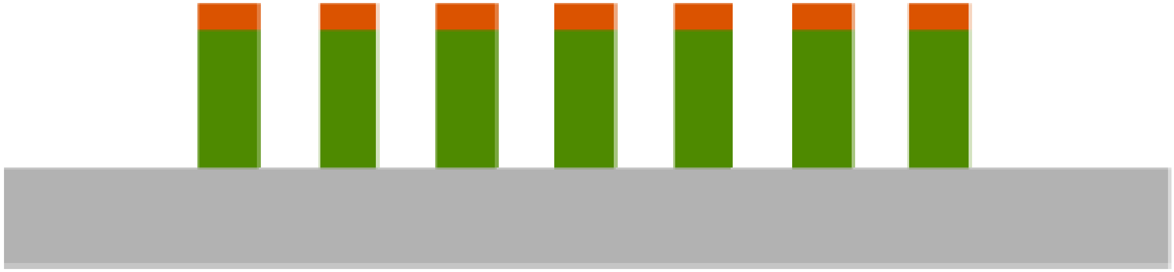

Template

Release layer

Transfer layer

Etch layer

SFIL zone plates: basic demonstration

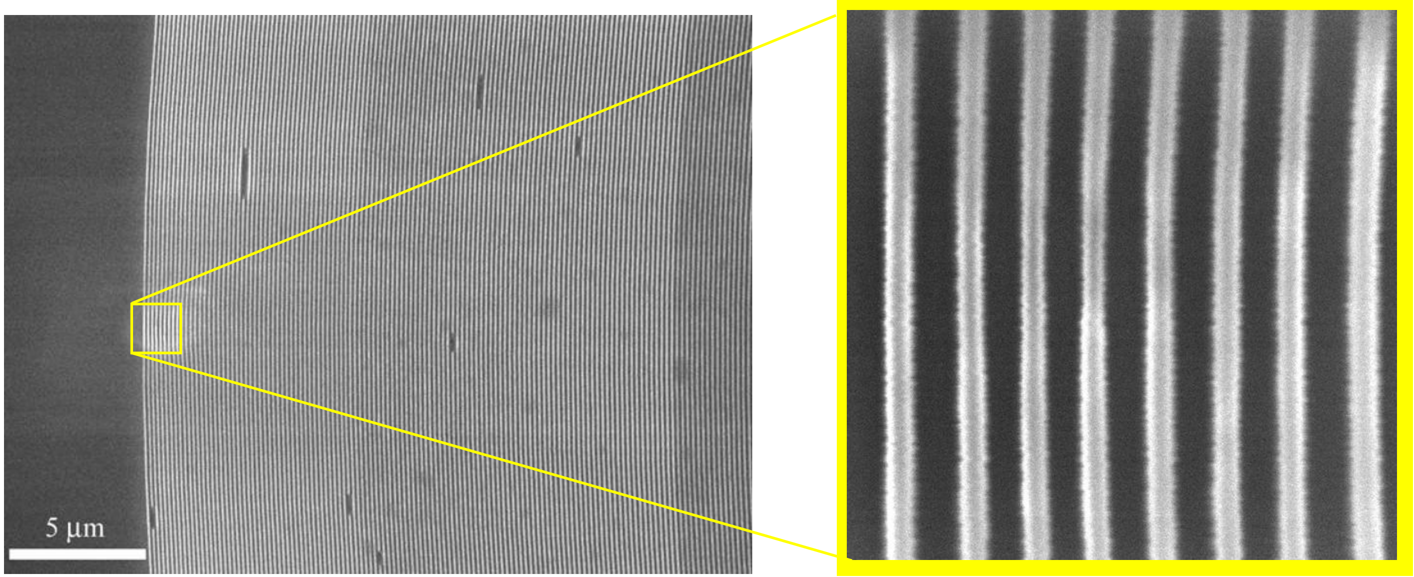

50 nm zones replicated in transfer layer from quartz wafer. Stein *et al.*, *JVST B* **21**, 214 (2003)

Sputter-sliced or “jelly roll” zone plates

- It’s easy to make thin layers! Successive layer deposition on a rotating wire. First proposed by Schmahl and Rudolph in 1980 (Ash, *Scanned Image Microscopy*).
- Many efforts, including Göttingen, Livermore, SPring-8, ESRF...
- Challenges: circularity, error accumulation....

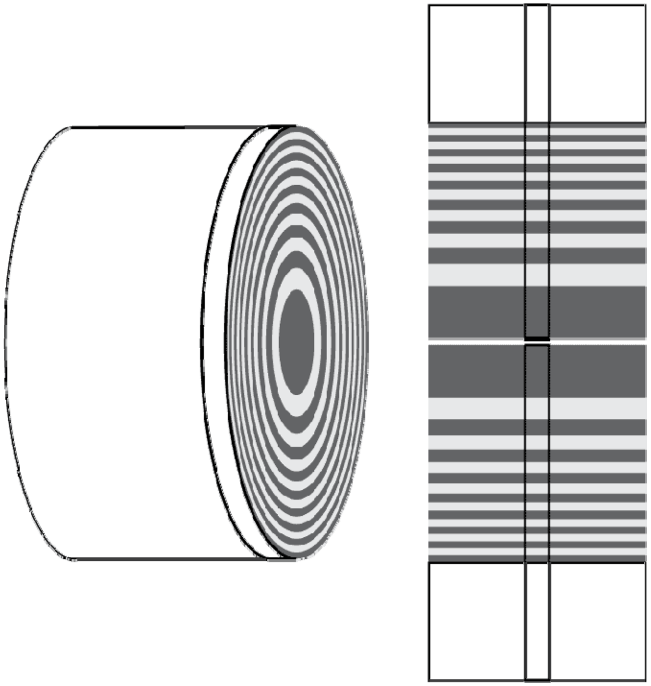

Multilayer Laue lenses

- Forget top-down circles, and go sideways! Start by depositing thinnest zones first on a flat substrate, and work your way up to thicker zones. Cross two 1D lenses for 2D focusing.
- For thick optics, you want to tilt to be on the Bragg condition anyway [Maser, PhD thesis; Maser and Schmahl, *Opt. Comm*. **89**, 355 (1992)]

NSLS II: stated goal is 1 nm resolution using MLLs (or kinoform refractive lenses)

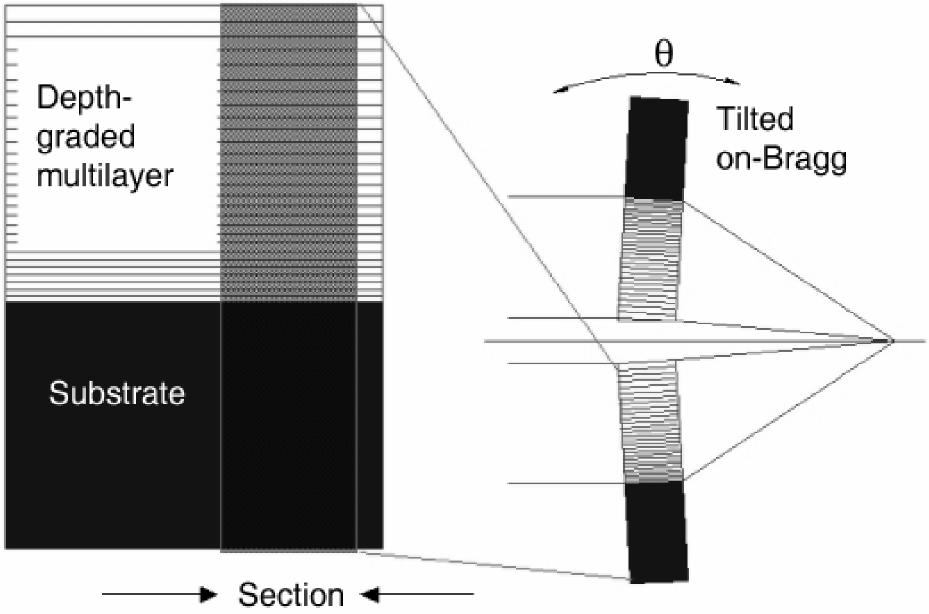

J. Maser et al., *SPIE* **5539**, 185 (2004); plus tests by Liu *et al*., *J. Appl. Phys*. **98**, 113519 (2005); Kang *et al*., *Appl. Phys. Lett*. **86**, 151109 (2005); Kang *et al*., *Phys. Rev. Lett*. **96**, 127401 (2006).

MLLs are not without challenges

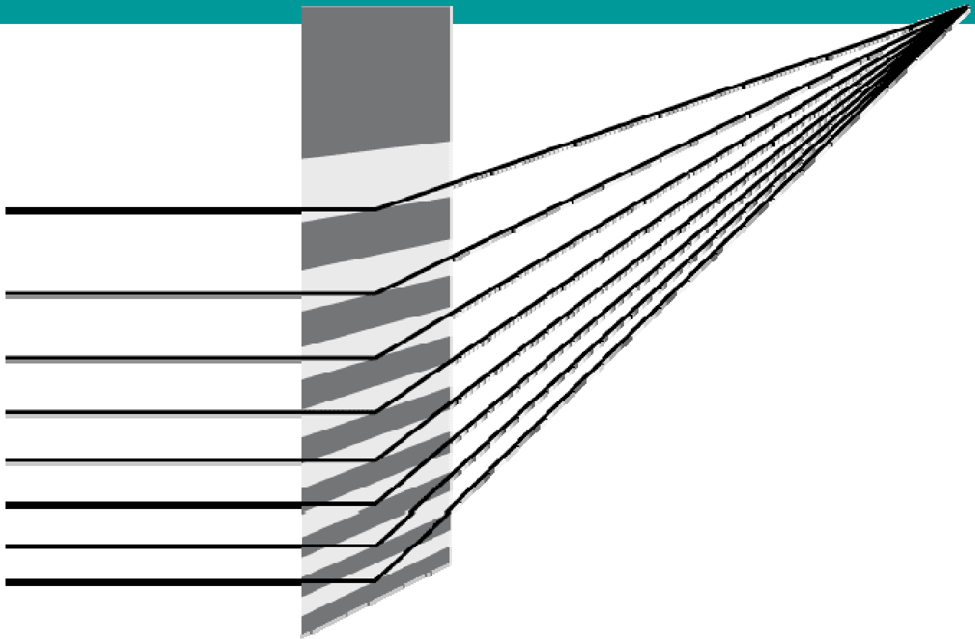

Must stay on-Bragg for
good efficiency

–

High resolution: lots of layers!

- ❑ Transverse resolution Δ_t=1.22Δ_{rN}, where Δ_{rN}=outermost zone width
- ❑ Diameter d=1.22 $\lambda f/\Delta_t$, # zones N=1.22^2 $\lambda f/\Delta_t^2$

Challenge at high resolution: depth of focus

- Depth of focus is 1.22λ/N.A., or $4.88(dr_N)^2/\lambda$ where dr_N is the outermost zone width

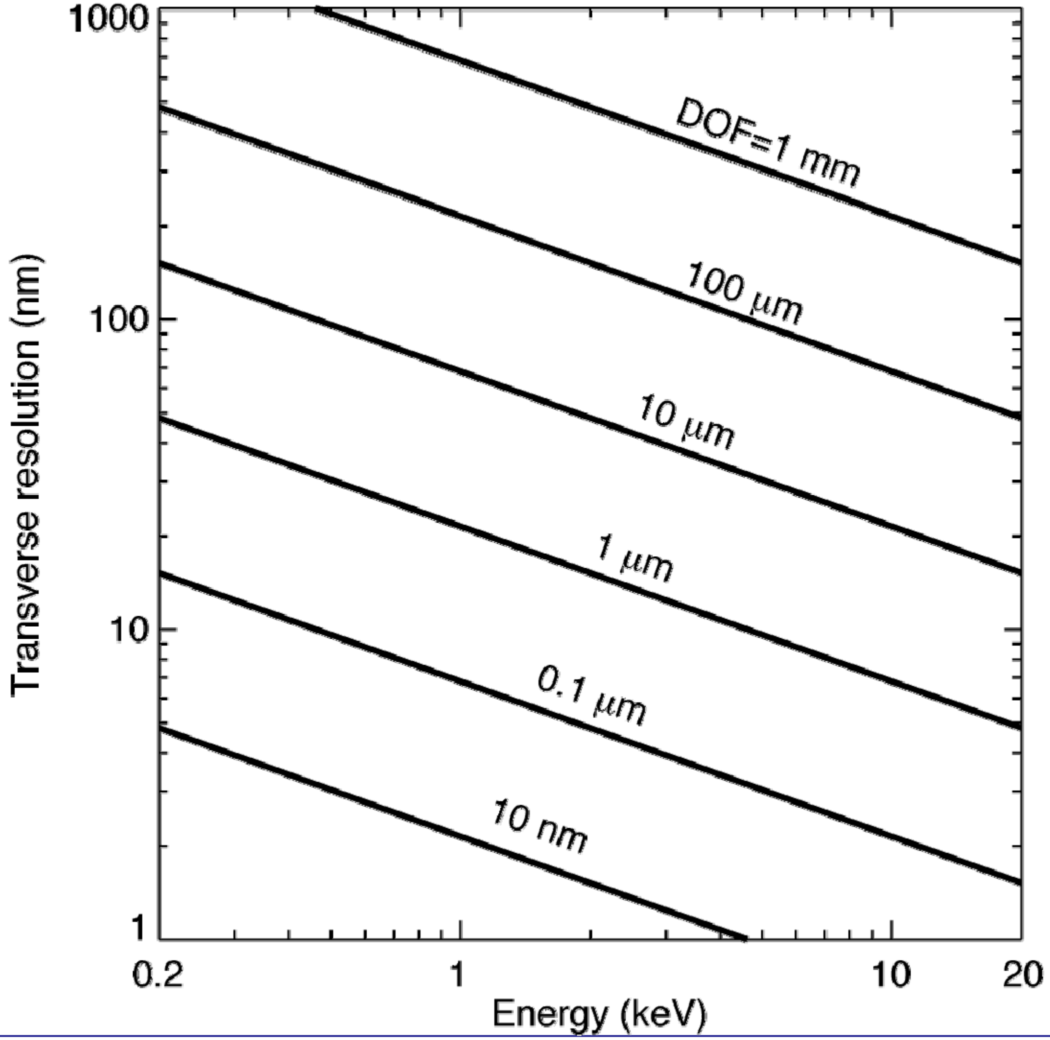

How clean is the focus?

- ☐ a=(central stop diameter)/(zone plate diameter)

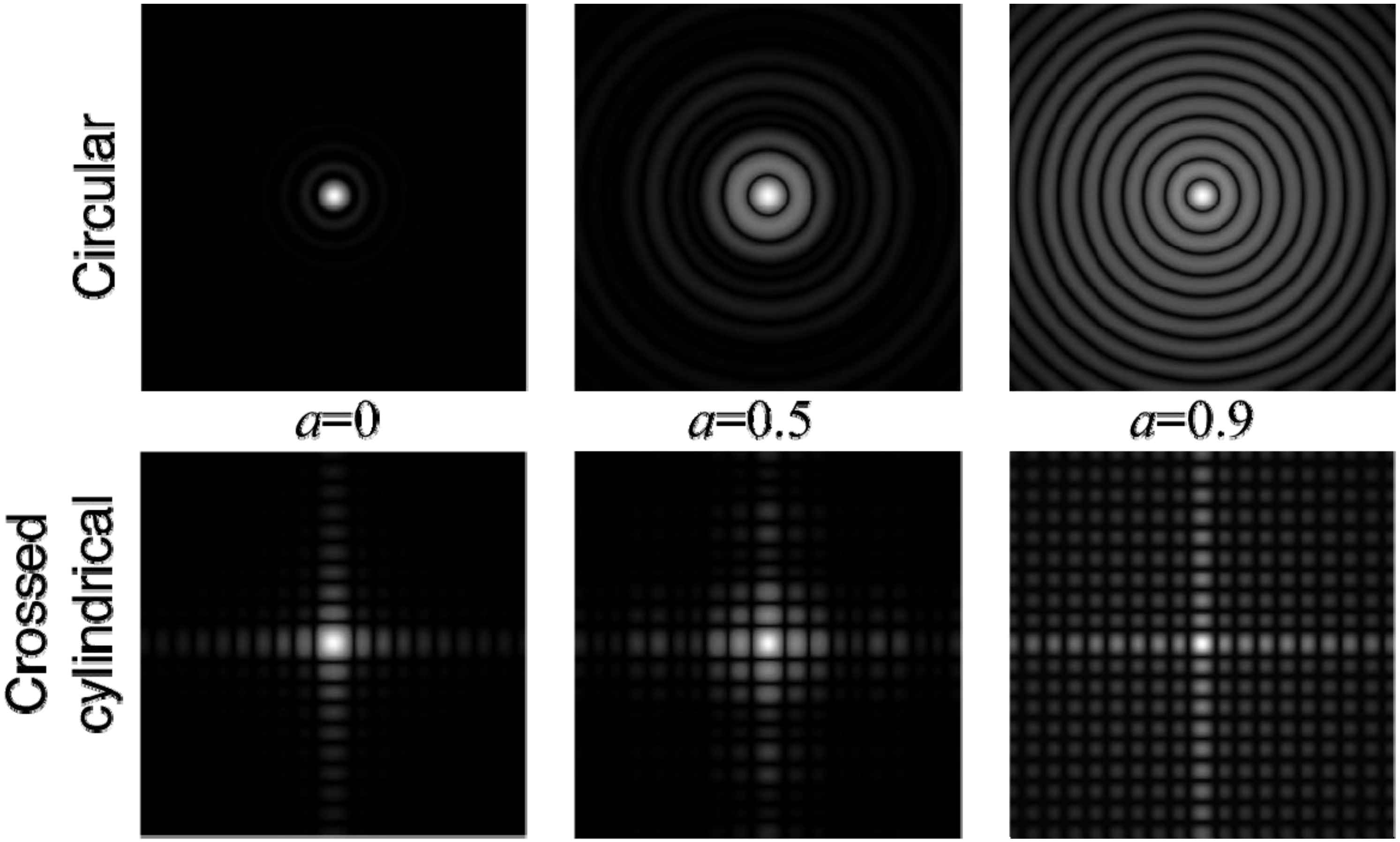

You really want all zones!

X-ray optics: best resolution

X-ray optics: best resolution

ZP Uses

- Microscope objective
- Condenser/monochromator
- Microprobe forming lens
- Beam splitter
- Works for any wave (including neutrons and atoms)

ZP based x-ray microscope

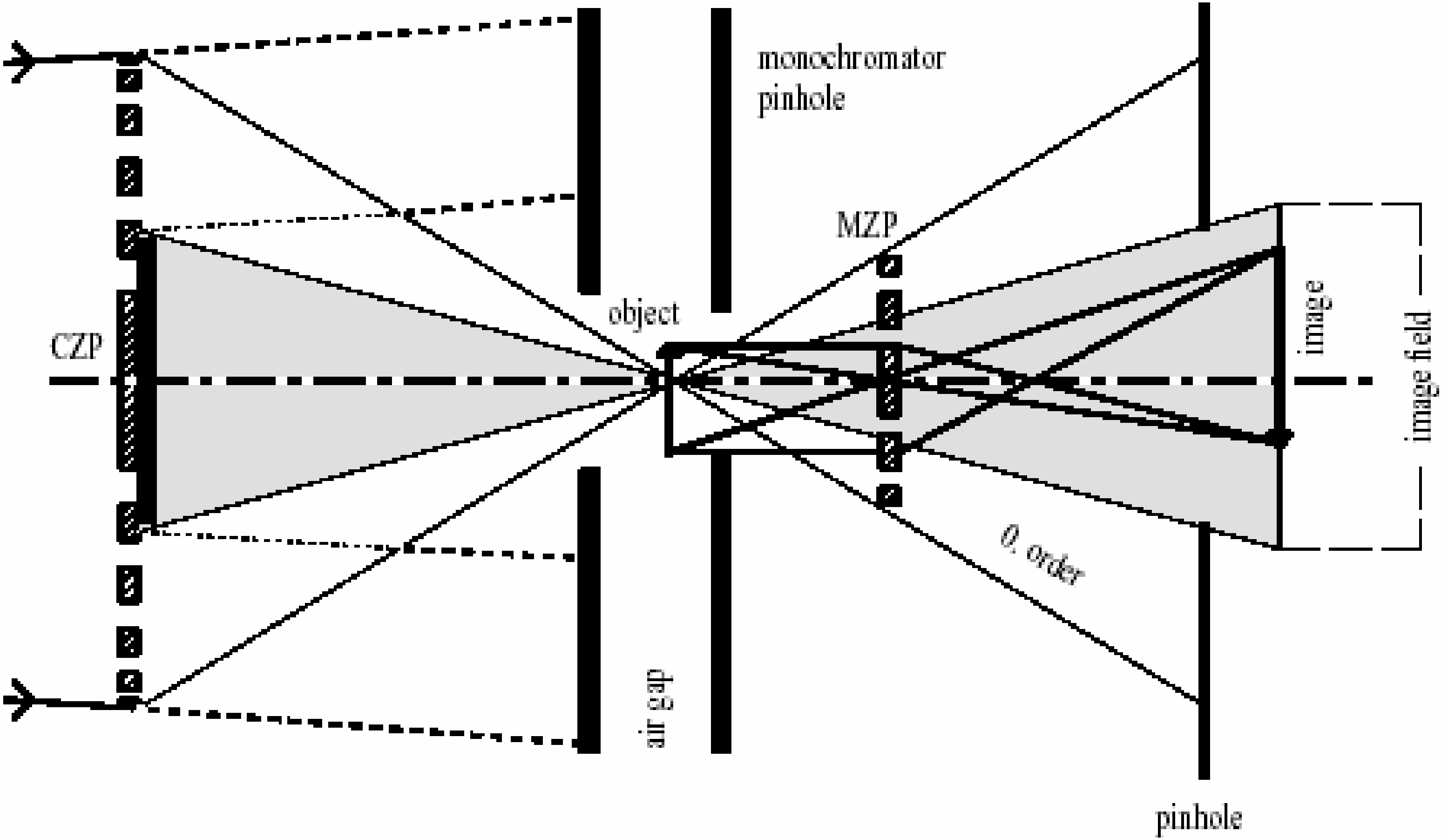

Full-field and scanning

- TXM
- Incoherent illumination; works well with a bending magnet, with fast imaging
- More pixels (e.g., 2048^2)
- Optic efficiency   specimen dose
- Moderate spectral resolution if zone plate condenser used - but most new TXMs use grating/crystal and reflective condenser!

STXM

- Coherent illumination; works best with an undulator
- Less dose to sample (~10% efficient ZP)
- Better suited to conventional grating monochromator [high E/(ΔE)]
- Microprobes: fluorescence etc.

TXM: transmission x-ray microscope

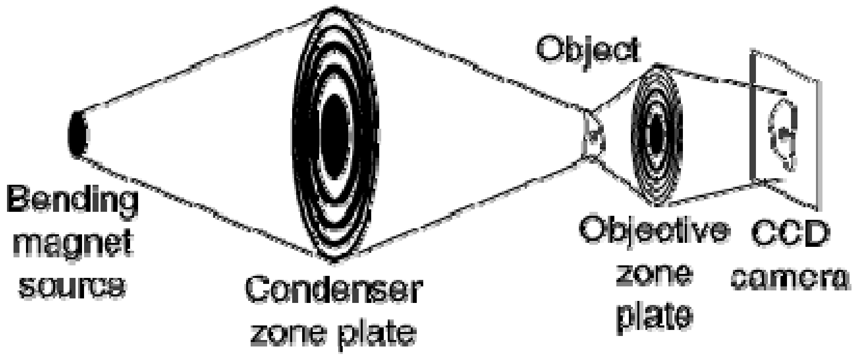

STXM: scanning transmission x-ray microscope

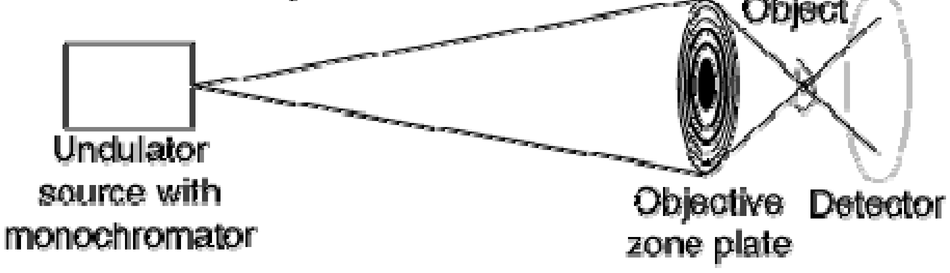

X-Ray Advantage:
High-resolution imaging of buried Structures

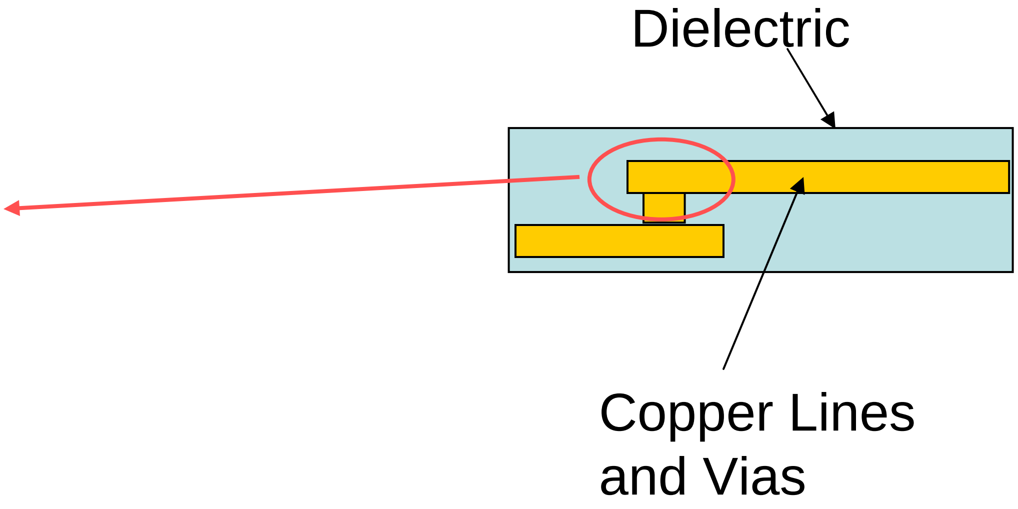

Computed Tomography

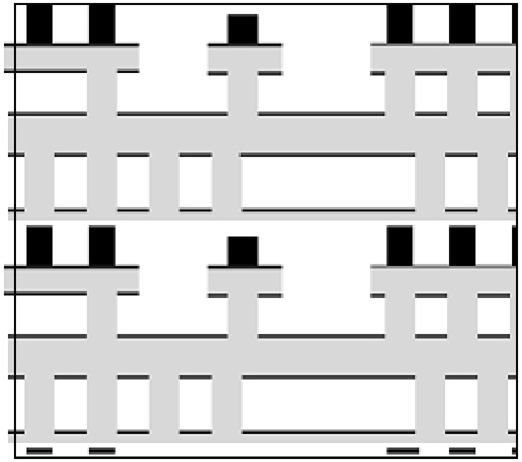

(1) Sample imaged at various angles to acquire tomographic projections.

Sinogram

(2) 3D reconstruction by backprojection results in 3D image of the sample.

Imaging Length Scale Coverage

Loss of contrast and throughput leads to a crossover at ~1um resolution

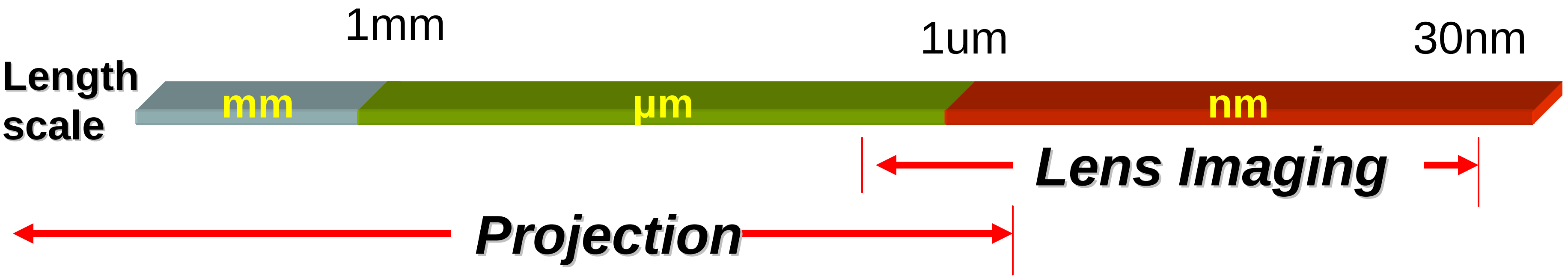

X-ray Imaging with High-resolution (nanoXCT) Optics and High Contrast

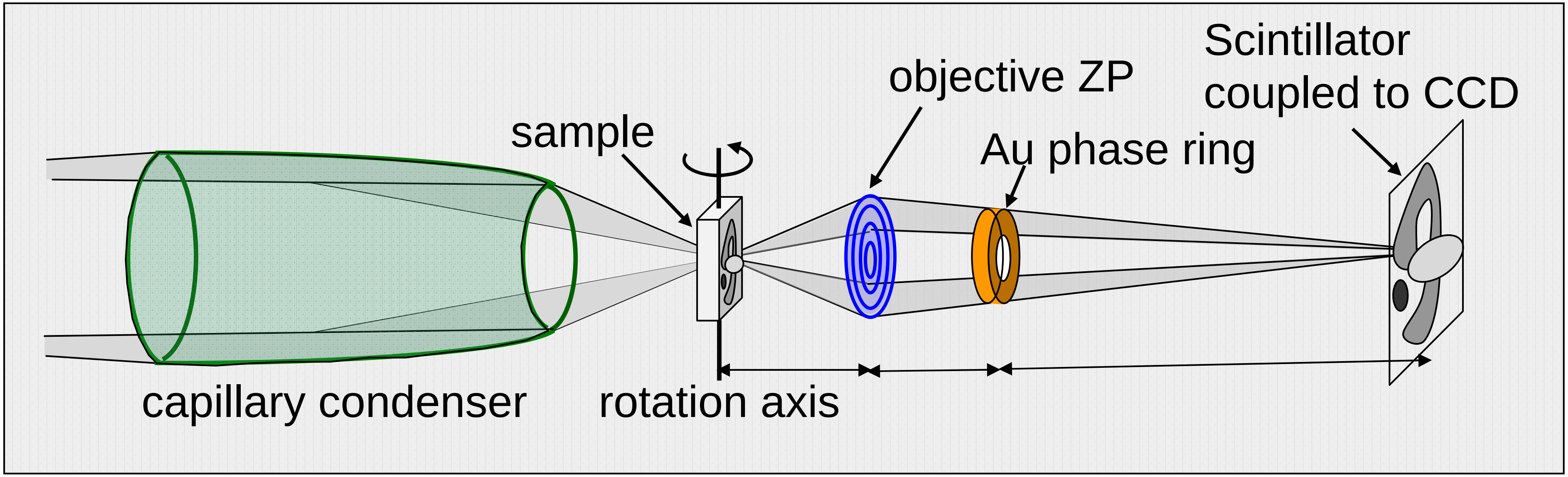

- Key components:
  - High efficiency, reflective ellipsoidal capillary condenser
  - High-resolution objective zone plate
  - Zernike phase contrast phase plate
  - High-efficiency, high resolution x-ray detector
  - Precision tomography stages

nm-scale: Tubular Fuel Cell (SOFC)

Courtesy of Dr. W. Chiu (U. Connecticut),, Adaptive Materials Inc.

2D transmission x-ray images

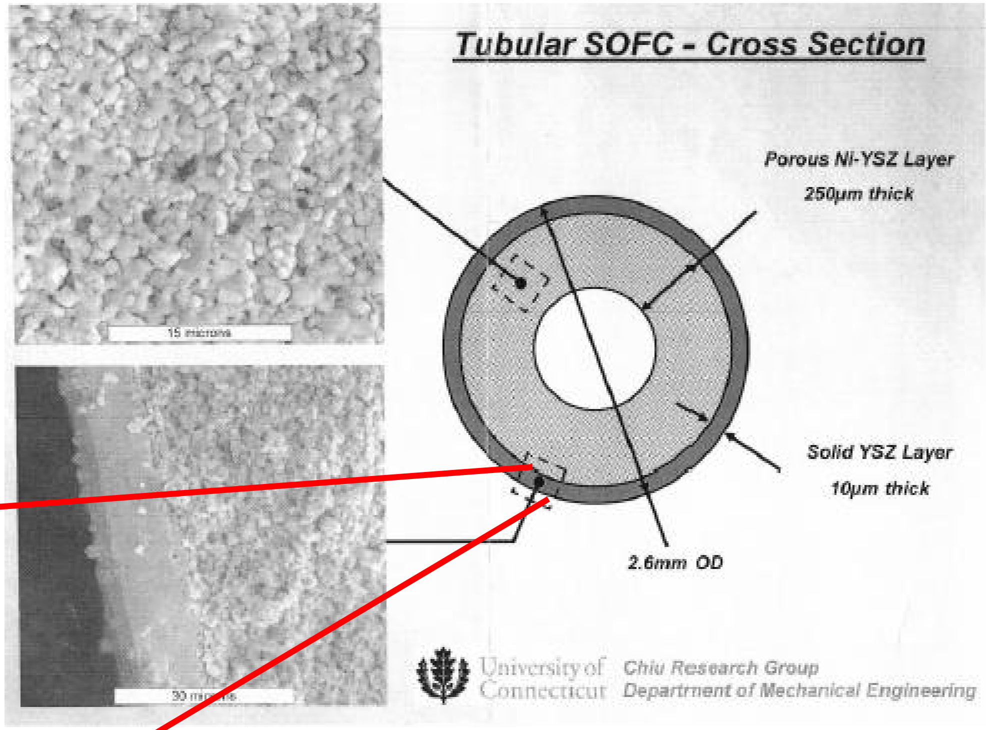

Xradia nanoXCT-8-50-Z
8keV x-ray energy (stand alone)
sub-50nm resolution
Zernike phase contrast

Tubular Fuel Cell (SOFC)

2D transmission x-ray projection images (0-90 degree rotation)

Reconstructed 3D volume

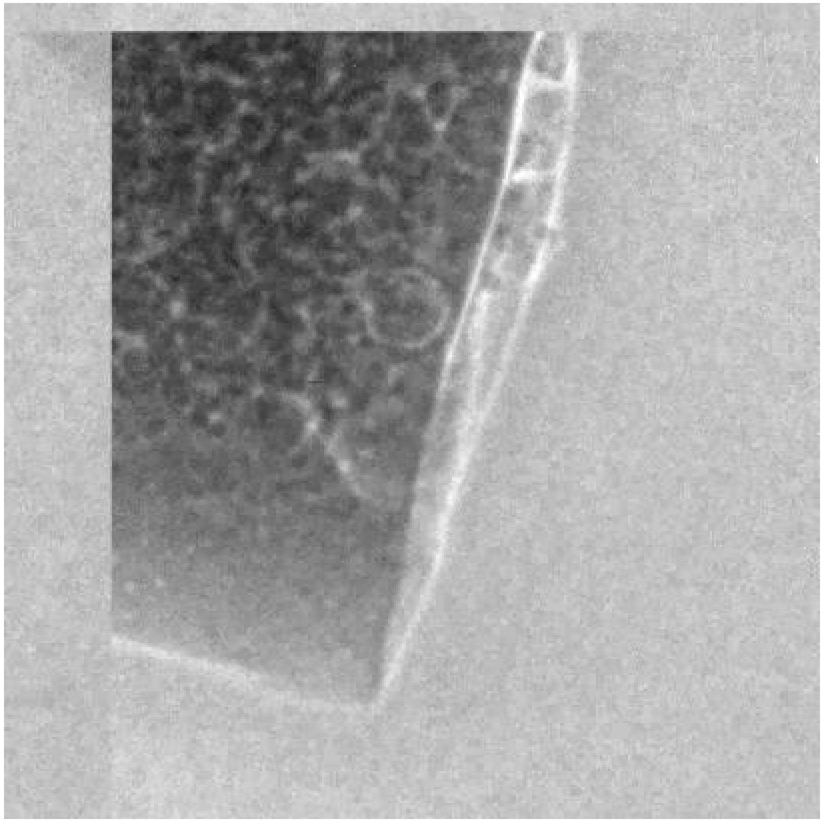

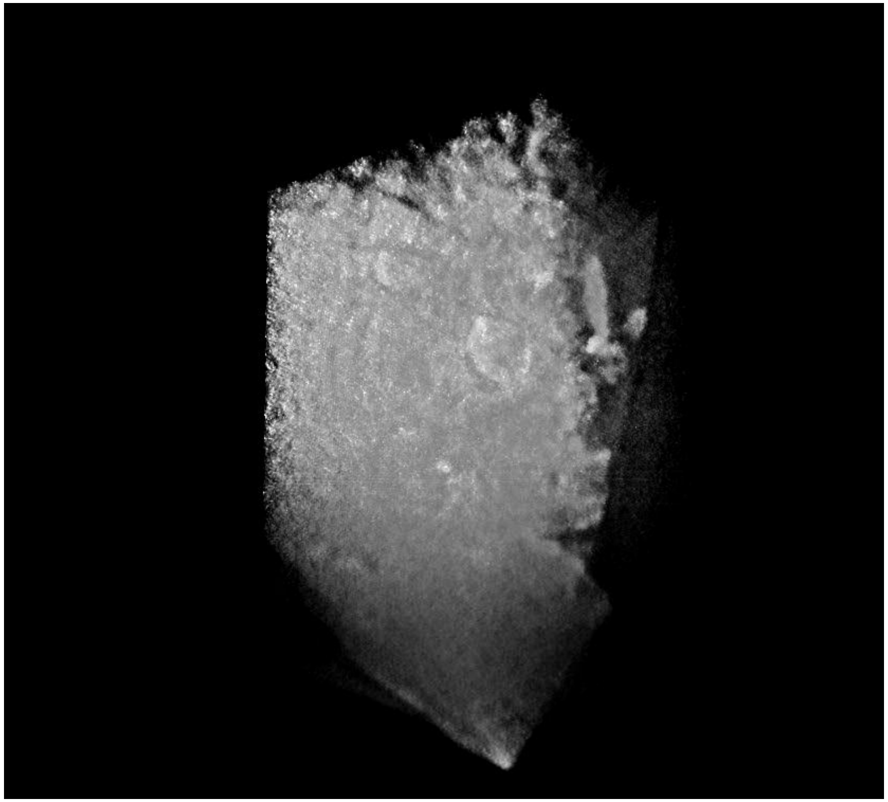

SOFC Pore Structure Imaging – cont'd

- **nanaoXCT Experiment details**
  - Xradia (Concord, CA)
  - 8 keV copper source
  - 181 projections at 300 sec per projection
  - 22.6 µm field of view
  - 50 nm resolution
  - 3-D tomographic reconstruction

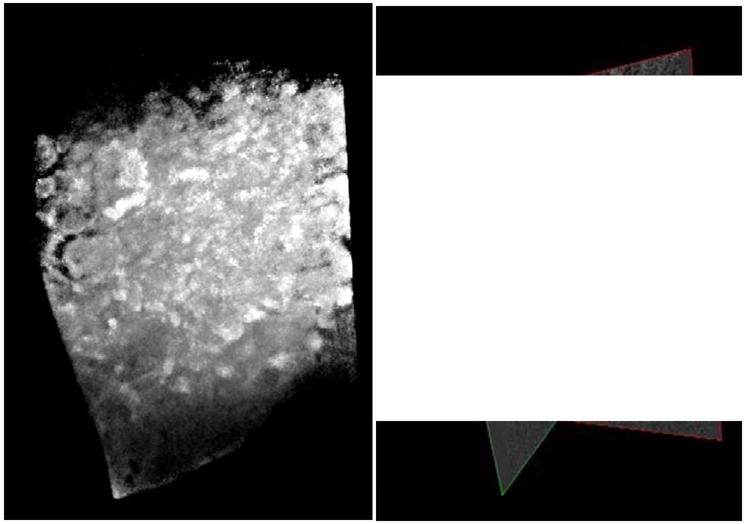

Source: Prof Wilson Chiu, University of Connecticut

Putting It All Together

nXCT-Imaged SOFC Anode

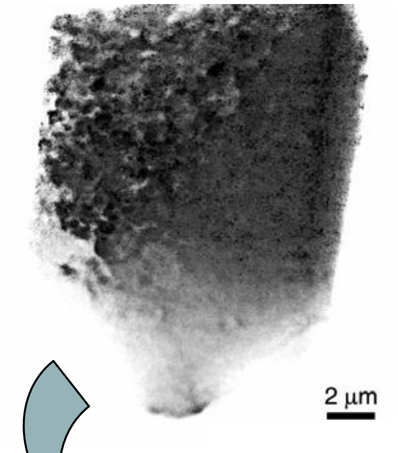

3D Reconstruction

Gas Transport, Reformation & Electrochemistry

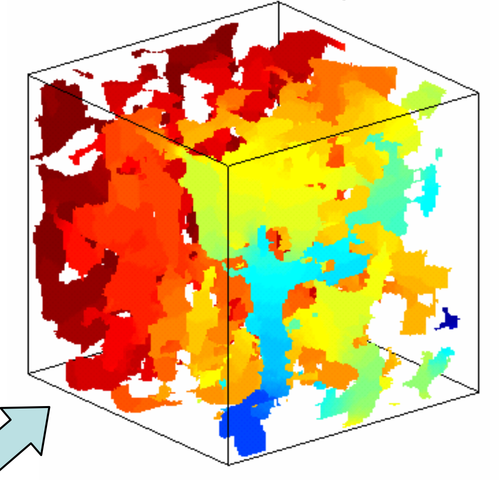

User Models

?

Optimum Structure

Parameters

ε τ <r> <r^2>

D_{ij} D^k_{ij} μ k

η_{ohm} η_{conc} ρ

[i_o β η_{act} L_{TPB}]

Ionic & Electronic Charge Transfer

Source: Prof Wilson Chiu, University of Connecticut

M1 Metal Layer IC Sample

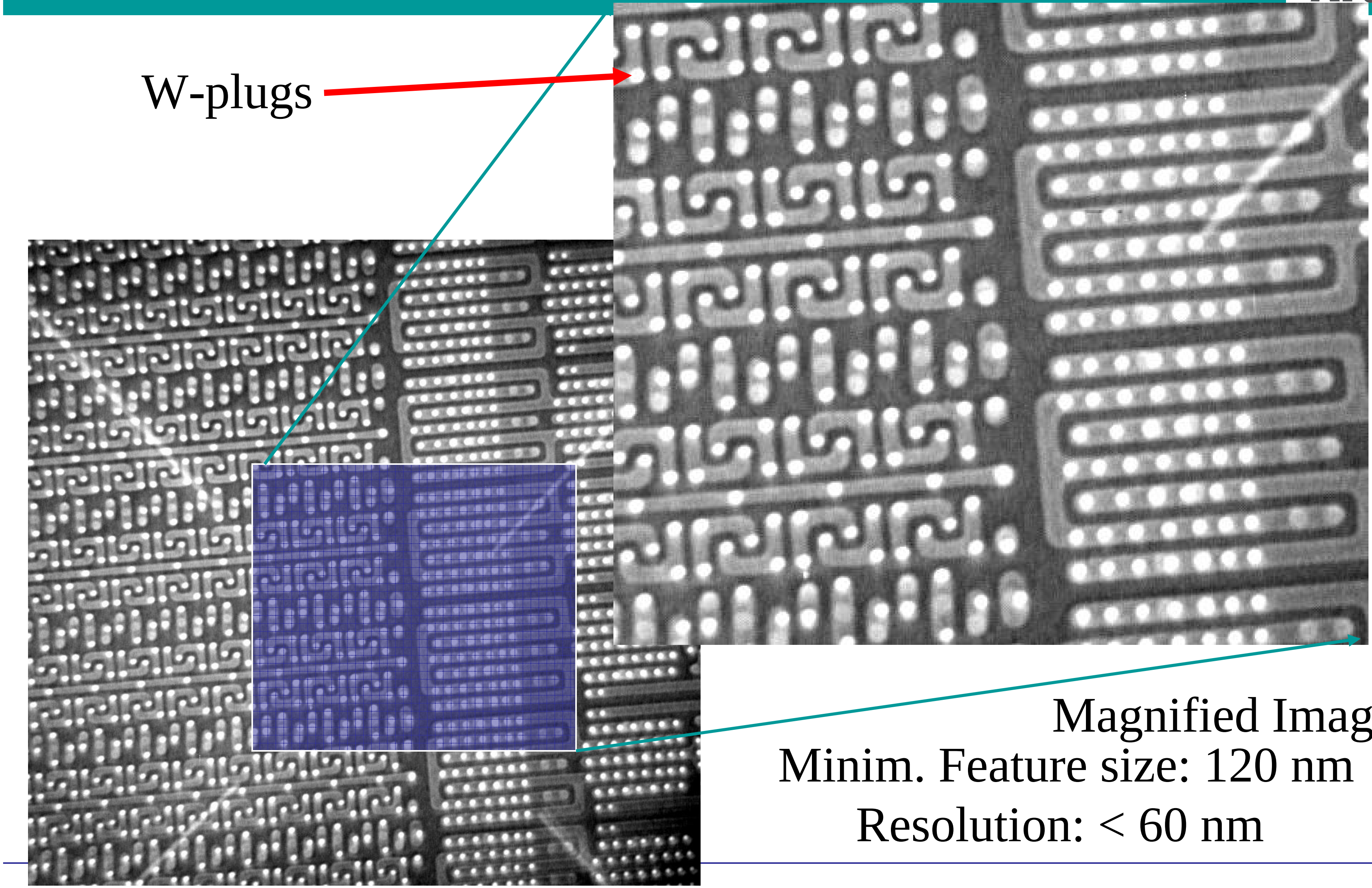

Magnified Image

Minim. Feature size: 120 nm

Resolution: < 60 nm

Raw Image Data of Cu-Interconnect

- Cr 5.4keV x-ray energy
- Cu interconnect sample with 5 layers of trenches and interconnecting vias
- 6 hr data collection time

- Bright structures are Cu

1μm

CT Reconstruction – Planar Slices

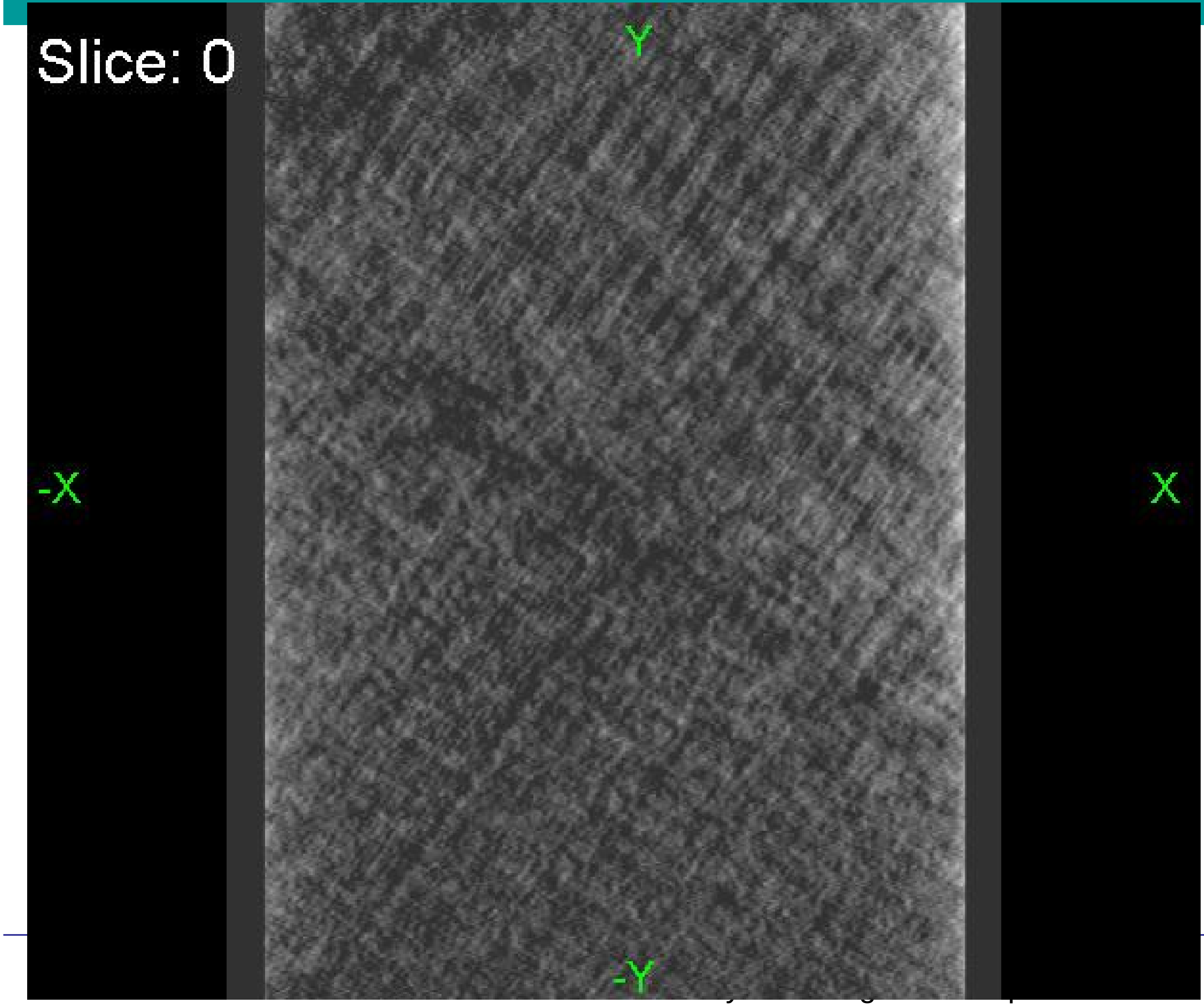

- Cu Layers, and W Layer clearly resolved

Extracted Layers of Pentium 4 chip (120nm node)

Cu (8 keV) Laboratory x-ray source
Zernike Phase contrast Imaging

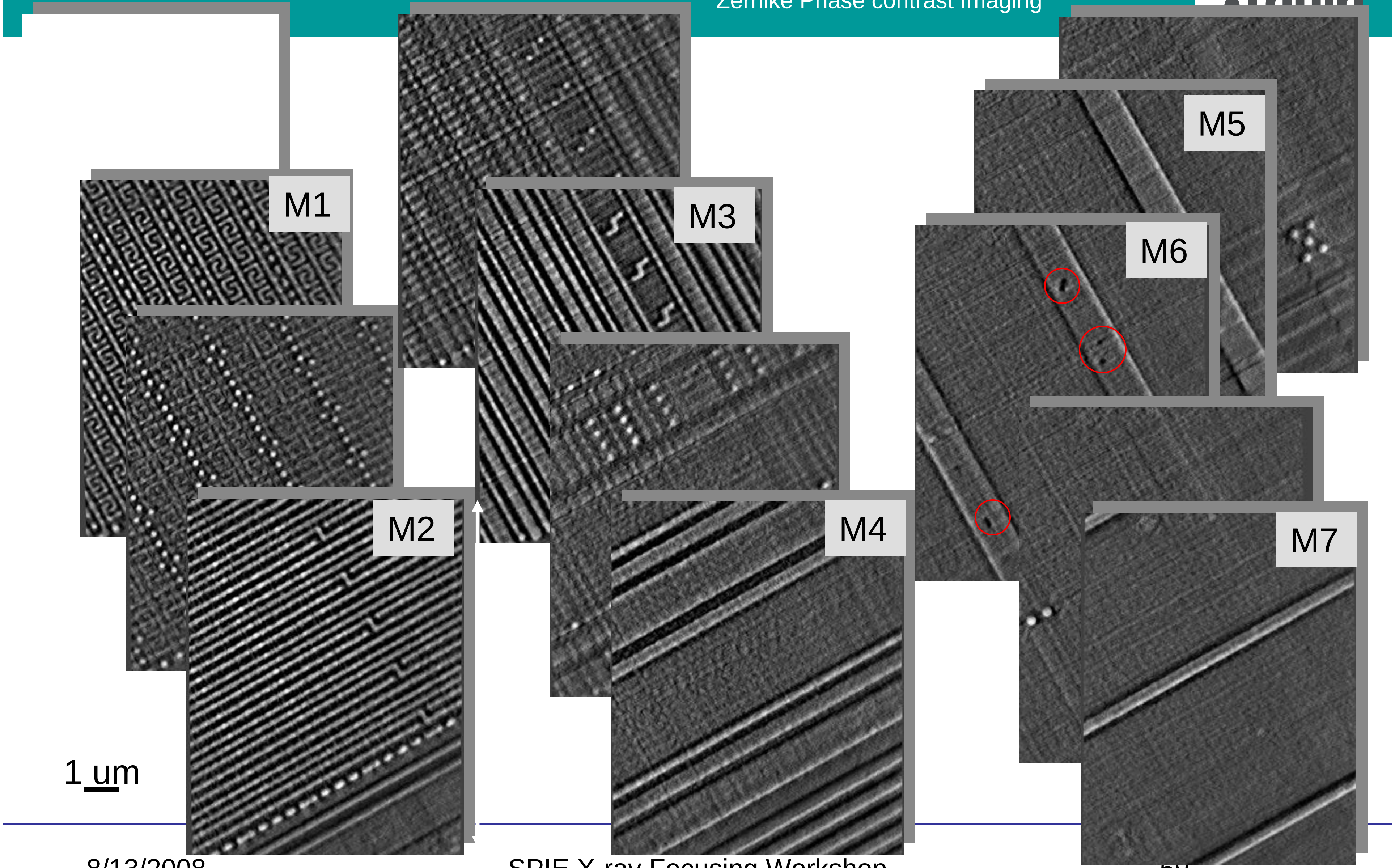

Technologically Relevant Application:
TSV - Through-Silicon Vias (10um Diameter)

10 µm vias tilted at 45 degree.
Tile of 3x3 images 66x66 µm each

All vias have missing electroplating (key hole) in center

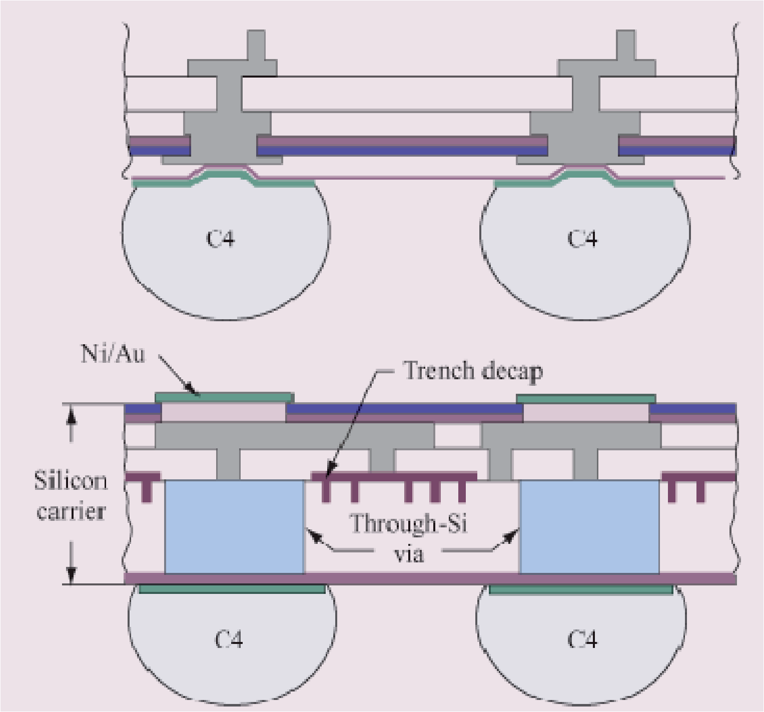

50 µm

Large field of view mode
2 minute exposure per tile

Detailed X-ray Tomography of Single Via

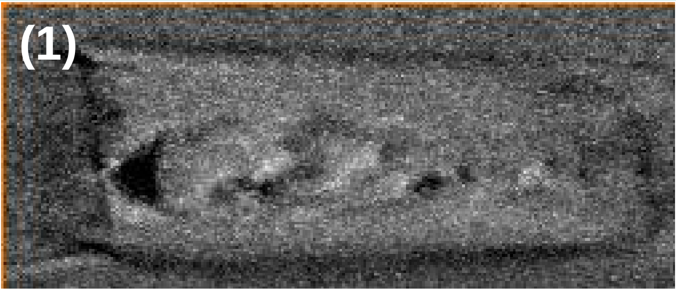

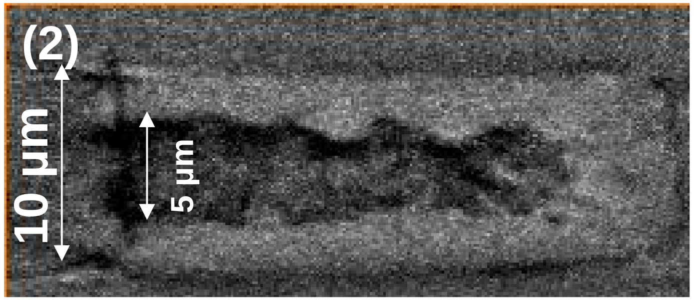

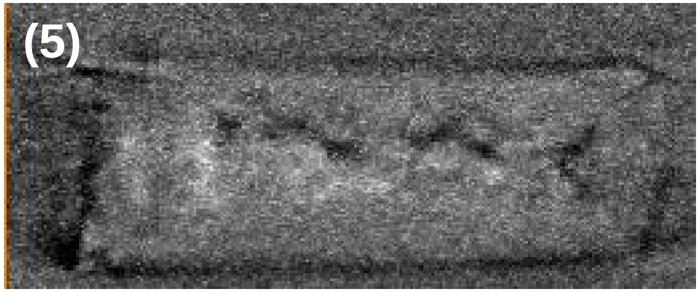

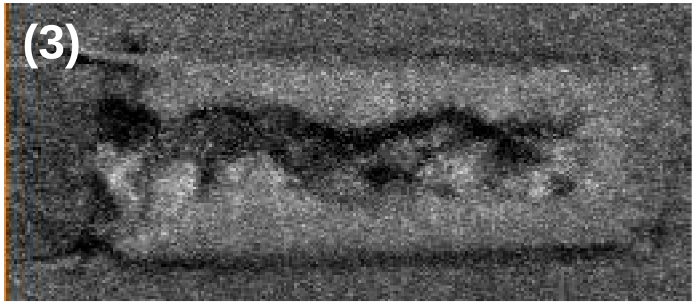

nanoXCT allows direct visualization of the key hole without physical cross-sectioning

Scanning Microscope Geometry and Detectors

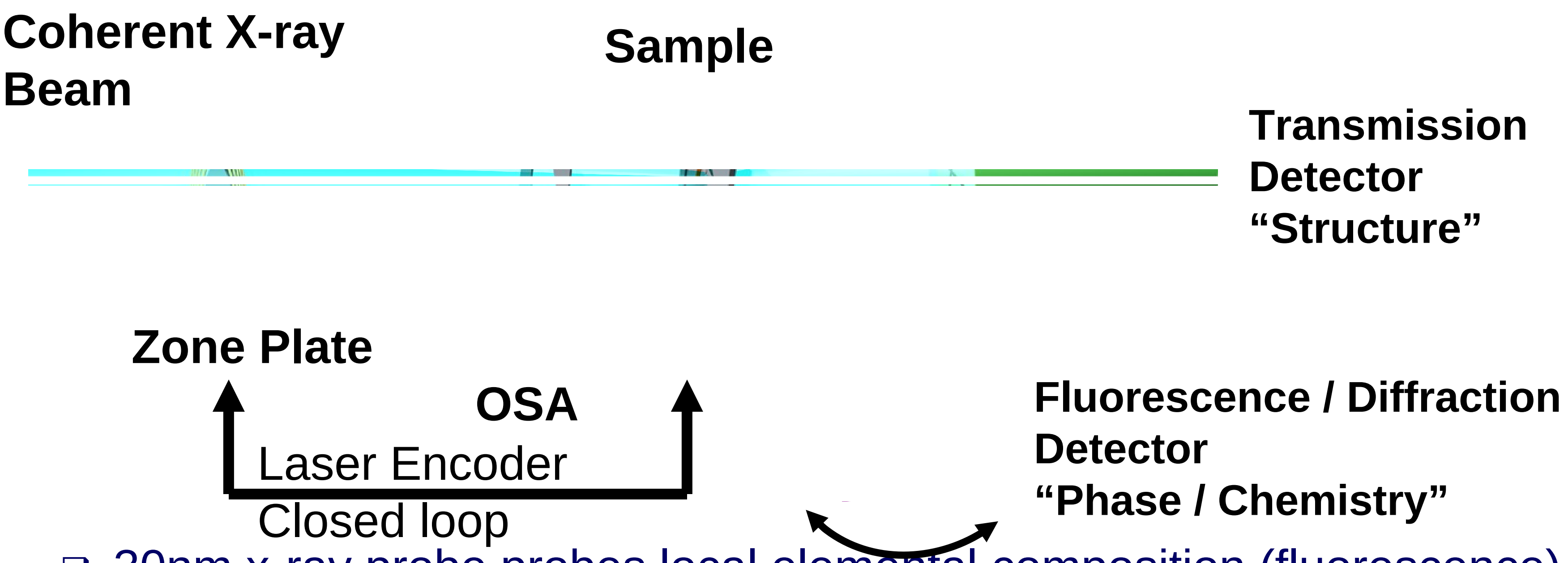

Coherent X-ray Beam

Sample

Transmission Detector “Structure”

Zone Plate

OSA

Laser Encoder Closed loop

Fluorescence / Diffraction Detector “Phase / Chemistry”

- 30nm x-ray probe probes local elemental composition (fluorescence) and crystallinity (diffraction)
- Vibration and drift stability between zone plate and sample are critical for performance
  - laser encoding and stiff stages needed!
- Platform also suited for other coherence based experiments such as diffraction imaging, zone plate holographic methods

Sub-nm Resolution Laser Doppler Encoder

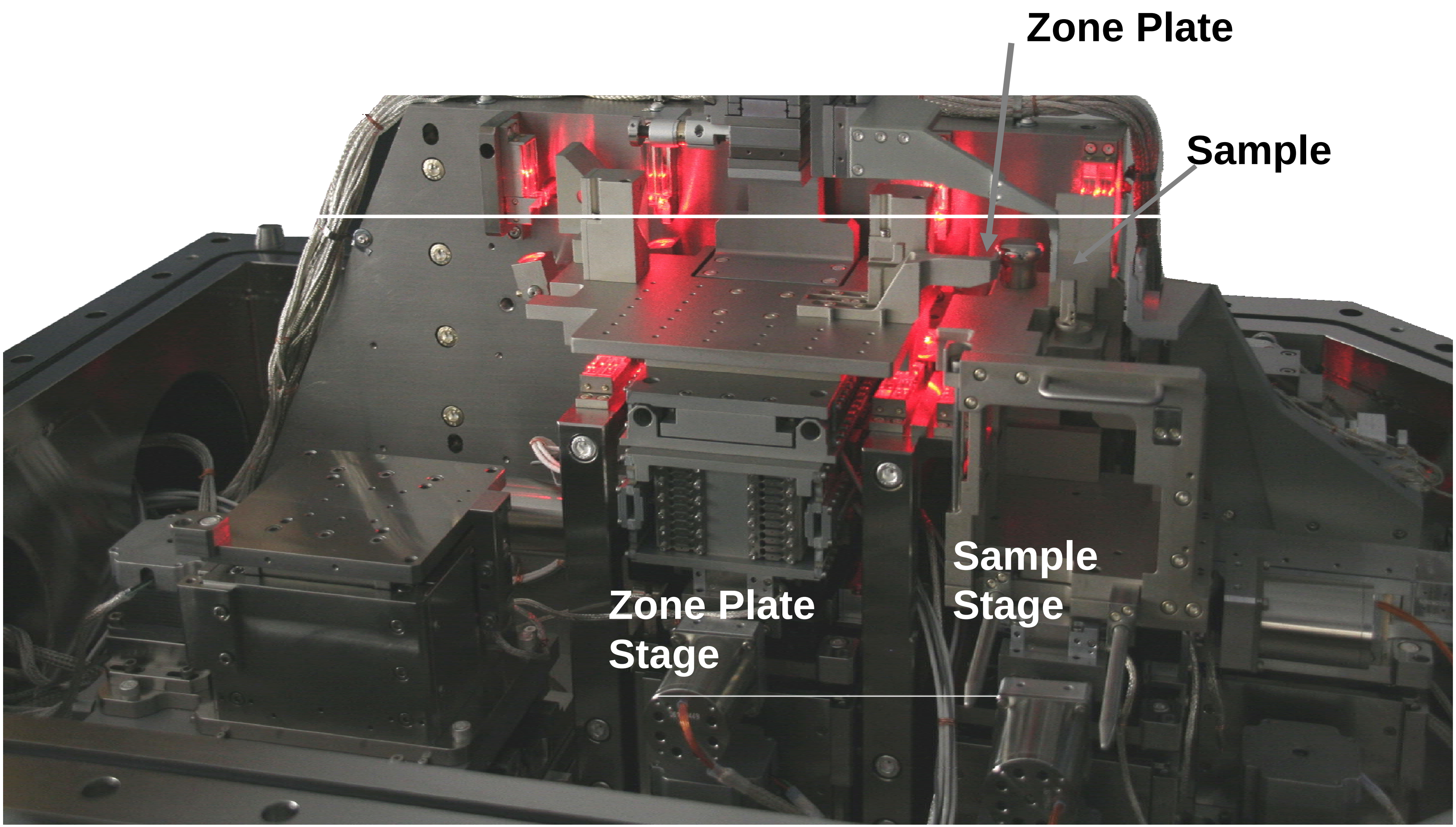

Application Example Fluorescence: Marine Biology
Trace Metals in Plankton and Global Carbon Balance

- Standard approach: bulk analysis
- X-ray microscopy: separate and study individual organism

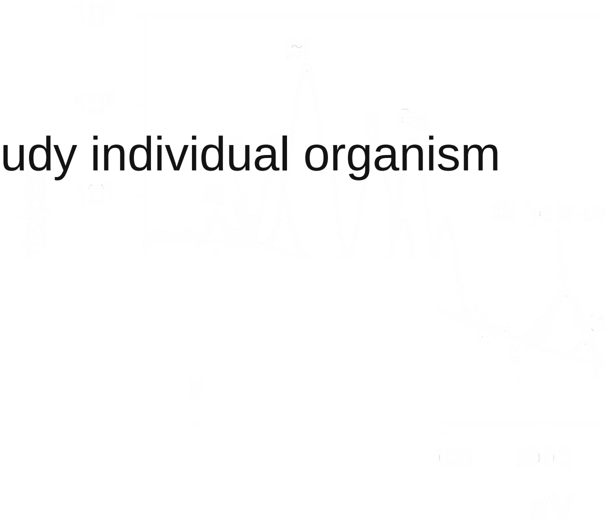

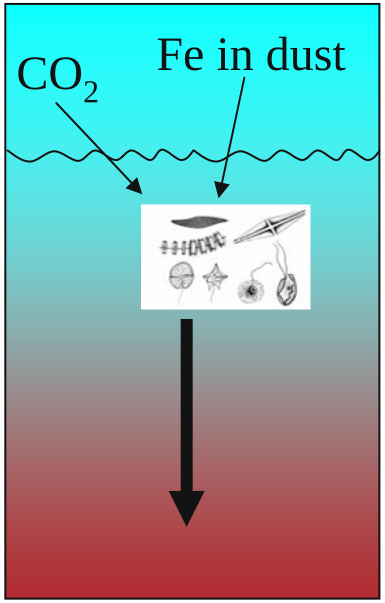

Visible light

- B. Twining, S. Baines *et al.*, Marine Sciences Research Center, SUNY Stony Brook
- A. Osanna, C. Vaa, B. Winn, S. Wirick, C. Jacobsen, Dept. of Physics & Astronomy, SUNY Stony Brook

Composite:
Cl, Fe, Cu

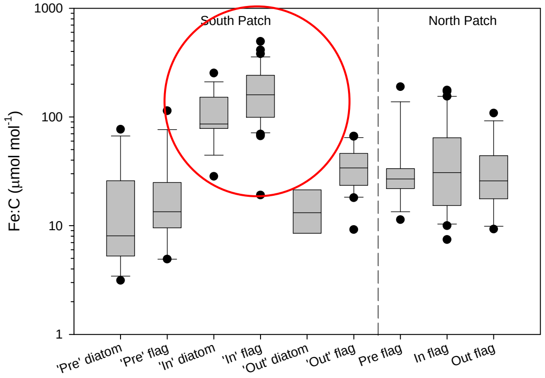

Application Example Diffraction: - Quantum dot stressors on Si Nanomembranes

Ge hut QD
30 nm Si
250 nm

Ge-Si Lattice Lattice Mismatch Distorts Si Membrane

Microdiffraction at
APS Sector 2
hν=11.2 keV
200 nm spot

Prediction: F. Liu, M. Huang, P. Rugheimer, D. E. Savage, and M. G. Lagally, Phys. Rev. Lett. (2002)

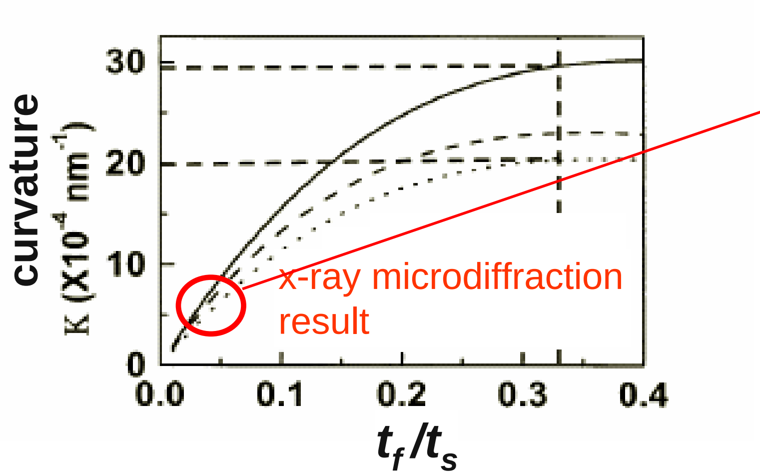

x-ray microdiffraction result

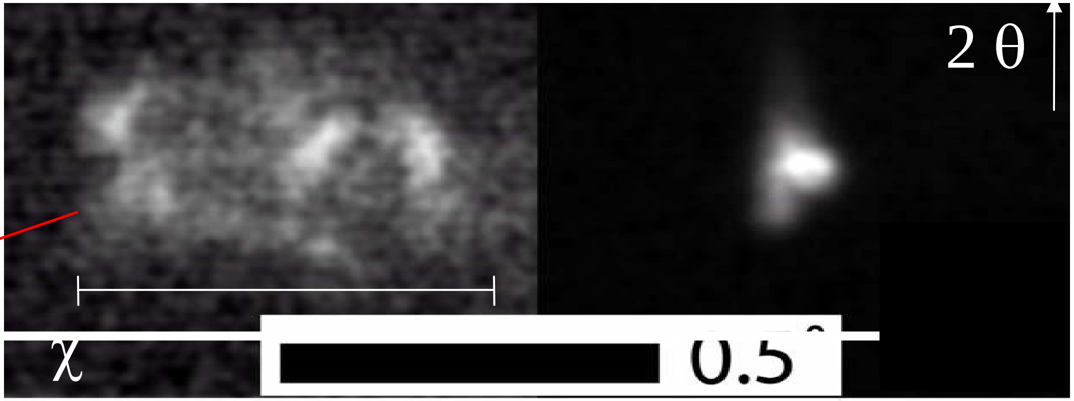

membrane Si (004) reflection with Ge huts

without Ge

University of Wisconsin MRSEC IRG1

P. G. Evans, D. S. Tinberg, M. M. Roberts, M. G. Lagally, Y. Xiao, B. Lai, and Z. Cai, *APL* ***87****, 073112 (2005).*

College of Engineering
University of Wisconsin-Madison

Summary / Outlook

Acknowledgments

NSRRC
Gung-Chian Yin, Y. Whu, K. Liang

SSRL
P. Pianetta, S. Brennan, K. Lüning

APS
Q. Shen, Y. Chu, W-K Lee,
J. Maser, S. Vogt, B. Lai

BSRF
Ziyu Wu, Peiping Zhu

UCSF, NASA Ames
E. Almeida

Cornell
M. van der Meulen

IBM
D. Valett

AMD
E. Zschech, A. Vairagar

Xradia, Inc. team

NSRRC (Taiwan)

SSRL BL-6-2
(Stanford, USA)

APS ID-32, ID-26
Argonne, USA

Acknowledgments

- Chris Jacobsen (Stony Brook), Janos Kirz (LBL) for supplying parts of the material for this presentation
- Customers, collaborators and colleagues for data and information

Thank you for your attention!